

Report on

# Damper System Identification and Change Detection

2 February 2005

Submitted to

California Department of Transportation  
Attention: Dr Allaoua Kartoum  
Division of Engineering Services  
P.O. Box 168041, MS #9-2/5I  
1801 - 30th Street, M.S. 9  
Sacramento, California 95816

## *Final Report*

Contract Number 59A0356  
Covering the Period  
1 October 2002 - 30 June 2004

submitted by

Sami F Masri, Haebum A Yun, Farzad Tasbihgoo, and John P Caffrey  
Department of Civil and Environmental Engineering  
University of Southern California  
Los Angeles, California 90089-2531  
masri@usc.edu

in collaboration with

Nicos Makris and Cameron Black  
Department of Civil and Environmental Engineering  
University of California  
Berkeley, California 94720



## Technical Report Documentation Page

1. Report No. USC-CEE-R2005-1	2. Government Accession No.	3. Recipient's Catalog No.	
4. Title and Subtitle Damper System Identification and Change Detection		5. Report Date 2 February 2005	
		6. Performing Organization Code USC	
7. Author(s) Sami F Masri, Haebum A Yun, Farzad Tasbihgoo, and John P Caffrey		8. Performing Organization Report No.	
9. Performing Organization Name and Address Department of Civil and Environmental Engineering University of Southern California Los Angeles, California 90089-2531		10. Work Unit No. (TRAIS)	
		11. Contract or Grant No. 59A0356	
12. Sponsoring Agency Name and Address California Department of Transportation Division of Engineering Services P.O. Box 168041, MS #9-2/5I 1801 – 30 <sup>th</sup> Street, M.S. 9 Sacramento, California 95816		13. Type of Report and Period Covered Final Report 1 October 2002 – 30 June 2004	
		14. Sponsoring Agency Code	
15. Supplementary Notes This report is submitted with the collaboration of Nicos Makris and Cameron Black of the Department of Civil and Environmental Engineering, University of California Berkeley, California 94720.			
16. Abstract  <p>The goals of this research project were to perform a sequence of analytical and experimental studies designed to shed more light on the numerous challenging technical issues encountered in the characterization of the physical phenomena exhibited by nonlinear viscous dampers, with the aim of evaluating some structural health monitoring approaches. Specific tasks of this project included: (1) Perform a sequence of experimental tests to gain insight into the most sensitive indicators of slight changes in the structural characteristics of the dampers; (2) Construct a theoretical framework to develop nonlinear, reduced-order, high-fidelity mathematical models from experimental structural response measurements, that can be used to detect, quantify, and locate slight changes in the structural system parameters; (3) Investigate the range of validity of nonparametric system identification techniques, such as neural networks, and their utility as a sensitive tool for detecting damage in a monitored structural damper without any a priori information about the topology, or failure modes of the underlying structure.</p> <p>Two typical nonlinear viscous dampers, one a 250 kip size and the other a 15 kip size, were tested at UCB, and the data were supplied to USC to perform detailed analysis using a variety of techniques for developing simplified mathematical models based on the corresponding damper response measures. USC used an adaptable ("smart") magnetorheological (MR) damper to generate vibration measurements corresponding to modified damper characteristics, which were used to mimic changes in the damper vibration signature. The nonparametric data analysis tools that were evaluated, in conjunction with the nonlinear viscous dampers, were subsequently used to detect and quantify the level of observed changes in the MR damper vibration signature.</p> <p>Two parametric (one on-line and the other off-line), and two nonparametric (the Restoring Force Method, and Artificial Neural Networks) system identification approaches are found to be powerful tools for developing reduced order nonlinear models of the tested nonlinear dampers. Provided that the damper state variables and induced force are available from measurements, high-fidelity mathematical models, of different forms and degrees of complexity, can be established and subsequently used for computational purposes, as well as for structural health monitoring applications.</p> <p>Due to the fact that the class of dampers under investigation consists of essentially a uniaxial member, whose force-deformation characteristics can be accurately and completely defined once the underlying state variables are obtained, the uncertainty bounds on the detected changes in such measurements are quite small. Hence, the methods provide an arsenal of powerful signal processing tools that offer the potential for being reliable indicators of small changes in the underlying physical damper characteristics, which can be detected through the application of real-time structural health monitoring methodologies based on vibration signature analysis.</p>			
17. Key Word Nonlinear viscous damper, magnetorheological damper, parametric identification, nonparametric identification, structural health monitoring, damage detection		18. Distribution Statement	
19. Security Classif. (of this report) none	20. Security Classif. (of this page) none	21. No. of Pages	22. Price



## DISCLAIMER

Any opinions, findings, conclusions, or recommendations expressed in this publication do not necessarily reflect the views of the CalTrans. Additionally, neither CalTrans or any of their respective employees make any warranty, expressed or implied, or assume any legal liability or responsibility for the accuracy, completeness, or usefulness of any information, product, or process included in this publication.



# Contents

<b>EXECUTIVE SUMMARY</b>	<b>xiii</b>
<b>ACKNOWLEDGEMENTS</b>	<b>xiii</b>
<b>List of Figures</b>	<b>xix</b>
<b>List of Tables</b>	<b>xxxix</b>
<b>1 INTRODUCTION</b>	<b>1</b>
1.1 Scope of Work . . . . .	2
1.1.1 Task 1: Component Testing of Dampers . . . . .	2
1.1.2 Task 2: Development of an Accurate Mathematical Model for an Individual Damper Element . . . . .	3
1.1.3 Task 3: Evaluation of Damper Modified States . . . . .	3
1.2 Report Organization . . . . .	4
<b>2 TECHNICAL BACKGROUND FOR DATA ANALYSIS TOOLS</b>	<b>5</b>
2.1 Introduction . . . . .	5
2.2 Parametric System Identification . . . . .	5
2.2.1 On-line Parametric System Identification . . . . .	6
2.2.2 Off-Line Parametric System Identification . . . . .	8
2.3 Nonparametric Identification Approaches . . . . .	9

2.3.1	Restoring Force Method . . . . .	9
2.3.2	Artificial Neural Networks . . . . .	13
<b>3</b>	<b>EXPERIMENTAL SETUP FOR THE 250 KIP VISCOUS DAMPER</b>	<b>19</b>
3.1	Damper Specifications . . . . .	19
3.2	Instrumentation . . . . .	19
3.3	Test Specifications . . . . .	21
<b>4</b>	<b>PRELIMINARY DATA PROCESSING FOR THE 250 KIP VISCOUS DAMPER</b>	<b>23</b>
4.1	Data Acquisition . . . . .	23
4.2	Preliminary Data Analysis . . . . .	23
<b>5</b>	<b>PARAMETRIC IDENTIFICATION OF THE 250 KIP VISCOUS DAMPER</b>	<b>27</b>
5.1	Data Sets . . . . .	27
5.2	Parametric Identification Results . . . . .	27
5.2.1	On-Line Parametric Identification Results . . . . .	27
5.2.2	Off-line Parametric Identification Results . . . . .	31
5.3	Summary of the Parametric Identification . . . . .	33
<b>6</b>	<b>NONPARAMETRIC RESTORING FORCE METHOD IDENTIFICATION FOR THE 250 KIP VISCOUS DAMPER</b>	<b>35</b>
6.1	Application of the Restoring Force Method to Collected Data Sets . . . . .	35
6.2	Validation of Restoring Force Method Results . . . . .	43
<b>7</b>	<b>IDENTIFICATION OF THE 250 KIP VISCOUS DAMPER USING ARTIFICIAL NEURAL NETWORKS</b>	<b>49</b>
7.1	Background . . . . .	49
7.2	Application of Artificial Neural Networks to Collected Data Sets . . . . .	49
<b>8</b>	<b>EXPERIMENTAL SETUP FOR THE 15 KIP VISCOUS DAMPER</b>	<b>57</b>

8.1 Damper Specifications . . . . . 57

8.2 Instrumentation . . . . . 57

8.3 Test Specifications . . . . . 59

**9 PRELIMINARY DATA PROCESSING FOR THE 15 KIP VISCOUS DAMPER 61**

9.1 Collection of Data Sets . . . . . 61

9.2 Sample Results of Preliminary Data Analysis . . . . . 61

**10 PARAMETRIC IDENTIFICATION OF THE 15 KIP VISCOUS DAMPER 67**

10.1 First Round of Testing . . . . . 67

10.2 Parametric Identification of the First Round of Testing . . . . . 68

10.2.1 On-line Parametric Identification of the First Round of Testing . . . . . 68

10.2.2 Off-line Parametric Identification of the First Round of Testing . . . . . 68

10.3 Second Round of Testing . . . . . 71

10.4 Parametric Identification of the Second Round of Testing . . . . . 73

10.4.1 On-line Parametric Identification of the Second Round of Testing . . . . . 73

10.4.2 Off-line Parametric Identification of the Second Round of Testing . . . . . 75

10.5 Summary of the Parametric Identification . . . . . 78

**11 NONPARAMETRIC RESTORING FORCE METHOD IDENTIFICATION FOR THE 15 KIP VISCOUS DAMPER 81**

11.1 Problem Formulation of the Restoring Force Method . . . . . 81

11.2 Application and Validation of the Restoring Force Method to Collected Data Sets . . 81

11.3 Statistical Study Using the Restoring Force Method . . . . . 84

**12 IDENTIFICATION OF THE 15 KIP VISCOUS DAMPER USING ARTIFICIAL NEURAL NETWORKS 93**

12.1 Problem Formulation of Artificial Neural Networks . . . . . 93

12.2 Application of Artificial Neural Networks to Collected Data Sets . . . . . 93

<b>13 EXPERIMENTAL SETUP OF THE MAGNETO-RHEOLOGICAL DAMPER</b>	<b>99</b>
13.1 Damper Specifications . . . . .	99
13.2 Test Setup and Instrumentation . . . . .	100
13.3 Test Specifications . . . . .	102
<b>14 MEASUREMENT OF THE MAGNETO-RHEOLOGICAL DAMPER RESPONSE UNDER BROADBAND EXCITATION</b>	<b>107</b>
14.1 Collection of Data Sets . . . . .	107
14.2 Sample Results of Preliminary Data Analysis . . . . .	107
<b>15 NONPARAMETRIC RESTORING FORCE METHOD IDENTIFICATION FOR THE MAGNETO-RHEOLOGICAL DAMPER</b>	<b>113</b>
15.1 Problem Formulation of the Restoring Force Method . . . . .	113
15.2 Application of the Restoring Force Method to Collected Data Sets . . . . .	113
<b>16 IDENTIFICATION OF THE MAGNETO-RHEOLOGICAL DAMPER USING ARTIFICIAL NEURAL NETWORKS</b>	<b>119</b>
16.1 Problem Formulation of Artificial Neural Networks . . . . .	119
16.2 Application of Artificial Neural Networks to Collected Data Sets . . . . .	119
<b>17 DETECTION OF CHANGES IN STRUCTURAL CHARACTERISTICS FOR THE MAGNETO-RHEOLOGICAL DAMPER</b>	<b>123</b>
17.1 Change Detection Using the Restoring Force Method . . . . .	123
17.2 Detection of Change for the Damper Dynamic Response Using the ANN . . . . .	124
<b>18 DISCUSSION</b>	<b>129</b>
18.1 Identification Results of the 250 Kip Viscous Damper . . . . .	129
18.2 Identification Results for the 15 Kip Viscous Damper . . . . .	133
18.2.1 Comparison of the identified manufacturer parameters the damping coefficient $C$ and the exponent $n$ . . . . .	136

18.3 Identification Results of the Magneto-Rheological Damper . . . . . 138

**19 SUMMARY AND CONCLUSIONS 141**

**REFERENCES 143**

**APPENDICES 147**

**A DATA ACQUISITION AND PRELIMINARY DATA PROCESSING FOR THE 250 KIP VISCOUS DAMPER 149**

A.1 Experimental Data (Raw) for the 250 Kip Viscous Damper . . . . . 149

A.2 Data Acquisition and Preliminary Data Processing . . . . . 150

**B PARAMETRIC IDENTIFICATION RESULTS OF THE 250 KIP VISCOUS DAMPER 181**

B.1 On-Line Parametric Identification . . . . . 182

B.2 Off-Line Parametric Identification . . . . . 198

**C NONPARAMETRIC IDENTIFICATION RESULTS FOR THE 250 KIP VISCOUS DAMPER 215**

C.1 Restoring Force Method . . . . . 215

C.2 Artificial Neural Networks . . . . . 231

**D DATA ACQUISITION FOR THE 15 KIP VISCOUS DAMPER - FIRST ROUND 263**

D.1 Experimental Data (Raw) for the 15 Kip Viscous Damper - First Round . . . . . 263

**E DATA ACQUISITION FOR THE 15 KIP VISCOUS DAMPER - SECOND ROUND 281**

E.1 Experimental Data (Raw) for the 15 Kip Viscous Damper - Second Round . . . . . 281

**F PARAMETRIC IDENTIFICATION RESULTS OF THE 15 KIP VISCOUS DAMPER 315**

F.1	Identification Results of 15 Kip Damper for the First Round of Testing . . . . .	316
F.1.1	On-Line Parametric Identification of the First Round of Testing . . . . .	316
F.1.2	Off-Line Parametric Identification of the First Round of Testing . . . . .	319
F.2	Identification Results of 15 kip Damper for the Second Round of Testing . . . . .	322
F.2.1	On-Line Parametric Identification Plots . . . . .	322
F.2.2	Off-Line Parametric Identification Plots . . . . .	327
<b>G NONPARAMETRIC IDENTIFICATION RESULTS FOR THE 15 KIP VIS- COUS DAMPER</b>		<b>333</b>
G.1	Restoring Force Method . . . . .	333
G.1.1	Comparison of Measured and Identified Force for the 15 Kip Damper Using RFM . . . . .	333
G.1.2	Histograms of Chebyshev and Power Series Coefficients for the 15 Kip Damper	344
G.1.3	Probability Density Functions of Chebyshev Coefficients for the 15 Kip Damper	353
G.2	Restoring Force Method . . . . .	362
G.2.1	Comparison of Measured and Identified Force for the 15 Kip Damper Using ANN . . . . .	362
<b>H NONPARAMETRIC IDENTIFICATION RESULTS FOR THE MR DAMPER</b>		<b>367</b>
H.1	Data Acquisition and Preliminary Data Processing . . . . .	367
H.1.1	Summary of Probability Density Functions for the MR Damper Excitation .	367
H.1.2	MR Damper Response for 1.0 Ampere Input Current (Nominal Case, 100%)	369
H.1.3	MR Damper Response for 0.95 Ampere Input Current (95%) . . . . .	373
H.1.4	MR Damper Response for 0.90 Ampere Input Current (90%) . . . . .	377
H.1.5	MR Damper Response for 0.75 Ampere Input Current (75%) . . . . .	381
H.2	Restoring Force Method . . . . .	385
H.2.1	Comparison of Measured and Identified MR Damper Force for 1.00 Ampere Input Current (100%) . . . . .	385

H.2.2 Comparison of Measured and Identified MR Damper Force for 0.95 Ampere  
Input Current (95%) . . . . . 389

H.2.3 Comparison of Measured and Identified MR Damper Force for 0.90 Ampere  
Input Current (90%) . . . . . 393

H.2.4 Comparison of Measured and Identified MR Damper Force for 0.75 Ampere  
Input Current (75%) . . . . . 397

H.2.5 Chebyshev Coefficients for the MR Damper . . . . . 401

H.3 Artificial Neural Networks . . . . . 405



## EXECUTIVE SUMMARY

### Background

Viscous dampers are integral components of the retrofit strategies that have been adopted for several California toll bridges. Design engineers have realized their economic and engineering advantage in dissipating the large anticipated wind and seismic forces. Viscous dampers are being specified more frequently in designs, allowing substantial reduction in member sizes, and subsequent economic savings.

Due to the significant role dampers play in the retrofit schemes, it is imperative that health monitoring applications be researched. Health monitoring processes provide potential remote sensing abilities to continuously evaluate the integrity of components. The goals of the research project reported herein were achieved by performing a sequence of analytical and experimental studies designed to shed more light on the numerous challenging technical issues encountered in the characterization of the physical phenomena exhibited by the structural damper components. Specific tasks of this research project included:

1. Perform a sequence of experimental tests to gain insight into the most sensitive indicators of slight changes in the structural characteristics of the dampers.
2. Construct a theoretical framework to develop nonlinear, reduced-order, high-fidelity mathematical models from experimental structural response measurements, that can be used to detect, quantify, and locate slight changes in the structural system parameters.
3. Investigate the range of validity of nonparametric system identification techniques, such as neural networks, and their utility as a sensitive tool for detecting damage in a monitored structural damper without any a priori information about the topology, or failure modes of the underlying structure.

### Accomplishments

Two typical nonlinear viscous dampers, one a 250 kip size and the other a 15 kip size, were tested at UCB, and the data were supplied to USC to perform detailed analysis using a variety of techniques for developing simplified mathematical models based on the corresponding damper response measures. The dampers examined were identified according to their force output when subjected to their peak design velocity. The peak design velocity was never reached during the tests presented in this report (i.e. the 250 kip damper outputs 250 kips at 42 in/sec piston velocity).

USC used an adaptable (“smart”) magnetorheological (MR) damper to generate vibration measurements corresponding to modified damper characteristics, which were used to mimic changes in

the damper vibration signature. The nonparametric data analysis tools that were evaluated, in conjunction with the nonlinear viscous dampers, were subsequently used to detect and quantify the level of observed changes in the MR damper vibration signature.

## **Findings**

Two parametric (one on-line and the other off-line), and two nonparametric (the Restoring Force Method, and Artificial Neural Networks) system identification approaches are found to be powerful tools for developing reduced order nonlinear models of the tested nonlinear dampers. Provided that the damper state variables and induced force are available from measurements, high-fidelity mathematical models, of different forms and degrees of complexity, can be established and subsequently used for computational purposes, as well as for structural health monitoring applications.

Due to the fact that the class of dampers under investigation consists of essentially a uniaxial member, whose force-deformation characteristics can be accurately and completely defined once the underlying state variables are obtained, the uncertainty bounds on the detected changes in such measurements are quite small. Hence, the methods provide an arsenal of powerful signal processing tools that offer the potential for being reliable indicators of small changes in the underlying physical damper characteristics, which can be detected through the application of real-time structural health monitoring methodologies based on vibration signature analysis.

## **Recommendations**

Tests should be conducted on full-scale nonlinear viscous dampers to assemble a catalogue of vibration signatures associated with induced plausible failure/damage states of varying type, location, magnitude, and rate of change. The availability of such information will enable Caltrans maintenance personnel to ascertain the nature of the inherent damper damage based on the mathematical representation of observed vibration measurements.

To achieve maximum reliability and sensitivity (threshold level) of change detection for the monitored damper characteristics, it is highly desirable to measure the time history of the monitored damper force. Suitable instrumentation should be incorporated in future installation of dampers, and similar response modification devices.

## ACKNOWLEDGMENTS

Partial financial support for this study was provided by the California Department of Transportation under Contract # 59A0356. The valuable input and comments of Caltrans engineers A Kartoum, M Keever and C Sikorsky are appreciated.

The 250 kip damper was donated by Caltrans, while the 15 kip damper was donated by Taylor Devices during a past research project at U.C. Berkeley funded by Caltrans.

The authors would like to acknowledge the assistance of E Kallinikidou in the preparation of the manuscript.



# List of Figures

- 2.1 Schematic of single degree-of-freedom system. . . . . 10
- 2.2 Damper simulation response polluted with noise signal. . . . . 12
- 2.3 Comparison of measured force (dashed line) and identified restoring force (solid line). 12
- 2.4 Dynamic response of a SDOF linear system. . . . . 15
- 2.5 Comparison of the reference and identified restoring forces for a SDOF linear system. 16
- 2.6 Dynamic response of a SDOF nonlinear system. . . . . 17
- 2.7 Comparison of the reference and identified restoring forces for a SDOF nonlinear system. . . . . 18
  
- 3.1 The 250 kip damper installed on the damper testing machine of the University of California. . . . . 20
  
- 4.1 Time history of the 250 kip damper response subjected to sinusoidal excitation. . . . 24
- 4.2 Time histories of the 250 kip damper response subjected to sinusoidal excitation after preliminary data processing. . . . . 25
- 4.3 Phase plots of the 250 kip damper response subjected to sinusoidal excitation after preliminary data processing. . . . . 26
  
- 5.1 Sample measured data of the 250 kip damper for data set UCB1\_17\_7 . . . . . 28
- 5.2 On-line parametric identification results of the 250 kip damper for data set UCB1\_17\_7 30
- 5.3 Off-line parametric identification results of the 250 kip damper for data set UCB1\_17\_7 32

6.1	The third order RFM identification results for the 250 kip damper response subjected to sinusoidal excitation. . . . .	36
6.2	The fifth order RFM identification results for the 250 kip damper response subjected to sinusoidal excitation. . . . .	37
6.3	Comparison of the measured and identified time history response of the 250 kip damper using RFM. . . . .	39
6.4	Comparison of the measured and identified response of the 250 kip damper in phase plot using RFM. . . . .	40
6.5	Identified RFM coefficients for the 250 kip damper subjected to sinusoidal excitation.	41
6.6	Low order stiffness and damping coefficients for the 250 kip damper subjected to sinusoidal excitation. . . . .	42
6.7	Comparison of normalized Chebyshev coefficients of the 250 kip damper subjected to sinusoidal excitations with different peak velocity. . . . .	46
6.8	Comparison of low order Chebyshev coefficients of the 250 kip damper subjected to sinusoidal excitations with different peak velocity. . . . .	47
7.1	The displacement, velocity and acceleration of the 250 kip damper as the input of the neural networks. . . . .	50
7.2	The force of the 250 kip damper as the output of the neural networks. . . . .	50
7.3	Ratio of the current error function normalized by the starting error function and the current optimal standard deviation of random step size. . . . .	52
7.4	Comparison of the measured and identified damper response to sinusoidal excitation in time history using ANN. . . . .	53
7.5	Comparison of the measured and identified damper response in phase plot to sinusoidal excitation using ANN. . . . .	54
8.1	The 15 kip viscous damper testing setup at the University of California, Berkeley. . .	58
9.1	Measured dynamic response of the 15 kip damper in the first round experiments for the data set Qrt1.01. . . . .	62

9.2 Measured oil and surface temperatures of the 15 kip damper in the first round experiments for the data set Qrt1\_01. . . . . 63

9.3 Measured dynamic response of the 15 kip damper in the second round experiments for the data set usc\_5\_400\_q4. . . . . 64

9.4 Measured oil and surface temperatures of the 15 kip damper in the second round experiments for the data set usc\_5\_400\_q4. . . . . 65

9.5 Sample result of the measured displacement (solid line) and the double-integrated displacement using the measured acceleration (dashed line) of the 15 kip damper. . . 66

10.1 sample measured data of the 15 kip damper for data set Qtr4\_0125 . . . . . 69

10.2 On-line parametric identification results of 15 kip damper for data set Qtr4\_0125 . . 70

10.3 Off-line parametric identification results of 15 kip damper for data set Qtr4\_0125 . . 72

10.4 Sample measured data of the 15 kip damper for data set usc\_5400\_q4 . . . . . 74

10.5 On-line parametric identification results of the 15 kip damper for data set usc\_5400\_q4 76

10.6 Off-line parametric identification results of the 15 kip damper for data set usc\_5400\_q4 77

11.1 Comparison of the measured and identified damper response to broadband excitation in time history using RFM. . . . . 83

11.2 The response of the 15 kip damper subjected to broadband excitation. . . . . 86

11.3 Comparison of the measured and identified 15 kip damper response using RFM. . . 87

11.4 Summary of the RFM identification of the 15 kip damper subjected to broadband excitation. . . . . 88

11.5 Histogram of the dc, stiffness and damping Chebyshev coefficients of 15 kip damper subjected to broadband excitation. . . . . 89

11.6 Probability density function of the damping and stiffness Chebyshev coefficients of the 15 kip damper for the data set Qtr1\_01. . . . . 90

11.7 Probability density function of the damping and stiffness Chebyshev coefficients of the 15 kip damper for the data set Qtr1\_0125. . . . . 91

12.1 Ratio of the current error function normalized by the starting error function and the current optimal standard deviation of random step size. . . . . 94

12.2 Comparison of the measured and identified damper response to broadband excitation using ANN. . . . .	96
13.1 Magneto-rheological damper and water-cooling system. . . . .	100
13.2 Magneto-rheological damper test setup at the Structural Dynamics Laboratory of the University of Southern California. . . . .	102
13.3 A schematic of sensor/actuator system of MR-damper test setup. . . . .	103
13.4 The data acquisition software interface programmed in Labview for the MR damper experiments. . . . .	104
13.5 Displacement time history of the shaker motion for MR damper experiments. . . . .	105
14.1 Probability density function of the MR damper excitation. . . . .	108
14.2 The displacement of the MR damper subjected to broadband excitation. . . . .	108
14.3 The velocity of the MR damper subjected to broadband excitation. . . . .	109
14.4 The acceleration of the MR damper subjected to broadband excitation. . . . .	109
14.5 The force of the MR damper subjected to broadband excitation. . . . .	110
14.6 MR damper response to broadband excitation in phase plot. . . . .	111
15.1 Comparison of the measured and identified damper response in time history using RFM for 1.0 ampere MR damper input current test No. 1. . . . .	114
15.2 Comparison of the measured and identified damper response in time history using RFM for 0.75 ampere MR damper input current test No. 1. . . . .	114
15.3 The averaged restoring force coefficients for 1.0 ampere MR damper input current. . . . .	117
16.1 Ratio of the current error function for the nominal case normalized by the starting error function (solid line) and the current optimal standard deviation of random step size (dashed line). The y-axis is plotted in log scale. . . . .	121
16.2 Comparison of the measured and identified damper response to broadband excitation using ANN. . . . .	122

17.1	The averaged normalized Chebyshev coefficients with the 5th order curve fitting for different MR-damper input currents. . . . .	125
17.2	The first and third order RFM coefficients of the MR-damper subjected to broadband excitation. . . . .	126
17.3	The ratio of the first and third order RFM coefficients of the MR-damper subjected to broadband excitation. . . . .	127
17.4	Comparison of the estimated and measured damping response using the ANN for different MR-damper input current levels. . . . .	128
18.1	Comparison of the estimated and measured damping response using the RFM for different MR-damper input current levels. . . . .	140
A.1	Time history plot of the 250 kip damper response subjected to sinusoidal excitation for the data set UCB1_10_4. . . . .	151
A.2	Phase plot of the 250 kip damper response subjected to sinusoidal excitation for the data set UCB1_10_4. . . . .	152
A.3	Time history plot of the 250 kip damper response subjected to sinusoidal excitation for the data set UCB1_10_5. . . . .	153
A.4	Phase plot of the 250 kip damper response subjected to sinusoidal excitation for the data set UCB1_10_5. . . . .	154
A.5	Time history plot of the 250 kip damper response subjected to sinusoidal excitation for the data set UCB1_10_6. . . . .	155
A.6	Phase plot of the 250 kip damper response subjected to sinusoidal excitation for the data set UCB1_10_6. . . . .	156
A.7	Time history plot of the 250 kip damper response subjected to sinusoidal excitation for the data set UCB1_12_4. . . . .	157
A.8	Phase plot of the 250 kip damper response subjected to sinusoidal excitation for the data set UCB1_12_4. . . . .	158
A.9	Time history plot of the 250 kip damper response subjected to sinusoidal excitation for the data set UCB1_12_5. . . . .	159

A.10 Phase plot of the 250 kip damper response subjected to sinusoidal excitation for the data set UCB1_12_5. . . . .	160
A.11 Time history plot of the 250 kip damper response subjected to sinusoidal excitation for the data set UCB1_12_6. . . . .	161
A.12 Phase plot of the 250 kip damper response subjected to sinusoidal excitation for the data set UCB1_12_6. . . . .	162
A.13 Time history plot of the 250 kip damper response subjected to sinusoidal excitation for the data set UCB1_12_7. . . . .	163
A.14 Phase plot of the 250 kip damper response subjected to sinusoidal excitation for the data set UCB1_12_7. . . . .	164
A.15 Time history plot of the 250 kip damper response subjected to sinusoidal excitation for the data set UCB1_15_4. . . . .	165
A.16 Phase plot of the 250 kip damper response subjected to sinusoidal excitation for the data set UCB1_15_4. . . . .	166
A.17 Time history plot of the 250 kip damper response subjected to sinusoidal excitation for the data set UCB1_15_5. . . . .	167
A.18 Phase plot of the 250 kip damper response subjected to sinusoidal excitation for the data set UCB1_15_5. . . . .	168
A.19 Time history plot of the 250 kip damper response subjected to sinusoidal excitation for the data set UCB1_15_6. . . . .	169
A.20 Phase plot of the 250 kip damper response subjected to sinusoidal excitation for the data set UCB1_15_6. . . . .	170
A.21 Time history plot of the 250 kip damper response subjected to sinusoidal excitation for the data set UCB1_15_7. . . . .	171
A.22 Phase plot of the 250 kip damper response subjected to sinusoidal excitation for the data set UCB1_15_7. . . . .	172
A.23 Time history plot of the 250 kip damper response subjected to sinusoidal excitation for the data set UCB1_17_4. . . . .	173
A.24 Phase plot of the 250 kip damper response subjected to sinusoidal excitation for the data set UCB1_17_4. . . . .	174

A.25 Time history plot of the 250 kip damper response subjected to sinusoidal excitation for the data set UCB1\_17\_5. . . . . 175

A.26 Phase plot of the 250 kip damper response subjected to sinusoidal excitation for the data set UCB1\_17\_5. . . . . 176

A.27 Time history plot of the 250 kip damper response subjected to sinusoidal excitation for the data set UCB1\_17\_6. . . . . 177

A.28 Phase plot of the 250 kip damper response subjected to sinusoidal excitation for the data set UCB1\_17\_6. . . . . 178

A.29 Time history plot of the 250 kip damper response subjected to sinusoidal excitation for the data set UCB1\_17\_7. . . . . 179

A.30 Phase plot of the 250 kip damper response subjected to sinusoidal excitation for the data set UCB1\_17\_7. . . . . 180

B.1 On-line parametric identification results of the 250 kip damper for data set UCB1\_10\_4183

B.2 On-line parametric identification results of the 250 kip damper for data set UCB1\_10\_5184

B.3 On-line parametric identification results of the 250 kip damper for data set UCB1\_10\_6185

B.4 On-line parametric identification results of the 250 kip damper for data set UCB1\_12\_4186

B.5 On-line parametric identification results of the 250 kip damper for data set UCB1\_12\_5187

B.6 On-line parametric identification results of the 250 kip damper for data set UCB1\_12\_6188

B.7 On-line parametric identification results of the 250 kip damper for data set UCB1\_12\_7189

B.8 On-line parametric identification results of the 250 kip damper for data set UCB1\_15\_4190

B.9 On-line parametric identification results of the 250 kip damper for data set UCB1\_15\_5191

B.10 On-line parametric identification results of the 250 kip damper for data set UCB1\_15\_6192

B.11 On-line parametric identification results of the 250 kip damper for data set UCB1\_15\_7193

B.12 On-line parametric identification results of the 250 kip damper for data set UCB1\_17\_4194

B.13 On-line parametric identification results of the 250 kip damper for data set UCB1\_17\_5195

B.14 On-line parametric identification results of the 250 kip damper for data set UCB1\_17\_6196

B.15 On-line parametric identification results of the 250 kip damper for data set UCB1\_17\_7197

B.16	Off-line parametric identification results of the 250 kip damper for data set UCB1_10.4199	
B.17	Off-line parametric identification results of the 250 kip damper for data set UCB1_10.5200	
B.18	Off-line parametric identification results of the 250 kip damper for data set UCB1_10.6201	
B.19	Off-line parametric identification results of the 250 kip damper for data set UCB1_12.4202	
B.20	Off-line parametric identification results of the 250 kip damper for data set UCB1_12.5203	
B.21	Off-line parametric identification results of the 250 kip damper for data set UCB1_12.6204	
B.22	Off-line parametric identification results of the 250 kip damper for data set UCB1_12.7205	
B.23	Off-line parametric identification results of the 250 kip damper for data set UCB1_15.4206	
B.24	Off-line parametric identification results of the 250 kip damper for data set UCB1_15.5207	
B.25	Off-line parametric identification results of the 250 kip damper for data set UCB1_15.6208	
B.26	Off-line parametric identification results of the 250 kip damper for data set UCB1_15.7209	
B.27	Off-line parametric identification results of the 250 kip damper for data set UCB1_17.4210	
B.28	Off-line parametric identification results of the 250 kip damper for data set UCB1_17.5211	
B.29	Off-line parametric identification results of the 250 kip damper for data set UCB1_17.6212	
B.30	Off-line parametric identification results of the 250 kip damper for data set UCB1_17.7213	
C.1	Comparison of the measured and identified damper response in time history using RFM for the data set UCB1_10.4. . . . .	216
C.2	Comparison of the measured and identified damper response in time history using RFM for the data set UCB1_10.5. . . . .	217
C.3	Comparison of the measured and identified damper response in time history using RFM for the data set UCB1_10.6. . . . .	218
C.4	Comparison of the measured and identified damper response in time history using RFM for the data set UCB1_12.4. . . . .	219
C.5	Comparison of the measured and identified damper response in time history using RFM for the data set UCB1_12.5. . . . .	220
C.6	Comparison of the measured and identified damper response in time history using RFM for the data set UCB1_12.6. . . . .	221

C.7 Comparison of the measured and identified damper response in time history using RFM for the data set UCB1\_12.7. . . . . 222

C.8 Comparison of the measured and identified damper response in time history using RFM for the data set UCB1\_15.4. . . . . 223

C.9 Comparison of the measured and identified damper response in time history using RFM for the data set UCB1\_15.5. . . . . 224

C.10 Comparison of the measured and identified damper response in time history using RFM for the data set UCB1\_15.6. . . . . 225

C.11 Comparison of the measured and identified damper response in time history using RFM for the data set UCB1\_15.7. . . . . 226

C.12 Comparison of the measured and identified damper response in time history using RFM for the data set UCB1\_17.4. . . . . 227

C.13 Comparison of the measured and identified damper response in time history using RFM for the data set UCB1\_17.5. . . . . 228

C.14 Comparison of the measured and identified damper response in time history using RFM for the data set UCB1\_17.6. . . . . 229

C.15 Comparison of the measured and identified damper response in time history using RFM for the data set UCB1\_17.7. . . . . 230

C.16 Comparison of the measured and identified damper response in time history using ANN for the data set UCB1\_10.4. . . . . 232

C.17 Comparison of measured and identified damper response in phase plot using ANN for the data set UCB1\_10.4. . . . . 233

C.18 Comparison of the measured and identified damper response in time history using ANN for the data set UCB1\_10.5. . . . . 234

C.19 Comparison of measured and identified damper response using ANN in phase plot for the data set UCB1\_10.5. . . . . 235

C.20 Comparison of the measured and identified damper response using ANN in time history for the data set UCB1\_10.6. . . . . 236

C.21 Comparison of measured and identified damper response using ANN in phase plot for the data set UCB1\_10.6. . . . . 237

C.22 Comparison of the measured and identified damper response using ANN in time history for the data set UCB1_12_4. . . . .	238
C.23 Comparison of measured and identified damper response using ANN in phase plot for the data set UCB1_12_4. . . . .	239
C.24 Comparison of the measured and identified damper response using ANN in time history for the data set UCB1_12_5. . . . .	240
C.25 Comparison of measured and identified damper response using ANN in phase plot for the data set UCB1_12_5. . . . .	241
C.26 Comparison of the measured and identified damper response using ANN in time history for the data set UCB1_12_6. . . . .	242
C.27 Comparison of measured and identified damper response using ANN in phase plot for the data set UCB1_12_6. . . . .	243
C.28 Comparison of the measured and identified damper response using ANN in time history for the data set UCB1_12_7. . . . .	244
C.29 Comparison of measured and identified damper response using ANN in phase plot for the data set UCB1_12_7. . . . .	245
C.30 Comparison of the measured and identified damper response using ANN in time history for the data set UCB1_15_4. . . . .	246
C.31 Comparison of measured and identified damper response using ANN in phase plot for the data set UCB1_15_4. . . . .	247
C.32 Comparison of the measured and identified damper response using ANN in time history for the data set UCB1_15_5. . . . .	248
C.33 Phase plots of measured and identified damper response using ANN in phase plot for the data set UCB1_15_5. . . . .	249
C.34 Comparison of the measured and identified damper response using ANN in time history for the data set UCB1_15_6. . . . .	250
C.35 Phase plots of measured and identified damper response using ANN in phase plot for the data set UCB1_15_6. . . . .	251
C.36 Comparison of the measured and identified damper response using ANN in time history for the data set UCB1_15_7. . . . .	252

C.37 Phase plots of measured and identified damper response using ANN in phase plot for the data set UCB1\_15\_7. . . . . 253

C.38 Comparison of the measured and identified damper response using ANN in time history for the data set UCB1\_17\_4. . . . . 254

C.39 Phase plots of measured and identified damper response using ANN in phase plot for the data set UCB1\_17\_4. . . . . 255

C.40 Comparison of the measured and identified damper response using ANN in time history for the data set UCB1\_17\_5. . . . . 256

C.41 Phase plots of measured and identified damper response using ANN in phase plot for the data set UCB1\_17\_5. . . . . 257

C.42 Comparison of the measured and identified damper response using ANN in time history for the data set UCB1\_17\_6. . . . . 258

C.43 Comparison of measured and identified damper response using ANN in phase plot for the data set UCB1\_17\_6. . . . . 259

C.44 Comparison of the measured and identified damper response using ANN in time history for the data set UCB1\_17\_7. . . . . 260

C.45 Phase plots of measured and identified damper response using ANN in phase plot for the data set UCB1\_17\_7. . . . . 261

D.1 Measured dynamic response of the 15 kip damper in the first round experiments for the data set Qrt1\_01. . . . . 265

D.2 Measured oil and surface temperatures of the 15 kip damper in the first round experiments for the data set Qrt1\_01. . . . . 266

D.3 Measured dynamic response of the 15 kip damper in the first round experiments for the data set Qrt2\_01. . . . . 267

D.4 Measured oil and surface temperatures of the 15 kip damper in the first round experiments for the data set Qrt2\_01. . . . . 268

D.5 Measured dynamic response of the 15 kip damper in the first round experiments for the data set Qrt3\_01. . . . . 269

D.6 Measured oil and surface temperatures of the 15 kip damper in the first round experiments for the data set Qrt3\_01. . . . . 270

D.7	Measured dynamic response of the 15 kip damper in the first round experiments for the data set Qrt4.01. . . . .	271
D.8	Measured oil and surface temperatures of the 15 kip damper in the first round experiments for the data set Qrt4.01. . . . .	272
D.9	Measured dynamic response of the 15 kip damper in the first round experiments for the data set Qrt1.0125. . . . .	273
D.10	Measured oil and surface temperatures of the 15 kip damper in the first round experiments for the data set Qrt1.0125. . . . .	274
D.11	Measured dynamic response of the 15 kip damper in the first round experiments for the data set Qrt2.0125. . . . .	275
D.12	Measured oil and surface temperatures of the 15 kip damper in the first round experiments for the data set Qrt2.0125. . . . .	276
D.13	Measured dynamic response of the 15 kip damper in the first round experiments for the data set Qrt3.0125. . . . .	277
D.14	Measured oil and surface temperatures of the 15 kip damper in the first round experiments for the data set Qrt3.0125. . . . .	278
D.15	Measured dynamic response of the 15 kip damper in the first round experiments for the data set Qrt4.0125. . . . .	279
D.16	Measured oil and surface temperatures of the 15 kip damper in the first round experiments for the data set Qrt4.0125. . . . .	280
E.1	Measured dynamic response of the 15 kip damper in the second round experiments for the data set usc_10.175_q1. . . . .	283
E.2	Measured oil and surface temperatures of the 15 kip damper in the second round experiments for the data set usc_10.175_q1. . . . .	284
E.3	Measured dynamic response of the 15 kip damper in the second round experiments for the data set usc_10.175_q2. . . . .	285
E.4	Measured oil and surface temperatures of the 15 kip damper in the second round experiments for the data set usc_10.175_q2. . . . .	286
E.5	Measured dynamic response of the 15 kip damper in the second round experiments for the data set usc_10.175_q3. . . . .	287

E.6 Measured oil and surface temperatures of the 15 kip damper in the second round experiments for the data set usc\_10\_175\_q3. . . . . 288

E.7 Measured dynamic response of the 15 kip damper in the second round experiments for the data set usc\_10\_175\_q4. . . . . 289

E.8 Measured oil and surface temperatures of the 15 kip damper in the second round experiments for the data set usc\_10\_175\_q4. . . . . 290

E.9 Measured dynamic response of the 15 kip damper in the second round experiments for the data set usc\_10\_200\_q1. . . . . 291

E.10 Measured oil and surface temperatures of the 15 kip damper in the second round experiments for the data set usc\_10\_200\_q1. . . . . 292

E.11 Measured dynamic response of the 15 kip damper in the second round experiments for the data set usc\_10\_200\_q2. . . . . 293

E.12 Measured oil and surface temperatures of the 15 kip damper in the second round experiments for the data set usc\_10\_200\_q2. . . . . 294

E.13 Measured dynamic response of the 15 kip damper in the second round experiments for the data set usc\_10\_200\_q3. . . . . 295

E.14 Measured oil and surface temperatures of the 15 kip damper in the second round experiments for the data set usc\_10\_200\_q3. . . . . 296

E.15 Measured dynamic response of the 15 kip damper in the second round experiments for the data set usc\_10\_200\_q4. . . . . 297

E.16 Measured oil and surface temperatures of the 15 kip damper in the second round experiments for the data set usc\_10\_200\_q4. . . . . 298

E.17 Measured dynamic response of the 15 kip damper in the second round experiments for the data set usc\_5\_300\_q1. . . . . 299

E.18 Measured oil and surface temperatures of the 15 kip damper in the second round experiments for the data set usc\_5\_300\_q1. . . . . 300

E.19 Measured dynamic response of the 15 kip damper in the second round experiments for the data set usc\_5\_300\_q2. . . . . 301

E.20 Measured oil and surface temperatures of the 15 kip damper in the second round experiments for the data set usc\_5\_300\_q2. . . . . 302

E.21 Measured dynamic response of the 15 kip damper in the second round experiments for the data set usc_5_300_q3. . . . .	303
E.22 Measured oil and surface temperatures of the 15 kip damper in the second round experiments for the data set usc_5_300_q3. . . . .	304
E.23 Measured dynamic response of the 15 kip damper in the second round experiments for the data set usc_5_300_q4. . . . .	305
E.24 Measured oil and surface temperatures of the 15 kip damper in the second round experiments for the data set usc_5_300_q4. . . . .	306
E.25 Measured dynamic response of the 15 kip damper in the second round experiments for the data set usc_5_400_q1. . . . .	307
E.26 Measured oil and surface temperatures of the 15 kip damper in the second round experiments for the data set usc_5_400_q1. . . . .	308
E.27 Measured dynamic response of the 15 kip damper in the second round experiments for the data set usc_5_400_q2. . . . .	309
E.28 Measured oil and surface temperatures of the 15 kip damper in the second round experiments for the data set usc_5_400_q2. . . . .	310
E.29 Measured dynamic response of the 15 kip damper in the second round experiments for the data set usc_5_400_q3. . . . .	311
E.30 Measured oil and surface temperatures of the 15 kip damper in the second round experiments for the data set usc_5_400_q3. . . . .	312
E.31 Measured dynamic response of the 15 kip damper in the second round experiments for the data set usc_5_400_q4. . . . .	313
E.32 Measured oil and surface temperatures of the 15 kip damper in the second round experiments for the data set usc_5_400_q4. . . . .	314
F.1 On-line parametric identification results of the 15 kip damper for data set Qtr4_01 .	317
F.2 On-line parametric identification results of the 15 kip damper for data set Qtr4_0125	318
F.3 Off-line parametric identification results of the 15 kip damper for data set Qtr4_01 .	320
F.4 Off-line parametric identification results of the 15 kip damper for data set Qtr4_0125	321
F.5 On-line parametric identification results of the 15 kip damper for data set usc_10175_q4323	

F.6 On-line parametric identification results of the 15 kip damper for data set usc\_10200\_q4324

F.7 On-line parametric identification results of the 15 kip damper for data set usc\_5300\_q4325

F.8 On-line parametric identification results of the 15 kip damper for data set usc\_5400\_q4326

F.9 Off-line parametric identification results of the 15 kip damper for data set usc\_10175\_q4328

F.10 Off-line parametric identification results of the 15 kip damper for data set usc\_10200\_q4329

F.11 Off-line parametric identification results of the 15 kip damper for data set usc\_5300\_q4330

F.12 Off-line parametric identification results of the 15 kip damper for data set usc\_5400\_q4331

G.1 Comparison of the measured and identified damper response using RFM for the data set Qtr1\_01, segment No. 1. . . . . 334

G.2 Summary of the RFM identification of the 15 kip damper subjected to broadband excitation for the data set Qtr1\_01, segment No. 1. . . . . 335

G.3 Comparison of the measured and identified damper response using RFM for the data set Qtr1\_01, segment No. 2. . . . . 336

G.4 Summary of the RFM identification of the 15 kip damper subjected to broadband excitation for the data set Qtr1\_01, segment No. 2. . . . . 337

G.5 Comparison of the measured and identified damper response using RFM for the data set Qtr1\_01, segment No. 3. . . . . 338

G.6 Summary of the RFM identification of the 15 kip damper subjected to broadband excitation for the data set Qtr1\_01, segment No. 3. . . . . 339

G.7 Comparison of the measured and identified damper response using RFM for the data set Qtr1\_01, segment No. 4. . . . . 340

G.8 Summary of the RFM identification of the 15 kip damper subjected to broadband excitation for the data set Qtr1\_01, segment No. 4. . . . . 341

G.9 Comparison of the measured and identified damper response using RFM for the data set Qtr1\_01, segment No. 5. . . . . 342

G.10 Summary of the RFM identification of the 15 kip damper subjected to broadband excitation for the data set Qtr1\_01, segment No. 5. . . . . 343

G.11 Histogram of Chebyshev and power series coefficients for the data set Qtr1\_01. . . . 345

G.12 Histogram of Chebyshev and power series coefficients for the data set Qtr2_01. . . .	346
G.13 Histogram of Chebyshev and power series coefficients for the data set Qtr3_01. . . .	347
G.14 Histogram of Chebyshev and power series coefficients for the data set Qtr4_01. . . .	348
G.15 Histogram of Chebyshev and power series coefficients for the data set Qtr1_0125. . .	349
G.16 Histogram of Chebyshev and power series coefficients for the data set Qtr2_0125. . .	350
G.17 Histogram of Chebyshev and power series coefficients for the data set Qtr3_0125. . .	351
G.18 Histogram of Chebyshev and power series coefficients for the data set Qtr4_0125. . .	352
G.19 Probability density function of the damping and stiffness Chebyshev coefficients for the data set Qtr1_01. . . . .	354
G.20 Probability density function of the damping and stiffness Chebyshev coefficients for the data set Qtr2_01. . . . .	355
G.21 Probability density function of the damping and stiffness Chebyshev coefficients for the data set Qtr3_01. . . . .	356
G.22 Probability density function of the damping and stiffness Chebyshev coefficients for the data set Qtr1_01. . . . .	357
G.23 Probability density function of the damping and stiffness Chebyshev coefficients for the data set Qtr1_0125. . . . .	358
G.24 Probability density function of the damping and stiffness Chebyshev coefficients for the data set Qtr2_0125. . . . .	359
G.25 Probability density function of the damping and stiffness Chebyshev coefficients for the data set Qtr3_0125. . . . .	360
G.26 Probability density function of the damping and stiffness Chebyshev coefficients for the data set Qtr4_0125. . . . .	361
G.27 Comparison of the measured and identified damper response using ANN in time history for the data set usc5400q4. . . . .	363
G.28 Comparison of the measured and identified damper response using ANN in time history for the data set usc5300q4. . . . .	364
G.29 Comparison of the measured and identified damper response using ANN in time history for the data set usc10200q4. . . . .	365

G.30 Comparison of the measured and identified damper response using ANN in time history for the data set usc10175q4. . . . . 366

H.1 Time history of the MR damper response subjected to broadband excitation for 1.0 ampere input current. . . . . 370

H.2 FFT of the MR damper response subjected to broadband excitation for 1.0 ampere input current. . . . . 371

H.3 Phase plot of the MR damper response subjected to broadband excitation for 1.0 ampere input current. . . . . 372

H.4 Time history of the MR damper response subjected to broadband excitation for 0.95 ampere input current. . . . . 374

H.5 FFT of the MR damper response subjected to broadband excitation for 0.95 ampere input current. . . . . 375

H.6 Phase plot of the MR damper response subjected to broadband excitation for 0.95 ampere input current. . . . . 376

H.7 Time history of the MR damper response subjected to broadband excitation for 0.90 ampere input current. . . . . 378

H.8 FFT of the MR damper response subjected to broadband excitation for 0.90 ampere input current. . . . . 379

H.9 Phase plot of the MR damper response subjected to broadband excitation for 0.90 ampere input current. . . . . 380

H.10 Time history of the MR damper response subjected to broadband excitation for 0.75 ampere input current. . . . . 382

H.11 FFT of the MR damper response subjected to broadband excitation for 0.75 ampere input current. . . . . 383

H.12 Phase plot of the MR damper response subjected to broadband excitation for 0.75 ampere input current. . . . . 384

H.13 Comparison of the measured and identified damper response in time history using RFM for 1.0 ampere MR damper input current test No. 1. . . . . 385

H.14 Comparison of the measured and identified damper response in time history using RFM for 1.0 ampere MR damper input current test No. 2. . . . . 385

H.15 Comparison of the measured and identified damper response in time history using RFM for 1.0 ampere MR damper input current test No. 3. . . . .	386
H.16 Comparison of the measured and identified damper response in time history using RFM for 1.0 ampere MR damper input current test No. 4. . . . .	386
H.17 Comparison of the measured and identified damper response in time history using RFM for 1.0 ampere MR damper input current test No. 5. . . . .	386
H.18 Comparison of the measured and identified damper response in time history using RFM for 1.0 ampere MR damper input current test No. 6. . . . .	387
H.19 Comparison of the measured and identified damper response in time history using RFM for 1.0 ampere MR damper input current test No. 7. . . . .	387
H.20 Comparison of the measured and identified damper response in time history using RFM for 1.0 ampere MR damper input current test No. 8. . . . .	387
H.21 Comparison of the measured and identified damper response in time history using RFM for 1.0 ampere MR damper input current test No. 9. . . . .	388
H.22 Comparison of the measured and identified damper response in time history using RFM for 1.0 ampere MR damper input current test No. 10. . . . .	388
H.23 Comparison of the measured and identified damper response in time history using RFM for 0.95 ampere MR damper input current test No. 1. . . . .	389
H.24 Comparison of the measured and identified damper response in time history using RFM for 0.95 ampere MR damper input current test No. 2. . . . .	389
H.25 Comparison of the measured and identified damper response in time history using RFM for 0.95 ampere MR damper input current test No. 3. . . . .	390
H.26 Comparison of the measured and identified damper response in time history using RFM for 0.95 ampere MR damper input current test No. 4. . . . .	390
H.27 Comparison of the measured and identified damper response in time history using RFM for 0.95 ampere MR damper input current test No. 5. . . . .	390
H.28 Comparison of the measured and identified damper response in time history using RFM for 0.95 ampere MR damper input current test No. 6. . . . .	391
H.29 Comparison of the measured and identified damper response in time history using RFM for 0.95 ampere MR damper input current test No. 7. . . . .	391

H.30 Comparison of the measured and identified damper response in time history using  
 RFM for 0.95 ampere MR damper input current test No. 8. . . . . 391

H.31 Comparison of the measured and identified damper response in time history using  
 RFM for 0.95 ampere MR damper input current test No. 9. . . . . 392

H.32 Comparison of the measured and identified damper response in time history using  
 RFM for 0.95 ampere MR damper input current test No. 10. . . . . 392

H.33 Comparison of the measured and identified damper response in time history using  
 RFM for 0.90 ampere MR damper input current test No. 1. . . . . 393

H.34 Comparison of the measured and identified damper response in time history using  
 RFM for 0.90 ampere MR damper input current test No. 2. . . . . 393

H.35 Comparison of the measured and identified damper response in time history using  
 RFM for 0.90 ampere MR damper input current test No. 3. . . . . 394

H.36 Comparison of the measured and identified damper response in time history using  
 RFM for 0.90 ampere MR damper input current test No. 4. . . . . 394

H.37 Comparison of the measured and identified damper response in time history using  
 RFM for 0.90 ampere MR damper input current test No. 5. . . . . 394

H.38 Comparison of the measured and identified damper response in time history using  
 RFM for 0.90 ampere MR damper input current test No. 6. . . . . 395

H.39 Comparison of the measured and identified damper response in time history using  
 RFM for 0.90 ampere MR damper input current test No. 7. . . . . 395

H.40 Comparison of the measured and identified damper response in time history using  
 RFM for 0.90 ampere MR damper input current test No. 8. . . . . 395

H.41 Comparison of the measured and identified damper response in time history using  
 RFM for 0.90 ampere MR damper input current test No. 9. . . . . 396

H.42 Comparison of the measured and identified damper response in time history using  
 RFM for 0.90 ampere MR damper input current test No. 10. . . . . 396

H.43 Comparison of the measured and identified damper response in time history using  
 RFM for 0.75 ampere MR damper input current test No. 1. . . . . 397

H.44 Comparison of the measured and identified damper response in time history using  
 RFM for 0.75 ampere MR damper input current test No. 2. . . . . 397

H.45 Comparison of the measured and identified damper response in time history using RFM for 0.75 ampere MR damper input current test No. 3. . . . .	398
H.46 Comparison of the measured and identified damper response in time history using RFM for 0.75 ampere MR damper input current test No. 4. . . . .	398
H.47 Comparison of the measured and identified damper response in time history using RFM for 0.75 ampere MR damper input current test No. 5. . . . .	398
H.48 Comparison of the measured and identified damper response in time history using RFM for 0.75 ampere MR damper input current test No. 6. . . . .	399
H.49 Comparison of the measured and identified damper response in time history using RFM for 0.75 ampere MR damper input current test No. 7. . . . .	399
H.50 Comparison of the measured and identified damper response in time history using RFM for 0.75 ampere MR damper input current test No. 8. . . . .	399
H.51 Comparison of the measured and identified damper response in time history using RFM for 0.75 ampere MR damper input current test No. 9. . . . .	400
H.52 Comparison of the measured and identified damper response in time history using RFM for 0.75 ampere MR damper input current test No. 10. . . . .	400
H.53 The averaged restoring force coefficients for 1.0 ampere MR damper input current. .	401
H.54 The averaged restoring force coefficients for 0.95 ampere MR damper input current.	402
H.55 The averaged restoring force coefficients for 0.90 ampere MR damper input current.	403
H.56 The averaged restoring force coefficients for 0.75 ampere MR damper input current.	404
H.57 Comparison of the measured and identified damper response in time history for 1.0 ampere MR damper input current. . . . .	405
H.58 Comparison of the measured and identified damper response in time history for 0.90 ampere MR damper input current. . . . .	406
H.59 Comparison of the measured and identified damper response in time history for 0.75 ampere MR damper input current. . . . .	407

# List of Tables

- 3.1 Manufacturer design parameters for the 250 kip viscous damper. . . . . 19
- 3.2 Test parameters of the UCB 250 kip damper . . . . . 21
  
- 5.1 Test matrix of the 250 kip damper data set . . . . . 29
- 5.2 On-line parametric identification results for the 250 kip damper data sets . . . . . 31
- 5.3 Off-line parametric identification results for the 250 kip damper data set . . . . . 33
- 5.4 Comparison of the maximum measured force, absolute equivalent design force, and identified force of the 250 kip viscous damper. . . . . 34
  
- 6.1 Test parameters of the UCB 250 kip damper. . . . . 38
- 6.2 Root mean square error and normalized mean square error of the measured and estimated damping forces. . . . . 43
- 6.3 Comparison of the maximum measured force, absolute equivalent design force, and maximum RFM-identified force of the 250 kip viscous damper. . . . . 44
- 6.4 Identified Chebyshev and power series coefficients of the 250 kip damper. . . . . 45
  
- 7.1 Training parameters for the response of the 250 kip damper using the adaptive random search method . . . . . 51
- 7.2 Normalized mean square error between the measured and identified force of the 250 kip viscous damper. . . . . 54
- 7.3 Comparison of the maximum measured force, absolute equivalent design force, and ANN-identified force of the 250 kip viscous damper. . . . . 55
  
- 8.1 Manufacturer design parameters for the 250 kip viscous damper. . . . . 57

8.2	Sensor configuration of data acquisition system for the 15 kip viscous damper. . . . .	58
8.3	First round test specifications. . . . .	59
8.4	Second round test specifications. . . . .	60
10.1	Test matrix of the first round of testing for the 15 kip damper . . . . .	67
10.2	On-line identification for the 15 kip damper first round of testing . . . . .	71
10.3	Off-line identification for the 15 kip damper first round of testing . . . . .	71
10.4	Test matrix for of the second round of testing of the 15 kip damper . . . . .	73
10.5	On-line identification for the 15 kip damper second round of testing . . . . .	75
10.6	Off-line identification for the 15 kip damper second round of testing . . . . .	78
10.7	Comparison of the maximum measured force, absolute equivalent design force, and identified force of the 15 kip viscous damper. . . . .	79
10.8	Comparison of the maximum measured force, absolute equivalent design force, and identified force of the 15 kip viscous damper. . . . .	79
11.1	Determining the optimal order of Chebyshev approximation of the 15 kip damper response. . . . .	82
11.2	Identified RFM coefficients for the 15 kip damper subjected to broadband excitation for the first round tests. . . . .	82
11.3	Identified RFM coefficients for the 15 kip damper subjected to broadband excitation for the second round tests. . . . .	84
11.4	Comparison of the maximum measured force, absolute equivalent design force, and maximum RFM-identified force of the 15 kip viscous damper. . . . .	85
11.5	The first and second order statistics of normalized Chebyshev coefficients of the 15 kip viscous damper subjected to broadband excitation. . . . .	90
12.1	Training parameters of ANN identification for the response of the 15 kip damper using adaptive random search method. . . . .	95
12.2	Normalized mean square error between measured and identified force of the 15 kip viscous damper. . . . .	95

12.3 Comparison of the maximum measured force, absolute equivalent design force, and maximum ANN-identified force of the 15 kip viscous damper. . . . . 97

13.1 Lord Corp. magneto-rheological damper (RD-1005-3) specifications. . . . . 101

13.2 Excitation characteristics for the MR damper experiments. . . . . 103

13.3 Characteristics of the MR damper excitation. . . . . 106

15.1 Parameters of RFM identification for the MR damper. . . . . 114

15.2 Normalized mean square error of the normalized Chebyshev coefficients of the MR damper response. . . . . 115

16.1 Training parameters of ANN identification for the response of the MR damper using adaptive random search method. . . . . 120

16.2 Normalized mean square error of the measured and identified force of the MR damper. 120

17.1 Stiffness and damping coefficients of MR-damper subjected to broadband excitation at different input current levels. . . . . 124

18.1 Comparison of the maximum measured force, equivalent design force, and identified force of the 250 kip viscous damper. . . . . 130

18.2 Normalized mean-square-error comparison of the various identification techniques for the 250 kip viscous damper . . . . . 131

18.3 Error comparison of the various identification techniques for the 250 kip viscous damper . . . . . 132

18.4 Comparison of the maximum measured force, absolute equivalent design force, and identified force of the 15 kip viscous damper. . . . . 134

18.5 Comparison of the maximum measured force, absolute equivalent design force, and identified force of the 15 kip viscous damper. . . . . 134

18.6 Comparison of the maximum measured force, absolute equivalent design force, and maximum RFM-identified force of the 15 kip viscous damper. . . . . 135

18.7 Normalized mean-square-error comparison of the various identification techniques for the 15 kip viscous damper . . . . . 135

18.8	On-line parametric identification results for the 250 kip damper data sets . . . . .	137
18.9	On-line identification results for the 15 kip damper first round of testing . . . . .	137
18.10	On-line identification for the 15 kip damper second round of testing . . . . .	138
18.11	Mean-square-error levels and normalized mean-square-error of the dynamic response for the change detection in the MR damper. . . . .	139
B.1	Test matrix of the 250 kip damper data set . . . . .	181
B.2	On-line parametric identification results for the 250 kip damper data sets . . . . .	182
B.3	Off-line parametric identification results for the 250 kip damper data set . . . . .	198
F.1	The identification data sets of the 15 kip damper first round of testing . . . . .	315
F.2	The identification data sets of the 15 kip damper second round of testing . . . . .	315
F.3	On-line identification for the 15 kip damper first round of testing . . . . .	316
F.4	Off-line identification for the 15 kip damper first round of testing . . . . .	319
F.5	On-line identification for the 15 kip damper second round of testing . . . . .	322
F.6	Off-line identification for the 15 kip damper second round of testing . . . . .	327
G.1	The first and second order statistics of normalized Chebyshev coefficients of 15 kip viscous damper. . . . .	353
H.1	Characteristics of the MR damper excitation. . . . .	368



# Chapter 1

## INTRODUCTION

Large-scale dampers are being specified for incorporation into several California toll bridge retrofit strategies. The reasons are obvious; energy dissipative devices decrease both member design demands, thereby allowing a subsequent reduction in member sizes, and displacement demands, thereby eliminating impact forces. Dramatic weight and cost savings are realized based on member size reductions. As such, the dampers are integral components of these structures. Failure of a damper can portend potentially catastrophic system failure, as the adjoining members have been sized based on the energy absorbed and displacements limited by the dampers.

The retrofit design of many large toll structures have already incorporated dampers to dissipate the large energy anticipated from seismic events. Examples include the Vincent Thomas suspension bridge, the Coronado bay bridge, the Richmond-San Rafael bridge, and the west spans of the San Francisco-Oakland bay bridge. Specification of these dampers was crucial to the success of the design in meeting the stipulated design criteria. Given the critical nature of the damper elements to the success of the retrofit strategies being implemented on these large-span structures, the development of analytical tools for evaluating their performance is imperative.

Several technical challenges play a major role in system identification applications to structural damage detection. For example, uniqueness and observability problems are inherent in many structural systems due to the presence of redundant structural members and limited sensor locations. In addition, the available physical measurements from the sensors always contain small amounts of noise superimposed on the desired signal. The presence of such noise can perturb the accuracy and reliability of various system identification algorithms. Finally, the available response measures of some structural systems are inherently insensitive to changes in structural parameters of interest, making it difficult to devise an adequate test arrangement. Further details about the numerous technical hurdles and potential approaches for structural health monitoring of infrastructure systems and components are available in the works of Housner *et al.* (1997); Makris & Zhang (2004);

Masri *et al.* (2004); Sikorsky *et al.* (2001).

## 1.1 Scope of Work

The project outline involved a sequence of analytical and experimental studies to assess the utility of some promising SHM approaches for application to individual viscous dampers of the type employed by Caltrans on several toll bridges.

The data analysis approaches employed state-of-the-art system identification methods (Worden & Tomlinson, 2001). These methods are broadly classified as parametric or nonparametric. Data collected from testing at the University of California, Berkeley, on two different dampers, were utilized to fully characterize the dynamics of the dampers, as a means of selection and optimization of the set of analytical tools previously developed.

Following is a brief overview of the three specific tasks that were accomplished as part of this research project. The first task was the responsibility of the University of California, Berkeley (UCB), while the latter two tasks were the responsibility of the University of Southern California (USC).

### 1.1.1 Task 1: Component Testing of Dampers

The component testings of a 15 kip and a 250 kip fluid dampers were conducted at UCB. The 15 kip damper was designed to deliver a nearly linear behavior ( $F = C \text{sign}(\dot{x})|\dot{x}|^n$ , with  $n \approx 1.0$  and  $C \approx 0.70 \text{ kip sec/in}$ ), whereas the 250 kip damper tested was designed to deliver a nonlinear behavior ( $n \approx 0.35$  and  $C \approx 60 \text{ kip sec/in}$ ). Selected displacement time histories were imposed on the fluid dampers via hydraulic actuators. The force recorded in the load cell of the test setup is the resulting force at the attachment of the damper that is needed to sustain the imposed displacement history. During the viscous dampers testings at UCB, in addition to force, time histories of the displacement, and temperature were recorded.

The imposed displacement histories included different levels of excitation and a wide spectral content capable of exciting all the relevant system parameters within the response range of interest.

The experimental tests included:

- broad-band stationary random excitations, one at a low amplitude level and another at a higher level.
- a swept-sine excitation straddling the frequency band of interest.

### 1.1.2 Task 2: Development of an Accurate Mathematical Model for an Individual Damper Element

Using data from tests at UCB, as defined in Task 1, parametric as well as nonparametric approaches were employed to furnish different formats of the member's characteristics.

Four specific approaches, two parametric and two nonparametric, were used to analyze and model the physical characteristics of the damper elements:

1. The parametric phase of this study employed an efficient technique to develop suitable nonlinear model(s) of varying degree of complexity. Among the more promising parametric models that were explored are:
  - (a) The off-line parametric identification based on the Bouc-Wen hysteretic model (Chassiakos *et al.* , 1995, 1998; Ma *et al.* , 2004; Smyth *et al.* , 1999, 2002).
  - (b) The on-line parametric identification based on the viscous dampers design model (Ioannou & Datta, 1991; Ioannou & Sun, 1996; Miyamoto & Hanson, 2002; Soong & Dargush, 1997).
2. The nonparametric phase of the investigation used two approaches:
  - (a) The method of Masri and Caughey (1979), whereby the effective restoring force of the element is analytically represented in terms of a doubly-indexed series of orthogonal polynomials involving appropriate basis functions that depend on the element's state variables.
  - (b) Artificial neural networks consisting of three-layer feedforward nets (Burton *et al.* , 1996; Garcia *et al.* , 1997; Masri *et al.* , 1992, 1993, 1996, 1999, 2000).

### 1.1.3 Task 3: Evaluation of Damper Modified States

Due to practical difficulties in inducing damage states of various types in real viscous dampers, it was not feasible to utilize the UCB dampers for this phase of the study. Instead, the USC researchers employed a "smart" magneto-rheological (MR) damper to investigate the detectability of relatively small changes in the physical properties of such adaptive dampers. The corresponding dynamic response was analyzed by USC in order to establish damage detection thresholds associated with the tested MR damper.

## 1.2 Report Organization

The technical background for the data analysis tools is presented in Chapter 2. The experimental tests and corresponding system identification studies (both parametric and nonparametric) of the two dampers tested at UCB are included in Chapters 3-12. The third major task of this study, the detection and quantification of changes in nonlinear dampers, is presented in Chapters 13-17. This phase of the investigation was accomplished by means of an MR damper. A summary and conclusions of the research, as well as recommendations for future studies, are provided in Chapter 19.

Several appendices are included in which supplementary detailed analysis results from the experimental studies are presented in a compact form.

## Chapter 2

# TECHNICAL BACKGROUND FOR DATA ANALYSIS TOOLS

### 2.1 Introduction

This section includes a brief overview of the analysis tools used for developing mathematical models based on the measured response of the tested nonlinear dampers reported in this study. The two broad classes of methods applied can be classified as *parametric* and *nonparametric* methods.

### 2.2 Parametric System Identification

The parametric system identification is based on physical models, with parameters either representing a physical characteristic of the system (stiffness and damping), or capturing the overall physical behavior of the system (hysteresis) with mathematical equations.

There are two main approaches for identifying the unknown parameters of a system. The first method is on-line identification, which is used when there is a need to track the values of the parameters at each time-step. This method has applications in control, health monitoring, time-varying systems, and etc. The second method is off-line identification, which is used when there is a need to find an optimum value of the parameters for a segment of the measured data. Applications of this method exist in simulation, modeling damage-detection, and etc.

The on-line identification method selected for this study is based on the adaptive least-squares with forgetting factor algorithm. This algorithm minimizes the least-squares error of the measured data with respect to the unknowns at every time step. The forgetting factor weights the previous values of the data in order to track the time-varying parameters.

The off-line identification method chosen for this study is based on adaptive random search

optimization. This technique searches for the optimum value of the parameters over a segment of the measurements by minimizing the mean-square error between the measured force and predicted force.

### 2.2.1 On-line Parametric System Identification

The on-line parametric system identification method is based on the adaptive least-squares algorithm with forgetting factor. This method is capable of identifying unknown parameters of nonlinear non-stationary models using a linear<sup>1</sup> Static Parametric Model (SPM) in real-time (tracking the parameters values at every time step). The general form of a SPM may be described by (Ioannou & Datta, 1991; Ioannou & Sun, 1996):

$$z = \theta^{*T} \phi \quad (2.1)$$

where  $z$  is the measurement vector,  $\phi$  is the signal (or regressor) vector, and  $\theta$  is the unknown parameters vector. For example, the equation of motion of a nonlinear duffing oscillator is given by:

$$f(t) = m\ddot{x} + c\dot{x} + kx + dx^3 \quad (2.2)$$

where  $m$ ,  $c$ , and  $k$  are the mass, damping, and stiffness values of the system, and  $x$ ,  $\dot{x}$ , and  $\ddot{x}$  are the system response, displacement, velocity, and acceleration. The SPM form of Eqn. 2.2 is:

$$\underbrace{[f(t)]}_z = \underbrace{\begin{bmatrix} m \\ c \\ k \\ d \end{bmatrix}}_{\theta^{*T}} \times \underbrace{\begin{bmatrix} \ddot{x} \\ \dot{x} \\ x \\ x^3 \end{bmatrix}}_{\phi} \quad (2.3)$$

where the  $\theta^*$  is the unknown parameters vector,  $\phi$  is the signal vector (regressor vector), and  $z$  is the measurement vector.

The adaptive least-squares algorithm with forgetting factor for identifying  $\theta(t)$ , the estimate of  $\theta^*$  in the SPM model (Eqn. 2.1), is obtained by solving  $\nabla J(\theta) = 0$ . The cost function  $J(\theta)$  for the recursive adaptive least-squares algorithm with forgetting-factor is defined as:

$$J(\theta) = \frac{1}{2} \int_0^t \exp^{-\beta(t-\tau)} \frac{[z(\tau) - \theta^T \phi(\tau)]^2}{m_s^2(\tau)} d\tau + \frac{1}{2} \exp^{-\beta t} (\theta - \theta_0)^T Q_0 (\theta - \theta_0) \quad (2.4)$$

---

<sup>1</sup>The word *linear* here means that the parameters of the system ( $\theta^*$ ) and the signal vectors of the system ( $\phi$ ) have linear relation, even though the system has nonlinear response.

where,  $Q_0 = Q_0^T > 0$ ,  $\beta \geq 0$ ,  $\theta_0 = \theta(0)$ . The recursive least-squares algorithm for continuous-time is:

$$\begin{aligned} \dot{\theta} &= P\epsilon\phi \\ \dot{P} &= \begin{cases} \beta P - P\frac{\phi\phi^T}{m_s^2}P, & \text{if } \|P(t)\| \leq R_0 \\ 0 & \text{otherwise} \end{cases} \end{aligned} \quad (2.5)$$

where,  $P(0) = P_0 = P_0^T$ ,  $\|P_0\| \leq R_0$ ,  $R_0$  is the upper bound for  $\|P\|$ ,  $m_s$  is the normalizing signal, and  $\beta \geq 0$  is the forgetting factor (Ioannou & Sun, 1996).

The condition for parameter convergence of the adaptive least-squares algorithm (Eqn. 2.5) is that the signal vector  $\phi$  of the SPM model (Eqn. 2.1) be persistently excited.

### Formulation of Viscous Dampers Design Model for the On-line Parametric Identification Method

The model used for the on-line identification of dampers is based on a design model which is extensively used by damper manufacturers (Miyamoto & Hanson, 2002; Soong & Dargush, 1997). The model is given by:

$$F = C \text{sign}(\dot{x})|\dot{x}|^n \quad (2.6)$$

where  $F$  is the damping force,  $\dot{x}$  is the damper velocity,  $C$  is the damping coefficient, and  $n$  is the exponent.

In order to identify the unknown parameters of Eqn. 2.6 with the adaptive least-square algorithm (Eqn. 2.5), the SPM form (Eqn. 2.1) of the model (Eqn. 2.6) must be derived. For numerical implementation (in order to avoid imaginary values), (Eqn. 2.6) is reformulated as:

$$\text{sign}(F)|F| = C \text{sign}(\dot{x})|\dot{x}|^n \quad (2.7)$$

where  $\text{sign}(\cdot)$  is the sign function, and  $|\cdot|$  is the absolute function. Eqn. 2.7 and 2.6 are mathematically identical in real number space ( $F \wedge \dot{x} \in R$ ). In viscous dampers the force  $F$  has the same sign with the velocity,  $\dot{x}$ . Therefore, the SPM form of the design model (Eqn. 2.7), which provides a linear relation between the unknown parameters  $\theta^*$  and measured signals  $\phi$  is:

$$\frac{\text{Log}(|F|)}{z} = \frac{\text{Log}(C)}{\theta^*} n \times \frac{1}{\phi} \left[ \frac{1}{\text{Log}(|\dot{x}|)} \right] \quad (2.8)$$

The unknown vector ( $\theta^*$ ) in Eqn. 2.8 can be identified by the on-line adaptive least-squares algorithm given by Eqn. 2.5.

### 2.2.2 Off-Line Parametric System Identification

The off-line parametric system identification method is based on the adaptive random search optimization algorithm (Andronikou *et al.*, 1982; Masri *et al.*, 1980). The method identifies a set of optimum parameters for a model by performing an adaptive random search on the parameters solution-space, which minimizes the normalized mean-square-error between the measured force and the predicted force. The random search starts with an initial condition and adaptively changes the variance of search steps, in order to find a new set of parameters that reduces the value of the objective function at every step. The normalized mean-square-error (NMSE) is defined as the ratio of the error variance to the signal variance, which may be computed by:

$$MSE(\hat{f}) = \frac{100}{N\sigma_f^2} \sum_{i=1}^N (f_i - \hat{f}_i)^2 \quad (2.9)$$

where  $f$  is the measured force,  $\hat{f}$  is the predicted force,  $N$  is the number of data points, and  $\sigma_f^2$  is the variance of the measured force. Note that, throughout this report,  $NMSE$  is used in the summary and comparison tables, since it is the recommended measure for goodness of fit in nonlinear system identifications (Worden & Tomlinson, 2001).

In order to compute the predicted force at each time step, the differential equation representing system dynamics is solved numerically. The differential equation of the damper used herein is widely used in the field of system identification (Soong & Dargush, 1997; Spencer Jr. *et al.*, 1997). The equation combines linear polynomial terms and an evolutionary term known as Bouc-Wen (Wen, 1976, 1980, 1989), which generates hysteresis in the response. The differential equation for this model is defined by:

$$\begin{aligned} f(t) &= c\dot{x} + kx + z \\ \dot{z} &= \frac{1}{\eta} [A\dot{x} - \nu(\beta|\dot{x}|z|z|^{n-1} - \gamma\dot{x}|z|^n)] \end{aligned} \quad (2.10)$$

where  $f(t)$  is the applied force on the system,  $x$  the displacement,  $\dot{x}$  the velocity,  $z$  the evolutionary Bouc-Wen term,  $\dot{z}$  is the derivative of  $z$ , and  $\eta$ ,  $A$ ,  $\nu$ ,  $\beta$ ,  $\gamma$ ,  $n$  are the Bouc-Wen model unknowns.

The unknown parameters in Eqn. 2.10 are not independent. For identification purposes the dependent parameters are clustered into independent terms as below:

$$\begin{aligned}
 f(t) &= c\dot{x} + kx + z \\
 \dot{z} &= \theta_1\dot{x} + \theta_2|\dot{x}|z|z|^{n-1} + \theta_3\dot{x}|z|^n
 \end{aligned}
 \tag{2.11}$$

The vector of independent unknown parameters is:

$$\theta^* = [c, k, n, \theta_1, \theta_2, \theta_3] \tag{2.12}$$

The identification procedure initializes the value for vector  $\theta^*$ , and the corresponding force with the measured system responses, are predicted. Then the normalized mean-square-error of the measured force and predicted force is computed. Based on the computed error, the adaptive random search algorithm generates a new set of values for the unknown parameters vector  $\theta^*$ . This procedure is repeated until the optimal value for the parameters in  $\theta^*$  are reached.

## 2.3 Nonparametric Identification Approaches

Two methods of nonparametric identification approaches are described in this section; the Restoring Force Method (RFM) and Artificial Neural Networks (ANN).

### 2.3.1 Restoring Force Method

The RFM provides a simple procedure of nonparametric identification to mitigate mathematical complexity, convergence difficulties, excessive computational effort, restrictions on the type of the dynamic systems (i.e., linear or nonlinear), and restrictions on the system excitations (Masri & Caughey, 1979). The advantages of the RFM are realized because:

1. The applicability of this method extends to linear, nonlinear, hysteretic, nonhysteretic and self-excited systems with limit cycles.
2. Virtually any type of probing signals can be utilized for system identification.
3. In the absence of *a priori* knowledge of the type and order of the nonlinearity, several of the orthogonal polynomials can be determined while the lower-order coefficients remain valid for the higher ones.
4. The approximation error, within the range of measurements, can be forced to oscillate between the limits with the application of Chebyshev polynomials (*equal-ripple property*).

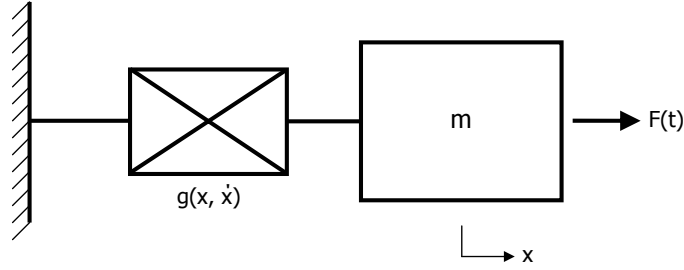


Figure 2.1: Schematic of single degree-of-freedom system.

5. The convergence rate is high, reducing execution time even for systems with non-polynomial linearity.

The development of the RFM is based on the generalized equation of motion for the response of a single degree of freedom (SDOF) system (Figure 2.1). Although the procedure described in this section is for a SDOF system, the multi-degree of freedom (MDOF) system can be identified in a similar manner (Worden & Tomlinson, 2001). The response of a SDOF system can be specified as:

$$m\ddot{x}(t) + r(x(t), \dot{x}(t)) = f(t) \quad (2.13)$$

where  $m$  is the system mass,  $x(t)$  is defined as the system displacement,  $r(x(t), \dot{x}(t))$  is the restoring force, and  $f(t)$  is the external excitation. The equation can be rewritten as:

$$r(x(t), \dot{x}(t)) = f(t) - m\ddot{x}(t) \quad (2.14)$$

The right-hand-side (RHS) terms of the above equation can be known or measurable, the time history of the restoring force  $r(x(t), \dot{x}(t))$  can be estimated. Let us write the estimated restoring force as  $\hat{r}(x, \dot{x})$ , then

$$r(x(t), \dot{x}(t)) \approx \hat{r}(x, \dot{x}) = \sum_{i=0}^{m2} \sum_{j=0}^{n2} C_{ij} T_i(x') T_j(\dot{x}') \quad (2.15)$$

where the  $T_i(x')$  and  $T_j(\dot{x}')$  are Chebyshev polynomials of displacement and velocity, respectively, and  $C_{ij}$  is the corresponding coefficient, so called Chebyshev coefficient. The Chebyshev polynomial is defined as:

$$T_n = \cos(n \arccos \xi) \quad -1 \leq \xi \leq 1 \quad (2.16)$$

satisfying the weighted orthogonality property

$$\int_{-1}^1 \frac{T_n(\xi)T_m(\xi)d\xi}{\sqrt{1-\xi^2}} = \begin{cases} 0 & : n \neq m \\ \pi/2 & : n = m \neq 0 \\ \pi & : n = m = 0 \end{cases} \quad (2.17)$$

The normalized displacement ( $x'$ ) and velocity ( $\dot{x}'$ ) values are defined as

$$x' = \frac{[x - (x_{max} + x_{min})/2]}{[(x_{max} - x_{min})/2]} \quad (2.18)$$

$$\dot{x}' = \frac{[\dot{x} - (\dot{x}_{max} + \dot{x}_{min})/2]}{[(\dot{x}_{max} - \dot{x}_{min})/2]} \quad (2.19)$$

The normalized Chebyshev coefficients are generated by fitting the computed restoring force from the prescribed data set containing the system displacement and velocity to the measured/simulated force response. One advantage of this method is that upon a relatively straightforward transformation of Equation 2.15 to a power series expansion, the coefficients can be correlated to recognizable physical dynamic systems. Therefore, the system degradation can be detected by monitoring the change of these coefficients.

The above algorithms were validated first using simulation data. Simulations were performed utilizing a nonlinear SDOF Duffing oscillator. The restoring force for this oscillator can be written as

$$f(x, \dot{x}) = m[2\zeta\omega\dot{x} + \omega^2(x + \varepsilon x^3)] \quad (2.20)$$

The simulated Duffing oscillator was designed with a unit mass and period, and a natural frequency of  $2\pi$ . This yielded a system stiffness of 39.48, a damping coefficient of 1.26, and a nonlinear term  $\varepsilon$  of 11.23. Resulting simulation data was corrupted with stationary, zero-mean noise having a standard deviation of 0.10. The superposition of the noise signal was introduced to replicate real-world noise sources, such as instrumentation susceptibility, cabling interface, acquisition hardware, etc. Figure 2.2 illustrates the system response to a stationary random excitation.

The identification simulations yielded normalized Chebyshev coefficients, in this case for a third order Chebyshev approximation of the nonlinear system. Correlation to recognizable physical systems required transforming the identified Chebyshev coefficients to a power series form. A comparison of the measured system restoring force to the identified one is charted in Figure 2.3.

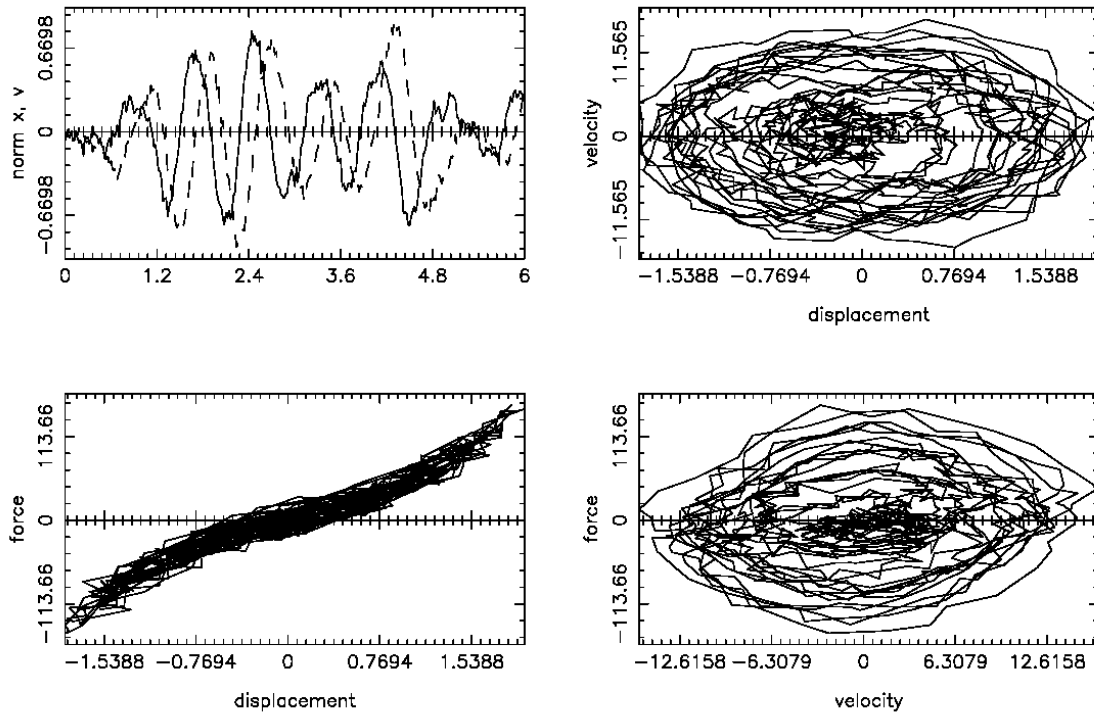


Figure 2.2: Damper simulation response polluted with noise signal.

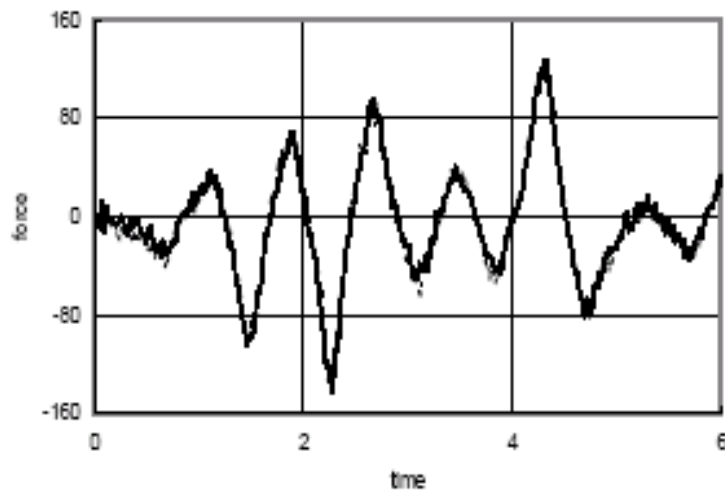


Figure 2.3: Comparison of measured force (dashed line) and identified restoring force (solid line).

### 2.3.2 Artificial Neural Networks

Artificial Neural Networks (ANN) have been shown to be a powerful tool for developing model-free representation of nonlinear systems on the basis of response measurements (Burton *et al.* , 1996; Masri *et al.* , 1993).

In this section, a brief outline is presented for how to use vibration data, obtained from a SDOF system such as a nonlinear viscous damper, to train a suitable network by using a robust stochastic optimization approach known as adaptive random search (Masri *et al.* , 1999). To illustrate the capability of ANN to model linear, as well as nonlinear systems with equal ease, two demonstration test problems will be presented: one involving the response of a linear SDOF system, and the other a nonlinear SDOF system.

Synthetic data were generated from a nonlinear finite element package to obtain numerical solution to the following differential equation

$$m\ddot{x}(t) + g(x, \dot{x}) = F(t) \quad (2.21)$$

which can be expressed as

$$g(x, \dot{x}) = F(t) - m\ddot{x}(t) \quad (2.22)$$

where  $x$  is the displacement,  $\dot{x}$  the velocity,  $\ddot{x}$  the acceleration,  $m$  the system mass,  $F(t)$  the excitation input, and  $g(x, \dot{x})$  the restoring force. The “measured” displacement and velocity signals were used as input, and the restoring force signal as output of the neural networks. The neural networks were trained to minimize the RMS error of the estimated restoring force  $g(t)$ , and the reference restoring force  $\hat{g}(t)$ . Therefore, the quality of training could be determined by the mean square value. The neural networks training was based on the adaptive random search method (ARS). Once the neural networks were trained, the weights of neural networks were validated with another time history segment of the dynamic response. A new segment of the displacement and velocity was fed to the neural networks, while the “trained” weights remained the same. The validation phase was completed by measuring the RMS error between the estimated and the reference restoring force.

#### *Linear SDOF System*

A single degree-of-freedom linear system was considered as illustrated in Figure 2.1. It was assumed that a sinusoidal excitation was applied to the system, and using the FEM module, its dynamic response was computed. The sinusoidal excitation and corresponding computed dynamic responses

are shown in Figure 2.4.

Once the dynamic response was obtained, it was used in the ANN module to train the neural networks. The first 300 out of a total 2000 time history data points were imported into the ANN module. The displacement and velocity data were the input, and the restoring force data the output of the ANN (Figure 2.4). After training the neural networks, the RMS error ( $f_i$ ) was evaluated for each statistical trial.

Once the training phase was completed, the trained neural networks were validated with a new set of dynamic response data. Another section of the dynamic time history response was selected as a new data set. By fixing the weight parameters, the new displacement and velocity data were fed to the neural networks, and the RMS error of the deviation between the estimated and reference restoring force was evaluated. The resulting RMS error was 3.62 %. The estimated and reference restoring forces are illustrated in Figure 2.5.

#### *Nonlinear SDOF System*

A Duffing SDOF oscillator model was considered to verify the ability of the ARS method to properly train neural networks for a nonlinear system. The restoring force  $g(x, \dot{x})$  is expressed as

$$\begin{aligned} m\ddot{x}(t) + g(x, \dot{x}) &= F(t) \\ g(x, \dot{x}) &= ax + bx^3 + c\dot{x} \end{aligned} \tag{2.23}$$

where  $m=1$ ,  $a=2\pi$ ,  $b=10$ ,  $c=1.25$ . The nonlinear dynamic response to a sinusoidal excitation is shown in Figure 2.6. The procedures of training and validation for the linear case were applied to the nonlinear case (Figure 2.7). The RMS error of the reference and estimated restoring forces was 4.06 % - 7.13 % in training, and a 6.15 % error was observed in the validation of the ANN identification.

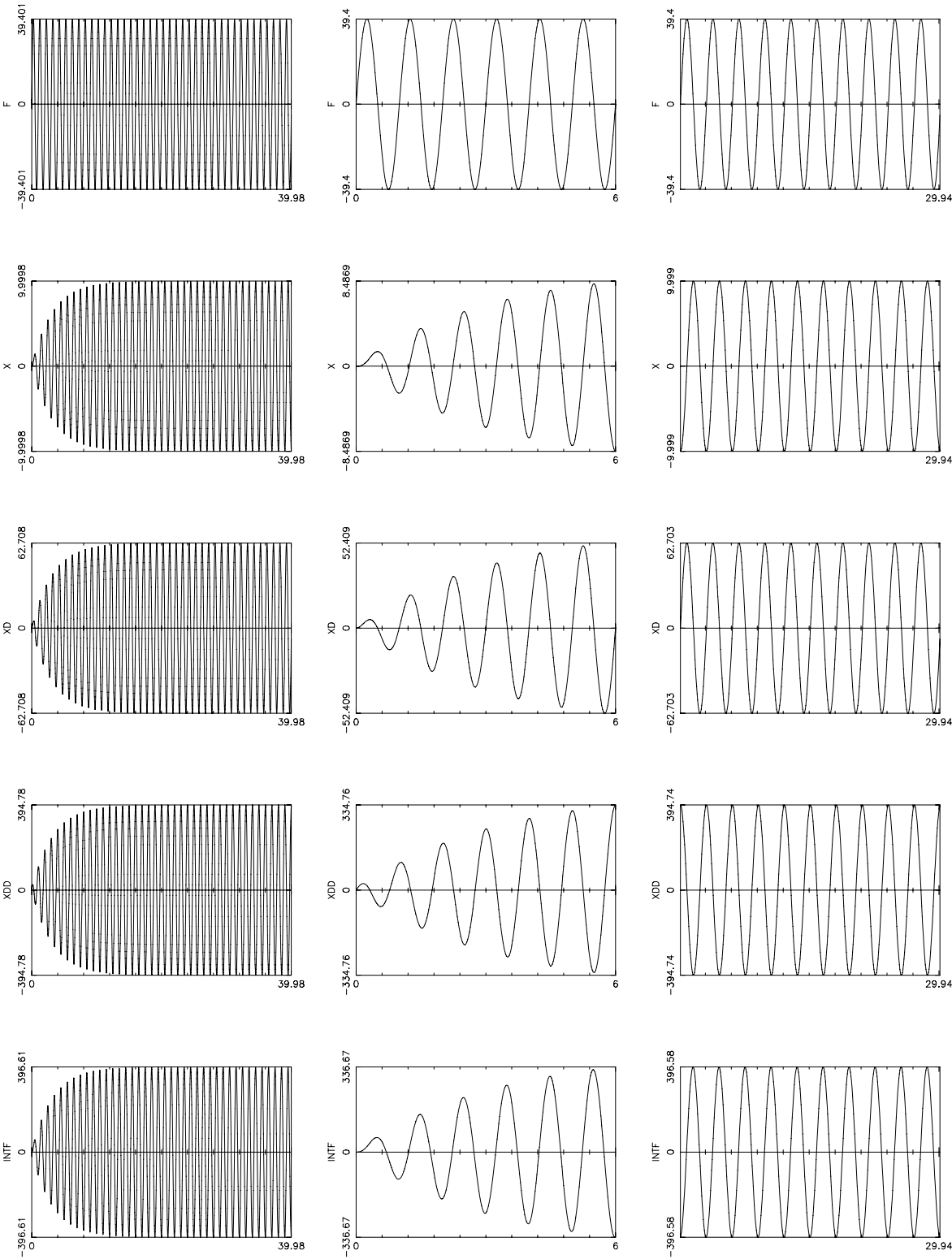


Figure 2.4: Dynamic response of a SDOF linear system.

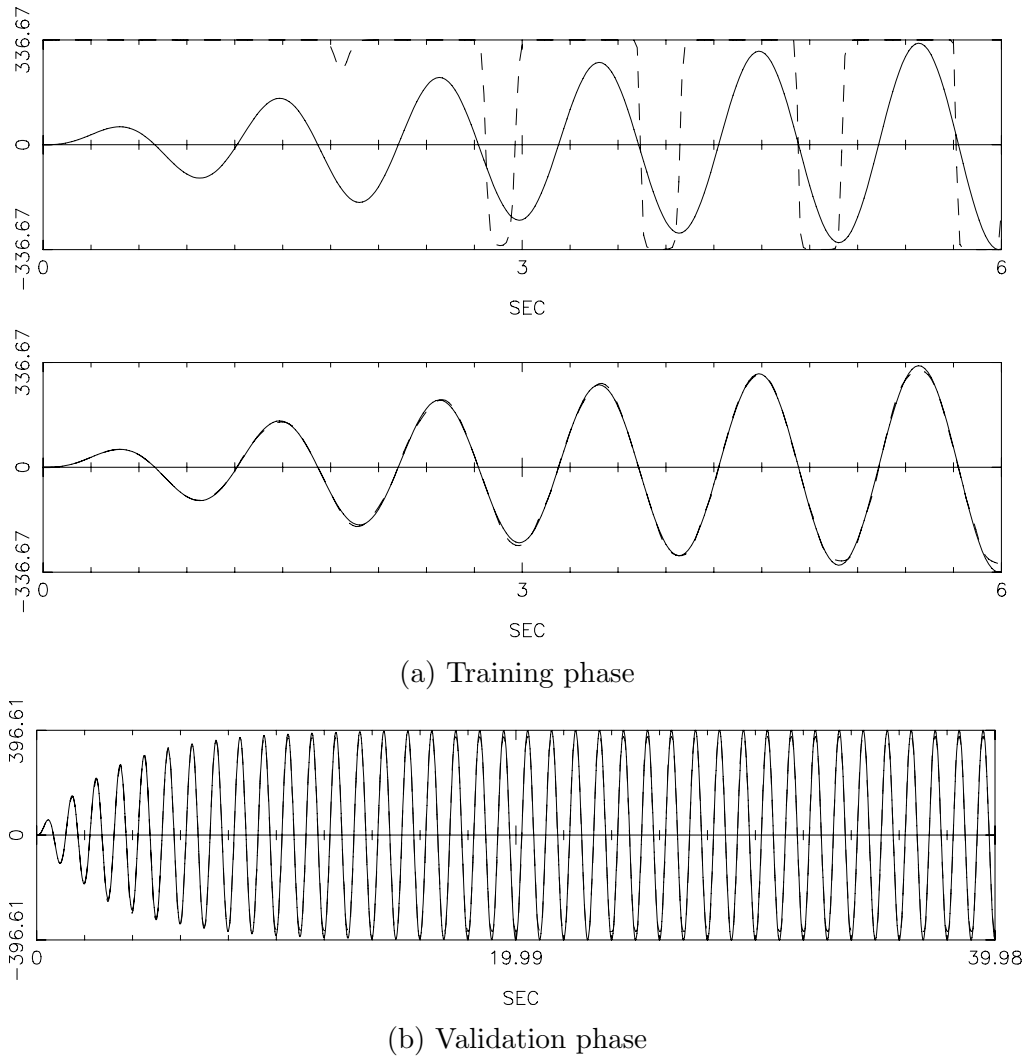


Figure 2.5: Comparison of the reference and identified restoring forces for a SDOF linear system.

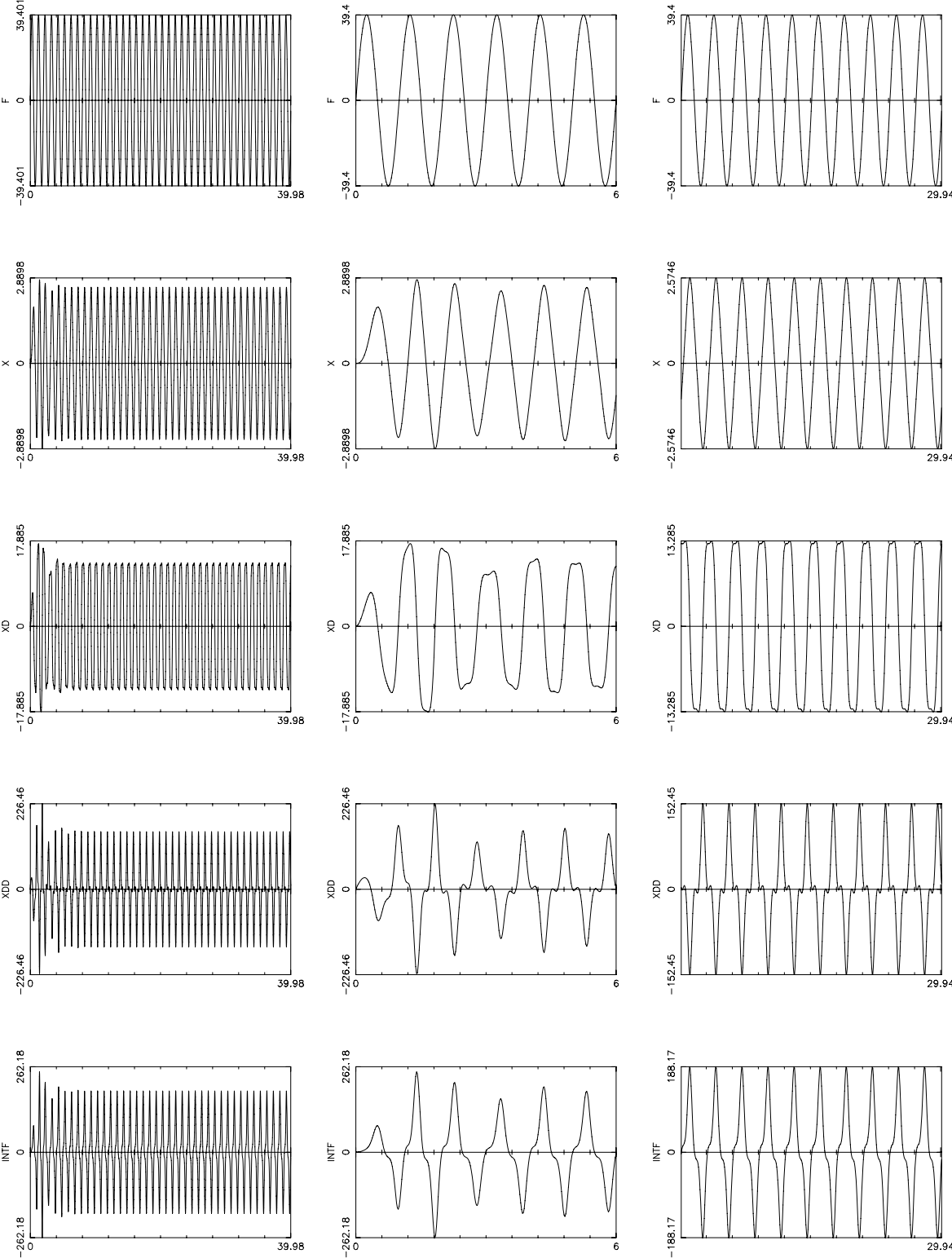


Figure 2.6: Dynamic response of a SDOF nonlinear system.

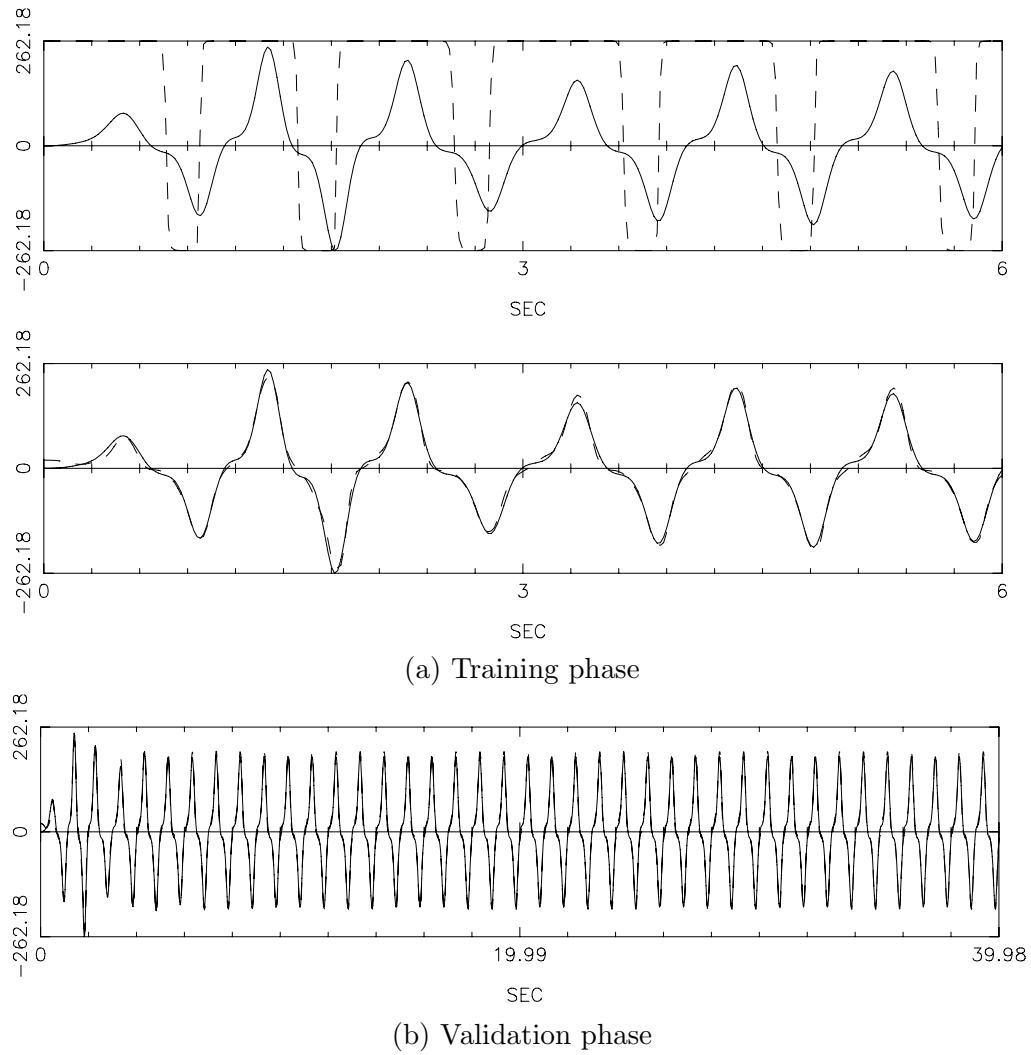


Figure 2.7: Comparison of the reference and identified restoring forces for a SDOF nonlinear system.

## Chapter 3

# EXPERIMENTAL SETUP FOR THE 250 KIP VISCOUS DAMPER

### 3.1 Damper Specifications

The 250 kip damper was tested at the Earthquake Engineering Research Center at the University of California, Berkeley. This damper is a sister damper of the eight dampers installed at the 91/5 overcrossing in Orange County, CA. It has a mid-stroke length of 72 in and a maximum stroke of  $\pm 8.0$  in. The damper behaves according to the nonlinear constitutive law given by Eqn. 2.6 with  $C = 60$  kip·sec/in with  $n = 0.35$ .

A series of tests was performed using the 250 kip viscous damper to obtain the data for parametric and nonparametric system identification. The experiments were conducted by graduate student Cameron Black with the assistance of the lab personnel of U.C. Berkeley under the direction of Professor Nicos Makris. The photo of the test setup is shown in Figure 3.1. The manufacturer design parameters are listed in Table 3.1.

Table 3.1: Manufacturer design parameters for the 250 kip viscous damper.

Damper Type	$C$ (kip sec/in)	$n$
250 Kip	60	0.35

### 3.2 Instrumentation

The setup comprises of a self-equilibrating reaction frame with a 300 kips actuator equipped with a 1000 gpm proportional valve. The bolted head-piece at the opposite side of the actuator can assume other positions to accommodate dampers with different length. In addition to the load-cell



(a)



(b)

Figure 3.1: The 250 kip damper installed on the damper testing machine of the University of California, Berkeley, built by Prof. N. Makris. This damper is a sister damper of the eight dampers installed at the 91/5 overcrossing in Orange County, CA.

and LVDT, the damper was instrumented with six thermocouple probes along its length as shown in Figure 3.1 (b).

A total of 15 tests were performed with the 250 kip viscous damper and the damper response was measured. The collected data were delivered to USC. The data files contained two channel readings; the first column contained displacement in inches, and the second column force in kips. The force was measured with an in-line load cell, and the displacement with a transducer measuring the displacement between the reaction frame and the clevis. The data files did not include a time column, but the sampling rate was conducted at 100 Hz.

### 3.3 Test Specifications

The specifications of the 15 tests are tabulated in Table 3.2. In the series of tests, the damper was excited with a sinusoidal time history. The velocity varied from 10 to 17.5 in/sec, and the displacement varied from 4 to 7 inches. All the data sets had a 6-cycle duration, except one that had a 10-cycle duration.

Table 3.2: Test parameters of the UCB 250 kip damper

No	Filename	Peak vel (in/s)	Freq (Hz)	Displacement (in)	No. cycles	Scan rate (Hz)
1	UCB1_10.4	10.0	0.398	4	6	100
2	UCB1_10.5	10.0	0.318	5	6	100
3	UCB1_10.6	10.0	0.265	6	6	100
4	UCB1_12.4	12.5	0.5	4	6	100
5	UCB1_12.5	12.5	0.4	5	6	100
6	UCB1_12.6	12.5	0.332	6	6	100
7	UCB1_12.7	12.5	0.284	7	6	100
8	UCB1_15.4	15.0	0.6	4	6	100
9	UCB1_15.5	15.0	0.477	5	6	100
10	UCB1_15.6	15.0	0.4	6	10	100
11	UCB1_15.7	15.0	0.341	7	6	100
12	UCB1_17.4	17.5	0.695	4	6	100
13	UCB1_17.5	17.5	0.557	5	6	100
14	UCB1_17.6	17.5	0.464	6	6	100
15	UCB1_17.7	17.5	0.399	7	6	100



## Chapter 4

# PRELIMINARY DATA PROCESSING FOR THE 250 KIP VISCOUS DAMPER

### 4.1 Data Acquisition

The 250 kip damper was excited with sinusoidal motion, and the response was measured in displacement and force. The measurement was sampled at 100 Hz. Each test contained more than 6 cycles of sinusoid, and the test duration varied from 18 to 75 seconds, depending on the velocity of the excitation motion. An example of the collected data sets is shown in Figure 4.1. A total of 15 tests were conducted as summarized in Table 3.2.

### 4.2 Preliminary Data Analysis

The measured data contained only displacement and force, therefore the velocity and acceleration of the damper were obtained by numerical differentiation from the measured displacement using the following procedures:

- Step 1:** *The DC was calculated and subtracted from the measured displacement and force.*
- Step 2:** *The starting and ending point of the excitation were measured, and the “zero-padding” range from the displacement and force were removed.*
- Step 3:** *The displacement was differentiated to obtain the velocity.*
- Step 4:** *A cosine tapered window was applied to the displacement time history, and then a band-pass filter was applied to the displacement. The cutoff frequency*

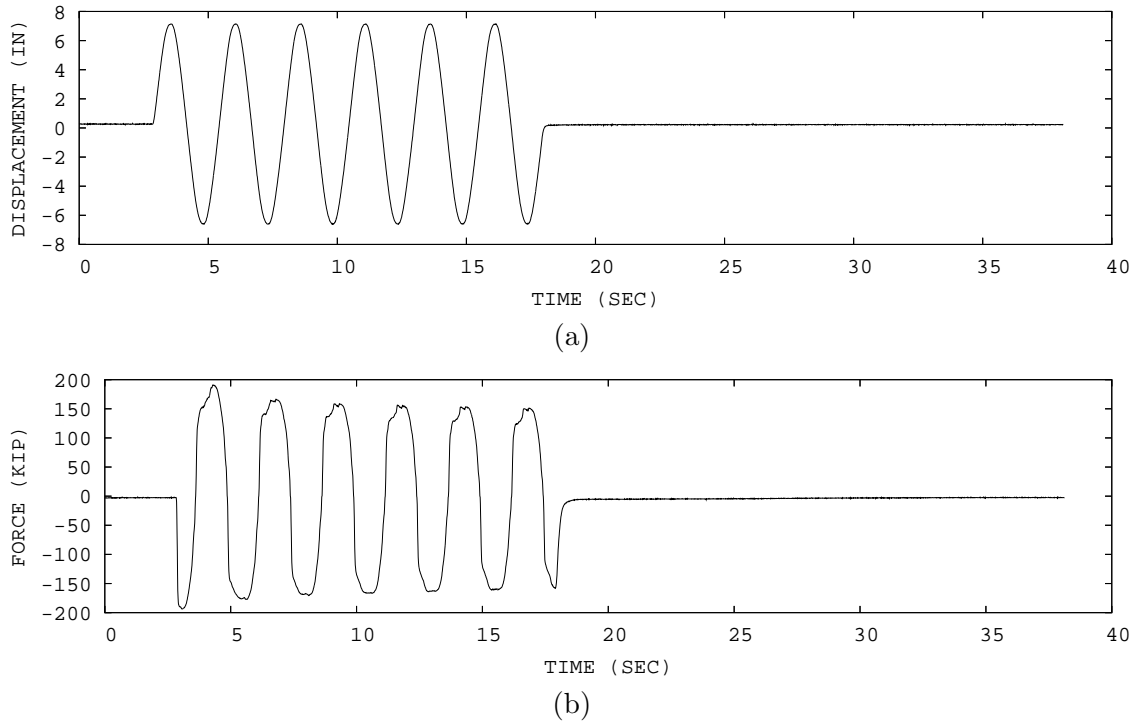


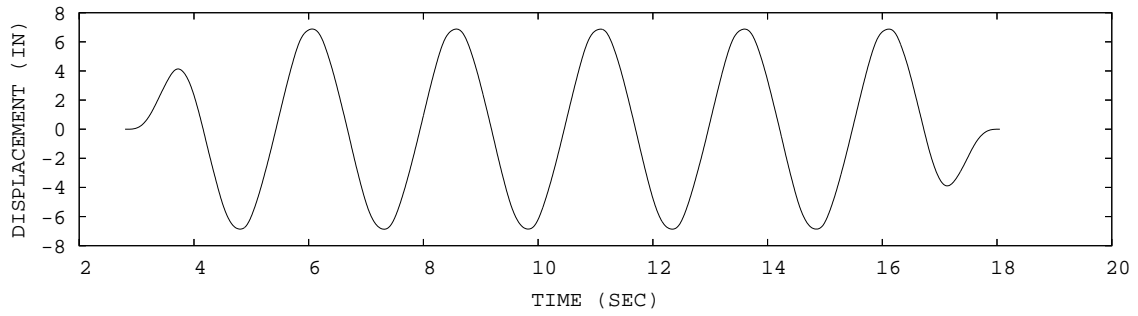
Figure 4.1: Time history of the 250 kip damper response subjected to sinusoidal excitation for the data set UCB1\_17\_7.

was 0.1 to 10 Hz. The resulting displacement is shown in Figure 4.2 (a).

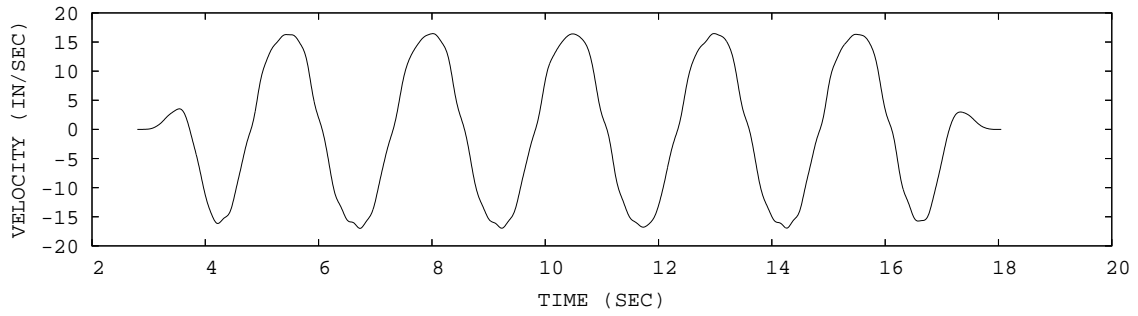
**Step 5:** With the velocity from step 3, steps 3 and 4 were repeated to obtain the acceleration. The resulting velocity and acceleration are shown in Figures 4.2 (b) and 4.2 (c).

**Step 6:** Step 4 was repeated for the measured force. The force is shown in Figure 4.2 (d).

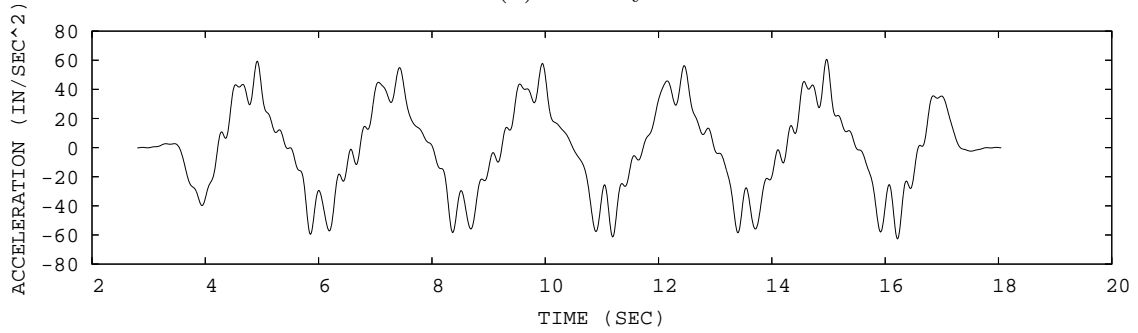
The phase plots corresponding to the data set UCB1\_17\_7 are shown in Figure 4.3. The entire data sets measured in Section 4.2 were processed; the time histories and phase plots of the data are shown in Figures A.1 - A.30 in Appendix A.



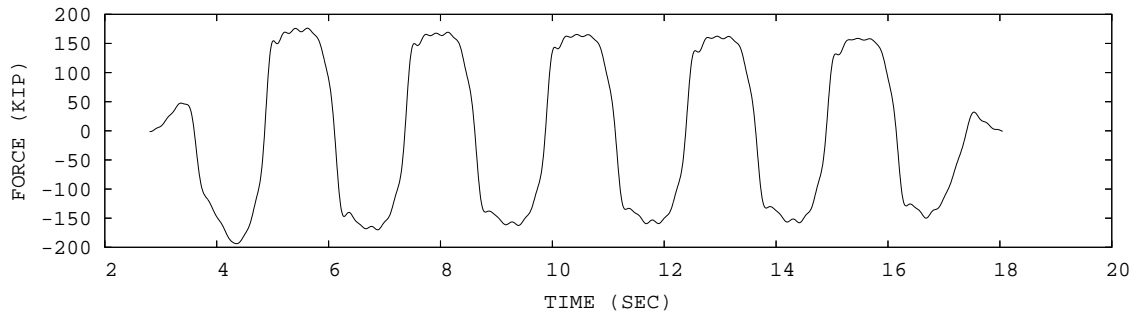
(a) Displacement



(b) Velocity



(c) Acceleration



(d) Force

Figure 4.2: Time histories of the 250 kip damper response subjected to sinusoidal excitation of the data set for UCB1\_17\_7. The displacement and force were measured, and the velocity and acceleration were obtained by differentiating the measured displacement.

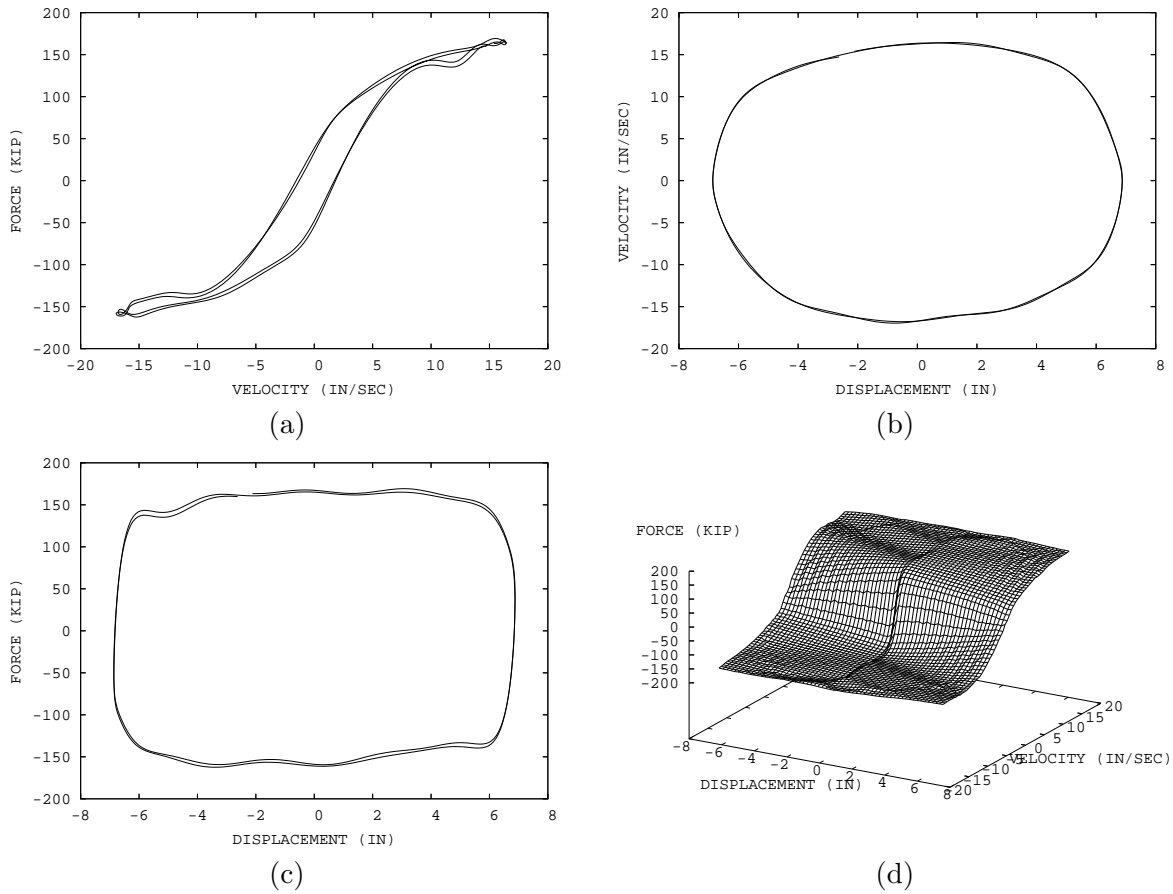


Figure 4.3: Phase plots of the 250 kip damper response subjected to sinusoidal excitation of the data set for UCB1\_17\_7. The displacement and force were measured, and the velocity and acceleration were obtained by differentiating the measured displacement.

## Chapter 5

# PARAMETRIC IDENTIFICATION OF THE 250 KIP VISCOUS DAMPER

### 5.1 Data Sets

The naming convention and test description for the tests performed on the 250 kip damper are summarized in Table 5.1. Figure 5.1 shows sample measured data of the 250 kip damper for the data set UCB1\_17\_7. Figs. 5.1 (a), (b), (c), and (d) are system time-history responses, displacement, velocity, acceleration, and measured force, respectively. Fig. 5.1 (e) is the displacement-force phase-plot, and Fig. 5.1 (f) is the velocity-force phase-plot.

### 5.2 Parametric Identification Results

One data set is selected to illustrate the results of the on-line and off-line parametric identification algorithms in detail. The identification results for the rest of the data sets are summarized in Tables 5.2 and 5.3. The plots of the parametric identification results for all data sets of the 250 kip viscous damper are provided in Appendix B.

#### 5.2.1 On-Line Parametric Identification Results

Data set UCB1\_17\_7 is selected to demonstrate the on-line parametric identification results. Figure 5.2 depicts the identification results of the selected test case. Figures 5.2 (a) and (b) show the time-history of the unknown parameters of the design model (Eqn. 2.6), Fig. 5.2(c) shows the time-history comparison of the measured force (solid line) and the predicted force (dash-dot line),

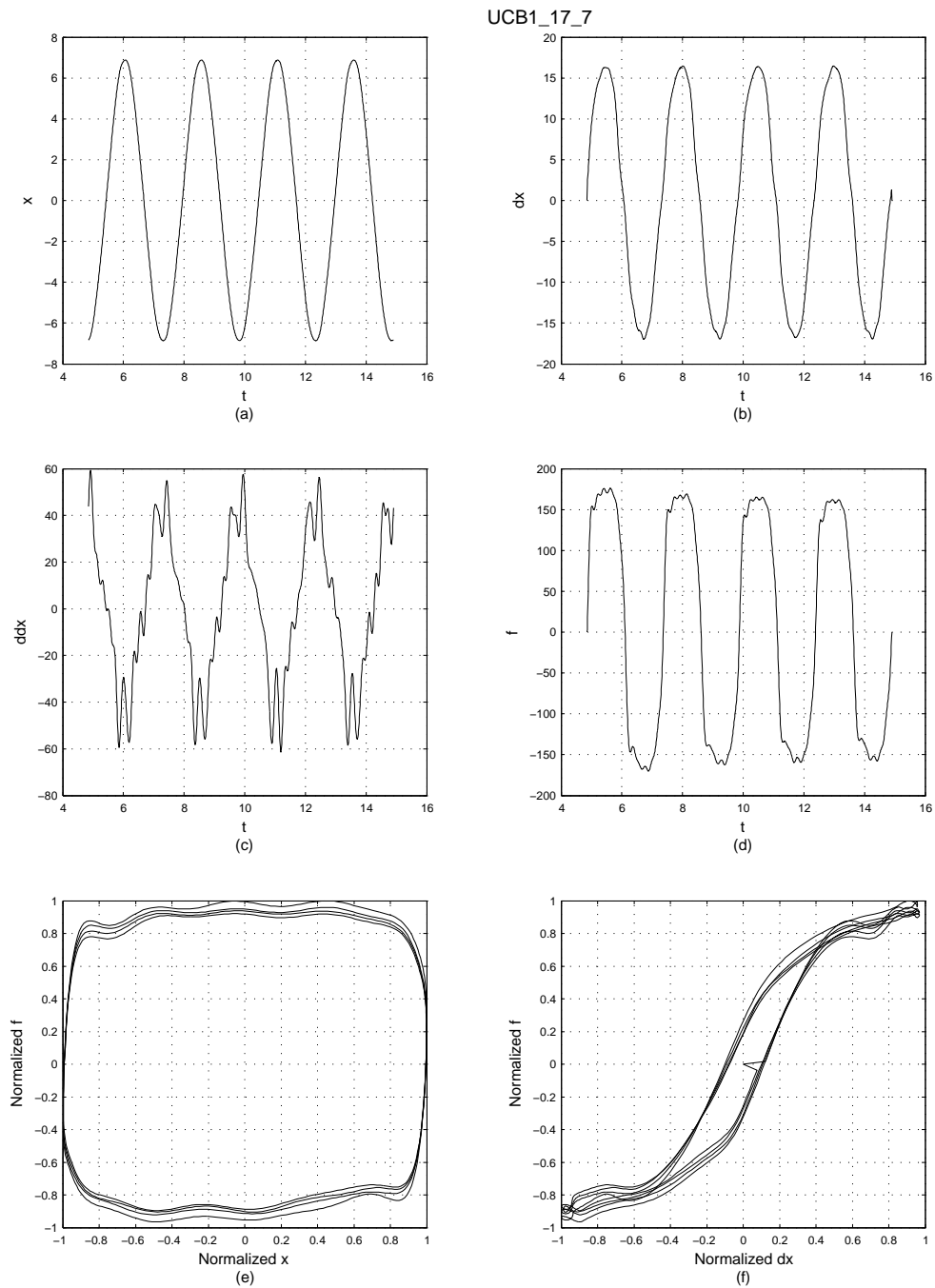


Figure 5.1: Sample measured data of the 250 kip damper for data set UCB1\_17\_7. Parts(a), (b), (c), and (d) are the system responses; displacement, velocity, acceleration, and measured force, respectively. Part (e) is the displacement-force phase-plot, and part (f) is the velocity-force phase-plot.

Table 5.1: Test matrix of the 250 kip damper data set.

Data set Name	Approx. Peak Velocity (in/sec)	Test Frequency (hz)	Test Amplitude (in)	Number of Cycle	Scan Rate (hz)
UCB1_10.4	10.00	0.398	4	6	100
UCB1_10.5	10.00	0.318	5	6	100
UCB1_10.6	10.00	0.265	6	6	100
UCB1_12.4	12.00	0.500	4	6	100
UCB1_12.5	12.50	0.400	5	6	100
UCB1_12.6	12.50	0.332	6	6	100
UCB1_12.7	12.50	0.284	7	6	100
UCB1_15.4	15.00	0.600	4	6	100
UCB1_15.5	15.00	0.477	5	6	100
UCB1_15.6	15.00	0.400	6	10	100
UCB1_15.7	15.00	0.341	7	6	100
UCB1_17.4	17.50	0.695	4	6	100
UCB1_17.5	17.50	0.557	5	6	100
UCB1_17.6	17.50	0.464	6	6	100
UCB1_17.7	17.50	0.399	7	6	100

Figs. 5.2 (d) and (e) depict the displacement-force and velocity-force phase-plane comparison of the measured force (solid line) and the predicted force (dash-dot line), for one cycle.

Table 5.2 summarizes the results of the on-line parametric identification for the 250 kip damper data sets. Column 1 is the data set name, column 2 is the manufacturer value for the damping coefficient  $C$ , column 3 is the average value of the identified damping coefficient  $\hat{C}$ , column 4 is the manufacturer specification value for the exponent  $n$ , column 5 is the average value of the identified exponent  $\hat{n}$  (Eqn. 2.6), column 6 is the selected value of the forgetting factor ( $\beta$ ) in the on-line identification algorithm (Eqn. 2.5), and column 7 is the normalized mean-square-error percentage of the difference between the predicted force and the measured force. The plots of all the identification results for the on-line algorithm are provided in Appendix B.1.

There is a spike in the value of the predicted force in its first cycle of identification (Fig. 5.2 (c)). The spike is caused by the initial values of the unknown parameters. After few steps of identification, when the parameters converge to their nominal values, the predicted force converges to the measured force.

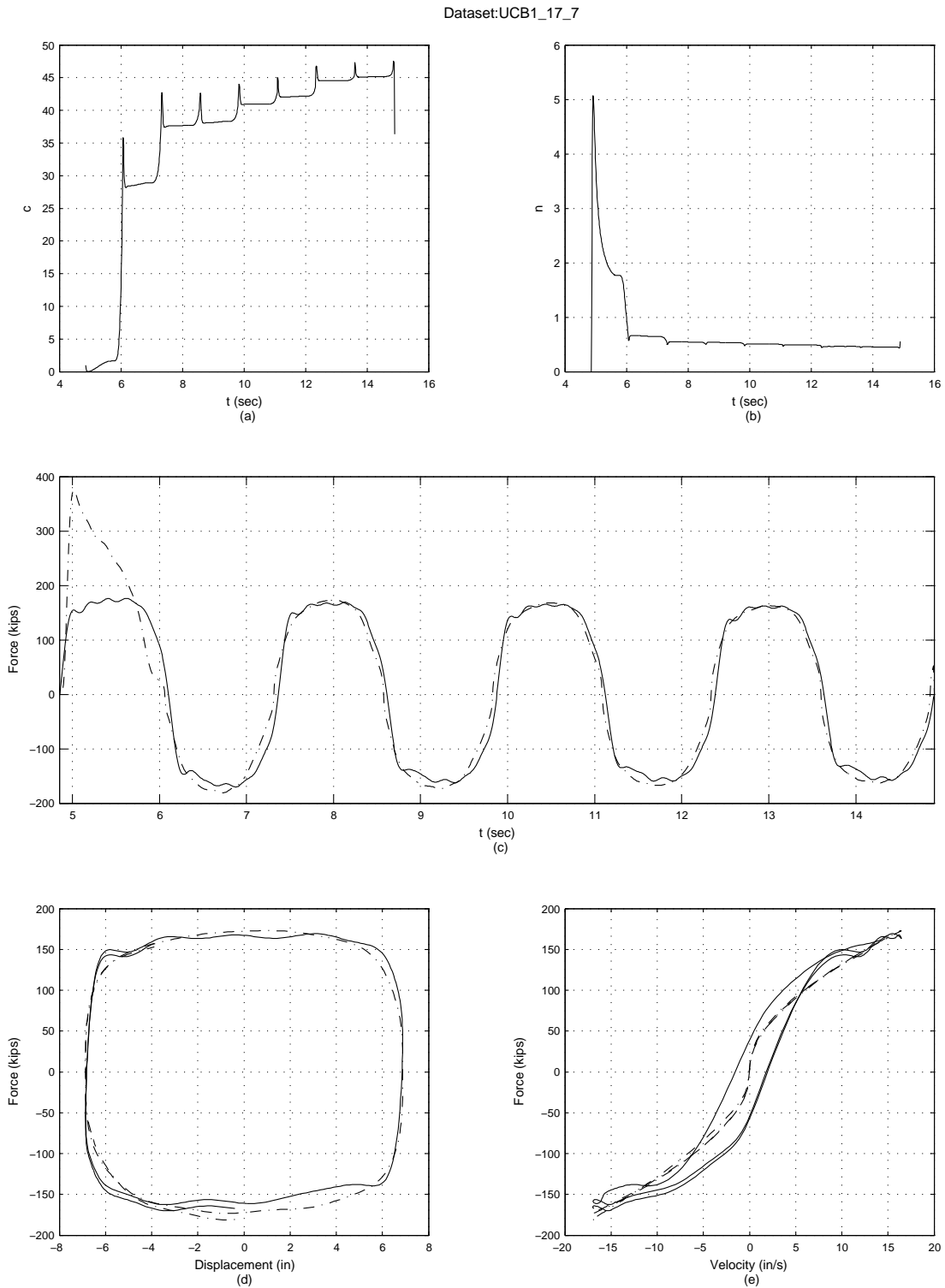


Figure 5.2: On-line parametric identification results of the 250 kip damper for data set UCB1\_17.7. Part (a) and (b) show the time-history of the unknown parameters, part (c) shows the time-history comparison of the measured force (solid line) and the predicted force (dash-dot line), part (d) is the displacement-force phase-plane comparison of the measured force (solid line) and the predicted force (dash-dot line), for one cycle, and part (e) is the velocity-force phase-plane comparison of the measured force (solid line) and the predicted force (dash-dot line), for one cycle.

Table 5.2: Summary of the on-line parametric identification results for the 250 kip damper data sets. Column 1 is the data set name, column 2 is the manufacturer value for the damping coefficient  $C$ , column 3 is the average value of the identified damping coefficient  $\hat{C}$ , column 4 is the manufacturer specification value for the exponent  $n$ , column 5 is the average value of the identified exponent  $\hat{n}$  (Eqn. 2.6), column 6 is the selected value of the forgetting factor ( $\beta$ ) in the on-line identification algorithm (Eqn. 2.5), and column 7 is the normalized mean-square-error percentage of the difference between the predicted force and the measured force.

Data set Name	Damping Coeff. $C$ (kip sec/in)		Exponent $n$		$\beta$ forgetting factor	% MSE error
	Damper Spec.	Identified	Damper Spec.	Identified		
UCB1_10_4	60.00	54.32	0.35	0.37	1.0	4.00
UCB1_10_5	60.00	48.55	0.35	0.44	1.0	5.74
UCB1_10_6	60.00	51.67	0.35	0.43	1.0	5.50
UCB1_12_4	60.00	49.72	0.35	0.41	1.0	6.22
UCB1_12_5	60.00	47.24	0.35	0.45	1.0	6.24
UCB1_12_6	60.00	47.90	0.35	0.45	1.0	5.79
UCB1_12_7	60.00	47.06	0.35	0.46	1.0	5.19
UCB1_15_4	60.00	44.58	0.35	0.45	1.0	6.25
UCB1_15_5	60.00	42.76	0.35	0.48	1.0	5.99
UCB1_15_6	60.00	44.60	0.35	0.46	1.0	4.79
UCB1_15_7	60.00	45.55	0.35	0.47	1.0	5.60
UCB1_17_4	60.00	42.91	0.35	0.46	1.0	6.19
UCB1_17_5	60.00	41.94	0.35	0.48	1.0	6.03
UCB1_17_6	60.00	40.69	0.35	0.49	1.0	6.06
UCB1_17_7	60.00	45.21	0.35	0.45	1.0	5.48

### 5.2.2 Off-line Parametric Identification Results

Data set UCB1\_17.7 is selected to demonstrate the results of the off-line parametric identification approach. Fig. 5.3 (a) shows the time-history comparison of the measured force (solid line) and the predicted force (dash-dot line), Fig. 5.3 (b) shows the displacement-force phase-plane comparison of the measured force (solid line) and the predicted force (dash-dot line), for one cycle, and Fig. 5.3 (c) depicts the velocity-force phase-plane comparison of the measured force (solid line) and the predicted force (dash-dot line), for one cycle.

Table 5.3 summarizes results of the off-line parametric identification method for the 250 kip damper data sets. Column 1 is the data set name, columns 2 to 7 give the optimum values of the initially unknown vector for the optimization model (Eqn. 2.10), and the last column is the normalized mean-square-error value of the difference between the predicted force and the measured force. The plots of the off-line parametric identification results for the 250 kip damper data sets are provided in Appendix B.2.

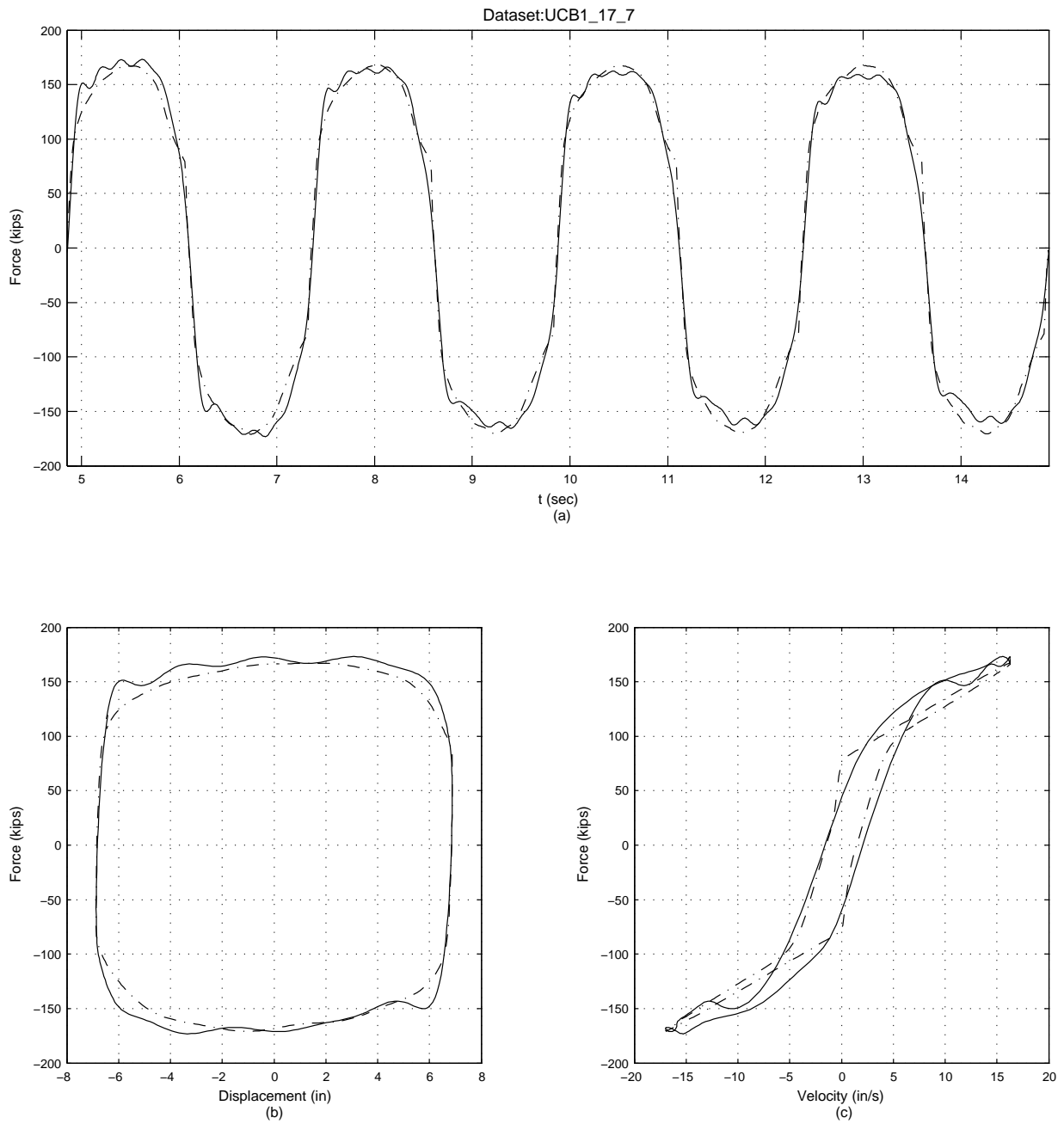


Figure 5.3: Off-line parametric identification results of the 250 kip damper for data set UCB1\_17\_7. Part (a) shows the time-history comparison of the measured force (solid line) and the predicted force (dash-dot line), part (b) shows the displacement-force phase-plane comparison of the measured force (solid line) and the predicted force (dash-dot line), for one cycle, and part (c) shows the velocity-force phase-plane comparison of the measured force (solid line) and the predicted force (dash-dot line), for one cycle.

Table 5.3: Summary of the off-line parametric identification results for the 250 kip damper data set. Column 1 is the data set name, columns 2 to 7 are the optimum values of the initially unknown parameters (Eqn. 2.11), column 8 is the normalized mean-square-error (Eqn. 2.9).

Data set	c (kip sec/in)	k (kip/in)	n	$\theta_1$	$\theta_2$	$\theta_3$	% MSE
UCB1_10_4	7.51	0.07	1.87	430.1	-1.06	0.89	2.00
UCB1_10_5	8.57	0.67	2.01	476.2	-0.77	0.65	3.49
UCB1_10_6	8.36	0.18	2.07	511.8	-0.96	0.86	3.27
UCB1_12_4	6.26	0.88	2.01	493.5	-0.41	0.32	2.87
UCB1_12_5	6.48	0.69	2.01	509.3	-0.86	0.77	3.07
UCB1_12_6	6.74	0.25	2.02	512.3	-0.83	0.74	3.04
UCB1_12_7	7.17	0.04	2.03	500.8	-1.02	0.91	3.15
UCB1_15_4	4.65	1.09	2.01	511.2	-0.29	2.15	2.78
UCB1_15_5	5.88	0.80	2.01	511.2	-0.47	0.39	2.86
UCB1_15_6	6.06	0.73	2.02	547.2	-0.97	0.87	3.01
UCB1_15_7	6.14	0.55	1.83	622.6	-3.29	3.00	2.94
UCB1_17_4	5.36	1.27	1.84	546.9	-0.45	0.27	2.75
UCB1_17_5	5.57	1.19	1.82	578.3	-1.31	1.10	2.82
UCB1_17_6	5.67	0.97	1.94	627.1	-1.74	1.60	2.81
UCB1_17_7	5.65	0.60	1.95	622.8	-1.69	1.55	2.82

### 5.3 Summary of the Parametric Identification

The maximum measured force, absolute equivalent design force, and the identified force from the parametric identification of 250 kip viscous damper are summarized and compared in Table 5.4. In Table 5.4, column 2 is the maximum measured force of each data set, column 3 is the absolute equivalent design force, which is calculated based on the design formula (Eqn. 2.6), the corresponding measured velocity for the maximum force in each test, and the manufacturer design parameters ( $C = 60$  (kip sec/in) and  $n = 0.35$ ), and columns 4 and 5 are the identified forces from the on-line and off-line parametric identification methods of the 250 kip viscous damper.

Table 5.4: Comparison of the maximum measured force, absolute equivalent design force, and identified force from the parametric identification methods of the 250 kip viscous damper. The equivalent design force is calculated based on the design formula (Eqn. 2.6), the corresponding measured velocity for the maximum force in each test, and the manufacturer design parameters ( $C = 60$  (kip sec/in) and  $n = 0.35$ ).

Test Name	Maximum Measured Force (kip)	Absolute Equivalent Design Force (kip)	Identified Force	
			On-line PI (kip)	Off-line PI (kip)
UCB1_10_4	152.55	132.24	135.70	141.45
UCB1_10_5	154.26	133.40	141.47	148.46
UCB1_10_6	158.57	133.84	147.43	145.83
UCB1_12_4	165.67	142.16	145.10	151.43
UCB1_12_5	163.18	144.32	151.94	153.98
UCB1_12_6	163.33	144.16	158.98	154.14
UCB1_12_7	163.38	144.81	157.63	153.99
UCB1_15_4	173.18	152.46	152.91	161.99
UCB1_15_5	171.89	151.39	159.91	163.38
UCB1_15_6	173.20	153.46	167.18	161.98
UCB1_15_7	171.81	152.23	170.50	164.79
UCB1_17_4	175.35	158.70	158.10	168.58
UCB1_17_5	175.66	159.28	167.67	171.67
UCB1_17_6	174.88	159.65	168.97	172.34
UCB1_17_7	176.22	156.80	173.32	170.93

## Chapter 6

# NONPARAMETRIC RESTORING FORCE METHOD IDENTIFICATION FOR THE 250 KIP VISCOUS DAMPER

### 6.1 Application of the Restoring Force Method to Collected Data Sets

The experimental data of the 250 kip damper response prepared in Chapter 4 were used in the RFM identification. The goals of the identification were to demonstrate that (1) the RFM can be used to identify a 250 kip viscous damper under harmonic excitation, and (2) the Chebyshev and power series coefficients determined with the RFM reflect the change of the peak velocity and displacement in the experiments.

To determine the proper Chebyshev order, the damper response was identified with different order numbers. The order number was limited to 5. The comparison of the 3rd and 5th orders of the identification results are shown in Figures 6.1 and 6.2. Figures 6.1 and 6.2 (a) show the comparison of the measured and estimated damping forces in the time domain. The error between the measured and estimated damping forces are also shown in Figures 6.1 and 6.2 (b). It was evident that the 3rd order identification missed the small and higher frequency ripples, while the 5th order identification detected the ripples. The estimation error is observed clearly in the force-velocity phase plots in 6.1 and 6.2 (d). The 3rd order identification under-estimates the damping force in the velocity ranges between approximately -5 and 5 in/sec. Therefore, the 5th-order Chebyshev identification was used in the RFM identification. The parameters of the RFM identification of the 250 kip viscous damper are summarized in Table 6.1.

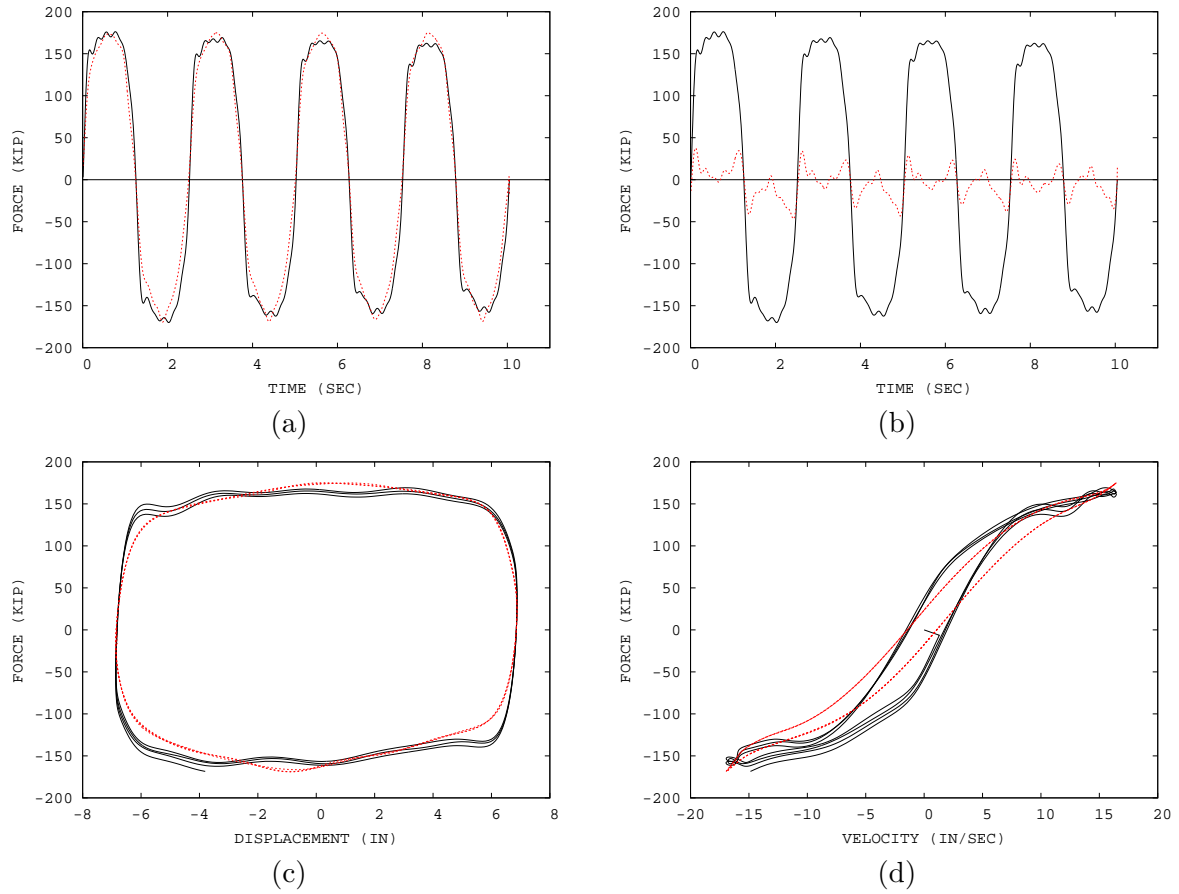


Figure 6.1: The third order RFM identification results for the damper response subjected to sinusoidal excitation for the data set of UCB1\_17\_7. The solid line is the measured force, and the dashed line is the identified force. Note that relative time was used for the identification segment.

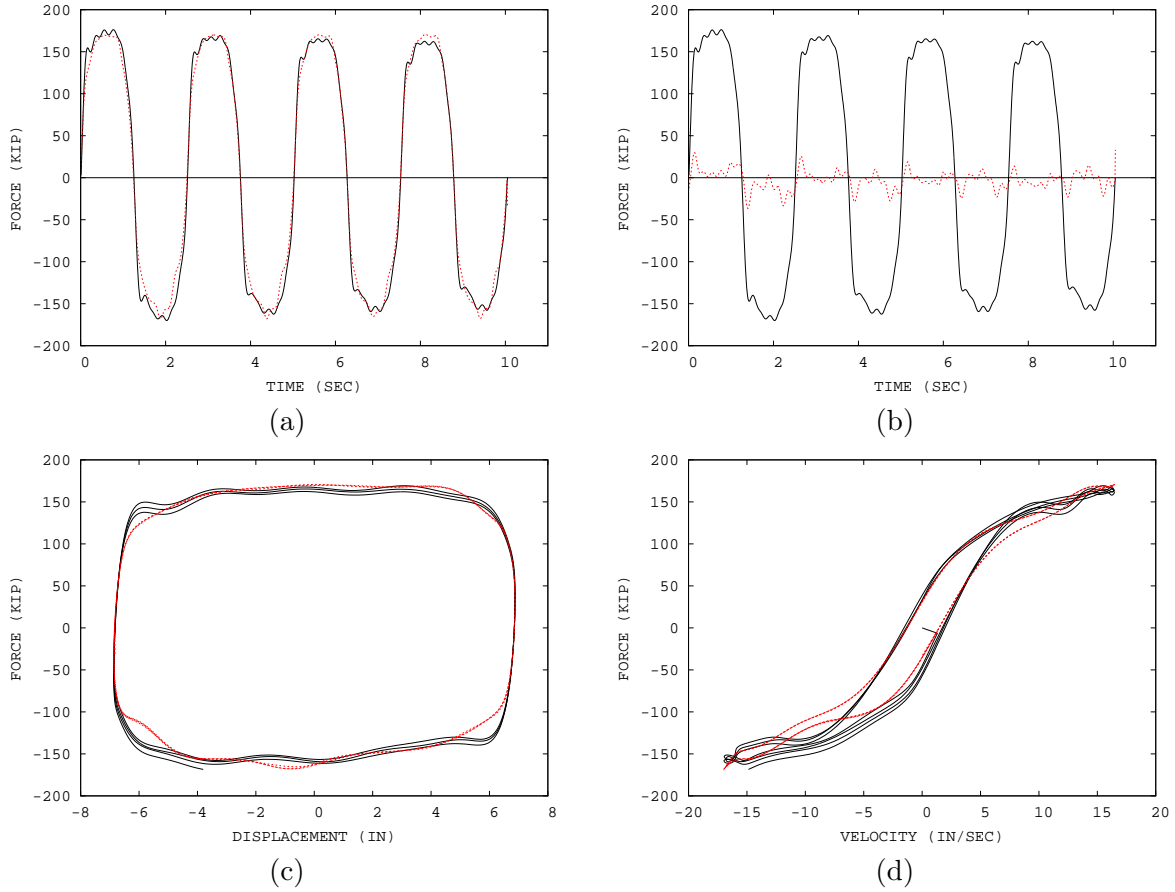


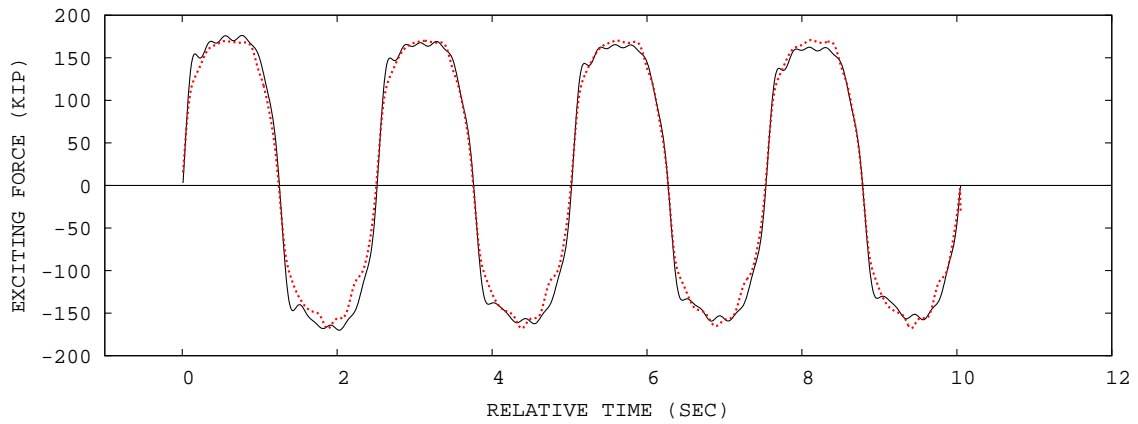
Figure 6.2: The fifth order RFM identification results of the 250 kip damper response subjected to sinusoidal excitation for the data set UCB1\_17\_7. The solid line is the measured force, and the dashed line is the identified force. Note that relative time was used for the identification segment.

Table 6.1: Test parameters of the UCB 250 kip damper.

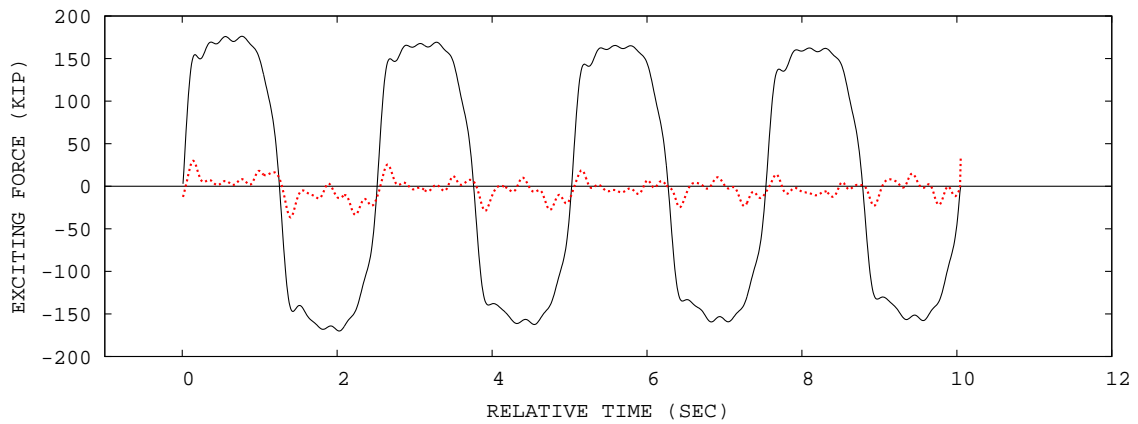
No	Filename	No of data pts	Sampling rate (Hz)	Order	Iteration
1	UCB1_10.4	1751	100	5	1
2	UCB1_10.5	1258			
3	UCB1_10.6	1509			
4	UCB1_12.4	806			
5	UCB1_12.5	1001			
6	UCB1_12.6	1206			
7	UCB1_12.7	1409			
8	UCB1_15.4	667			
9	UCB1_15.5	839			
10	UCB1_15.6	1751			
11	UCB1_15.7	1173			
12	UCB1_17.4	575			
13	UCB1_17.5	718			
14	UCB1_17.6	648			
15	UCB1_17.7	1006			

With the identification parameters, a total of 15 sets of the 250 kip damper response data were identified, and sample identification results are shown in Figures 6.3 and 6.4. The identification results for the other data sets are shown in Figures C.1 - C.15 in Appendix C.1. The normalized Chebyshev coefficients, normalized power series coefficients, and de-normalized power series coefficients were also determined, and are shown in Figures 6.5 (a), (b) and (c), respectively. The coefficients are also tabulated in Table 6.4. The first and third terms of the stiffness and damping coefficients are summarized in Figure 6.6. The results showed that the dominant terms of the damper response were the first order of stiffness and damping coefficients. This was similarly observed in all the other 14 data sets. The root mean square error and mean square error ratio of the measured and estimated damping forces of the 15 data sets are shown in Table 6.2. The results demonstrate that the characteristics of the 250 kip viscous damper were successfully identified with the RFM.

The maximum measured, absolute equivalent design, and maximum RFM-identified forces are calculated and compared in Table 6.3. The absolute equivalent design force is calculated based on the design formula (Eqn. 2.6), the corresponding measured velocity for the maximum force in each test, and the manufacturer design parameters ( $C = 60$  (kip sec/in) and  $n = 0.35$ ). The results showed that the absolute equivalent design forces were slightly underestimated than the maximum measured forces with the ratio of 0.85 - 0.91. The maximum RFM-identified forces were very close to the maximum measured force with the ratio of 0.90 - 0.90.

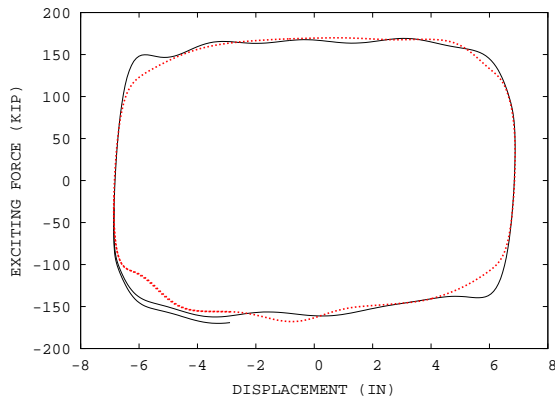


(a) Estimated force

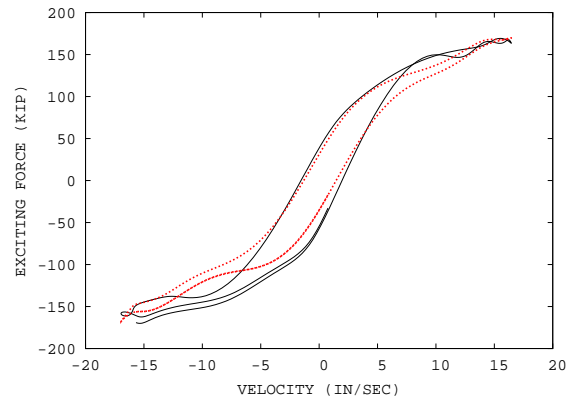


(b) Error between estimated and measured force

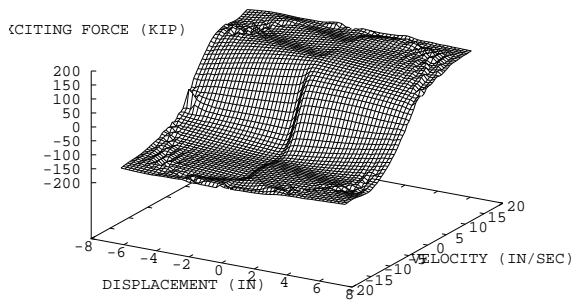
Figure 6.3: Comparison of the measured and identified time history response of the 250 kip damper using RFM for the data set UCB1\_17.7. The solid line is the measured force, and the dashed line is the identified force. Note that relative time was used for the identification segment.



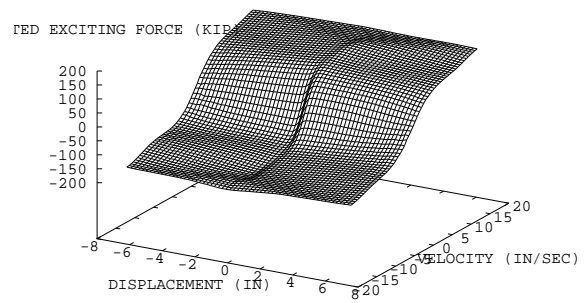
(a)



(b)

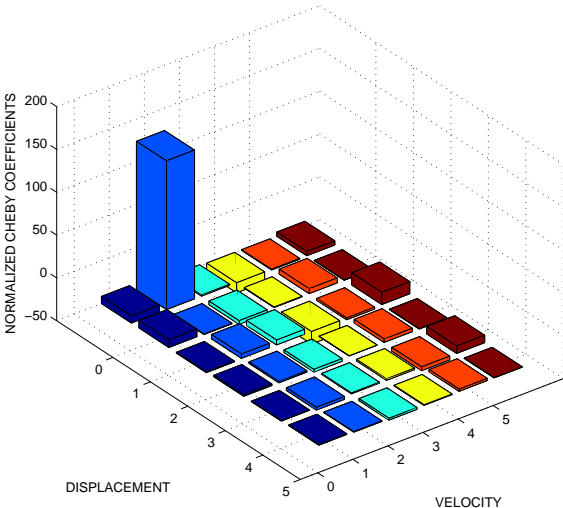


(c)

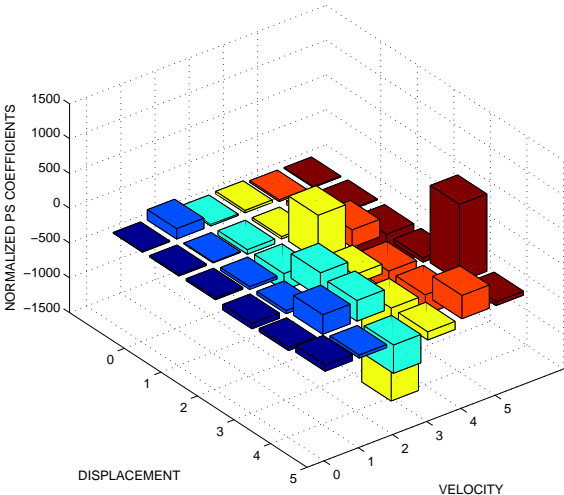


(d)

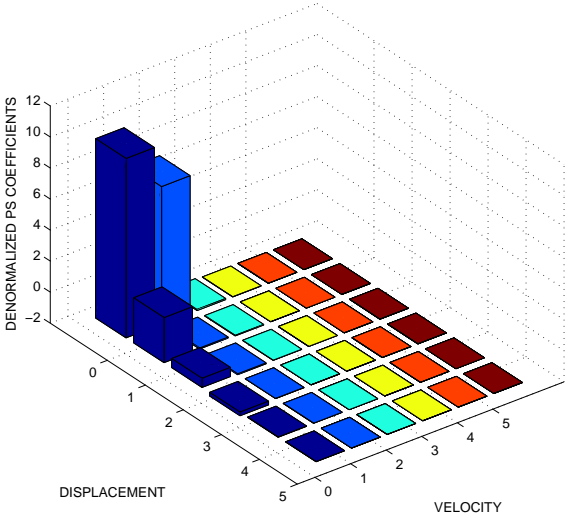
Figure 6.4: Comparison of the measured and identified response of the 250 kip damper in phase plot using RFM for the data set UCB1\_17.7. The solid line is the measured force, and the dashed line is the identified force.



(a) Chebyshev coefficients



(b) Normalized power series coefficients



(c) Denormalized power series coefficients

Figure 6.5: Identified RFM coefficients for the 250 kip damper subjected to sinusoidal excitation for the data set UCB1\_17\_7.

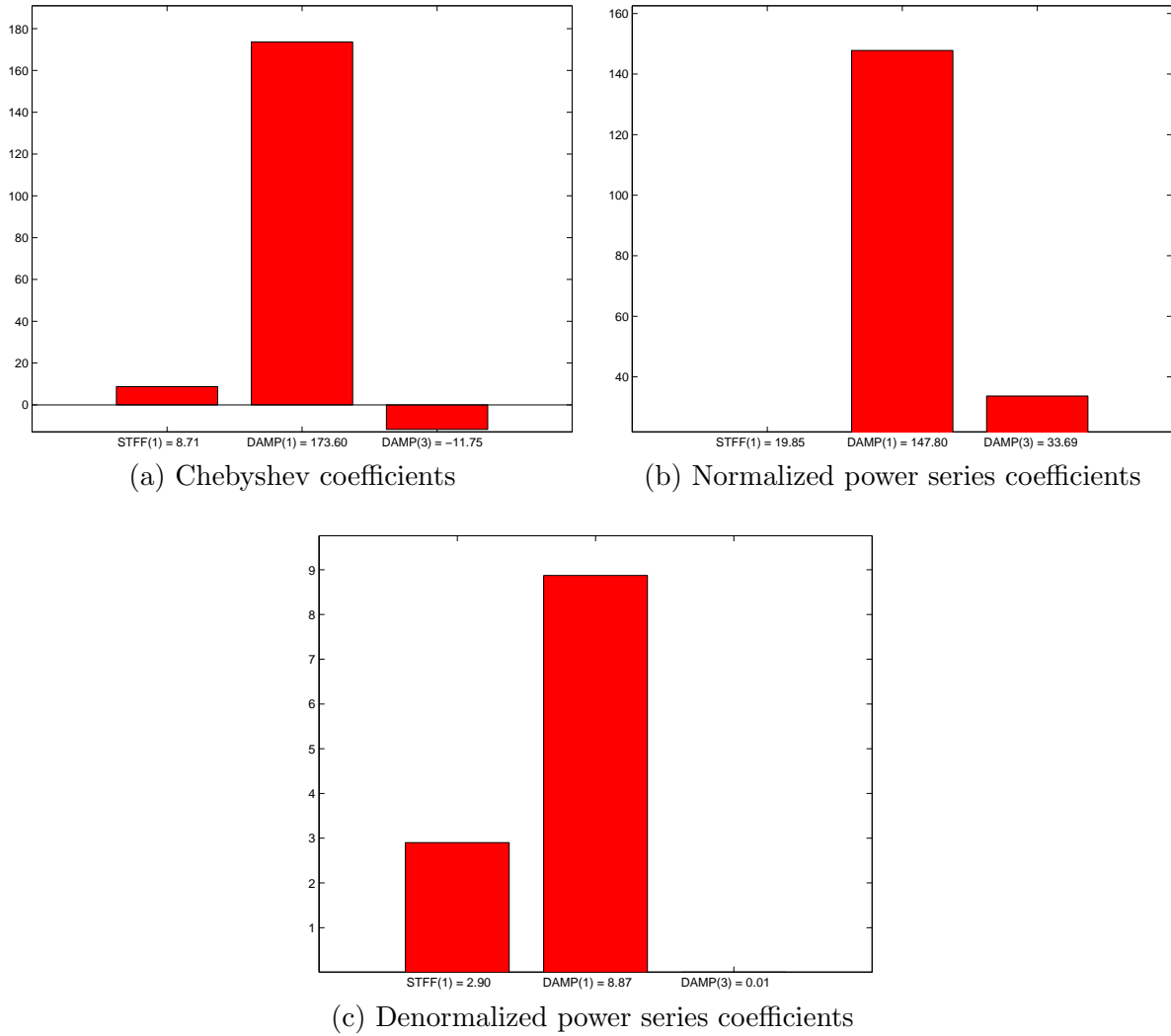


Figure 6.6: Low order stiffness and damping coefficients for the 250 kip damper subjected to sinusoidal excitation for the data set UCB1\_17\_7.

Table 6.2: Root mean square error and normalized mean square error of the measured and estimated damping forces.

No	Filename	RMS error	Normalized MSE (%)
1	UCB1_10.4	130.02	0.74
2	UCB1_10.5	112.93	1.61
3	UCB1_10.6	117.16	1.56
4	UCB1_12.4	122.56	1.69
5	UCB1_12.5	124.33	1.08
6	UCB1_12.6	124.63	2.31
7	UCB1_12.7	123.55	1.66
8	UCB1_15.4	130.58	1.32
9	UCB1_15.5	132.09	1.02
10	UCB1_15.6	130.02	0.74
11	UCB1_15.7	133.41	1.64
12	UCB1_17.4	136.47	0.74
13	UCB1_17.5	138.52	0.66
14	UCB1_17.6	138.89	0.72
15	UCB1_17.7	138.42	0.67

## 6.2 Validation of Restoring Force Method Results

As discussed in Section 6.1, the second goal of the RFM identification on the 250 kip viscous damper was to demonstrate that the change of the RFM coefficients can be used as an indicator of the damper's restoring force alteration. Because the restoring force of a viscous damper is linearly or nonlinearly proportional to the magnitude of the excitation velocity. Three test cases with the same displacement, but different peak velocities were chosen, and compared with their normalized Chebyshev coefficients. The three test cases included: (1) 17.5 in/sec and 7 in, (2) 15.0 in/sec and 7 in, and (3) 12.5 in/sec and 7 in. The normalized Chebyshev coefficients are shown in Figure 6.7. In all these cases, the dominant coefficient of the damping force was the first order damping term. It was also observed that the dominant first damping coefficient decreased as the peak excitation velocity decreased (Figure 6.8). The same observations were valid for the 3rd order damping coefficient.

Table 6.3: Comparison of the maximum measured force, absolute equivalent design force, and maximum RFM-identified force of the 250 kip viscous damper. The equivalent design force is calculated based on the design formula (Eqn. 2.6), the corresponding measured velocity for the maximum force in each test, and the manufacturer design parameters ( $C = 60$  (kip sec/in) and  $n = 0.35$ ). The ratio of each force respect to the maximum measured force are shown in the parenthesis.

Test No.	Test name	Max measured force (kip)	Absolute equivalent design force (kip)	RFM-identified force (kip)
1	UCB1_10_4	152.55	132.24 (0.87)	144.13 (0.94)
2	UCB1_10_5	154.26	134.17 (0.87)	149.91 (0.97)
3	UCB1_10_6	158.57	134.17 (0.85)	146.47 (0.92)
4	UCB1_12_4	165.67	143.82 (0.87)	157.65 (0.95)
5	UCB1_12_5	163.18	144.86 (0.89)	150.52 (0.92)
6	UCB1_12_6	163.33	144.23 (0.88)	159.62 (0.98)
7	UCB1_12_7	163.38	144.85 (0.89)	152.17 (0.93)
8	UCB1_15_4	173.18	152.62 (0.88)	156.29 (0.90)
9	UCB1_15_5	171.89	152.57 (0.89)	168.08 (0.98)
10	UCB1_15_6	173.20	153.59 (0.89)	160.74 (0.93)
11	UCB1_15_7	171.81	153.87 (0.90)	166.36 (0.97)
12	UCB1_17_4	175.35	158.70 (0.91)	166.64 (0.95)
13	UCB1_17_5	175.66	159.36 (0.91)	171.55 (0.98)
14	UCB1_17_6	174.88	159.90 (0.91)	168.62 (0.96)
15	UCB1_17_7	176.22	159.91 (0.91)	167.83 (0.95)

Table 6.4: Identified Chebyshev and power series coefficients of the 250 kip damper for the data set UCB1\_17\_7.

(a) Chebyshev coefficients

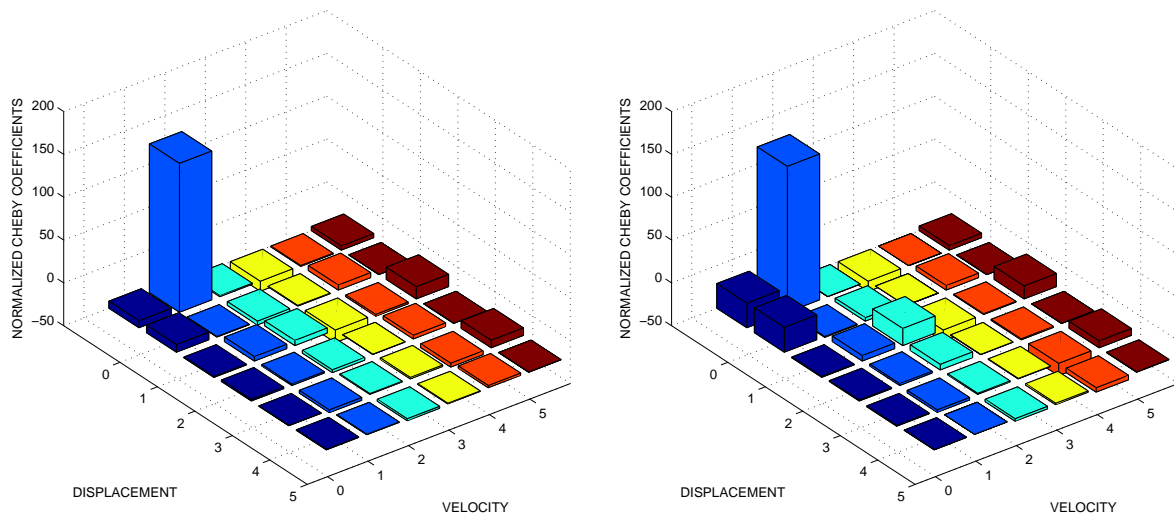
$x/\dot{x}$	0	1	2	3	4	5
0	8.20	173.60	1.21	-11.75	-0.86	4.80
1	8.72	-0.51	-4.41	-0.57	5.75	0.14
2	-0.92	5.07	5.83	-14.64	-2.02	14.25
3	1.70	1.60	-3.08	0.18	4.10	0.17
4	-0.41	-3.23	0.89	1.67	-4.40	8.67
5	0.65	-0.54	-2.26	-0.71	2.61	0.22

(b) Normalized power series coefficients

$x/\dot{x}$	0	1	2	3	4	5
0	9.21	147.80	18.40	33.69	-25.86	-12.39
1	19.85	9.75	-65.04	-33.56	52.16	11.87
2	28.07	-40.77	-240.10	647.70	249.20	-654.40
3	-74.92	-46.46	352.40	134.60	-286.80	-59.83
4	-45.62	281.20	295.80	-1335.00	-281.60	1110.00
5	88.33	43.18	-406.50	-115.90	334.30	56.34

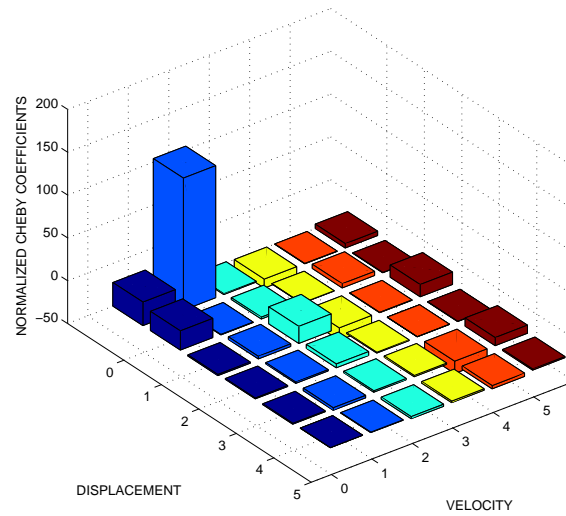
(c) Denormalized power series coefficients

$x/\dot{x}$	0	1	2	3	4	5
0	11.56	8.87	0.07	0.01	0.00	0.00
1	2.90	0.07	-0.03	0.00	0.00	0.00
2	0.58	-0.06	-0.02	0.00	0.00	0.00
3	-0.23	-0.01	0.00	0.00	0.00	0.00
4	-0.02	0.01	0.00	0.00	0.00	0.00
5	0.01	0.00	0.00	0.00	0.00	0.00



(a) 17.5 in/sec

(b) 15.0 in/sec



(c) 12.5 in/sec

Figure 6.7: Comparison of normalized Chebyshev coefficients of the 250 kip damper subjected to sinusoidal excitations with different peak velocity; (a) 17.5 in/sec, (b) 15.0 in/sec and (c) 12.5 in/sec. The displacement was 7 in in all cases.

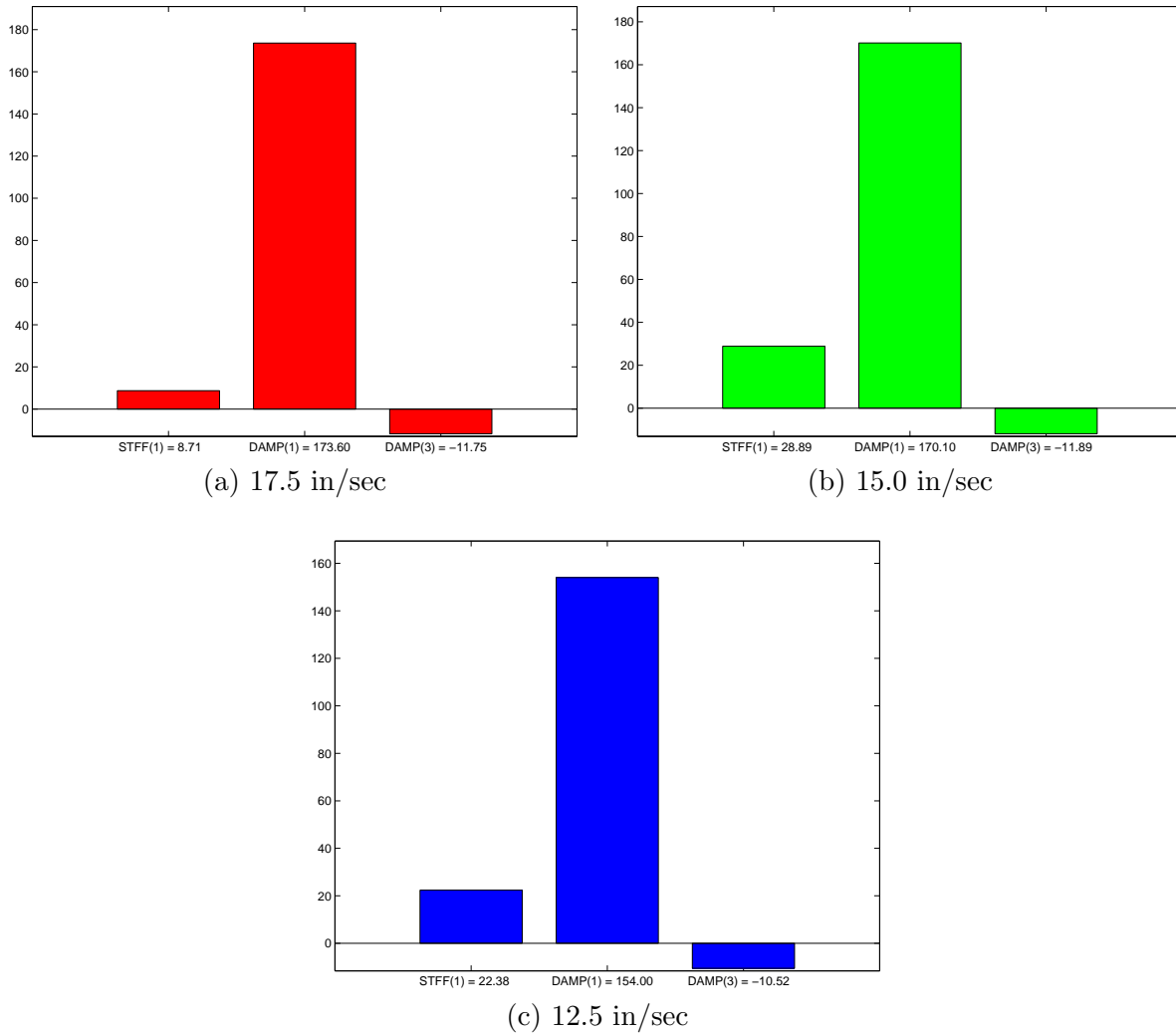


Figure 6.8: Comparison of low order Chebyshev coefficients of the 250 kip damper subjected to sinusoidal excitations with different peak velocity; (a) 17.5 in/sec, (b) 15.0 in/sec and (c) 12.5 in/sec. The displacement was 7 in in all cases.



## Chapter 7

# IDENTIFICATION OF THE 250 KIP VISCOUS DAMPER USING ARTIFICIAL NEURAL NETWORKS

### 7.1 Background

One of the objectives of the present research was to demonstrate that the damper can be identified by ANN. Unlike RFM, no prior investigation was undertaken to explore the relationship between the restoring force and the weights and bias of the neural networks; it is much more challenging to extract meaningful analytical relationships between the physical change of the system and the weights and bias of the neural networks. The data sets in Chapter 4 were used in the ANN identification. An example of the damper response used in the identification is illustrated in Figures 7.1 and 7.2. The ANN had three inputs and one output: the displacement, velocity and acceleration were used as the input, and the force was used as the output.

### 7.2 Application of Artificial Neural Networks to Collected Data Sets

The neural networks were trained using the measured response of the 250 kip damper. The displacement, velocity and acceleration were used as the neural networks input, and the force was fitted as the output of the neural networks. The training was performed with the ARS method. A description of the ARS method is provided in Section 2.3.2. The training parameters for the 250 kip damper are summarized in Table 7.1. During the training, the weights and bias of the neural

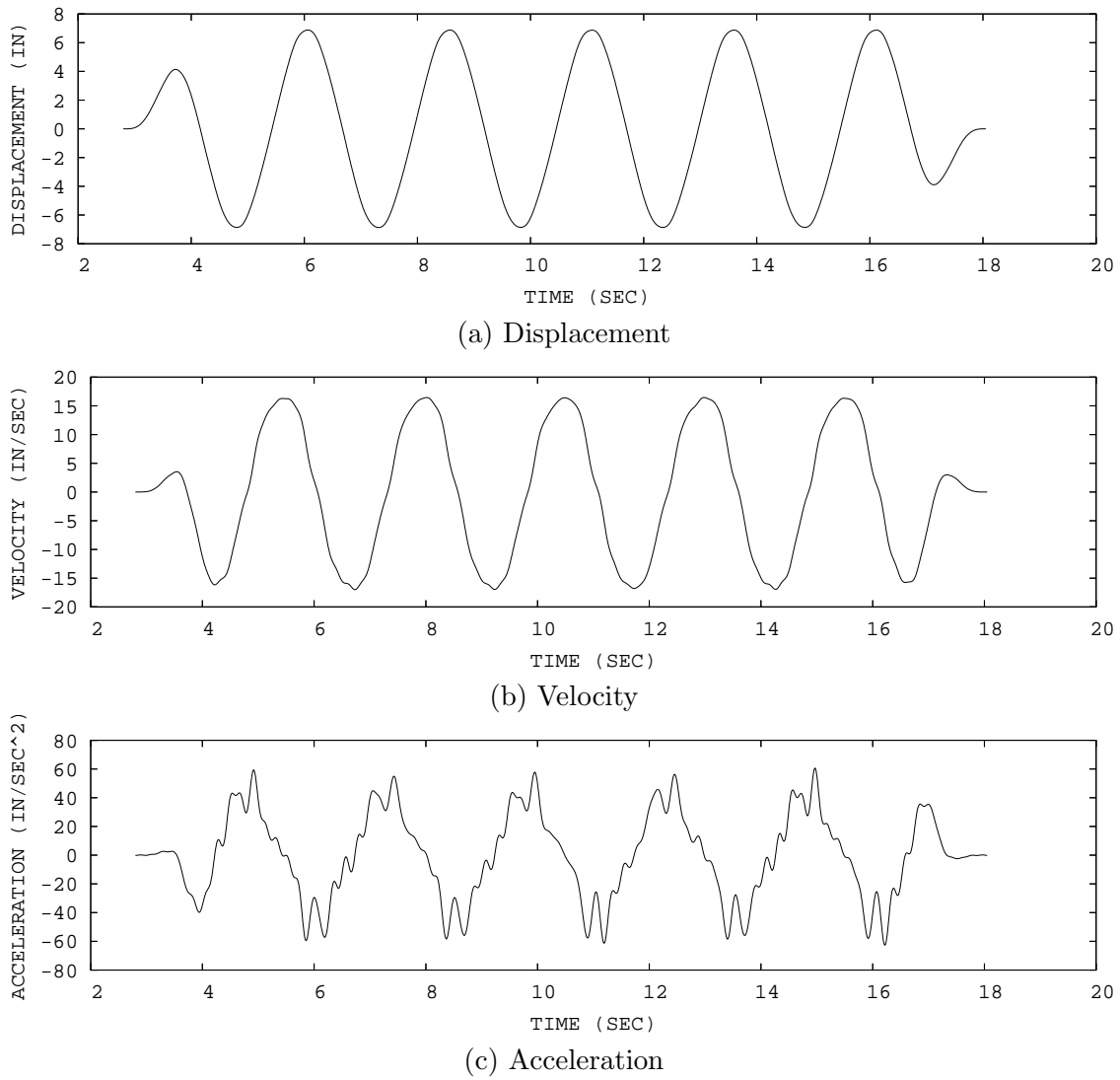


Figure 7.1: The displacement, velocity and acceleration of the 250 kip damper as the input of the neural networks.

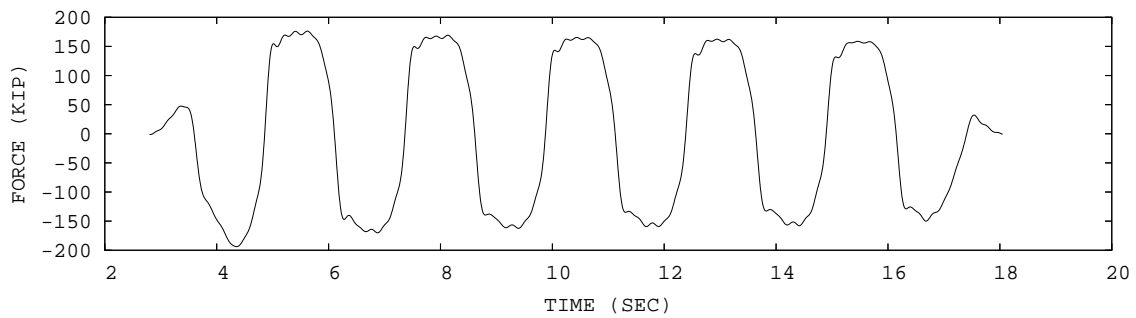


Figure 7.2: The force of the 250 kip damper as the output of the neural networks.

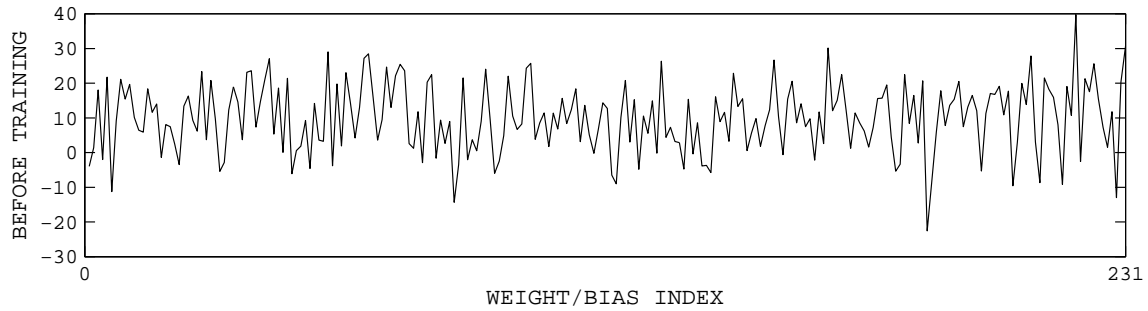
Table 7.1: Training parameters for the response of the 250 kip damper using the adaptive random search method

Number of global search	10
Number of local search	500
Number of statistical averaging	3
Number of nodes in the 1st layer	15
Number of nodes in the 2nd layer	10
neural networks input	Displacement Velocity Acceleration
neural networks output	Force

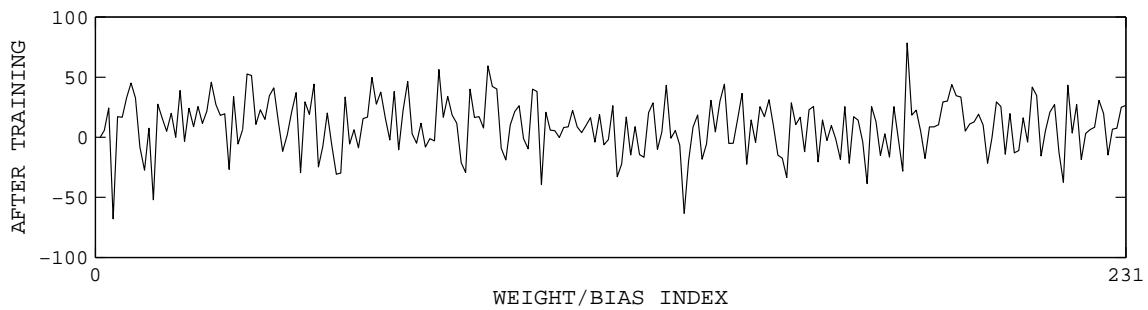
networks were changed to minimize the root-mean-square error between the measured and the identified force as shown in Figures 7.3 (a) and (b). In Figure 7.3 (c), the ratio of the current error function normalized by the starting error function (solid line), and the current optimal standard deviation of the random step size (dashed line) are shown in the log scale. As the global loops were executed in the adaptive random search, both the error ratio and step size converged.

The results of the ANN training are shown in Figure 7.4 (the measured force with a solid line and the identified response with a dashed line). Figures 7.4 (a) and (b) depict the measured and identified damper force before and after network training, respectively. It was observed that there was a very good agreement between the identified and the measured force. The estimation error between the measured and identified force is shown in Figure 7.4 (c). For all the 15 data sets, the quality of the force data fitting was excellent. The mean square error ratio ranged from 0.09 % to 0.23% (Table 7.2). The training results from the rest of the data sets are shown in Figures C.16 to C.45. Therefore, based on the above results, it was verified that ANN can be used to identify the response of the 250 kip viscous damper under sinusoidal excitation.

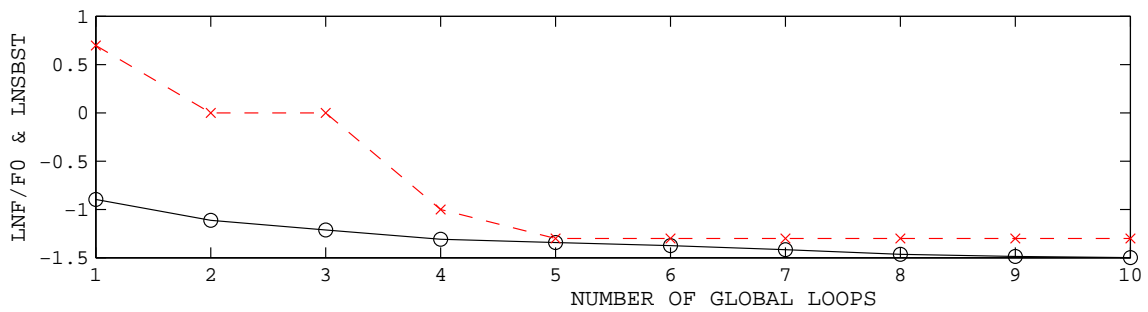
The maximum measured, absolute equivalent design and maximum ANN-identified forces were compared in Table 7.3. In the table, The equivalent design force is calculated based on the design formula (Eqn. 2.6), the corresponding measured velocity for the maximum force in each test, and the manufacturer design parameters ( $C = 60$  (kip sec/in) and  $n = 0.35$ ).



(a) Weights and bias before training

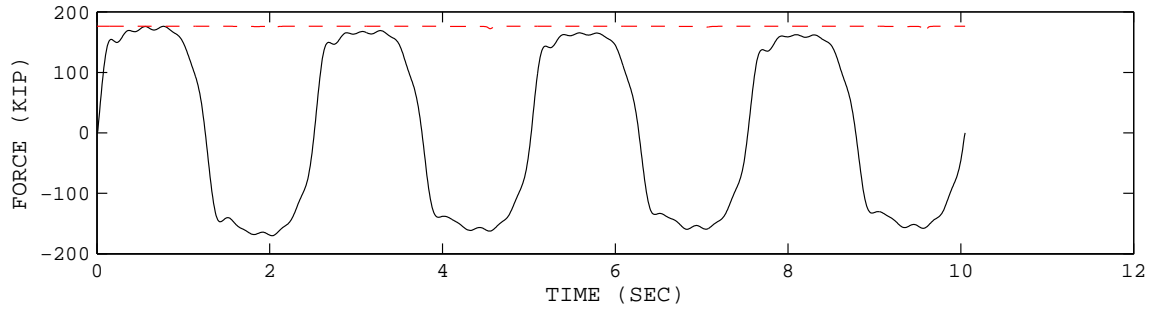


(b) Weights and bias after training

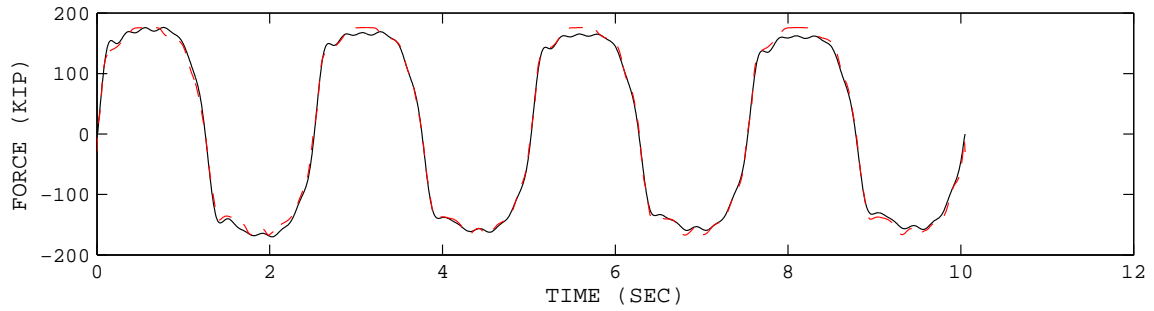


(c) RMSE ratio after training

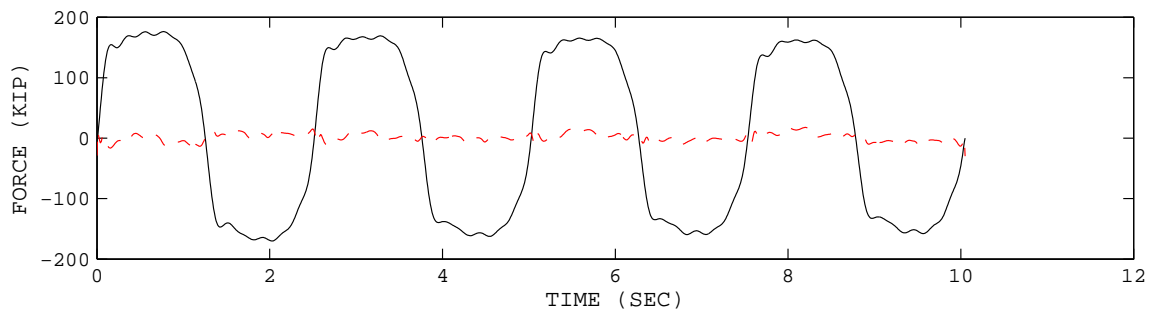
Figure 7.3: Ratio of the current error function normalized by the starting error function (solid line) and the current optimal standard deviation of random step size (dashed line) for the data set UCB1.17.7. The y-axis is plotted in log scale.



(a) Force before training



(b) Force after training



(c) Error after training

Figure 7.4: Comparison of the measured and identified damper response to sinusoidal excitation for in time history using ANN for the data set UCB1\_17.7. The solid line is the measured force, and the dashed line is the identified force.

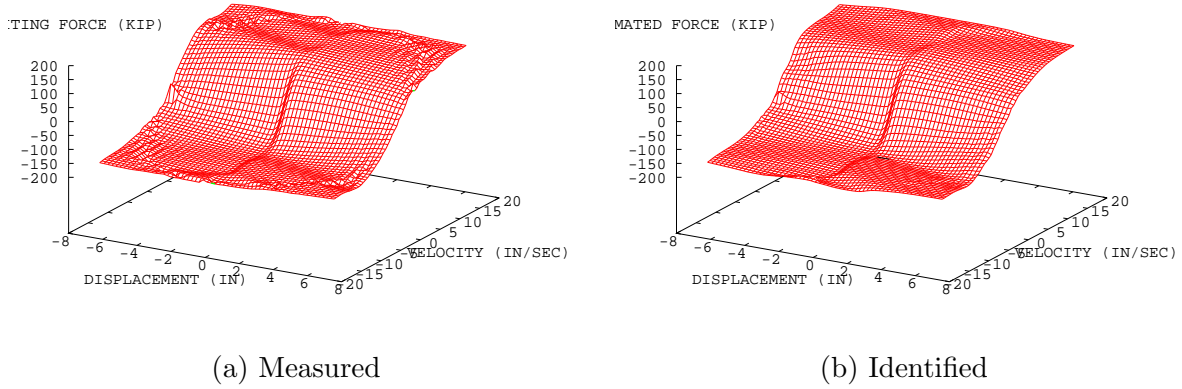


Figure 7.5: Comparison of the measured and identified damper response in phase plot to sinusoidal excitation using ANN for the data set UCB1\_17\_7. The solid line is the measured force, and the dashed line is the identified force.

Table 7.2: Normalized mean square error between the measured and identified force of the 250 kip viscous damper.

No.	Test name	Normalized MSE (%)
1	UCB1_10_4	0.13
2	UCB1_10_5	0.09
3	UCB1_10_6	0.10
4	UCB1_12_4	0.10
5	UCB1_12_5	0.10
6	UCB1_12_6	0.15
7	UCB1_12_7	0.09
8	UCB1_15_4	0.23
9	UCB1_15_5	0.12
10	UCB1_15_6	0.12
11	UCB1_15_7	0.10
12	UCB1_17_4	0.15
13	UCB1_17_5	0.11
14	UCB1_17_6	0.23
15	UCB1_17_7	0.10

Table 7.3: Comparison of the maximum measured force, equivalent design force, and ANN-identified force from the parametric identification methods of the 250 kip viscous damper. The absolute equivalent design force is calculated based on the design formula (Eqn. 2.6), the corresponding measured velocity for the maximum force in each test, and the manufacturer design parameters ( $C = 60$  (kip sec/in) and  $n = 0.35$ ).

Test No.	Test name	Max measured force (kip)	Equivalent design force (kip)	ANN-identified force (kip)
1	UCB1_10_4	152.55	132.24	154.37
2	UCB1_10_5	154.26	134.17	148.76
3	UCB1_10_6	158.57	134.17	152.17
hline 4	UCB1_12_4	165.67	143.82	150.17
5	UCB1_12_5	163.18	144.86	150.23
6	UCB1_12_6	163.33	144.23	151.44
7	UCB1_12_7	163.38	144.85	156.59
8	UCB1_15_4	173.18	152.62	170.89
9	UCB1_15_5	171.89	152.57	157.26
10	UCB1_15_6	173.20	153.59	159.33
11	UCB1_15_7	171.81	153.87	168.02
12	UCB1_17_4	175.35	158.70	165.75
13	UCB1_17_5	175.66	159.36	164.39
14	UCB1_17_6	174.88	159.90	174.88
15	UCB1_17_7	176.22	159.91	167.83



## Chapter 8

# EXPERIMENTAL SETUP FOR THE 15 KIP VISCOUS DAMPER

### 8.1 Damper Specifications

A series of tests was performed at U.C. Berkeley using a 15 kip viscous damper as shown in Figure 8.1. The 15 kip damper has a linear viscous behavior ( $F(t) = C \text{sign}(\dot{x}(t))|\dot{x}(t)|^n$ , where  $n \approx 1$  and  $C \approx 0.70$  kip sec/in), and has been tested previously by Chang *et al.* (2002) within the context of a previous Caltrans project. The experimental setup of the 15 kip damper is shown in Figure 8.1. Contrary to the 250 kip damper, the force developed in the damper is measured through a stationary load cell that is connected between the damper and the reaction frame. The imposed displacement history is measured with a linear variable differential transducer (LVDT). The manufacturer design parameters are listed in Table 8.1.

Table 8.1: Manufacturer design parameters for the 250 kip viscous damper.

Damper Type	$C$ (kip sec/in)	$n$
15 Kip	0.7	1.0

### 8.2 Instrumentation

A total of twelve channels of raw data were collected measuring force, displacement, damper oil temperature, damper surface temperature, acceleration, and input displacement signal. The sensor configuration of the data acquisition system for the 15 kip damper is shown in Table 8.2. The data were sampled at 1000 Hz, and approximately two minutes of data were acquired for each test.



Figure 8.1: The 15 kip viscous damper testing setup at the University of California, Berkeley.

Table 8.2: Sensor configuration of data acquisition system for the 15 kip viscous damper.

Channel No	Name	Unit	Description
1	Time	sec	-
2	Load	kip	Measured force
3	Stroke	inch	Measured displacement
4	Oil temp 1	F	Internal oil temperature
5	Oil temp 2	F	Internal temperature at 90 degrees around cylinder
6	Ext temp 1	F	External temperature in-line with internal probes
7	Ext temp 2	F	External temperature in-line with internal probes
8	Ext temp 3	F	External temperature 2 in closer to center of damper
9	Ext temp 4	F	External temperature 2 in closer to center of damper
10	Accel. damper	G	Acceleration attached to the damper housing
11	Accel. actuator	G	Acceleration attached to the actuator
12	Command	inch	Input displacement signal

### 8.3 Test Specifications

A total of 24 tests were conducted by UCB personnel using the 15 kip viscous damper (Tables 8.3 and 8.4). Each test was displacement-controlled.

In the first round of tests, a total of eight tests were performed. A broadband signal truncated at the upper bound of 15 Hz was the damper specimen excitation input. A cosine taper was applied at the upper and lower bounds of the truncated signal. The taper was applied to the first and last 0.1 Hz range of the windowed signal. A two-minute time history signal was generated with this frequency content. The amplitude of the first round of tests was set to be 0.1 and 0.125 inches. Each amplitude level was tested four times. The duration of each test was approximately two minutes with 1000 Hz sampling rate.

A total of 16 tests were performed in the second round of tests. The second round of tests utilized a similar broadband excitation, but with two different lower cutoff frequencies: 5 Hz and 10 Hz. In the second round tests, the damper was excited with 0.175, 0.2, 0.3 and 0.4 inch amplitudes. Each amplitude level was tested four times, as in the first round of testing.

Table 8.3: First round test specifications.

Test No.	Name	Amplitude (in)	Cutoff Freq (Hz)
1	Qtr1_01	0.1	15
2	Qtr2_01	0.1	15
3	Qtr3_01	0.1	15
4	Qtr4_01	0.1	15
5	Qtr1_0125	0.125	15
6	Qtr2_0125	0.125	15
7	Qtr3_0125	0.125	15
8	Qtr4_0125	0.125	15

Table 8.4: Second round test specifications.

Test No.	Name	Amplitude (in)	Cutoff Freq (Hz)
1	usc_10175_q1	0.175	10
2	usc_10175_q2	0.175	10
3	usc_10175_q3	0.175	10
4	usc_10175_q4	0.175	10
5	usc_10200_q1	0.200	10
6	usc_10200_q2	0.200	10
7	usc_10200_q3	0.200	10
8	usc_10200_q4	0.200	10
9	usc_5300_q1	0.300	5
10	usc_5300_q2	0.300	5
11	usc_5300_q3	0.300	5
12	usc_5300_q4	0.300	5
13	usc_5400_q1	0.400	5
14	usc_5400_q2	0.400	5
15	usc_5400_q3	0.400	5
16	usc_5400_q4	0.400	5

## Chapter 9

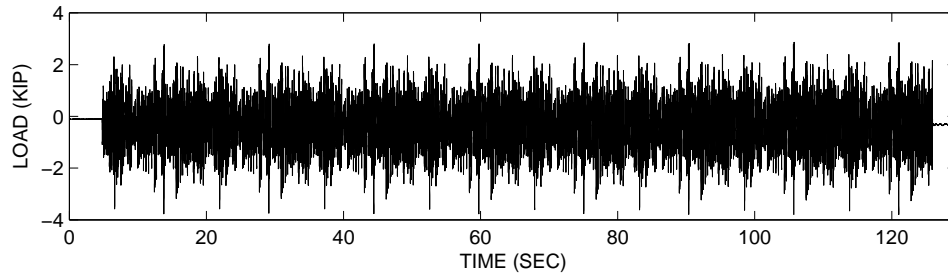
# PRELIMINARY DATA PROCESSING FOR THE 15 KIP VISCOUS DAMPER

### 9.1 Collection of Data Sets

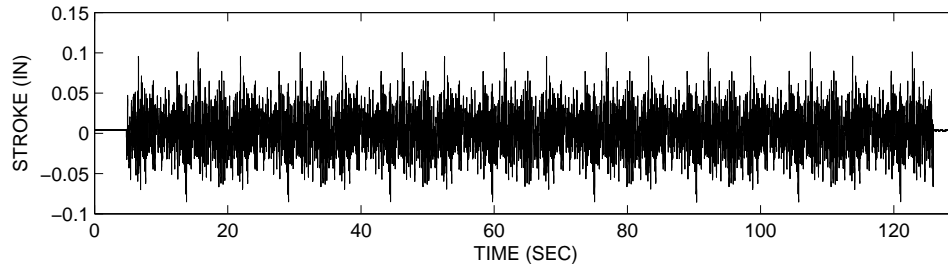
The time histories of dynamic response and temperature in the first and second round tests are shown in Figures 9.1 to 9.4. The complete data sets of the measured time histories are shown in Figures D.1 to D.16 in Appendix D.1 for the first round tests, and Figures E.1 to E.32 in Appendix E.1 for the second round. The first 20 rows of the measured data for usc\_5\_400\_q4 are shown in Sections D.1 and E.1, respectively. The ASCII data files for the entire data sets are provided in the accompanying CD under \data\UCB2\_2\raw\.

### 9.2 Sample Results of Preliminary Data Analysis

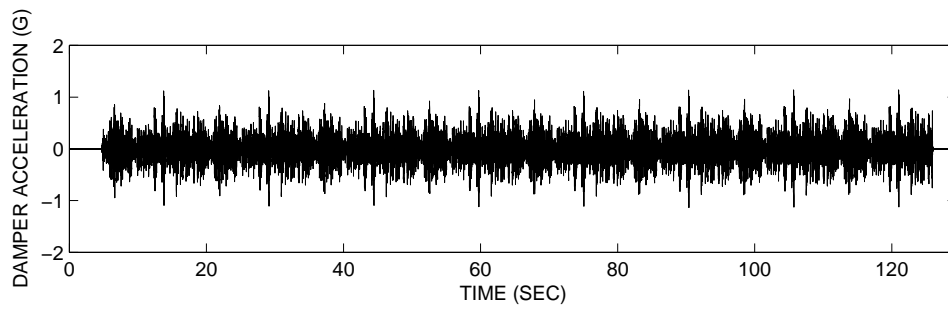
The identification procedures used in this study require displacement and velocity time histories for the RFM and displacement, velocity and acceleration time histories for the ANN. The time-history of the displacement and acceleration data were provided by UCB; to obtain velocity data, a software module was developed to integrate the acceleration data. The velocity data were then bandpass-filtered between 2 and 100 Hz. The validity of the integration results was confirmed by differentiating the measured actuator stroke. A second integration step was performed to validate the correlation between the measured and the computed displacement (i.e., double integrated acceleration data). Figure 9.5 shows the comparison between the measured displacement (solid line) and double integrated acceleration (dashed line) of the 15 kip damper.



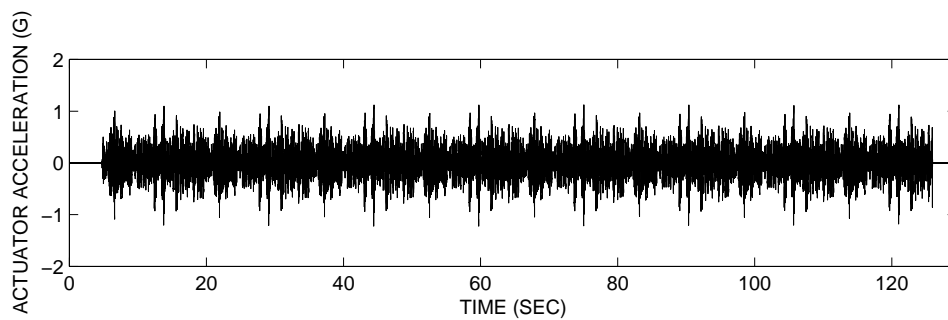
(a) Load (Force)



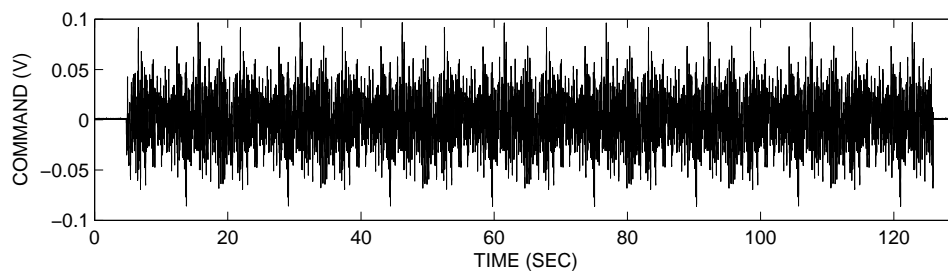
(b) Stroke (Displacement)



(c) Damper acceleration

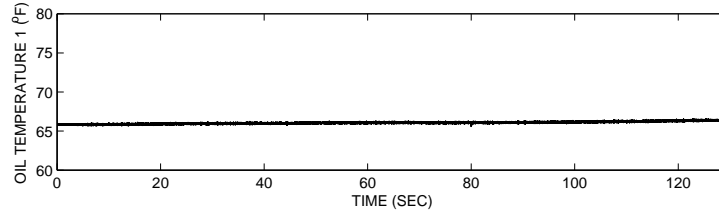


(d) Actuator acceleration

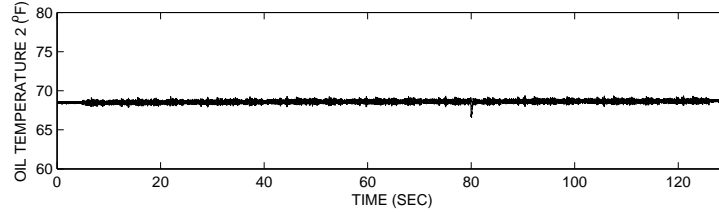


(e) Command Signal

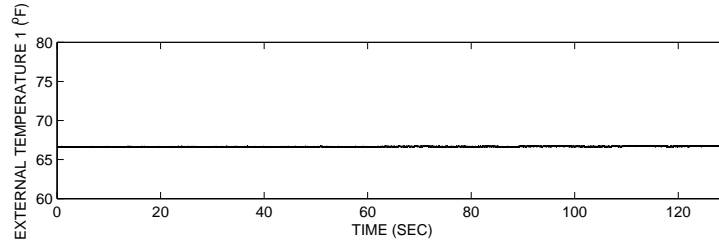
Figure 9.1: Measured data of the 15 kip damper in the first round experiments for the data set Qrt1.01.



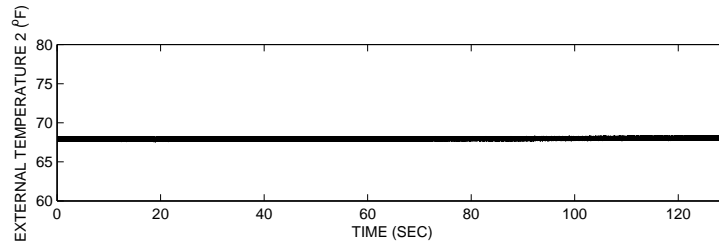
(a) Oil temperature 1



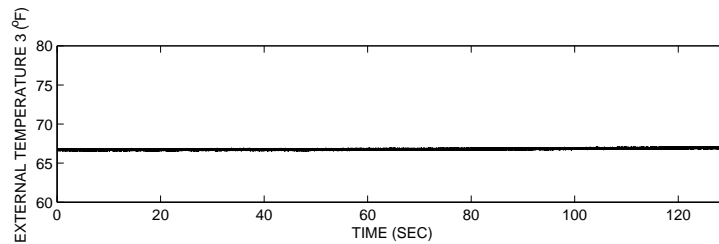
(b) Oil temperature 2



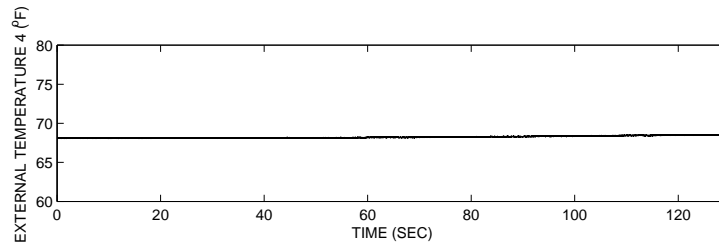
(c) Surface temperature 1



(d) Surface temperature 2

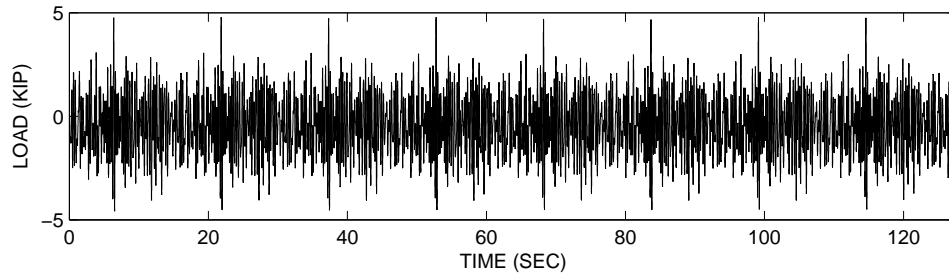


(e) Surface temperature 3

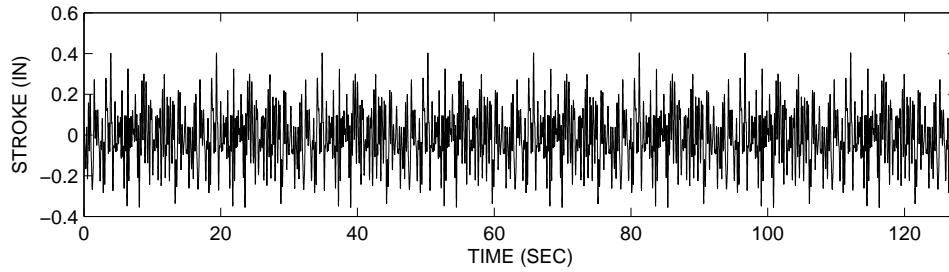


(f) Surface temperature 4

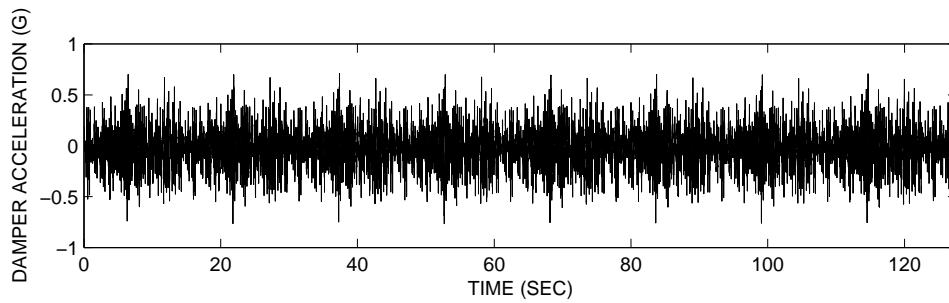
Figure 9.2: Measured oil and surface temperatures of the 15 kip damper in the first round experiments for the data set Qrt1.01.



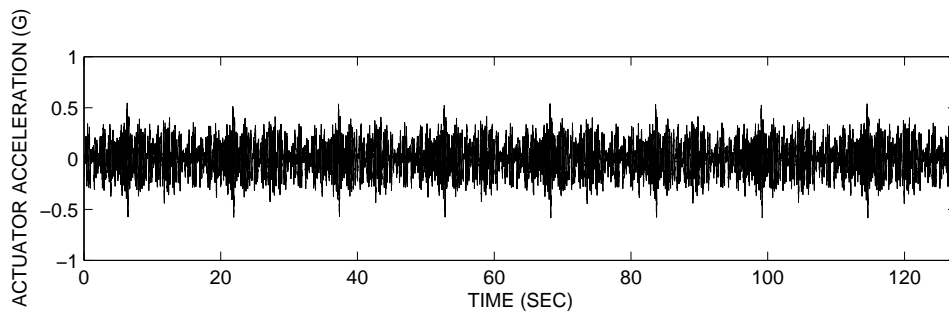
(a) Load (Force)



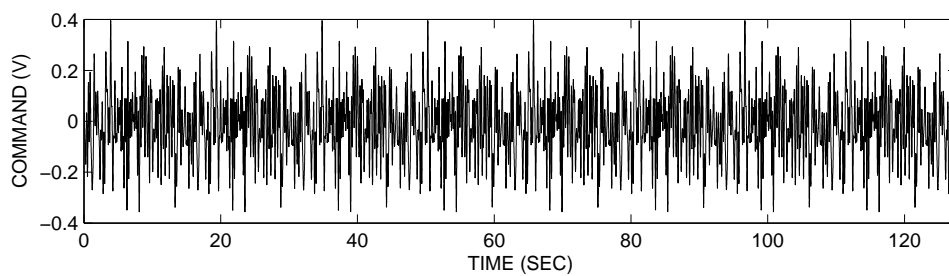
(b) Stroke (Displacement)



(c) Damper acceleration

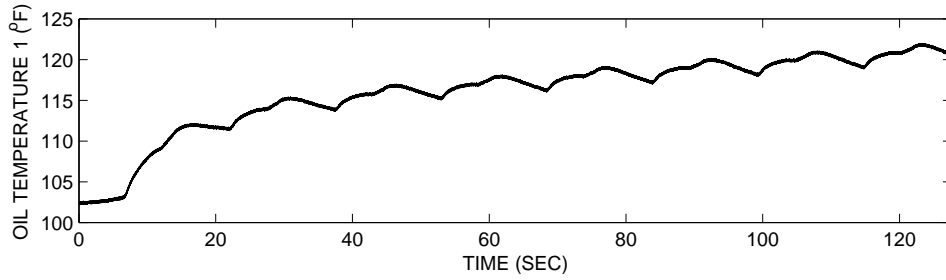


(d) Actuator acceleration

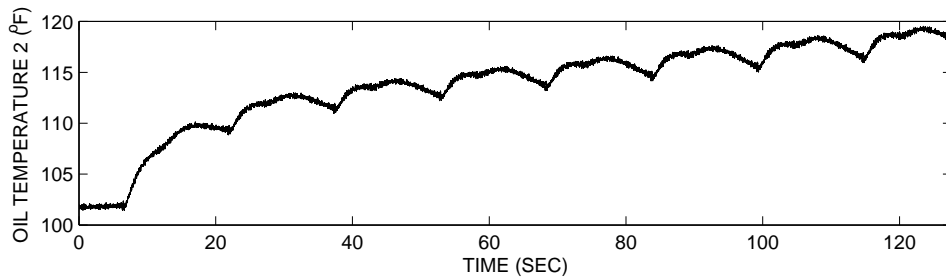


(e) Command Signal

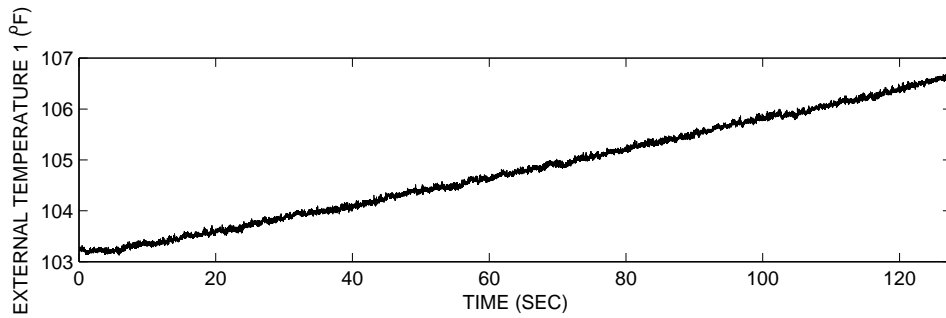
Figure 9.3: Measured data of the 15 kip damper in the second round experiments for the data set usc\_5\_400\_q4.



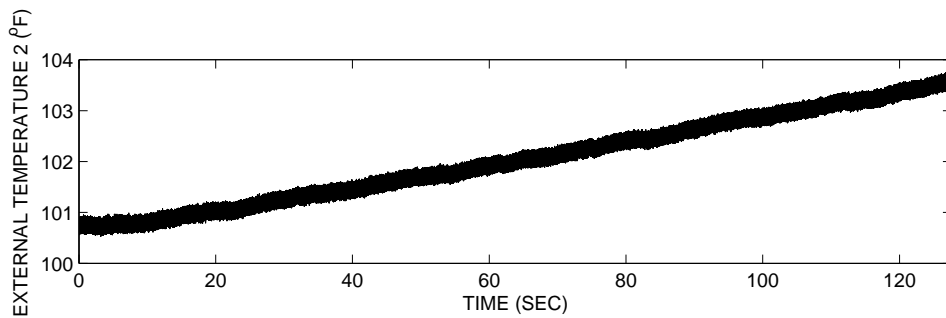
(a) Oil temperature 1



(b) Oil temperature 2



(c) Surface temperature 1



(d) Surface temperature 2

Figure 9.4: Measured oil and surface temperatures of the 15 kip damper in the second round experiments for the data set usc\_5\_400\_q4.

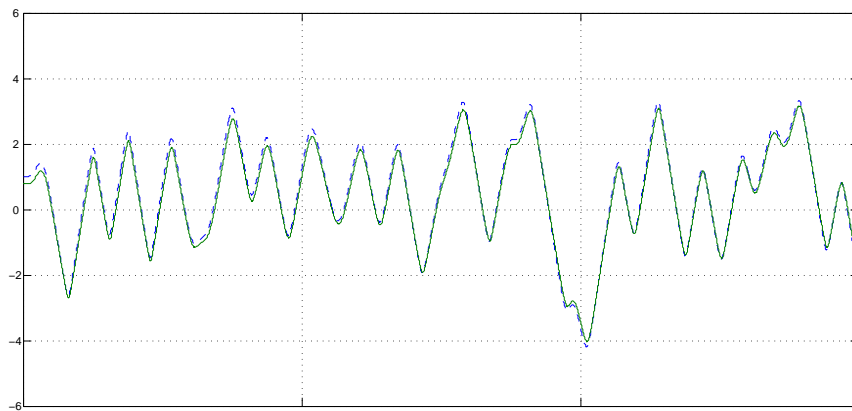


Figure 9.5: Sample result of the measured displacement (solid line) and the double-integrated displacement using the measured acceleration (dashed line) of the 15 kip damper.

## Chapter 10

# PARAMETRIC IDENTIFICATION OF THE 15 KIP VISCOUS DAMPER

The 15 kip damper was tested with broad-band random excitation signals, in two rounds. For the first round of testing, the excitation signal was filtered at the cut-off frequency of 15 Hz; for the second round of testing, the cut-off frequencies were 5 Hz and 10 Hz. One data set is selected from each round of testing to illustrate the on-line and the off-line parametric identification plots in this chapter. The rest of the parametric identification plots are provided in Appendix F.

### 10.1 First Round of Testing

The naming convention for the data sets from the first round of testing are shown in Table 10.1. The data were recorded in four individual files for each test.

Table 10.1: Test matrix and naming convention of the first round of testing for the 15 kip damper.

Data set Name	Test Amplitude (in)	Cutoff Frequency (Hz)
Qtr1_01	0.1	15
Qtr2_01	0.1	15
Qtr3_01	0.1	15
Qtr4_01	0.1	15
Qtr1_0125	0.125	15
Qtr2_0125	0.125	15
Qtr3_0125	0.125	15
Qtr4_0125	0.125	15

Figure 10.1 shows sample measured data of the 15 kip damper for data set Qtr4.0125. Fig-

ures 10.1 (a), (b), (c), and (d) are the system responses, displacement, velocity, acceleration, and measured force, respectively. Fig. 10.1 (e) is the displacement-force phase-plot, and Fig. 10.1 (f) is the velocity-force phase-plot.

## 10.2 Parametric Identification of the First Round of Testing

The on-line and off-line parametric identification methods under discussion were applied to all data sets, and the plots of the identification results for one data set are presented in this section. The parametric identification results for all data sets are provided in Appendix F.1. The summary of the on-line identification results is shown in Table 10.2, and the summary of the off-line identification results is shown in Table 10.3.

### 10.2.1 On-line Parametric Identification of the First Round of Testing

Data set Qtr4\_0125 is selected to demonstrate the on-line parametric identification results of the first round of testing. Figure 10.2 shows the on-line identification results for the data set Qtr4\_0125. Figs. 10.2 (a) and 10.2 (b) show the filtered time-history of the unknown parameters of the design model (Eqn. 2.6), Fig. 10.2 (c) shows the time-history comparison of the measured force (solid line) and the predicted force (dash-dot line), Fig. 10.2 (d) is the displacement-force phase-plane comparison of the measured force (solid line) and the predicted force (dash-dot line), for one cycle, and Fig. 10.2 (e) is the velocity-force phase-plane comparison of the measured force (solid line) and the predicted force (dash-dot line), for one cycle.

The on-line parametric identification results of the 15 kip damper for the first round of testing are summarized in Table 10.2. Column 1 is the data set name, column 2 is the manufacturer value for the damping coefficient  $C$ , column 3 is the average value of the identified damping coefficient  $\hat{C}$ , column 3 is the manufacturer specification value for the exponent  $n$ , column 4 is the average value of the identified exponent  $\hat{n}$  (Eqn. 2.6), column 5 is the selected value of the forgetting factor ( $\beta$ ) in the on-line identification algorithm (Eqn. 2.5), and column 6 is the normalized mean-square-error percentage of the difference between the predicted force and the measured force. The plots of the on-line identification for the first round of testing are provided in Appendix F.1.1.

### 10.2.2 Off-line Parametric Identification of the First Round of Testing

Data set Qtr4\_0125 is selected to demonstrate the results of the off-line parametric identification for the first round of testing. Fig. 10.3 (a) shows the time-history comparison of the measured force (solid line) and the predicted force (dash-dot line), Fig. 10.3 (b) shows the displacement-force

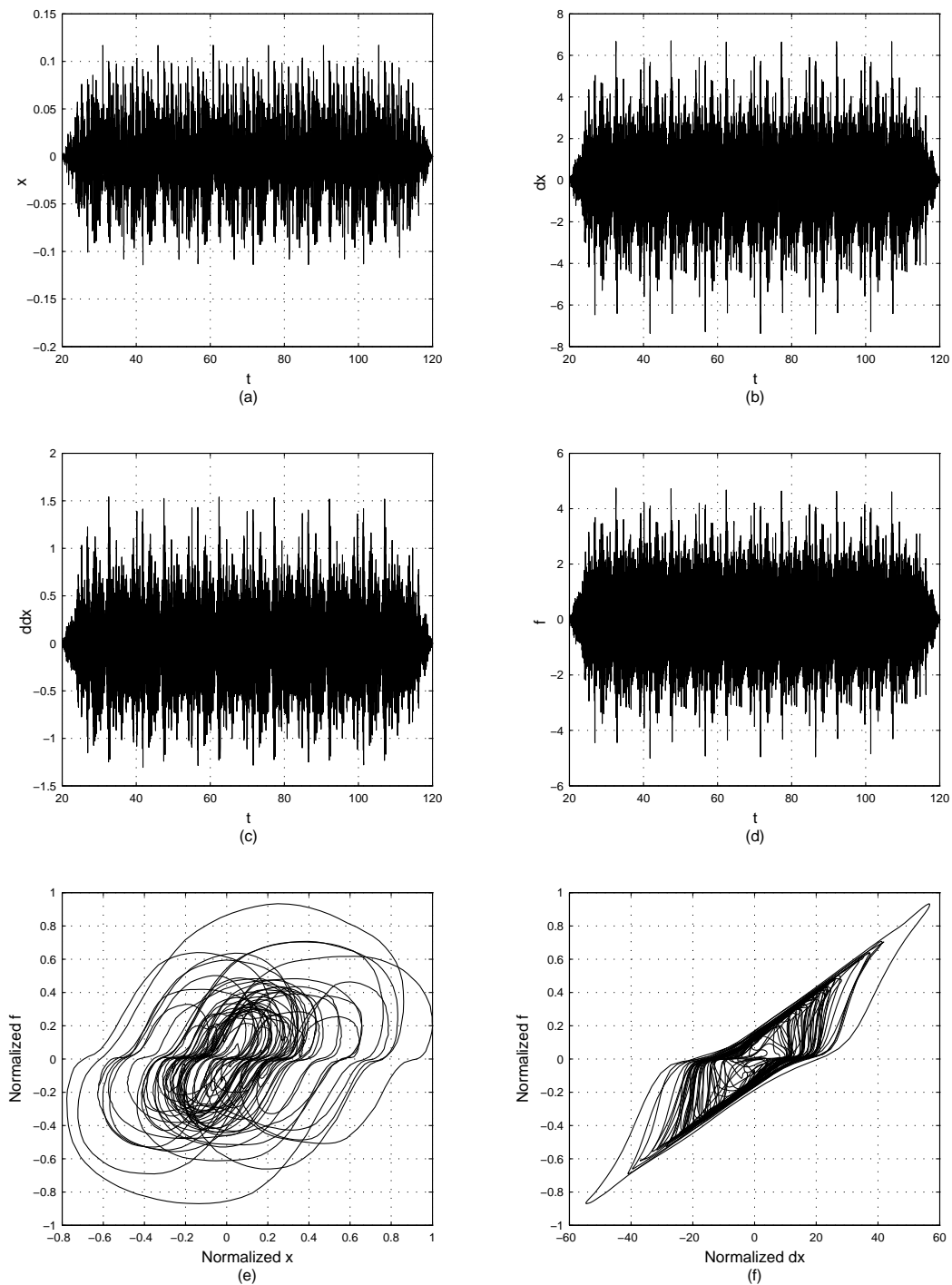


Figure 10.1: Sample measured data of the 15 kip damper for data set Qtr4\_0125. Part(a), (b), (c), and (d) are the system responses; displacement, velocity, acceleration, and measured force, respectively. Part (e) is the displacement-force phase-plot, and part (f) is the velocity-force phase-plot.

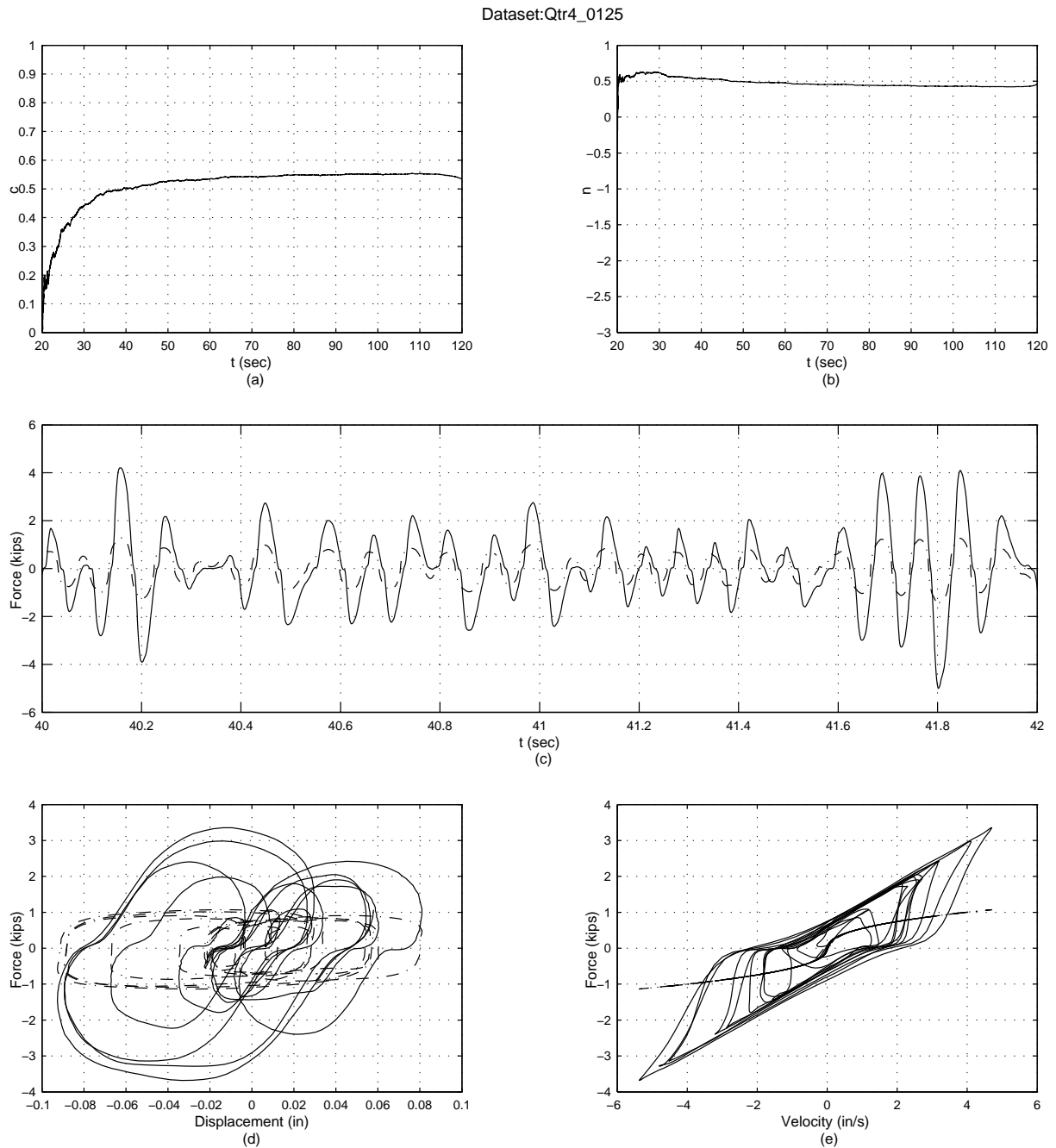


Figure 10.2: On-line parametric identification results of the 15 kip damper for data set Qtr4\_0125. Part (a) and (b) show the filtered time-history of the unknown parameters, part (c) shows the time-history comparison of the measured force (solid line) and the predicted force (dash-dot line), part (d) is the displacement-force phase-plane comparison of the measured force (solid line) and the predicted force (dash-dot line), for one cycle, and part (e) is the velocity-force phase-plane comparison of the measured force (solid line) and the predicted force (dash-dot line), for one cycle.

Table 10.2: Summary of the on-line parametric identification results for the 15 kip damper of the data sets in the first round of testing. Column 1 is the data set name, column 2 is the manufacturer value for the damping coefficient  $C$ , column 3 is the average value of the identified damping coefficient  $\hat{C}$ , column 4 is the manufacturer specification value for the exponent  $n$ , column 5 is the average value of the identified exponent  $\hat{n}$  (Eqn. 2.6), column 6 is the selected value of the forgetting factor ( $\beta$ ) in the on-line identification algorithm (Eqn. 2.5), and column 7 is the normalized mean-square-error percentage of the difference between the predicted force and the measured force.

Data set Name	Damping Coeff. $C$ (kip sec/in)		Exponent $n$		$\beta$ forgetting factor	% MSE error
	Damper Spec.	Identified	Damper Spec.	Identified		
Qtr4.01	0.70	0.50	1.00	0.26	0.8	6.1
Qtr4.0125	0.70	0.59	1.00	0.34	0.8	6.4

phase-plane comparison of the measured force (solid line) and the predicted force (dash-dot line), for one cycle, and Fig. 10.3 (c) shows the velocity-force phase-plane comparison of the measured force (solid line) and the predicted force (dash-dot line), for one cycle.

The off-line parametric identification results of the 15 kip damper for the first round of testing are summarized in Table 10.3, where column 1 is the data set name, columns 2 to 7 give the optimum values of the initially unknown parameters for the optimization model (Eqn. 2.10), and the last column is the normalized mean-square-error value of the difference between the predicted force and the measured force. The plots of the off-line parametric identification results for the 15 kip damper of the first round of testing are provided in Appendix F.1.2.

Table 10.3: Summary of the off-line parametric identification results for the 15 kip damper of the data sets in the first round of testing. Column 1 is the data set name, columns 2 to 7 give the optimum values of the initially unknown parameters (Eqn. 2.11), column 8 is the normalized mean-square-error (Eqn. 2.9).

Data set	$c$ (kip sec/in)	$k$ (kip/in)	$n$	$\theta_1$	$\theta_2$	$\theta_3$	% MSE
Qtr4_01	0.39	2.49	1.92	32.09	-216.10	162.00	4.72
Qtr4_0125	0.43	2.75	1.89	32.59	-197.10	160.00	4.62

### 10.3 Second Round of Testing

The naming convention for the data sets from the second round of testing are shown in Table 10.4. The data were recorded in four individual files for each test.

Figure 10.4 shows sample measured data of the 15 kip damper for the data set usc\_5400\_q4. Figures 10.4 (a), (b), (c), and (d) are the system response, displacement, velocity, acceleration, and

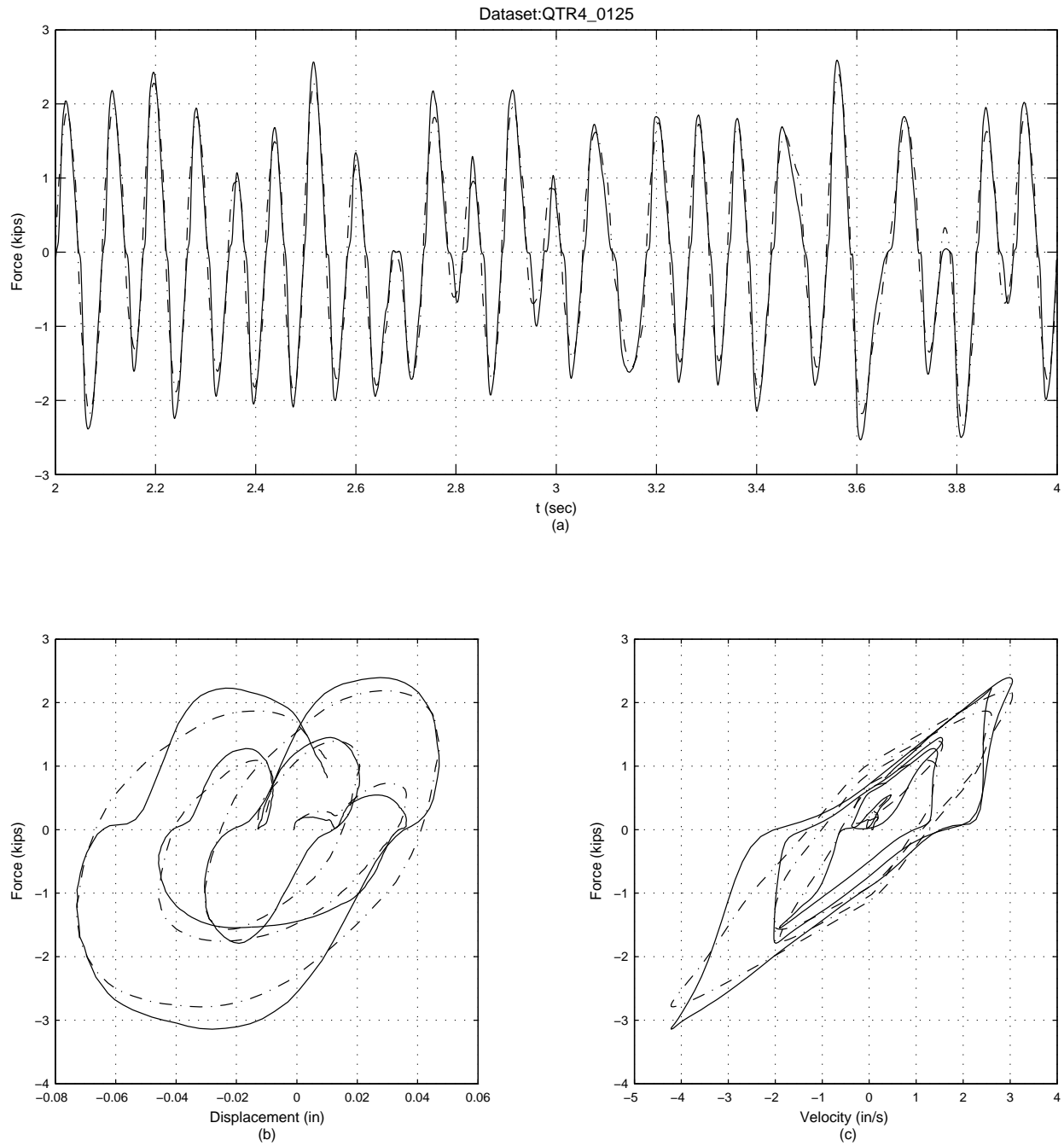


Figure 10.3: Off-line parametric identification results of the 15 kip damper for data set Qtr4\_0125. Part (a) shows the time-history comparison of the measured force (solid line) and the predicted force (dash-dot line), part (b) shows the displacement-force phase-plane comparison of the measured force (solid line) and the predicted force (dash-dot line), for one cycle, and part (c) shows the velocity-force phase-plane comparison of the measured force (solid line) and the predicted force (dash-dot line), for one cycle.

Table 10.4: Test matrix and naming convention of the 15 kip damper for the second round of testing.

Data set Name	Test Amplitude (in)	Cutoff Frequency (Hz)
usc_10175_q1	0.175	10
usc_10175_q2	0.175	10
usc_10175_q3	0.175	10
usc_10175_q4	0.175	10
usc_10200_q1	0.200	10
usc_10200_q2	0.200	10
usc_10200_q3	0.200	10
usc_10200_q4	0.200	10
usc_5300_q1	0.300	5
usc_5300_q2	0.300	5
usc_5300_q3	0.300	5
usc_5300_q4	0.300	5
usc_5400_q1	0.400	5
usc_5400_q2	0.400	5
usc_5400_q3	0.400	5
usc_5400_q4	0.400	5

measured force, respectively. Fig. 10.4 (e) is the displacement-force phase plot, and Fig. 10.4 (f) is the velocity-force phase plot.

## 10.4 Parametric Identification of the Second Round of Testing

The on-line and off-line parametric identification methods under discussion were applied to all data sets, and the plots of the identification results for one data set are presented in this section. The parametric identification results for all data sets are provided in Appendix F.2. The summary of the on-line identification results is shown in Table 10.5, and the summary of the off-line identification results is shown in Table 10.6.

### 10.4.1 On-line Parametric Identification of the Second Round of Testing

Data set usc\_5400\_q4 is selected to demonstrate the on-line parametric identification results for the second round of testing. Figure 10.5 shows the on-line identification results for the data set usc\_5400\_q4. Figs. 10.5 (a) and 10.5 (b) show the filtered time-history of the unknown parameters of the design model (Eqn. 2.6), Fig. 10.5 (c) shows the time-history comparison of the measured force (solid line) and the predicted force (dash-dot line), Fig. 10.5 (d) is the displacement-force phase-plane comparison of the measured force (solid line) and the predicted force (dash-dot line),

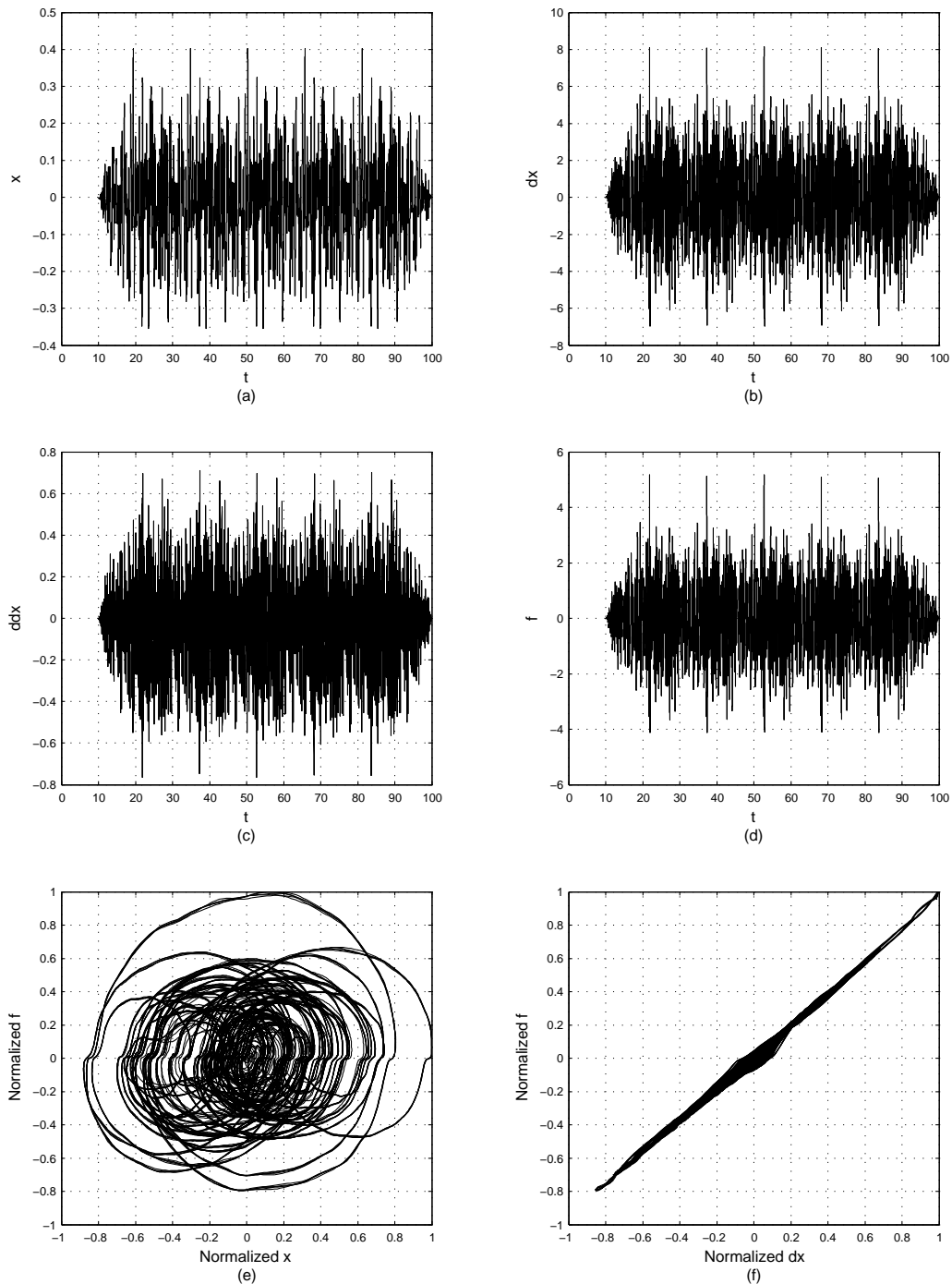


Figure 10.4: Sample measured data of the 15 kip damper for data set usc\_5400-q4. Part (a), (b), (c), and (d) are the system responses; displacement, velocity, acceleration, and measured force, respectively. Part (e) is the displacement-force phase-plot, and part (f) is the velocity-force phase-plot.

for one cycle, and Fig. 10.5 (e) is the velocity-force phase-plane comparison of the measured force (solid line) and the predicted force (dash-dot line), for one cycle.

The on-line parametric identification results of the 15 kip damper for the second round of testing are summarized in Table 10.5. Column 1 is the data set name, column 2 is the manufacturer value for the damping coefficient  $C$ , column 3 is the average value of the identified damping coefficient  $\hat{C}$ , column 3 is the manufacturer specification value for the exponent  $n$ , column 4 is the average value of the identified exponent  $\hat{n}$  (Eqn. 2.6), column 5 is the selected value of the forgetting factor ( $\beta$ ) in the on-line identification algorithm (Eqn. 2.5), and column 6 is the normalized mean-square-error percentage of the difference between the predicted force and the measured force. The plots of the on-line identification results for the second round of testing are provided in Appendix F.2.1.

Table 10.5: Summary of the on-line parametric identification results for the 15 kip damper of the data sets in the first second of testing. Column 1 is the data set name, column 2 is the manufacturer value for the damping coefficient  $C$ , column 3 is the average value of the identified damping coefficient  $\hat{C}$ , column 3 is the manufacturer specification value for the exponent  $n$ , column 4 is the average value of the identified exponent  $\hat{n}$  (Eqn. 2.6), column 5 is the selected value of the forgetting factor ( $\beta$ ) in the on-line identification algorithm (Eqn. 2.5), and column 6 is the normalized mean-square-error percentage of the difference between the predicted force and the measured force.

Data set Name	Damping Coeff. $C$ (kip sec/in)		Exponent $n$		$\beta$ forgetting factor	% MSE error
	Damper Spec.	Identified	Damper Spec.	Identified		
usc_10175_q4	0.70	0.50	1.00	0.83	0.8	6.7
usc_10200_q4	0.70	0.80	1.00	0.69	0.8	6.4
usc_5300_q4	0.70	0.80	1.00	0.69	0.8	4.4
usc_5400_q4	0.70	0.50	1.00	0.89	0.8	6.0

#### 10.4.2 Off-line Parametric Identification of the Second Round of Testing

Data set usc\_5400\_q4 is selected to demonstrate the results of the off-line parametric identification for the second round of testing. Fig. 10.6 (a) shows the time-history comparison of the measured force (solid line) and the predicted force (dash-dot line), Fig. 10.6 (b) shows the displacement-force phase-plane comparison of the measured force (solid line) and the predicted force (dash-dot line), for one cycle, and Fig. 10.6 (c) shows the velocity-force phase-plane comparison of the measured force (solid line) and predicted force (dash-dot line), for one cycle.

The off-line parametric identification results of the 15 kip damper for the second round of testing are summarized in Table 10.6, where column 1 is the data set name, columns 2 to 6 give the optimum values of the initially unknown parameters for the optimization model (Eqn. 2.10), and the last column is the normalized mean-square-error value of the difference between the predicted

Dataset:usc\_5400\_q4

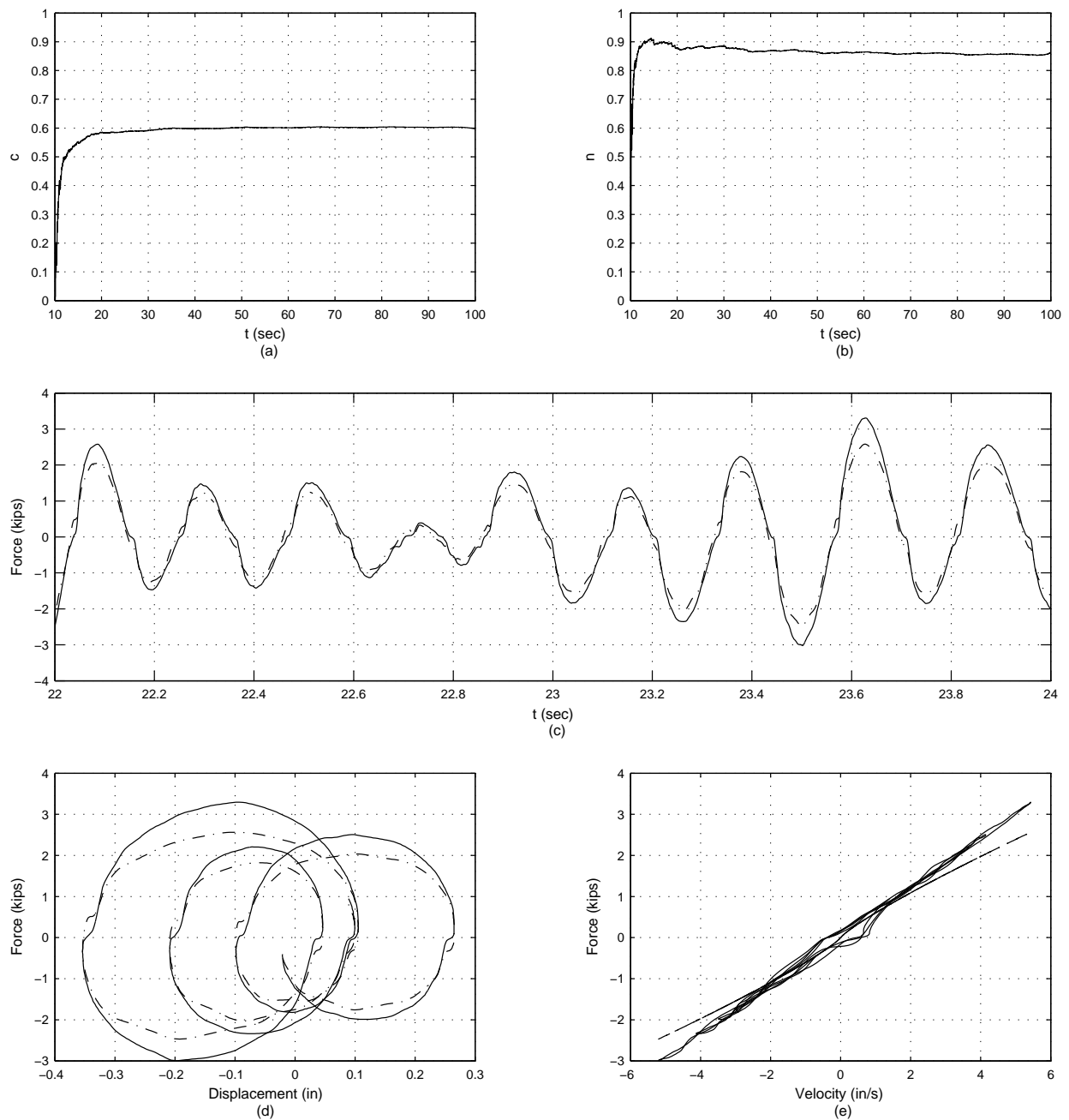


Figure 10.5: On-line parametric identification results of the 15 kip damper for data set usc\_5400\_q4. Part (a) and (b) show the filtered time-history of the unknown parameters, part (c) shows the time-history comparison of the measured force (solid line) and the predicted force (dash-dot line), part (d) is the displacement-force phase-plane comparison of the measured force (solid line) and the predicted force (dash-dot line), for one cycle, and part (e) is the velocity-force phase-plane comparison of the measured force (solid line) and the predicted force (dash-dot line), for one cycle.

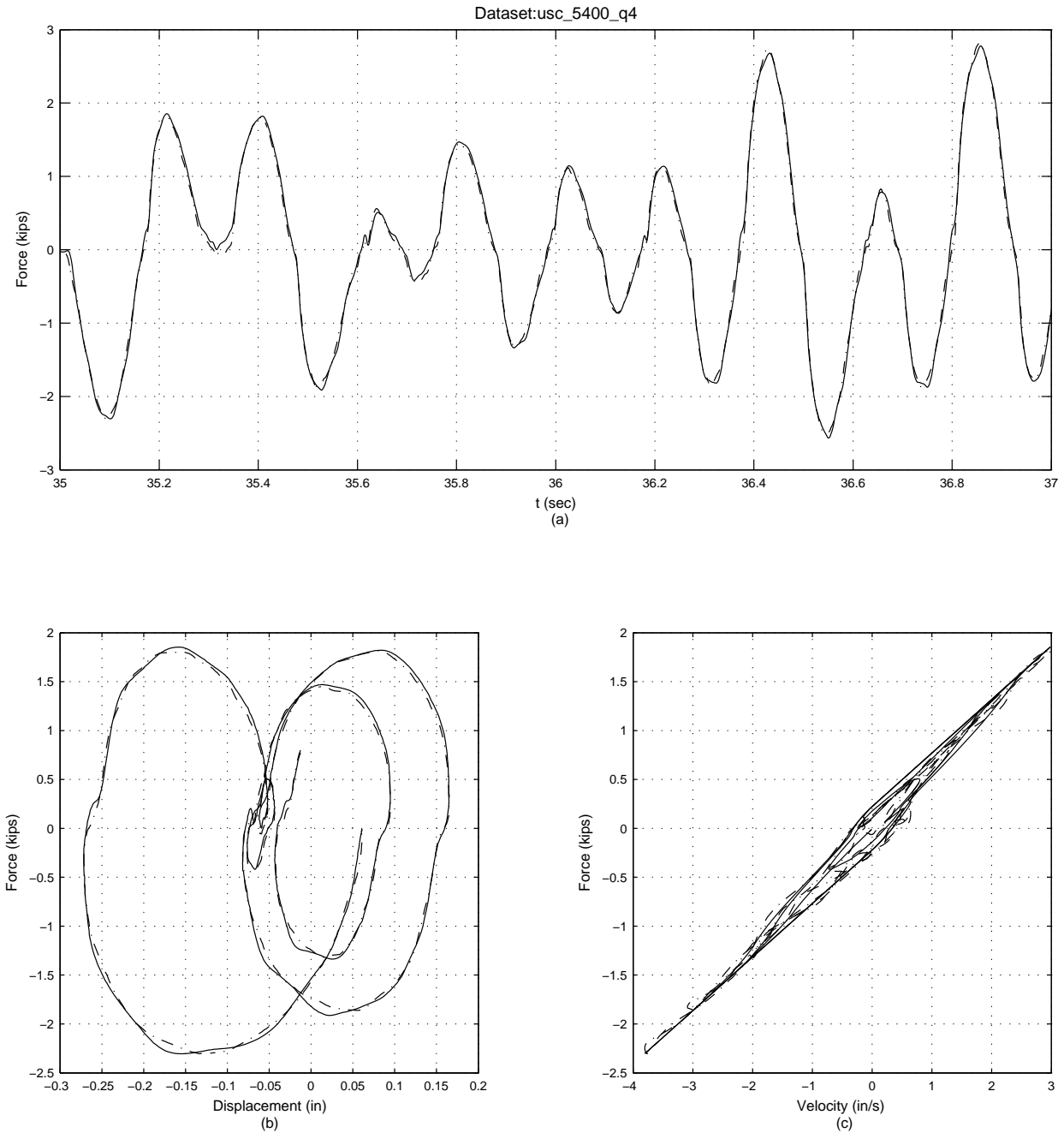


Figure 10.6: Off-line parametric identification results of the 15 kip damper for data set usc\_5400\_q4. Part (a) shows the time-history comparison of the measured force (solid line) and the predicted force (dash-dot line), part (b) shows the displacement-force phase-plane comparison of the measured force (solid line) and the predicted force (dash-dot line), for one cycle, and part (c) shows the velocity-force phase-plane comparison of the measured force (solid line) and the predicted force (dash-dot line), for one cycle.

force and the measured force. The plots of the off-line parametric identification results for the second round of testing of the 15 kip damper are provided in Appendix F.2.2.

Table 10.6: Summary of the off-line parametric identification results of the 15 kip damper for the data sets in the second round of testing. Column 1 is the data set name, columns 2 to 7 are the unknown parameters (Eqn. 2.11), column 8 is the normalized mean-square-error (Eqn. 2.9).

Data set	$c$ (kip sec/in)	$k$ (kip/in)	$n$	$\theta_1$	$\theta_2$	$\theta_3$	% MSE
usc_10175_q4	0.56	0.09	1.90	23.74	-411.40	153.80	3.26
usc_10200_q4	0.52	0.00	1.93	13.24	-362.80	162.00	3.28
usc_5300_q4	0.58	0.00	1.92	12.99	-402.80	164.10	2.47
usc_5400_q4	0.55	0.00	1.93	12.20	-384.60	163.10	2.38

## 10.5 Summary of the Parametric Identification

The maximum measured force, absolute equivalent design force, and the identified force from the parametric identification of the 15 kip viscous damper are summarized and compared in Tables 10.7 and 10.8. In Tables 10.7 and 10.8, column 1 is the maximum measured force of each data set, column 2 is the absolute equivalent design force, which is calculated based on the design formula (Eqn. 2.6), the corresponding measured velocity for the maximum force in each test, and the manufacturer design parameters ( $C = 60$  (kip sec/in) and  $n = 0.35$ ), and column 4 is the identified force from the parametric identification methods of the 15 kip viscous damper.

Table 10.7: Comparison of the maximum measured force, absolute equivalent design force, and identified force from the on-line parametric identification method of the 15 kip viscous damper. The equivalent design force is calculated based on the design formula (Eqn. 2.6), the corresponding measured velocity for the maximum force in each test, and the manufacturer design parameters ( $C = 0.70$  kip sec/in and  $n = 1.00$ ).

Test Name	Maximum Measured Force (kip)	Absolute Equivalent Design Force (kip)	On-line Identified Force (kip)
First round of testing			
Qtr4.01	3.79	4.05	3.28
Qtr4.0125	5.00	5.12	4.35
Second round of testing			
usc_10175_q4	4.32	4.99	4.44
usc_10200_q4	4.72	5.63	4.90
usc_5300_q4	3.96	4.32	3.96
usc_5400_q4	5.17	5.66	5.16

Table 10.8: Comparison of the maximum measured force, absolute equivalent design force, and identified force from the off-line parametric identification method of the 15 kip viscous damper. The equivalent design force is calculated based on the design formula (Eqn. 2.6), the corresponding measured velocity for the maximum force in each test, and the manufacturer design parameters ( $C = 0.70$  kip sec/in and  $n = 1.00$ ).

Test Name	Maximum Measured Force (kip)	Absolute Equivalent Design Force (kip)	Off-line Identified Force (kip)
First round of testing			
Qtr4.01	2.49	2.40	2.08
Qtr4.0125	3.86	3.68	3.20
Second round of testing			
usc_10175_q4	3.04	3.32	2.93
usc_10200_q4	4.50	4.88	3.93
usc_5300_q4	3.96	4.35	3.82
usc_5400_q4	5.12	5.63	4.63



## Chapter 11

# NONPARAMETRIC RESTORING FORCE METHOD IDENTIFICATION FOR THE 15 KIP VISCOUS DAMPER

### 11.1 Problem Formulation of the Restoring Force Method

The restoring force method (RFM) identification was performed using the experimental data of the 15 kip damper obtained in Chapter 9. The RFM is a nonparametric identification method, and a detailed description of the method was given in Section 2.3.1. Two objectives were pursued from the RFM identification: (1) to demonstrate that the RFM can be used to identify a 15 kip viscous damper subjected to a broadband excitation, and (2) to demonstrate that the Chebyshev and power series coefficients of the RFM can reflect the change of stroke amplitude, and the cutoff frequency of the broadband excitation.

### 11.2 Application and Validation of the Restoring Force Method to Collected Data Sets

The first and second round data sets of the 15 kip damper were used in the RFM identification. To find the optimal order of Chebyshev approximation, the entire two-minute data set was processed with the identification algorithm. Parametric studies were conducted to determine the optimal-order polynomial used in the identification scheme, as well as whether a 1-D or 2-D surface fit of the data set was appropriate. Selected results are presented in Table 11.1. The optimal Chebyshev approximation was found at the seventh order without iteration.

Table 11.1: Determining the optimal order of Chebyshev approximation of the 15 kip damper response for the data set Qtr1.1.

No.	Polynomial order	No. points	Iteration applied	Normalized MSE (%)
1	3	10,000	No	13.25
2	3	20,000	No	12.32
3	7	10,000	No	11.70
4	15	10,000	No	12.39
5	15	10,000	Yes	12.32
6	7	10,000	Yes	13.69

Table 11.2: Identified RFM coefficients for the 15 kip damper subjected to broadband excitation for the first round tests (Qtr1.01).

(a) Normalized Chebyshev coefficients

$x/\dot{x}$	0	1	2	3
0	-0.80	3.11	-0.16	0.10
1	0.06	-0.07	0.00	-0.01
2	0.77	0.04	0.05	-0.04
3	-0.01	0.01	0.02	0.02

(b) Normalized power series coefficients

$x/\dot{x}$	0	1	2	3
0	-1.15	0.54	-0.01	0.01
1	-1.83	0.05	-0.11	-0.03
2	188.36	10.67	0.34	-0.55
3	-163.37	-48.52	14.26	4.53

Using the optimal order of the Chebyshev approximation, the 15 kip viscous damper was identified. Figure 11.1 depicts the measured and identified results from the first 10,000 points of the Qtr1.01 data set used in the identification (the first data subset began at point 5,001 and concluded at point 15,000). Figure 11.1 displays the data in time history format and illustrates the excellent comparison between the measured and identified restoring force for a seventh order Chebyshev polynomial fit.

The identified Chebyshev and power series coefficients from the Qtr1.01 identification are tabulated in Table 11.2. Similar identification procedures were applied to the data set of usc.10200\_q1. The identified coefficients are tabulated in Table 11.3.

The maximum measured, absolute equivalent design and maximum RFM-identified forces are compared in Table 11.4 for the test duration 50 - 70 seconds. The absolute equivalent design force is calculated based on the design formula (Eqn. 2.6), the corresponding measured velocity for the

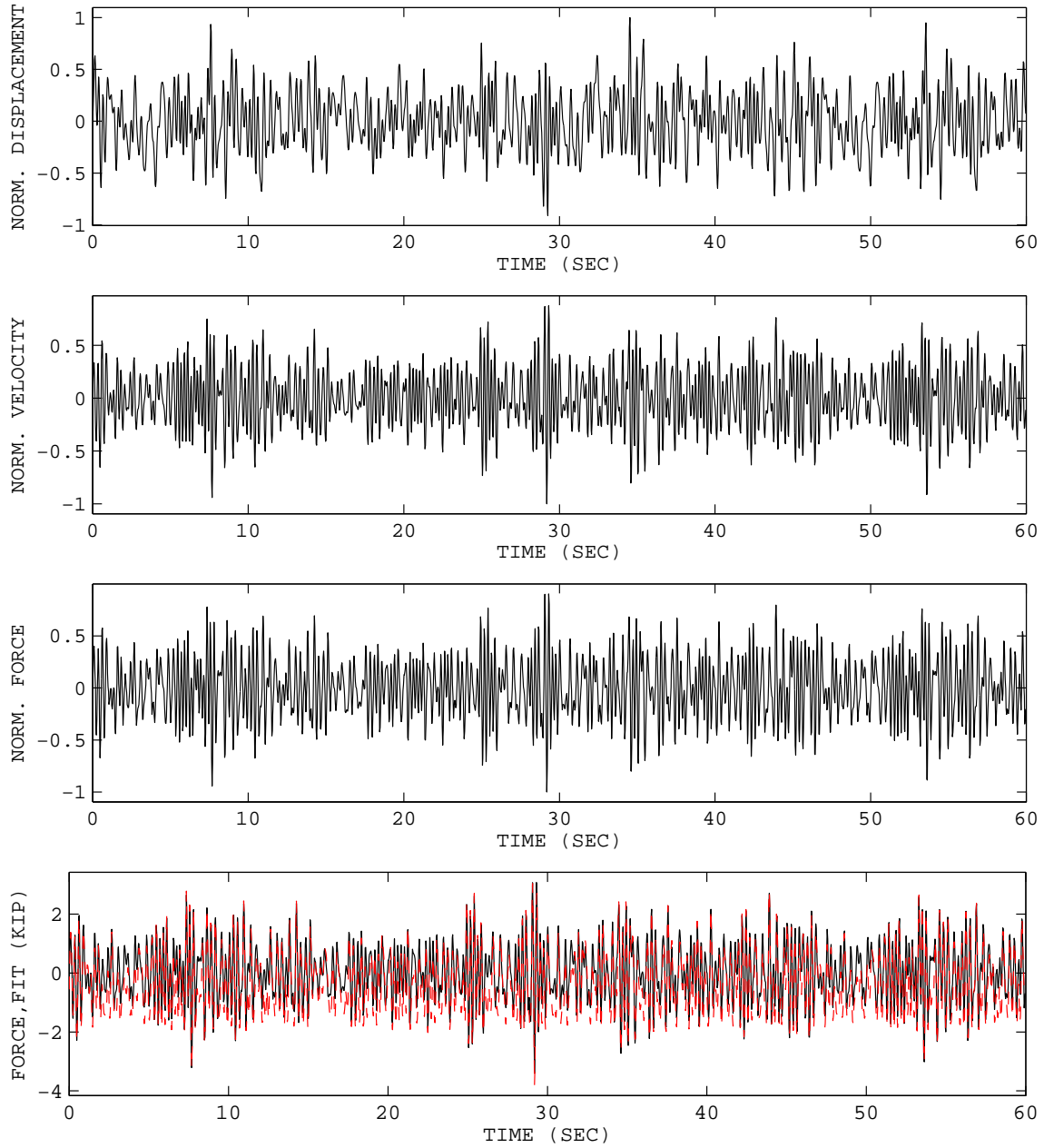


Figure 11.1: Comparison of the measured and identified damper response to broadband excitation in time history using RFM for the data set Qtr1.01. The solid line is the measured force, and the dashed line is the identified force.

Table 11.3: Identified RFM coefficients for the 15 kip damper subjected to broadband excitation for the second round tests (usc\_10200.q1).

(a) Normalized Chebyshev coefficients

$x/\dot{x}$	0	1	2	3
0	-0.66	-4.01	-0.12	-0.02
1	0.00	0.03	0.00	0.02
2	0.36	-0.04	0.16	0.04
3	0.00	-0.03	-0.05	0.02

(b) Normalized power series coefficients

$x/\dot{x}$	0	1	2	3
0	-0.62	-0.62	-0.02	0.00
1	-1.07	0.06	0.01	0.05
2	12.68	-2.09	0.69	0.15
3	39.29	-5.50	-1.47	-1.41

maximum force in each test, and the manufacturer design parameters ( $C = 0.7$  kip sec/in and  $n = 1.0$ ).

### 11.3 Statistical Study Using the Restoring Force Method

Once it was demonstrated that the RFM can be used to identify the 15 kip damper, a study was performed to derive the Chebyshev coefficients statistically from multiple measurements of the damper response. To explain the concept of the study, we will introduce the dynamic model in Equation 2.2 again as

$$f(t) = m\ddot{x} + c\dot{x} + kx + dx^3 \quad (11.1)$$

where  $m$ ,  $c$ , and  $k$  are the mass, damping, and stiffness values of system, and  $x$ ,  $\dot{x}$ , and  $\ddot{x}$  are the system's response, displacement, velocity, and acceleration, respectively. Equation 11.1 can be rewritten as

$$\underset{z}{\underline{f(t)}} = \underset{\theta^{*T}}{\underline{\begin{bmatrix} m \\ c \\ k \\ d \end{bmatrix}}}^T \times \underset{\phi}{\underline{\begin{bmatrix} \ddot{x} \\ \dot{x} \\ x \\ x^3 \end{bmatrix}}} \quad (11.2)$$

Table 11.4: Comparison of the maximum measured force, absolute equivalent design force, and maximum RFM-identified force of the 15 kip viscous damper for the test duration of 50 - 70 seconds. The absolute equivalent design force is calculated based on the design formula (Eqn. 2.6), the corresponding measured velocity for the maximum force in each test, and the manufacturer design parameters ( $C = 0.7$  kip sec/in and  $n = 1.0$ ).

Test No.	Test name	Max measured force (kip)	Absolute equivalent design force (kip)	RFM-identified force (kip)
1	Qtr1_01	3.08	1.20	2.62
2	Qtr2_01	3.68	1.24	3.97
3	Qtr3_01	3.70	1.27	3.98
4	Qtr4_01	3.57	1.24	3.68
5	Qtr1_0125	4.08	1.30	3.97
6	Qtr2_0125	4.44	1.35	4.73
7	Qtr3_0125	5.35	1.39	5.40
8	Qtr4_0125	4.45	1.33	4.68

where the  $\theta^*$  is the unknown parameter vector,  $\phi$  is the signal vector (regressor vector), and  $z$  is the measurement vector (Mendel, 1995). In the measurement of damper response, the measurement vector  $z$  and the signal parameter  $\phi$  are random, the parameter vector  $\theta^*$  determined with RFM is also random. Therefore, the goal of this statistical study was to investigate how to derive deterministic parameter values from the random parameter values.

First, statistical data were derived from each data set. Subsets of 2000 data points were processed starting at the point 10001. A total of 108 identifications were derived by defining the data subsets sequentially with a 50% overlapping (i.e., 1000 points) of the previous data subset; i.e., 10001 to 12000, and then 11001 to 13000, and so forth. One of the test data sets is shown in Figure 11.2, and an example of the identification results is shown in Figures 11.3 and 11.4.

Once 108 identifications were completed, the Chebyshev coefficients determined from the identifications were plotted in a histogram as shown in Figure 11.5. A total of 864 identifications were performed over eight sets of test data (Qtr1\_01 to Qtr4\_0125). It was observed that the determined Chebyshev coefficients followed Gaussian distribution. The probability density functions (pdf) of the Chebyshev coefficients for all the sets were determined (Figures 11.6 and 11.7). The rest of the plots are illustrated in Figures G.19 to G.23 in Appendix G.1. The first and second order statistics were calculated and are summarized in Table 11.5.

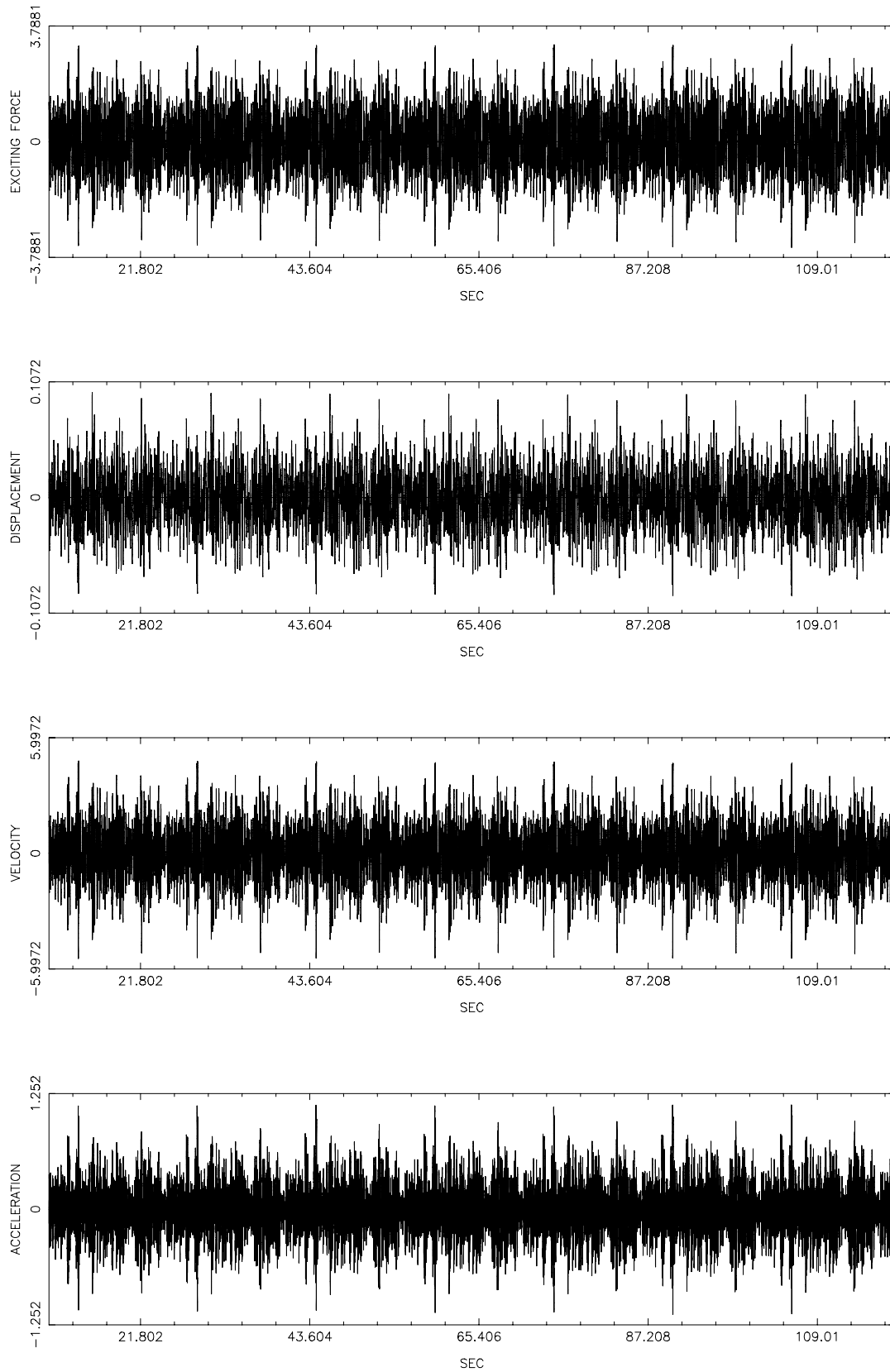


Figure 11.2: The response of the 15 kip damper subjected to broadband excitation for the data set Qtr1.01. The displacement, acceleration and force were measured. The velocity was obtained by differentiating the measured displacement. The acceleration was obtained by double-differentiating the measured displacement.

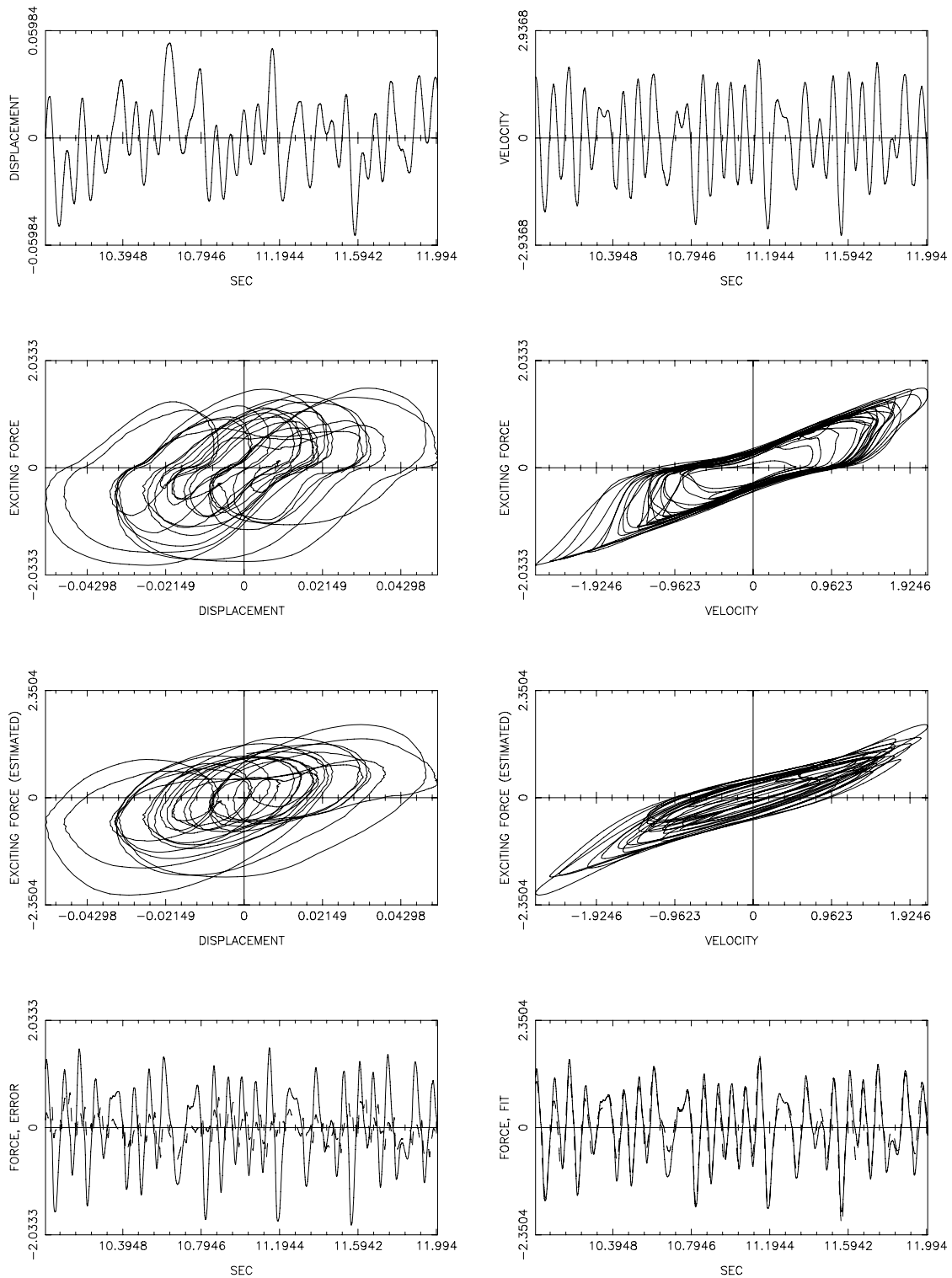


Figure 11.3: Comparison of the measured and identified 15 kip damper response using RFM for the data set Qtr1.01, segment No. 1. The solid line is the measured force, and the dashed line is the identified force.

## Restoring Force Method Analysis Results

---

Process Name	=	UCB-QTR1-01
Process Symbol	=	A00
Process Number	=	001
File Name	=	TBLA00001.ps
Process Date	=	Feb-02-2004 Mon
Process Time	=	03:32:11 PM

---

Starting data point	=	10001
Ending data point	=	12000
Data point increment	=	1

Min. displacement	=	-0.05
Max. displacement	=	0.05
Min. velocity	=	-2.67
Max. velocity	=	2.14
RMS level	=	0.73
Normalized RMS error	=	0.32

---

Normalized Chebyshev Coefficients				
I/J	0	1	2	3
0	-0.225	1.580	-0.097	0.167
1	0.464	0.000	-0.070	0.027
2	-0.023	0.061	0.013	0.067
3	-0.053	-0.008	0.087	-0.014

Normalized Power Series Coefficients				
I/J	0	1	2	3
0	-0.092	1.219	-0.220	0.399
1	0.957	-0.185	-0.664	0.280
2	-0.072	-0.277	0.051	0.533
3	-0.564	0.140	0.699	-0.231

De-Normalized Power Series Coefficients				
I/J	0	1	2	3
0	0.052	0.491	-0.017	0.029
1	17.250	-2.529	-1.821	0.393
2	-42.190	-33.940	14.990	13.050
3	-3486.000	764.500	695.100	-106.800

Figure 11.4: Summary of the RFM identification of the 15 kip damper subjected to broadband excitation for the data set Qtr1\_01, segment No. 1.

PROCESS NAME : UCB-QTR1-01  
 PROCESS SYMBOL: A00  
 PROCESS DATE : FEB-03-2004 TUE  
 NO. PROCESSES : 108  
 START DATA PTS: 10,000  
 END DATA PTS : 119,000  
 DATA INCREMENT: 1  
 DATA OVERLAP : 50%

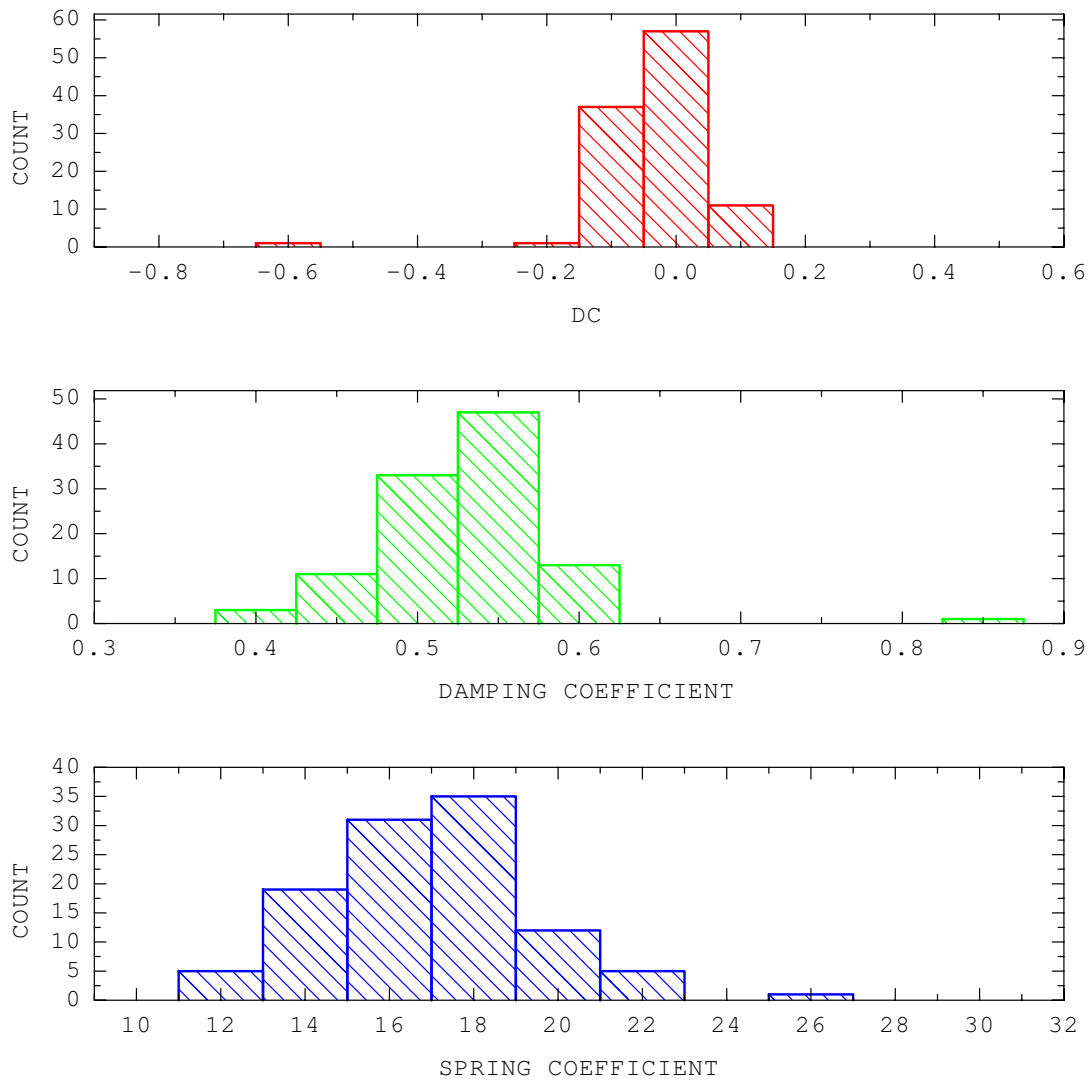
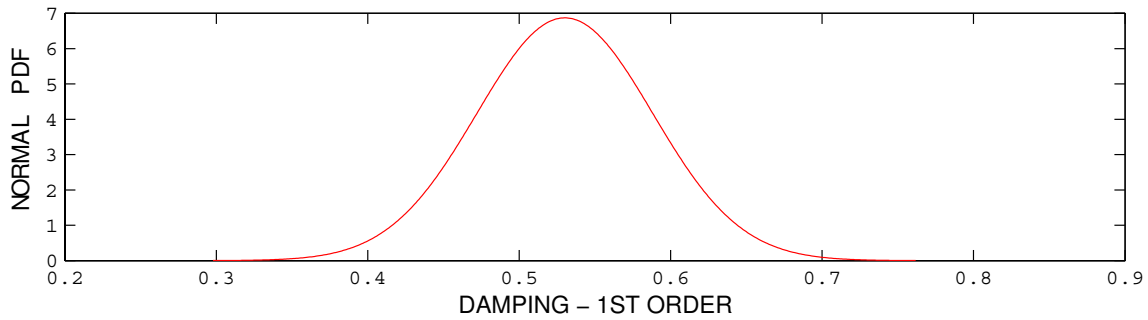
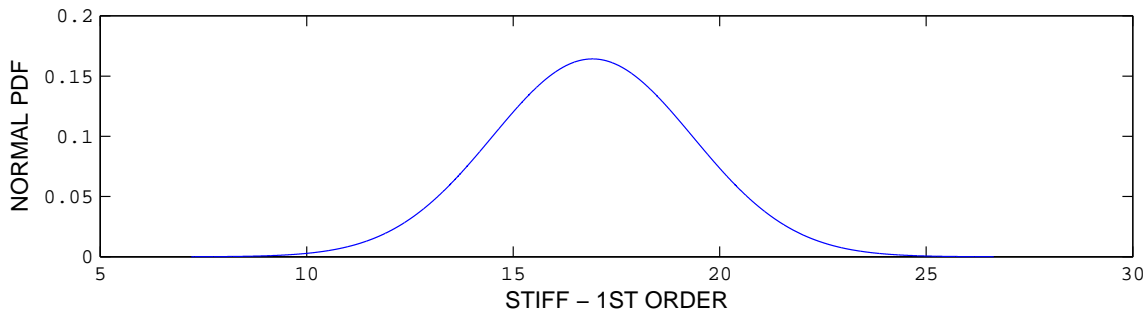


Figure 11.5: Histogram of the dc, stiffness and damping Chebyshev coefficients of 15 kip damper subjected to broadband excitation for the data set Qtr1\_01.



(a) First order damping coefficient

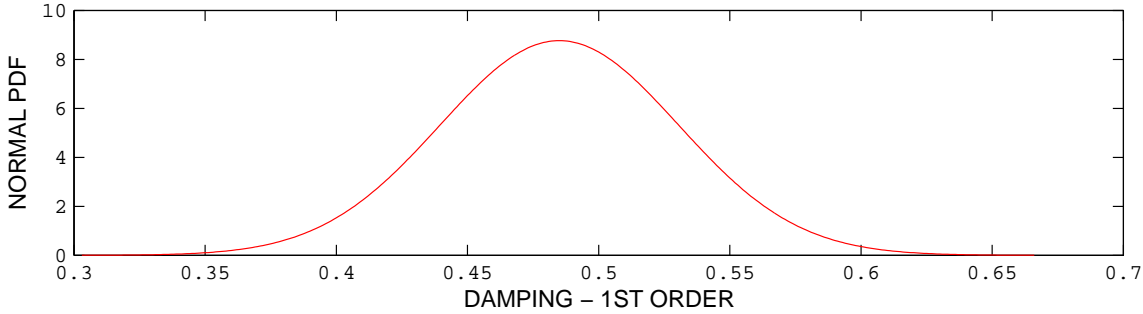


(b) First order stiffness coefficient

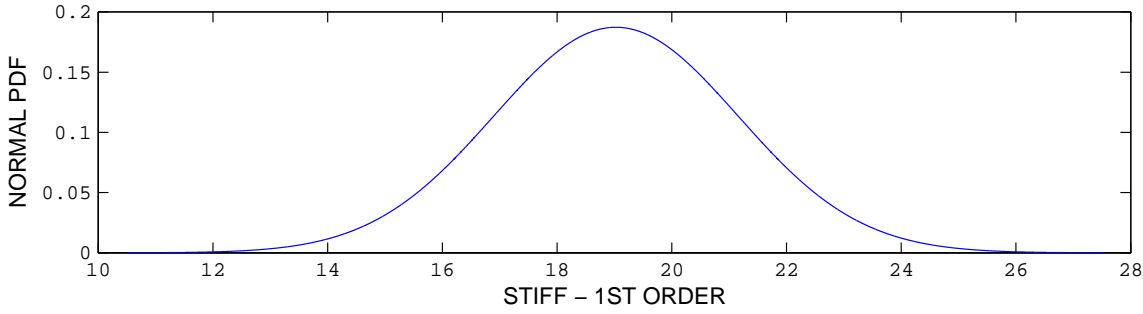
Figure 11.6: Probability density function of the damping and stiffness Chebyshev coefficients of the 15 kip damper for the data set Qtr1.01.

Table 11.5: The first and second order statistics of normalized Chebyshev coefficients of the 15 kip viscous damper subjected to broadband excitation.

NO	Name	Coeff	Mean	STDV	Median	Max	Min
1	Qtr1.01	damp	0.5301	0.0581	0.5315	0.8620	0.3930
		stiff	16.9209	2.4287	16.9850	25.4500	11.9700
2	Qtr2.01	damp	0.5621	0.0494	0.5665	0.6750	0.4300
		stiff	18.3347	2.2832	18.5000	25.1900	13.4300
3	Qtr3.01	damp	0.5242	0.0419	0.5170	0.7000	0.4330
		stiff	20.6677	2.3276	21.0300	26.3600	14.9600
4	Qtr4.01	damp	0.5825	0.0805	0.5710	1.3020	0.4820
		stiff	15.7455	7.2014	16.3350	24.1800	-53.5800
5	Qtr1.0125	damp	0.4850	0.0455	0.4795	0.7450	0.3860
		stiff	19.0266	2.1301	18.8750	28.6600	15.1200
6	Qtr2.0125	damp	0.6865	0.1069	0.6735	1.3900	0.5380
		stiff	25.3739	6.3576	24.1900	72.2000	18.8900
7	Qtr3.0125	damp	0.4848	0.0460	0.4875	0.5810	0.3680
		stiff	18.5428	2.7797	17.8300	26.1000	13.2500
8	Qtr4.0125	damp	0.6008	0.0394	0.5985	0.7380	0.5150
		stiff	19.0851	3.2532	18.1450	30.2800	14.4000



(a) First order damping coefficient



(b) First order stiffness coefficient

Figure 11.7: Probability density function of the damping and stiffness Chebyshev coefficients of the 15 kip damper for the data set Qtr1.0125.



## Chapter 12

# IDENTIFICATION OF THE 15 KIP VISCOUS DAMPER USING ARTIFICIAL NEURAL NETWORKS

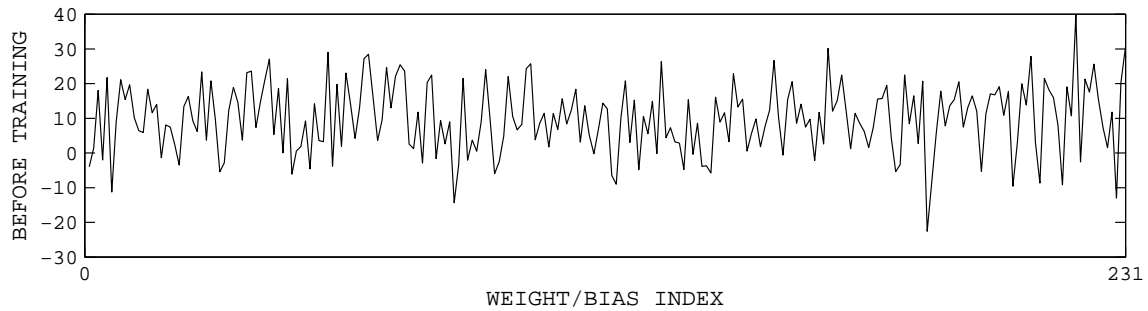
### 12.1 Problem Formulation of Artificial Neural Networks

The second round test of the 15 kip damper response data were used in the ANN identification. The goal of this identification process was to demonstrate that ANN can be utilized to identify the 15 kip damper under broadband excitation. Details of the ANN technique were discussed in Section 2.3.2.

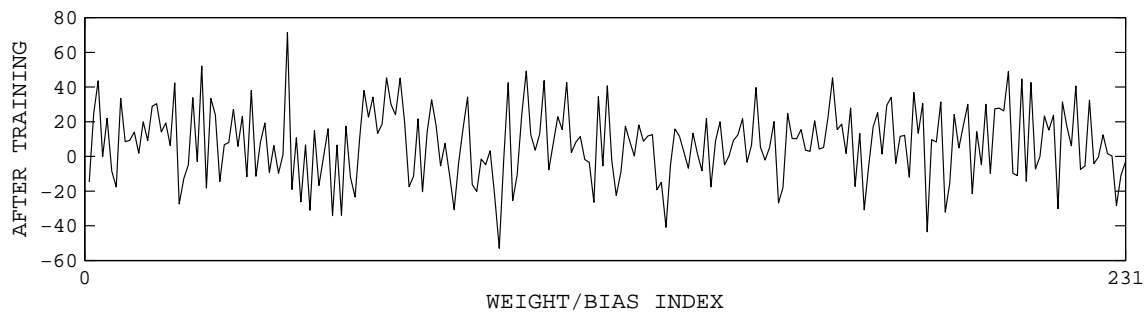
### 12.2 Application of Artificial Neural Networks to Collected Data Sets

The neural networks was trained using the second round of the collected data sets of the 15 kip damper response. Test parameters of the second round tests were shown in Section 8.3. During the training, the displacement, velocity and acceleration of the damper were used as the input of the neural networks, and the force as the output of the network. The identification parameters of the ANN are summarized in Table 12.1. Figures 12.1 (a) and (b) show the weights and bias of the neural networks before and after the training. Figure 12.1 illustrates the change of the error function and the standard deviation of the random step during the training. The error function and the step size were reduced, and eventually converged as the global loop was executed.

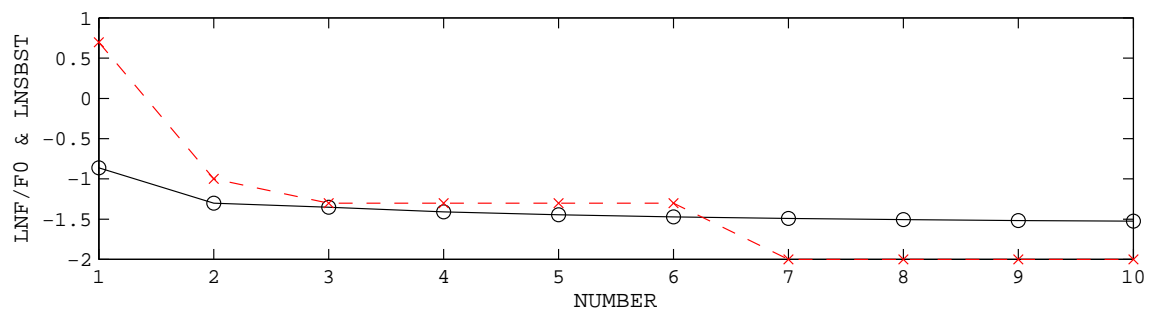
A total of four sets from the second round tests were identified, and an example of the identifica-



(a) Weights and bias before training



(b) Weights and bias after training



(c) RMSE ratio after training

Figure 12.1: The ratio of current error function normalized by the starting error function (solid line) and the current optimal standard deviation of random step size (dashed line) for the data set usc5400q4. The y-axis is plotted in log scale.

Table 12.1: Training parameters of ANN identification for the response of the 15 kip damper using adaptive random search method.

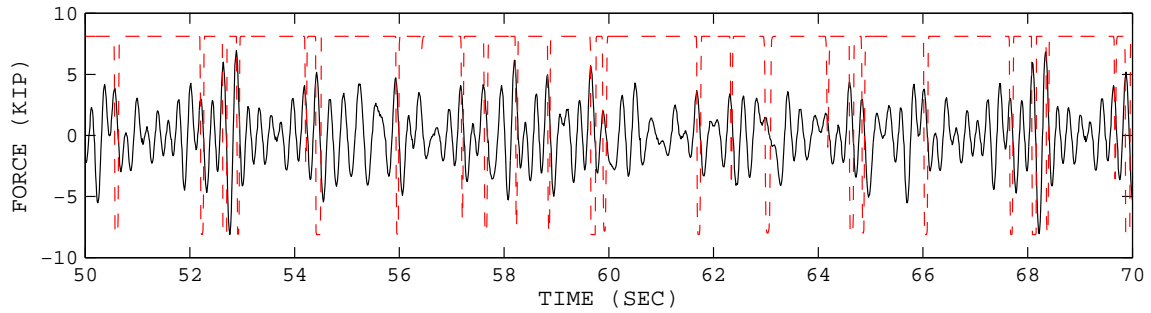
Number of global search	10
Number of local search	500
Number of statistical averaging	1
Number of nodes in the 1st layer	15
Number of nodes in the 2nd layer	10
neural networks input	Displacement Velocity Acceleration
neural networks output	Force

Table 12.2: Normalized mean square error between measured and identified force of the 15 kip viscous damper.

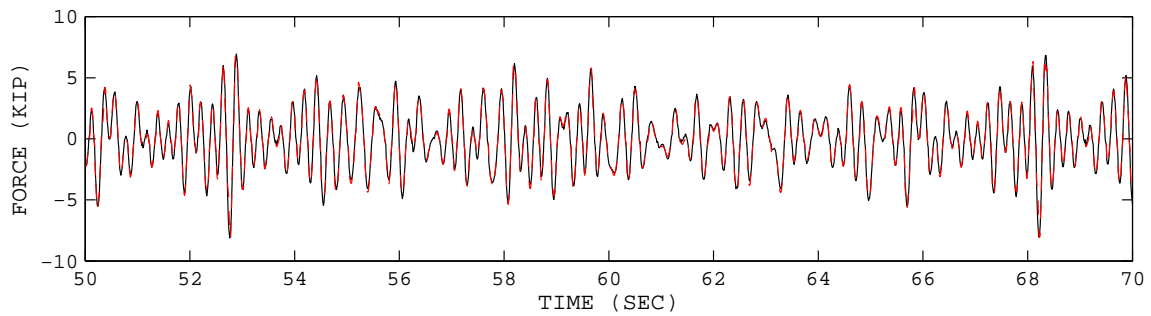
No.	Test name	Normalized MSE (%)
1	usc10175q4	2.53
2	usc10200q4	2.38
3	usc5300q4	2.05
4	usc5400q4	1.19

tion results is shown in Figure 12.2. The rest of the identification results are shown in Figures G.27 to G.30. The mean square error ratio of the measured and identified force was calculated to evaluate the identification performance (Table 12.2). The mean square error ratio varied from 0.09% to 0.16%. Therefore, based on the above results, the ANN can successfully identify the 15 kip viscous damper response under broadband excitation. The identification results of the entire data sets are provided in Section G.2.1 in Appendix G.

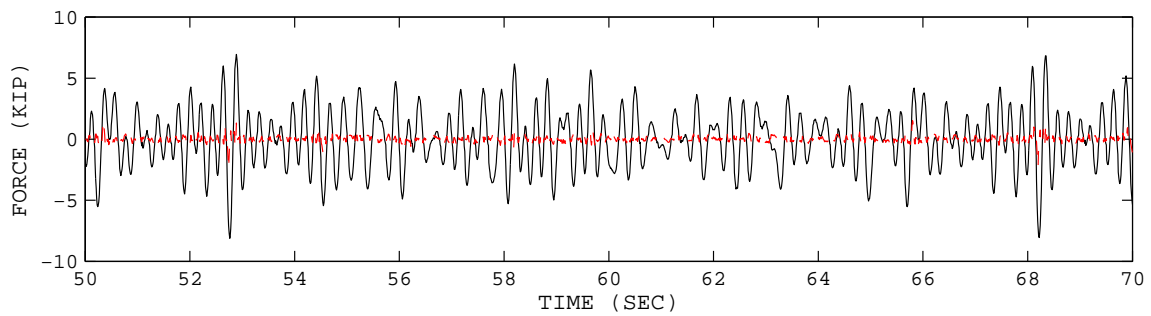
The maximum measured, absolute equivalent design and maximum RFM-identified forces were in Table 12.3. The absolute equivalent design force is calculated based on the design formula (Eqn. 2.6), the corresponding measured velocity for the maximum force in each test, and the manufacturer design parameters ( $C = 0.7$  kip sec/in and  $n = 1.0$ ).



(a) Force before training



(b) Force after training



(c) Error after training

Figure 12.2: Comparison of the measured and identified damper response to broadband excitation using ANN for the data set usc5400q4. The solid line is the measured force and the dot line is the identified force.

Table 12.3: Comparison of the maximum measured force, absolute equivalent design force, and maximum ANN-identified force from the parametric identification methods of the 15 kip viscous damper. The equivalent design force is calculated based on the design formula (Eqn. 2.6), the corresponding measured velocity for the maximum force in each test, and the manufacturer design parameters ( $C = 0.7$  kip sec/in and  $n = 1.0$ ).

Test No.	Test name	Max measured force (kip)	Absolute equivalent design force (kip)	ANN-identified force (kip)
1	usc_10175_q4	7.02	3.25	6.87
2	usc_10200_q4	8.05	3.59	7.88
3	usc_5300_q4	5.29	2.49	4.97
4	usc_5400_q4	6.95	3.15	6.79



## Chapter 13

# EXPERIMENTAL SETUP OF THE MAGNETO-RHEOLOGICAL DAMPER

### 13.1 Damper Specifications

A commercially available magneto-rheological (MR) damper was used in this test (Figure 13.1 (a)). As a magnetic field is applied to the MR fluid inside the monotube housing, the damping characteristics of the fluid increase with precision and no time delay. The damping characteristics can be controlled with the input current controller (Figure 13.1 (b)). The controller provides two modes, manual and external. In the manual mode, the operator can control the input current by using the knob on the unit. In the external mode, the operator can control the input current more precisely using an external function generator, or computer-based data acquisition system. Detailed specifications of the MR damper are shown in Table 13.1.

Similar to a classical viscous damper, the MR damper dissipates some of the input energy in the form of heat. As a result, a significant amount of heat can be accumulated inside the MR fluid and the monotube, especially after long time of operation. The accumulated heat is harmful to the MR damper's durability, hence it changes the properties of the MR liquid, which results in the change of the damper response. Therefore, it is critical that the temperature change remains minimum for a reliable test result. A water-cooling system was fabricated at USC to minimize the temperature effect on the experimental results. The cooling system mounted on the MR damper is shown in Figures 13.1 (c) and (d). Pressured water is supplied into the cooling system via one of two barbs. Then, the water flows through the gap between the damper surface and the cooler body. While the water flows around the damper surface, the heat is transferred to the circulated water, and then the heated water flows out through the other barb. By changing the speed of the

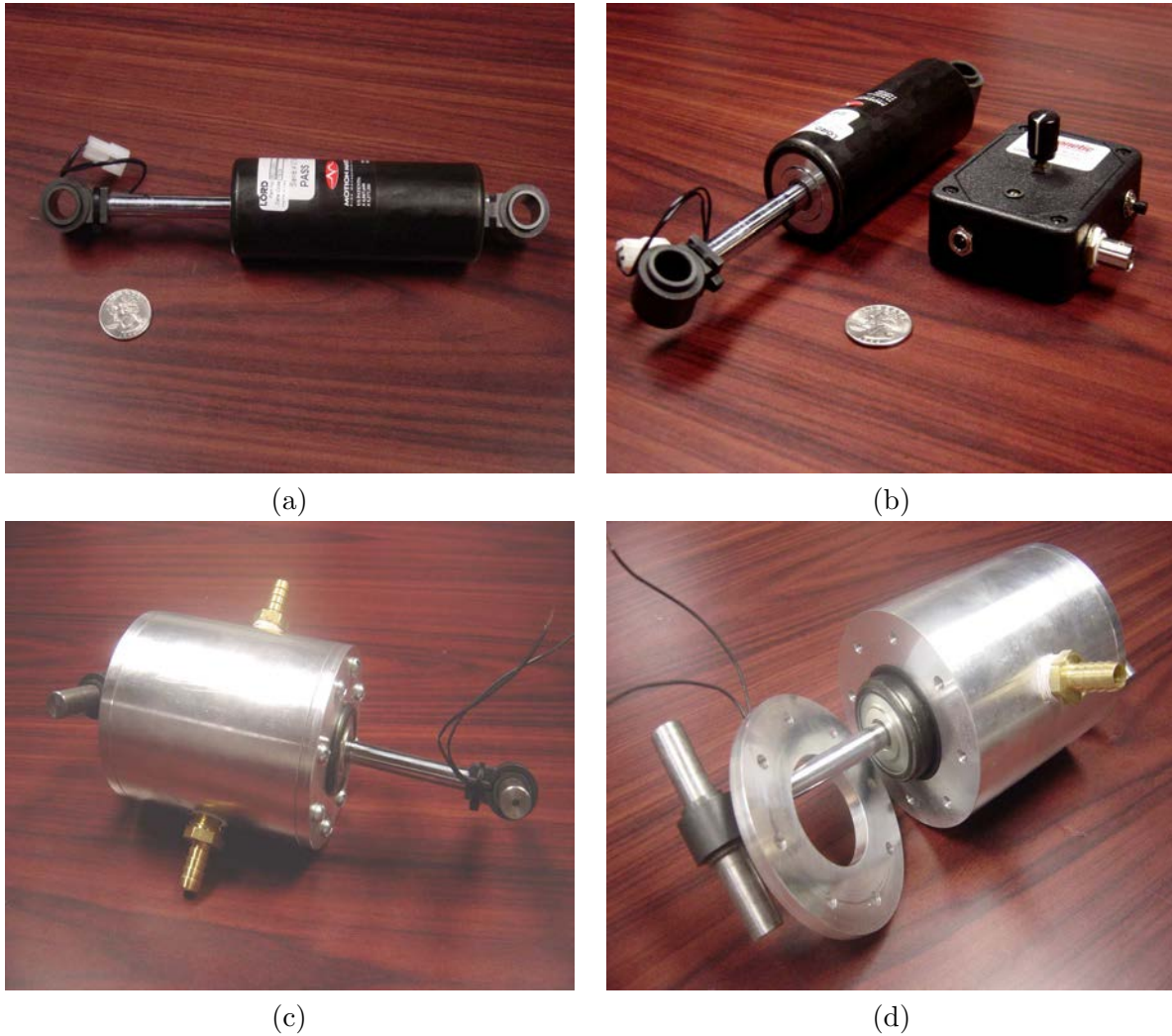


Figure 13.1: Magneto-rheological damper and water-cooling system.

water pump, the pressure of the circulated water can be adjusted to achieve the optimal efficiency during the heat transfer.

## 13.2 Test Setup and Instrumentation

An experimental setup was built to measure the response of the MR damper under various excitation types. The MR damper was installed with the test setup, as shown in Figure 13.2; one end of the damper was connected to the shaker, and the other end was connected to the fixture mounted firmly to the ground. The shaker was displacement-controlled by a personal computer. The MR damper was connected to the computer, for the control of the damping characteristics. A total of six sensors were recording the displacement, velocity, acceleration, force and temperature of the MR damper.

Table 13.1: Lord Corp. magneto-rheological damper (RD-1005-3) specifications.

Damper dimensions: - Compressed length - Extended length - Body diameter - Shaft diameter - Weight - For installation on pin	6.1 inches (155 mm) 8.2 inches (208 mm) 1.63 inches (41.4 mm) 0.390 inches (10 mm) 1.8 pounds (800 g) 0.47 inches (12 mm)
Electrical characteristics: - Input current - Input voltage - Resistance	2 amps max 12 V DC 5 ohms at ambient temp, 7 ohms at 160F (71C)
Damper forces (peak-to peak): - 2 in/sec at 1 amp - 8 in/sec at 0 amp	greater than 500 pounds (2224 N) less than 150 pounds (667 N)
Mechanical characteristics: - Min tensile strength - Max operating temperature - Storage temperature limits	1000 pounds (4448 N) 160F (71C) 212F to -40F (100C to -40C)
Durability	2 million cycles at $\pm 0.5$ inches ( $\pm 13$ mm), 2hertz with input current varying between 0 and 0.8 amps
Response time (amplifier & power supply dependent)	Less than 25 msec - time to reach 90% of max level during a 0 to 1 amp step input at 2 in /sec (51 mm/sec)
Damper connector (2 pin)	Body: Molex # 03-06-2023 Pins: Molex # 02-06-2103
Mating connector (2 pin)	Body: Molex # 03-06-1023 Pins: Molex # 02-06-1103

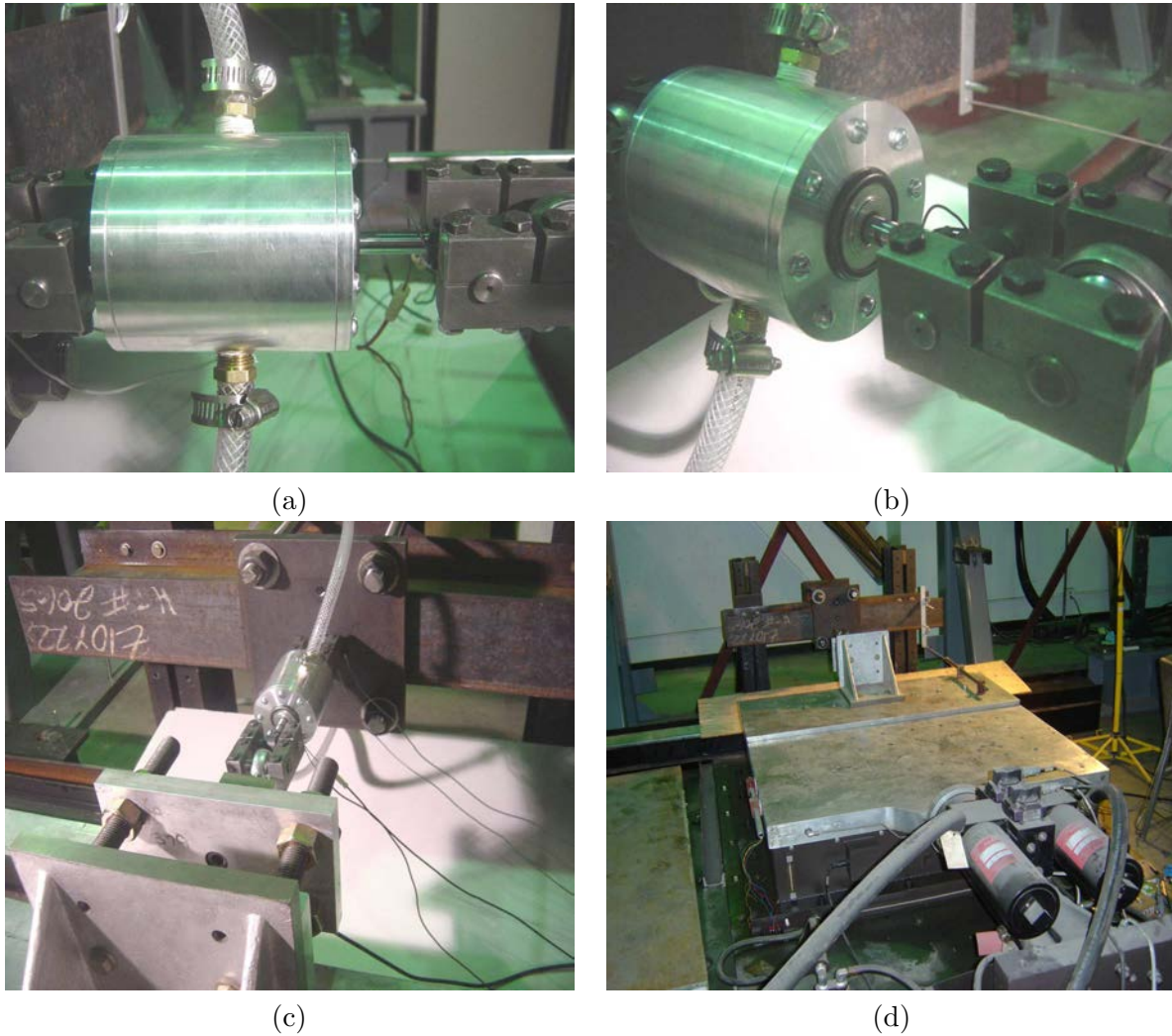


Figure 13.2: Magneto-rheological damper test setup at the Structural Dynamics Laboratory of the University of Southern California.

The schematic of the sensor-actuator system is illustrated in Figure 13.3, and the detailed sensor configuration is tabulated in Table 13.2. A data acquisition (DAQ) software was programmed in LabView to control the actuator and sensors from the computer. The DAQ software is illustrated in Figure 13.4.

### 13.3 Test Specifications

A series of tests was performed to obtain the data sets for parametric and nonparametric identification of the MR damper. The shaker was controlled in displacement mode to excite the MR damper. A total of 40 tests were performed with four different levels of MR damper input current;

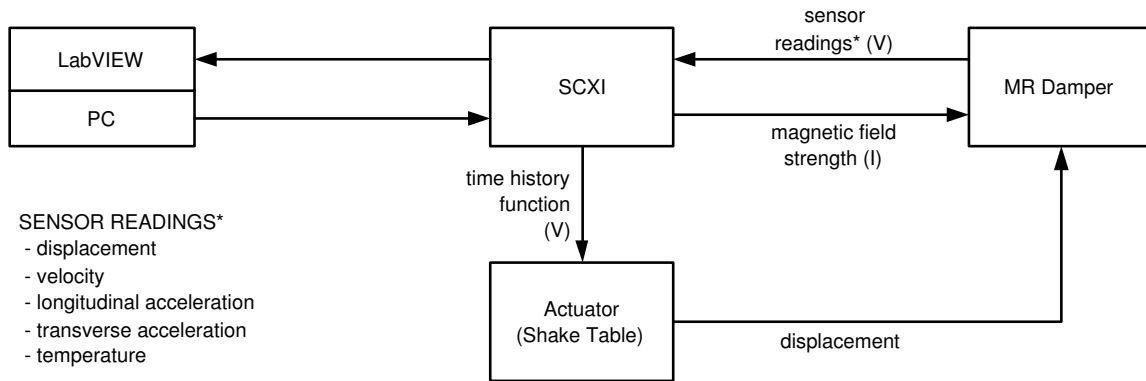


Figure 13.3: A schematic of sensor/actuator system of MR-damper test setup.

Table 13.2: Excitation characteristics for the MR damper experiments.

No.	Name	Unit	Description
1	EXCIT	lb	Damping force
2	DISP	inch	Damper displacement
3	VEL	inch/sec	Damper velocity
4	ACC	G	Damper acceleration
5	ACCf	G	Fixture acceleration
6	TEMP	F	Damper surface temperature
7	CMD	volt	Input signal to the actuator controller

1.0, 0.95, 0.90, and 0.75 ampere. The 1.0-ampere was used as the nominal case (i.e. 100%), and the rest of the current levels were compared to it (i.e. 95, 90, and 75%). For each current level, a total of ten tests were conducted with different sets of broadband shaker motion. The motion signal was generated as follows:

1. A long array of Gaussian random number was created.
2. The array was divided into ten sub-arrays. Each of the sub-arrays contained 30,000 data points. The length of each array corresponds to 30 seconds with 1,000 Hz sampling rate.
3. Each sub-array was windowed with cosine-tapered window in the time domain.
4. Then, the sub-arrays were filtered with a butterworth filter. The bandwidth was 0.1 to 5.0 Hz.
5. The same cosine-tapered window was applied again to the filtered sub-arrays.
6. Steps 1-5 were repeated until the first sub-array had standard deviation of 1.0 after the windowing and filtering.

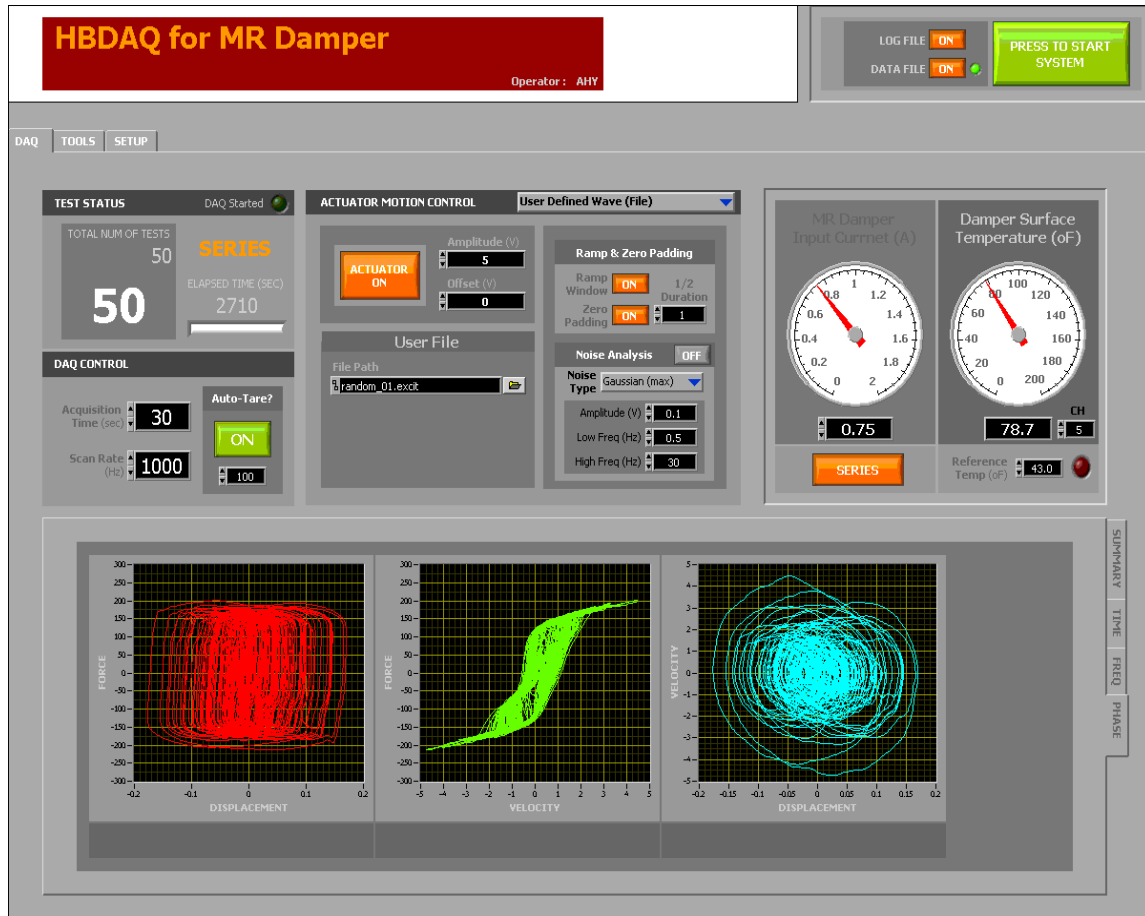


Figure 13.4: The data acquisition software interface programmed in Labview for the MR damper experiments.

7. The sub-arrays were used as the input signal of the shaker controller. At the beginning and end of the signal, zero voltage was added for two seconds (2,000 points), increasing the total length of the excitation to 32 seconds.

The time history shaker motion for the data set MRD1\_X11V\_M100\_S00\_00001 is shown in Figure 13.5. The mean, standard deviation, minimum and maximum of the shaker motions for all the tests are summarized in Table13.3.

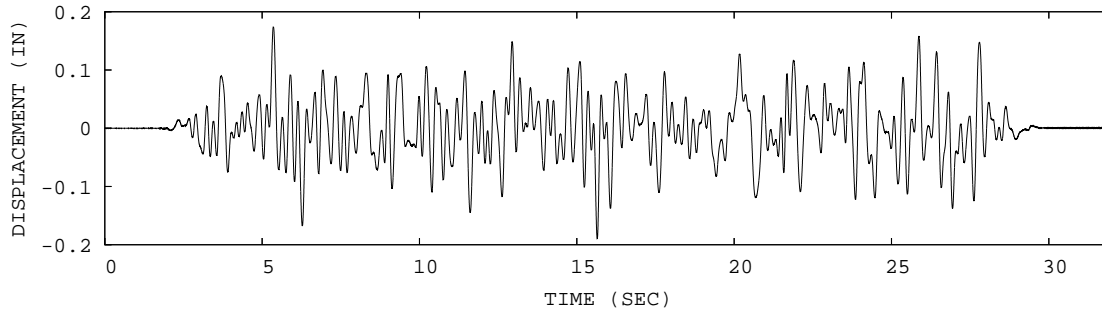


Figure 13.5: Displacement time history of the shaker motion for MR damper in the data set of MRD1\_X11V\_M100\_S00\_00001.

Table 13.3: Characteristics of the MR damper excitation. The unit of the input current was ampere, and the rest were inches. The excitation had a Gaussian distribution, and the bandwidth was from 0.1 to 5.0 Hz, with approximately  $\pm 0.2$  inch displacement. The shaker was controlled in displacement mode.

No.	Name	Mean	STDV	Max	Min	Input Current
1	MRD1_X11V_M100_S00_00001	0.0005	0.0498	0.1739	-0.1893	1.0
2	MRD1_X11V_M100_S00_00002	0.0005	0.0473	0.1526	-0.1797	
3	MRD1_X11V_M100_S00_00003	0.0003	0.0459	0.1588	-0.1929	
4	MRD1_X11V_M100_S00_00004	0.0006	0.0478	0.1858	-0.1535	
5	MRD1_X11V_M100_S00_00005	0.0011	0.0453	0.1689	-0.1600	
6	MRD1_X11V_M100_S00_00006	0.0010	0.0473	0.1868	-0.1337	
7	MRD1_X11V_M100_S00_00007	0.0007	0.0495	0.1764	-0.1517	
8	MRD1_X11V_M100_S00_00008	0.0005	0.0470	0.1527	-0.1951	
9	MRD1_X11V_M100_S00_00009	0.0001	0.0453	0.1801	-0.1835	
10	MRD1_X11V_M100_S00_00010	0.0001	0.0481	0.1658	-0.1559	
11	MRD1_X11V_M095_S00_00001	0.0006	0.0498	0.1739	-0.1893	0.95
12	MRD1_X11V_M095_S00_00002	0.0006	0.0474	0.1525	-0.1798	
13	MRD1_X11V_M095_S00_00003	0.0004	0.0459	0.1590	-0.1928	
14	MRD1_X11V_M095_S00_00004	0.0007	0.0479	0.1858	-0.1534	
15	MRD1_X11V_M095_S00_00005	0.0010	0.0453	0.1687	-0.1601	
16	MRD1_X11V_M095_S00_00006	0.0006	0.0473	0.1863	-0.1341	
17	MRD1_X11V_M095_S00_00007	0.0002	0.0496	0.1760	-0.1520	
18	MRD1_X11V_M095_S00_00008	0.0002	0.0469	0.1523	-0.1953	
19	MRD1_X11V_M095_S00_00009	0.0001	0.0453	0.1800	-0.1833	
20	MRD1_X11V_M095_S00_00010	0.0001	0.0481	0.1658	-0.1558	
21	MRD1_X11V_M090_S00_00001	0.0007	0.0498	0.1740	-0.1892	0.90
22	MRD1_X11V_M090_S00_00002	0.0007	0.0474	0.1527	-0.1796	
23	MRD1_X11V_M090_S00_00003	0.0006	0.0460	0.1591	-0.1925	
24	MRD1_X11V_M090_S00_00004	0.0009	0.0478	0.1861	-0.1531	
25	MRD1_X11V_M090_S00_00005	0.0013	0.0453	0.1690	-0.1597	
26	MRD1_X11V_M090_S00_00006	0.0013	0.0474	0.1872	-0.1333	
27	MRD1_X11V_M090_S00_00007	0.0010	0.0496	0.1767	-0.1513	
28	MRD1_X11V_M090_S00_00008	0.0010	0.0470	0.1530	-0.1945	
29	MRD1_X11V_M090_S00_00009	0.0007	0.0453	0.1808	-0.1829	
30	MRD1_X11V_M090_S00_00010	0.0005	0.0481	0.1660	-0.1555	
31	MRD1_X11V_M075_S00_00001	0.0007	0.0499	0.1739	-0.1891	0.75
32	MRD1_X11V_M075_S00_00002	0.0007	0.0474	0.1527	-0.1795	
33	MRD1_X11V_M075_S00_00003	0.0005	0.0460	0.1591	-0.1924	
34	MRD1_X11V_M075_S00_00004	0.0009	0.0479	0.1860	-0.1532	
35	MRD1_X11V_M075_S00_00005	0.0012	0.0453	0.1690	-0.1598	
36	MRD1_X11V_M075_S00_00006	0.0012	0.0474	0.1870	-0.1334	
37	MRD1_X11V_M075_S00_00007	0.0010	0.0496	0.1767	-0.1515	
38	MRD1_X11V_M075_S00_00008	0.0010	0.0470	0.1530	-0.1946	
39	MRD1_X11V_M075_S00_00009	0.0009	0.0453	0.1808	-0.1826	
40	MRD1_X11V_M075_S00_00010	0.0009	0.0481	0.1665	-0.1550	

## Chapter 14

# MEASUREMENT OF THE MAGNETO-RHEOLOGICAL DAMPER RESPONSE UNDER BROADBAND EXCITATION

### 14.1 Collection of Data Sets

With the test setup described in Chapter 13, a total of 40 experiments were conducted. Details of the test parameters were described in Section 13.3. The MR damper was excited with a broadband excitation motion, and the damper response was measured. An example of the broadband excitation histogram is shown in Figure 14.1.

### 14.2 Sample Results of Preliminary Data Analysis

During the experiments, displacement, velocity, acceleration and force were measured at the sampling rate of 1 kHz. The sensor readings were prefiltered at 100 Hz to prevent aliasing. The duration of each test was 32 seconds, consisting of 30-seconds excitation and 2-second cosine taper at the beginning and end of the excitation. Samples of the measurements time histories are shown in Figures 14.2 to 14.5. The corresponding phase plots are illustrated in Figure 14.6. The entire group of data sets for the 40 experiments are illustrated in Figures H.1 to H.12.

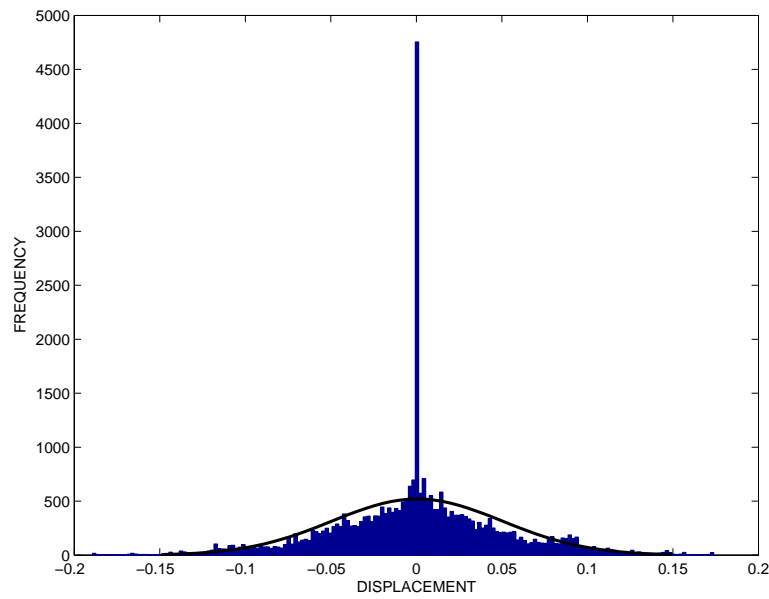
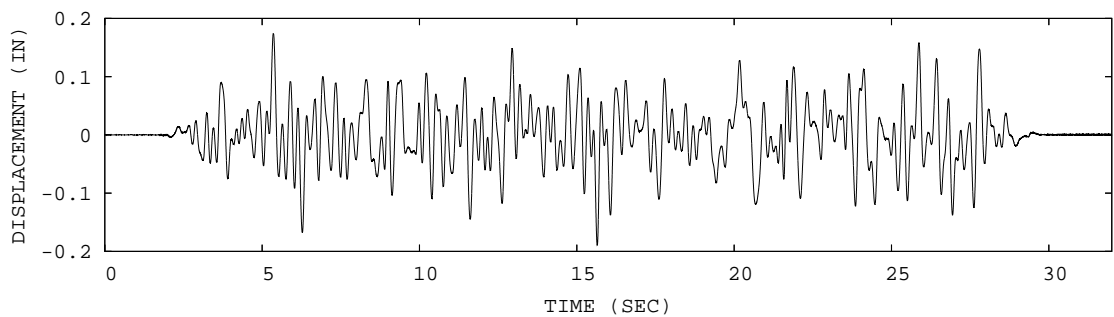
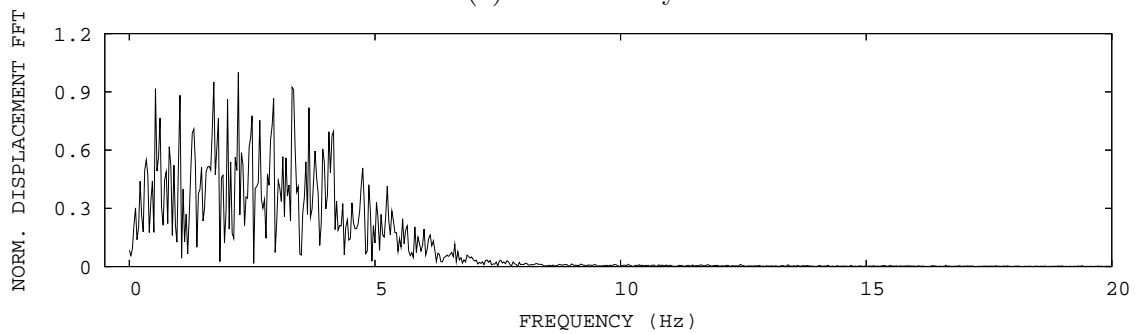


Figure 14.1: Probability density function of the MR damper excitation for the data set MRD1\_X11V\_M100\_S00\_00001. The test was displacement-controlled, and the unit of the displacement was in inch.



(a) Time history



(b) FFT

Figure 14.2: The displacement of the MR damper subjected to broadband excitation for the data set MRD1\_X11V\_M100\_S00\_00001.

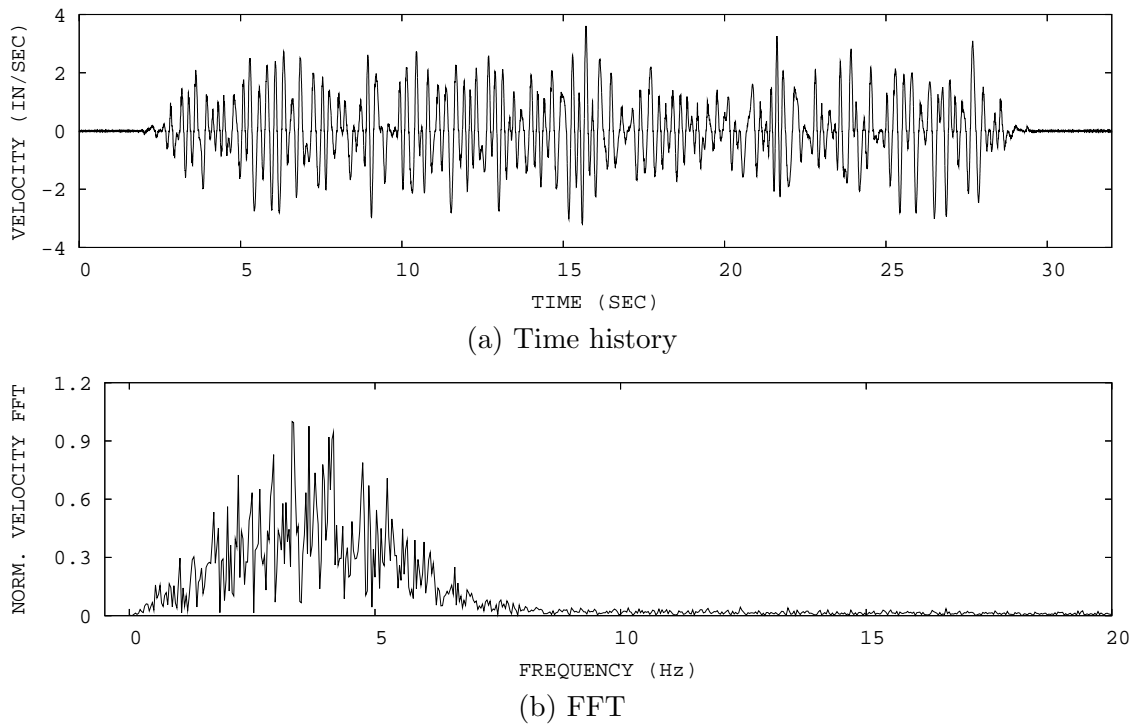


Figure 14.3: The velocity of the MR damper subjected to broadband excitation for the data set MRD1\_X11V\_M100\_S00\_00001.

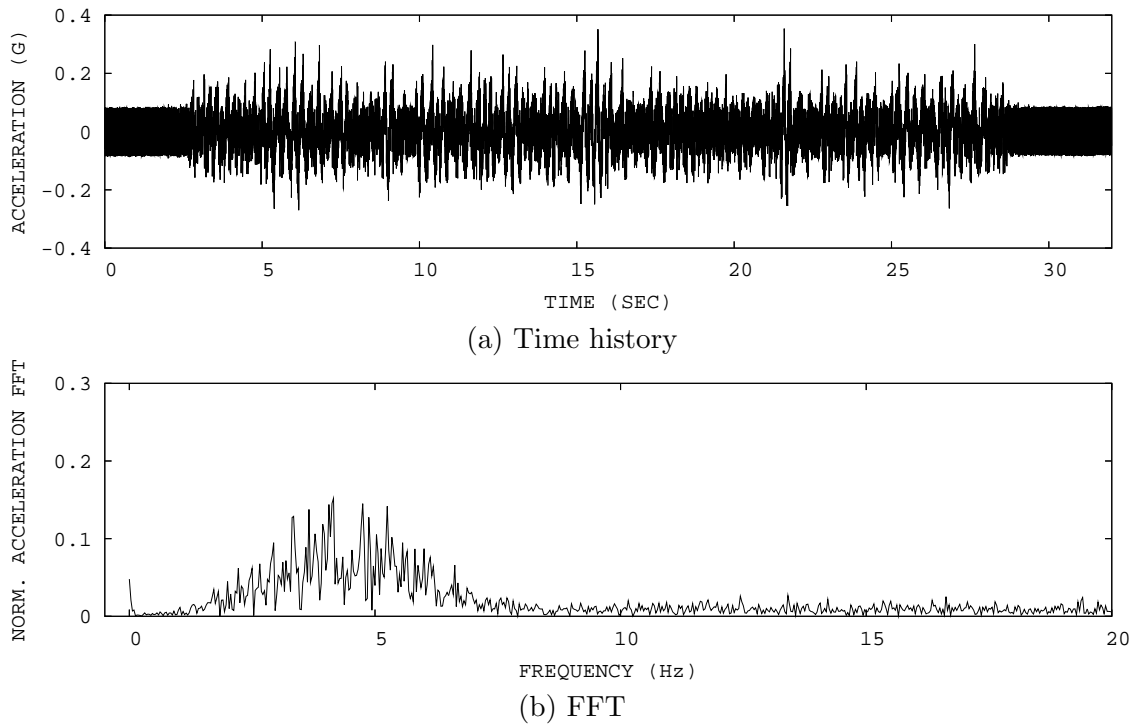


Figure 14.4: The acceleration of the MR damper subjected to broadband excitation for the data set MRD1\_X11V\_M100\_S00\_00001.

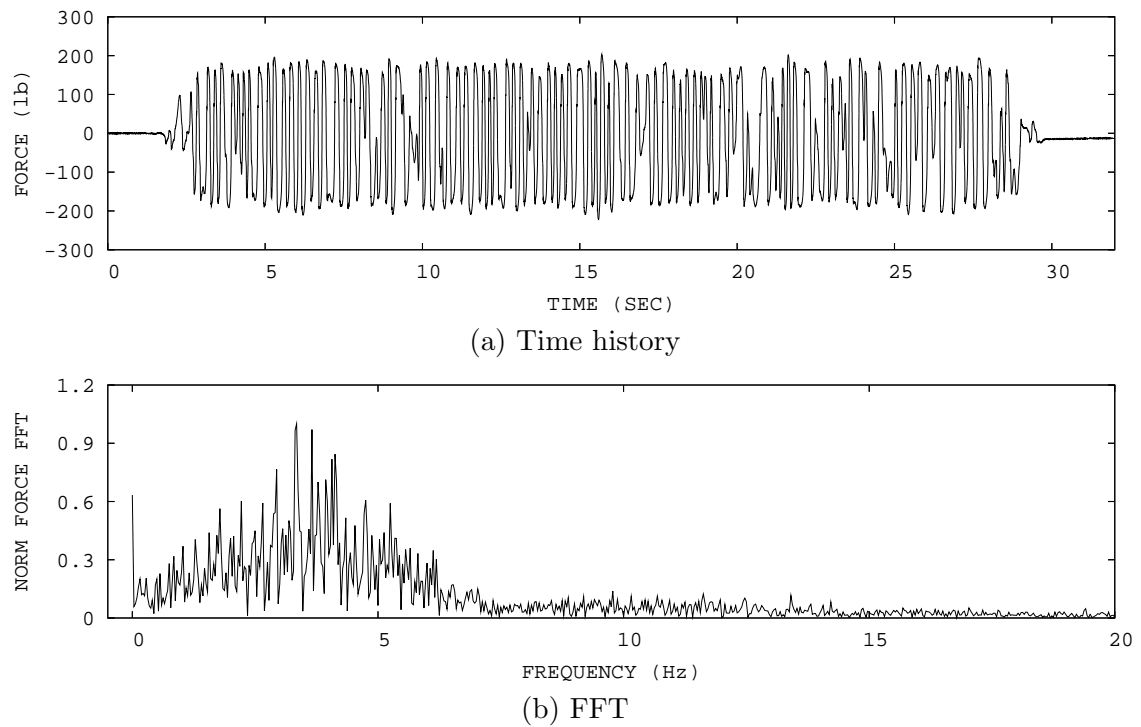


Figure 14.5: The force of the MR damper subjected to broadband excitation for the data set MRD1\_X11V\_M100\_S00\_00001.

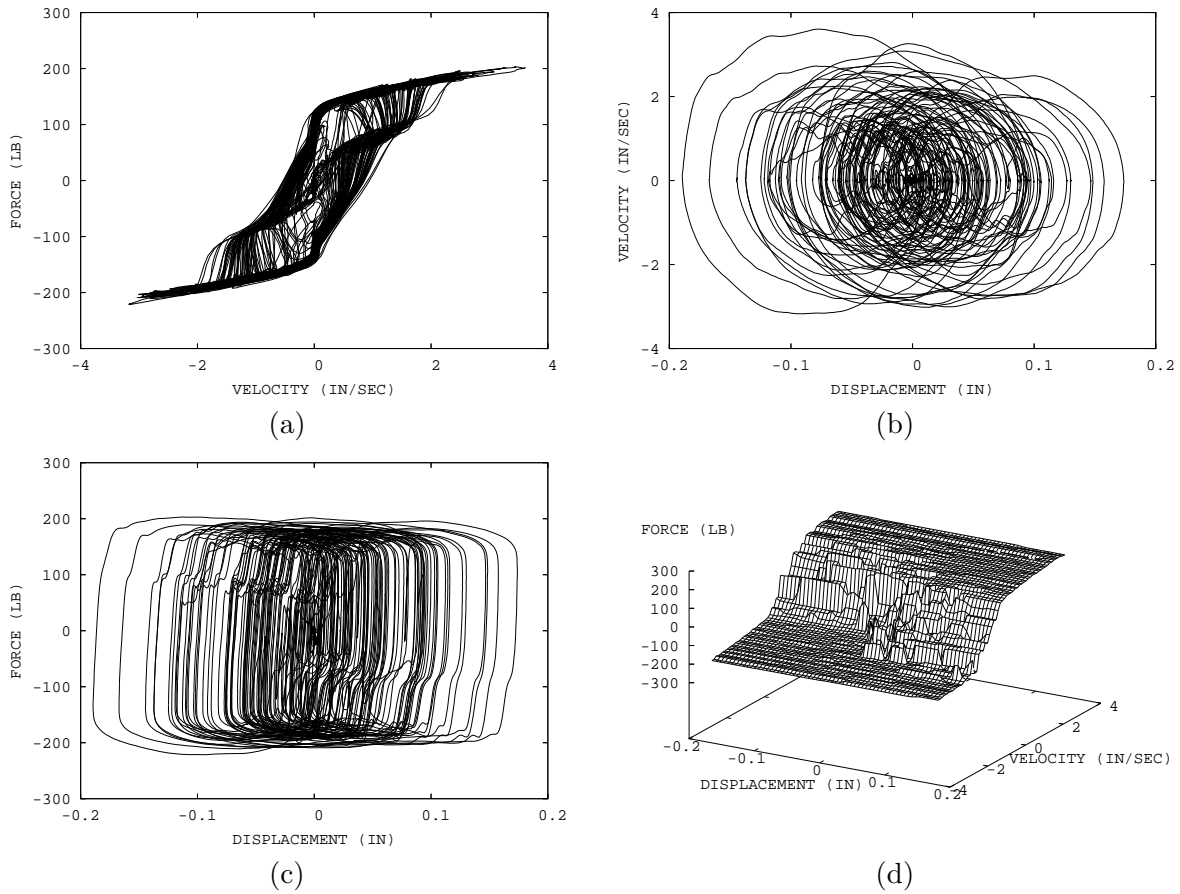


Figure 14.6: MR damper response to broadband excitation in phase plot for the data set MRD1\_X11V\_M100\_S00\_00001.



## Chapter 15

# NONPARAMETRIC RESTORING FORCE METHOD IDENTIFICATION FOR THE MAGNETO-RHEOLOGICAL DAMPER

### 15.1 Problem Formulation of the Restoring Force Method

The restoring force method (RFM) was used to identify the response of the MR damper under broadband excitation. The goal of this identification procedure was to demonstrate that the RFM can be used to identify the MR damper, when excited with the random actuator motion. The technical details of the RFM are provided in Section 2.3.1.

### 15.2 Application of the Restoring Force Method to Collected Data Sets

The RFM was applied to the MR damper response to identify the damper force. The identification parameters of the RFM are tabulated in Table 15.2. The MR damper force was successfully identified with the RFM, and examples are shown in Figures 15.1 and 15.2; the solid line is the measured force and the dashed line is the identified force. The rest of the RFM identification results can be found in Figures H.13 to H.52. The mean square error ratio of the identified Chebyshev coefficients were determined, and are listed in Table 15.2 for all the tests. The RMS error ratio of the RFM identification varied from 9.99% to 14.59%.

Table 15.1: Parameters of RFM identification for the MR damper.

Parameter	Value
Max. order of displacement	5
Max. order of velocity	5
No. of statistical averaging	1
Starting data points	6001
End data points	26000
Increment	10
No. of data points	2000

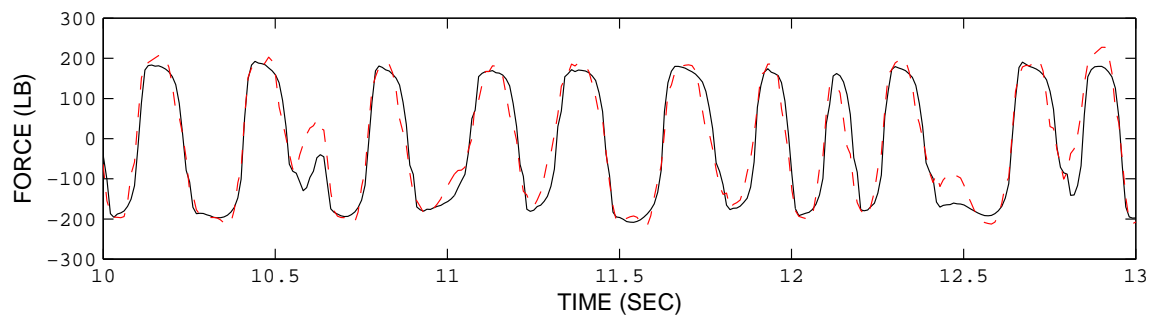


Figure 15.1: Comparison of the measured and identified damper response in time history using RFM for 1.0 ampere MR damper input current test No. 1 (MRD1\_X11V\_M100\_S00\_00001\_001). The solid line is the measured force and the dashed line is the identified force.

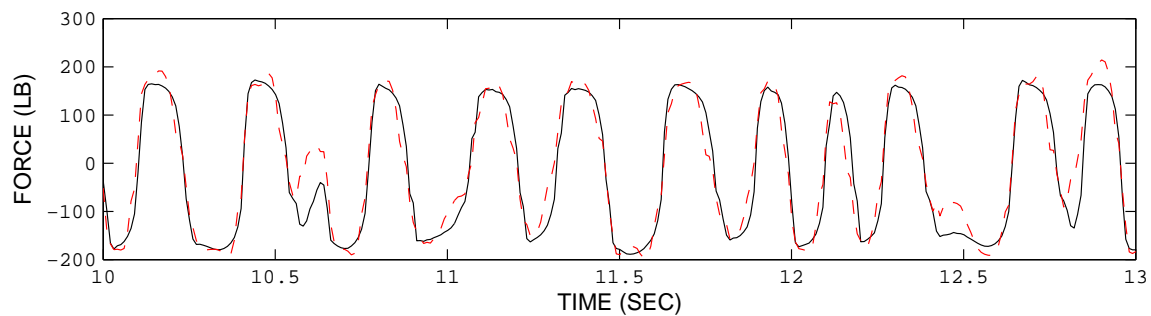


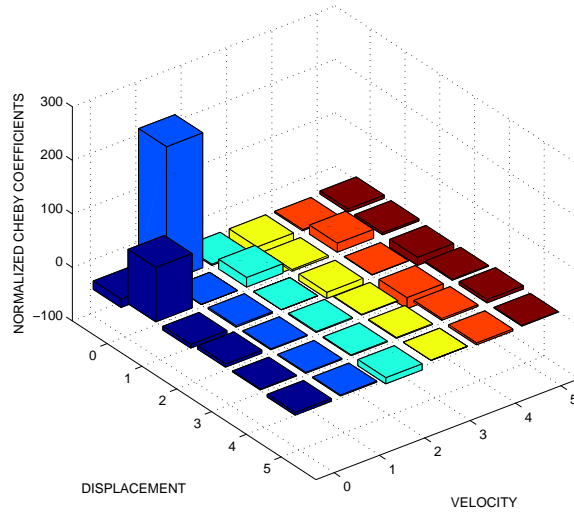
Figure 15.2: Comparison of the measured and identified damper response in time history using RFM for 0.75 ampere MR damper input current test No. 1 (MRD1\_X11V\_M075\_S00\_00001\_001). The solid line is the measured force and the dashed line is the identified force.

Table 15.2: Normalized mean square error of the normalized Chebyshev coefficients of the MR damper response.

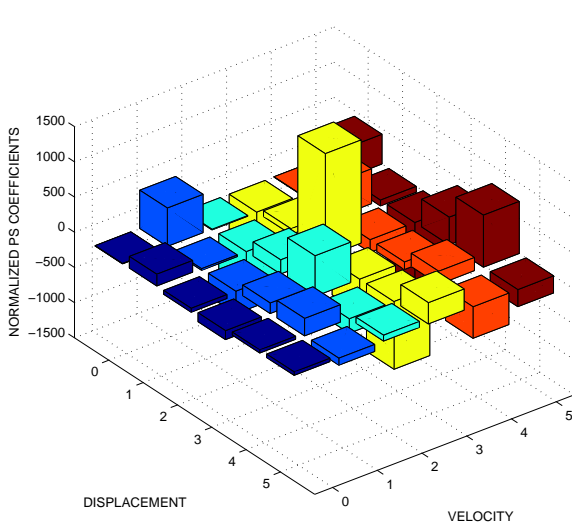
No.	Name	Normalized MSE (%)
1	MRD1_X11V_M100_S00_00001	10.43
2	MRD1_X11V_M100_S00_00002	11.77
3	MRD1_X11V_M100_S00_00003	14.21
4	MRD1_X11V_M100_S00_00004	11.56
5	MRD1_X11V_M100_S00_00005	13.25
6	MRD1_X11V_M100_S00_00006	11.63
7	MRD1_X11V_M100_S00_00007	12.32
8	MRD1_X11V_M100_S00_00008	14.59
9	MRD1_X11V_M100_S00_00009	13.25
10	MRD1_X11V_M100_S00_00010	11.29
11	MRD1_X11V_M095_S00_00001	10.50
12	MRD1_X11V_M095_S00_00002	11.90
13	MRD1_X11V_M095_S00_00003	14.21
14	MRD1_X11V_M095_S00_00004	11.77
15	MRD1_X11V_M095_S00_00005	13.32
16	MRD1_X11V_M095_S00_00006	11.56
17	MRD1_X11V_M095_S00_00007	12.53
18	MRD1_X11V_M095_S00_00008	14.14
19	MRD1_X11V_M095_S00_00009	13.32
20	MRD1_X11V_M095_S00_00010	11.02
21	MRD1_X11V_M090_S00_00001	10.24
22	MRD1_X11V_M090_S00_00002	11.56
23	MRD1_X11V_M090_S00_00003	14.21
24	MRD1_X11V_M090_S00_00004	11.42
25	MRD1_X11V_M090_S00_00005	13.91
26	MRD1_X11V_M090_S00_00006	12.04
27	MRD1_X11V_M090_S00_00007	12.75
28	MRD1_X11V_M090_S00_00008	14.14
29	MRD1_X11V_M090_S00_00009	13.10
30	MRD1_X11V_M090_S00_00010	10.89
31	MRD1_X11V_M075_S00_00001	9.99
32	MRD1_X11V_M075_S00_00002	13.91
33	MRD1_X11V_M075_S00_00003	13.69
34	MRD1_X11V_M075_S00_00004	11.22
35	MRD1_X11V_M075_S00_00005	13.10
36	MRD1_X11V_M075_S00_00006	11.18
37	MRD1_X11V_M075_S00_00007	12.32
38	MRD1_X11V_M075_S00_00008	13.84
39	MRD1_X11V_M075_S00_00009	12.82
40	MRD1_X11V_M075_S00_00010	13.47

Once the MR damper, excited with random motion was identified (Chapter 14), 10 sets of the RFM coefficients for each MR damper current input level were averaged. The input current of 1 ampere was used as the nominal case. The RFM coefficients of the nominal case are shown in Figure 15.3. The rest of the RFM coefficients for the other current input levels are shown in Figures H.53 to H.56. Based on the above results, it is inferred that the RFM can be used to identify, with reasonable accuracy, the MR damper under broadband excitation.

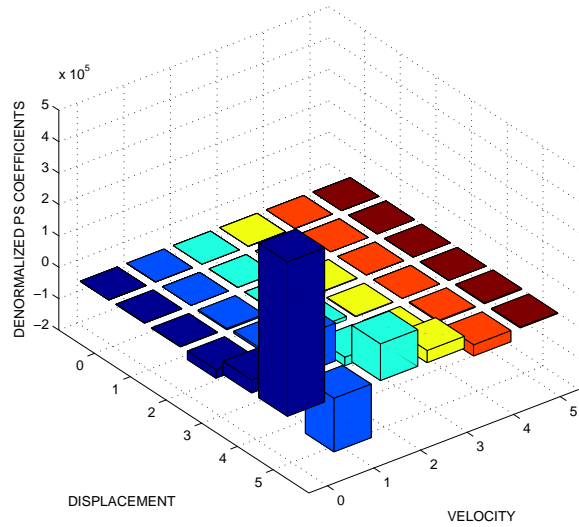
NOMINAL CASE - 1.00 AMPERE



(a) Normalized Chebyshev coefficients



(b) Normalized power series coefficients



(c) Denormalized power series coefficients

Figure 15.3: The averaged restoring force coefficients for 1.0 ampere MR damper input current. The coefficients were averaged over data sets MRD1\_X11V\_M100\_S00\_00001 to MRD1\_X11V\_M100\_S00\_00010.



## Chapter 16

# IDENTIFICATION OF THE MAGNETO-RHEOLOGICAL DAMPER USING ARTIFICIAL NEURAL NETWORKS

### 16.1 Problem Formulation of Artificial Neural Networks

The MR damper response data presented in Chapter 14 were used in the ANN identification. The goal of the identification was to demonstrate that ANN can be utilized to identify the MR damper under random excitation. The technical details of the ANN technique are provided in Section 2.3.2.

### 16.2 Application of Artificial Neural Networks to Collected Data Sets

The ANN were utilized to identify the MR damper response under random excitation. The inputs of the neural networks were displacement, velocity and acceleration, and the output was the force. The adaptive random search method was used to train the network with 10 global searches and 500 local searches. The first layer of the neural networks consisted of 15 nodes, and the second layer consisted of 10 nodes. The number of statistical averaging was 1. The identification parameters are tabulated in Table 16.1.

A total of three data sets were used in the ANN identification for the MR damper input currents of 1.00, 0.90 and 0.75. As shown in Figures 16.1 (a) and (b), the weights and bias of the neural networks were changed during the training to minimize the error between the measured and identified force. The error function and the step size of the optimization routine of the adaptive

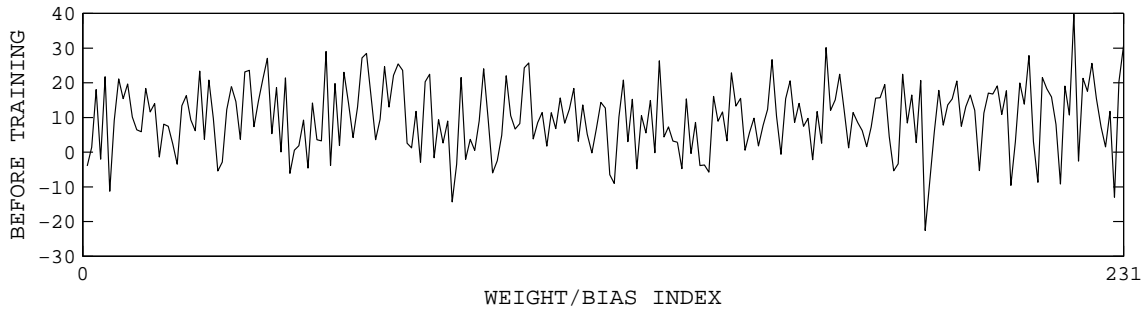
Table 16.1: Training parameters of ANN identification for the response of the MR damper using adaptive random search method.

Number of global search	10
Number of local search	500
Number of statistical averaging	1
Number of nodes in the 1st layer	15
Number of nodes in the 2nd layer	10
neural networks input	Displacement Velocity Acceleration
neural networks output	Force

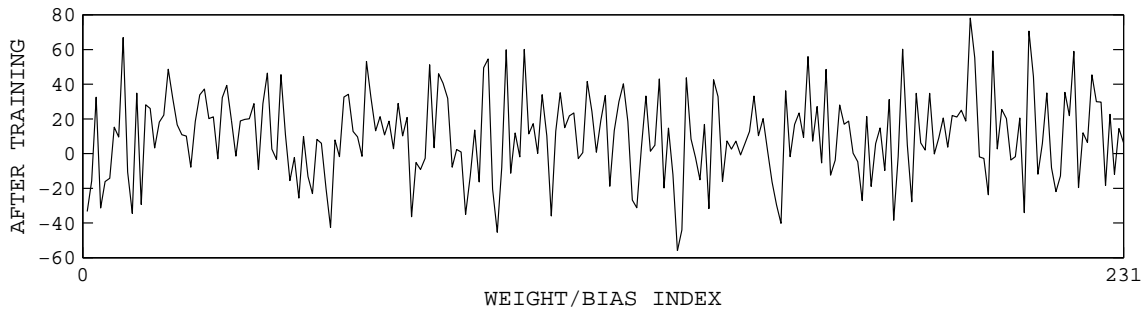
random search decreased and converged during the training phase (Figure 16.1 (c)). An example of the identification results is shown in Figure 16.2, and the normalized mean square errors are summarized in Table 16.2. The mean square error ratio varied from 1.88% to 2.05%. The entire set of the identification results are shown in Figures H.57 to H.59. Consequently, from the above results, it is inferred that the ANN can be used to identify the MR damper subjected to broadband excitation.

Table 16.2: Normalized mean square error of the measured and identified force of the MR damper.

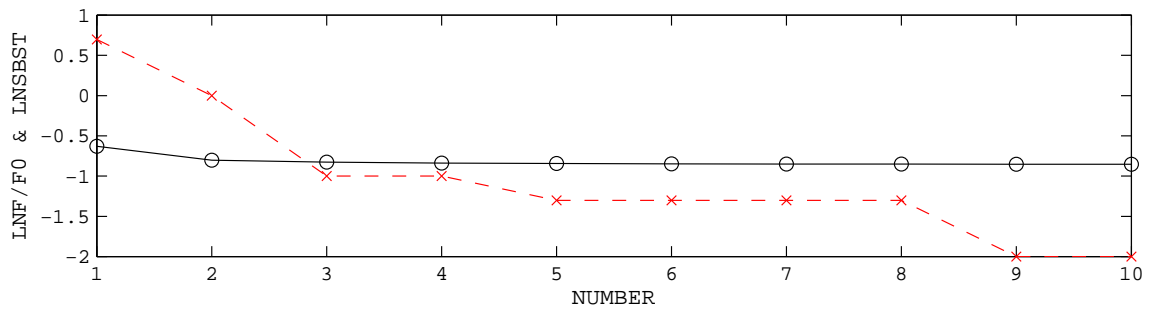
No.	Test name	Normalized MSE (%)
1	MRD1_X11V_M100_S00_00001	1.96
2	MRD1_X11V_M090_S00_00001	2.05
3	MRD1_X11V_M075_S00_00001	1.88



(a) Weights and bias before training

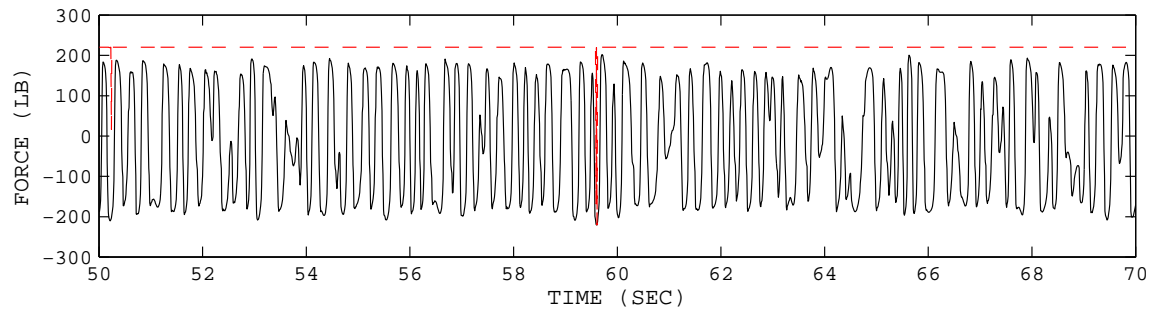


(b) Weights and bias after training

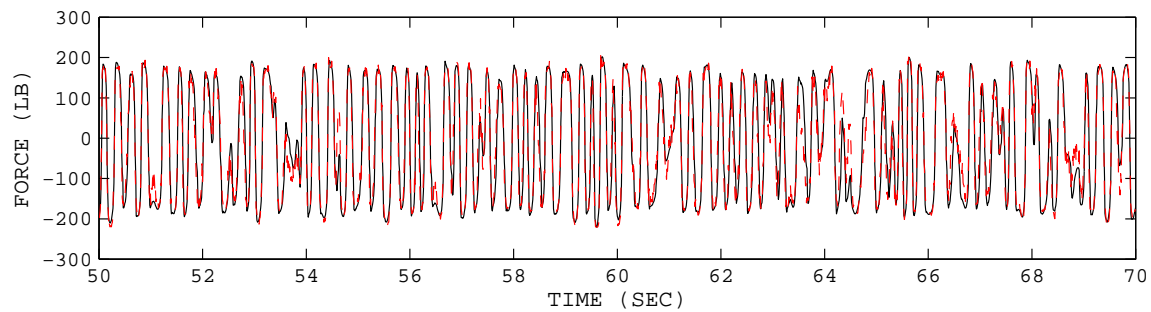


(c) RMSE ratio after training

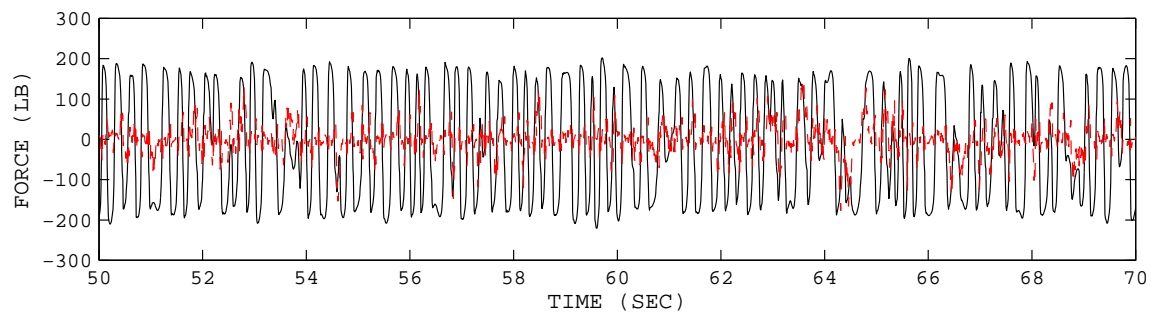
Figure 16.1: Ratio of the current error function for the nominal case normalized by the starting error function (solid line) and the current optimal standard deviation of random step size (dashed line). The y-axis is plotted in log scale.



(a) Force before training



(b) Force after training



(c) Error after training

Figure 16.2: Comparison of the measured and identified damper response to broadband excitation using ANN for 1.0 ampere input current (MRD1\_X11V\_M100\_S00\_00001\_001). The solid line is the measured force, and the dashed line is the identified force.

## Chapter 17

# DETECTION OF CHANGES IN STRUCTURAL CHARACTERISTICS FOR THE MAGNETO-RHEOLOGICAL DAMPER

One of the main goals of this study was to demonstrate that the proposed nonparametric identification techniques can be used to detect relatively small changes in the damper characteristics. Two methods of detecting the MR damper response change were tested: (1) the restoring force method and (2) the artificial neural networks.

### 17.1 Change Detection Using the Restoring Force Method

To verify that the damper characteristics can be detected using the restoring force method, the Chebyshev coefficients for three levels of the MR damper input cases were tested: 100% (1.0 ampere, nominal), 90% (0.9 ampere), and 75% (0.75 ampere) input current. As described in Section 13.1, ten tests for each current level were identified by the RFM (Figure 17.1). Once the identification was completed for all 30 tests (3 input current levels, each tested 10 times), the corresponding Chebyshev coefficients were averaged for each input current level. The first order stiffness and damping coefficients, as well as the third order damping term, are summarized in Table 17.1 and Figure 17.2. As shown in the figure, the dominant term for the damper response was the first order damping coefficient of 252.20. The first order stiffness and third order damping coefficients were also measured as 101.38 and -65.21, respectively. Once the averaged Chebyshev coefficients were obtained, the ratio of each coefficient was calculated with respect to the nominal case. The

Table 17.1: Stiffness and damping coefficients of MR-damper subjected to broadband excitation at different input current levels.

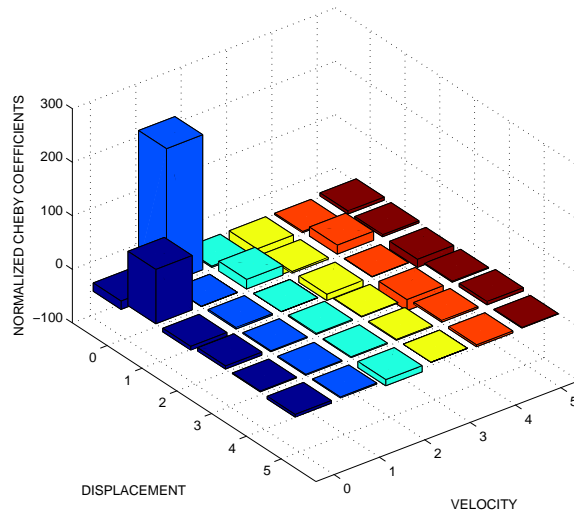
INPUT CURRENT LEVEL	STIFFNESS( $C_{10}$ )		DAMPING ( $C_{01}$ )		DAMPING ( $C_{03}$ )	
	value	ratio	value	ratio	value	ratio
100%	101.38	1.000	252.20	1.000	-65.21	1.000
90%	98.61	0.973	243.43	0.965	-61.79	0.948
75%	86.07	0.849	228.88	0.901	-59.40	0.911

ratio of the lower order Chebyshev coefficients is shown in Figure 17.3. The figure shows that both the stiffness and damping coefficients decreased, as the input current decreased. With the 25% reduction of the input current, the first order stiffness was reduced by 15%, while the first and third order damping were reduced by 10%. It was found that the change of the MR damper input current was proportional to the change of the Chebyshev coefficients, but not linearly proportional.

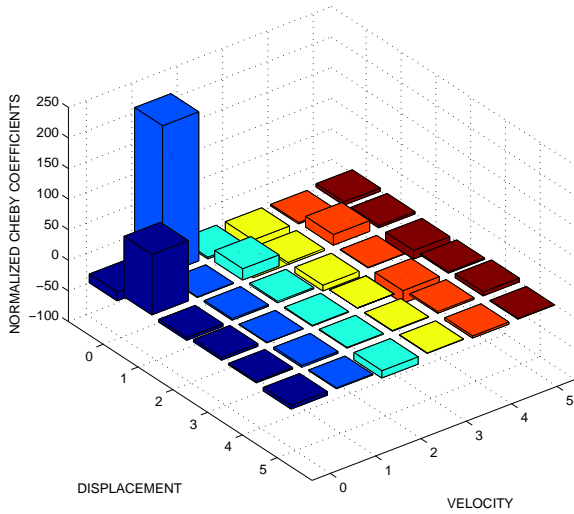
## 17.2 Detection of Change for the Damper Dynamic Response Using the ANN

The ANN method was also applied to detect the change of structural characteristics (i.e., the input current change) for the MR damper. The same data sets of the nominal (100%), 90%, and 75% cases for the RFM identification were used in the ANN identification. First, the neural networks were trained with the data set for the nominal case. The training result for the nominal case is shown in Figure 17.4 (a). Once the neural networks were trained with the nominal case data set, the trained networks were used to identify the MR damper for the 90% and 75% cases. The identification results for the 90% and 75% cases are shown in Figures 17.4 (b) and (c). The measured damper response is shown in a solid line in blue/red, and the identified response is a dotted line in black. Unlike the RFM, the ANN identification results show that the change of the MR damper is not detectable for the tested levels of the MR damper changes.

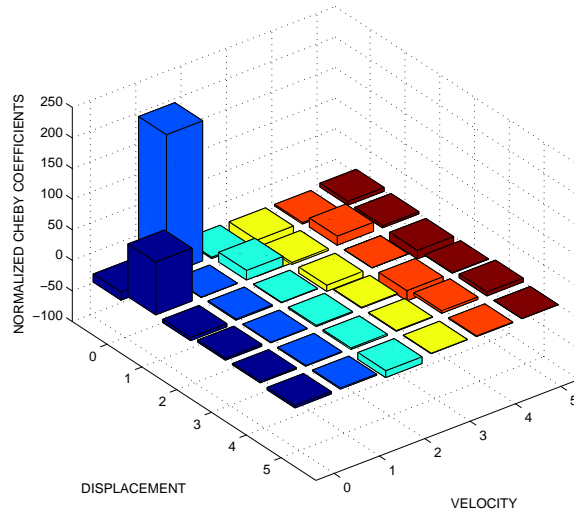
AVERAGED NORMALIZED CHEBYSHEV COEFFICIENTS



(a) 1.00 ampere (100%, nominal case)



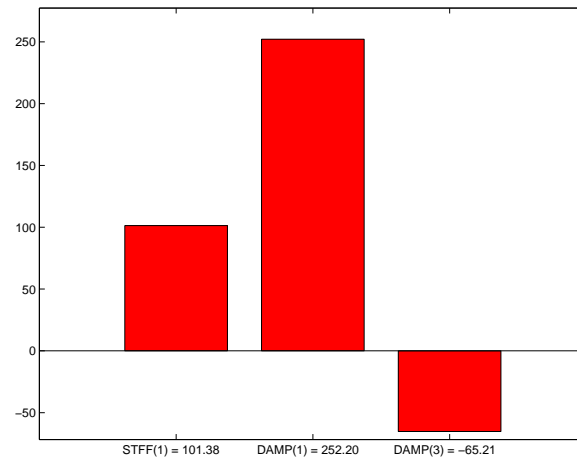
(b) 0.90 ampere (90%)



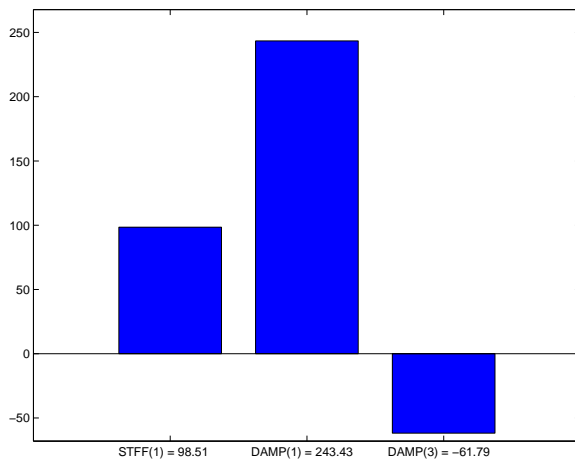
(c) 0.75 ampere (75%)

Figure 17.1: The averaged normalized Chebyshev coefficients with the 5th order curve fitting for different MR-damper input currents. The tested input currents were 1, 0.90 and 0.75 amperes for 100%, 90% and 75%, respectively.

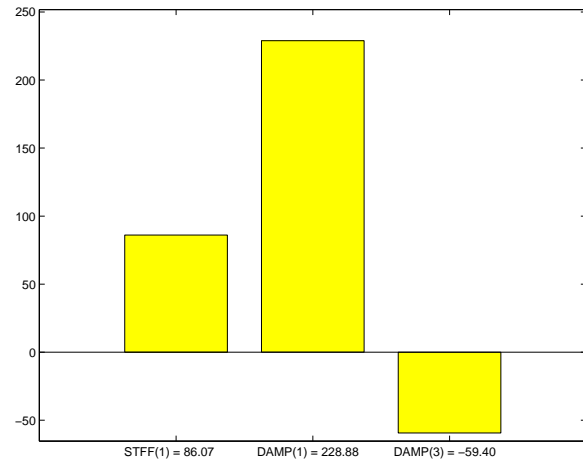
## AVERAGED NORMALIZED CHEBYSHEV COEFFICIENTS



(a) 1.00 ampere (100%, nominal case)



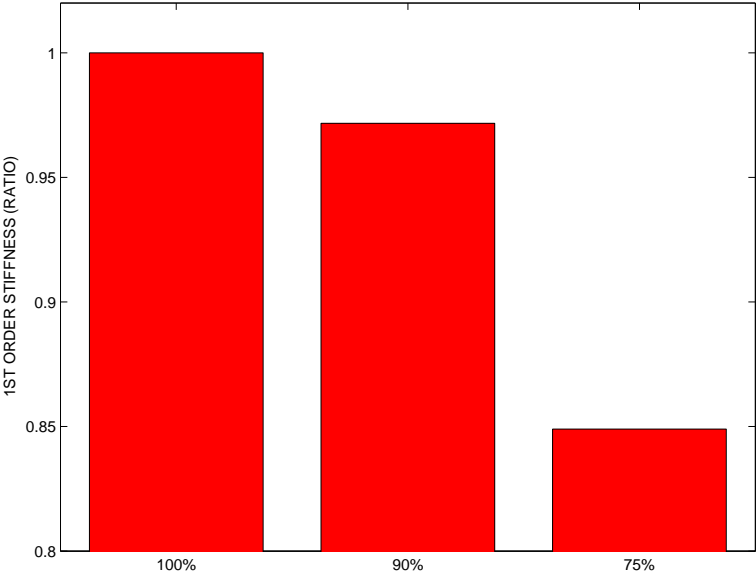
(b) 0.90 ampere (90%)



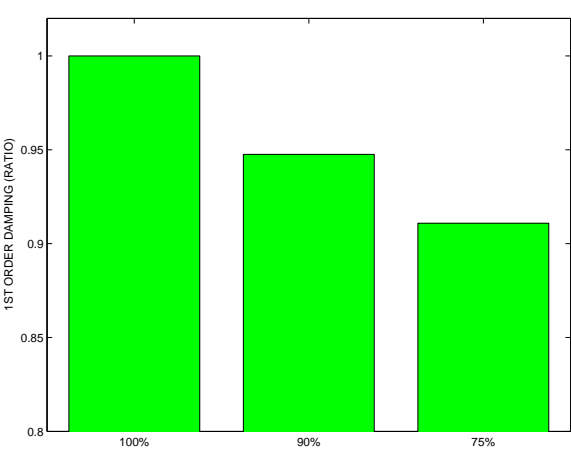
(c) 0.75 ampere (75%)

Figure 17.2: The first and third order RFM coefficients of the MR-damper subjected to broadband excitation for 1.0, 0.9 and 0.75 ampere input currents. The 1.0 ampere is the nominal case.

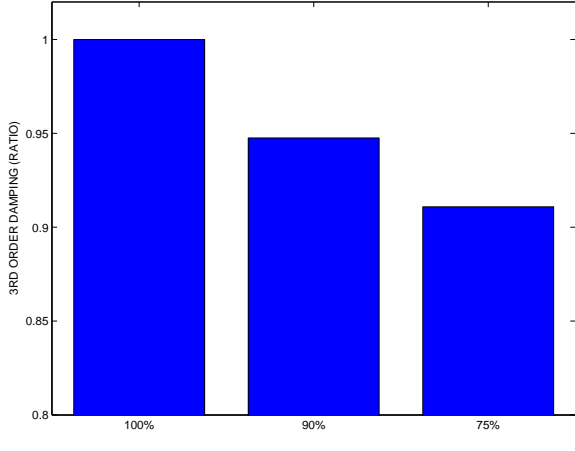
RATIO OF AVERAGED NORMALIZED CHEBYSHEV COEFFICIENTS



(a) 1st order stiffness

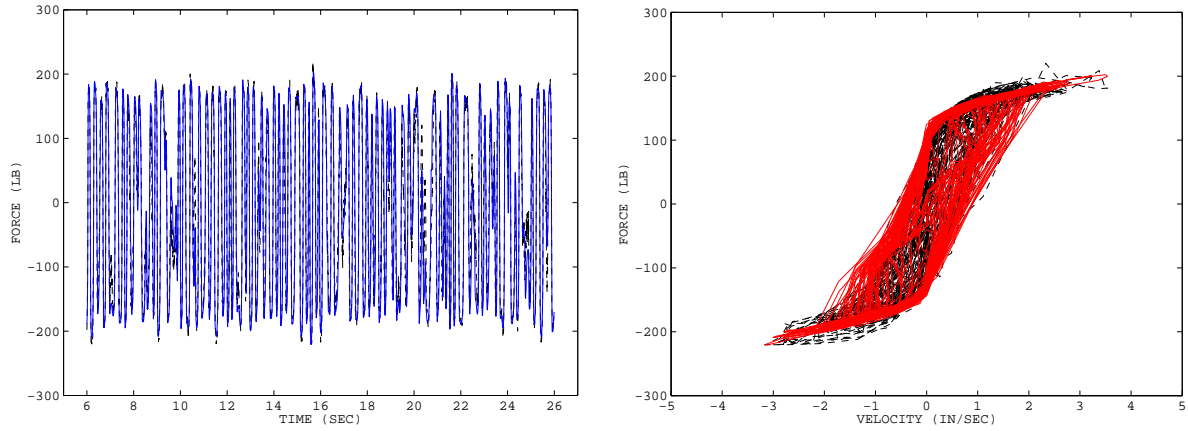


(b) 1st order damping

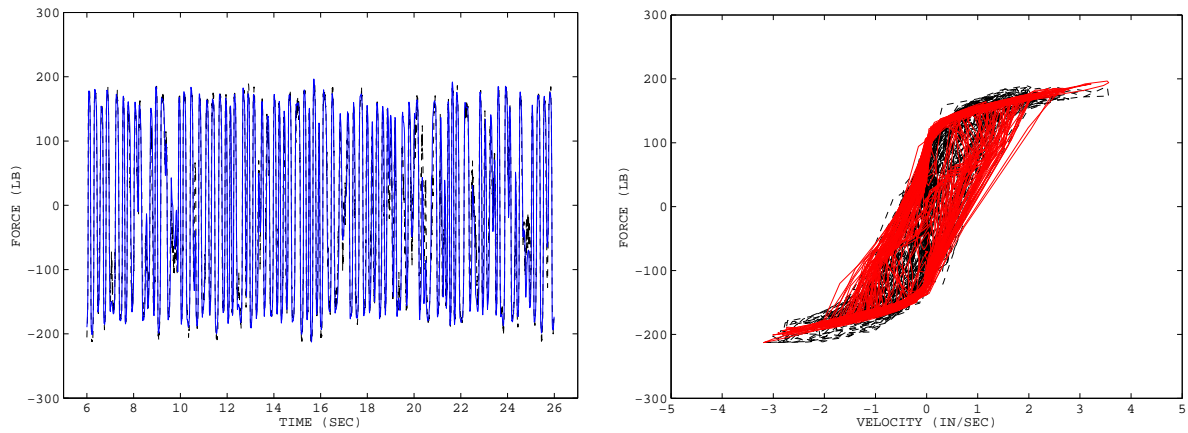


(c) 3rd order damping

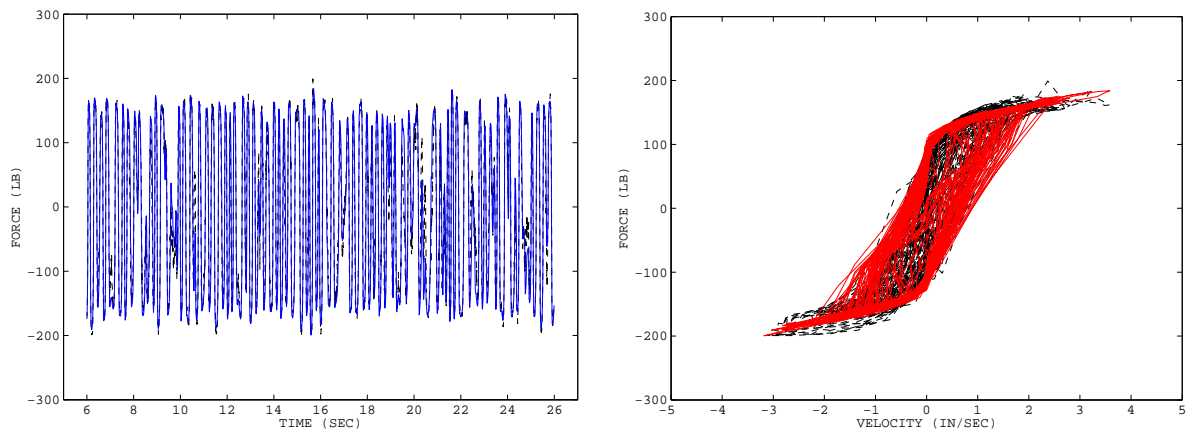
Figure 17.3: The ratio of the first and third order RFM coefficients of the MR-damper subjected to broadband excitation for 1.0 ampere input current (nominal case).



(a) 1.00 ampere (100%, nominal case)



(b) 0.90 ampere (90%)



(c) 0.75 ampere (75%)

Figure 17.4: Comparison of the estimated and measured damping response using the ANN for different MR-damper input current levels. The measured damper response is a solid line (blue and red), and the estimated damper response is a dotted line (black).

# Chapter 18

## DISCUSSION

### 18.1 Identification Results of the 250 Kip Viscous Damper

In order to compare the identification results of the 250 kip damper, the maximum measured force in each data set has been compared to the absolute equivalent design force, and the maximum identified force from the identification techniques. Table 18.1 summarizes the force comparison of all data sets, where column 1 is the data set name, column 2 is the maximum measured force, column 3 is the absolute equivalent design force, columns 4 to 7 are the maximum identified force from the parametric identifications (on-line/off-line methods), the artificial neural network identification, and the restoring force method of the 250 kip viscous damper. The equivalent design force is calculated based on the design formula (Eqn. 2.6), the corresponding measured velocity for the maximum force in each test, and the manufacturer design parameters ( $C = 60$  kip sec/in and  $n = 0.35$ ).

The normalized errors with respect to the maximum measured force are summarized in Table 18.2. The normalized mean-square-error (Eqn. 2.9) of the measured force, and the estimated forces calculated by using the proposed parametric and nonparametric identification techniques (Chapter 2) are summarized in Table 18.3. The comparative data from Table 18.3 indicate that the method which resulted in the smallest identification error was the artificial neural network method, whereas the on-line parametric identification using the design model resulted in the largest error. The following observations are derived from the results in Tables 18.2 and 18.3:

1. The largest mean-square error for the on-line parametric identification may be due to using constant coefficients (i.e.,  $C = 60$  and  $n = 0.35$ ). Although the design specifications (usually maximum velocity and maximum displacement in damper design) are satisfied using these coefficients, the actual dynamic behavior of a constructed damper could be highly non-linear. That is, the coefficients  $C$  and  $n$  could vary at different damper velocities and displacements.

Table 18.1: Comparison of the maximum measured force, absolute equivalent design force, identified force from the parametric identifications (on-line/off-line methods), the artificial neural network identification, and the restoring force method of the 250 kip viscous damper. The equivalent design force is calculated based on the design formula (Eqn. 2.6), the corresponding measured velocity for the maximum force in each test, and the manufacturer design parameters ( $C = 60$  kip sec/in and  $n = 0.35$ ).

Test Name	Maximum Measured Force (kip)	Absolute Eqv. Design Force (kip)	Identified Force			
			On-line PI (kip)	Off-line PI (kip)	RFM (kip)	ANN (kip)
UCB1_10.4	152.55	132.24	135.70	141.45	144.13	154.37
UCB1_10.5	154.26	133.40	141.47	148.46	149.91	148.76
UCB1_10.6	158.57	133.84	147.43	145.83	146.47	152.17
UCB1_12.4	165.67	142.16	145.10	151.43	157.65	150.17
UCB1_12.5	163.18	144.32	151.94	153.98	150.52	150.23
UCB1_12.6	163.33	144.16	158.98	154.14	159.62	151.44
UCB1_12.7	163.38	144.81	157.63	153.99	152.17	156.59
UCB1_15.4	173.18	152.46	152.91	161.99	156.29	170.89
UCB1_15.5	171.89	151.39	159.91	163.38	168.08	157.26
UCB1_15.6	173.20	153.46	167.18	161.98	160.74	159.33
UCB1_15.7	171.81	152.23	170.50	164.79	166.36	168.02
UCB1_17.4	175.35	158.70	158.10	168.58	166.64	165.75
UCB1_17.5	175.66	159.28	167.67	171.67	171.55	164.39
UCB1_17.6	174.88	159.65	168.97	172.34	168.62	174.88
UCB1_17.7	176.22	156.80	173.32	170.93	167.83	167.83

Table 18.2: Normalized mean-square-error comparison of the various identification techniques for the 250 kip viscous damper. The error is computed based on the difference between the measured force and the identified force, in percent.

Test Name	Maximum Measured Force	Absolute Eqv. Design Force	Identification Technique			
			On-line	Off-line	RFM	ANN
UCB1_10_4	0.00%	13.31%	11.05%	7.28%	5.52%	1.19%
UCB1_10_5	0.00%	13.52%	8.29%	3.76%	2.82%	3.57%
UCB1_10_6	0.00%	15.60%	7.03%	8.03%	7.63%	4.04%
UCB1_12_4	0.00%	14.19%	12.42%	8.60%	4.84%	9.36%
UCB1_12_5	0.00%	11.56%	6.89%	5.64%	7.76%	7.94%
UCB1_12_6	0.00%	11.74%	2.66%	5.63%	2.27%	7.28%
UCB1_12_7	0.00%	11.37%	3.52%	5.75%	6.86%	4.16%
UCB1_15_4	0.00%	11.96%	11.70%	6.46%	9.75%	1.32%
UCB1_15_5	0.00%	11.93%	6.97%	4.95%	2.22%	8.51%
UCB1_15_6	0.00%	11.40%	3.48%	6.48%	7.19%	8.01%
UCB1_15_7	0.00%	11.40%	0.76%	4.09%	3.17%	2.21%
UCB1_17_4	0.00%	9.50%	9.84%	3.86%	4.97%	5.47%
UCB1_17_5	0.00%	9.32%	4.55%	2.27%	2.34%	6.42%
UCB1_17_6	0.00%	8.71%	3.38%	1.45%	3.58%	0.00%
UCB1_17_7	0.00%	11.02%	1.65%	3.00%	4.76%	4.76%
Average	0.00%	11.77%	6.28%	5.15%	5.05%	4.95%

The varying coefficients for the constructed damper are usually unknown. In this case, the nonparametric identification techniques, such as the restoring force method and the artificial neural networks, can be more adequate than the parametric identification techniques. The identification results in Table 18.3 confirm this explanation.

2. The nonparametric identification techniques are recommended for the identification of the 250 kip viscous damper. It is known that the nonparametric identification techniques are suitable for the applications of health monitoring, vibration signature analysis and damage detection, while the parametric identification techniques are suitable for design and control applications (Soong, 1998).
3. Comparing *only* the maximum measured force and the maximum identified force would mislead engineers in the interpretation of the identification results. For example, the error of the maximum forces for the data set UCB1\_15.7 in Table 18.2 is the smallest (0.76%) for the on-line identification, which is contrary to the normalized mean-square-error (5.60%) in Table 18.3.

Table 18.3: Error comparison of the various identification techniques for the 250 kip viscous damper. The error is computed based on the difference between the maximum measured force and the maximum identified force in percents.

Test Name	Identification Technique			
	MSE On-line Identification	MSE Off-line Identification	MSE Restoring Force Method	MSE Artificial Neural Networks
UCB1_10_4	4.00%	2.00%	0.74%	0.13%
UCB1_10_5	5.74%	3.49%	1.61%	0.09%
UCB1_10_6	5.50%	3.27%	1.56%	0.10%
UCB1_12_4	6.22%	2.87%	1.69%	0.10%
UCB1_12_5	6.24%	3.07%	1.08%	0.10%
UCB1_12_6	5.79%	3.04%	2.31%	0.15%
UCB1_12_7	5.19%	3.15%	1.66%	0.09%
UCB1_15_4	6.25%	2.78%	1.32%	0.23%
UCB1_15_5	5.99%	2.86%	1.02%	0.12%
UCB1_15_6	4.79%	3.01%	0.74%	0.12%
UCB1_15_7	5.60%	2.94%	1.64%	0.10%
UCB1_17_4	6.19%	2.75%	0.74%	0.15%
UCB1_17_5	6.03%	2.82%	0.66%	0.11%
UCB1_17_6	6.06%	2.81%	0.72%	0.23%
UCB1_17_7	5.48%	2.82%	0.67%	0.10%
Average	5.67%	2.91%	1.21%	0.13%

## 18.2 Identification Results for the 15 Kip Viscous Damper

With the proposed identification techniques (Chapter 2), the maximum measured force in each data set has been compared to the absolute equivalent design force, and the maximum identified forces (Tables 18.4, 18.5, 18.6 for on-line parametric identification, off-line parametric identification, and nonparametric identification, respectively). The results from each identification technique are presented in separate tables because (unlike the 250 kip damper case) the damper was subjected to broadband excitation for longer duration, and different data ranges had to be used in the identification due to the nature of each technique, which resulted in different maximum measured forces for each technique.

The normalized mean-square-error (Eqn. 2.9) for the 15 kip viscous damper data sets for each identification technique are provided in Table 18.7. The average normalized mean-square-errors for all data sets are shown in the last row in Table 18.7. Based on the above results, the following observation can be made:

1. Overall, the artificial neural networks provide the best fit, while the on-line parametric identification technique provides the worst, in terms of normalized mean-square-error.
2. It is highly recommended to use random excitation in the identification of a viscous damper. For the purpose of reliable damper identification, a damper must be excited in a broad band to obtain various amplitude and frequency damper responses within the ranges of interest. By combining “chirp” excitation (fixed amplitude and varying frequency) and “beating” excitation (fixed frequency and varying amplitude), wide ranges of amplitude and frequency responses can be obtained. Using random excitation (varying frequency and amplitude), an experiment can be conducted much faster.
3. It is recommended to use the nonparametric identification techniques for the 15 kip damper. As shown in Tables 18.4 to 18.6, better identification results are derived from the artificial neural networks and the restoring force method. These observations agree with similar ones obtained from the 250 kip damper identification. It is known that the nonparametric identification methods are more efficient than the parametric identification ones in structural health monitoring, vibration signature analysis and damage detection (Soong, 1998).

Table 18.4: Comparison of the maximum measured force, absolute equivalent design force, and identified force from the on-line parametric identification method of the 15 kip viscous damper. The equivalent design force is calculated based on the design formula (Eqn. 2.6), the corresponding measured velocity for the maximum force in each test, and the manufacturer design parameters ( $C = 0.70$  kip sec/in and  $n = 1.00$ ).

Test Name	Maximum Measured Force (kip)	Absolute Equivalent Design Force (kip)	On-line Identified Force (kip)
First round of testing			
Qtr4.01	3.79	4.05	3.28
Qtr4.0125	5.00	5.12	4.35
Second round of testing			
usc_10175_q4	4.32	4.99	4.44
usc_10200_q4	4.72	5.63	4.90
usc_5300_q4	3.96	4.32	3.96
usc_5400_q4	5.17	5.66	5.16

Table 18.5: Comparison of the maximum measured force, absolute equivalent design force, and identified force from the off-line parametric identification method of the 15 kip viscous damper. The equivalent design force is calculated based on the design formula (Eqn. 2.6), the corresponding measured velocity for the maximum force in each test, and the manufacturer design parameters ( $C = 0.70$  kip sec/in and  $n = 1.00$ ).

Test Name	Maximum Measured Force (kip)	Absolute Equivalent Design Force (kip)	Off-line Identified Force (kip)
First round of testing			
Qtr4.01	2.49	2.40	2.08
Qtr4.0125	3.86	3.68	3.20
Second round of testing			
usc_10175_q4	3.04	3.32	2.93
usc_10200_q4	4.50	4.88	3.93
usc_5300_q4	3.96	4.35	3.82
usc_5400_q4	5.12	5.63	4.63

Table 18.6: Comparison of the maximum measured force, absolute equivalent design force, and maximum RFM-identified force of the 15 kip viscous damper for the test duration of 50 - 70 seconds. The absolute equivalent design force is calculated based on the design formula (Eqn. 2.6), the corresponding measured velocity for the maximum force in each test, and the manufacturer design parameters ( $C = 0.7$  kip sec/in and  $n = 1.0$ ).

Test Name	Max measured force (kip)	Absolute equivalent design force (kip)	Identified force (kip)
First round of testing - Using RFM			
Qtr1.01	3.08	1.20	2.62
Qtr2.01	3.68	1.24	3.97
Qtr3.01	3.70	1.27	3.98
Qtr4.01	3.57	1.24	3.68
Qtr1.0125	4.08	1.30	3.97
Qtr2.0125	4.44	1.35	4.73
Qtr3.0125	5.35	1.39	5.40
Qtr4.0125	4.45	1.33	4.68
Second round of testing - Using ANN			
usc_10175_q4	7.02	3.25	6.87
usc_10200_q4	8.05	3.59	7.88
usc_5300_q4	5.29	2.49	4.97
usc_5400_q4	6.95	3.15	6.79

Table 18.7: Normalized mean-square-error comparison of the various identification techniques for the 15 kip viscous damper. The error is computed based on the difference between the maximum measured force and the maximum identified force, in percent.

Test Name	Identified Force			
	On-line PI (kip)	Off-line PI (kip)	RFM (kip)	ANN (kip)
Qtr4.01	6.10%	4.72%	5.29%	—
Qtr4.0125	6.40%	4.62%	6.76%	—
usc_10175_q4	6.70%	3.26%	—	2.53%
usc_10200_q4	6.40%	3.28%	—	2.38%
usc_5300_q4	4.40%	2.47%	—	2.05%
usc_5400_q4	6.00%	2.38%	—	1.19%
Average	6.00%	3.46%	6.03%	2.04%

### 18.2.1 Comparison of the identified manufacturer parameters the damping coefficient $C$ and the exponent $n$

Tables 18.8 to 18.10 show the identified parameters of the 250 kip damper for the on-line identification technique (Section 2.2.1). The following issues are worth noting, based on the identification results:

1. The identification results show that the identified damping coefficients are under-estimated by 28%, and the identified exponent is over-estimated by 29% with respect to the design coefficients. It is also found that the under-estimation of the damping coefficient, and the over-estimation of the exponent increase, as the excitation velocity increases.
2. By the nature of the technique, the on-line identification requires long test durations for the coefficient values to reach their asymptotic values. The available test data for the 250 kip damper had mostly 6 cycles, and only 4 cycles were used in the identification, after the signal processing work-steps to obtain the velocity and acceleration by differentiating the measured displacement. The identification results can be more reliable with longer test durations and “richer” frequencies (Ioannou & Sun, 1996).

Table 18.8: Summary of the on-line parametric identification results for the 250 kip damper data sets. Column 1 is the data set name, column 2 is the manufacturer value for the damping coefficient  $C$ , column 3 is the average value of the identified damping coefficient  $\hat{C}$ , column 4 is the manufacturer specification value for the exponent  $n$ , column 5 is the average value of the identified exponent  $\hat{n}$  (Eqn. 2.6), column 6 is the selected value of the forgetting factor ( $\beta$ ) in the on-line identification algorithm (Eqn. 2.5), and column 7 is the normalized mean-square-error percentage of the difference between the predicted force and the measured force.

Data set Name	Damping Coeff. $C$ (kip sec/in)		Exponent $n$		$\beta$ forgetting factor	% MSE error
	Damper Spec.	Identified	Damper Spec.	Identified		
UCB1_10_4	60.00	54.32	0.35	0.37	1.0	4.00
UCB1_10_5	60.00	48.55	0.35	0.44	1.0	5.74
UCB1_10_6	60.00	51.67	0.35	0.43	1.0	5.50
UCB1_12_4	60.00	49.72	0.35	0.41	1.0	6.22
UCB1_12_5	60.00	47.24	0.35	0.45	1.0	6.24
UCB1_12_6	60.00	47.90	0.35	0.45	1.0	5.79
UCB1_12_7	60.00	47.06	0.35	0.46	1.0	5.19
UCB1_15_4	60.00	44.58	0.35	0.45	1.0	6.25
UCB1_15_5	60.00	42.76	0.35	0.48	1.0	5.99
UCB1_15_6	60.00	44.60	0.35	0.46	1.0	4.79
UCB1_15_7	60.00	45.55	0.35	0.47	1.0	5.60
UCB1_17_4	60.00	42.91	0.35	0.46	1.0	6.19
UCB1_17_5	60.00	41.94	0.35	0.48	1.0	6.03
UCB1_17_6	60.00	40.69	0.35	0.49	1.0	6.06
UCB1_17_7	60.00	45.21	0.35	0.45	1.0	5.48

Table 18.9: Summary of the on-line parametric identification results for the 15 kip damper of the data sets in the first round of testing. Column 1 is the data set name, column 2 is the manufacturer value for the damping coefficient  $C$ , column 3 is the average value of the identified damping coefficient  $\hat{C}$ , column 4 is the manufacturer specification value for the exponent  $n$ , column 5 is the average value of the identified exponent  $\hat{n}$  (Eqn. 2.6), column 6 is the selected value of the forgetting factor ( $\beta$ ) in the on-line identification algorithm (Eqn. 2.5), and column 7 is the normalized mean-square-error percentage of the difference between the predicted force and the measured force.

Data set Name	Damping Coeff. $C$ (kip sec/in)		Exponent $n$		$\beta$ forgetting factor	% MSE error
	Damper Spec.	Identified	Damper Spec.	Identified		
Qtr4.01	0.70	0.50	1.00	0.26	0.8	6.1
Qtr4.0125	0.70	0.59	1.00	0.34	0.8	6.4

Table 18.10: Summary of the on-line parametric identification results for the 15 kip damper of the data sets in the first second of testing. Column 1 is the data set name, column 2 is the manufacturer value for the damping coefficient  $C$ , column 3 is the average value of the identified damping coefficient  $\hat{C}$ , column 4 is the manufacturer specification value for the exponent  $n$ , column 5 is the average value of the identified exponent  $\hat{n}$  (Eqn. 2.6), column 6 is the selected value of the forgetting factor ( $\beta$ ) in the on-line identification algorithm (Eqn. 2.5), and column 7 is the normalized mean-square-error percentage of the difference between the predicted force and the measured force.

Data set Name	Damping Coeff. $C$ (kip sec/in)		Exponent $n$		$\beta$ forgetting factor	% MSE error
	Damper Spec.	Identified	Damper Spec.	Identified		
usc_10175_q4	0.70	0.50	1.00	0.83	0.8	6.7
usc_10200_q4	0.70	0.80	1.00	0.69	0.8	6.4
usc_5300_q4	0.70	0.80	1.00	0.69	0.8	4.4
usc_5400_q4	0.70	0.50	1.00	0.89	0.8	6.0

### 18.3 Identification Results of the Magneto-Rheological Damper

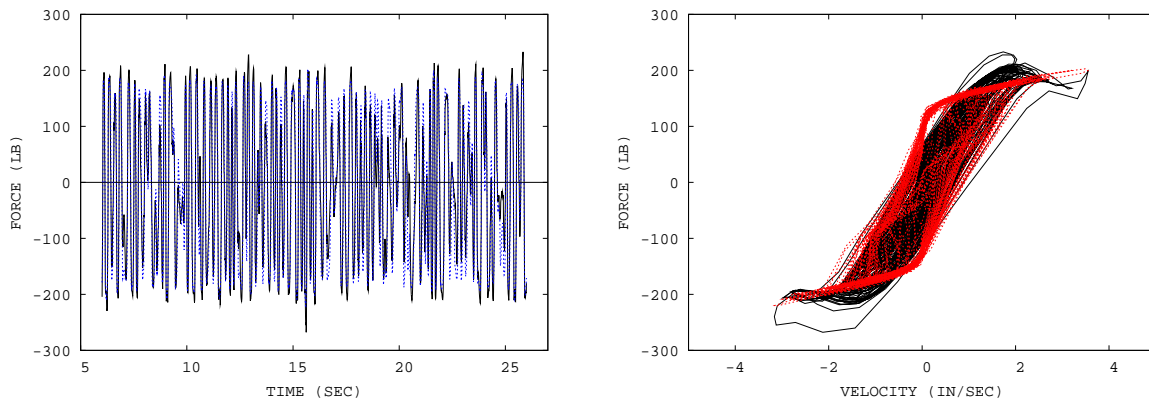
Two methods of the system change detection were discussed in Chapter 17: (1) the restoring force method (RFM), and (2) the artificial neural networks (ANN). The following can be noted from the MR damper identification results:

1. The change of the measured force was proportional to the change of the MR damper input current (not necessarily linear).
2. The change of the dynamic response for different MR damper input currents was detectable graphically (Figure 18.1). Mean-square-error levels (MSE), and normalized mean-square-errors (NMSE) of the dynamic response for the change detection in the MR damper are presented in Table 18.11. The MSE and NMSE for the training mode were calculated as  $\|f - \hat{f}\|$  and  $\|f - \hat{f}\|/\|f\|$ , respectively, where  $f$  is the measured force, and  $\hat{f}$  is the identified force using the Chebyshev coefficients (determined using the displacement and velocity for the tested data set). The MSE and NMSE for the validation mode were calculated as  $\|f - \hat{f}_{100}\|$ , and  $\|f - \hat{f}_{100}\|/\|f\|$ , respectively, where  $\hat{f}_{100}$  is the identified force using the Chebyshev coefficients (determined using the displacement and velocity for the nominal data set). The NMSE can be misleading regarding the change detection in the MR damper. That is, the NMSE in validation mode stays constant, as the MR damper input level changes, which implies that the system change is undetectable. A more appropriate measure for detecting the change of the system is the MSE ratio of  $\|f - \hat{f}_{100}\|/\|f - \hat{f}\|$ . The MSE ratio shows approximately 4% increase, as the MR damper input current decreases by 25%.
3. Using the ANN, the system change was undetectable, at the tested level of system change.

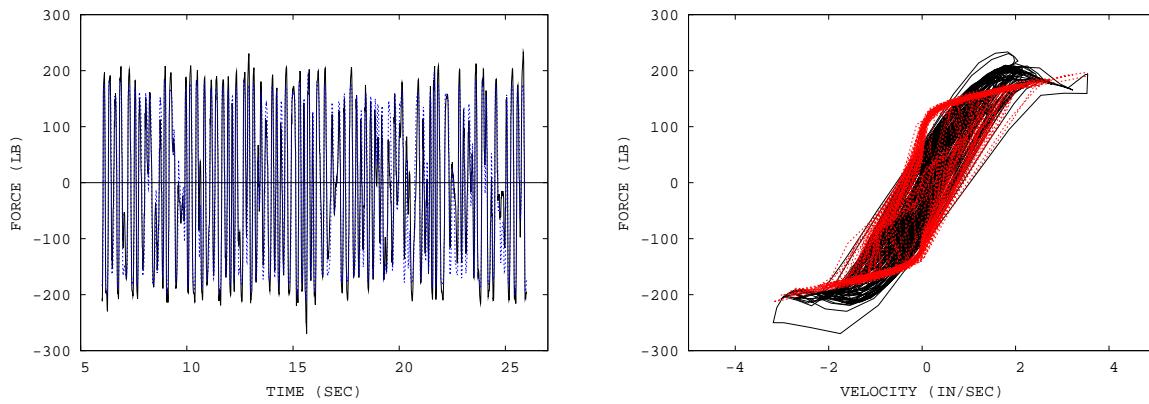
4. The change of the MR damper was most effectively detected by detecting the change of the Chebyshev coefficients at different levels of MR damper input current.

Table 18.11: Mean-square-error levels (MSE) and normalized mean-square-errors (NMSE) of the dynamic response for the change detection in the MR damper. The MSE and NMSE for the train mode are calculated as  $\|f - \hat{f}\|$ , and  $\|f - \hat{f}\|/\|f\|$ , respectively, where  $f$  is the measured force and  $\hat{f}$  is the identified force using the Chebyshev coefficients (determined using the displacement and velocity for the tested data set). The MSE and NMSE for the validation mode were calculated as  $\|f - \hat{f}_{100}\|$  and  $\|f - \hat{f}_{100}\|/\|f\|$ , respectively, where  $\hat{f}_{100}$  is the identified force using the Chebyshev coefficients (determined using the displacement and velocity for the nominal data set). The MSE ratio is calculated as  $\|f - \hat{f}_{100}\|/\|f - \hat{f}\|$ .

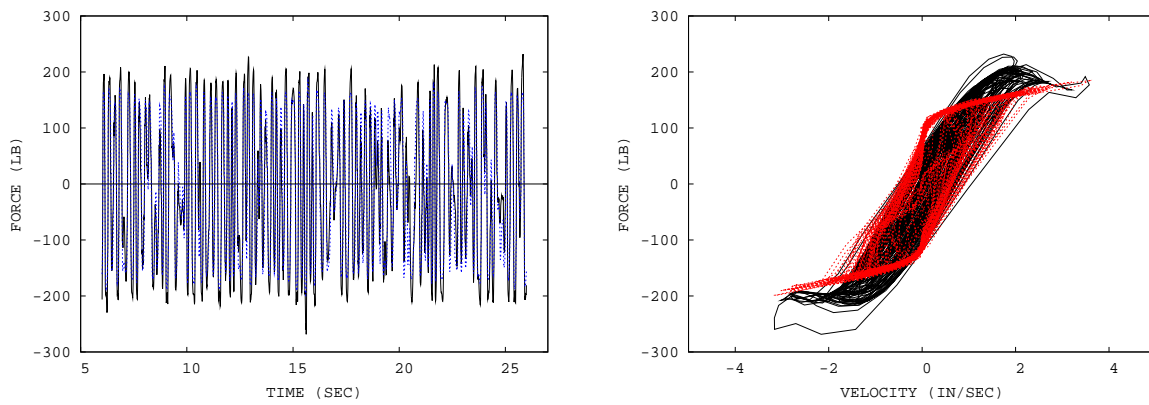
Test case	MSE - train ( $lb^2$ )	NMSE - train (%)	MSE - valid ( $lb^2$ )	NMSE - valid (%)	MSE ratio (%)
Nominal	$4.076 \times 10^6$	10.54	$4.076 \times 10^6$	10.54	100.00
90%	$3.706 \times 10^6$	10.35	$3.702 \times 10^6$	10.34	99.91
75%	$3.195 \times 10^6$	10.09	$3.319 \times 10^6$	10.48	103.87



(a) 1.00 ampere (100%, nominal case)



(b) 0.90 ampere (90%)



(c) 0.75 ampere (75%)

Figure 18.1: Comparison of the estimated and measured damping response using the RFM for different MR-damper input current levels. The measured damper response is a solid line (blue or red), and the estimated damper response is a dotted line (black). The estimated damping force was calculated with the normalized Chebyshev coefficients of the nominal case for all three cases.

## Chapter 19

# SUMMARY AND CONCLUSIONS

The goals of the project reported herein were to perform a sequence of analytical and experimental studies designed to shed more light on the numerous challenging technical issues encountered in the characterization of the physical phenomena exhibited by the nonlinear damper's structural components. Specific tasks of this research project included:

1. Perform a sequence of experimental tests to gain insight into the most sensitive indicators of slight changes in the structural characteristics of the dampers.
2. Develop a theoretical framework for processing the experimental structural response measurements to develop nonlinear, reduced-order, high-fidelity mathematical models which can be used to detect, quantify, and locate slight changes in the structural system parameters.
3. Investigate the range of validity of nonparametric system identification techniques, such as neural networks, and their utility as a sensitive tool for detecting damage in a monitored structural damper, without any a priori information about the topology or failure modes of the underlying structure.

To accomplish the goals of the project, two typical nonlinear viscous dampers, one a 250 kip size, and the other a 15 kip size, were tested at UCB, and the data were supplied to USC to perform detailed analyses using a variety of techniques for developing simplified mathematical models based on the corresponding damper response measurements.

USC also used an adaptable (“smart”) magneto-rheological (MR) damper to generate vibration measurements corresponding to modified damper characteristics, which were used to mimic changes in the damper vibration signature. The nonparametric data analysis tools that were evaluated in conjunction with the nonlinear viscous dampers, were subsequently used to detect and quantify the level of observed changes in the MR damper vibration signature.

## Findings

Two parametric (one on-line, and the other off-line), and two nonparametric (the Restoring Force Method, and Artificial Neural Networks) system identification approaches are found to be powerful tools for developing reduced order nonlinear models of the tested nonlinear dampers. Provided that the damper state variables, and induced force are available from measurements, high-fidelity mathematical models, of different forms and degrees of complexity, can be established and subsequently used for computational purposes, as well as for structural health monitoring applications.

Overall, it was found that the nonparametric identification approach provides better results for the identification and health monitoring of the tested viscous dampers, than the parametric identification method. Because of the nonlinearity of the viscous damper, it is not recommended to use the design parameters for the identification of the viscous damper's dynamic behavior.

Due to the fact that the class of dampers under investigation consists of essentially a uniaxial member whose force-deformation characteristics can be accurately and completely defined once the underlying state variables are obtained, the uncertainty bounds on the detected changes in such measurements are quite small. Hence, the methods examined in this study provide an arsenal of powerful signal processing tools that offer the potential for being reliable indicators of small changes in the underlying physical damper characteristics, which can be detected through the application of real-time structural health monitoring methodologies based on vibration signature analysis.

# REFERENCES

- ANDRONIKOU, A. M., BEKEY, G. A., & MASRI, S. F. 1982 (7-11 June). Identification of Nonlinear Hysteretic System Using Random Search. *Page 10721073 of: Proceedings of 6th IFAC Symposium on Identification and System Parameter Estimation.*
- BURTON, S. A., MAKRIS, N., KONSTANTOPOULOS, I., & ANTSAKLIS, P. J. 1996. Modeling the Response of ER Damper: Phenomenology and Emulation. *ASCE, Journal of Engineering Mechanics*, **122**(9), 897–906.
- CHANG, S.-P., MAKRIS, N., WHITTAKER, A. S., & THOMPSON, A. C. T. 2002. Experimental and analytical studies on the performance of hybrid isolation systems. *Earthquake Engineering and Structural Dynamics*, **31**(2), 421–443.
- CHASSIAKOS, A. G., MASRI, S. F., SMYTH, A. W., & ANDERSON, J. C. 1995 (June). Adaptive Methods For Identification of Hysteretic Structures. *Pages 2349–53 of: Proceedings of American Control Conference*, vol. TM15.
- CHASSIAKOS, A. G., MASRI, S. F., SMYTH, A. W., & CAUGHEY, T. K. 1998. On-Line Identification of Hysteretic Systems. *ASME, Journal of Applied Mechanics*, **65**(1), 194–203.
- GARCIA, G., BUTLER, K., & STUBBS, N. 1997. Relative performance of clustering-based neural network and statistical pattern recognition model for nondestructive damage detection. *Smart Materials and Structures*, **6**, 415–424.
- HOUSNER, G. W., BERGMAN, L. A., CAUGHEY, T. K., CHASSIAKOS, A. G., CLAUS, R. O., MASRI, S. F., SKELTON, R. E., SOONG, T. T., SPENCER, B. F., & YAO, J. T. P. 1997. SPECIAL ISSUE: Structural Control: Past, Present and Future. *ASCE, Journal of Engineering Mechanics*, **123**(9), 897–971.
- IOANNOU, P. A., & DATTA, A. 1991. Robust Adaptive Control: A Unified Approach. *Proceedings of the IEEE*, **79**(12), 1736–1768.

- IOANNOU, P. A., & SUN, J. 1996. *Robust Adaptive Control*. Prentice-Hall, Upper Saddle River, NJ.
- MA, F., ZHANG, H., BOCKSTEDTE, A., FOLIENSTE, G. C., & PAEVERE, P. 2004. Parameter Analysis of the Differential Model of Hysteresis. *Journal of Applied Mechanics*, **71**(May), 342–349.
- MAKRIS, N., & ZHANG, J. 2004. Seismic Response Analysis of a Highway Overcrossing Equipped with Elastomeric Bearing and Fluid Dampers. *ASCE, Journal of Structural Engineering*, **130**(6), 830–845.
- MASRI, S. F., & CAUGHEY, T. K. 1979. A Nonparametric Identification Technique for Nonlinear Dynamic Problems. *Journal of Applied Mechanics*, **46**(2), 433–447.
- MASRI, S. F., BEKEY, G. A., & SAFFORD, F. B. 1980. A Global Optimization Algorithm Using Adaptive Random Search. *Applied Mathematics and Computation*, **7**, 353–375.
- MASRI, S. F., CHASSIAKOS, A. G., & CAUGHEY, T. K. 1992. Structure-unknown non-linear dynamic systems: identification through neural networks. *Smart Materials and Structures*, **1**(1), 45–56.
- MASRI, S. F., CHASSIAKOS, A. G., & CAUGHEY, T. K. 1993. Identification of Nonlinear Dynamic Systems Using Neural Networks. *ASME, Journal of Applied Mechanics*, **60**(March), 123–133.
- MASRI, S. F., NAKAMURA, M., CHASSIAKOS, A. G., & CAUGHEY, T. K. 1996. Neural Network Approach to Detection of Changes in Structural Parameters. *Journal of Engineering Mechanics*, **122**(4), 350–360.
- MASRI, S. F., SMYTH, A. W., CHASSIAKOS, A. G., NAKAMURA, M., & CAUGHEY, T. K. 1999. Training Neural Networks By Adaptive Random Search Techniques. *ASCE, Journal of Engineering Mechanics*, **125**(2), 123–132.
- MASRI, S. F., SMYTH, A. W., CHASSIAKOS, A. G., CAUGHEY, T. K., & HUNTER, N. F. 2000. Application of Neural Networks for Detection of Changes in Nonlinear Systems. *ASCE, Journal of Engineering Mechanics*, **126**(7), 666–676.
- MASRI, S. F., SHENG, L. H., CAFFREY, J. P., NIGBOR, R. L., WAHBEH, M., & ABDEL-GHAFFAR, A. M. 2004. Application of a Web-enabled real-time structural health monitoring system for civil infrastructure systems. *Smart Materials and Structures*, **13**(6), 1269–1283.
- MENDEL, J. M. 1995. *Lessons in Estimation Theory for Signal Processing, Communications, and Control*. 2 edn. Prentice Hall.

- MIYAMOTO, K., & HANSON, D. R. 2002 (9-12 October). U. S. Design of Structures With Damping Systems. *In: Proceedings of Structural Engineers World Congress (SEWC 2002)*.
- SIKORSKY, C. S., STUBBS, N., BOLTON, R., CHOI, S., KARBHARI, V. M., & SEIBLE, F. 2001. Measuring bridge performance using a structural health monitoring system. *Pages 179–190 of: LIU, S.-C. (ed), Proceedings of SPIE, Smart Structures and Materials 2001: Smart Systems for Bridges, Structures, and Highways*, vol. 4330.
- SMYTH, A. W., MASRI, S. F., CHASSIAKOS, A. G., & CAUGHEY, T. K. 1999. On-line Parametric Identification of MDOF Nonlinear Hysteretic Systems. *ASCE, Journal of Engineering Mechanics*, **125**(2), 133–142.
- SMYTH, A. W., MASRI, S. F., KOSMATOPOULOS, E. B., CHASSIAKOS, A. G., & CAUGHEY, T. K. 2002. Development of Adaptive Modeling Techniques for Nonlinear Hysteretic Systems. *International Journal of Non-Linear Mechanics*, **37**, 1435–51.
- SOONG, T. T. 1998. Experimental Simulation of Degrading Structures Through Active Control. *Earthquake Engineering and Structural Dynamics*, **27**, 143–154.
- SOONG, T. T., & DARGUSH, G. F. 1997. *Passive Energy Dissipation Systems in Structural Engineering*. John Wiley & Sons.
- SPENCER JR., B. F., DYKE, S. J., SAIN, M. K., & CARLSON, J. D. 1997. Phenomenological Model of a Magnetorheological Damper. *ASCE, Journal of Engineering Mechanics*, **123**(3), 230–238.
- WEN, Y. K. 1976. Methods of Random Vibration of Hysteretic Systems. *ASCE, Journal of Engineering Mechanics*, **102**(EM2), 249–263.
- WEN, Y. K. 1980. Equivalent Linearization for Hysteretic Systems Under Random Excitation. *Journal of Applied Mechanics*, **47**(March), 150–154.
- WEN, Y. K. 1989. Methods of Random Vibration for inelastic Structures. *ASME, Journal of Applied Mechanics*, **42**(2), 39–52.
- WORDEN, K., & TOMLINSON, G. R. 2001. *Nonlinearity in Structural Dynamics: Detection, Identification and Modelling*. Institute of Physics Pub.



# Appendices



## Appendix A

# DATA ACQUISITION AND PRELIMINARY DATA PROCESSING FOR THE 250 KIP VISCOUS DAMPER

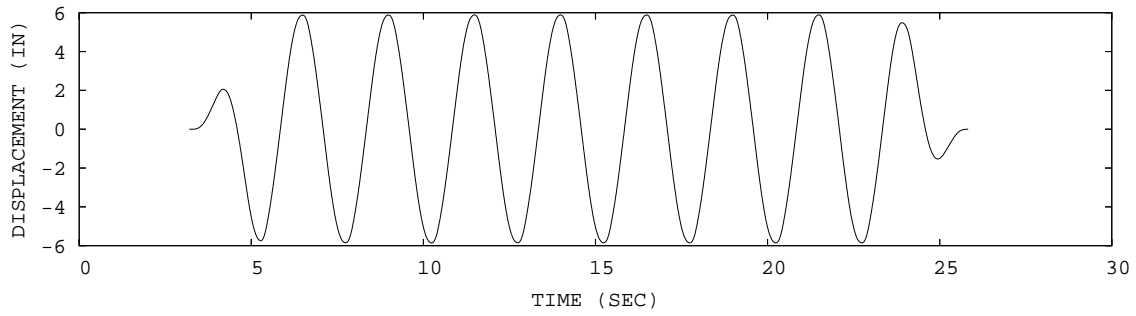
### A.1 Experimental Data (Raw) for the 250 Kip Viscous Damper

The dynamic response of the 250 kip viscous damper was obtained at the University of California, Berkeley by measuring the displacement and force. The first 20 rows of the obtained data (UCB1\_10\_4) is shown below. The entire data sets are provided in the accompanying CD in \data\UCB1\raw\ folder.

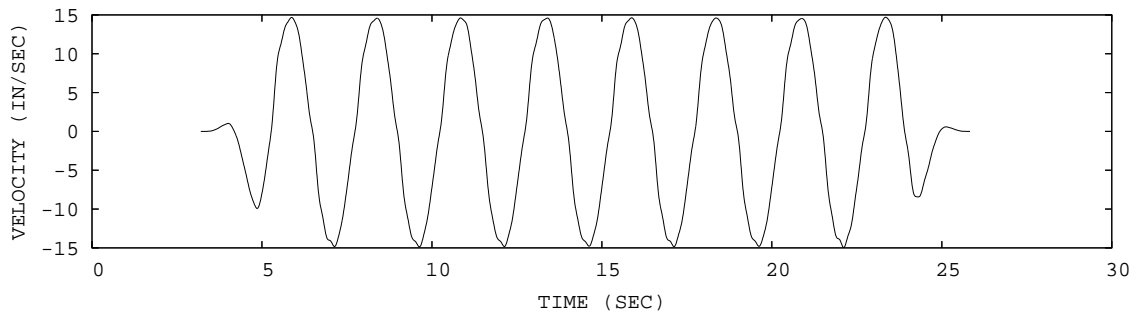
```
Disp_WP Load
in Kip
0.270152 -1.12843
0.270152 -1.12843
0.25708 -1.37024
0.283224 -1.37024
0.270152 -1.12843
0.270152 -1.37024
0.283224 -0.644819
0.270152 -1.37024
0.25708 -1.37024
0.25708 -1.37024
0.270152 -1.37024
0.309368 -1.12843
0.25708 -1.37024
0.283224 -1.12843
0.25708 -1.37024
0.25708 -1.37024
0.283224 -1.12843
0.283224 -1.85385
0.283224 -1.12843
0.25708 -1.37024
```

## A.2 Data Acquisition and Preliminary Data Processing

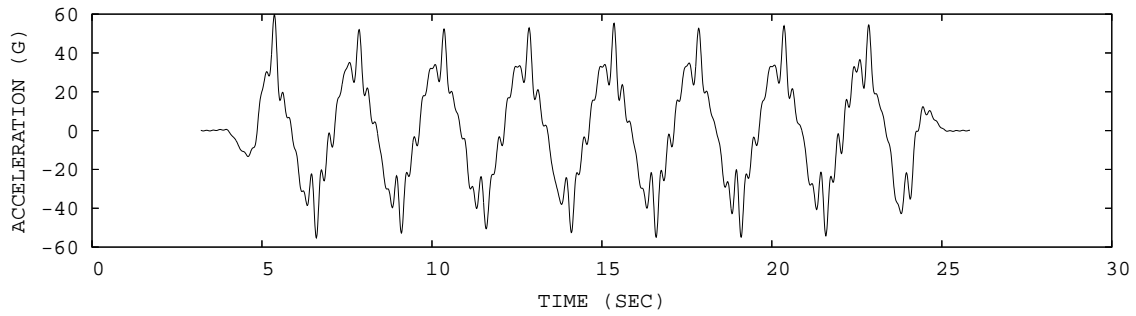
The time histories and phase plots of the 250 kip viscous damper response after preliminary data processing are shown in this section (Figs. A.1 to A.30).



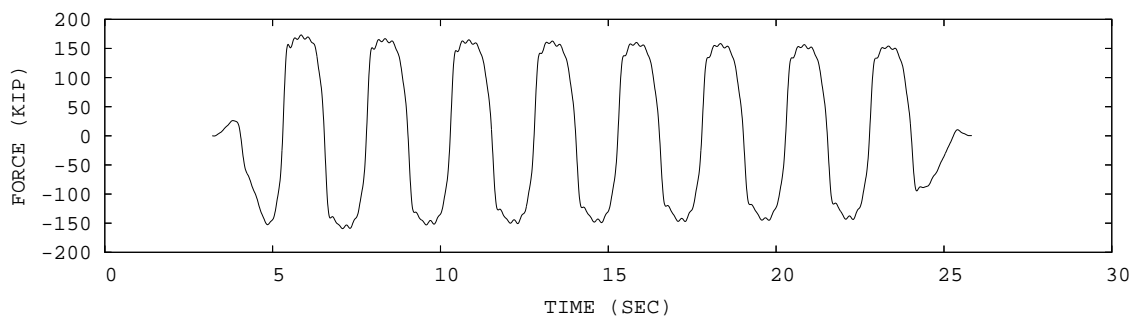
(a) Displacement



(b) Velocity



(c) Acceleration



(d) Force

Figure A.1: Time history plot of the 250 kip damper response subjected to sinusoidal excitation for the data set UCB1\_10\_4. The displacement and force were measured, and the velocity and acceleration were integrated from the displacement.

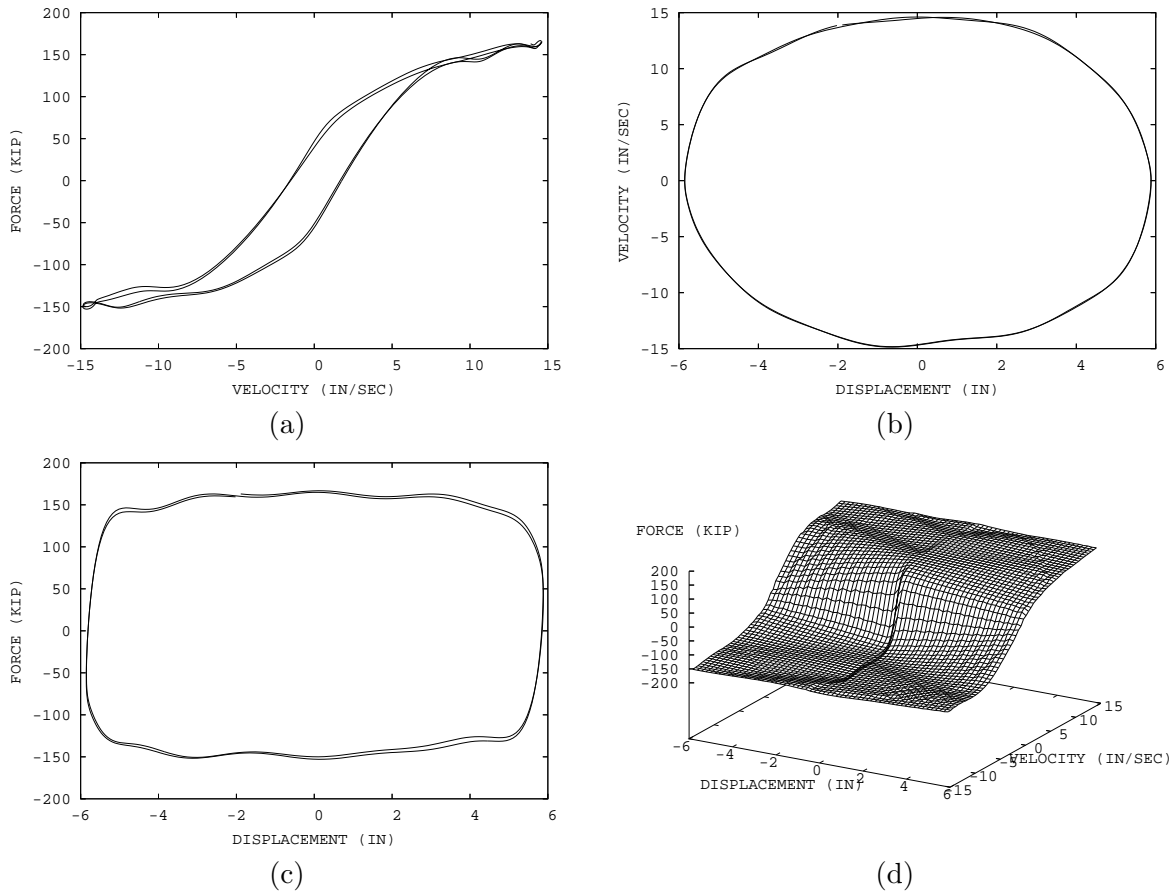
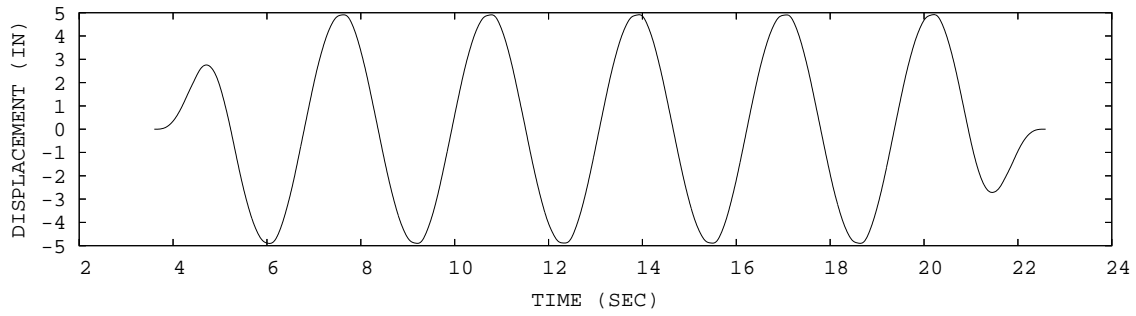
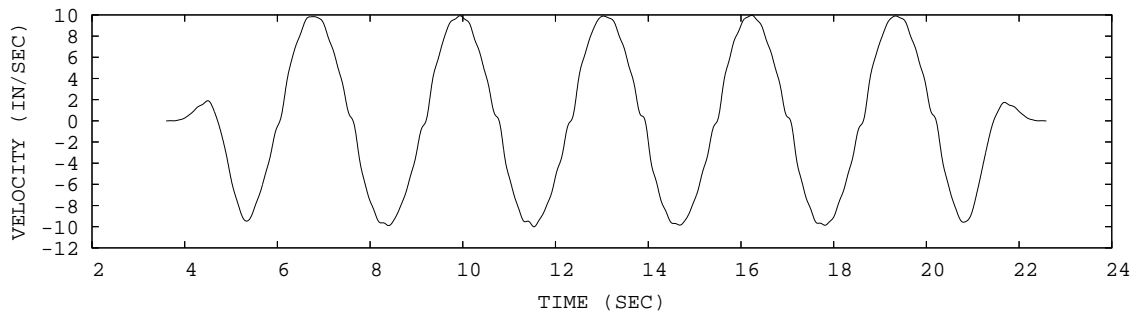


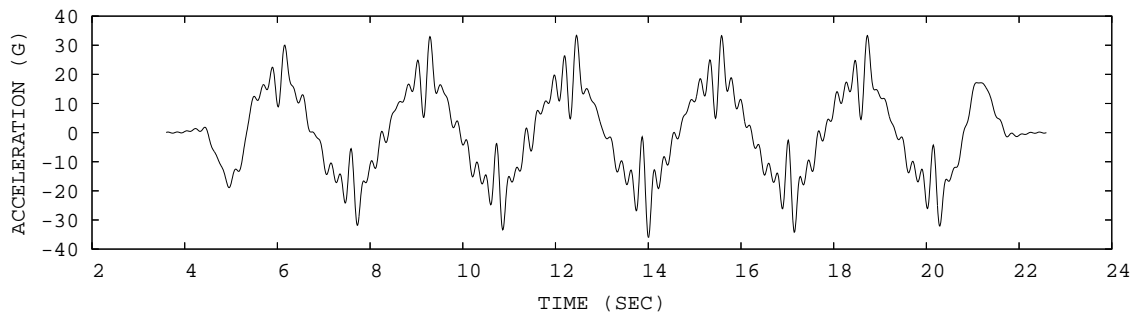
Figure A.2: Phase plot of the 250 kip damper response subjected to sinusoidal excitation for the data set UCB1\_10\_4. The displacement and force were measured, and the velocity and acceleration were integrated from the displacement.



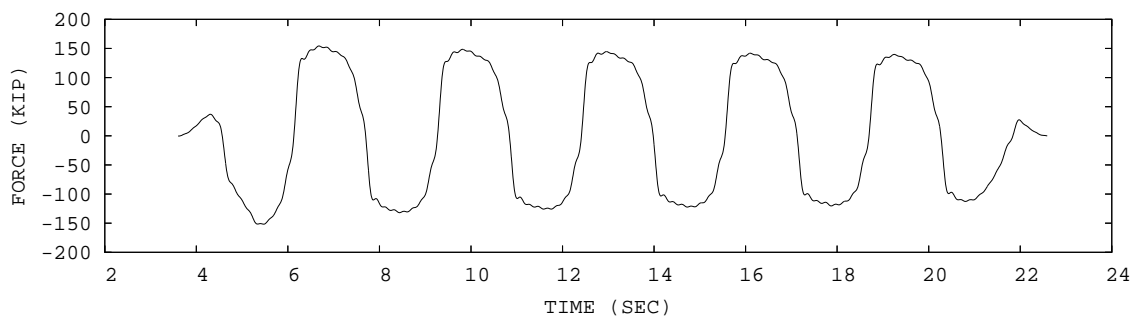
(a) Displacement



(b) Velocity



(c) Acceleration



(d) Force

Figure A.3: Time history plot of the 250 kip damper response subjected to sinusoidal excitation for the data set UCB1\_10\_5. The displacement and force were measured, and the velocity and acceleration were integrated from the displacement.

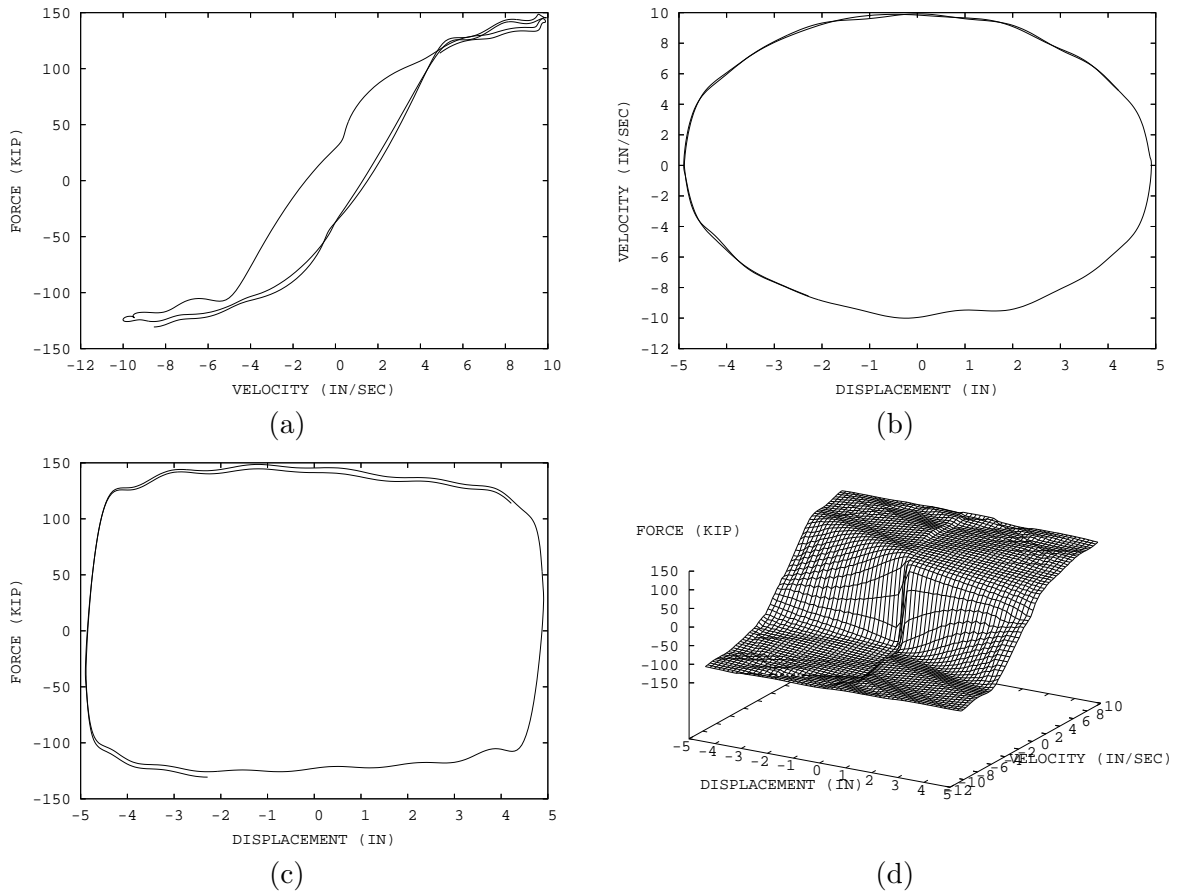


Figure A.4: Phase plot of the 250 kip damper response subjected to sinusoidal excitation for the data set UCB1\_10\_5. The displacement and force were measured, and the velocity and acceleration were integrated from the displacement.

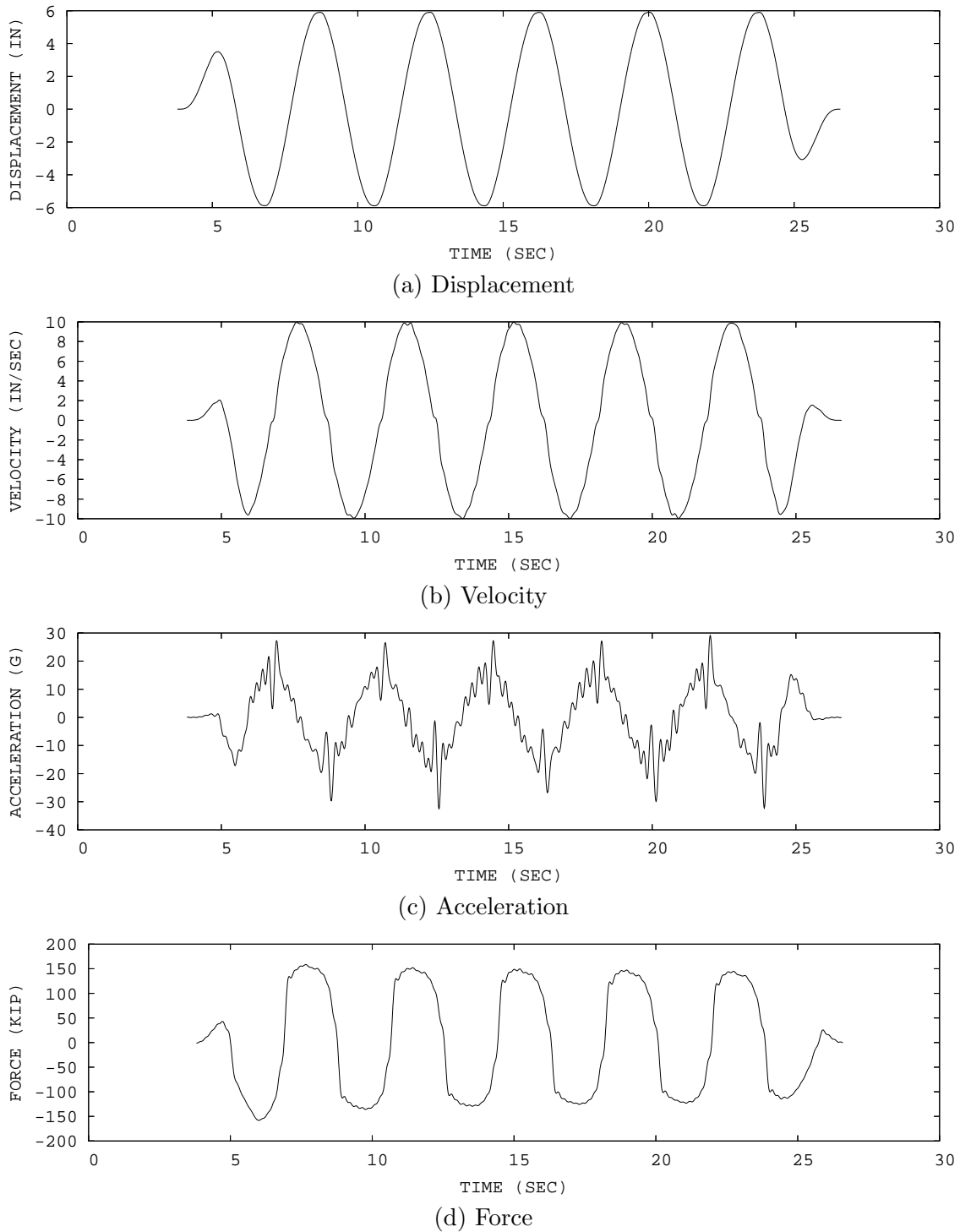


Figure A.5: Time history plot of the 250 kip damper response subjected to sinusoidal excitation for the data set UCB1\_10\_6. The displacement and force were measured, and the velocity and acceleration were integrated from the displacement.

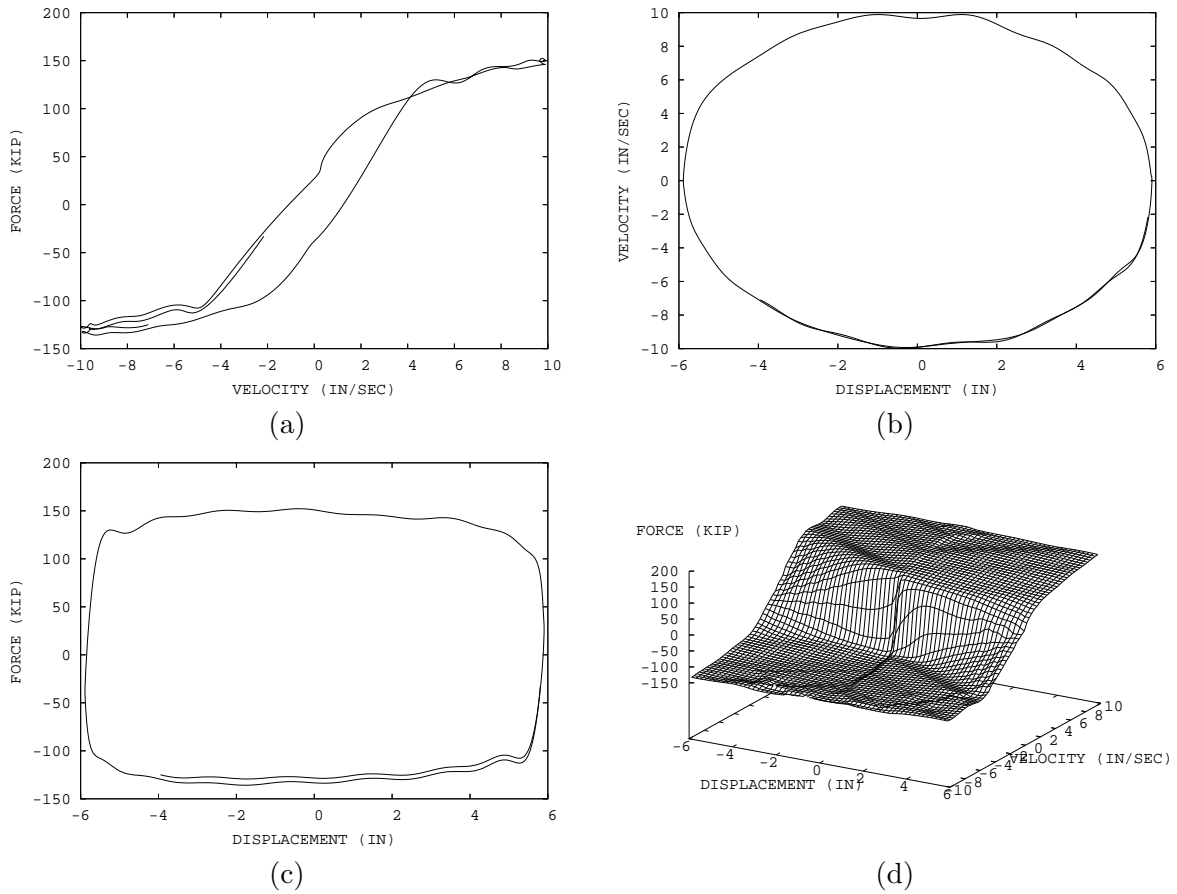
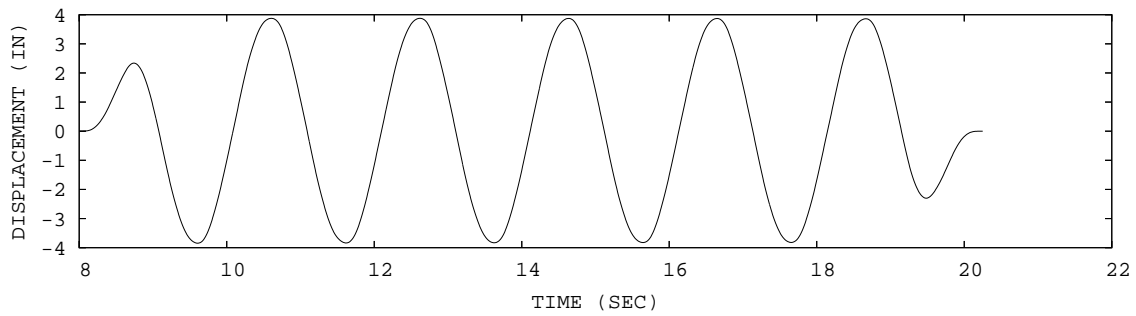
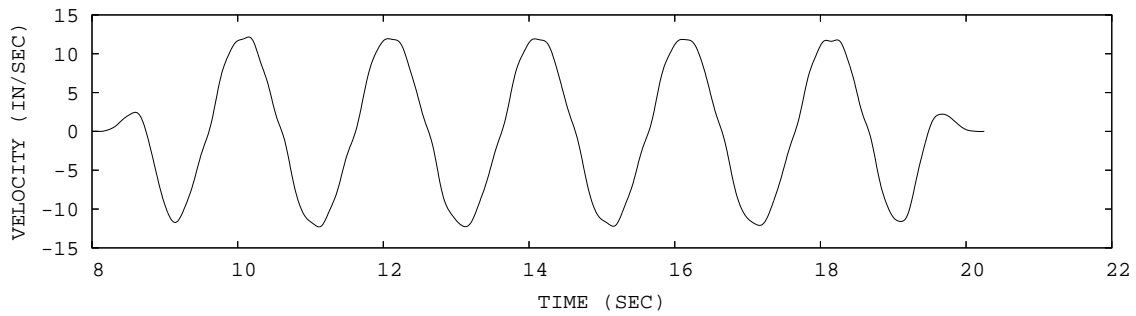


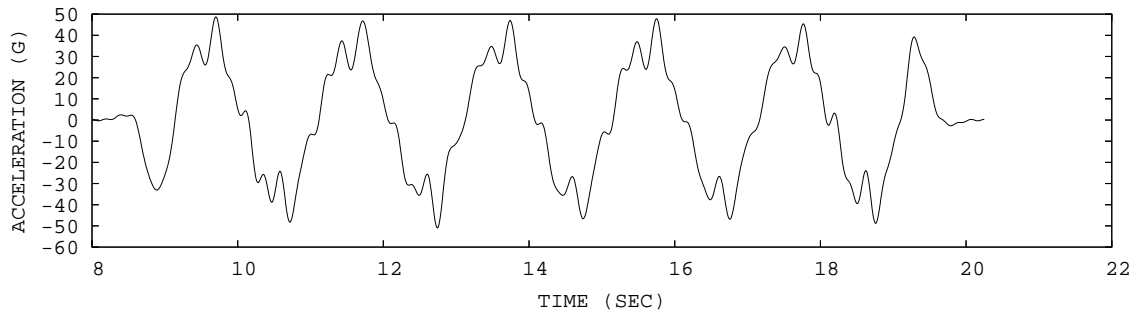
Figure A.6: Phase plot of the 250 kip damper response subjected to sinusoidal excitation for the data set UCB1\_10\_6. The displacement and force were measured, and the velocity and acceleration were integrated from the displacement.



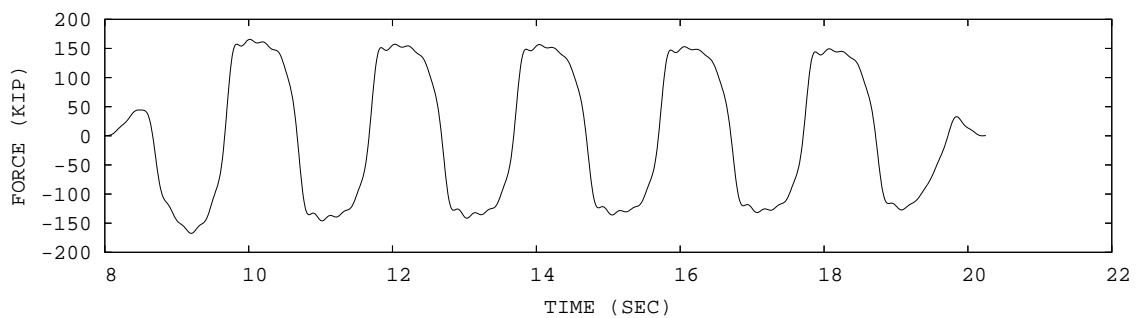
(a) Displacement



(b) Velocity



(c) Acceleration



(d) Force

Figure A.7: Time history plot of the 250 kip damper response subjected to sinusoidal excitation for the data set UCB1\_12\_4. The displacement and force were measured, and the velocity and acceleration were integrated from the displacement.

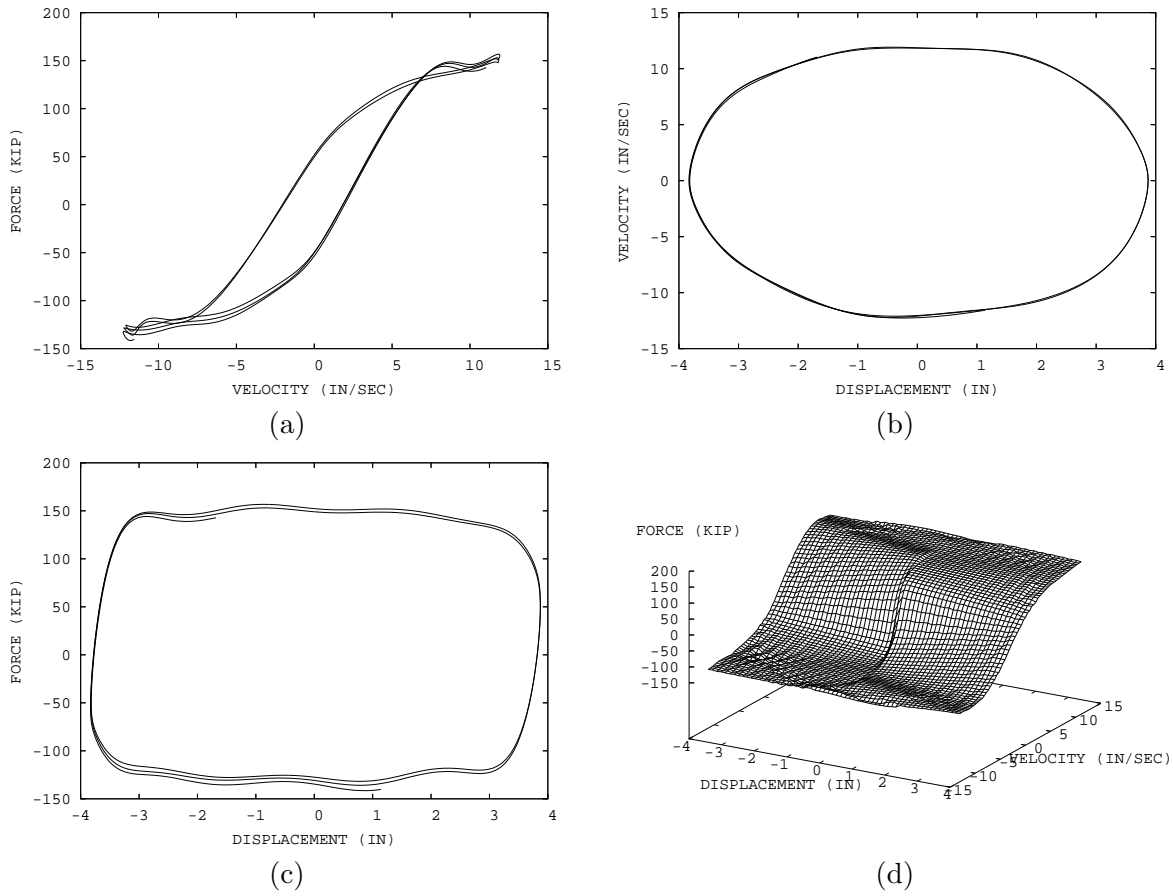


Figure A.8: Phase plot of the 250 kip damper response subjected to sinusoidal excitation for the data set UCB1\_12\_4. The displacement and force were measured, and the velocity and acceleration were integrated from the displacement.

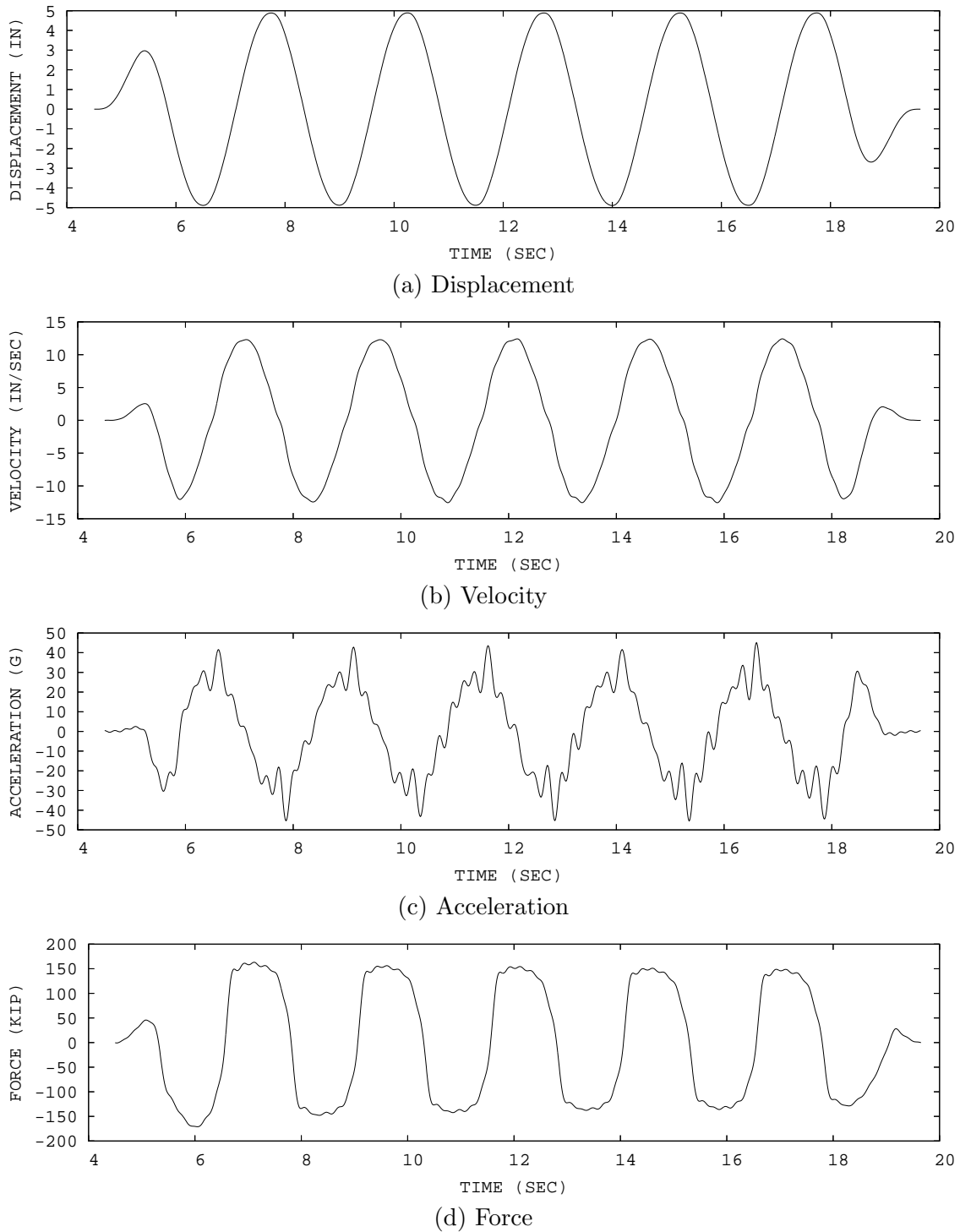


Figure A.9: Time history plot of the 250 kip damper response subjected to sinusoidal excitation for the data set UCB1\_12\_5. The displacement and force were measured, and the velocity and acceleration were integrated from the displacement.

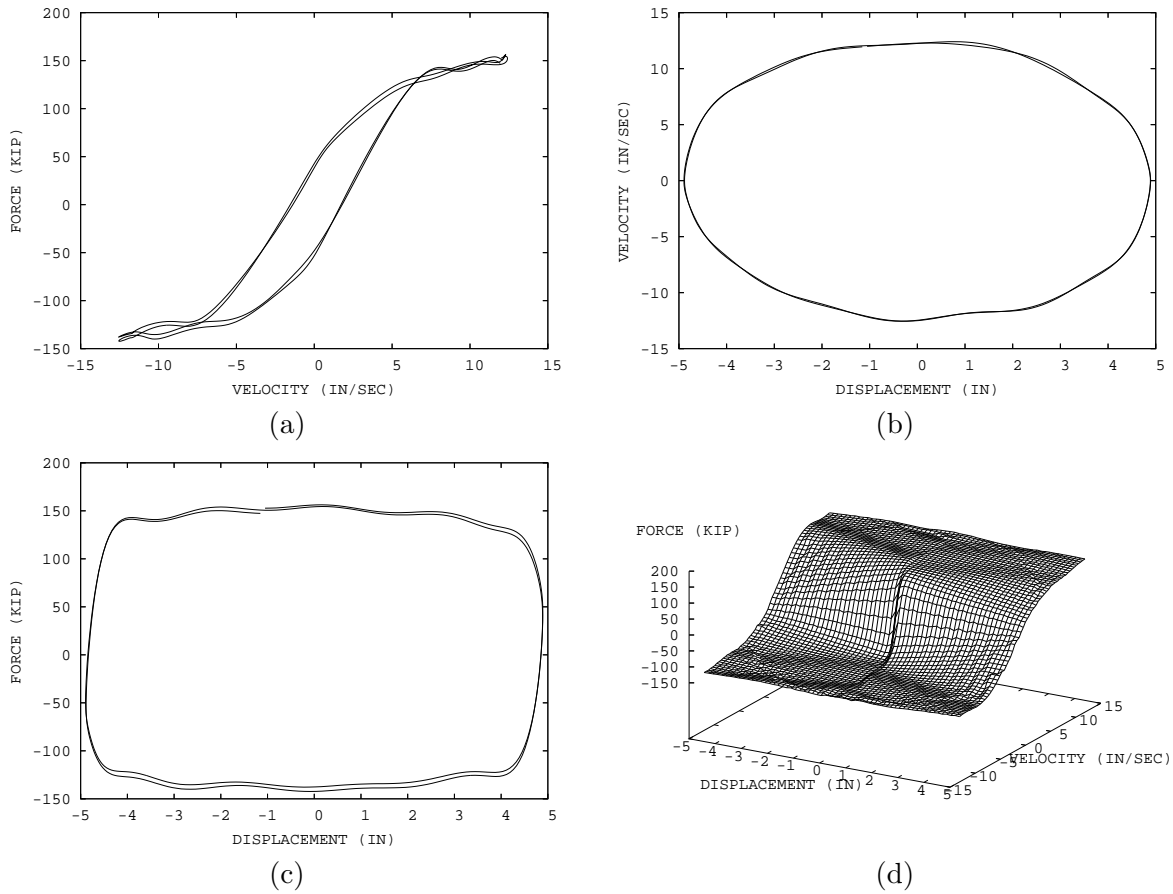
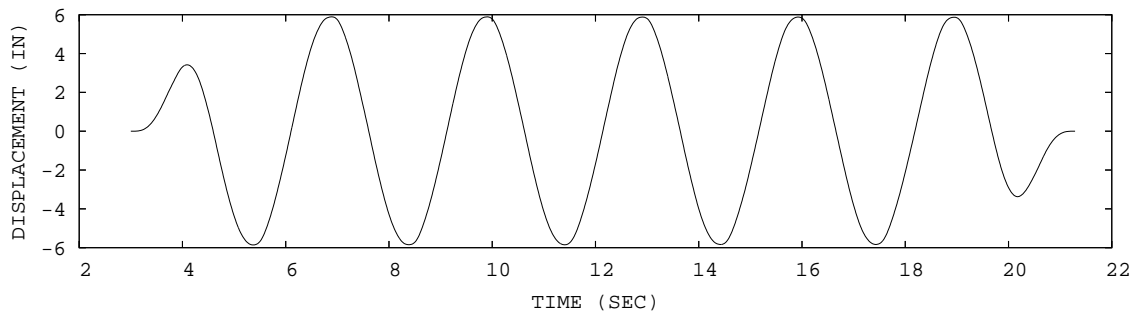
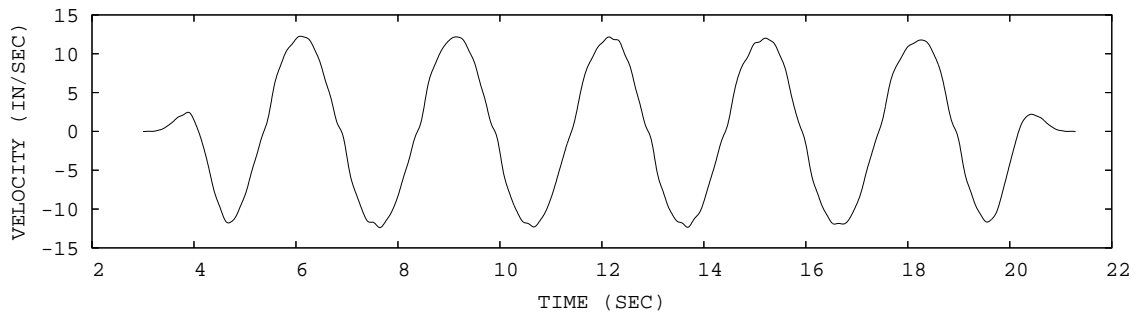


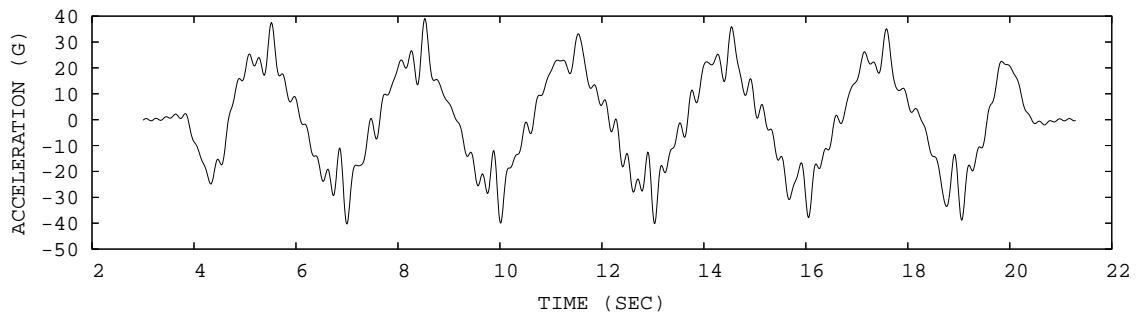
Figure A.10: Phase plot of the 250 kip damper response subjected to sinusoidal excitation for the data set UCB1\_12\_5. The displacement and force were measured, and the velocity and acceleration were integrated from the displacement.



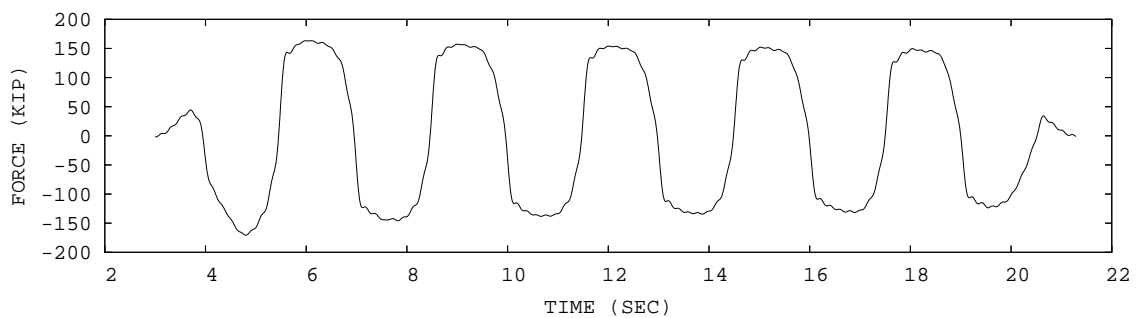
(a) Displacement



(b) Velocity



(c) Acceleration



(d) Force

Figure A.11: Time history plot of the 250 kip damper response subjected to sinusoidal excitation for the data set UCB1\_12\_6. The displacement and force were measured, and the velocity and acceleration were integrated from the displacement.

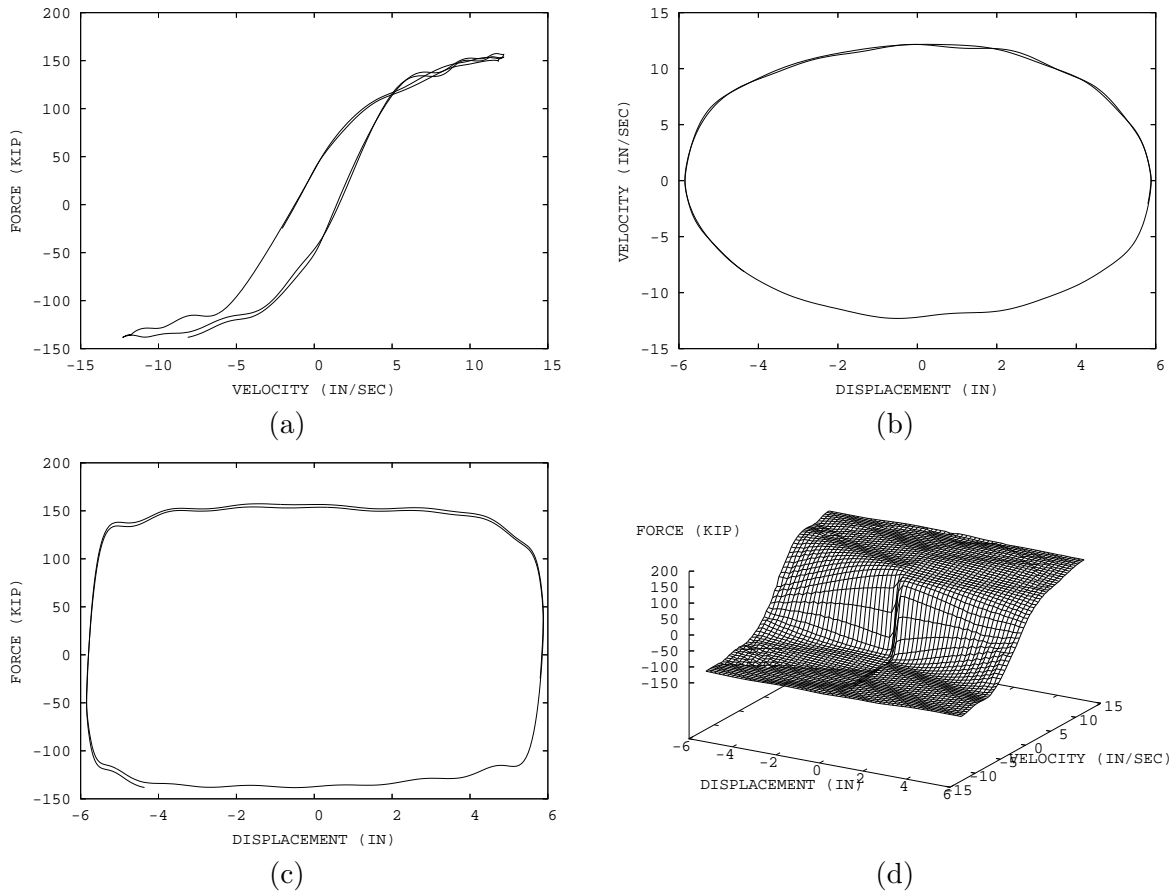


Figure A.12: Phase plot of the 250 kip damper response subjected to sinusoidal excitation for the data set UCB1\_12\_6. The displacement and force were measured, and the velocity and acceleration were integrated from the displacement.

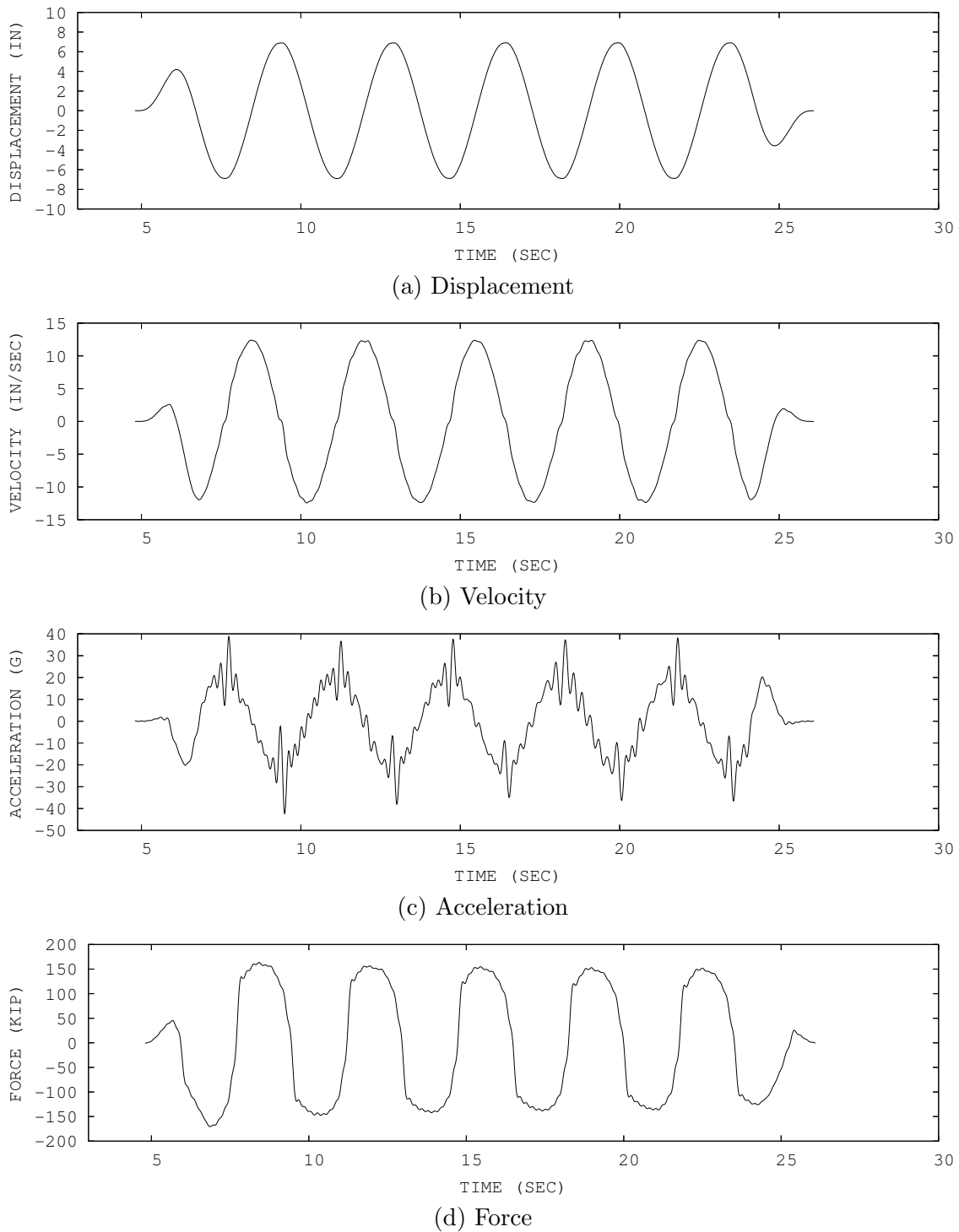


Figure A.13: Time history plot of the 250 kip damper response subjected to sinusoidal excitation for the data set UCB1\_12\_7. The displacement and force were measured, and the velocity and acceleration were integrated from the displacement.

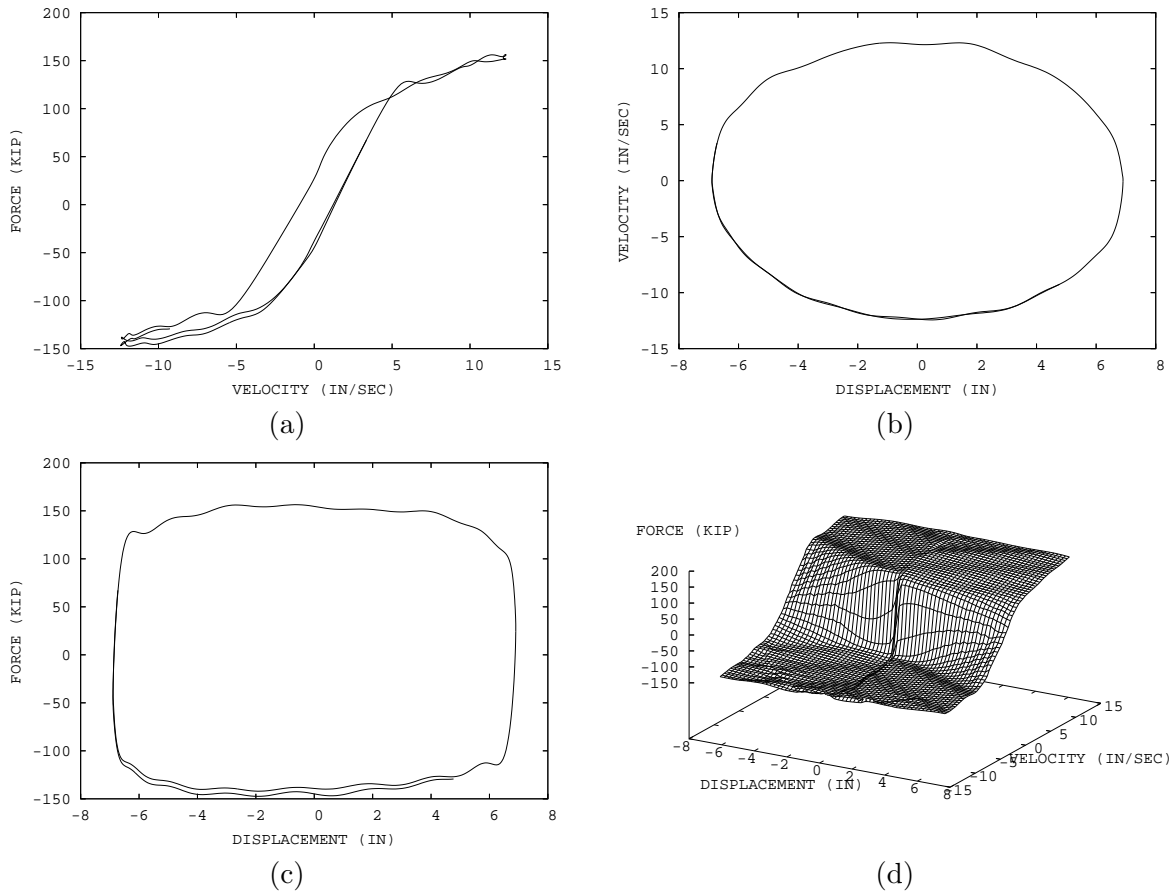
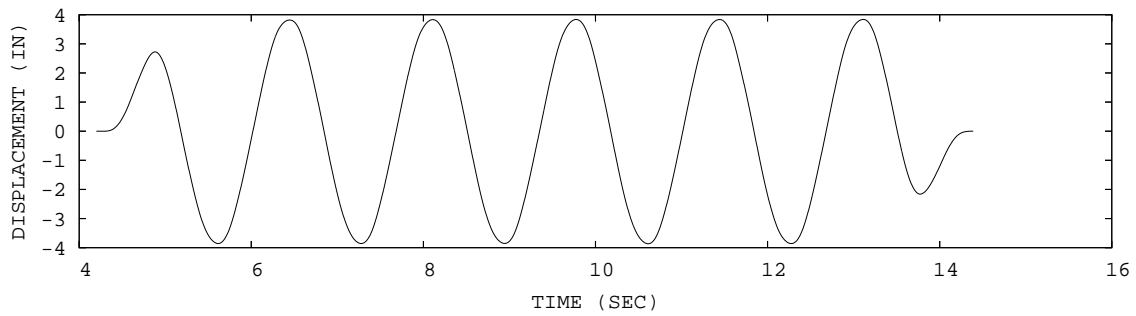
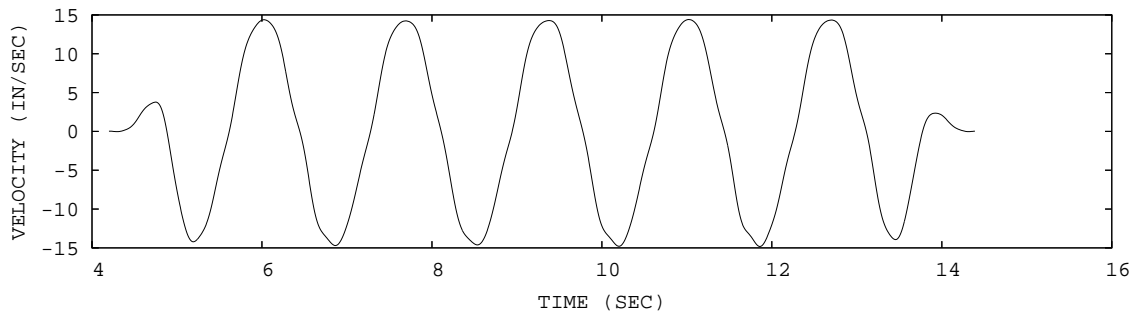


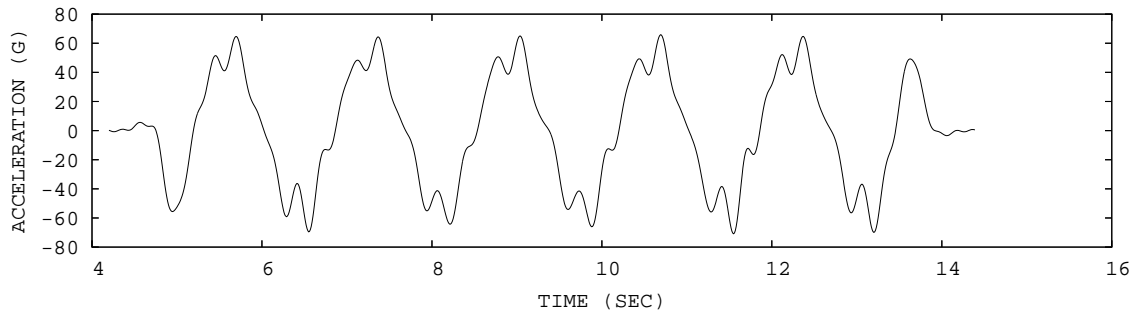
Figure A.14: Phase plot of the 250 kip damper response subjected to sinusoidal excitation for the data set UCB1\_12\_7. The displacement and force were measured, and the velocity and acceleration were integrated from the displacement.



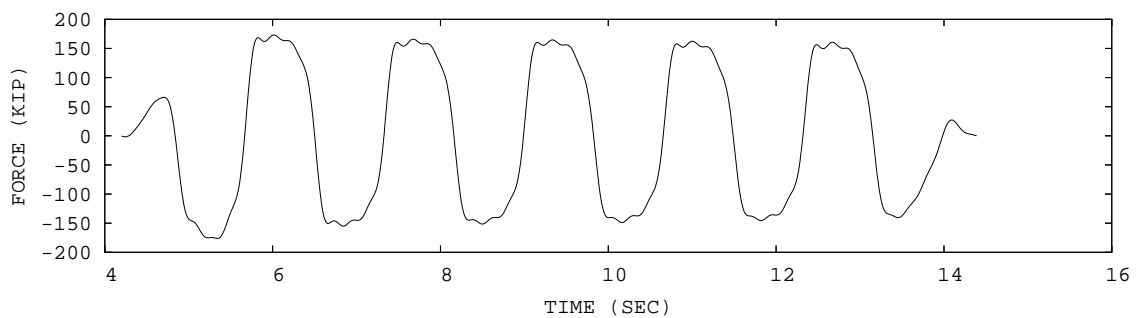
(a) Displacement



(b) Velocity



(c) Acceleration



(d) Force

Figure A.15: Time history plot of the 250 kip damper response subjected to sinusoidal excitation for the data set UCB1\_15\_4. The displacement and force were measured, and the velocity and acceleration were integrated from the displacement.

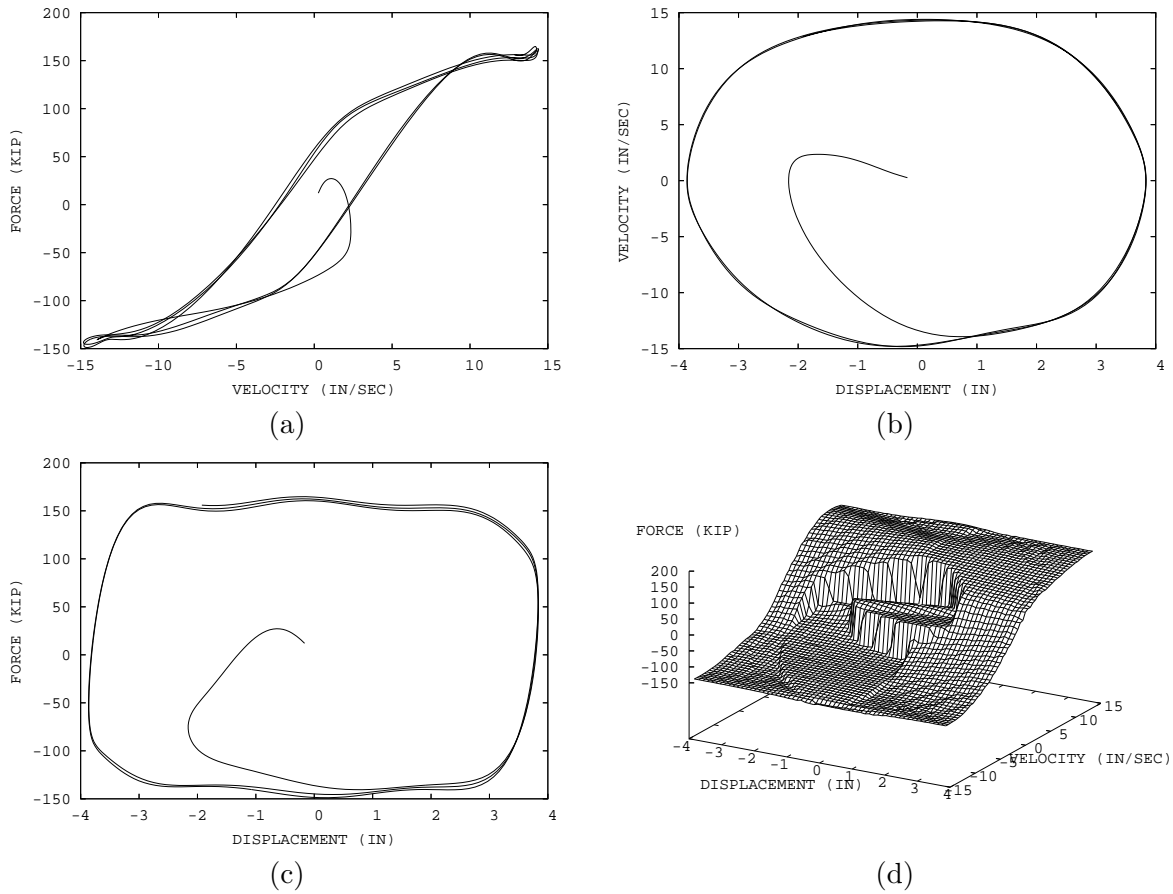
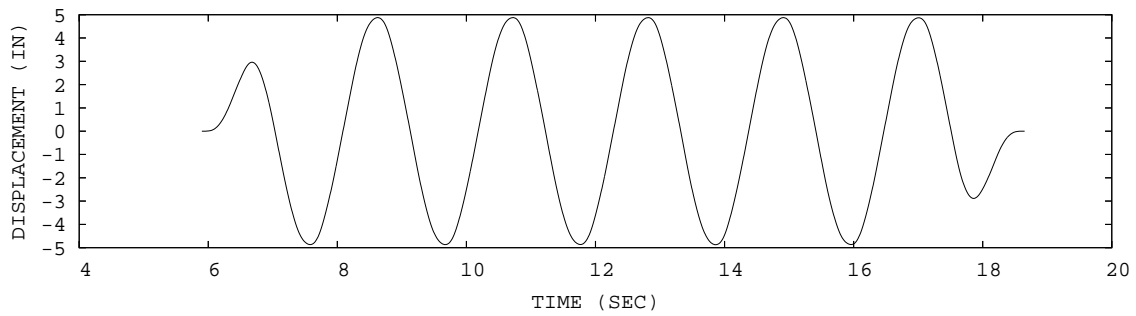
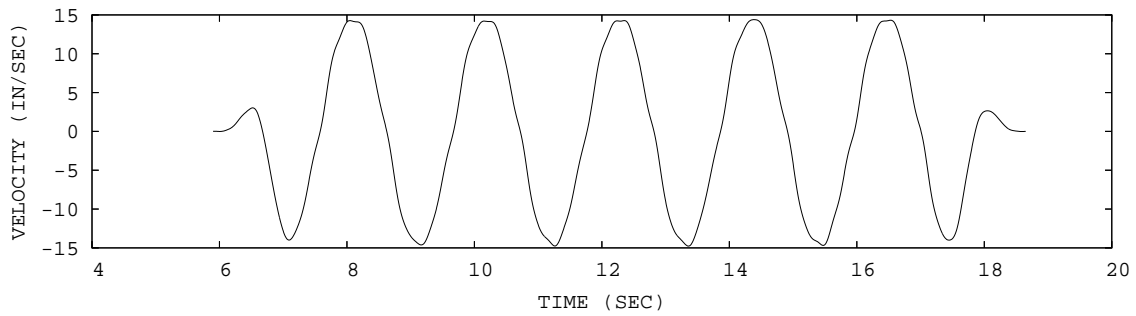


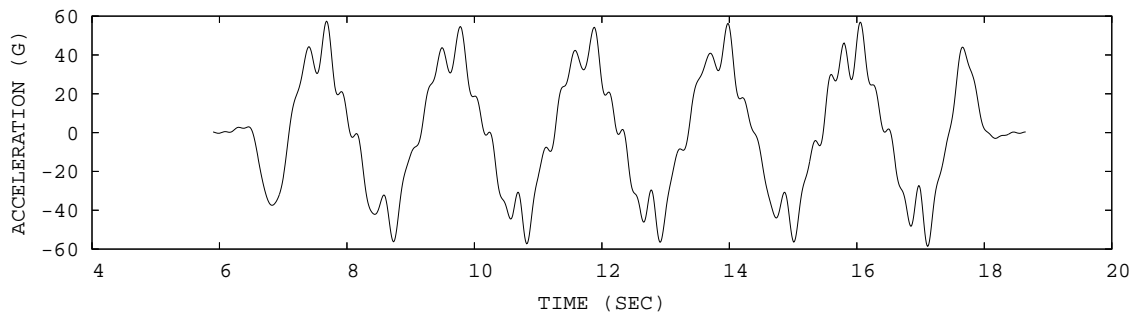
Figure A.16: Phase plot of the 250 kip damper response subjected to sinusoidal excitation for the data set UCB1\_15\_4. The displacement and force were measured, and the velocity and acceleration were integrated from the displacement.



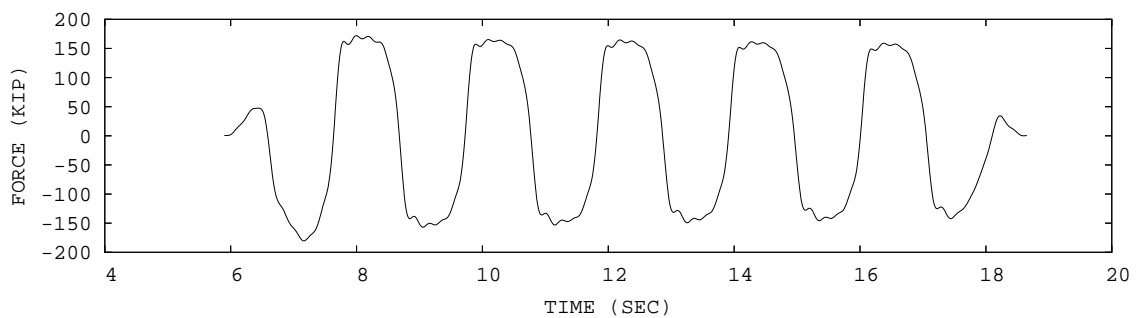
(a) Displacement



(b) Velocity



(c) Acceleration



(d) Force

Figure A.17: Time history plot of the 250 kip damper response subjected to sinusoidal excitation for the data set UCB1\_15\_5. The displacement and force were measured, and the velocity and acceleration were integrated from the displacement.

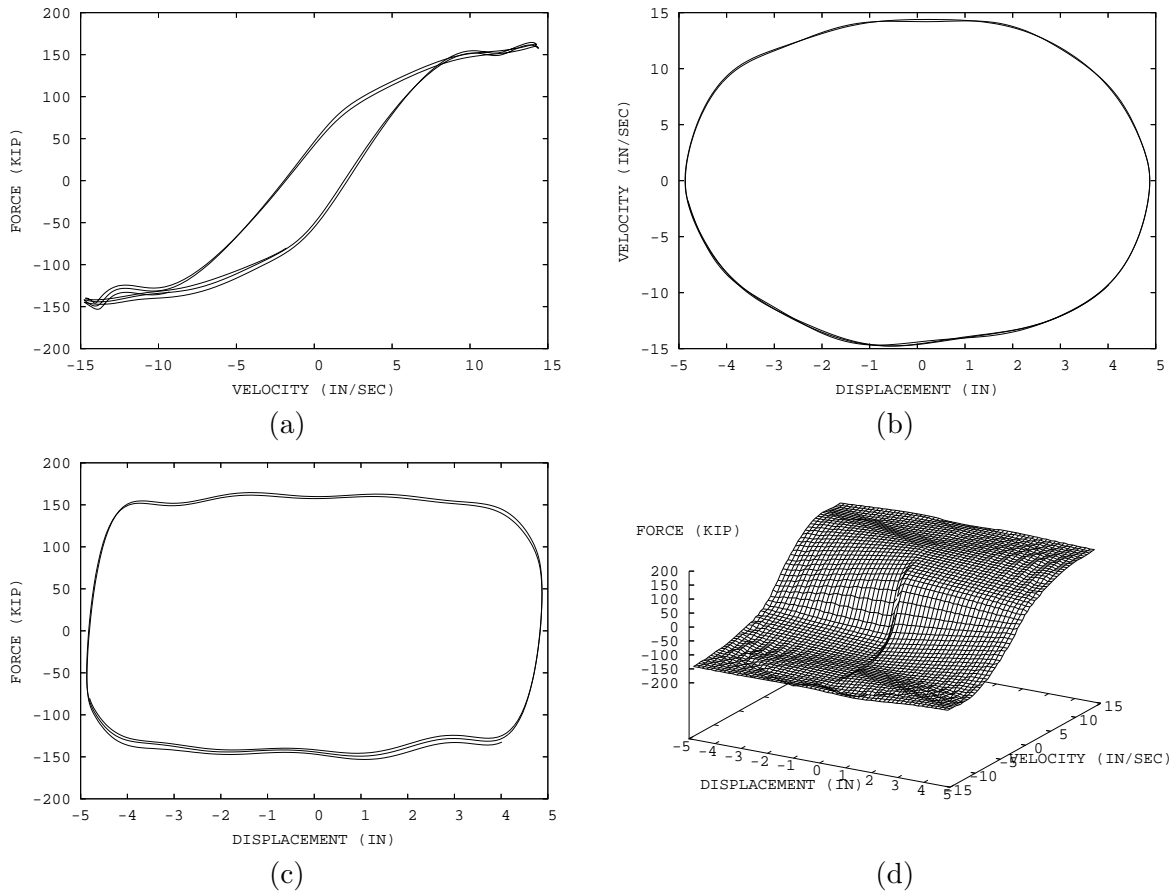
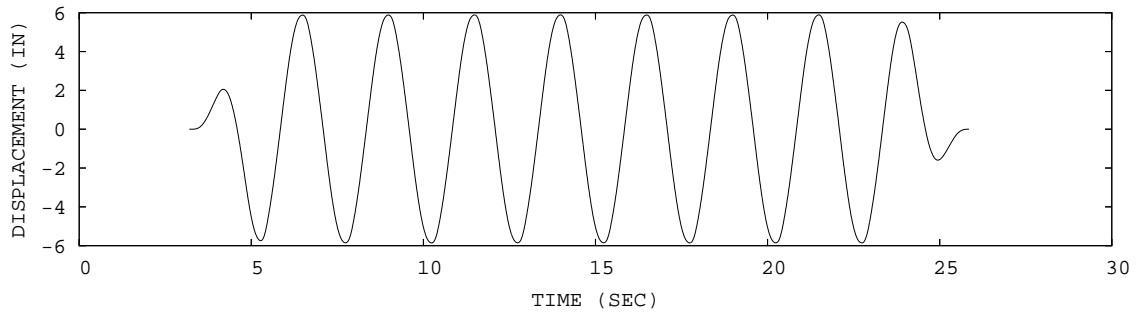
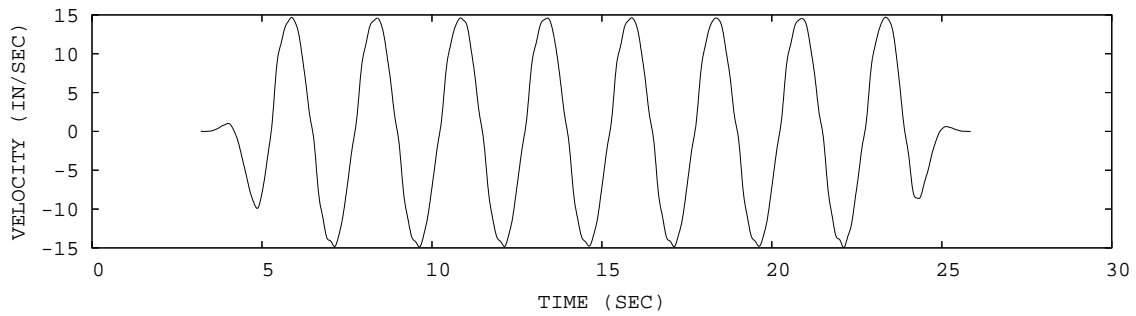


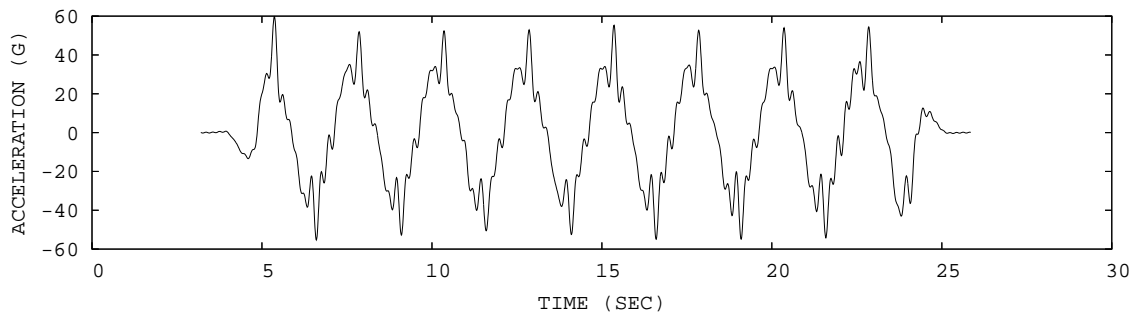
Figure A.18: Phase plot of the 250 kip damper response subjected to sinusoidal excitation for the data set UCB1\_15\_5. The displacement and force were measured, and the velocity and acceleration were integrated from the displacement.



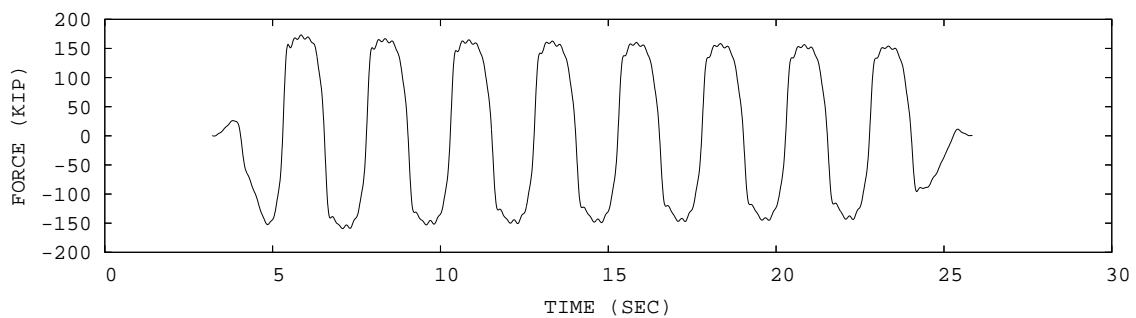
(a) Displacement



(b) Velocity



(c) Acceleration



(d) Force

Figure A.19: Time history plot of the 250 kip damper response subjected to sinusoidal excitation for the data set UCB1\_15\_6. The displacement and force were measured, and the velocity and acceleration were integrated from the displacement.

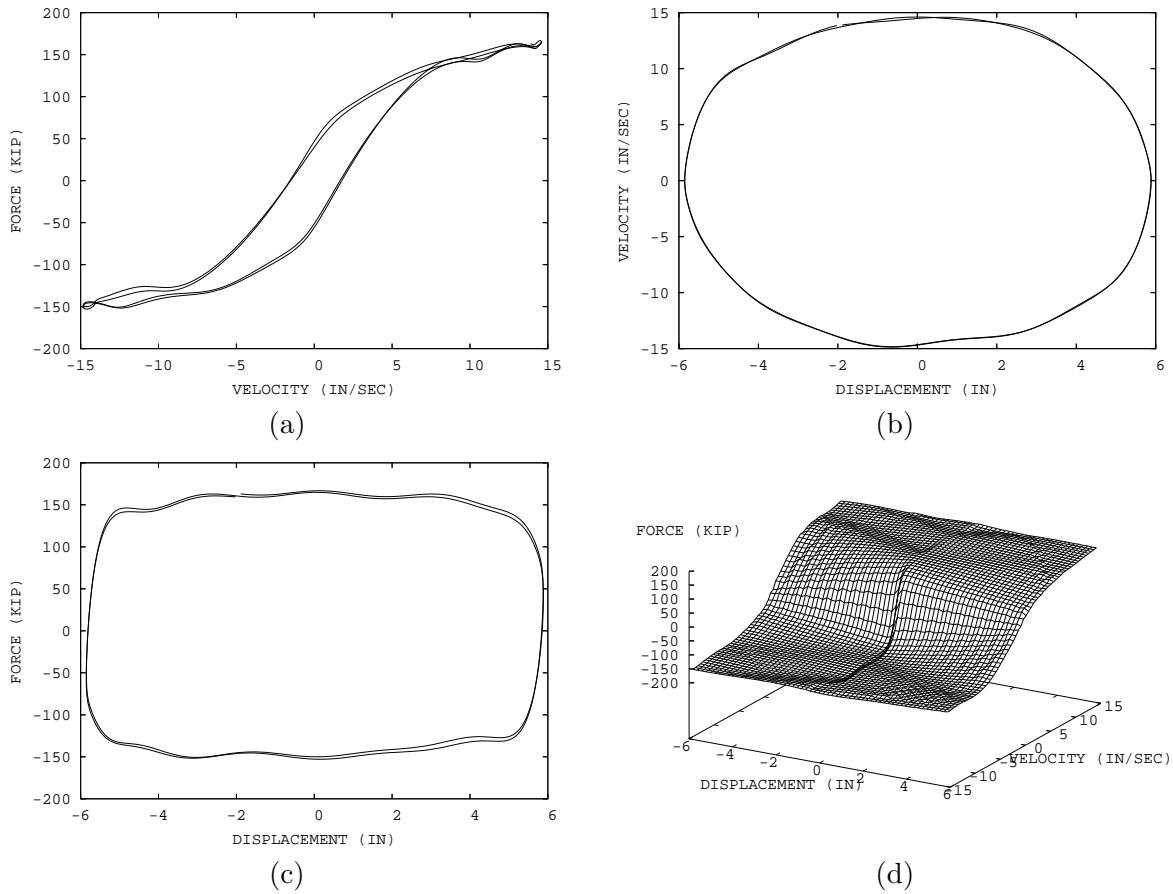
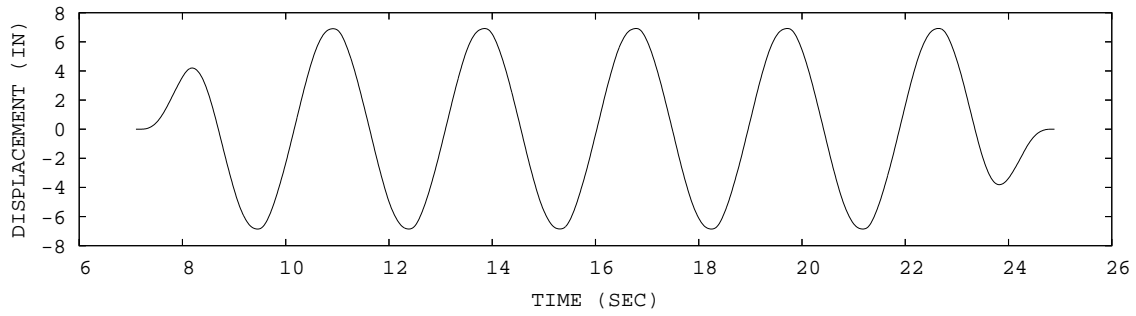
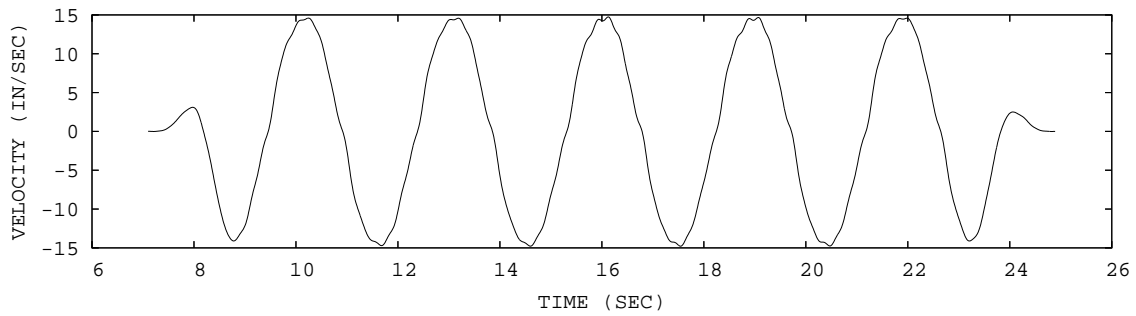


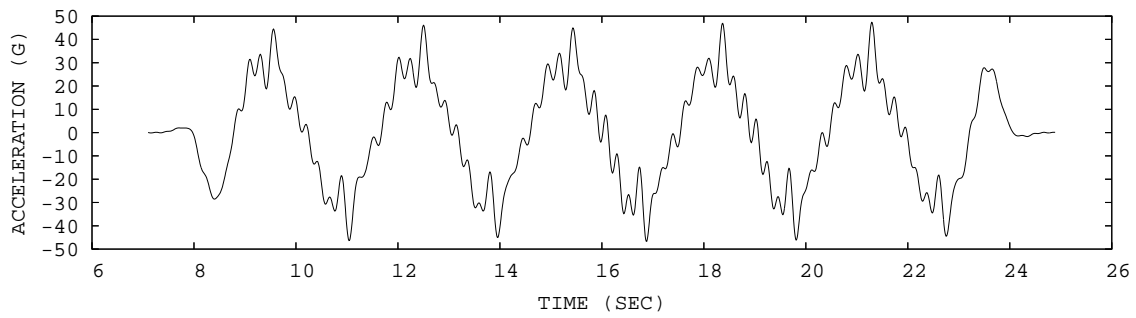
Figure A.20: Phase plot of the 250 kip damper response subjected to sinusoidal excitation for the data set UCB1\_15\_6. The displacement and force were measured, and the velocity and acceleration were integrated from the displacement.



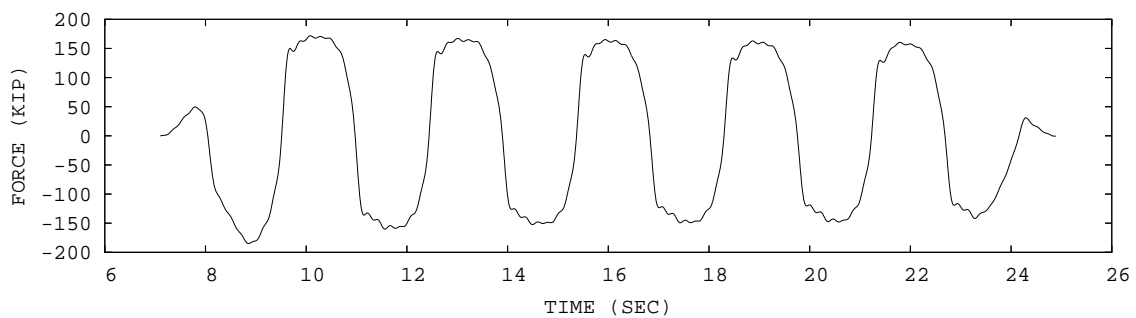
(a) Displacement



(b) Velocity



(c) Acceleration



(d) Force

Figure A.21: Time history plot of the 250 kip damper response subjected to sinusoidal excitation for the data set UCB1\_15\_7. The displacement and force were measured, and the velocity and acceleration were integrated from the displacement.

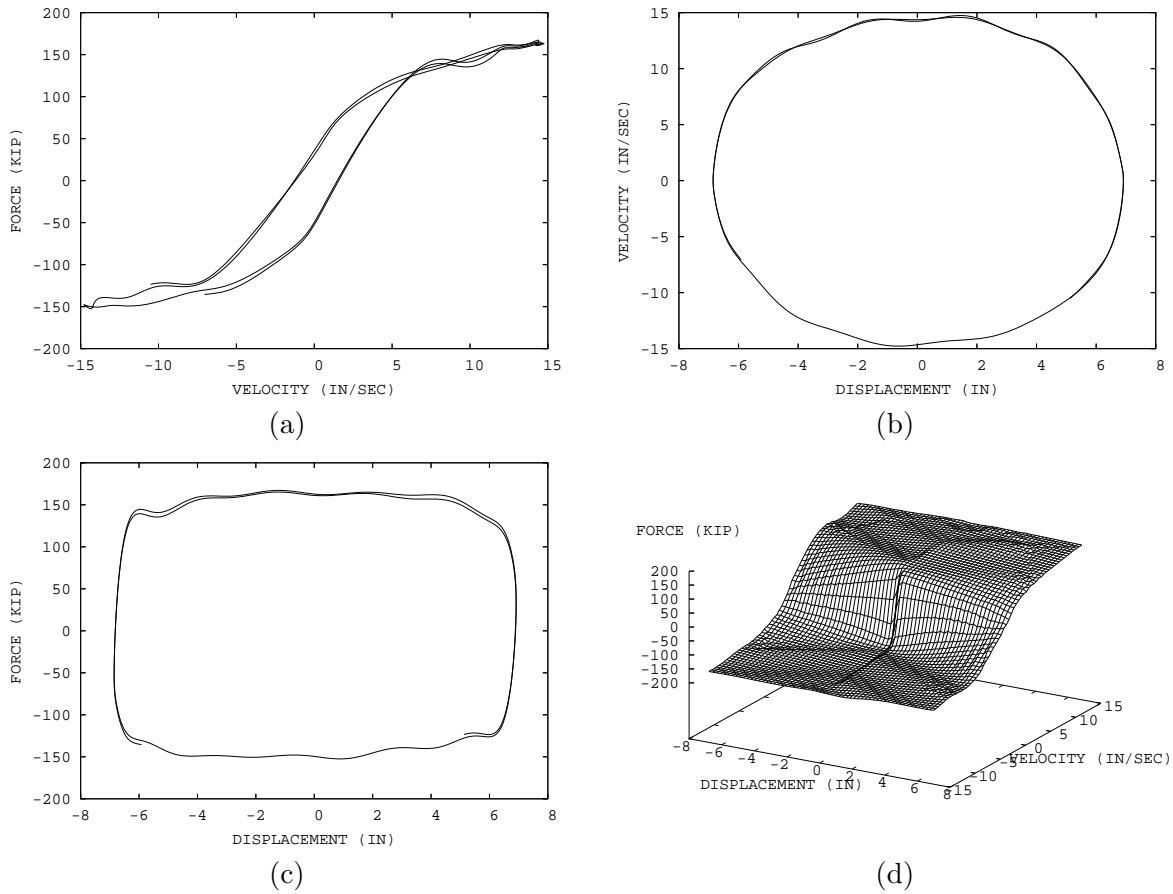


Figure A.22: Phase plot of the 250 kip damper response subjected to sinusoidal excitation for the data set UCB1\_15\_7. The displacement and force were measured, and the velocity and acceleration were integrated from the displacement.

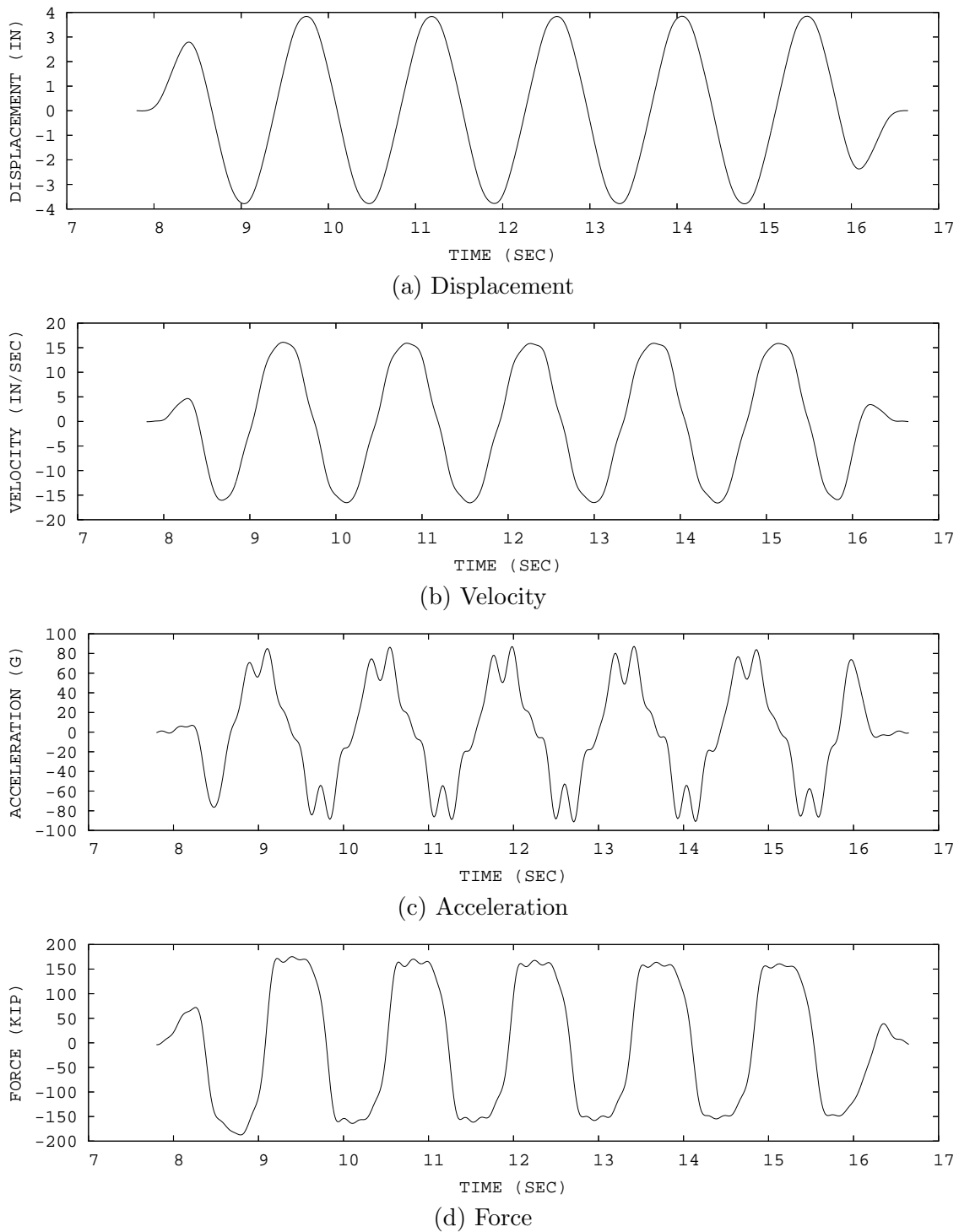


Figure A.23: Time history plot of the 250 kip damper response subjected to sinusoidal excitation for the data set UCB1\_17\_4. The displacement and force were measured, and the velocity and acceleration were integrated from the displacement.

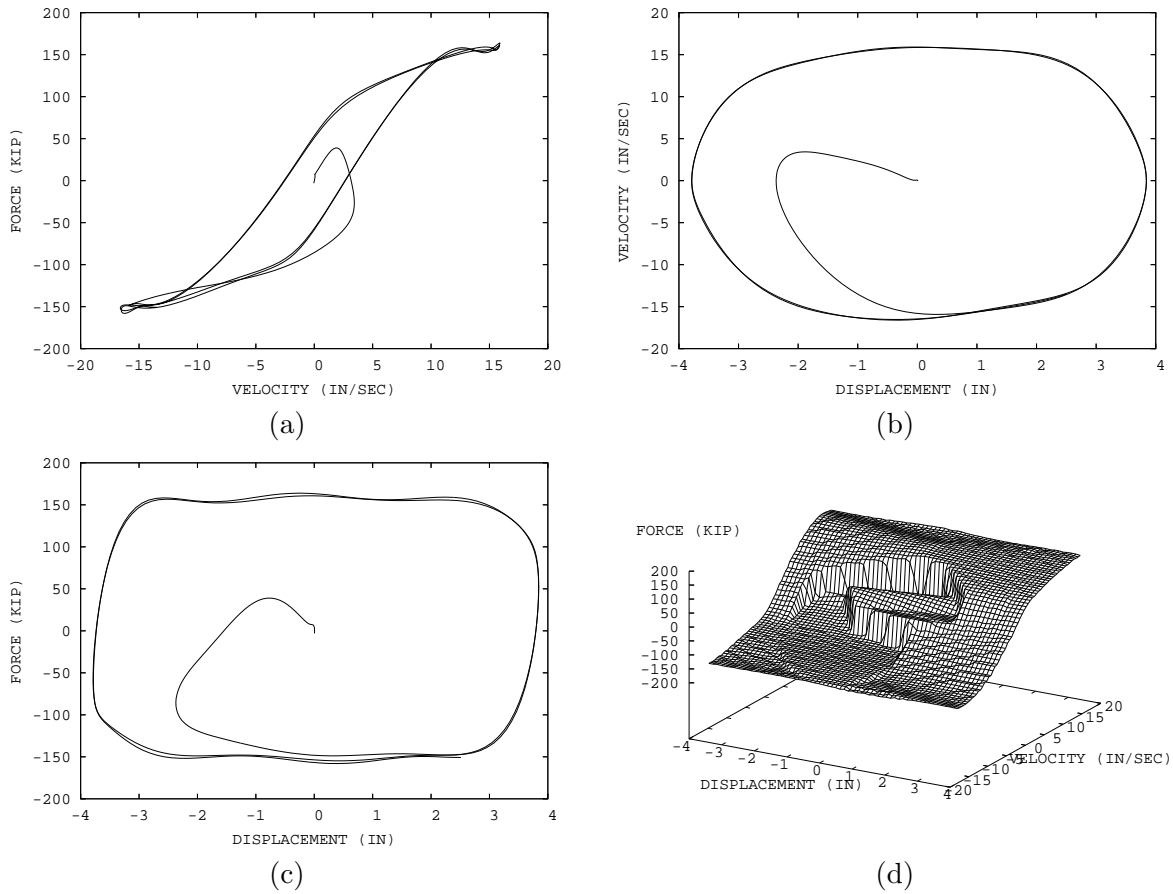
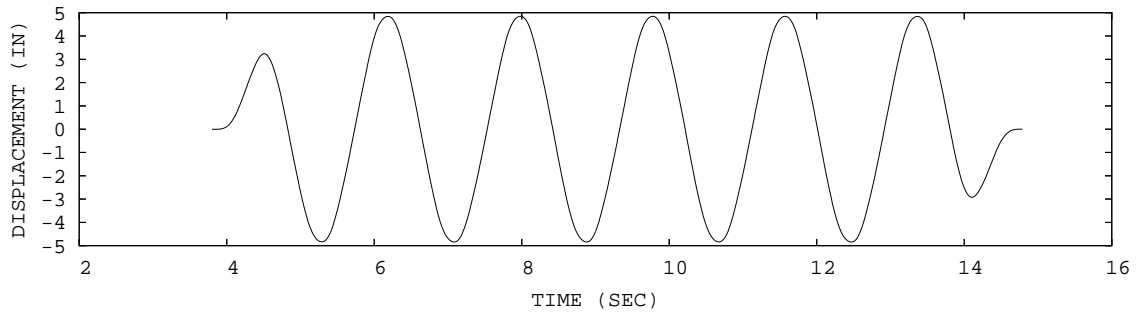
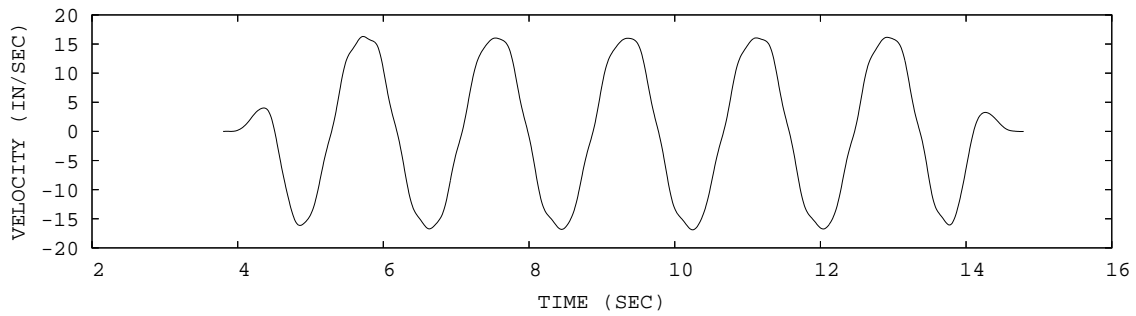


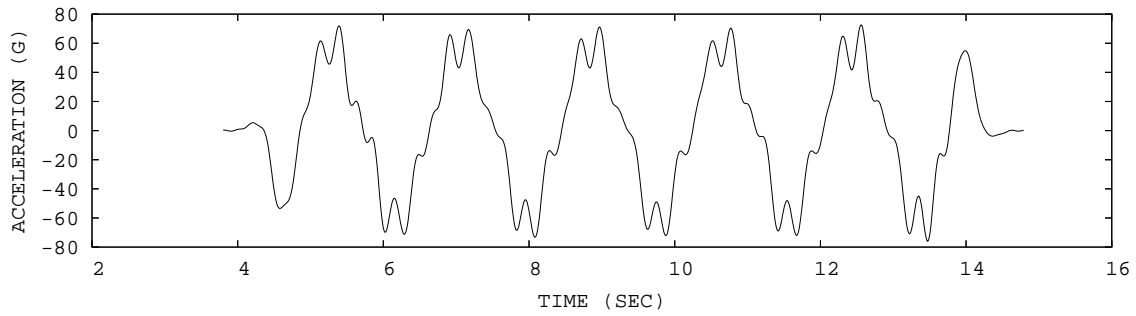
Figure A.24: Phase plot of the 250 kip damper response subjected to sinusoidal excitation for the data set UCB1\_17\_4. The displacement and force were measured, and the velocity and acceleration were integrated from the displacement.



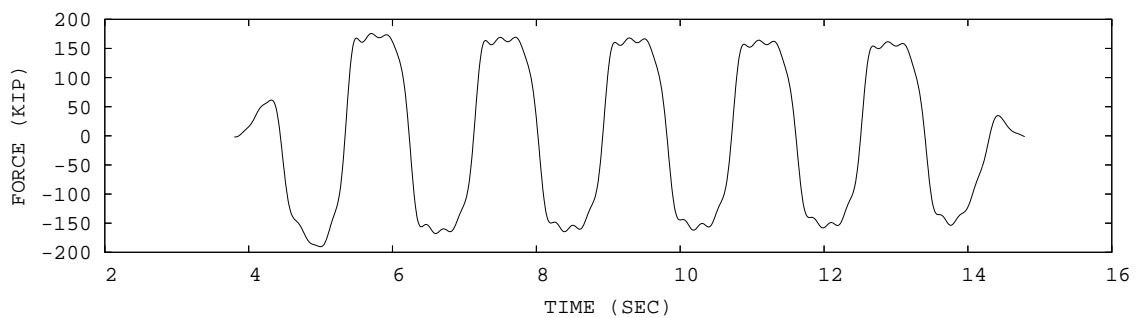
(a) Displacement



(b) Velocity



(c) Acceleration



(d) Force

Figure A.25: Time history plot of the 250 kip damper response subjected to sinusoidal excitation for the data set UCB1\_17\_5. The displacement and force were measured, and the velocity and acceleration were integrated from the displacement.

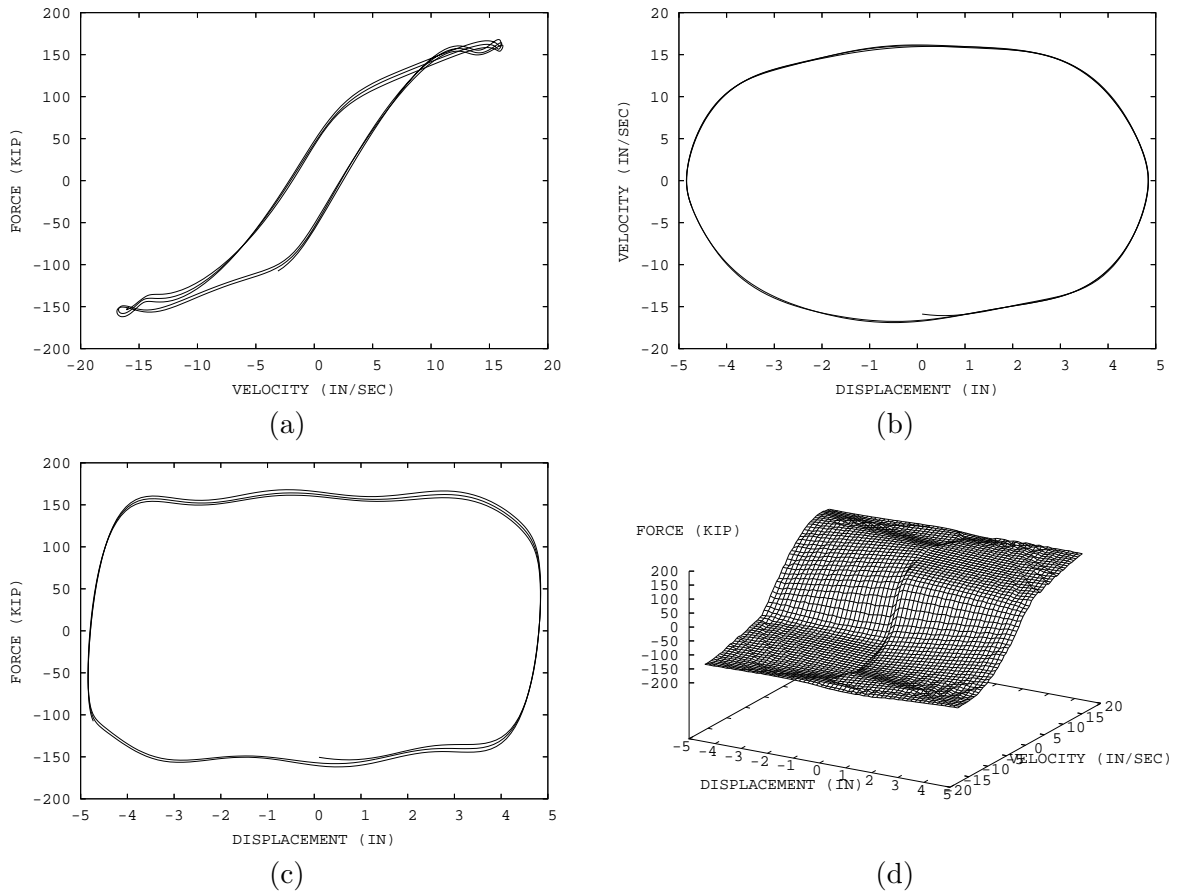


Figure A.26: Phase plot of the 250 kip damper response subjected to sinusoidal excitation for the data set UCB1\_17\_5. The displacement and force were measured, and the velocity and acceleration were integrated from the displacement.

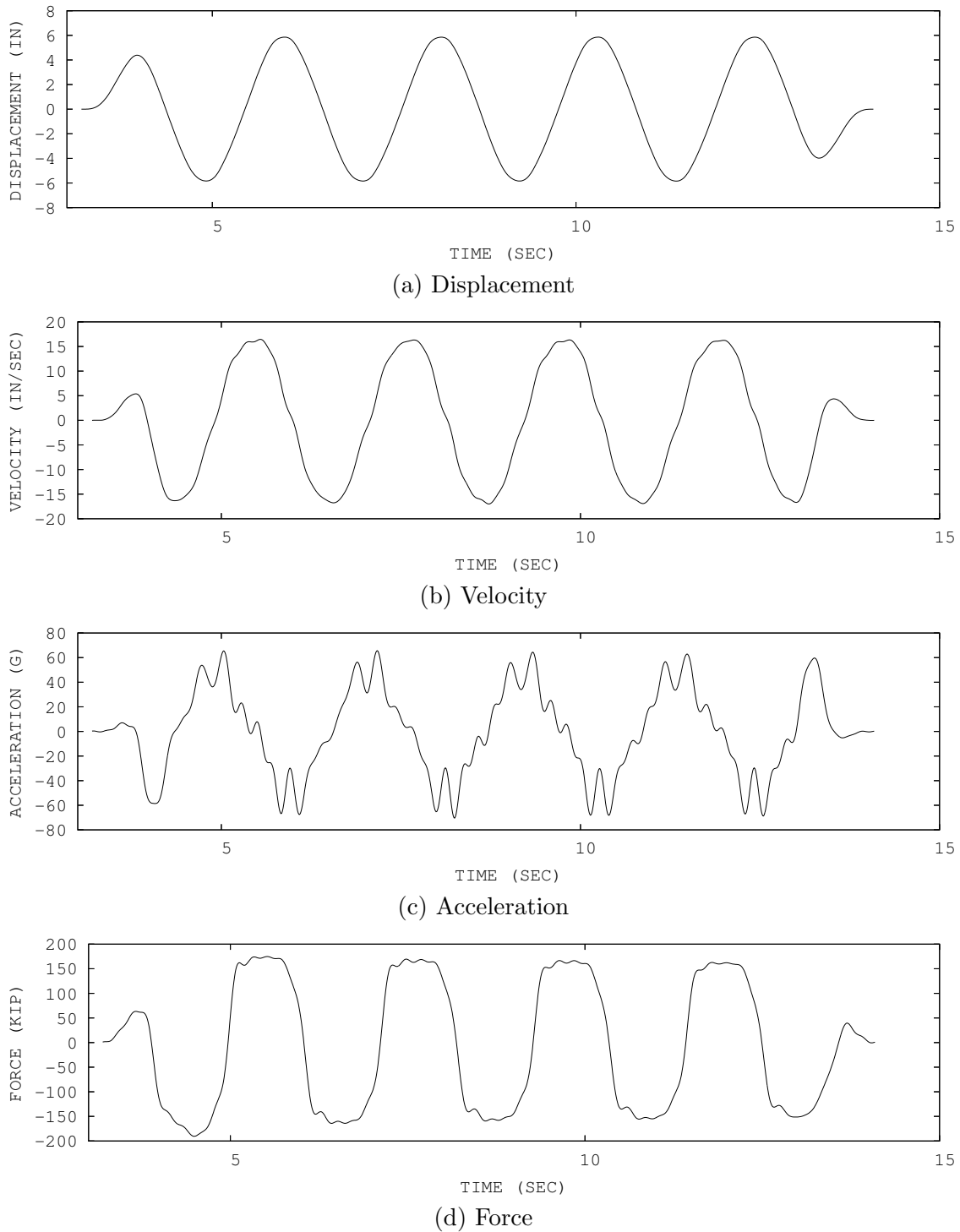


Figure A.27: Time history plot of the 250 kip damper response subjected to sinusoidal excitation for the data set UCB1\_17\_6. The displacement and force were measured, and the velocity and acceleration were integrated from the displacement.

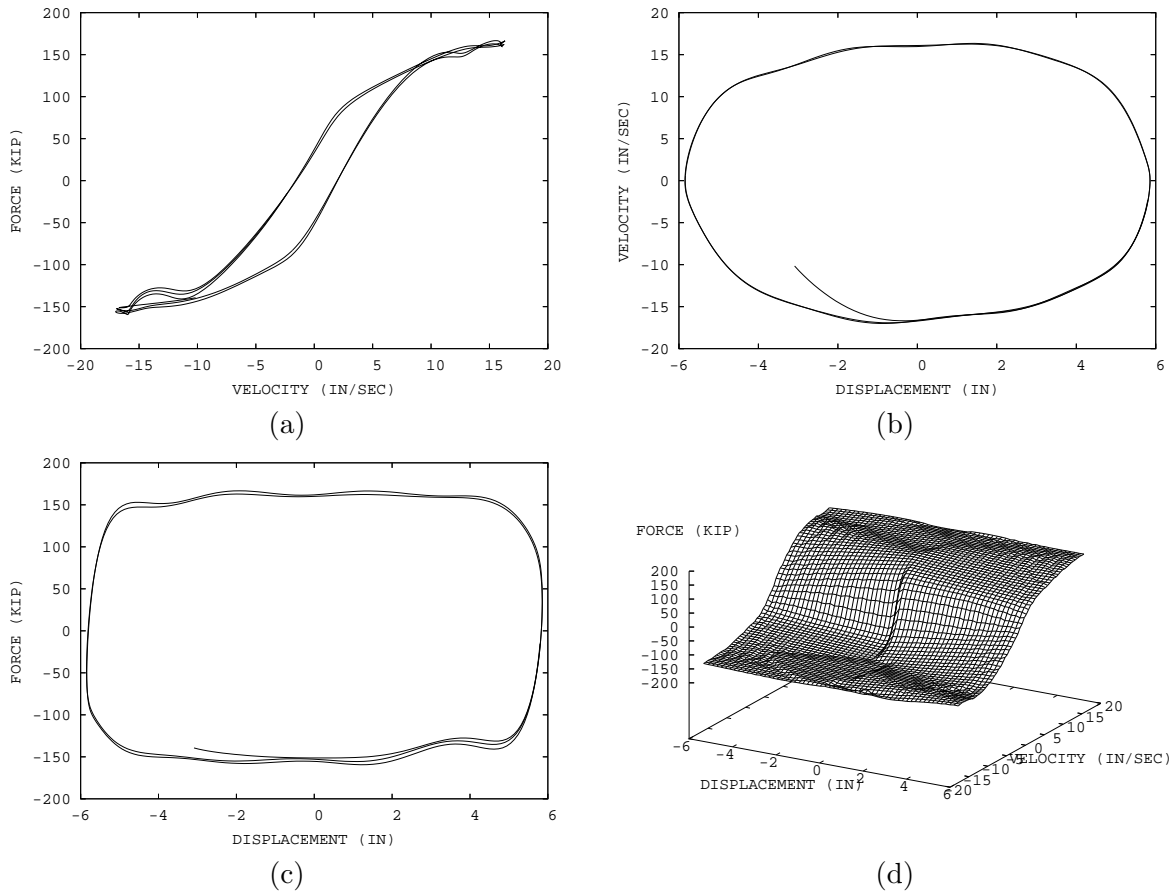
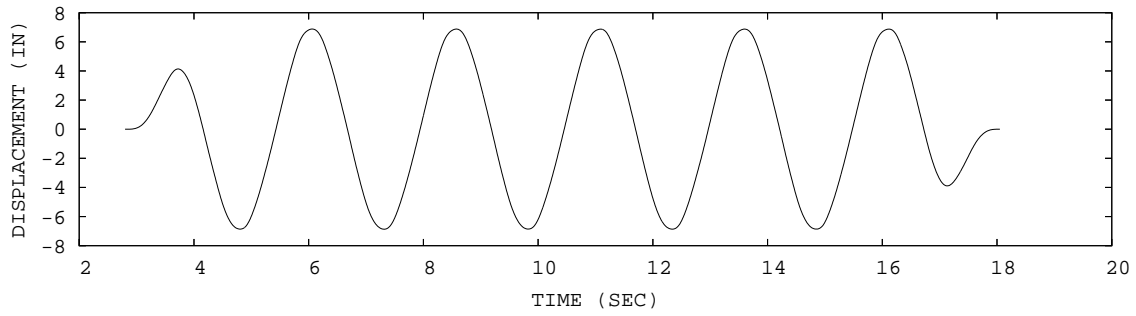
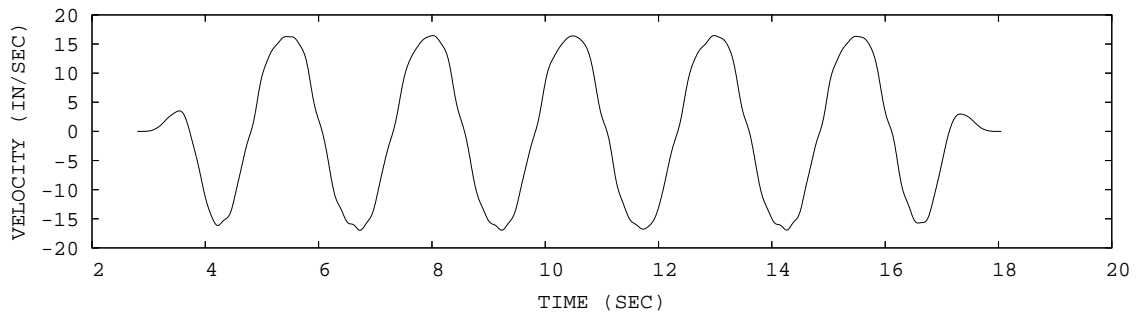


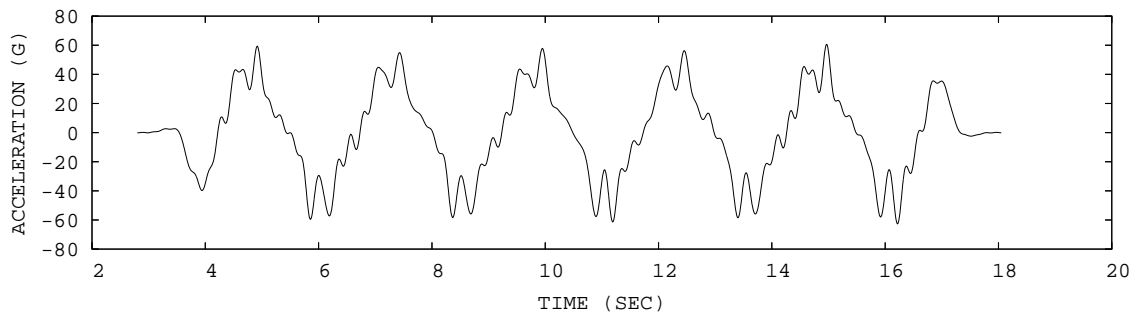
Figure A.28: Phase plot of the 250 kip damper response subjected to sinusoidal excitation for the data set UCB1\_17\_6. The displacement and force were measured, and the velocity and acceleration were integrated from the displacement.



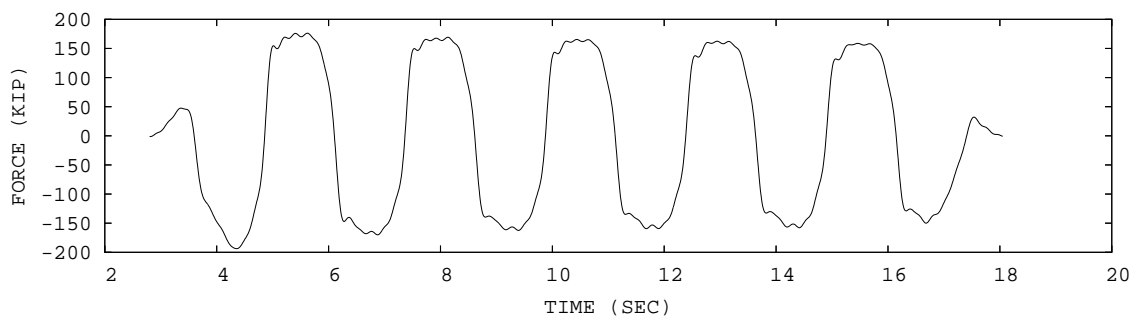
(a) Displacement



(b) Velocity



(c) Acceleration



(d) Force

Figure A.29: Time history plot of the 250 kip damper response subjected to sinusoidal excitation for the data set UCB1\_17\_7. The displacement and force were measured, and the velocity and acceleration were integrated from the displacement.

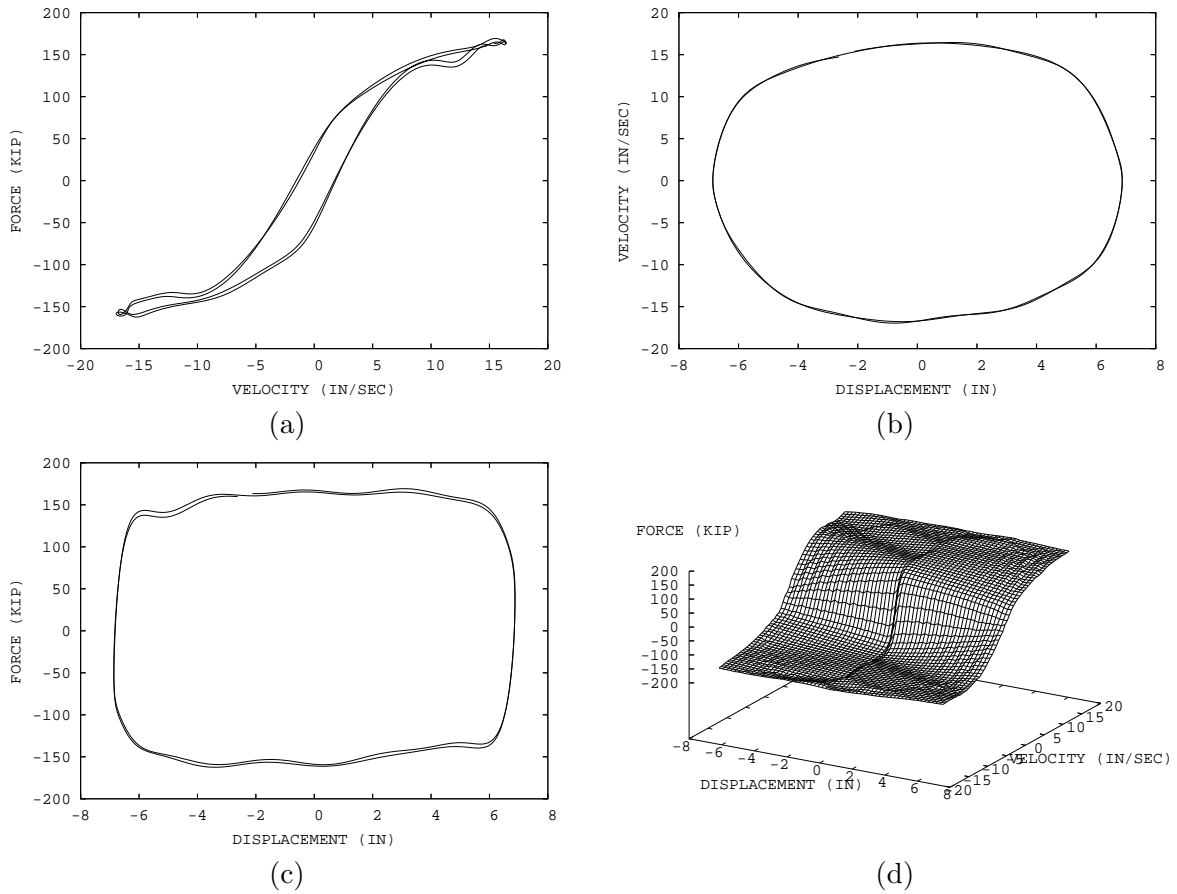


Figure A.30: Phase plot of the 250 kip damper response subjected to sinusoidal excitation for the data set UCB1\_17\_7. The displacement and force were measured, and the velocity and acceleration were integrated from the displacement.

## Appendix B

# PARAMETRIC IDENTIFICATION RESULTS OF THE 250 KIP VISCOUS DAMPER

The results of the off-line and the on-line parametric identifications for the 250 kip viscous damper data sets are provided in this appendix. The test matrix of the data sets is summarized in Table B.1.

Table B.1: Test matrix of the 250 kip damper data set.

Data set Name	Approx. Peak Velocity (in/sec)	Test Frequency (hz)	Test Amplitude (in)	Number of Cycle	Scan Rate (hz)
UCB1_10.4	10.00	0.398	4	6	100
UCB1_10.5	10.00	0.318	5	6	100
UCB1_10.6	10.00	0.265	6	6	100
UCB1_12.4	12.00	0.500	4	6	100
UCB1_12.5	12.50	0.400	5	6	100
UCB1_12.6	12.50	0.332	6	6	100
UCB1_12.7	12.50	0.284	7	6	100
UCB1_15.4	15.00	0.600	4	6	100
UCB1_15.5	15.00	0.477	5	6	100
UCB1_15.6	15.00	0.400	6	10	100
UCB1_15.7	15.00	0.341	7	6	100
UCB1_17.4	17.50	0.695	4	6	100
UCB1_17.5	17.50	0.557	5	6	100
UCB1_17.6	17.50	0.464	6	6	100
UCB1_17.7	17.50	0.399	7	6	100

## B.1 On-Line Parametric Identification

The plots of the on-line identification results are provided in this section. The results of the on-line identification of the 250 kip viscous damper are summarized in Table B.2.

Table B.2: Summary of the on-line parametric identification for the 250 kip damper data sets. Column 1 is the data set name, column 2 is the manufacturer value for the damping coefficient  $C$ , column 3 is the average value of the identified damping coefficient  $\hat{C}$ , column 4 is the manufacturer specification value for the exponent  $n$ , column 5 is the average value of the identified exponent  $\hat{n}$  (Eqn. 2.6), column 6 is the selected value of the forgetting factor ( $\beta$ ) in the on-line identification algorithm (Eqn. 2.5), and column 7 is the normalized mean-square-error percentage of the difference between the predicted force and the measured force.

Data set Name	Damping Coeff. $C$ (kip sec/in)		Exponent $n$		$\beta$ forgetting factor	% MSE error
	Damper Spec.	Identified	Damper Spec.	Identified		
UCB1_10_4	60.00	54.32	0.35	0.37	1.0	4.00
UCB1_10_5	60.00	48.55	0.35	0.44	1.0	5.74
UCB1_10_6	60.00	51.67	0.35	0.43	1.0	5.50
UCB1_12_4	60.00	49.72	0.35	0.41	1.0	6.22
UCB1_12_5	60.00	47.24	0.35	0.45	1.0	6.24
UCB1_12_6	60.00	47.90	0.35	0.45	1.0	5.79
UCB1_12_7	60.00	47.06	0.35	0.46	1.0	5.19
UCB1_15_4	60.00	44.58	0.35	0.45	1.0	6.25
UCB1_15_5	60.00	42.76	0.35	0.48	1.0	5.99
UCB1_15_6	60.00	44.60	0.35	0.46	1.0	4.79
UCB1_15_7	60.00	45.55	0.35	0.47	1.0	5.60
UCB1_17_4	60.00	42.91	0.35	0.46	1.0	6.19
UCB1_17_5	60.00	41.94	0.35	0.48	1.0	6.03
UCB1_17_6	60.00	40.69	0.35	0.49	1.0	6.06
UCB1_17_7	60.00	45.21	0.35	0.45	1.0	5.48

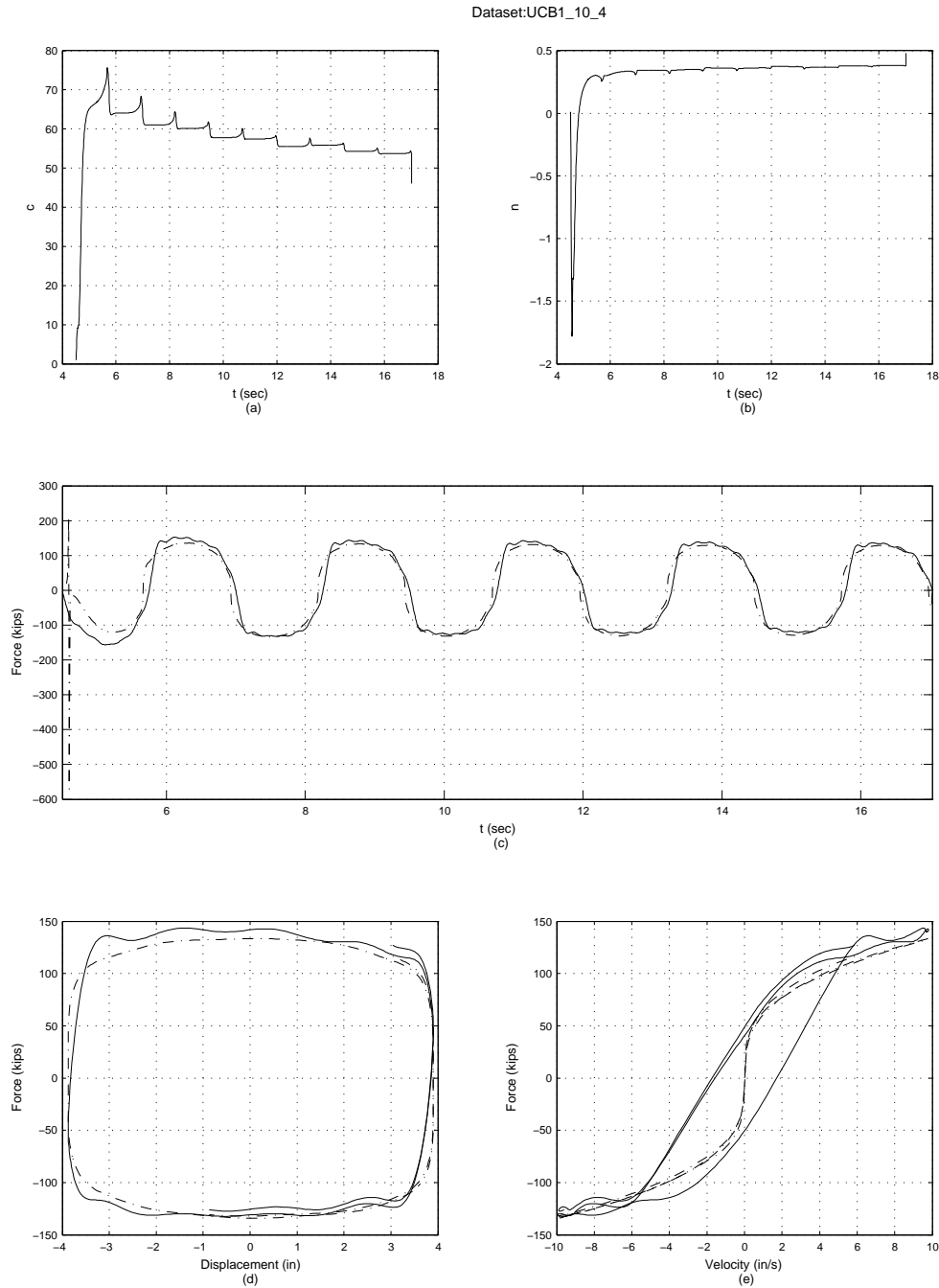


Figure B.1: On-line parametric identification results of 250 kips damper for data set UCB1\_10\_4. Part (a) and (b) show the time-history of the unknown parameters, part (c) shows the time-history comparison of the measured force (solid line) and the predicted force (dash-dot line), part (d) is the displacement-force phase-plane comparison of the measured force (solid line) and the predicted force (dash-dot line), for one cycle, and part (e) is the velocity-force phase-plane comparison of the measured force (solid line) and the predicted force (dash-dot line), for one cycle.

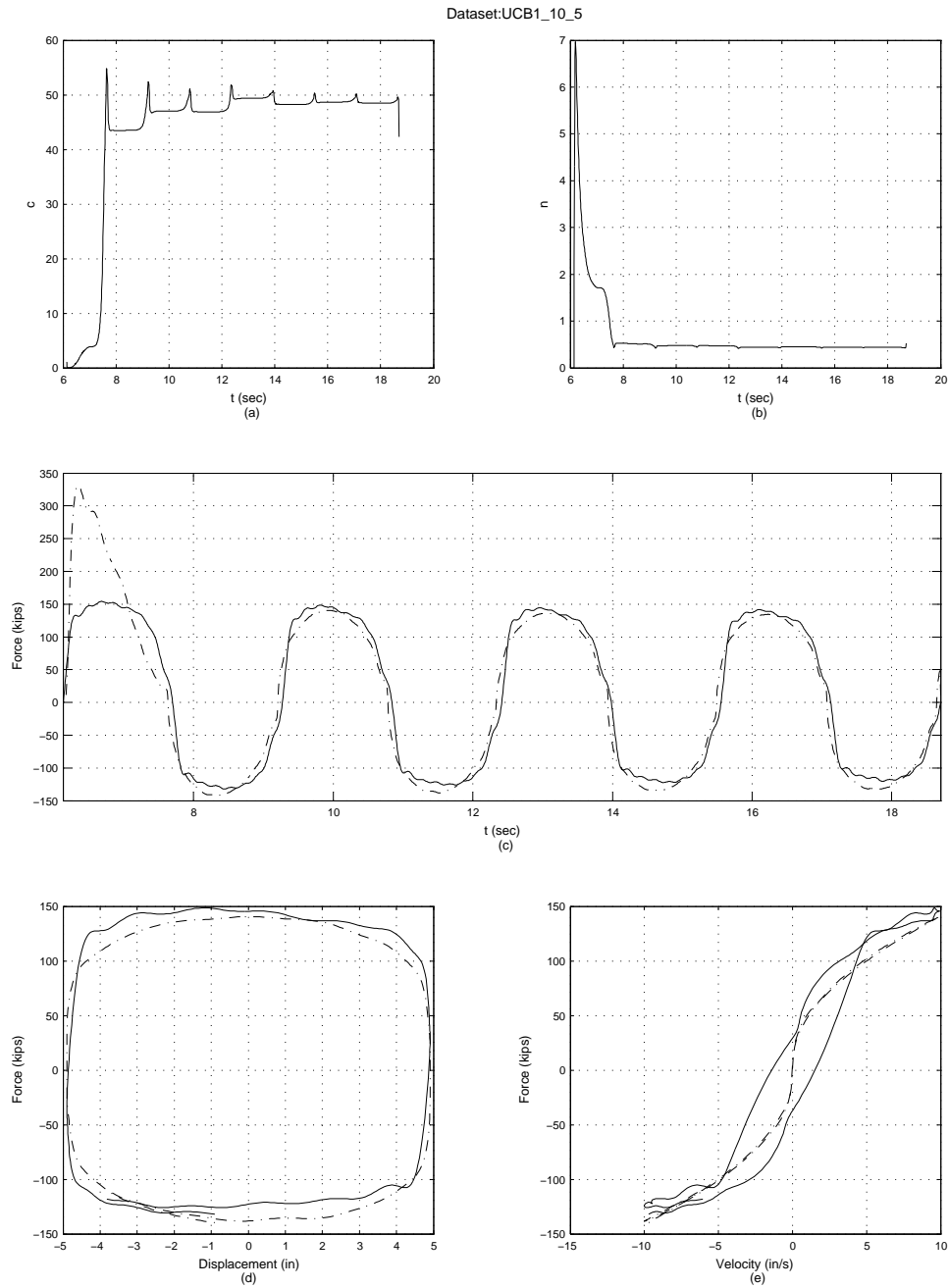


Figure B.2: On-line parametric identification results of 250 kips damper for data set UCB1\_10\_5. Part (a) and (b) show the time-history of the unknown parameters, part (c) shows the time-history comparison of the measured force (solid line) and the predicted force (dash-dot line), part (d) is the displacement-force phase-plane comparison of the measured force (solid line) and the predicted force (dash-dot line), for one cycle, and part (e) is the velocity-force phase-plane comparison of the measured force (solid line) and the predicted force (dash-dot line), for one cycle.

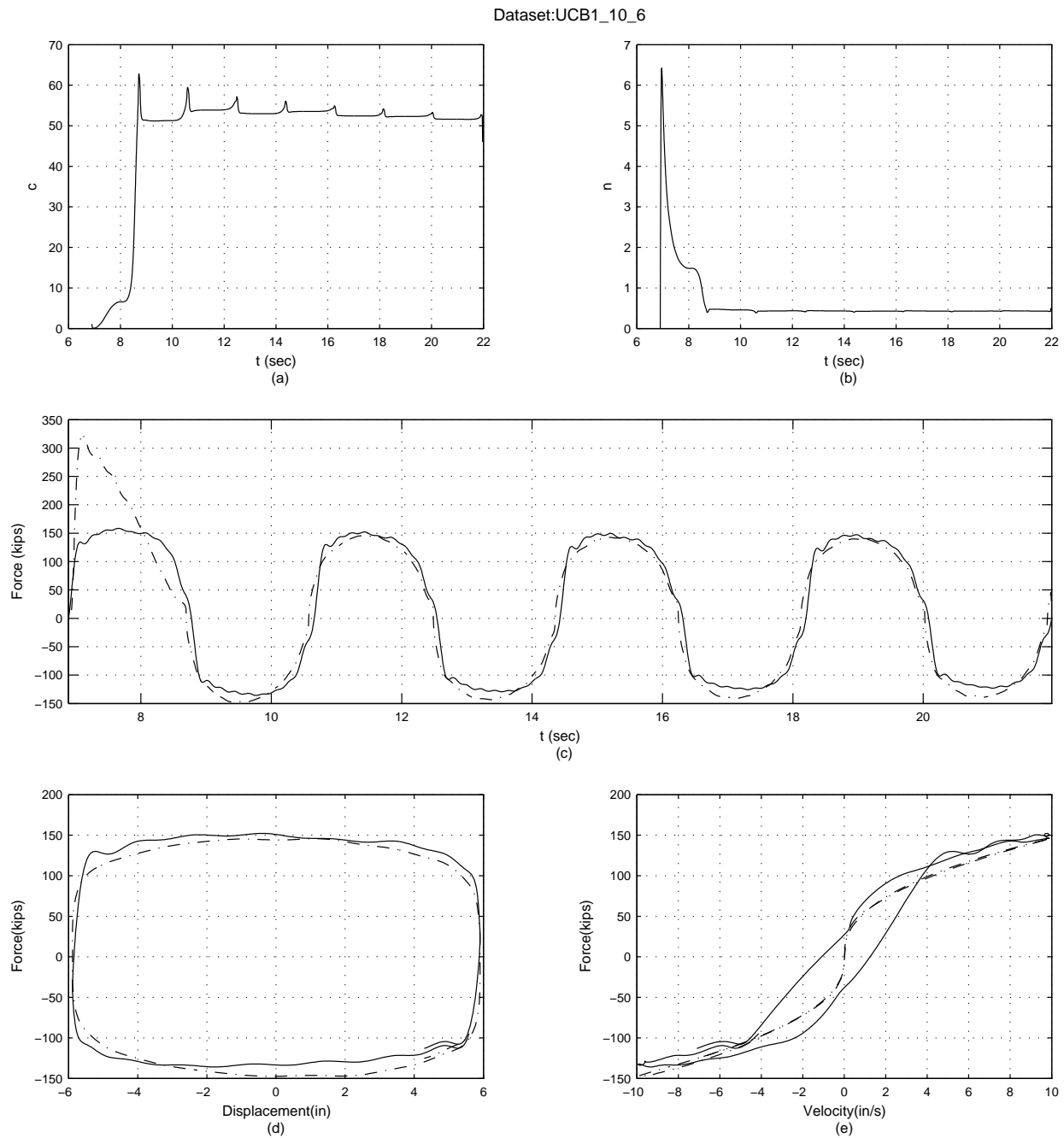


Figure B.3: On-line parametric identification results of 250 kips damper for data set UCB1\_10.6. Part (a) and (b) show the time-history of the unknown parameters, part (c) shows the time-history comparison of the measured force (solid line) and the predicted force (dash-dot line), part (d) is the displacement-force phase-plane comparison of the measured force (solid line) and the predicted force (dash-dot line), for one cycle, and part (e) is the velocity-force phase-plane comparison of the measured force (solid line) and the predicted force (dash-dot line), for one cycle.

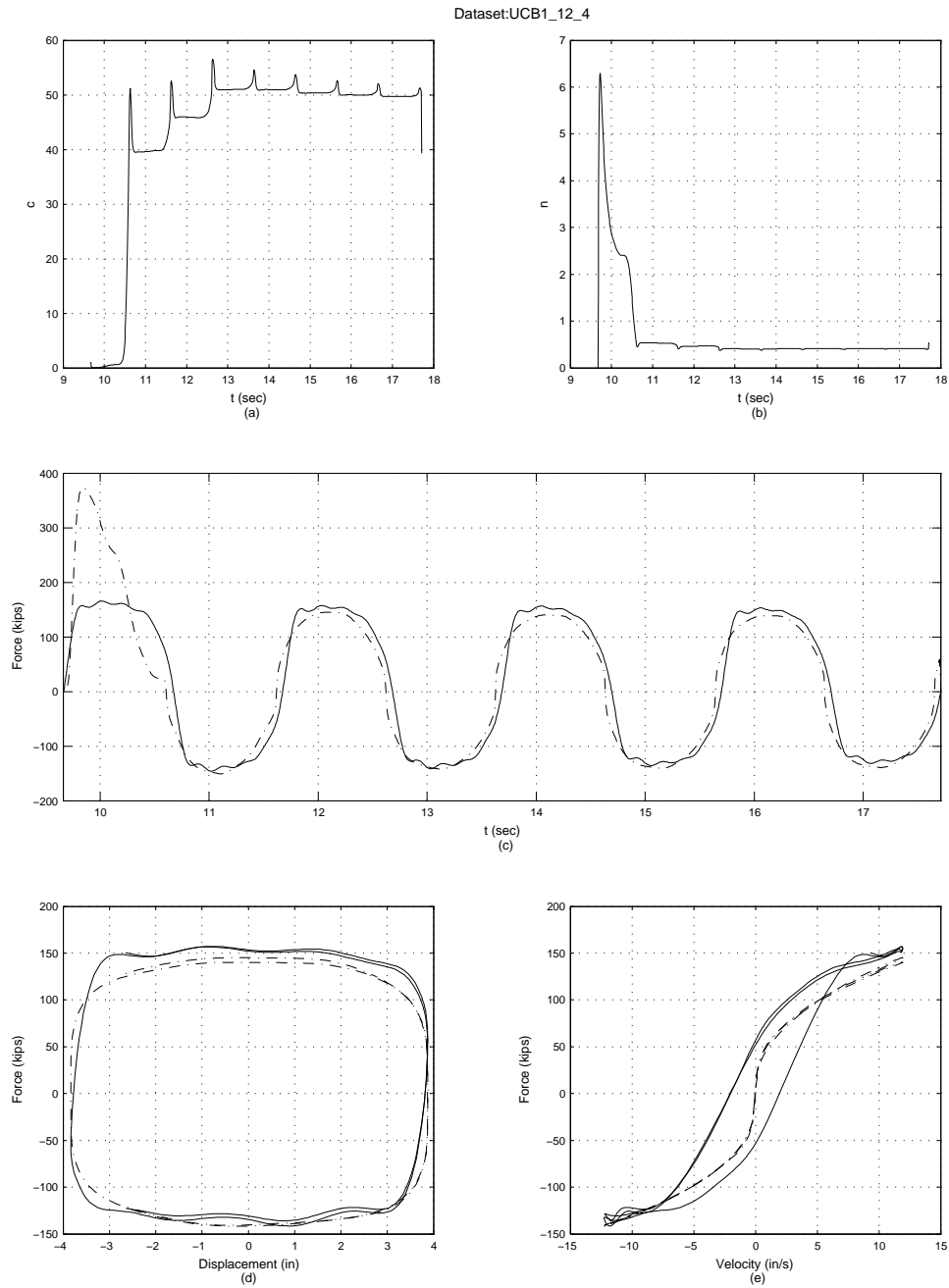


Figure B.4: On-line parametric identification results of 250 kips damper for data set UCB1\_12\_4. Part (a) and (b) show the time-history of the unknown parameters, part (c) shows the time-history comparison of the measured force (solid line) and the predicted force (dash-dot line), part (d) is the displacement-force phase-plane comparison of the measured force (solid line) and the predicted force (dash-dot line), for one cycle, and part (e) is the velocity-force phase-plane comparison of the measured force (solid line) and the predicted force (dash-dot line), for one cycle.

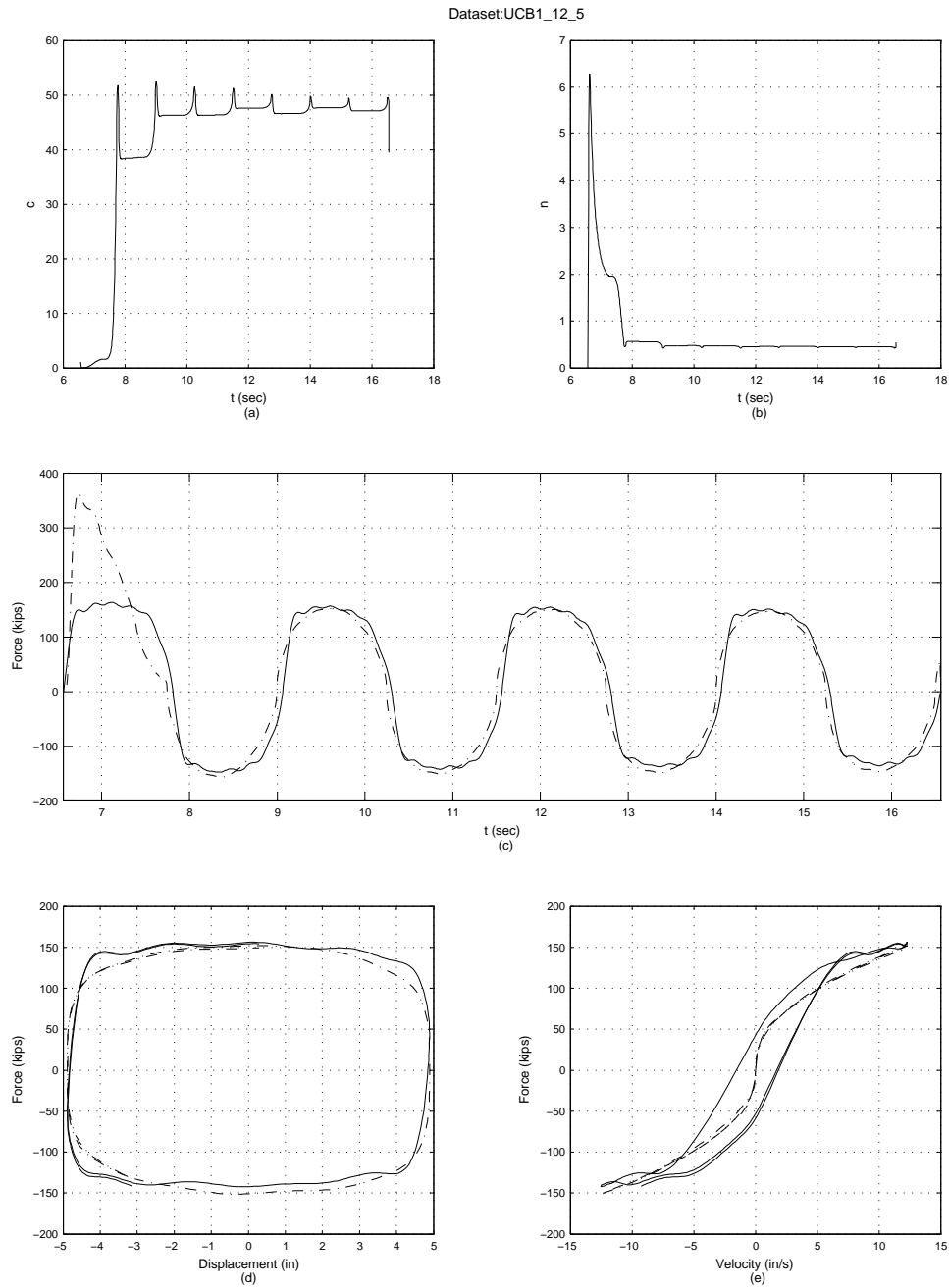


Figure B.5: On-line parametric identification results of 250 kips damper for data set UCB1\_12\_5. Part (a) and (b) show the time-history of the unknown parameters, part (c) shows the time-history comparison of the measured force (solid line) and the predicted force (dash-dot line), part (d) is the displacement-force phase-plane comparison of the measured force (solid line) and the predicted force (dash-dot line), for one cycle, and part (e) is the velocity-force phase-plane comparison of the measured force (solid line) and the predicted force (dash-dot line), for one cycle.

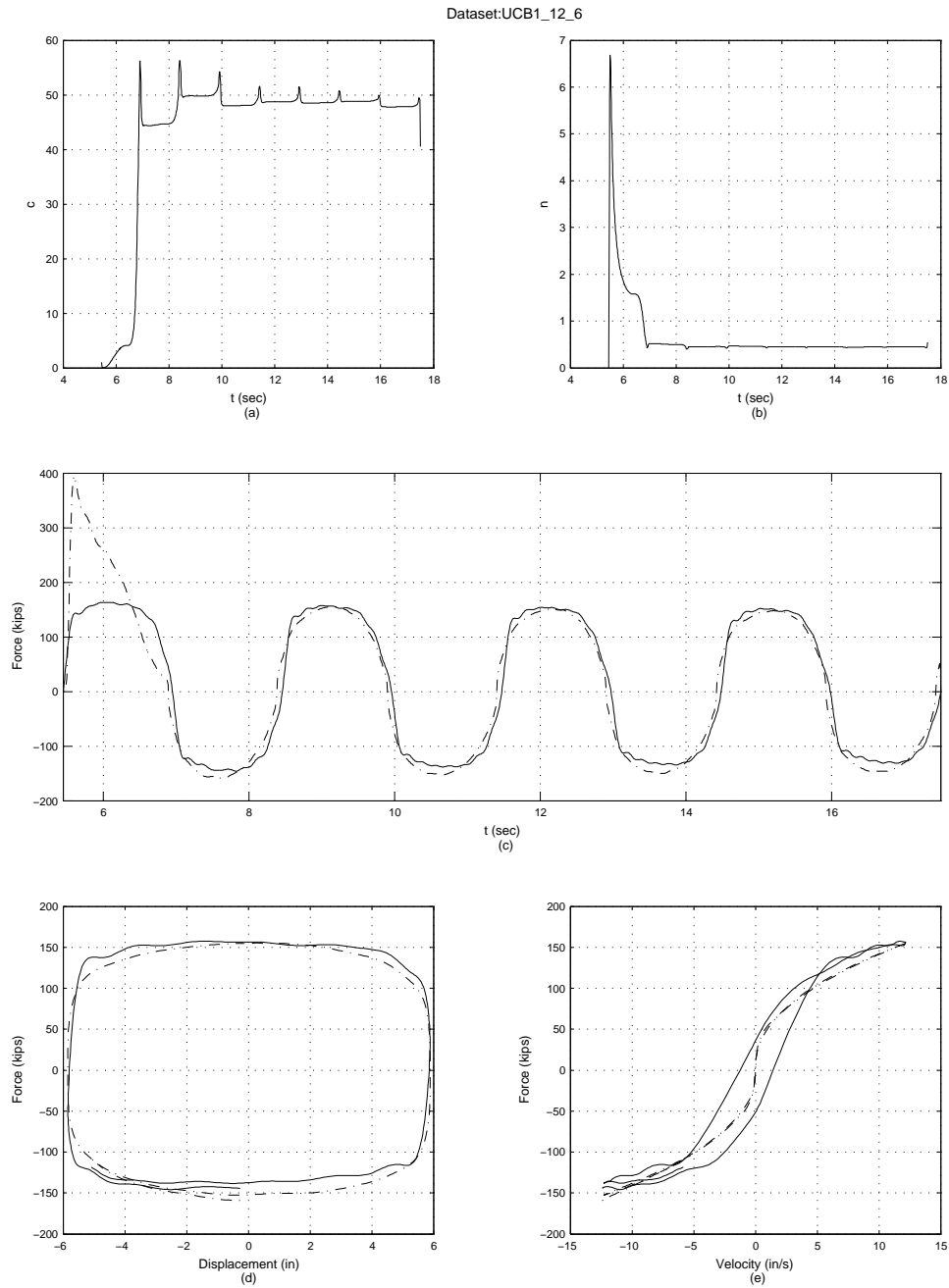


Figure B.6: On-line parametric identification results of 250 kips damper for data set UCB1\_12.6. Part (a) and (b) show the time-history of the unknown parameters, part (c) shows the time-history comparison of the measured force (solid line) and the predicted force (dash-dot line), part (d) is the displacement-force phase-plane comparison of the measured force (solid line) and the predicted force (dash-dot line), for one cycle, and part (e) is the velocity-force phase-plane comparison of the measured force (solid line) and the predicted force (dash-dot line), for one cycle.

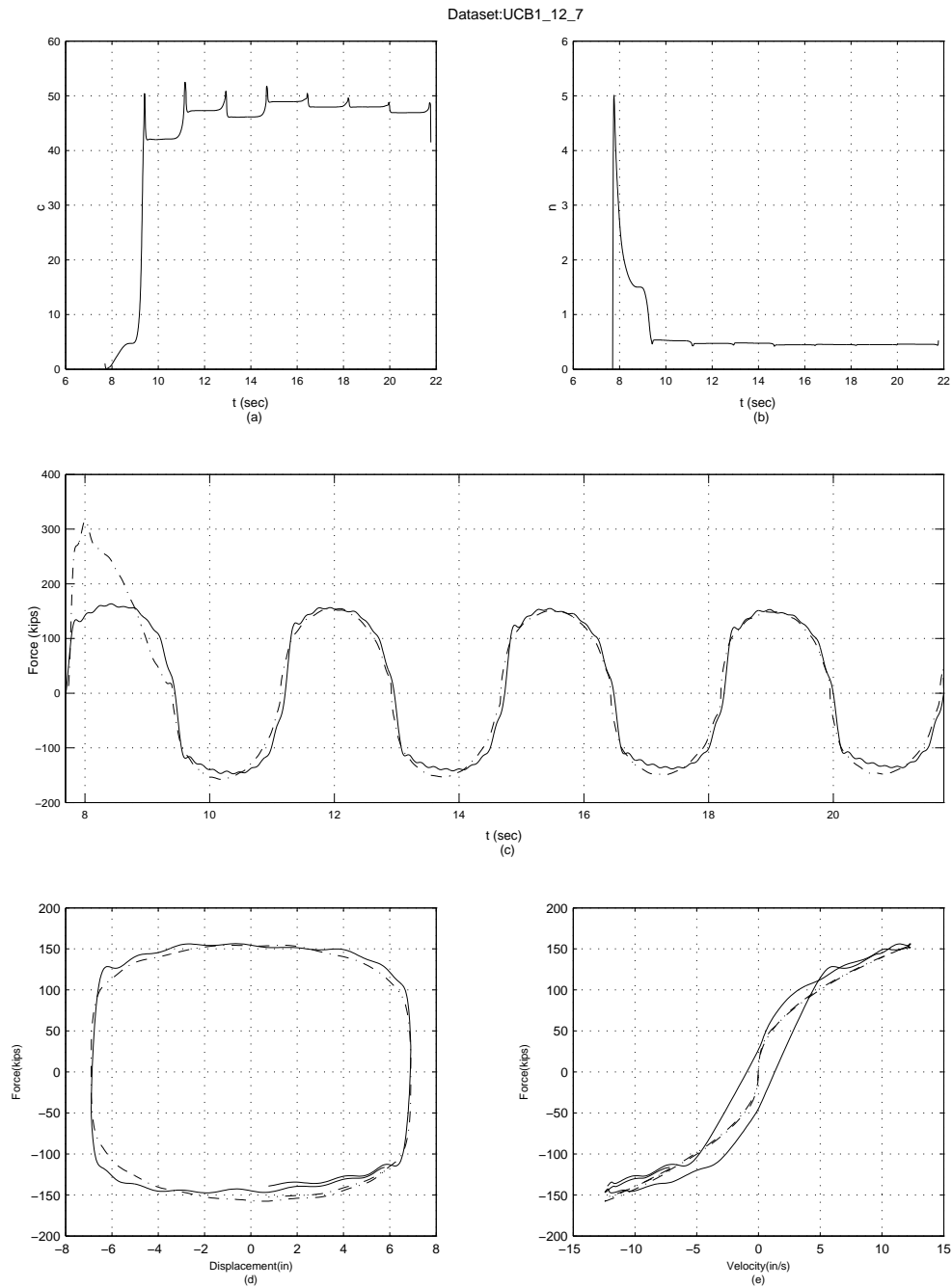


Figure B.7: On-line parametric identification results of 250 kips damper for data set UCB1\_12.7. Part (a) and (b) show the time-history of the unknown parameters, part (c) shows the time-history comparison of the measured force (solid line) and the predicted force (dash-dot line), part (d) is the displacement-force phase-plane comparison of the measured force (solid line) and the predicted force (dash-dot line), for one cycle, and part (e) is the velocity-force phase-plane comparison of the measured force (solid line) and the predicted force (dash-dot line), for one cycle.

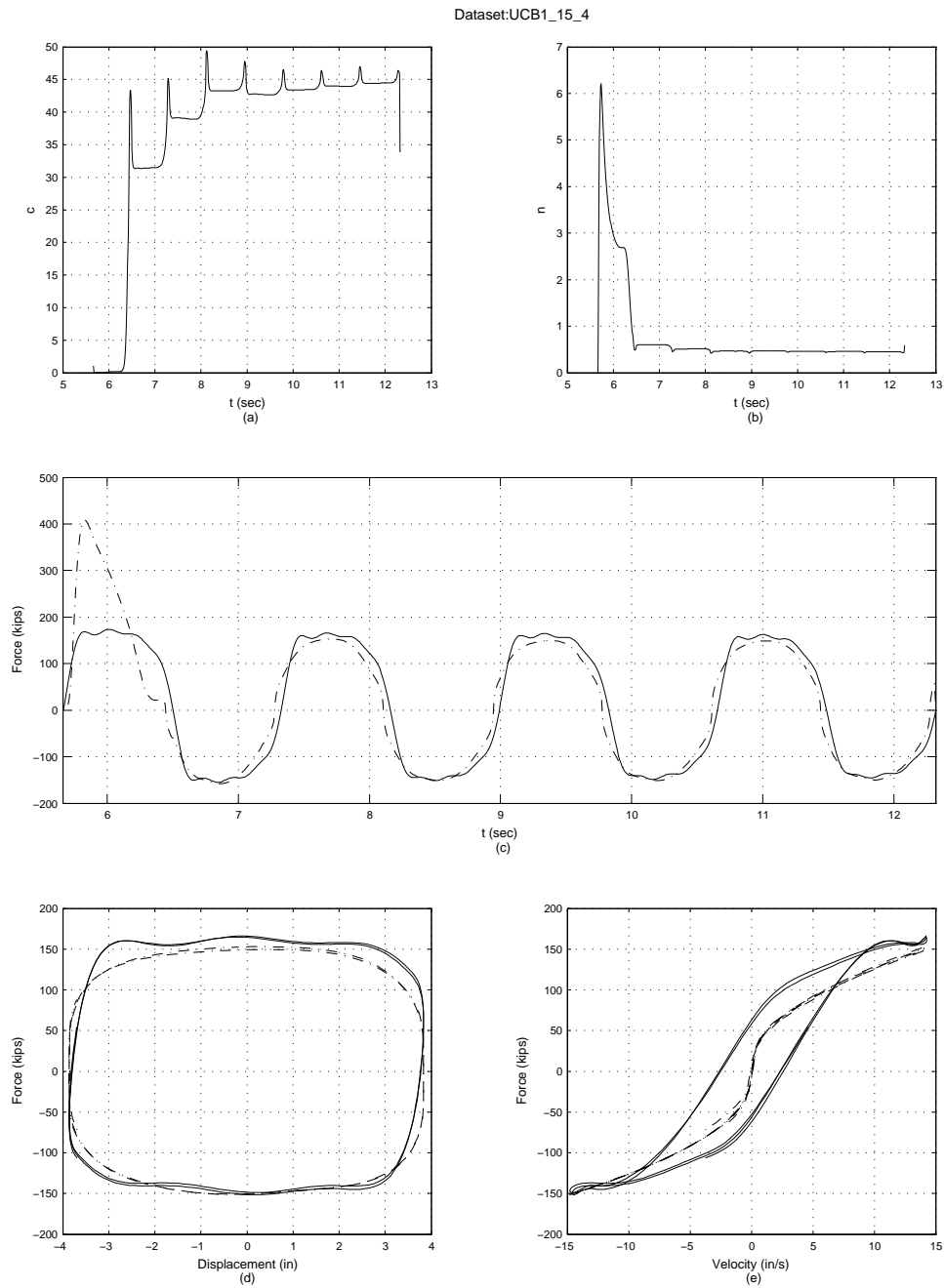


Figure B.8: On-line parametric identification results of 250 kips damper for data set UCB1\_15\_4. Part (a) and (b) show the time-history of the unknown parameters, part (c) shows the time-history comparison of the measured force (solid line) and the predicted force (dash-dot line), part (d) is the displacement-force phase-plane comparison of the measured force (solid line) and the predicted force (dash-dot line), for one cycle, and part (e) is the velocity-force phase-plane comparison of the measured force (solid line) and the predicted force (dash-dot line), for one cycle.

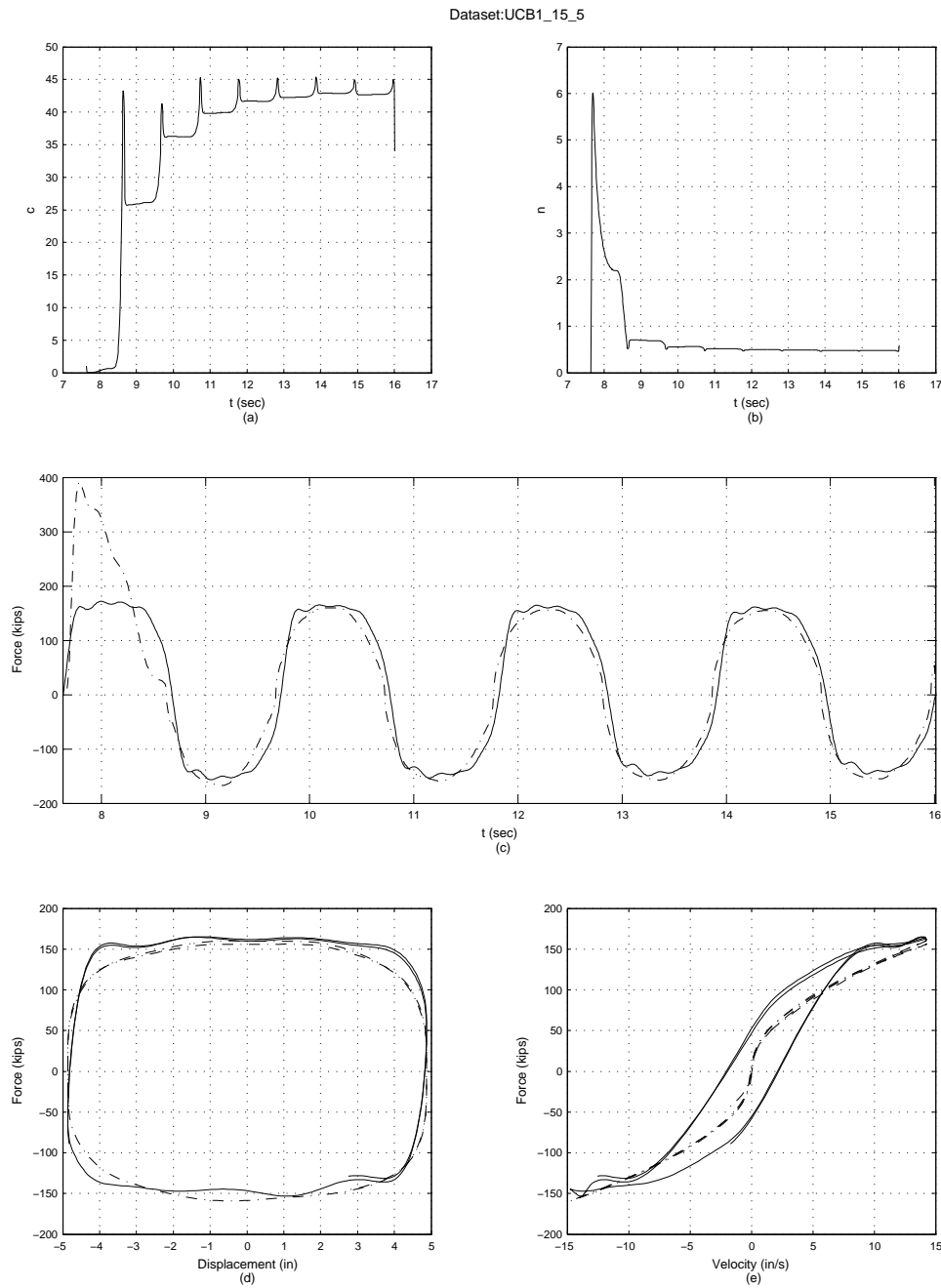


Figure B.9: On-line parametric identification results of 250 kips damper for data set UCB1\_15\_5. Part (a) and (b) show the time-history of the unknown parameters, part (c) shows the time-history comparison of the measured force (solid line) and the predicted force (dash-dot line), part (d) is the displacement-force phase-plane comparison of the measured force (solid line) and the predicted force (dash-dot line), for one cycle, and part (e) is the velocity-force phase-plane comparison of the measured force (solid line) and the predicted force (dash-dot line), for one cycle.

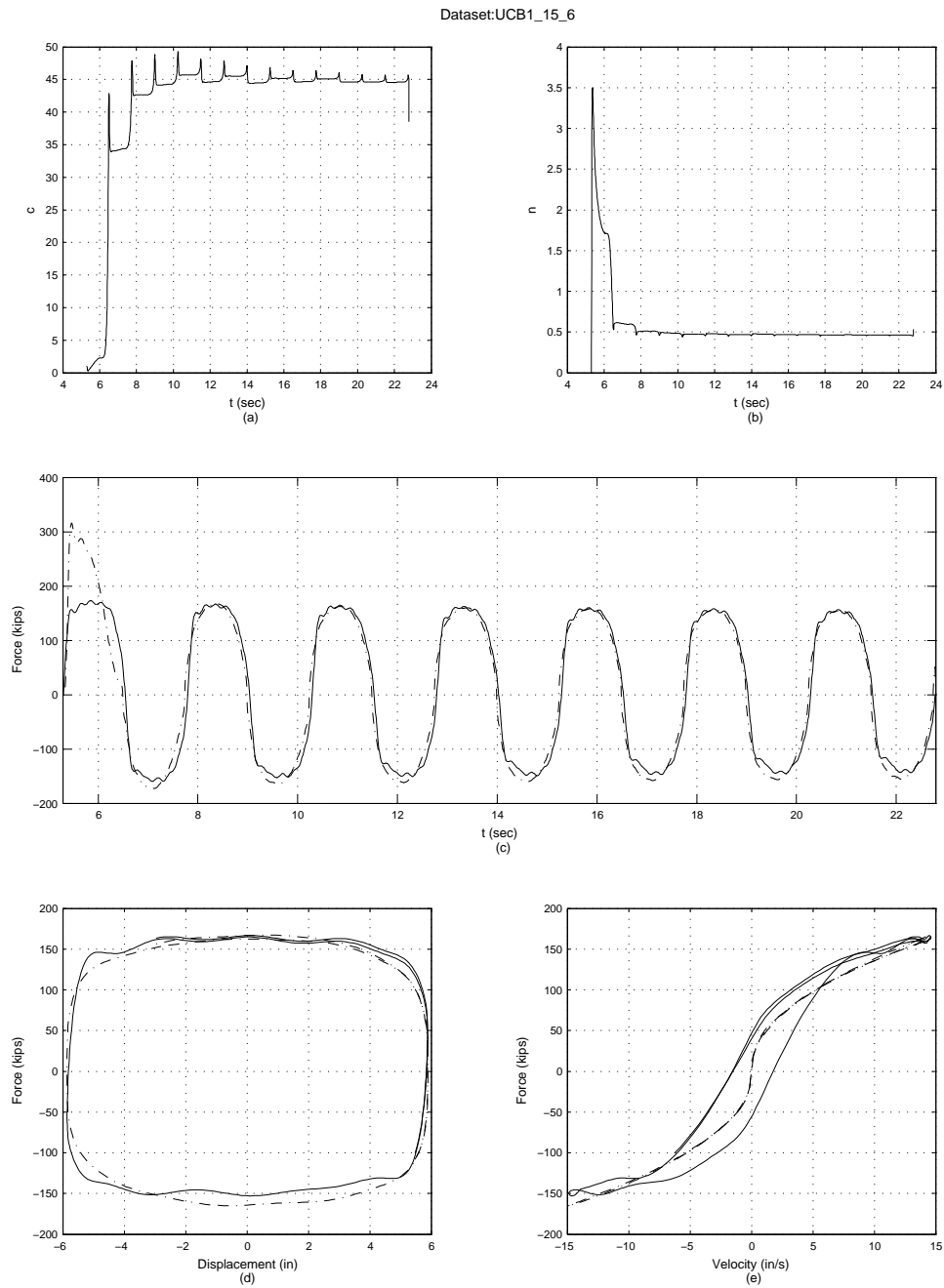


Figure B.10: On-line parametric identification results of 250 kips damper for data set UCB1\_15.6. Part (a) and (b) show the time-history of the unknown parameters, part (c) shows the time-history comparison of the measured force (solid line) and the predicted force (dash-dot line), part (d) is the displacement-force phase-plane comparison of the measured force (solid line) and the predicted force (dash-dot line), for one cycle, and part (e) is the velocity-force phase-plane comparison of the measured force (solid line) and the predicted force (dash-dot line), for one cycle.

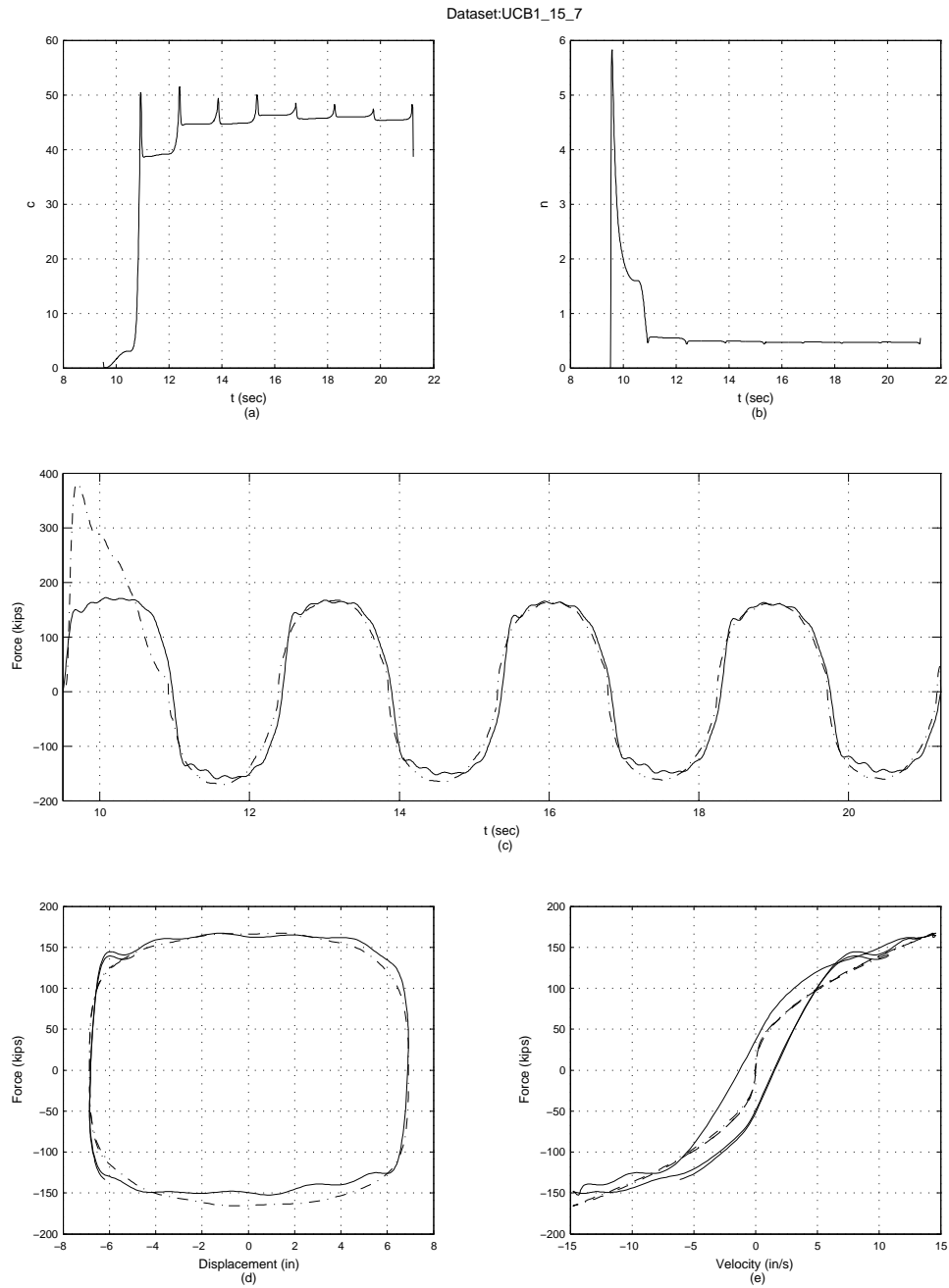


Figure B.11: On-line parametric identification results of 250 kips damper for data set UCB1\_15\_7. Part (a) and (b) show the time-history of the unknown parameters, part (c) shows the time-history comparison of the measured force (solid line) and the predicted force (dash-dot line), part (d) is the displacement-force phase-plane comparison of the measured force (solid line) and the predicted force (dash-dot line), for one cycle, and part (e) is the velocity-force phase-plane comparison of the measured force (solid line) and the predicted force (dash-dot line), for one cycle.

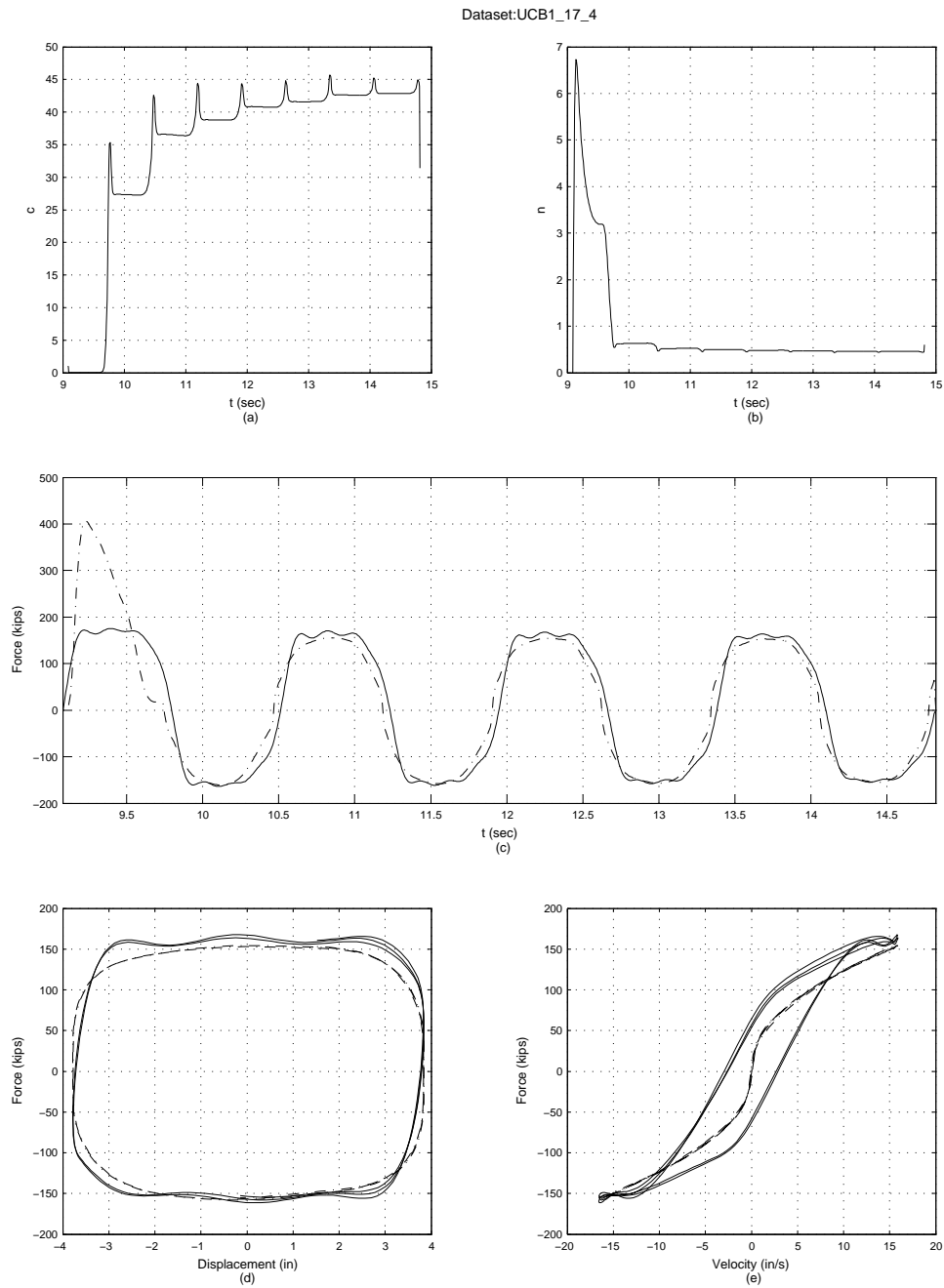


Figure B.12: On-line parametric identification results of 250 kips damper for data set UCB1\_17\_4. Part (a) and (b) show the time-history of the unknown parameters, part (c) shows the time-history comparison of the measured force (solid line) and the predicted force (dash-dot line), part (d) is the displacement-force phase-plane comparison of the measured force (solid line) and the predicted force (dash-dot line), for one cycle, and part (e) is the velocity-force phase-plane comparison of the measured force (solid line) and the predicted force (dash-dot line), for one cycle.

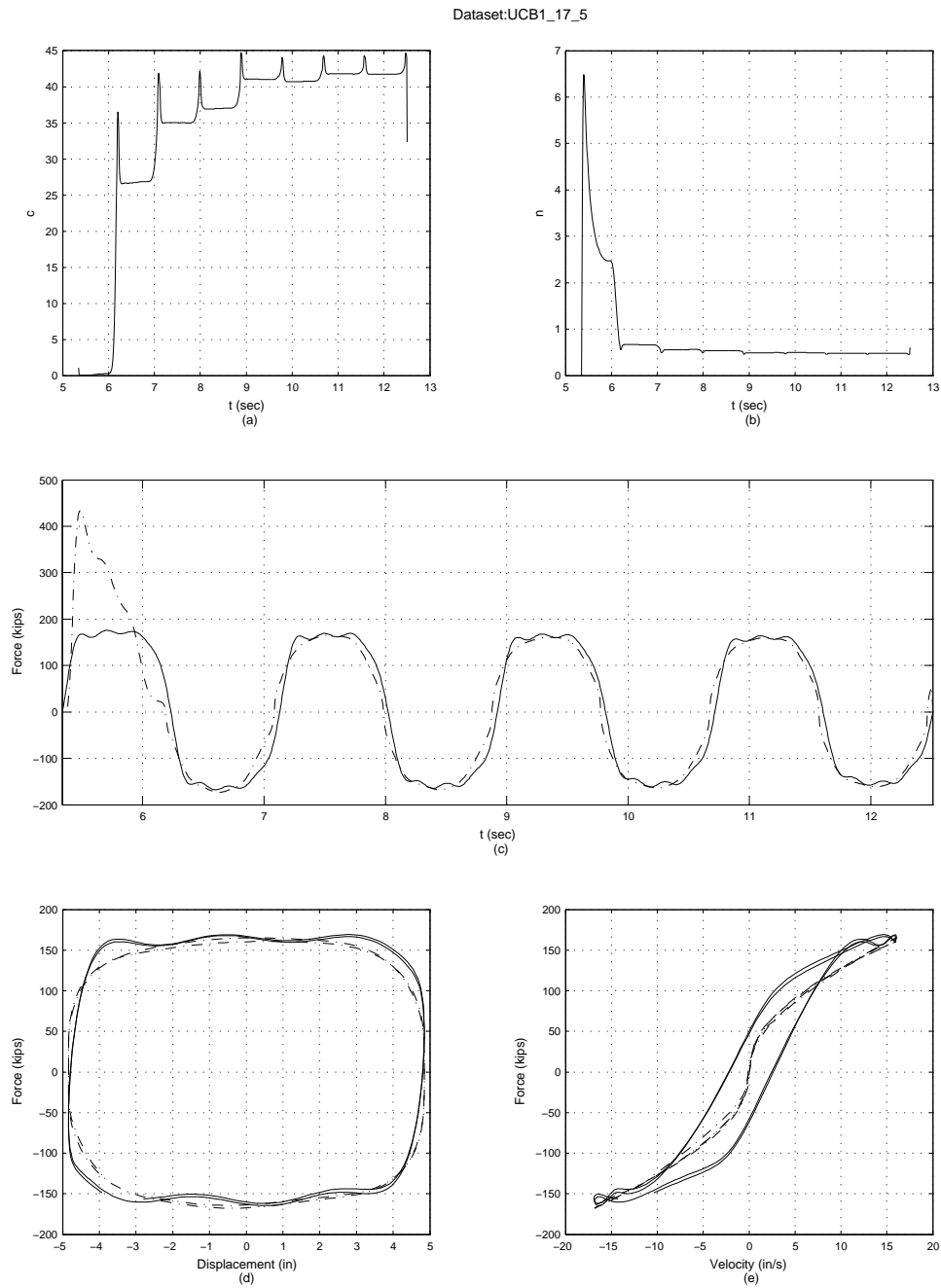


Figure B.13: On-line parametric identification results of 250 kips damper for data set UCB1\_17\_5. Part (a) and (b) show the time-history of the unknown parameters, part (c) shows the time-history comparison of the measured force (solid line) and the predicted force (dash-dot line), part (d) is the displacement-force phase-plane comparison of the measured force (solid line) and the predicted force (dash-dot line), for one cycle, and part (e) is the velocity-force phase-plane comparison of the measured force (solid line) and the predicted force (dash-dot line), for one cycle.

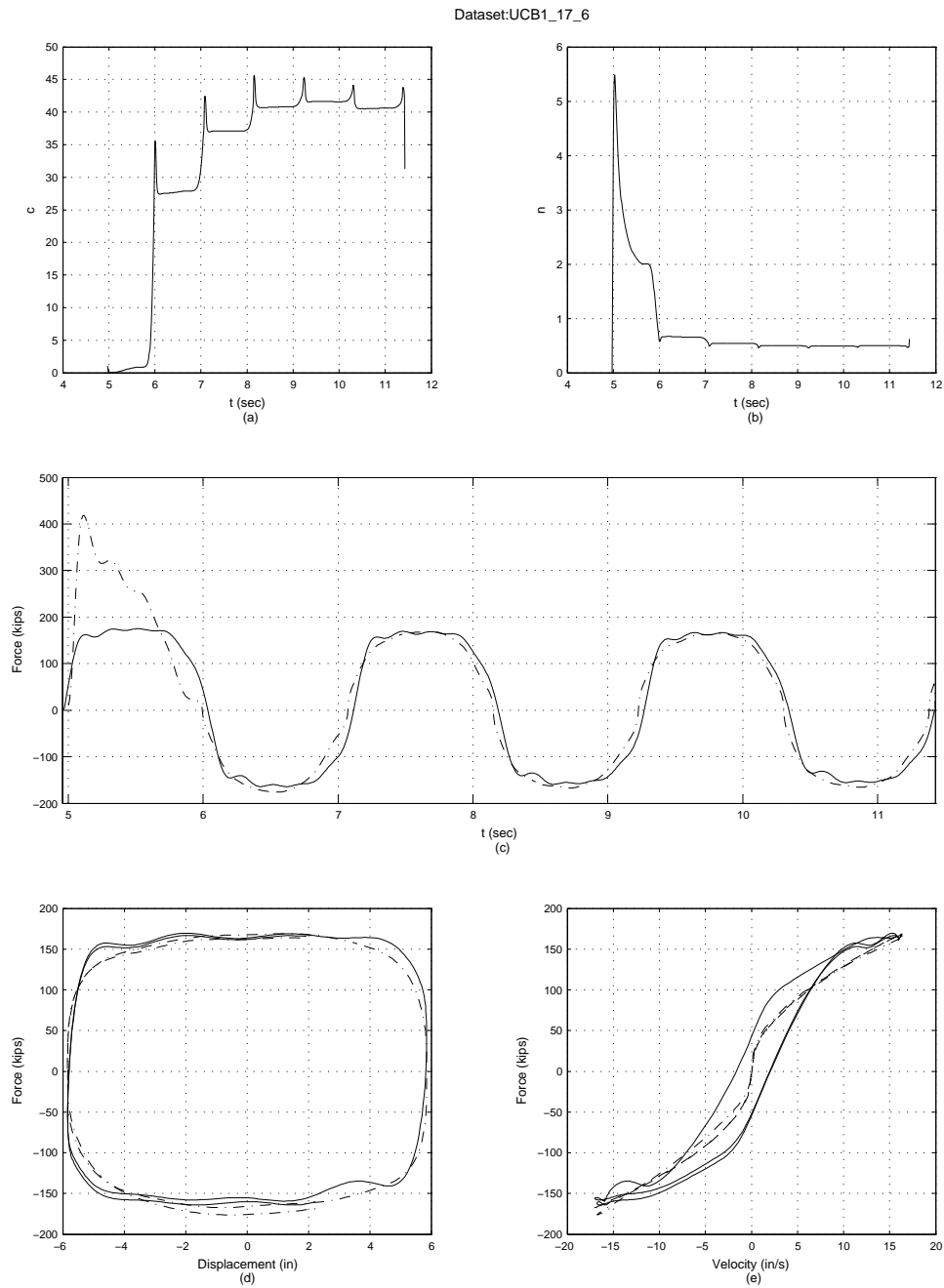


Figure B.14: On-line parametric identification results of 250 kips damper for data set UCB1\_17.6. Part (a) and (b) show the time-history of the unknown parameters, part (c) shows the time-history comparison of the measured force (solid line) and the predicted force (dash-dot line), part (d) is the displacement-force phase-plane comparison of the measured force (solid line) and the predicted force (dash-dot line), for one cycle, and part (e) is the velocity-force phase-plane comparison of the measured force (solid line) and the predicted force (dash-dot line), for one cycle.

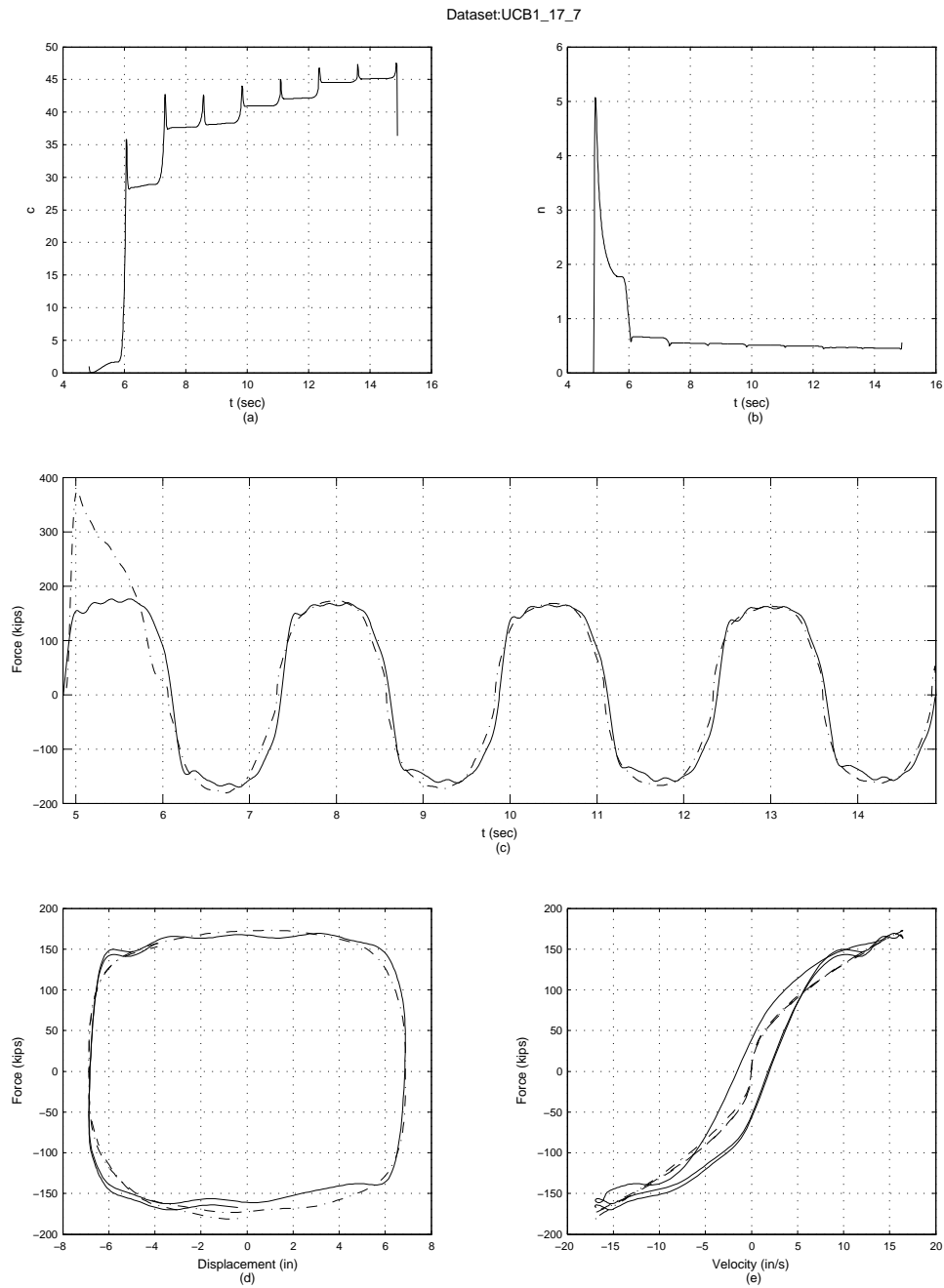


Figure B.15: On-line parametric identification results of 250 kips damper for data set UCB1\_17.7. Part (a) and (b) show the time-history of the unknown parameters, part (c) shows the time-history comparison of the measured force (solid line) and the predicted force (dash-dot line), part (d) is the displacement-force phase-plane comparison of the measured force (solid line) and the predicted force (dash-dot line), for one cycle, and part (e) is the velocity-force phase-plane comparison of the measured force (solid line) and the predicted force (dash-dot line), for one cycle.

## B.2 Off-Line Parametric Identification

The plots of the off-line identification results for the 250 kip viscous damper are provided in this section. The results of the off-line identification of the 250 kip viscous damper are summarized in Table B.3.

Table B.3: Summary of the off-line parametric identification results for the 250 kip damper data set. Column 1 is the data set name, columns 2 to 7 are the optimum values of the initially unknown parameters (Eqn. 2.11), column 8 is the normalized mean-square-error (Eqn. 2.9).

Data set	c (kip sec/in)	k (kip/in)	n	$\theta_1$	$\theta_2$	$\theta_3$	% MSE
UCB1_10_4	7.51	0.07	1.87	430.1	-1.06	0.89	2.00
UCB1_10_5	8.57	0.67	2.01	476.2	-0.77	0.65	3.49
UCB1_10_6	8.36	0.18	2.07	511.8	-0.96	0.86	3.27
UCB1_12_4	6.26	0.88	2.01	493.5	-0.41	0.32	2.87
UCB1_12_5	6.48	0.69	2.01	509.3	-0.86	0.77	3.07
UCB1_12_6	6.74	0.25	2.02	512.3	-0.83	0.74	3.04
UCB1_12_7	7.17	0.04	2.03	500.8	-1.02	0.91	3.15
UCB1_15_4	4.65	1.09	2.01	511.2	-0.29	2.15	2.78
UCB1_15_5	5.88	0.80	2.01	511.2	-0.47	0.39	2.86
UCB1_15_6	6.06	0.73	2.02	547.2	-0.97	0.87	3.01
UCB1_15_7	6.14	0.55	1.83	622.6	-3.29	3.00	2.94
UCB1_17_4	5.36	1.27	1.84	546.9	-0.45	0.27	2.75
UCB1_17_5	5.57	1.19	1.82	578.3	-1.31	1.10	2.82
UCB1_17_6	5.67	0.97	1.94	627.1	-1.74	1.60	2.81
UCB1_17_7	5.65	0.60	1.95	622.8	-1.69	1.55	2.82

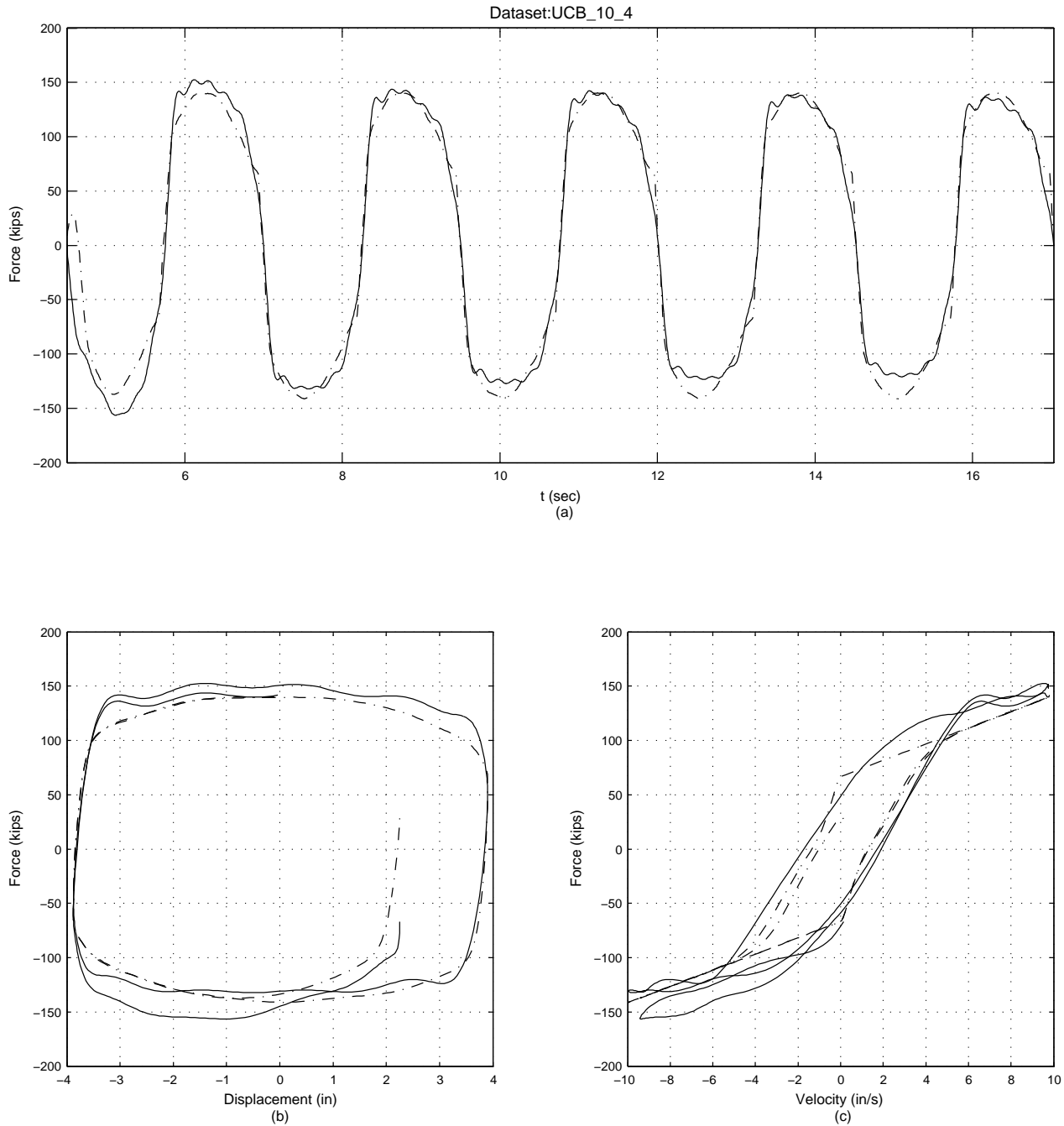


Figure B.16: Off-line parametric identification results of 250 kips damper for data set UCB1\_10.4. Part (a) shows the time-history comparison of the measured force (solid line) and the predicted force (dash-dot line), part (b) shows the displacement-force phase-plane comparison of the measured force (solid line) and the predicted force (dash-dot line), for one cycle, and part (c) shows the velocity-force phase-plane comparison of the measured force (solid line) and the predicted force (dash-dot line), for one cycle.

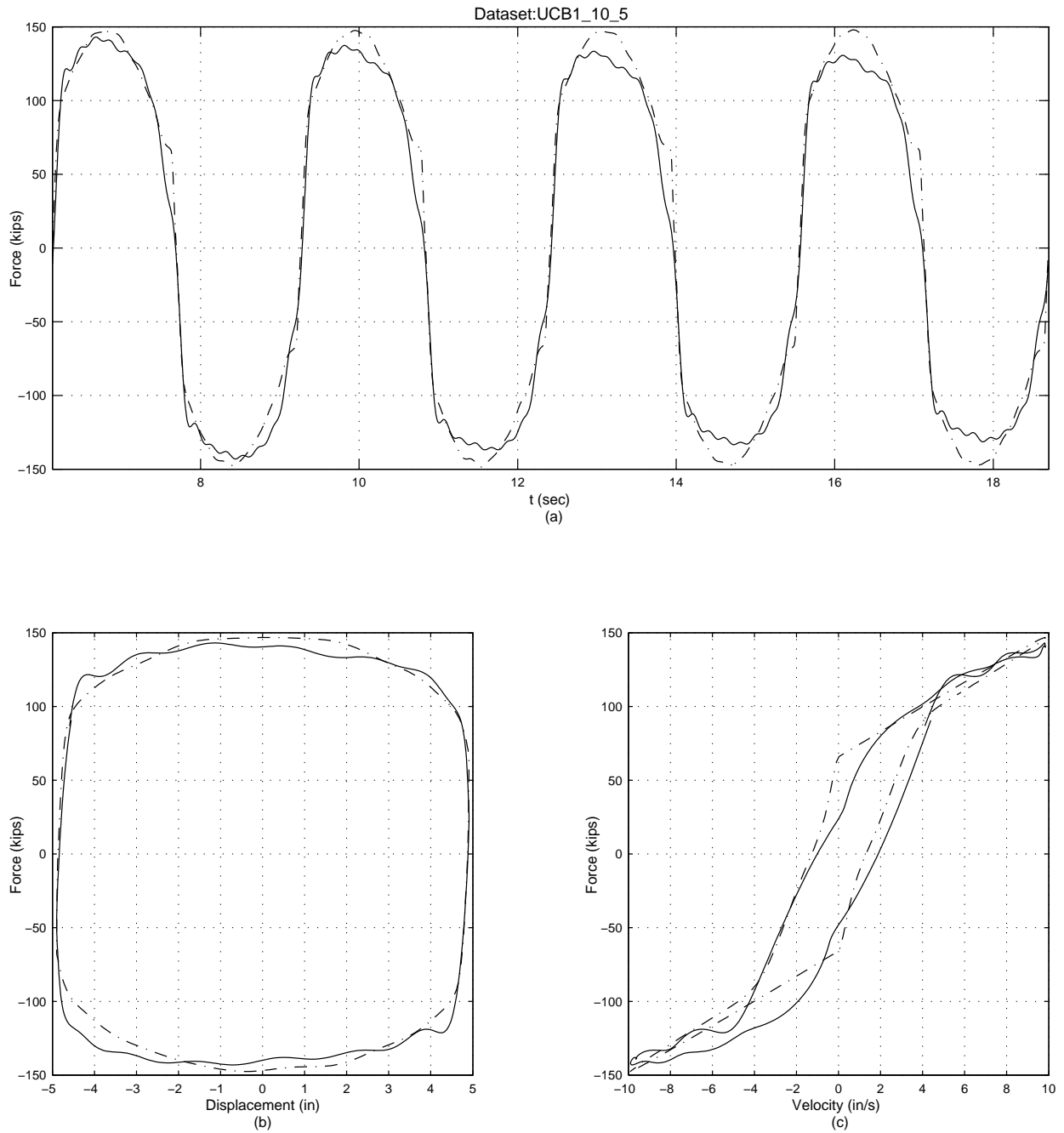


Figure B.17: Off-line parametric identification results of 250 kips damper for data set UCB1\_10\_5. Part (a) shows the time-history comparison of the measured force (solid line) and the predicted force (dash-dot line), part (b) shows the displacement-force phase-plane comparison of the measured force (solid line) and the predicted force (dash-dot line), for one cycle, and part (c) shows the velocity-force phase-plane comparison of the measured force (solid line) and the predicted force (dash-dot line), for one cycle.

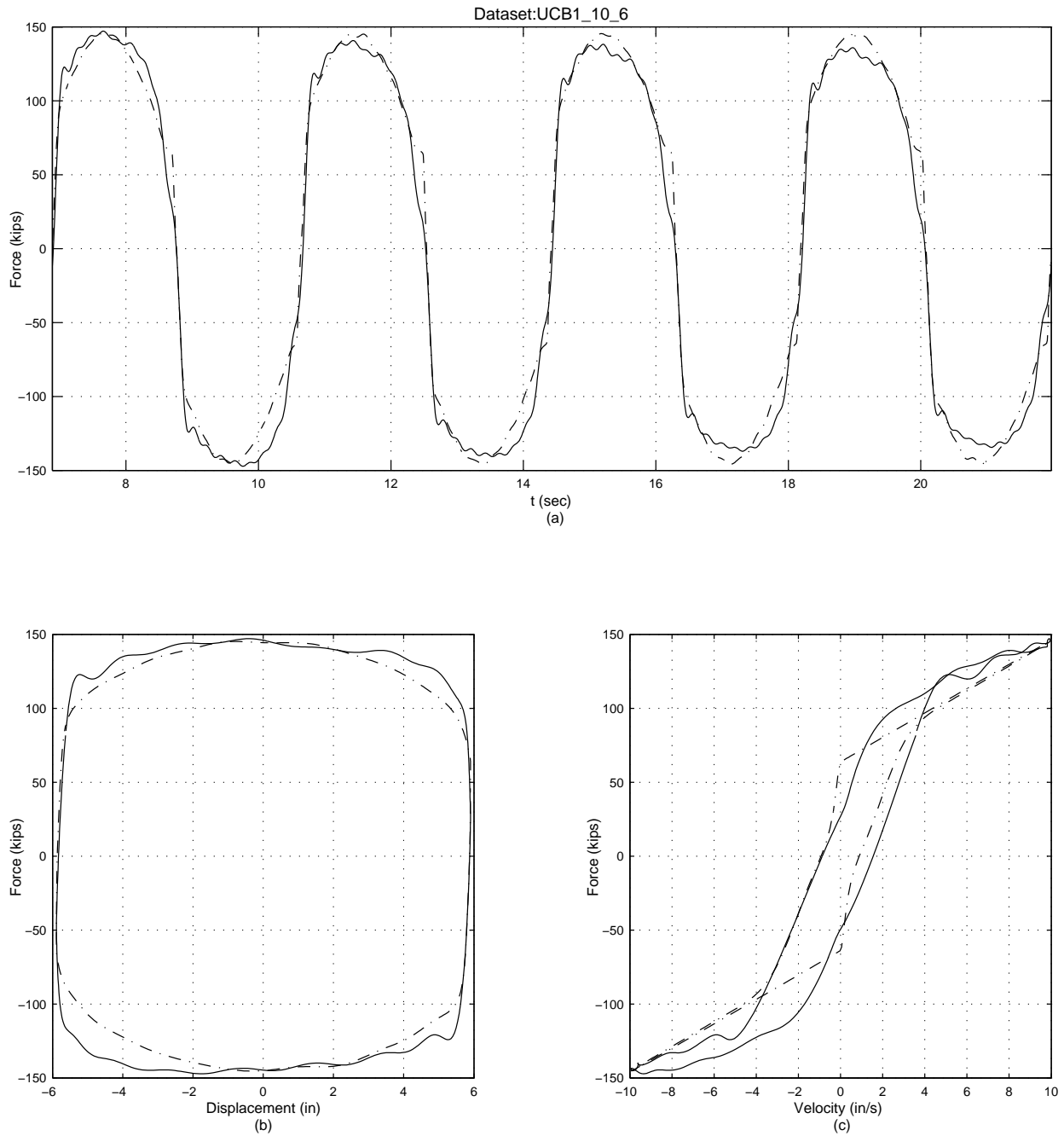


Figure B.18: Off-line parametric identification results of 250 kips damper for data set UCB1\_10.6. Part (a) shows the time-history comparison of the measured force (solid line) and the predicted force (dash-dot line), part (b) shows the displacement-force phase-plane comparison of the measured force (solid line) and the predicted force (dash-dot line), for one cycle, and part (c) shows the velocity-force phase-plane comparison of the measured force (solid line) and the predicted force (dash-dot line), for one cycle.

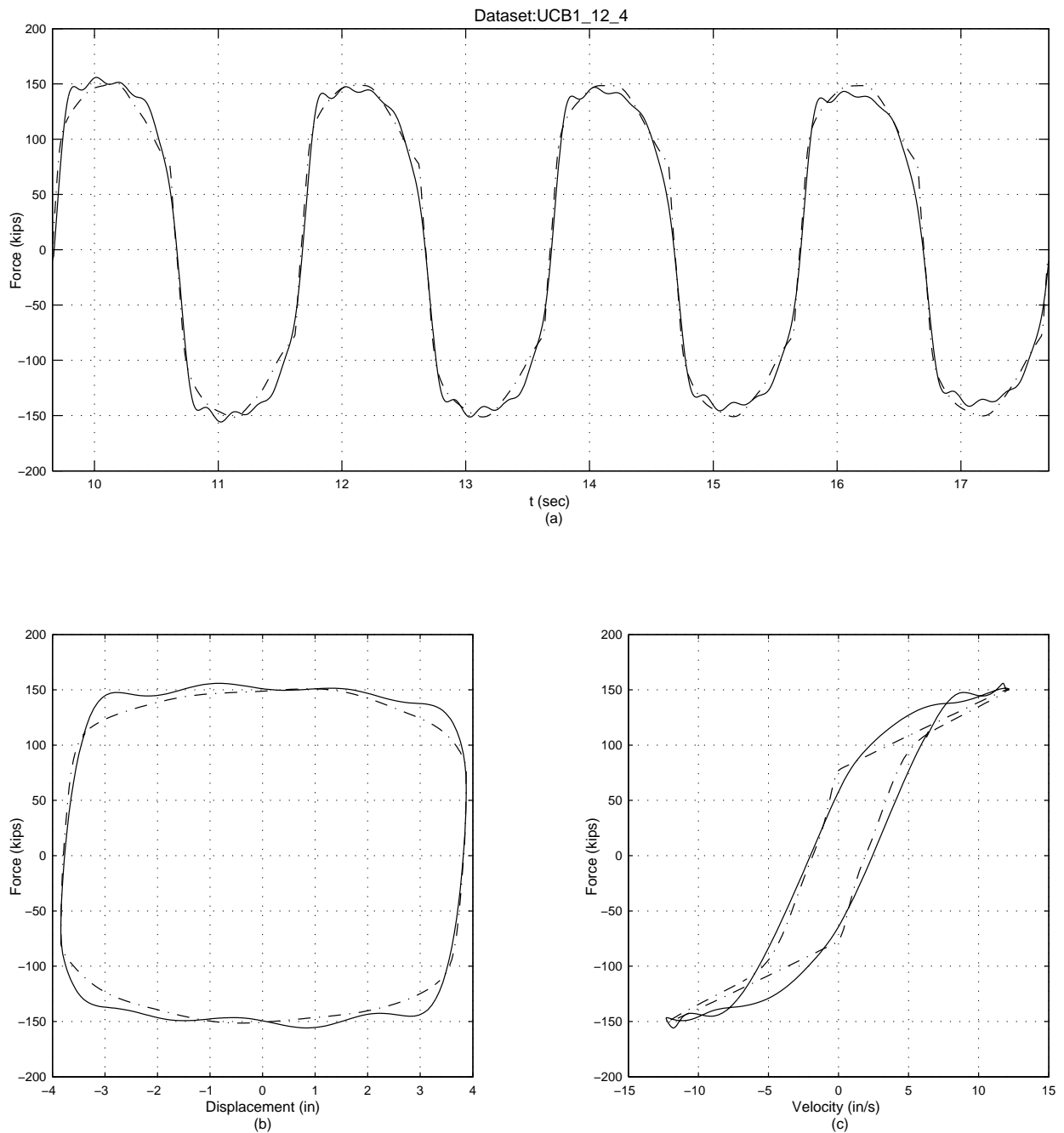


Figure B.19: Off-line parametric identification results of 250 kips damper for data set UCB1\_12\_4. Part (a) shows the time-history comparison of the measured force (solid line) and the predicted force (dash-dot line), part (b) shows the displacement-force phase-plane comparison of the measured force (solid line) and the predicted force (dash-dot line), for one cycle, and part (c) shows the velocity-force phase-plane comparison of the measured force (solid line) and the predicted force (dash-dot line), for one cycle.

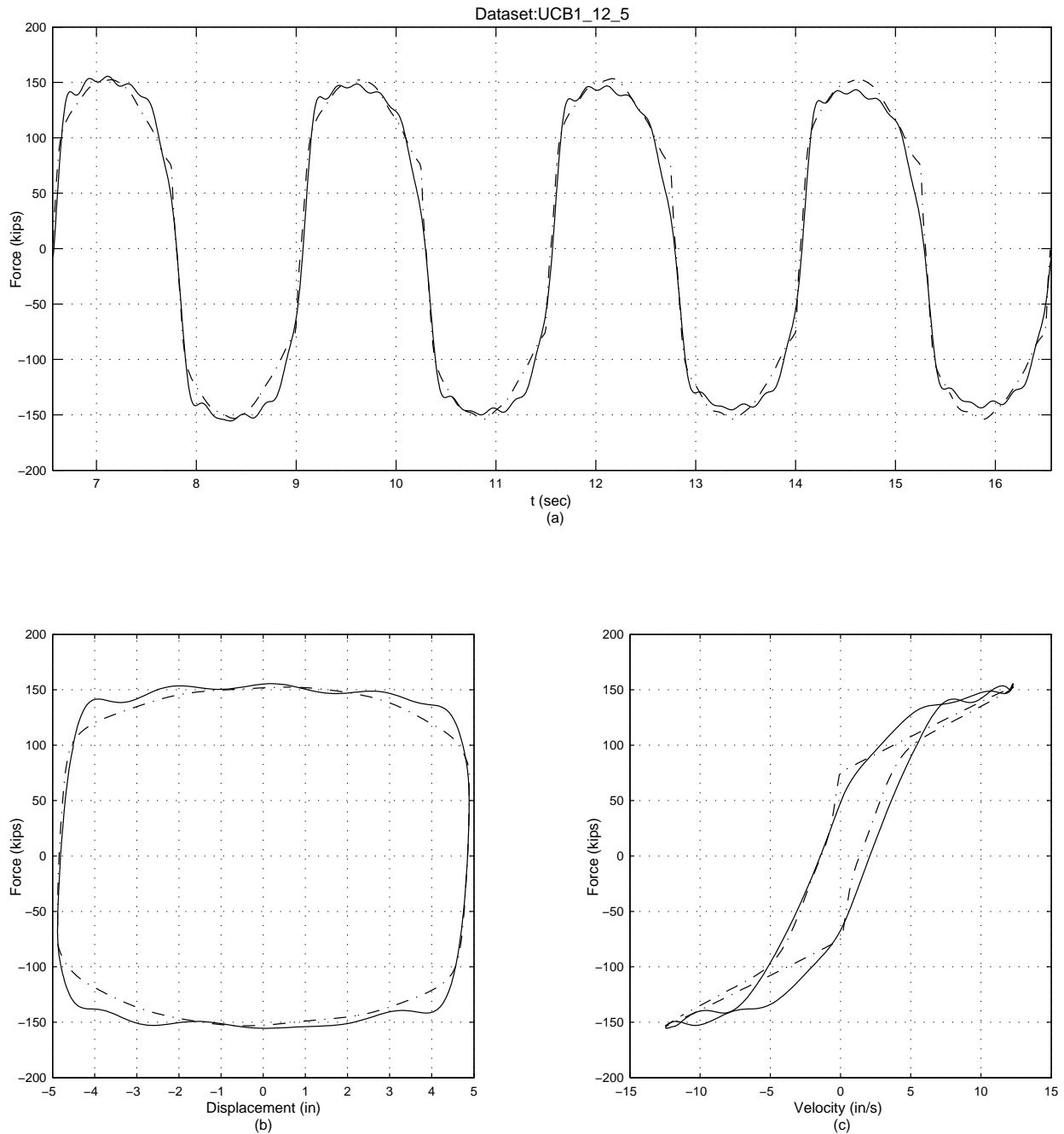


Figure B.20: Off-line parametric identification results of 250 kips damper for data set UCB1\_12\_5. Part (a) shows the time-history comparison of the measured force (solid line) and the predicted force (dash-dot line), part (b) shows the displacement-force phase-plane comparison of the measured force (solid line) and the predicted force (dash-dot line), for one cycle, and part (c) shows the velocity-force phase-plane comparison of the measured force (solid line) and the predicted force (dash-dot line), for one cycle.

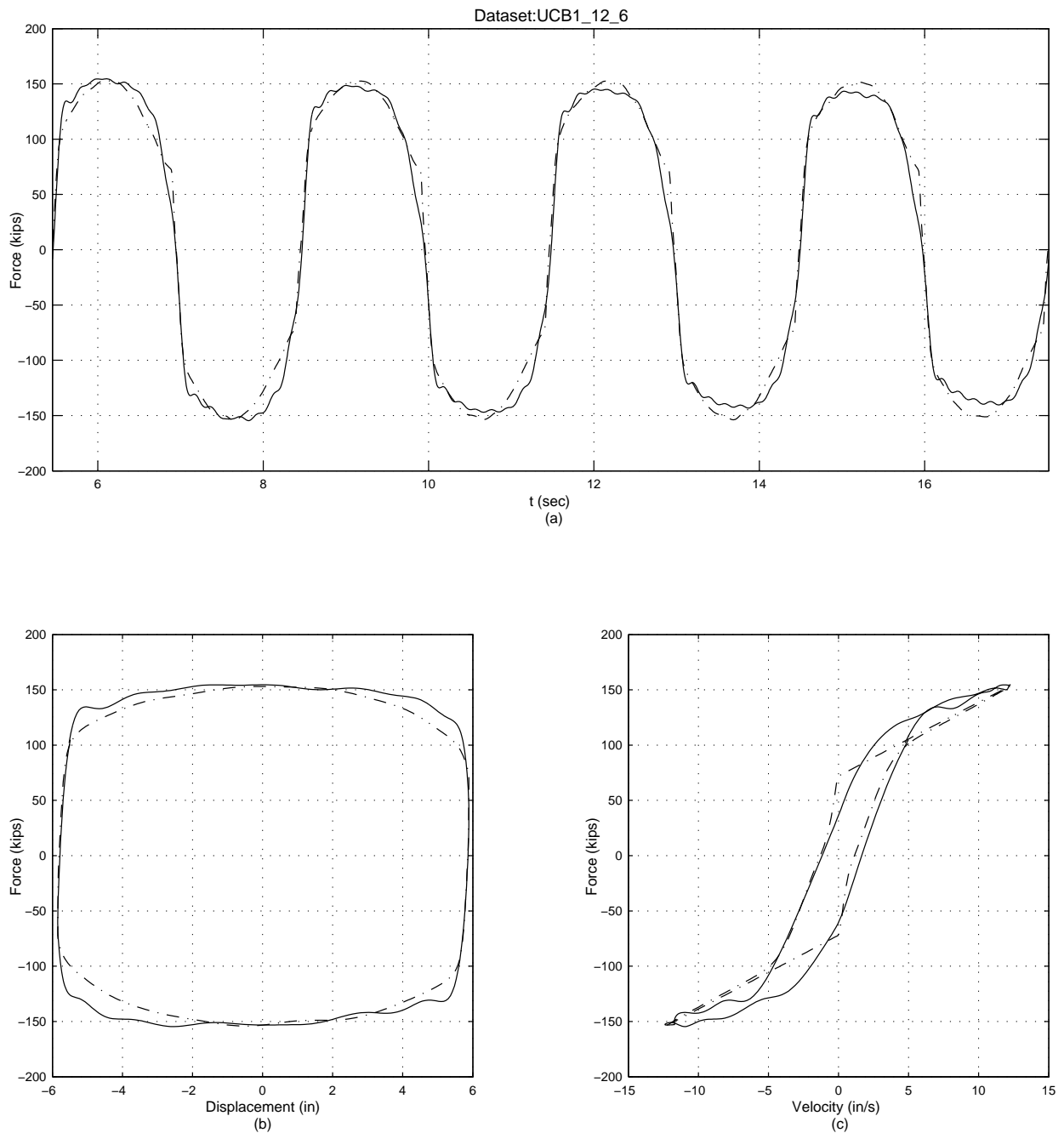


Figure B.21: Off-line parametric identification results of 250 kips damper for data set UCB1\_12.6. Part (a) shows the time-history comparison of the measured force (solid line) and the predicted force (dash-dot line), part (b) shows the displacement-force phase-plane comparison of the measured force (solid line) and the predicted force (dash-dot line), for one cycle, and part (c) shows the velocity-force phase-plane comparison of the measured force (solid line) and the predicted force (dash-dot line), for one cycle.

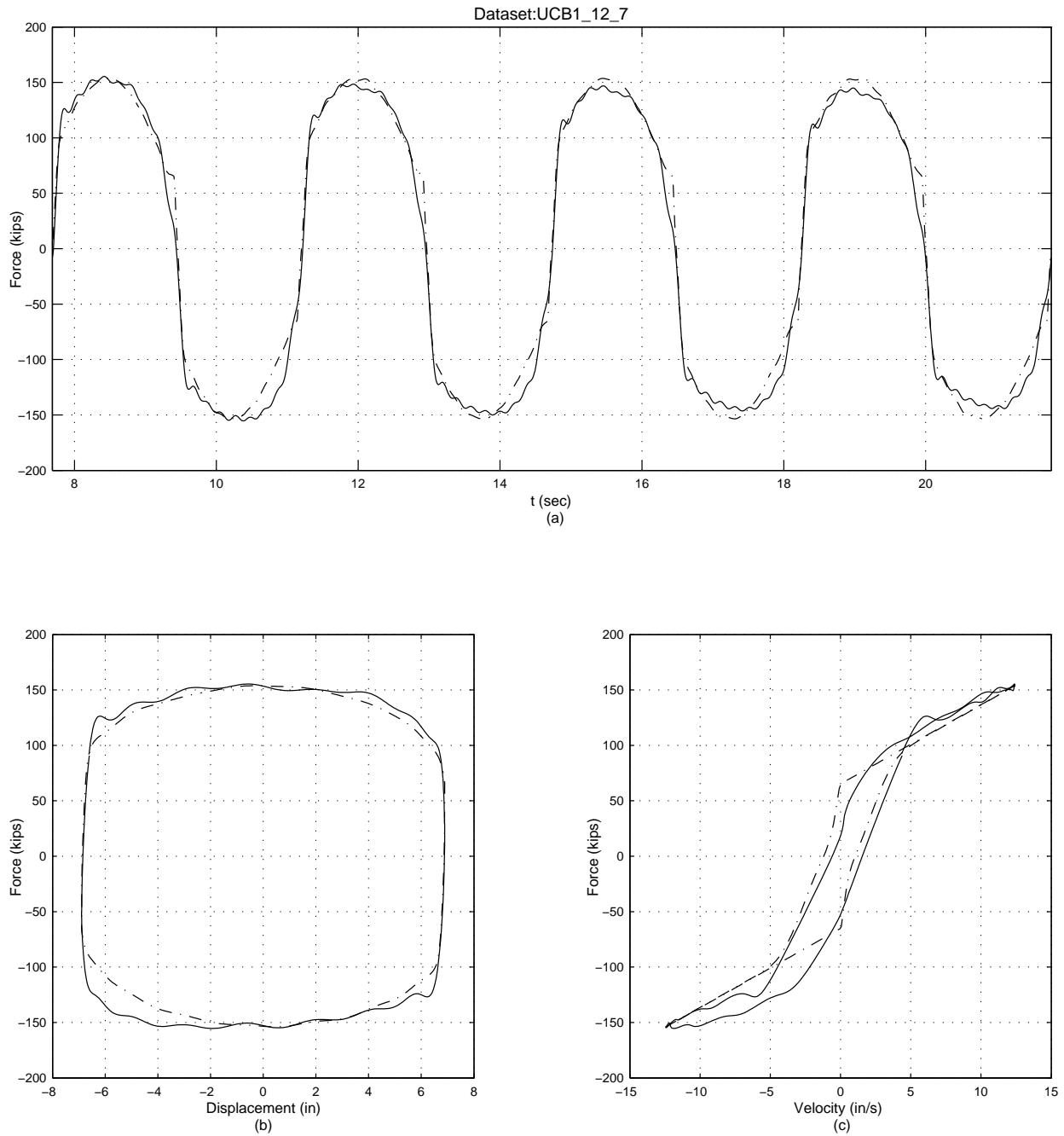


Figure B.22: Off-line parametric identification results of 250 kips damper for data set UCB1\_12.7. Part (a) shows the time-history comparison of the measured force (solid line) and the predicted force (dash-dot line), part (b) shows the displacement-force phase-plane comparison of the measured force (solid line) and the predicted force (dash-dot line), for one cycle, and part (c) shows the velocity-force phase-plane comparison of the measured force (solid line) and the predicted force (dash-dot line), for one cycle.

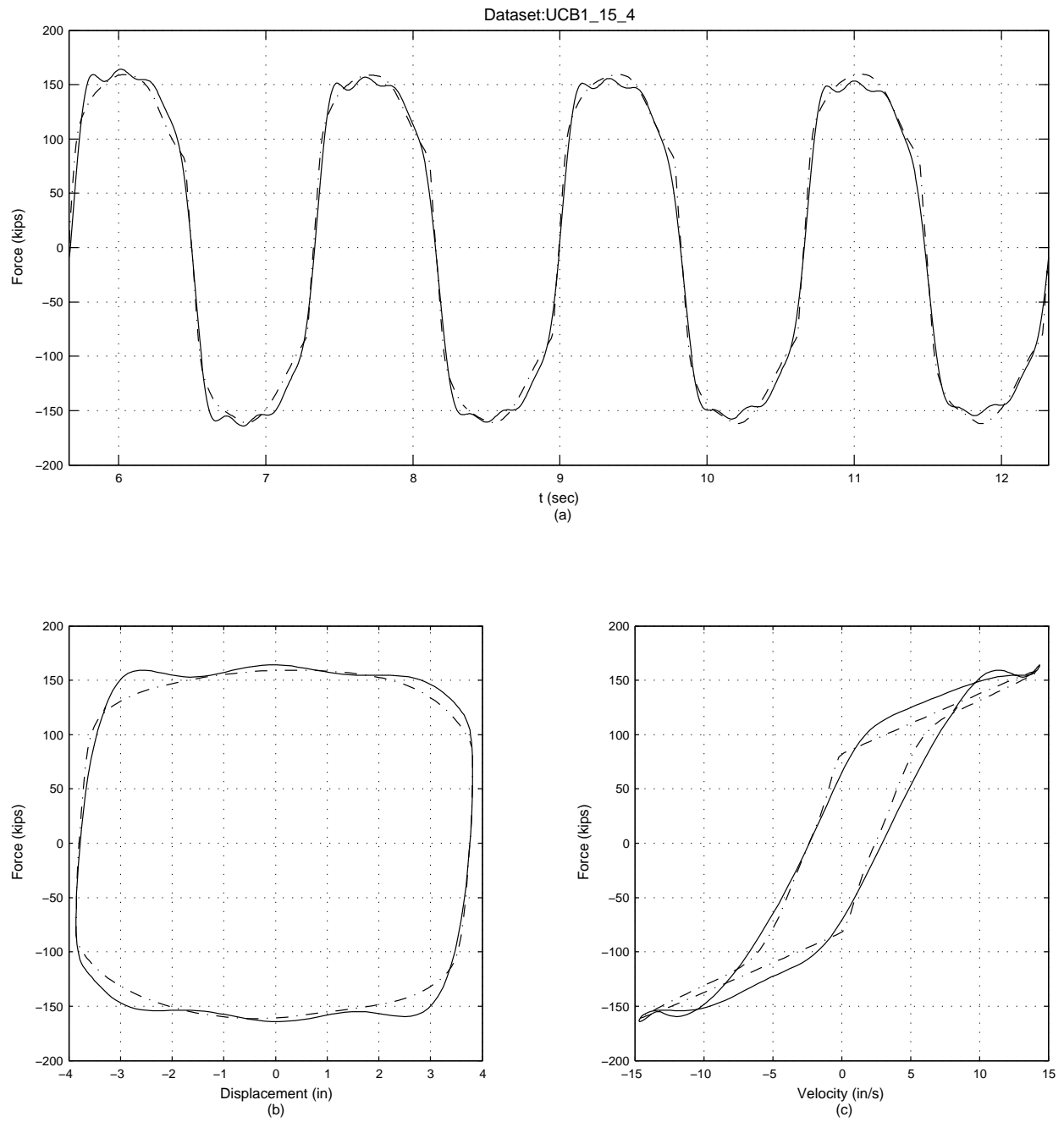


Figure B.23: Off-line parametric identification results of 250 kips damper for data set UCB1\_15\_4. Part (a) shows the time-history comparison of the measured force (solid line) and the predicted force (dash-dot line), part (b) shows the displacement-force phase-plane comparison of the measured force (solid line) and the predicted force (dash-dot line), for one cycle, and part (c) shows the velocity-force phase-plane comparison of the measured force (solid line) and the predicted force (dash-dot line), for one cycle.

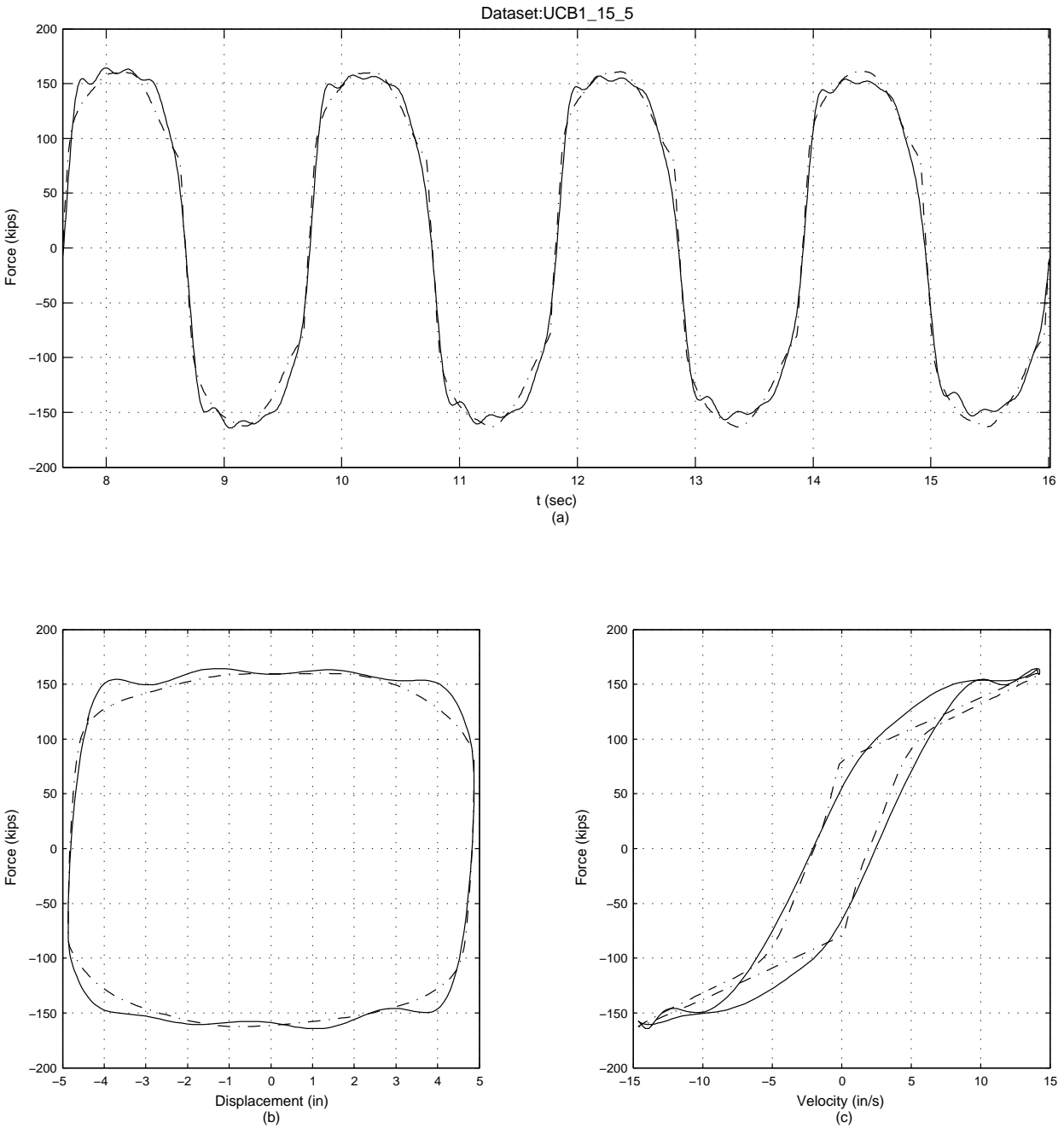


Figure B.24: Off-line parametric identification results of 250 kips damper for data set UCB1\_15\_5. Part (a) shows the time-history comparison of the measured force (solid line) and the predicted force (dash-dot line), part (b) shows the displacement-force phase-plane comparison of the measured force (solid line) and the predicted force (dash-dot line), for one cycle, and part (c) shows the velocity-force phase-plane comparison of the measured force (solid line) and the predicted force (dash-dot line), for one cycle.

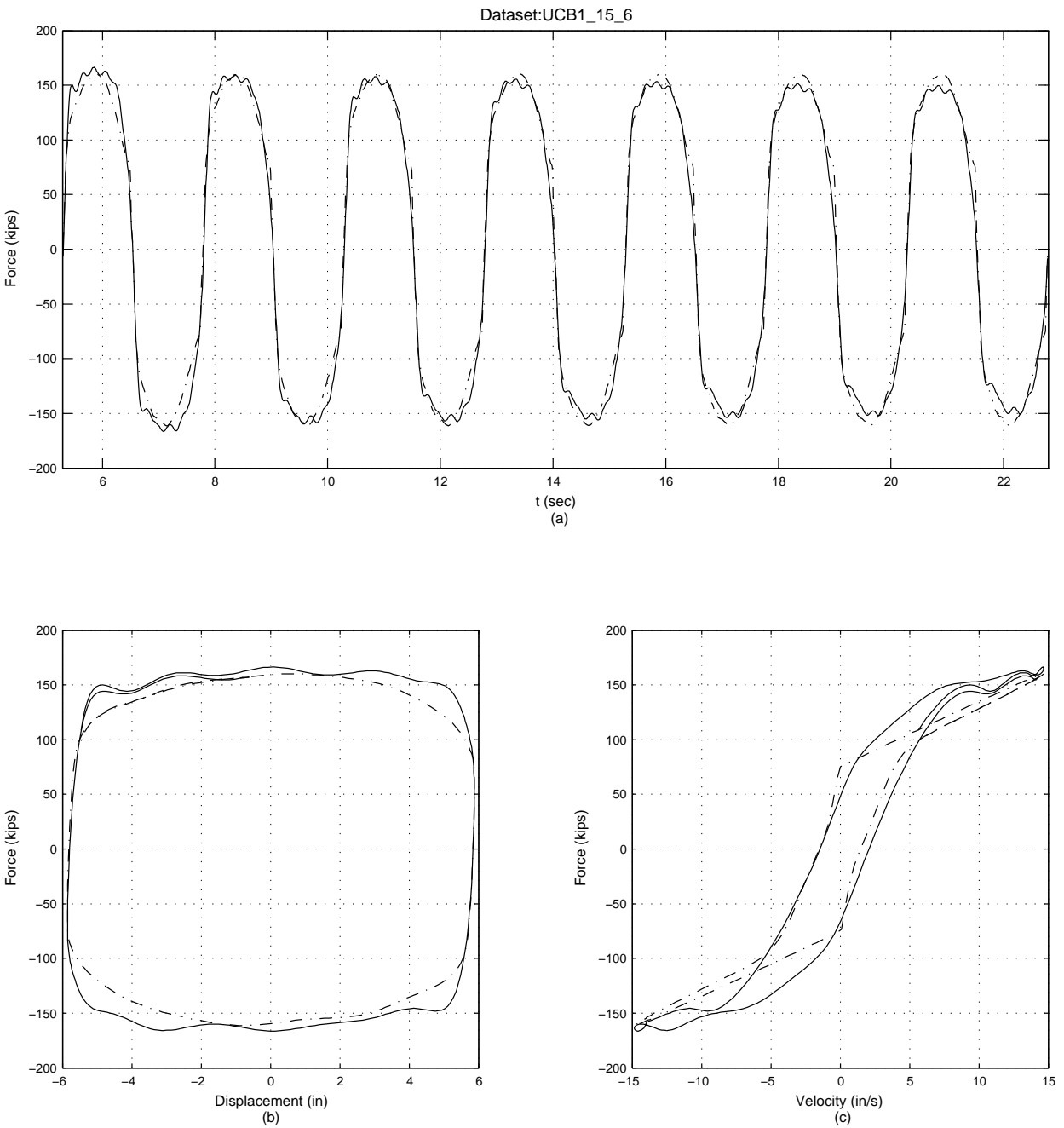


Figure B.25: Off-line parametric identification results of 250 kips damper for data set UCB1\_15.6. Part (a) shows the time-history comparison of the measured force (solid line) and the predicted force (dash-dot line), part (b) shows the displacement-force phase-plane comparison of the measured force (solid line) and the predicted force (dash-dot line), for one cycle, and part (c) shows the velocity-force phase-plane comparison of the measured force (solid line) and the predicted force (dash-dot line), for one cycle.

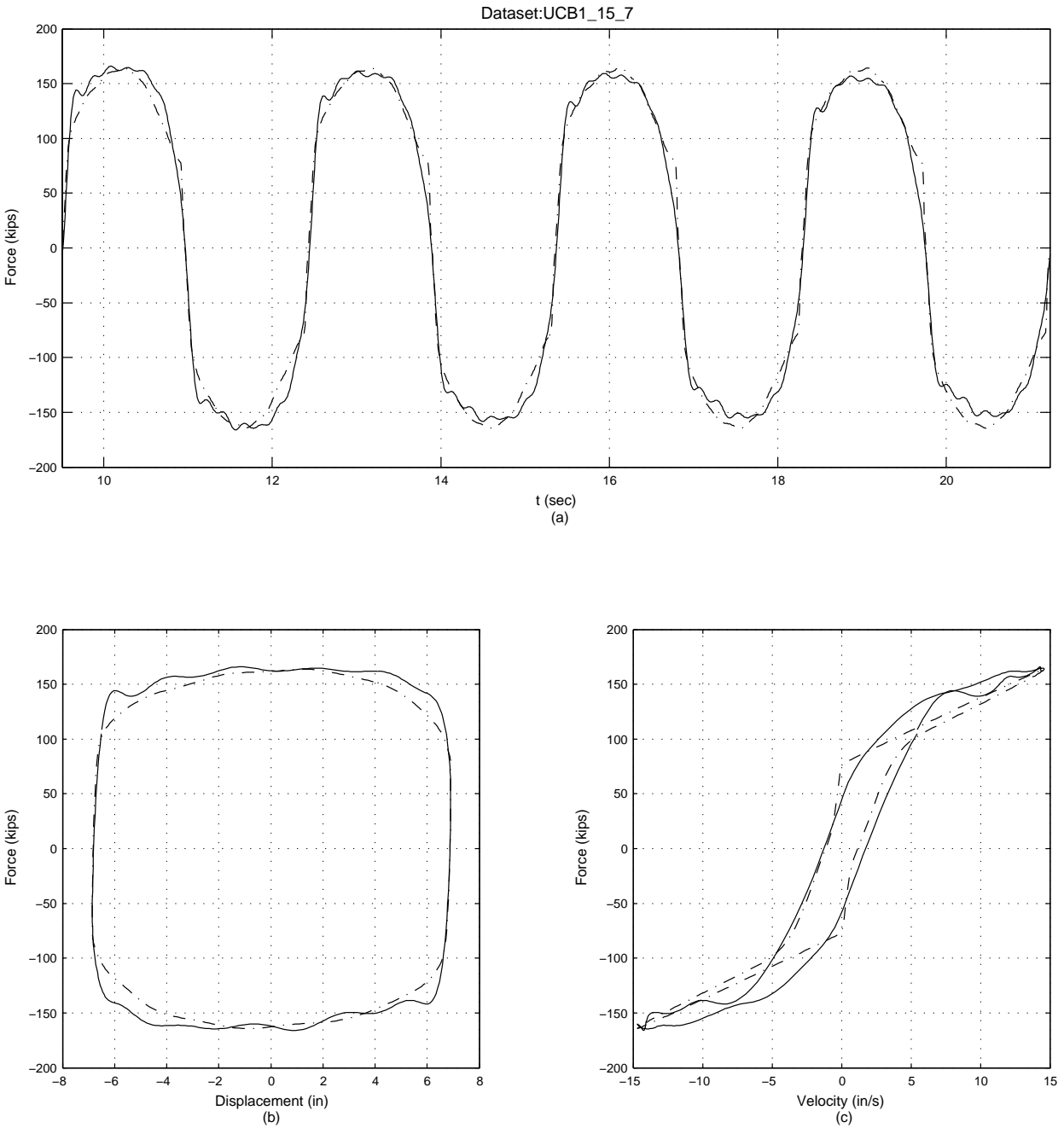


Figure B.26: Off-line parametric identification results of 250 kips damper for data set UCB1\_15.7. Part (a) shows the time-history comparison of the measured force (solid line) and the predicted force (dash-dot line), part (b) shows the displacement-force phase-plane comparison of the measured force (solid line) and the predicted force (dash-dot line), for one cycle, and part (c) shows the velocity-force phase-plane comparison of the measured force (solid line) and the predicted force (dash-dot line), for one cycle.

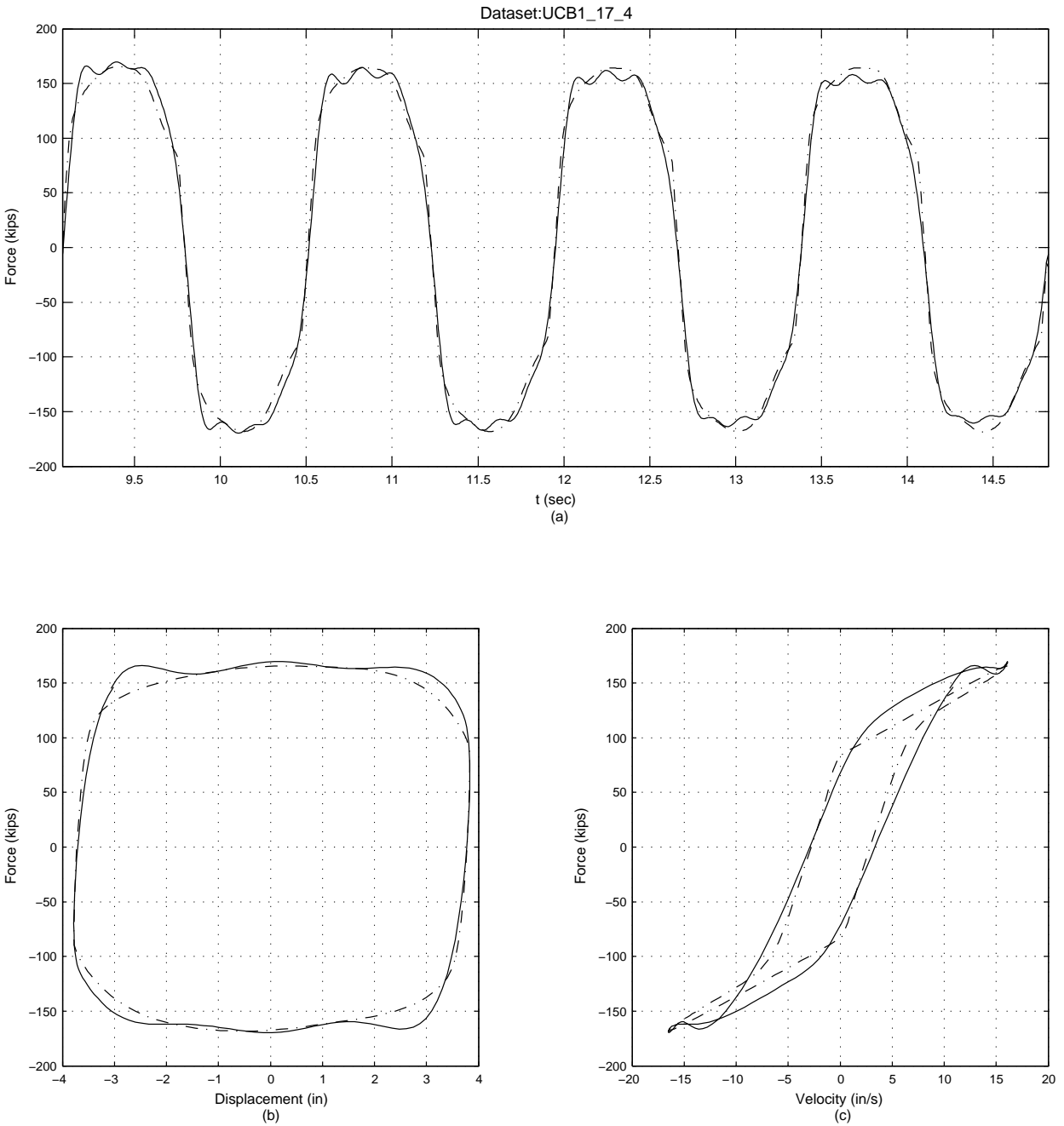


Figure B.27: Off-line parametric identification results of 250 kips damper for data set UCB1\_17\_4. Part (a) shows the time-history comparison of the measured force (solid line) and the predicted force (dash-dot line), part (b) shows the displacement-force phase-plane comparison of the measured force (solid line) and the predicted force (dash-dot line), for one cycle, and part (c) shows the velocity-force phase-plane comparison of the measured force (solid line) and the predicted force (dash-dot line), for one cycle.

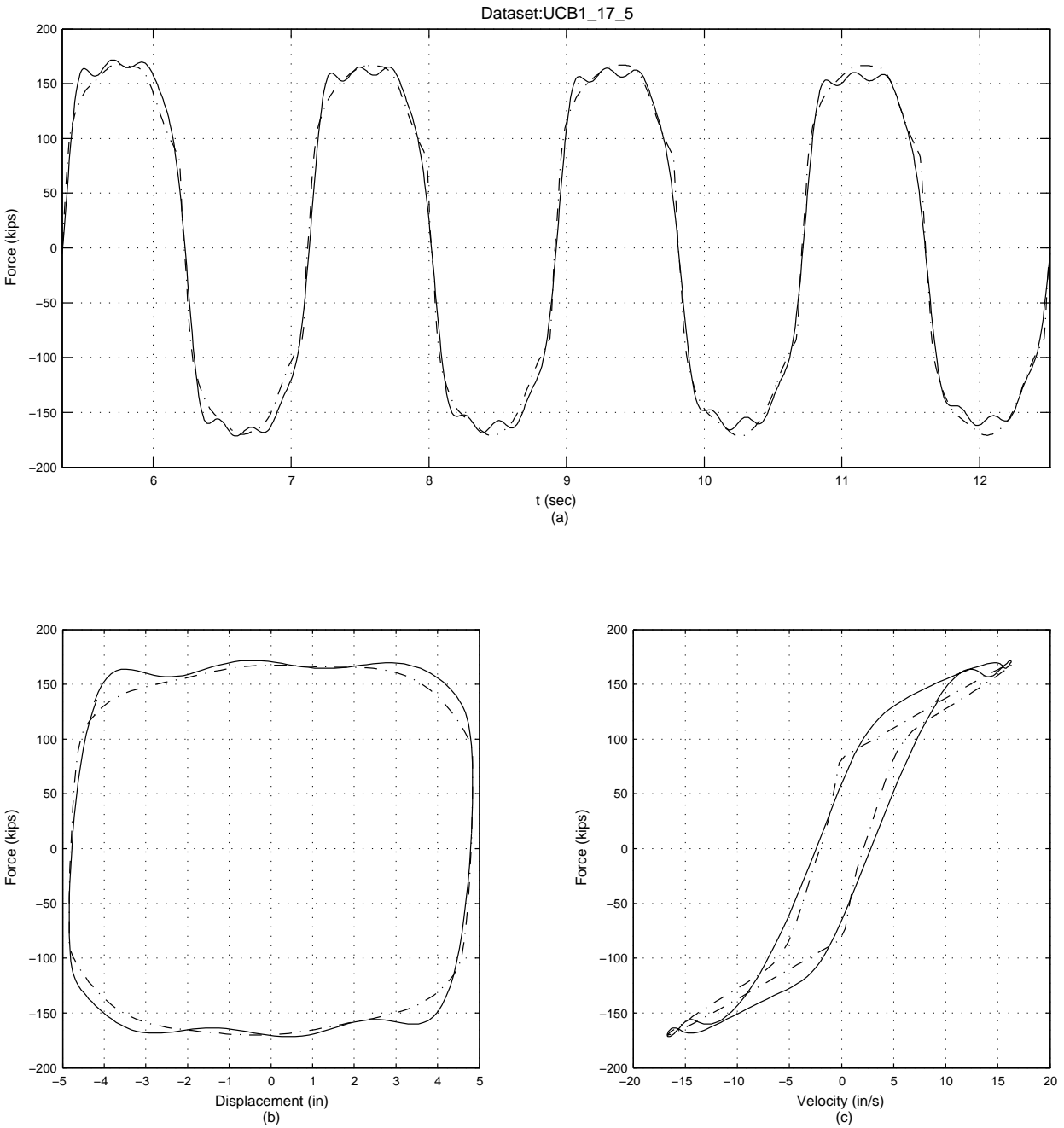


Figure B.28: Off-line parametric identification results of 250 kips damper for data set UCB1\_17\_5. Part (a) shows the time-history comparison of the measured force (solid line) and the predicted force (dash-dot line), part (b) shows the displacement-force phase-plane comparison of the measured force (solid line) and the predicted force (dash-dot line), for one cycle, and part (c) shows the velocity-force phase-plane comparison of the measured force (solid line) and the predicted force (dash-dot line), for one cycle.

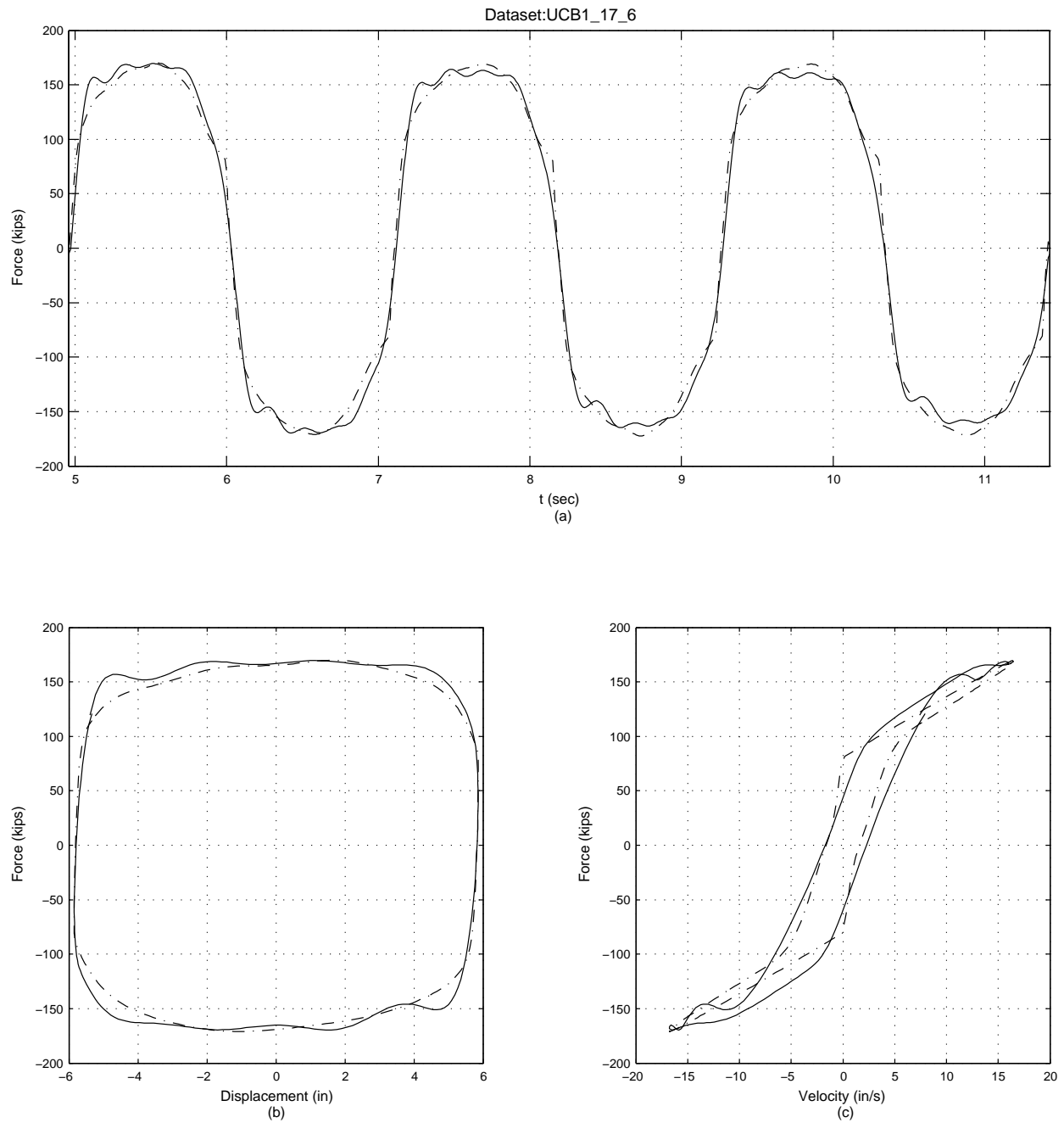


Figure B.29: Off-line parametric identification results of 250 kips damper for data set UCB1\_17.6. Part (a) shows the time-history comparison of the measured force (solid line) and the predicted force (dash-dot line), part (b) shows the displacement-force phase-plane comparison of the measured force (solid line) and the predicted force (dash-dot line), for one cycle, and part (c) shows the velocity-force phase-plane comparison of the measured force (solid line) and the predicted force (dash-dot line), for one cycle.

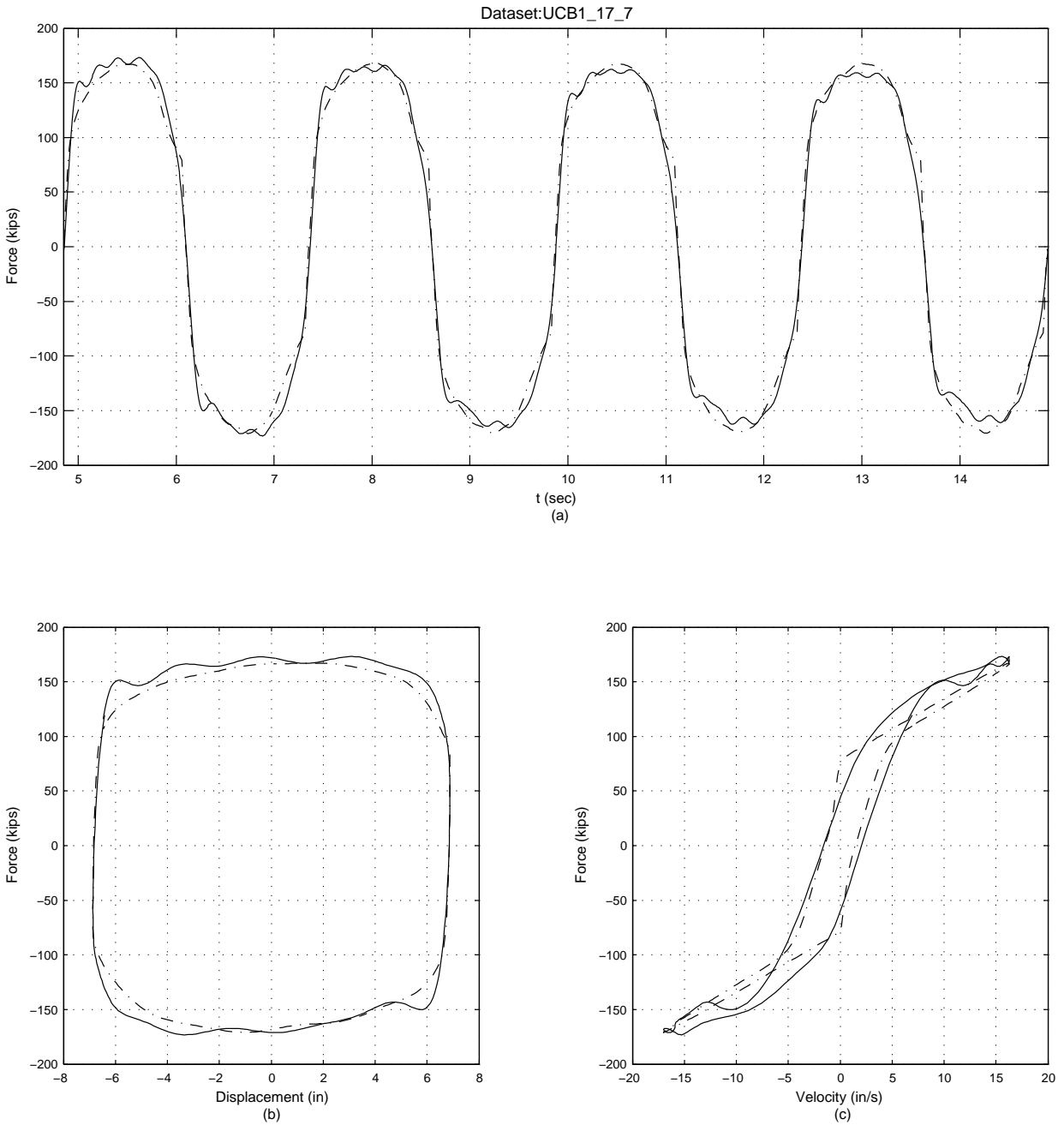


Figure B.30: Off-line parametric identification results of 250 kips damper for data set UCB1\_17.7. Part (a) shows the time-history comparison of the measured force (solid line) and the predicted force (dash-dot line), part (b) shows the displacement-force phase-plane comparison of the measured force (solid line) and the predicted force (dash-dot line), for one cycle, and part (c) shows the velocity-force phase-plane comparison of the measured force (solid line) and the predicted force (dash-dot line), for one cycle.

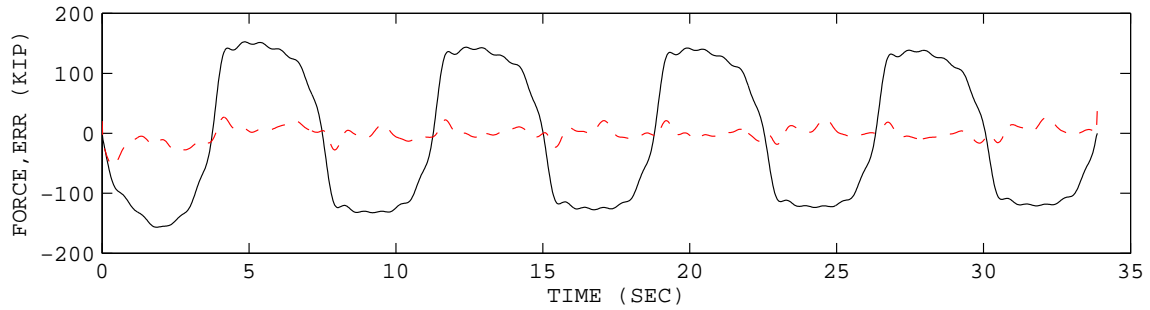


## Appendix C

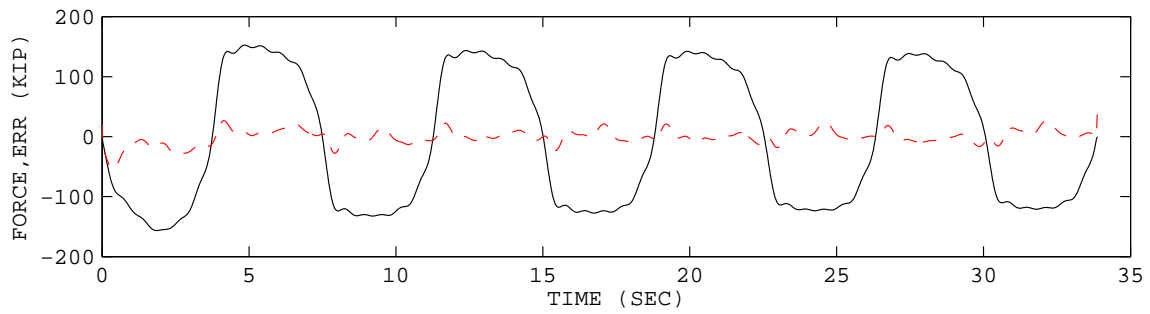
# NONPARAMETRIC IDENTIFICATION RESULTS FOR THE 250 KIP VISCOUS DAMPER

### C.1 Restoring Force Method

The plot comparisons of the measured and the identified force for the 250 kip viscous damper using the restoring force method are shown in this section (Figs.C.1 to C.15).

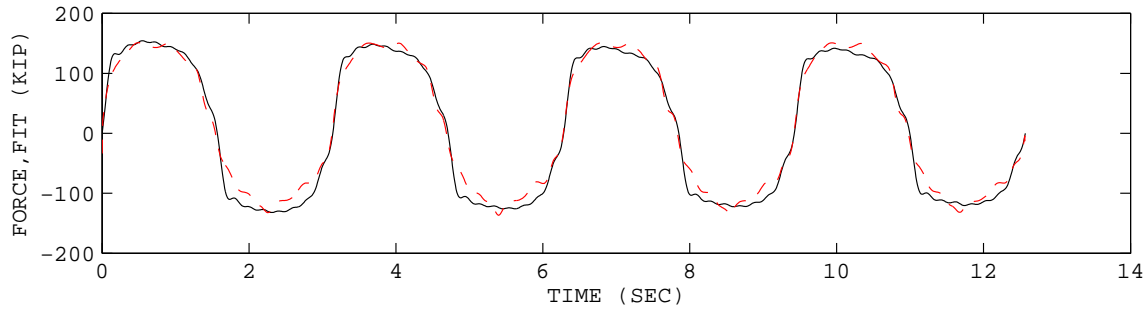


(a) Estimated force

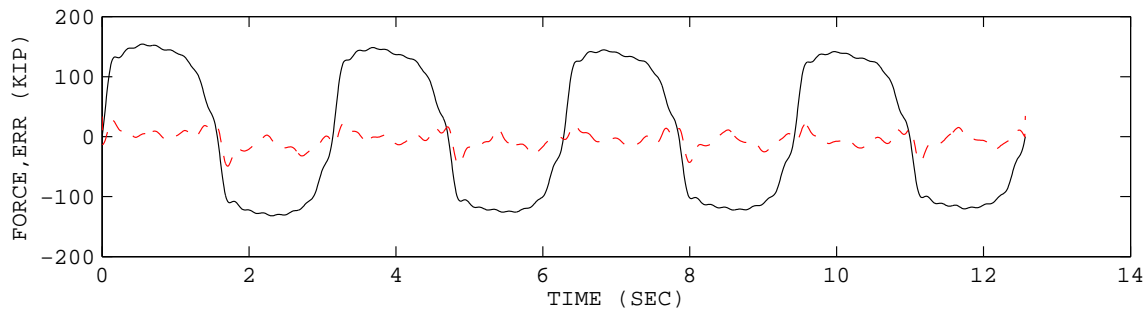


(b) Error between estimated and measured force

Figure C.1: Comparison of the measured and identified damper response in time history using RFM for the data set UCB1\_10\_4. The solid line is the measured force, and the dashed line is the identified force.

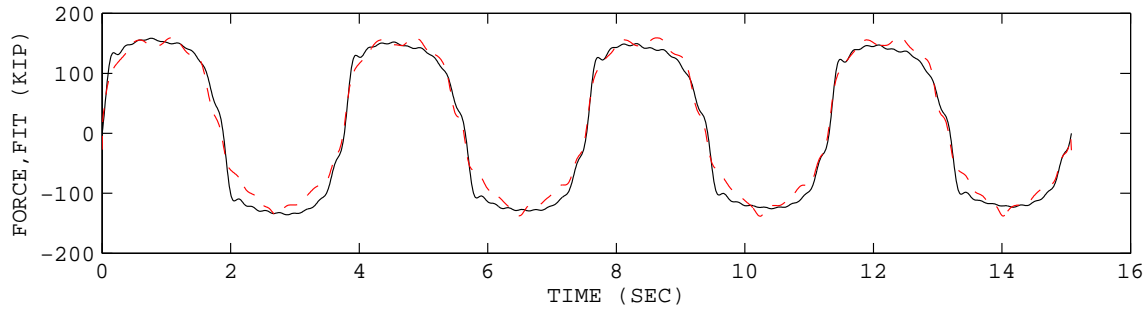


(a) Estimated force

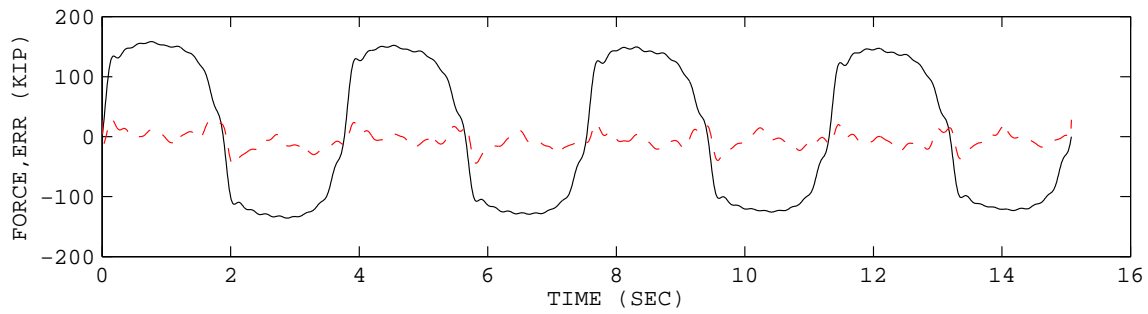


(b) Error between estimated and measured force

Figure C.2: Comparison of the measured and identified damper response in time history using RFM for the data set UCB1\_10\_5. The solid line is the measured force, and the dashed line is the identified force.

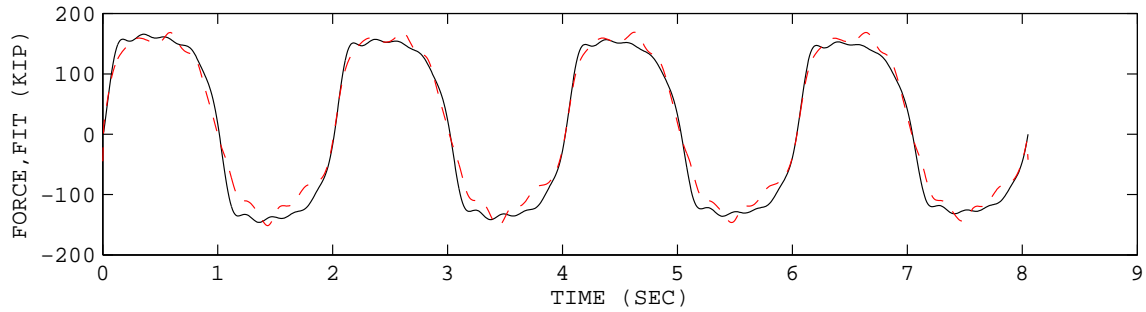


(a) Estimated force

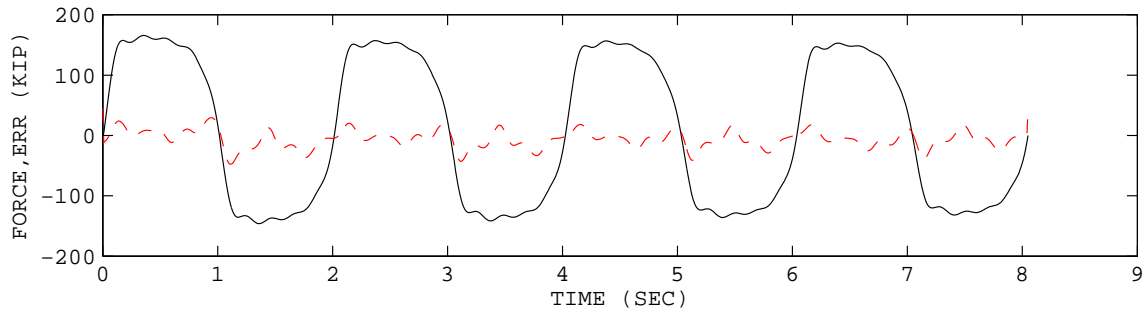


(b) Error between estimated and measured force

Figure C.3: Comparison of the measured and identified damper response in time history using RFM for the data set UCB1\_10\_6. The solid line is the measured force, and the dashed line is the identified force.

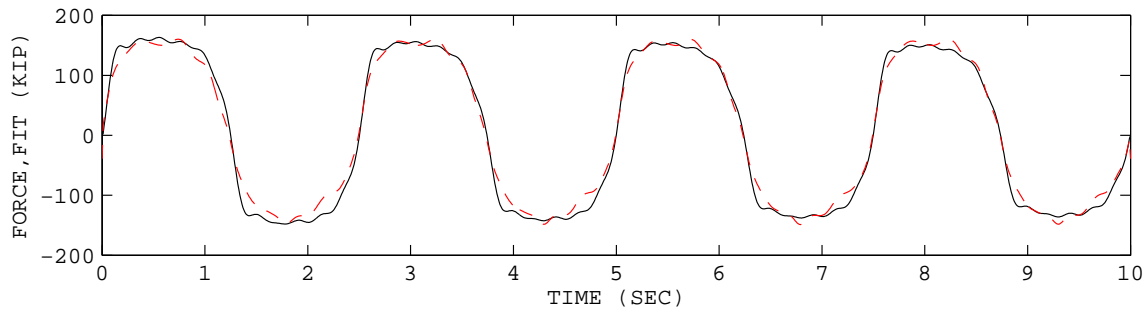


(a) Estimated force

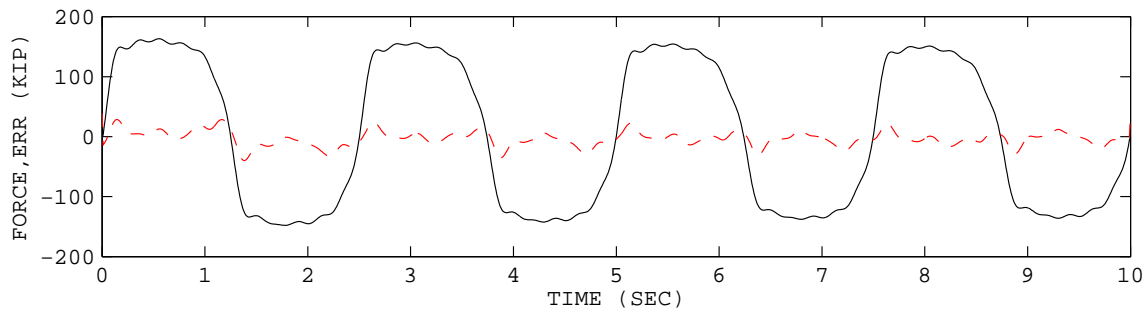


(b) Error between estimated and measured force

Figure C.4: Comparison of the measured and identified damper response in time history using RFM for the data set UCB1\_12\_4. The solid line is the measured force, and the dashed line is the identified force.

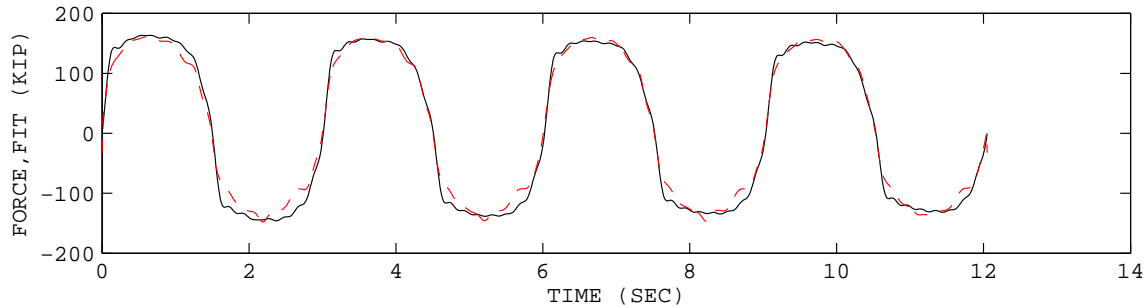


(a) Estimated force

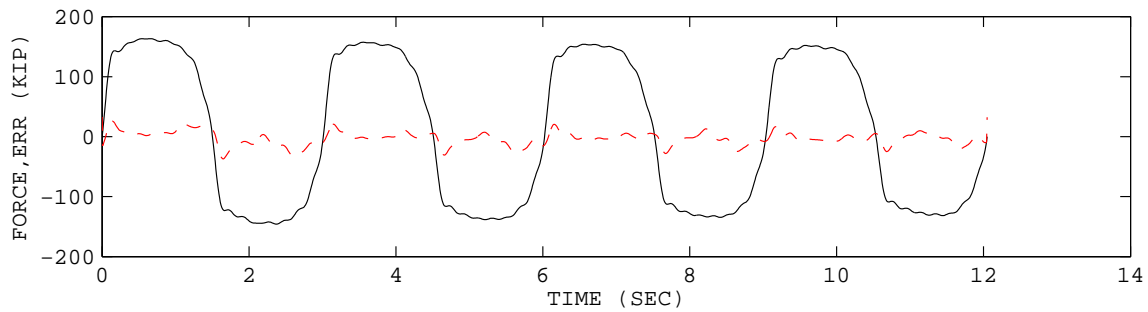


(b) Error between estimated and measured force

Figure C.5: Comparison of the measured and identified damper response in time history using RFM for the data set UCB1\_12\_5. The solid line is the measured force, and the dashed line is the identified force.

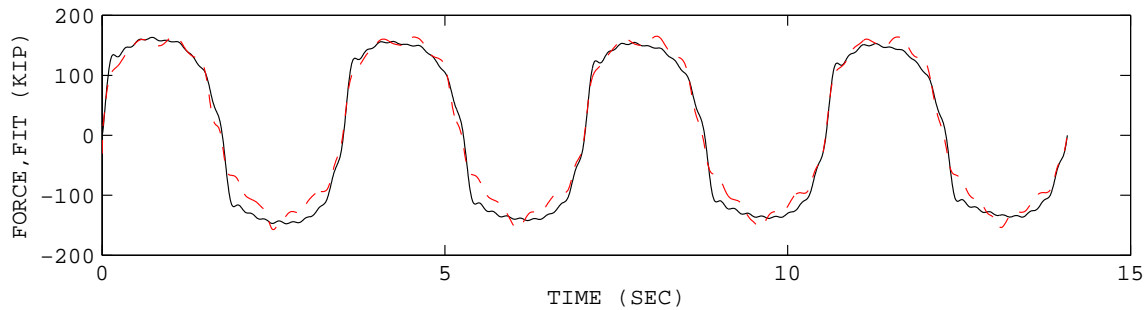


(a) Estimated force

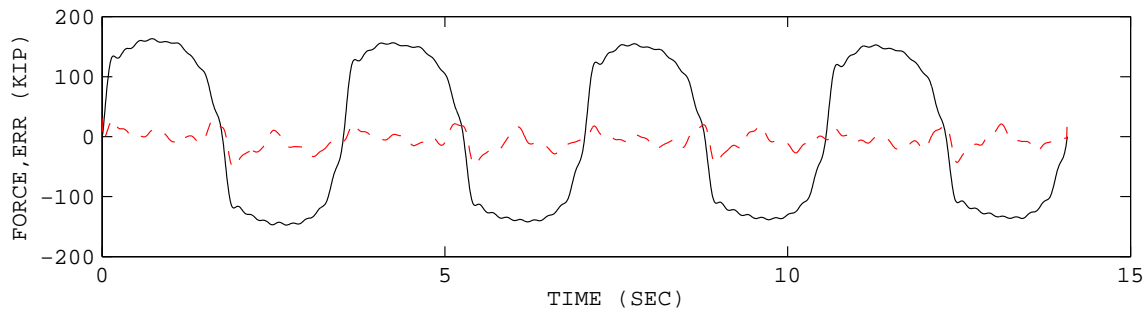


(b) Error between estimated and measured force

Figure C.6: Comparison of the measured and identified damper response in time history using RFM for the data set UCB1\_12\_6. The solid line is the measured force, and the dashed line is the identified force.

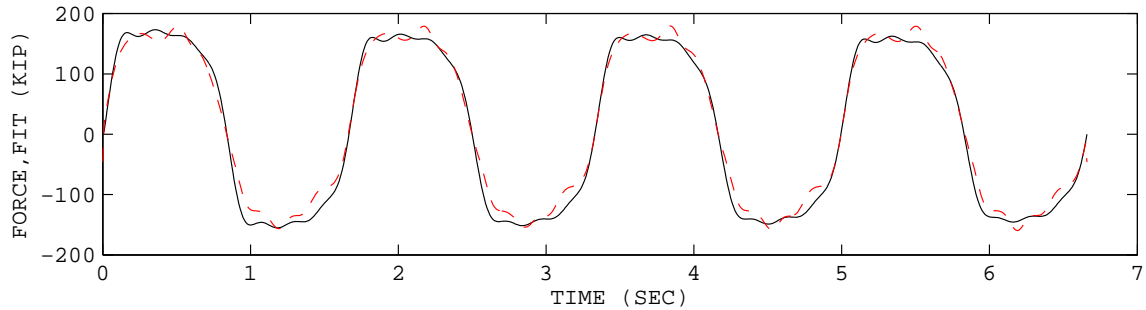


(a) Estimated force

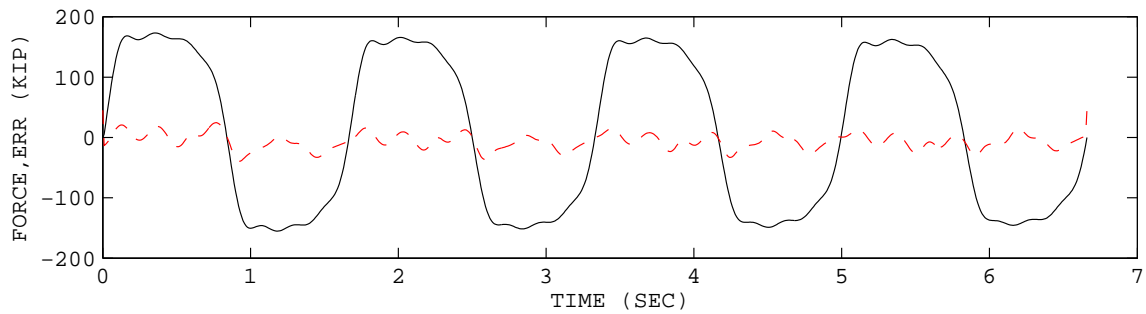


(b) Error between estimated and measured force

Figure C.7: Comparison of the measured and identified damper response in time history using RFM for the data set UCB1\_12\_7. The solid line is the measured force, and the dashed line is the identified force.

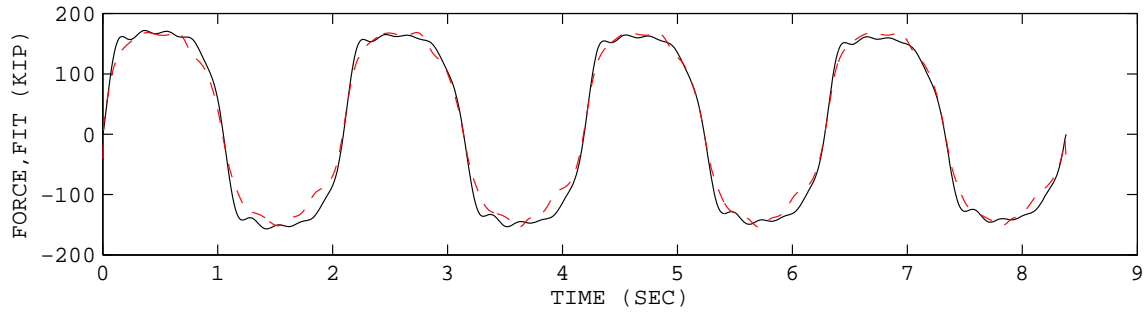


(a) Estimated force

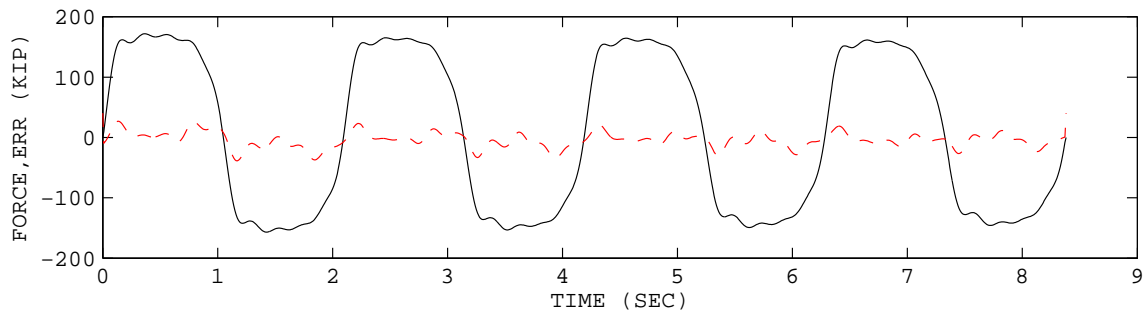


(b) Error between estimated and measured force

Figure C.8: Comparison of the measured and identified damper response in time history using RFM for the data set UCB1\_15\_4. The solid line is the measured force, and the dashed line is the identified force.

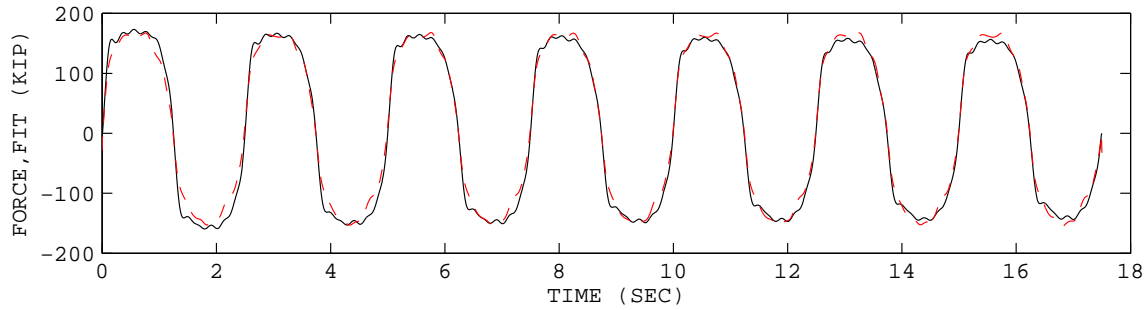


(a) Estimated force

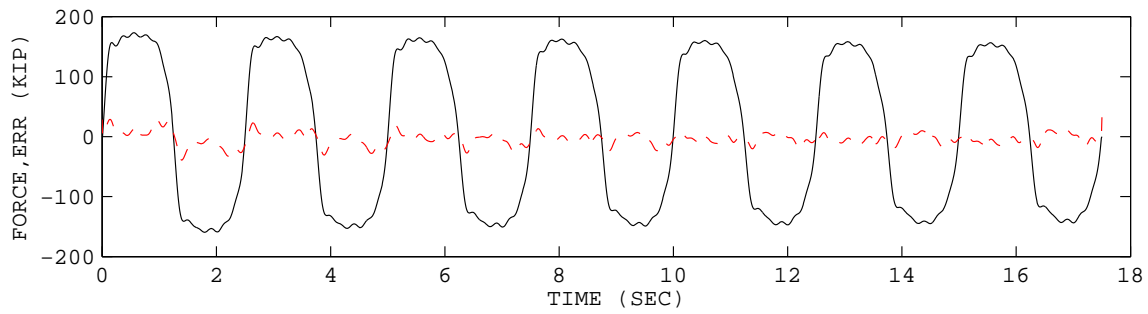


(b) Error between estimated and measured force

Figure C.9: Comparison of the measured and identified damper response in time history using RFM for the data set UCB1\_15.5. The solid line is the measured force, and the dashed line is the identified force.

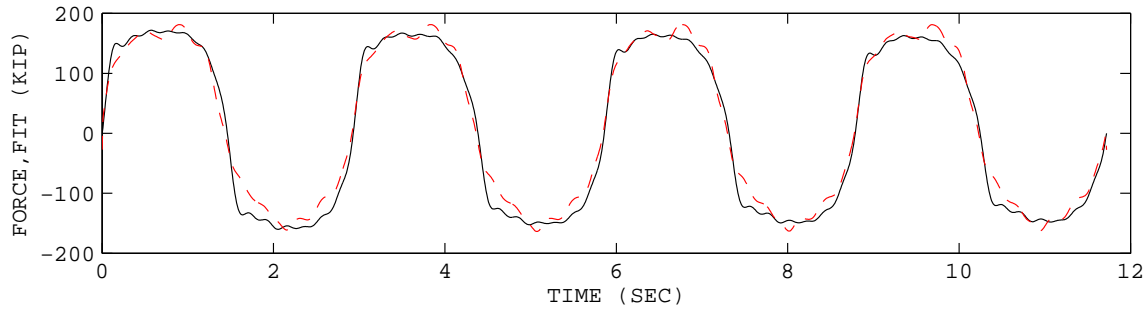


(a) Estimated force

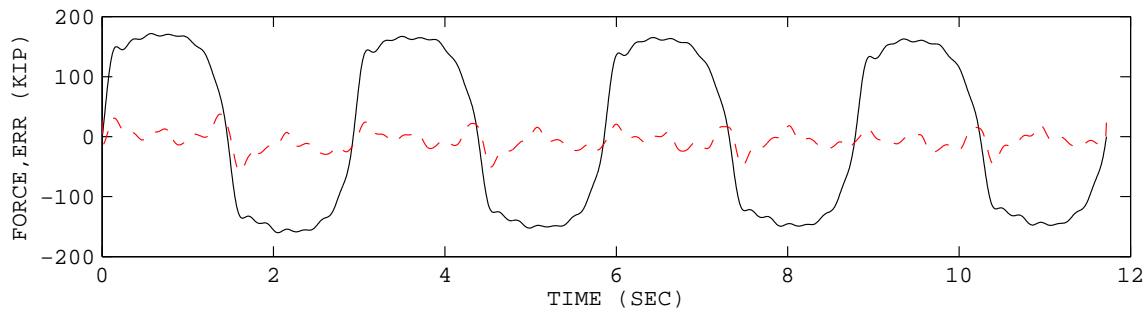


(b) Error between estimated and measured force

Figure C.10: Comparison of the measured and identified damper response in time history using RFM for the data set UCB1\_15\_6. The solid line is the measured force, and the dashed line is the identified force.

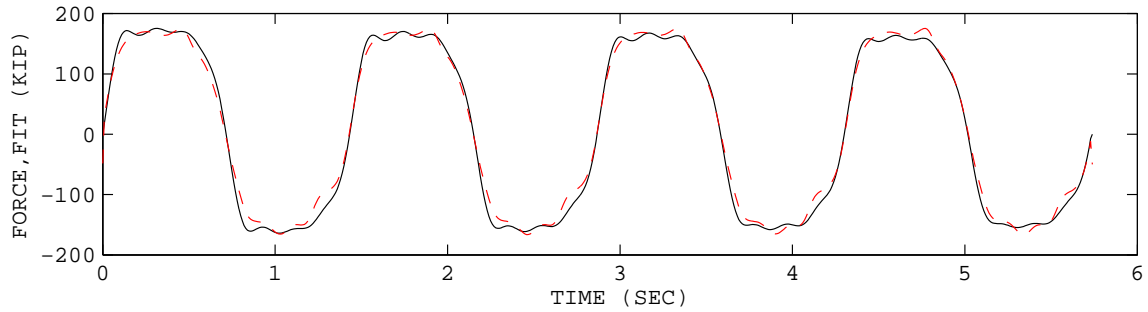


(a) Estimated force

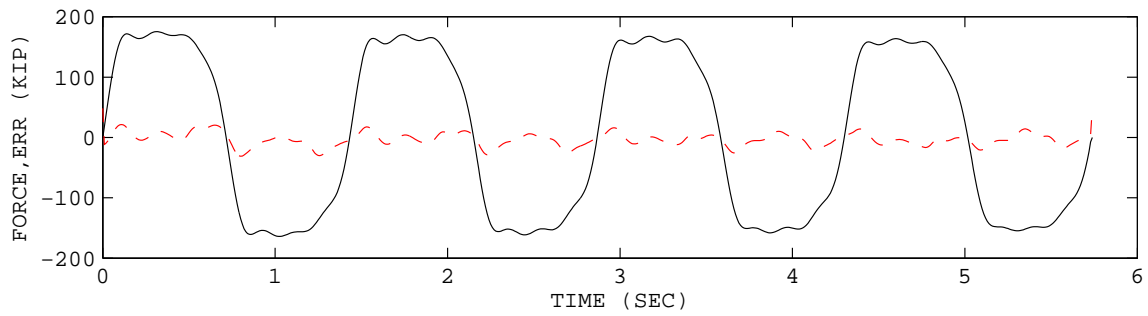


(b) Error between estimated and measured force

Figure C.11: Comparison of the measured and identified damper response in time history using RFM for the data set UCB1\_15\_7. The solid line is the measured force, and the dashed line is the identified force.

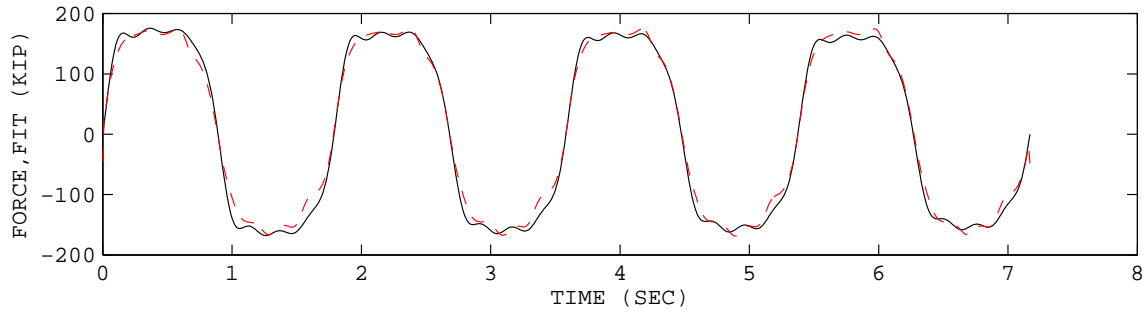


(a) Estimated force

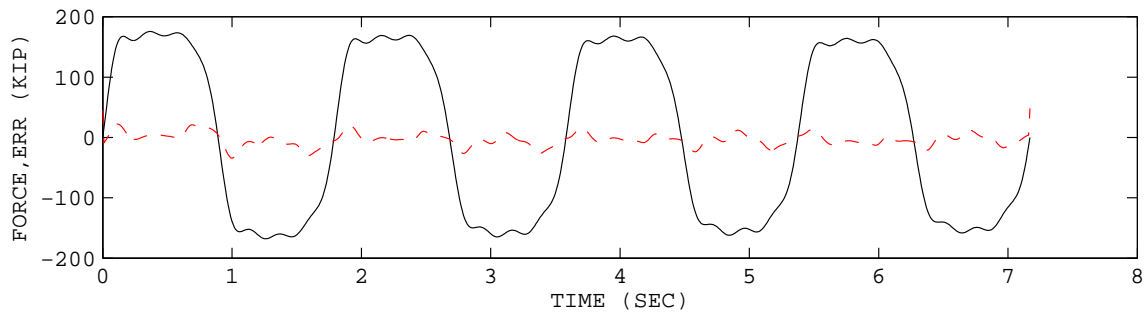


(b) Error between estimated and measured force

Figure C.12: Comparison of the measured and identified damper response in time history using RFM for the data set UCB1\_17\_4. The solid line is the measured force, and the dashed line is the identified force.

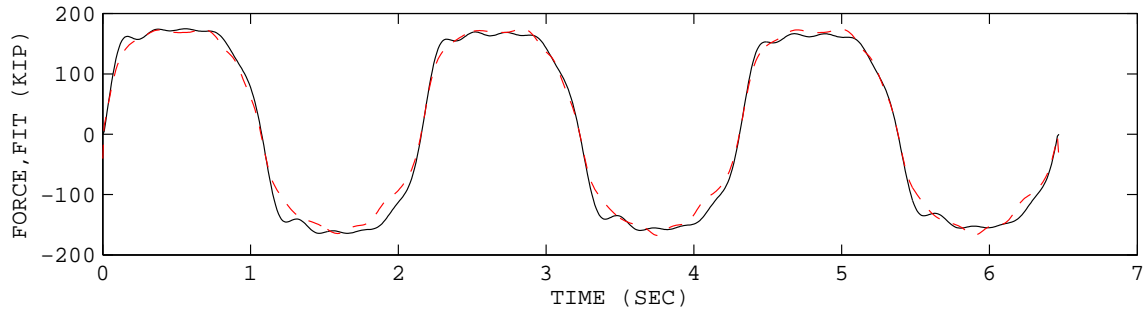


(a) Estimated force

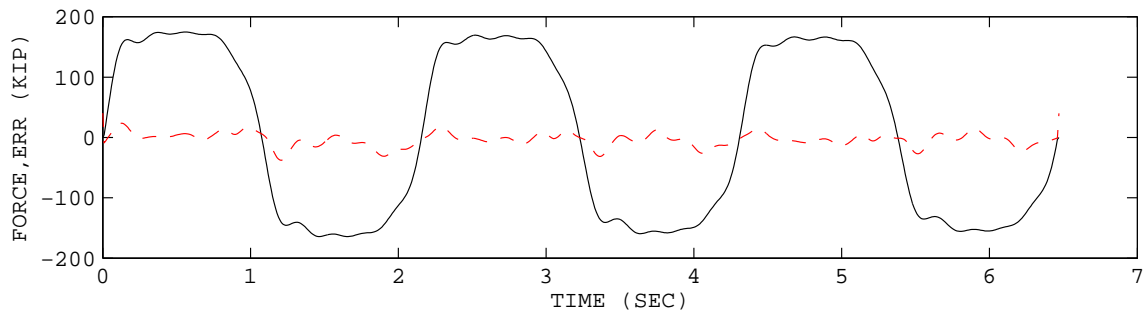


(b) Error between estimated and measured force

Figure C.13: Comparison of the measured and identified damper response in time history using RFM for the data set UCB1\_17.5. The solid line is the measured force, and the dashed line is the identified force.

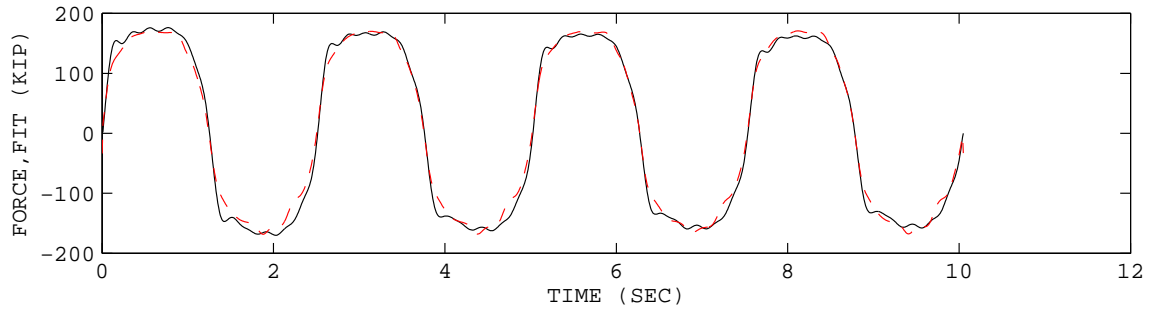


(a) Estimated force

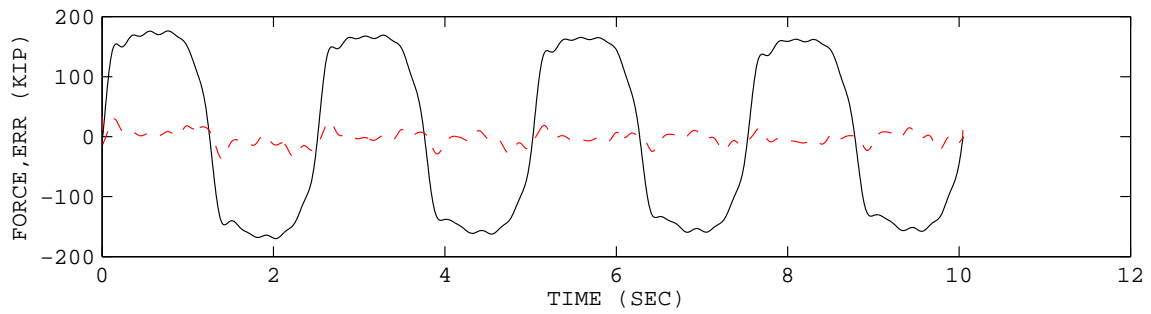


(b) Error between estimated and measured force

Figure C.14: Comparison of the measured and identified damper response in time history using RFM for the data set UCB1\_17\_6. The solid line is the measured force, and the dashed line is the identified force.



(a) Estimated force

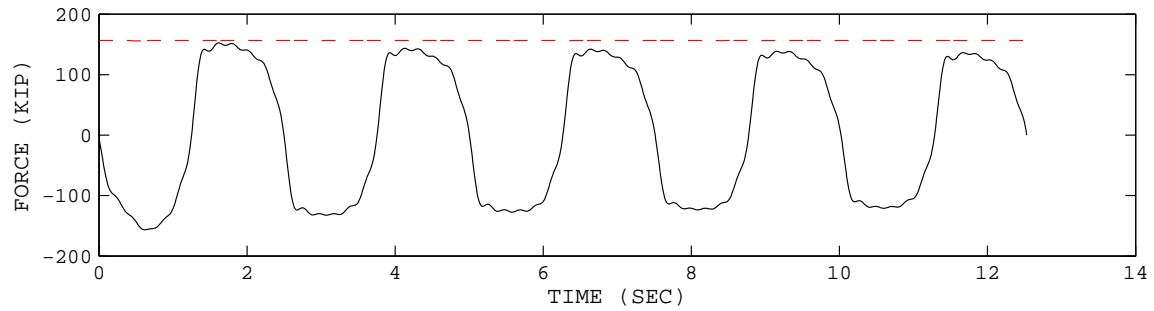


(b) Error between estimated and measured force

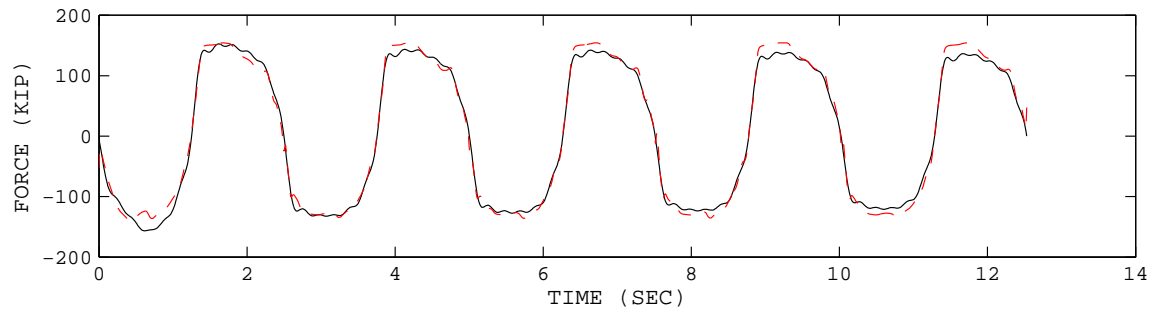
Figure C.15: Comparison of the measured and identified damper response in time history using RFM for the data set UCB1\_17\_7. The solid line is the measured force, and the dashed line is the identified force.

## C.2 Artificial Neural Networks

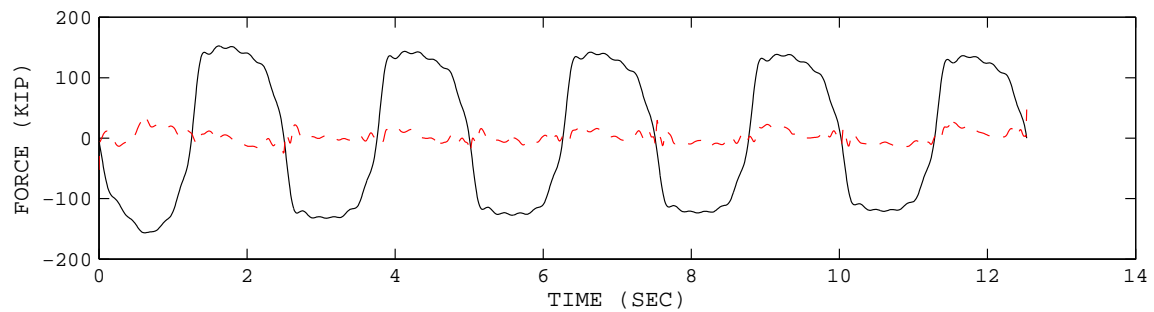
The plot comparisons of the measured and the identified force for the 250 kip viscous damper using the artificial neural networks are shown in this section (Figs. C.16 to C.45).



(a) Force before training



(b) Force after training



(c) Error after training

Figure C.16: Comparison of the measured and identified damper response in time history using ANN for the data set UCB1\_10.4.

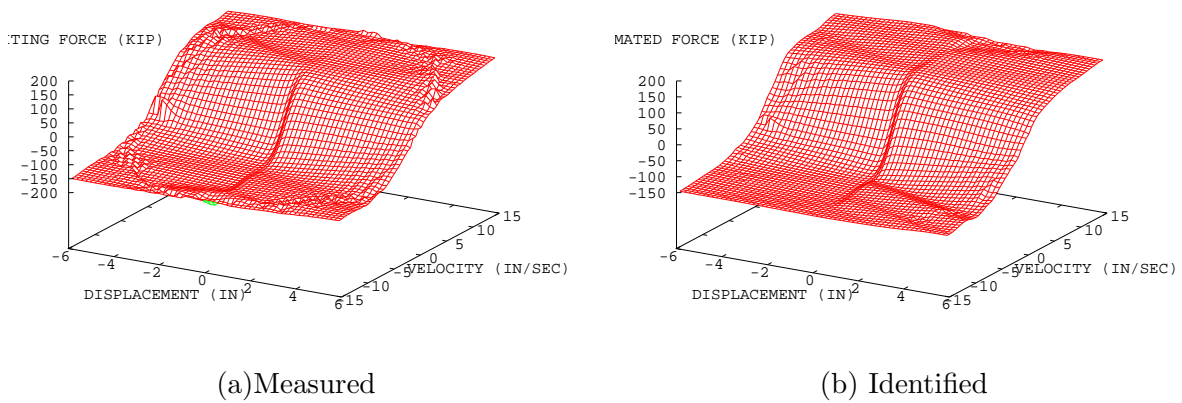
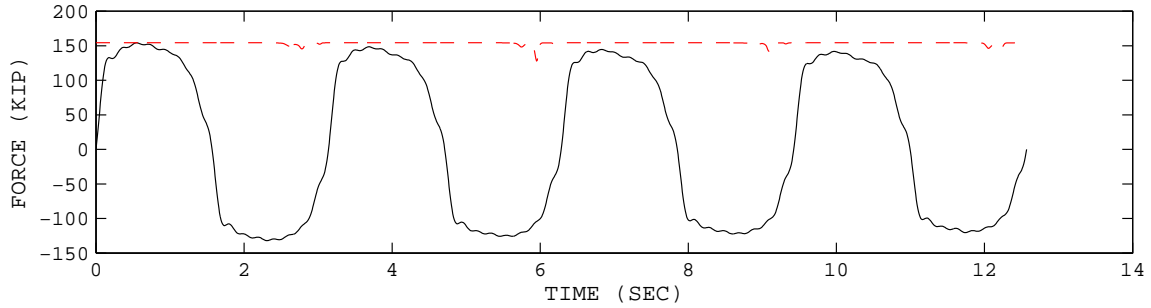
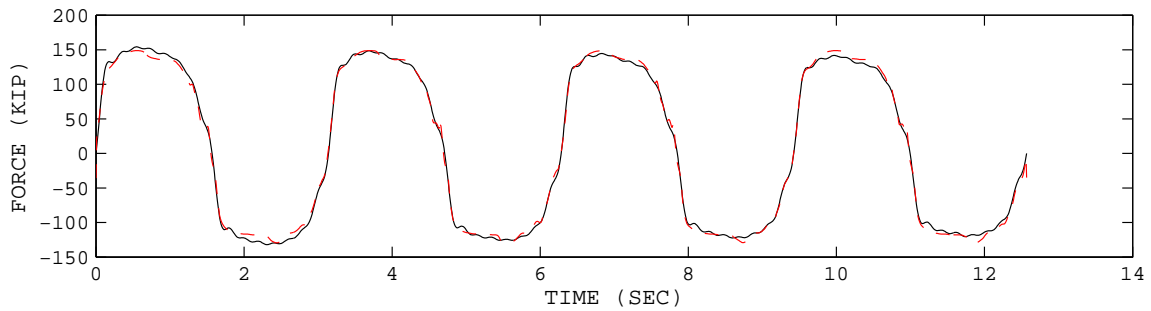


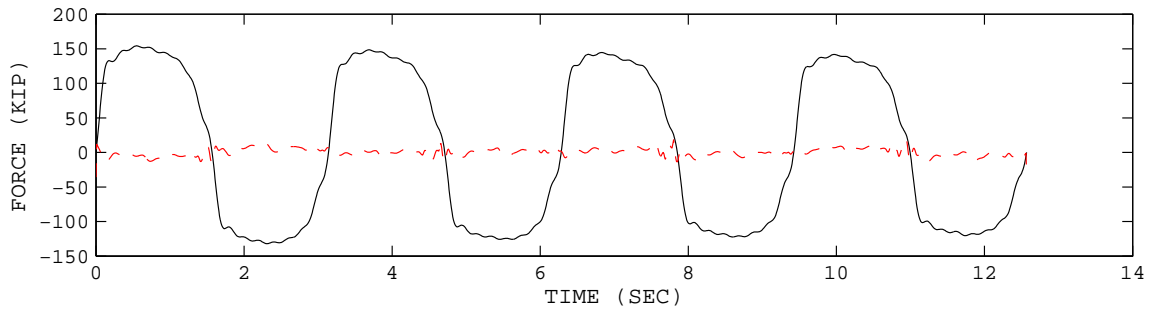
Figure C.17: Comparison of measured and identified damper response in phase plot using ANN for the data set UCB1\_10\_4.



(a) Force before training

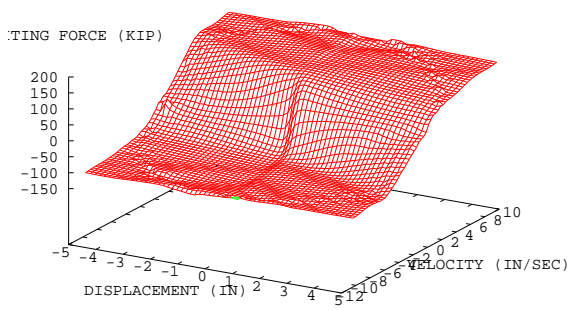


(b) Force after training

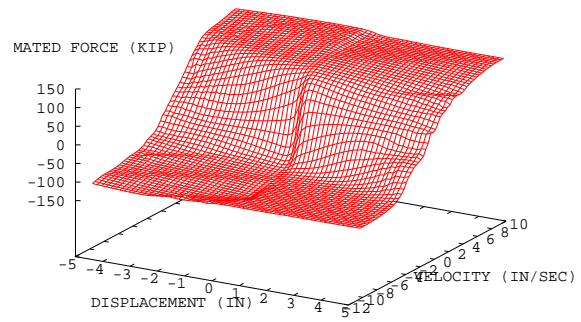


(c) Error after training

Figure C.18: Comparison of the measured and identified damper response in time history using ANN for the data set UCB1\_10.5.

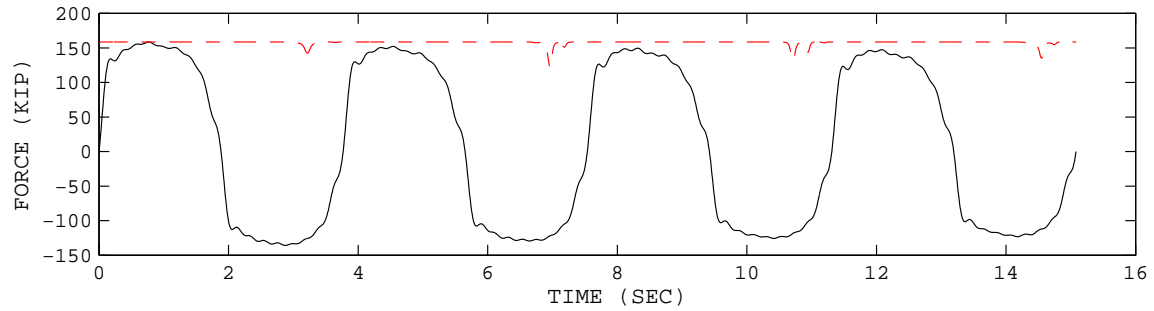


(a) Measured

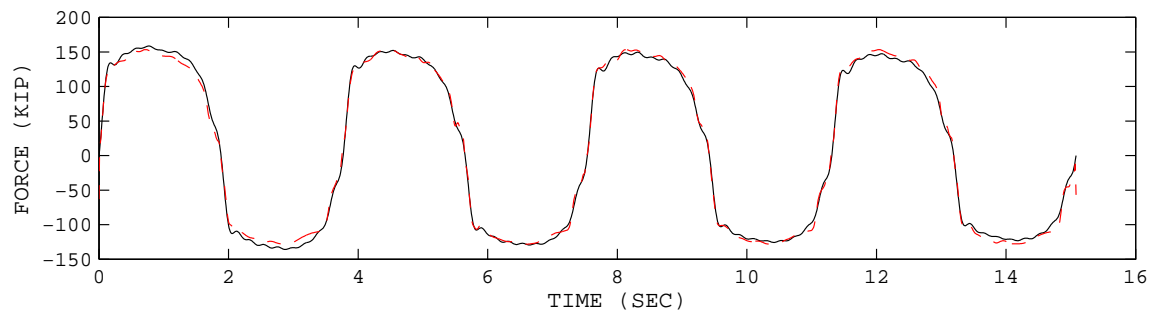


(b) Identified

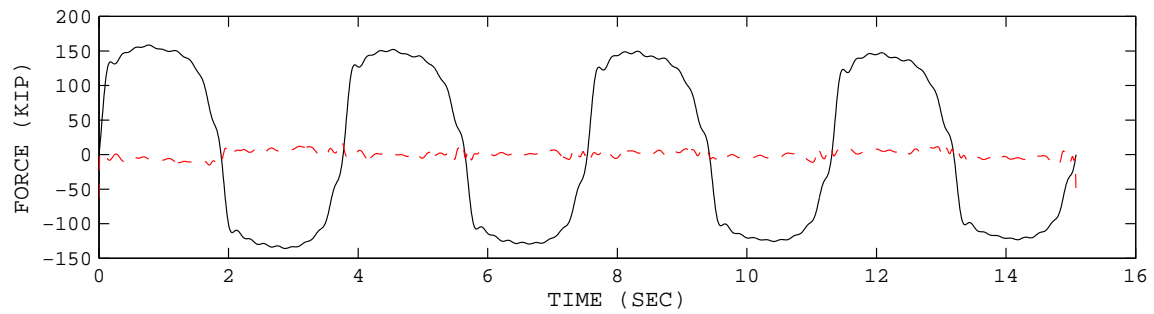
Figure C.19: Comparison of measured and identified damper response using ANN in phase plot for the data set UCB1\_10\_5.



(a) Force before training

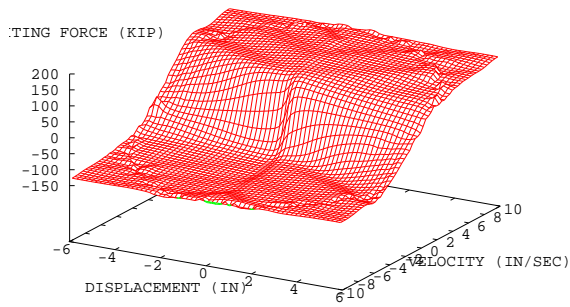


(b) Force after training

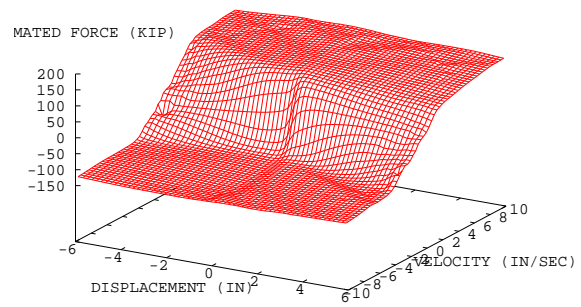


(c) Error after training

Figure C.20: Comparison of the measured and identified damper response using ANN in time history for the data set UCB1\_10\_6.

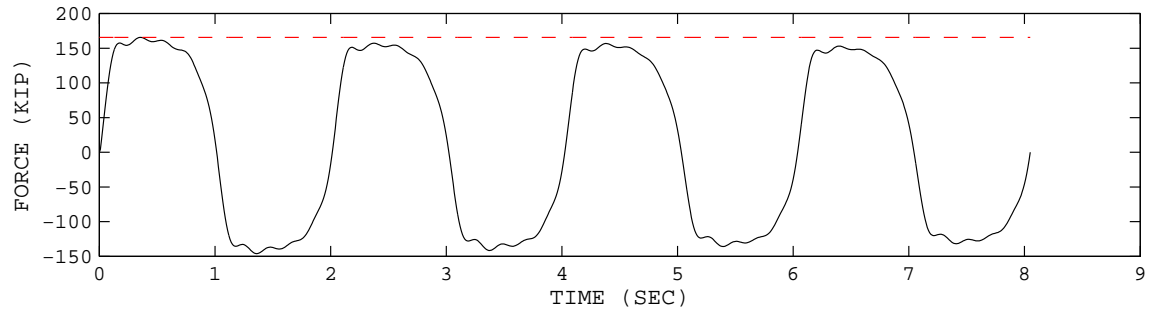


(a) Measured

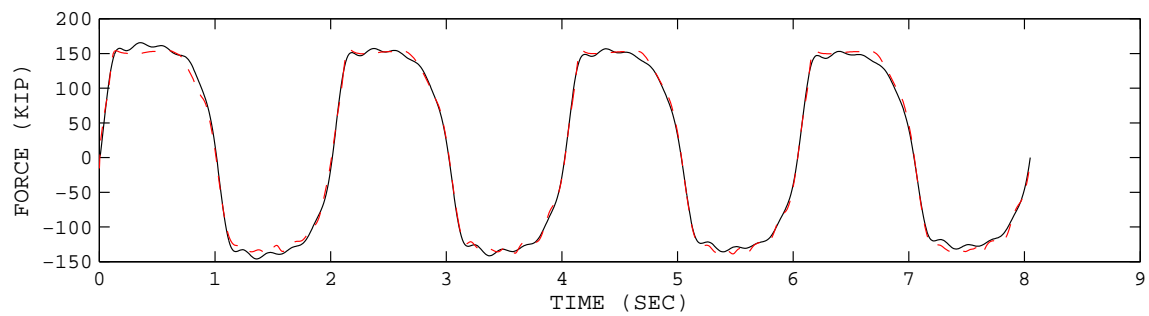


(b) Identified

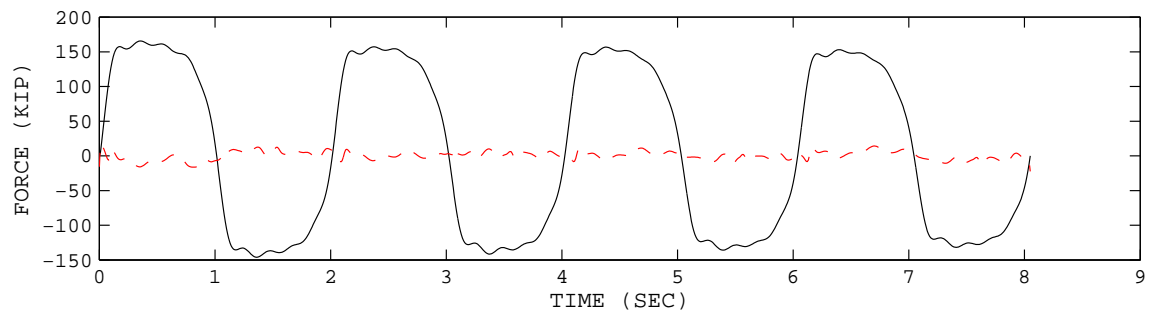
Figure C.21: Comparison of measured and identified damper response using ANN in phase plot for the data set UCB1\_10\_6.



(a) Force before training



(b) Force after training



(c) Error after training

Figure C.22: Comparison of the measured and identified damper response using ANN in time history for the data set UCB1.12.4.

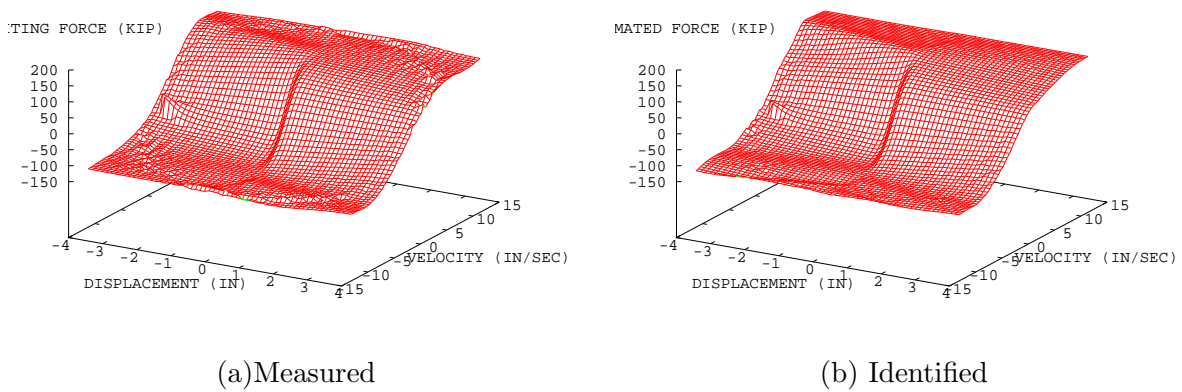
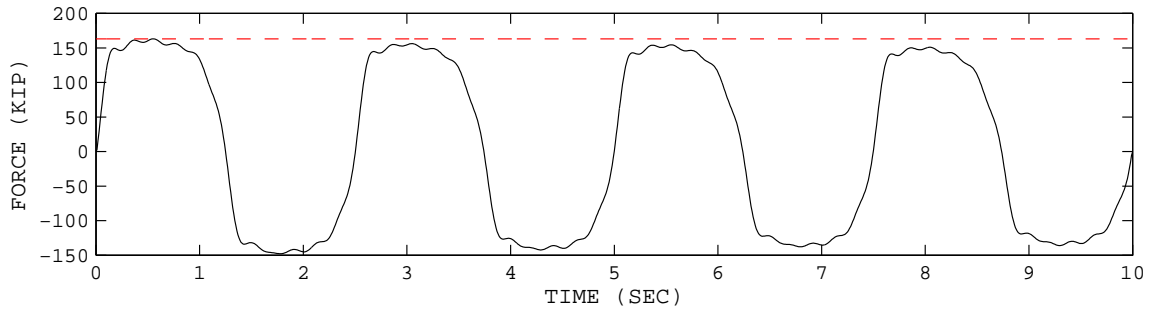
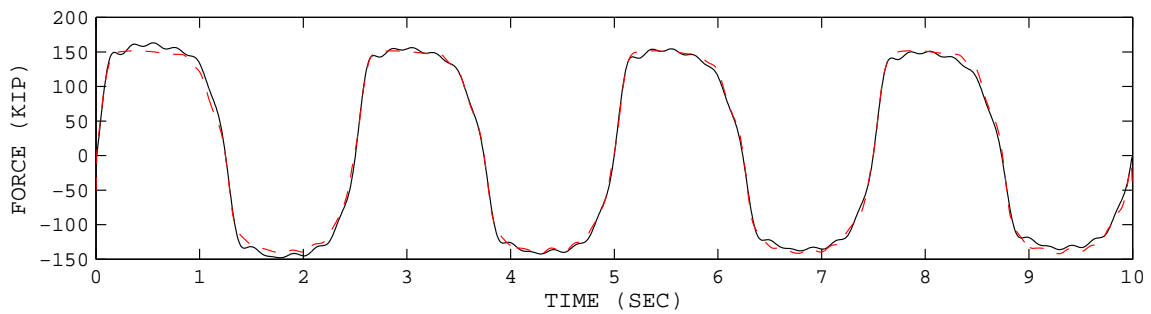


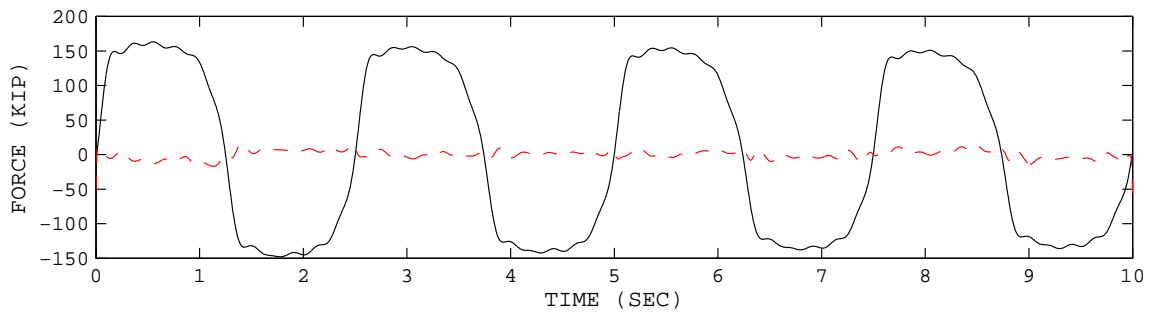
Figure C.23: Comparison of measured and identified damper response using ANN in phase plot for the data set UCB1\_12\_4.



(a) Force before training

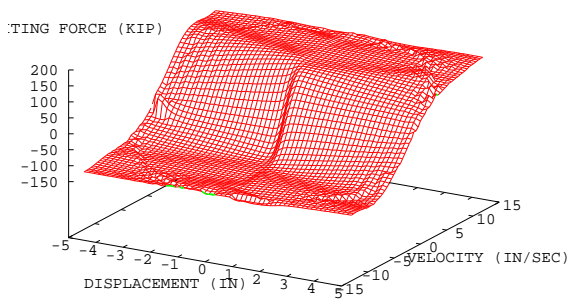


(b) Force after training

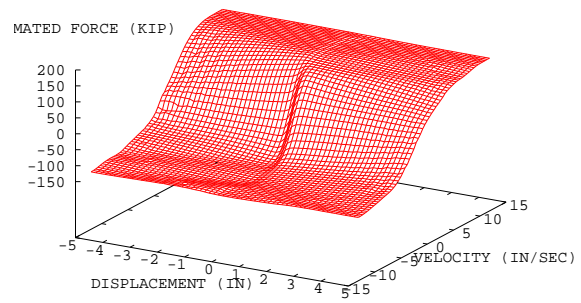


(c) Error after training

Figure C.24: Comparison of the measured and identified damper response using ANN in time history for the data set UCB1\_12\_5.

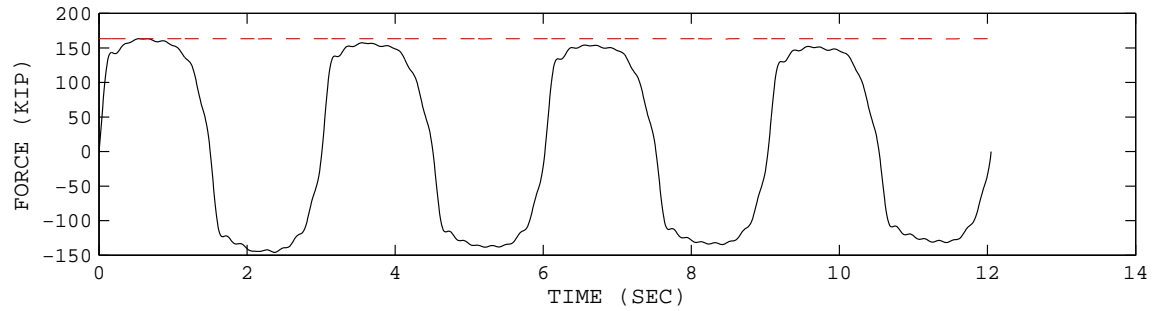


(a) Measured

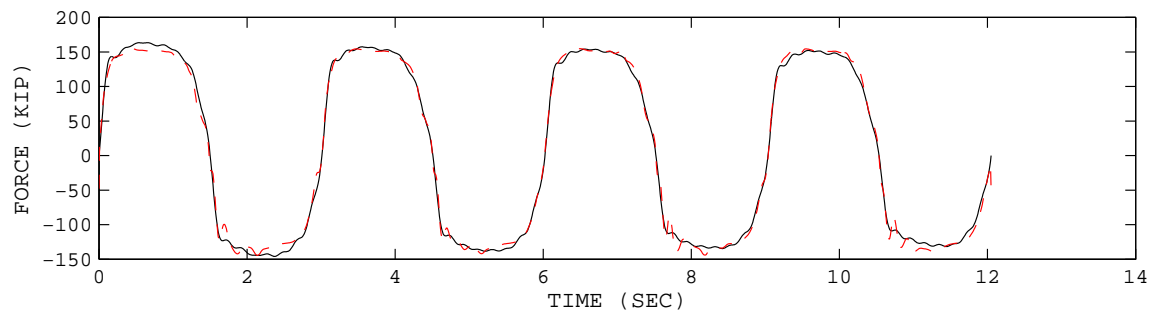


(b) Identified

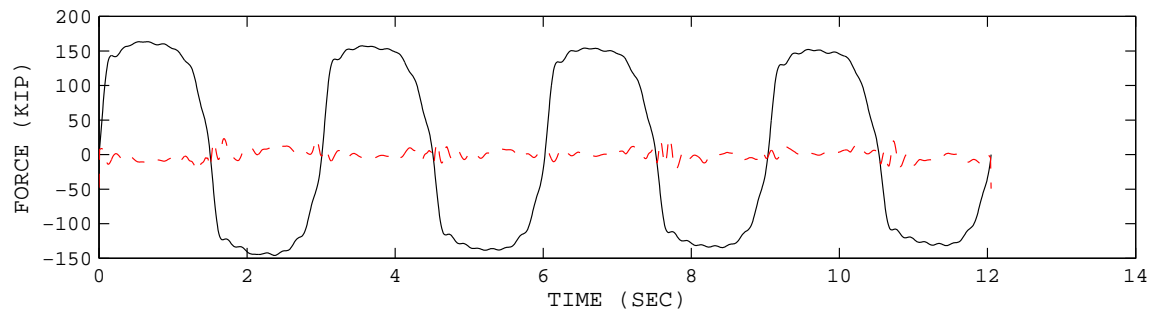
Figure C.25: Comparison of measured and identified damper response using ANN in phase plot for the data set UCB1\_12\_5.



(a) Force before training

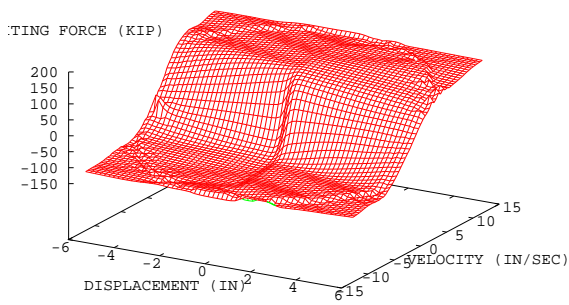


(b) Force after training

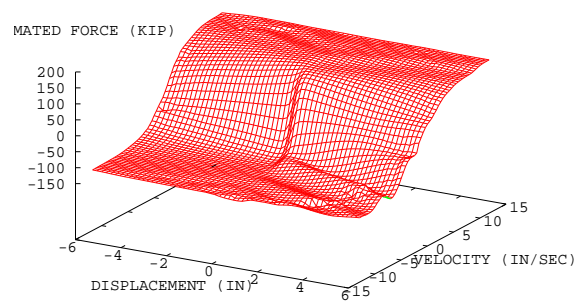


(c) Error after training

Figure C.26: Comparison of the measured and identified damper response using ANN in time history for the data set UCB1\_12\_6.

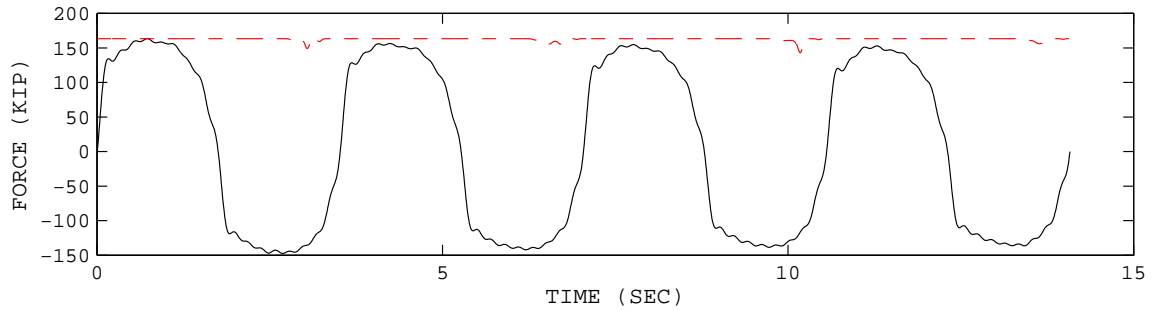


(a) Measured

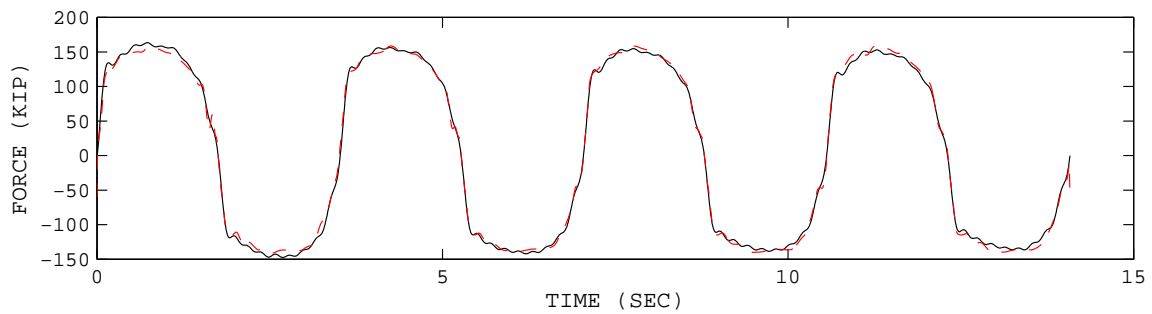


(b) Identified

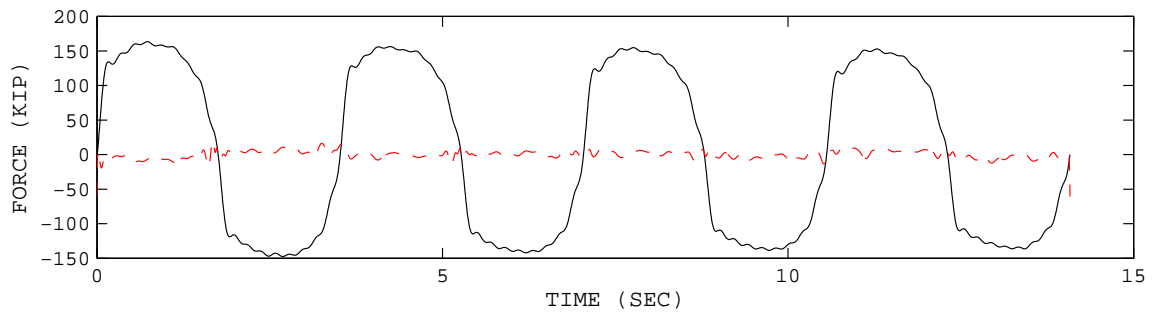
Figure C.27: Comparison of measured and identified damper response using ANN in phase plot for the data set UCB1\_12\_6.



(a) Force before training

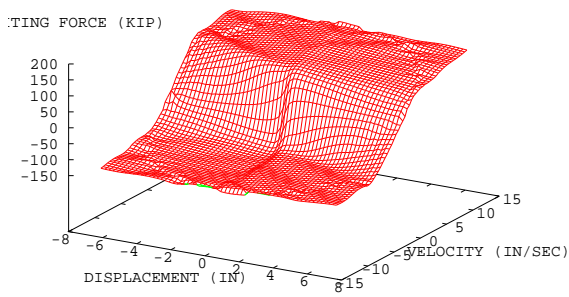


(b) Force after training

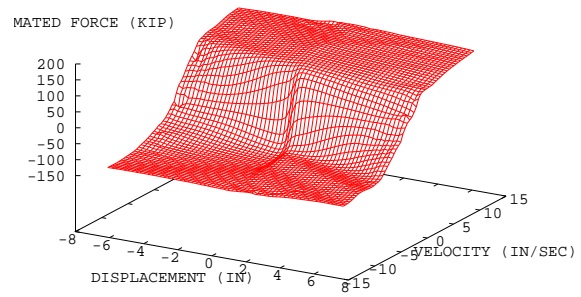


(c) Error after training

Figure C.28: Comparison of the measured and identified damper response using ANN in time history for the data set UCB1\_12\_7.

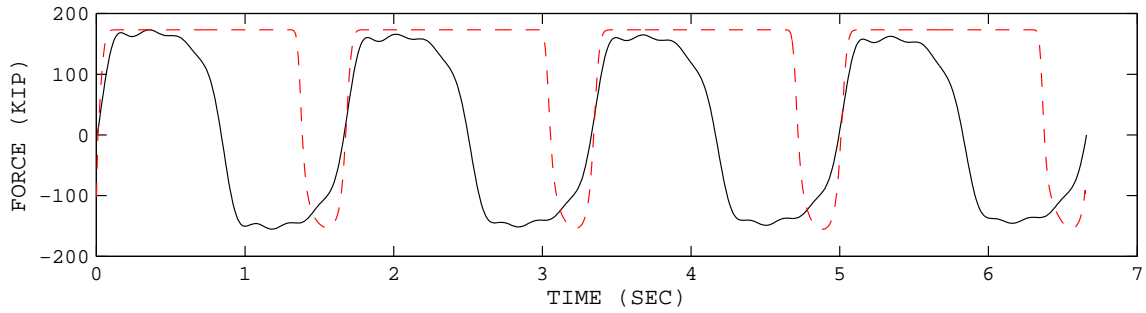


(a) Measured

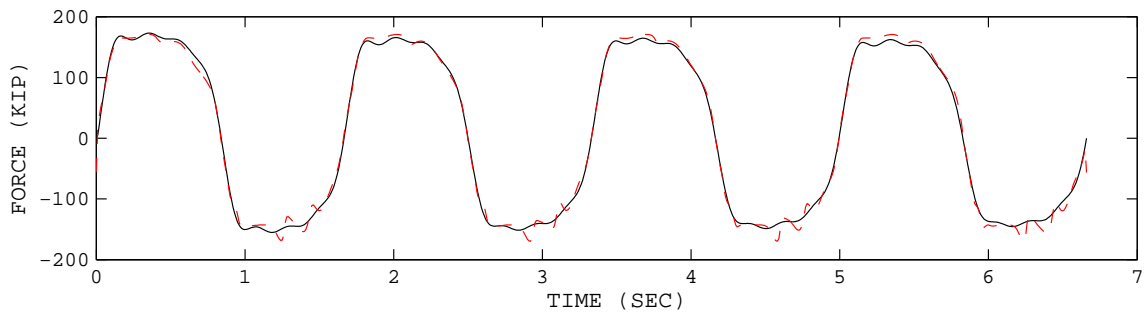


(b) Identified

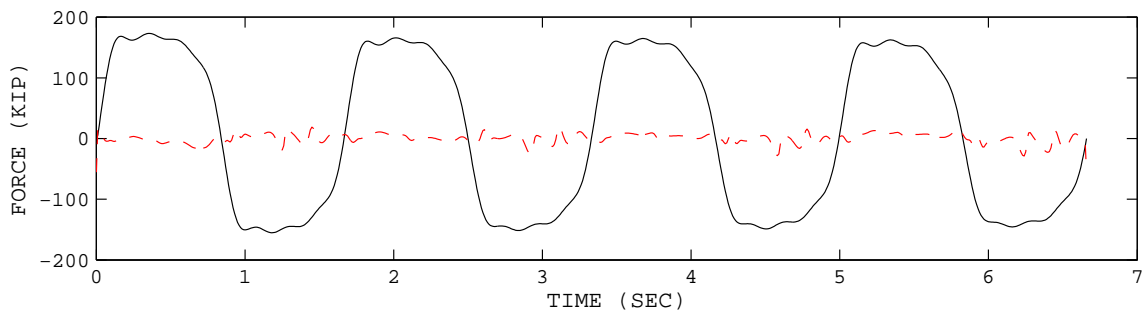
Figure C.29: Comparison of measured and identified damper response using ANN in phase plot for the data set UCB1\_12\_7.



(a) Force before training



(b) Force after training



(c) Error after training

Figure C.30: Comparison of the measured and identified damper response using ANN in time history for the data set UCB1.15.4.

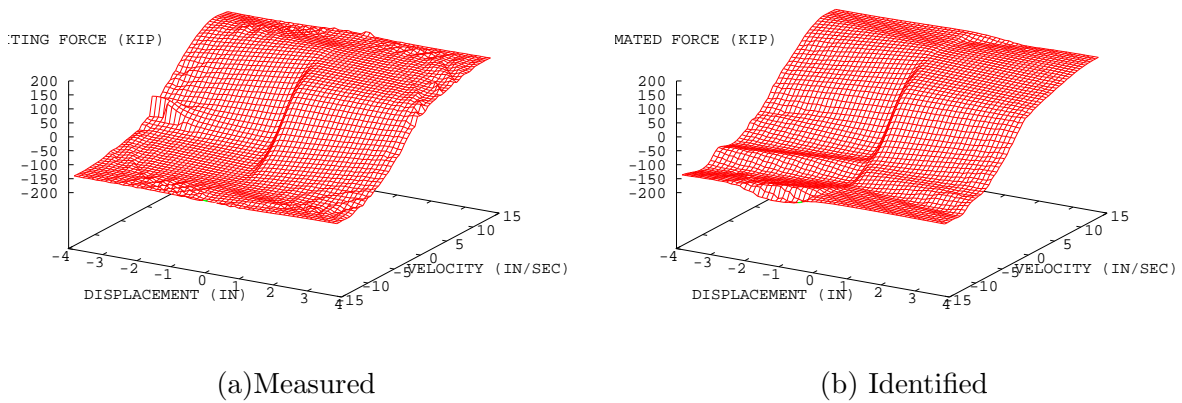
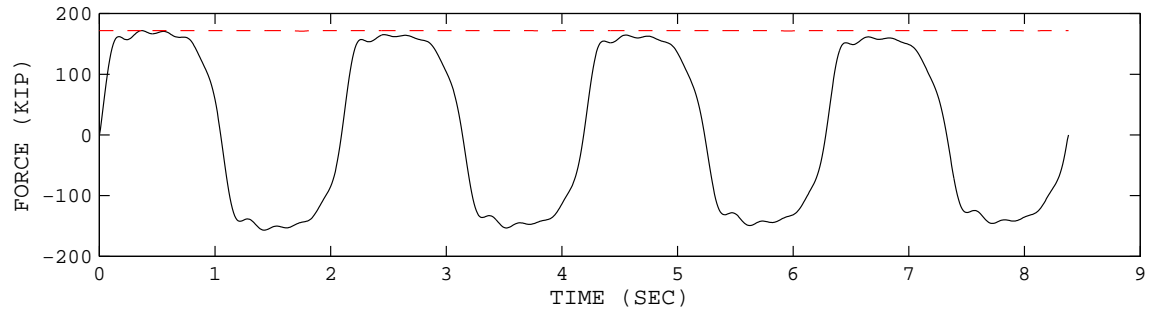
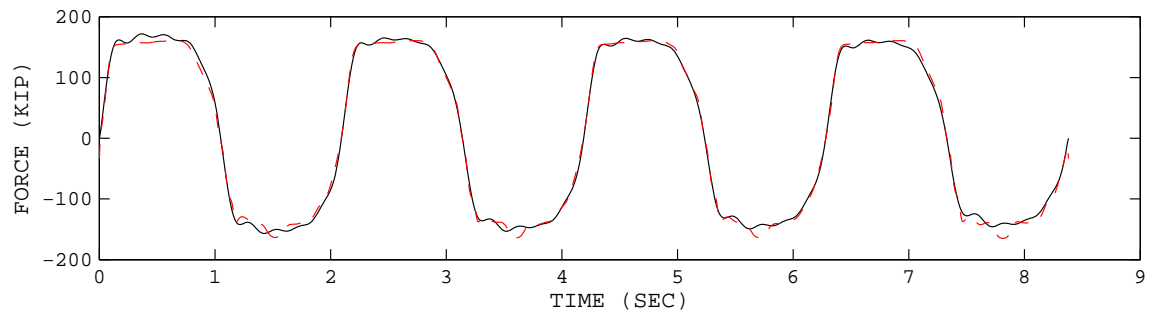


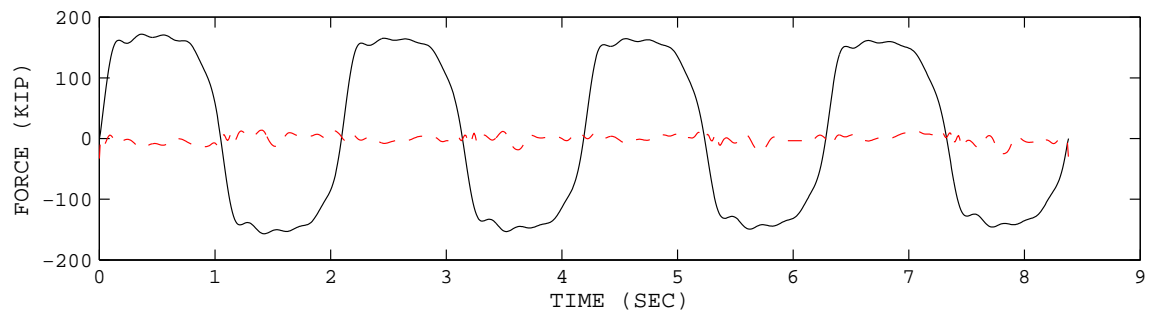
Figure C.31: Comparison of measured and identified damper response using ANN in phase plot for the data set UCB1\_15\_4.



(a) Force before training



(b) Force after training



(c) Error after training

Figure C.32: Comparison of the measured and identified damper response using ANN in time history for the data set UCB1.15.5.

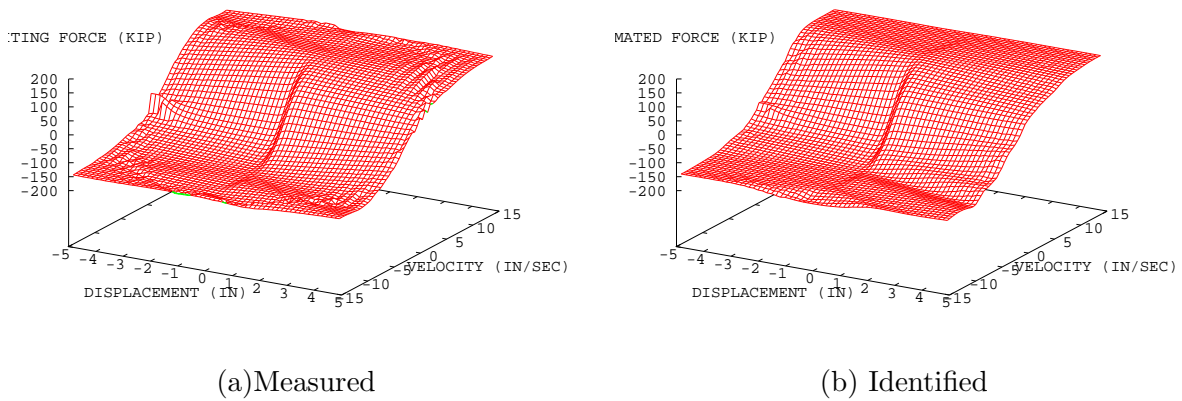
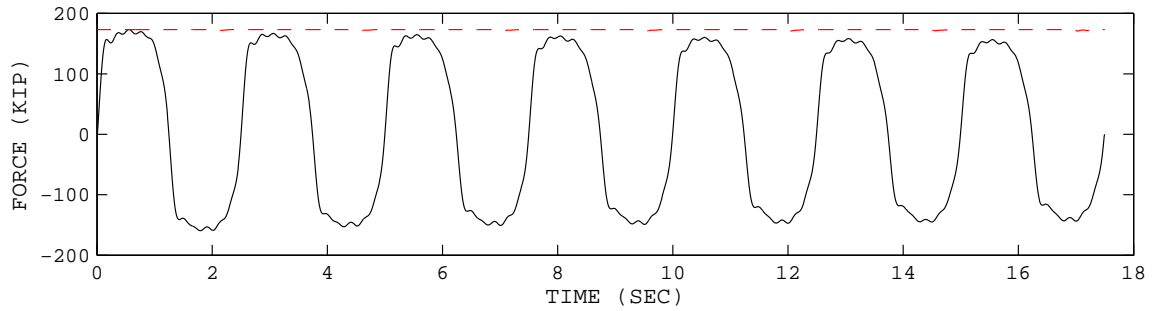
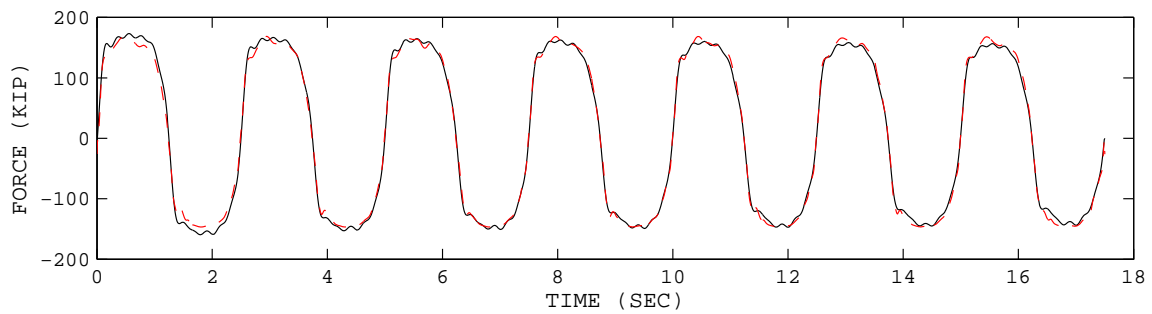


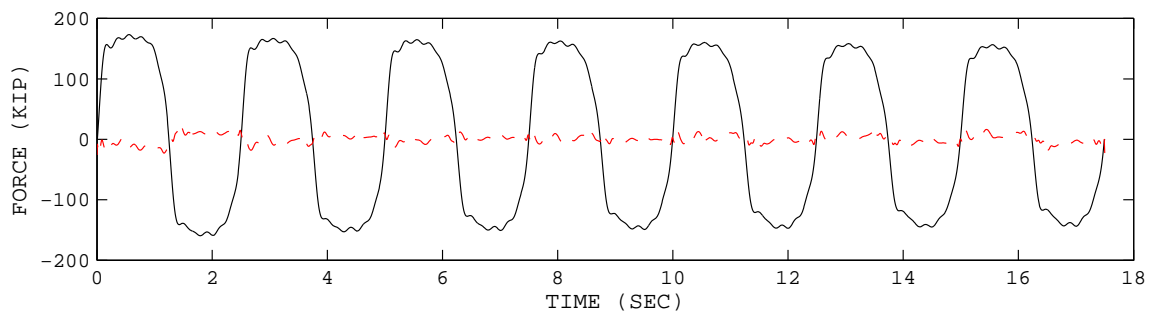
Figure C.33: Phase plots of measured and identified damper response using ANN in phase plot for the data set UCB1\_15\_5.



(a) Force before training

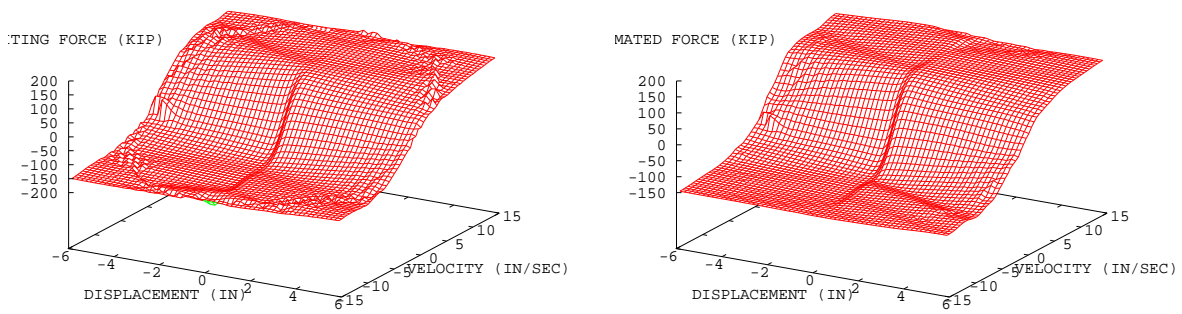


(b) Force after training



(c) Error after training

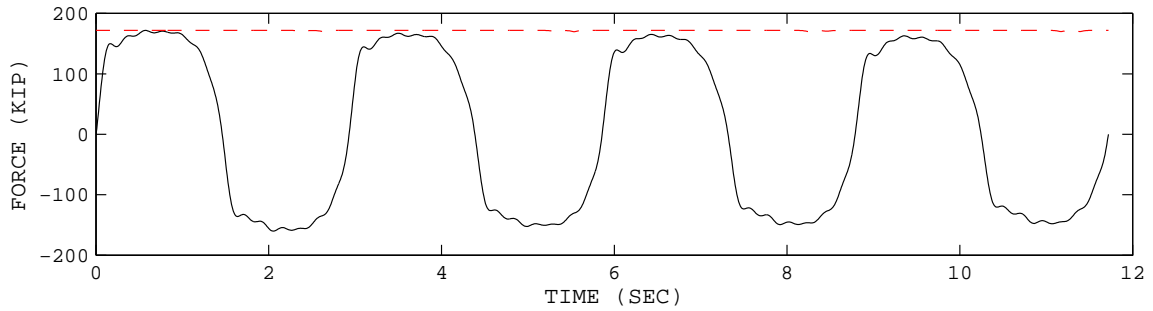
Figure C.34: Comparison of the measured and identified damper response using ANN in time history for the data set UCB1\_15\_6.



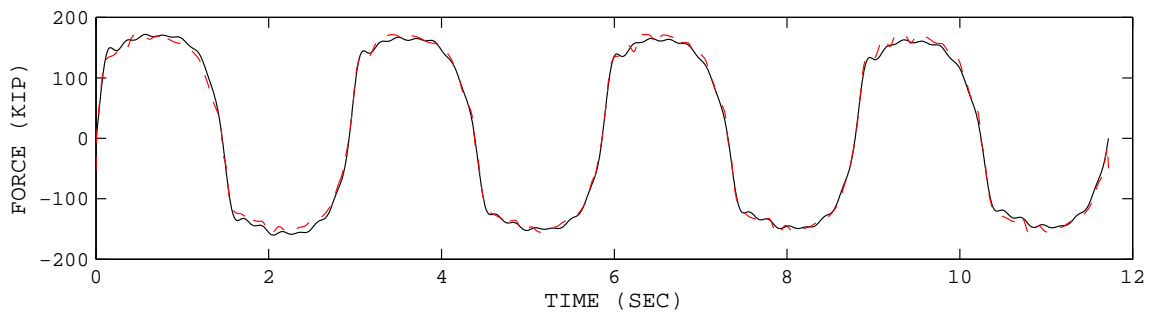
(a) Measured

(b) Identified

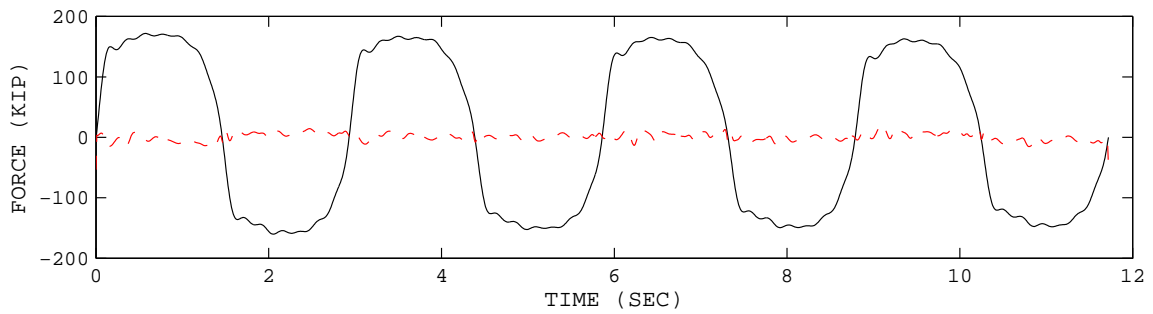
Figure C.35: Phase plots of measured and identified damper response using ANN in phase plot for the data set UCB1\_15\_6.



(a) Force before training

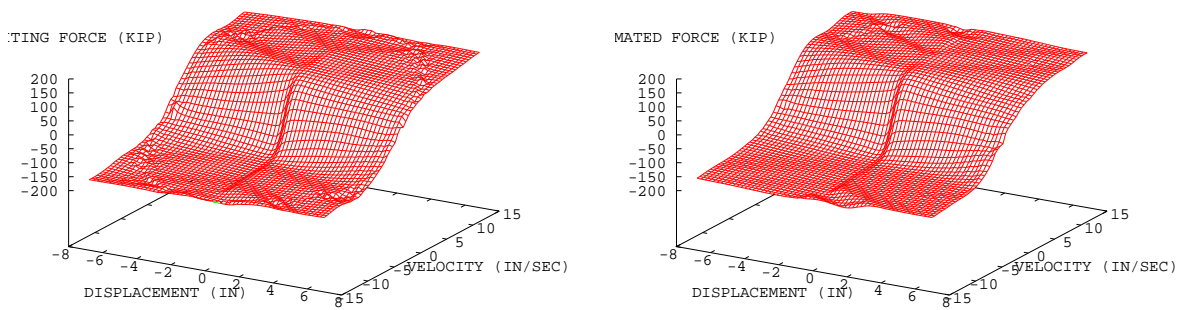


(b) Force after training



(c) Error after training

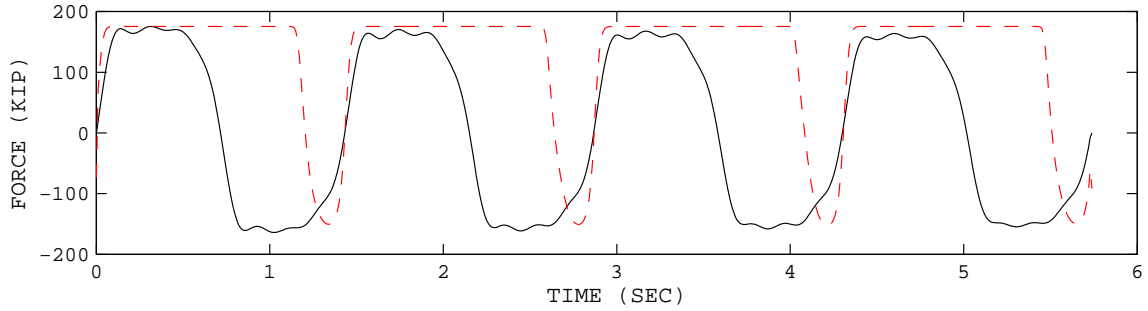
Figure C.36: Comparison of the measured and identified damper response using ANN in time history for the data set UCB1\_15\_7.



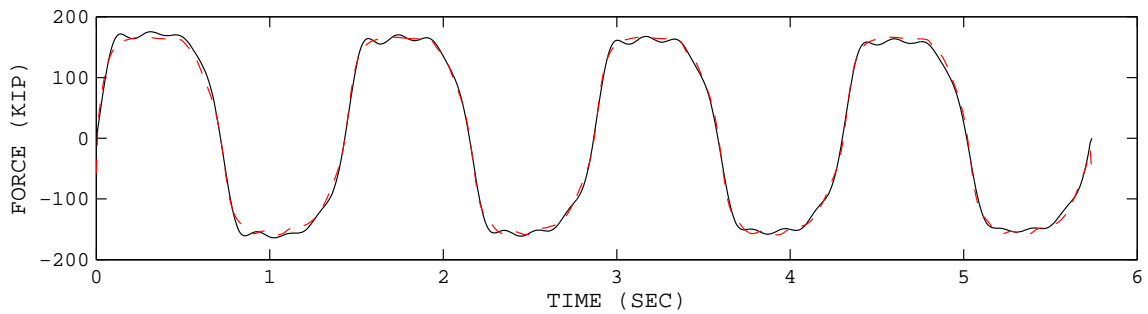
(a) Measured

(b) Identified

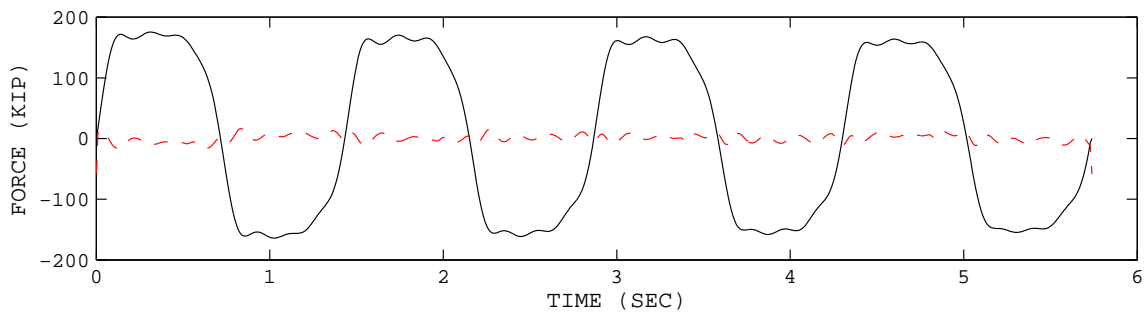
Figure C.37: Phase plots of measured and identified damper response using ANN in phase plot for the data set UCB1\_15\_7.



(a) Force before training

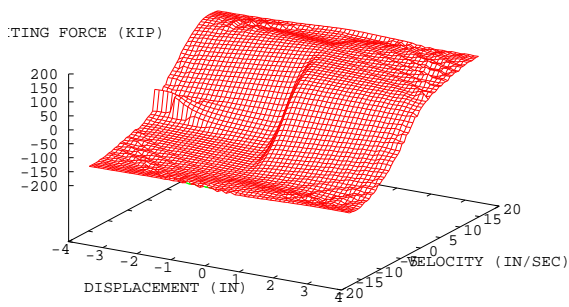


(b) Force after training

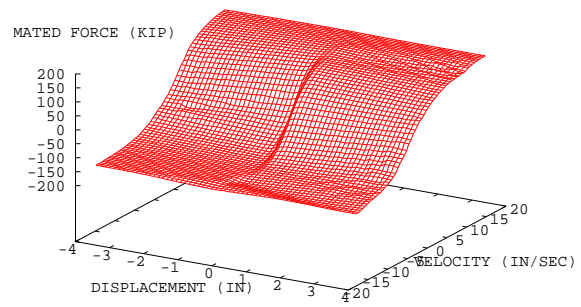


(c) Error after training

Figure C.38: Comparison of the measured and identified damper response using ANN in time history for the data set UCB1.17.4.

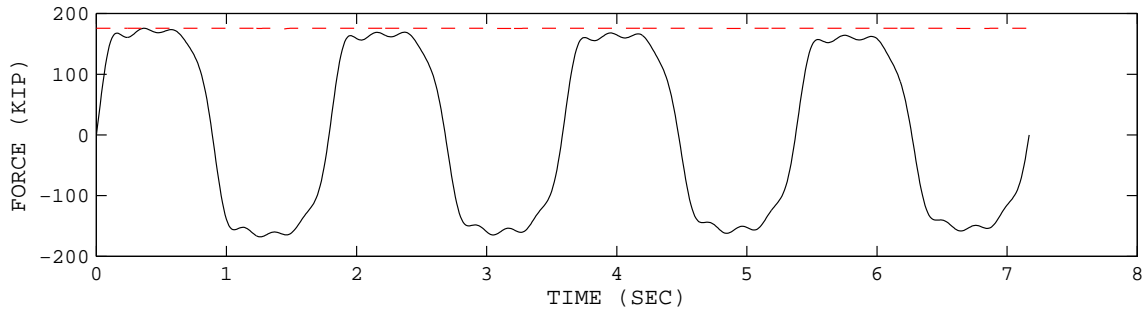


(a) Measured

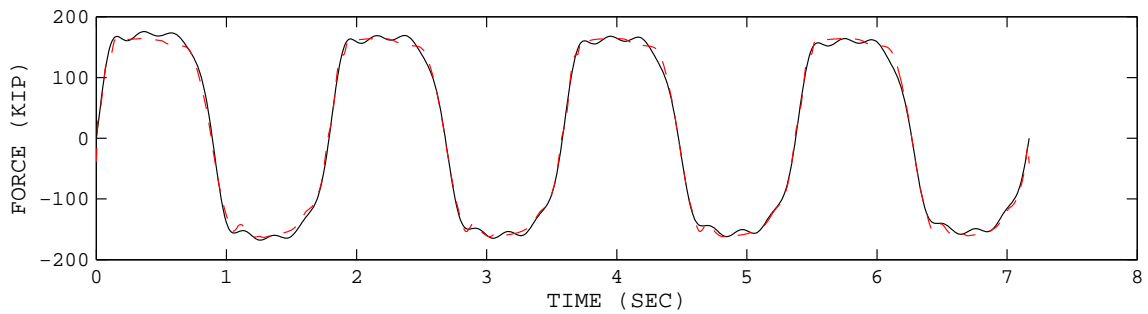


(b) Identified

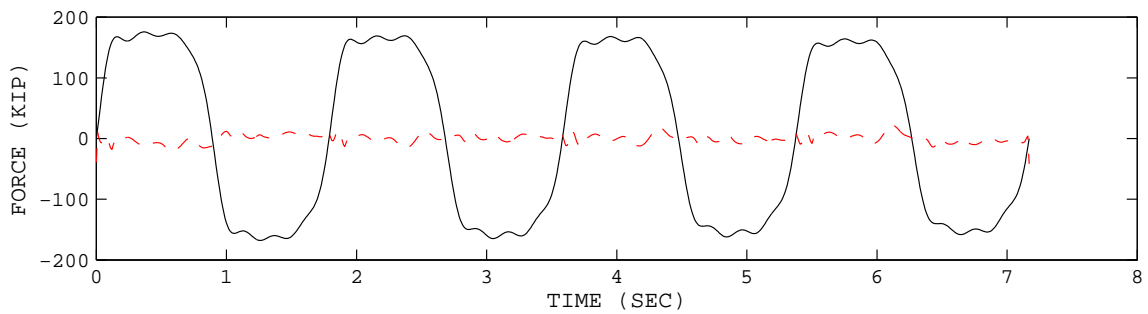
Figure C.39: Phase plots of measured and identified damper response using ANN in phase plot for the data set UCB1\_17\_4.



(a) Force before training

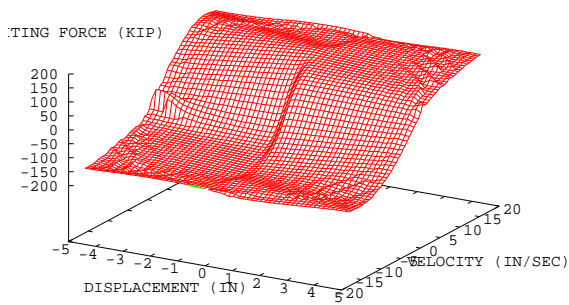


(b) Force after training

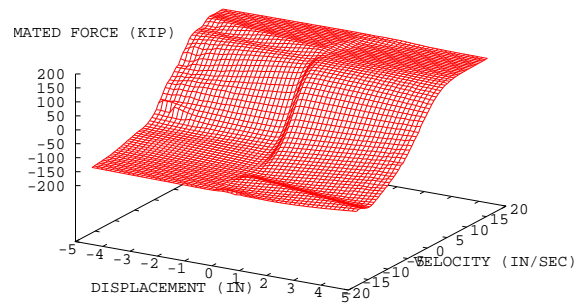


(c) Error after training

Figure C.40: Comparison of the measured and identified damper response using ANN in time history for the data set UCB1.17.5.

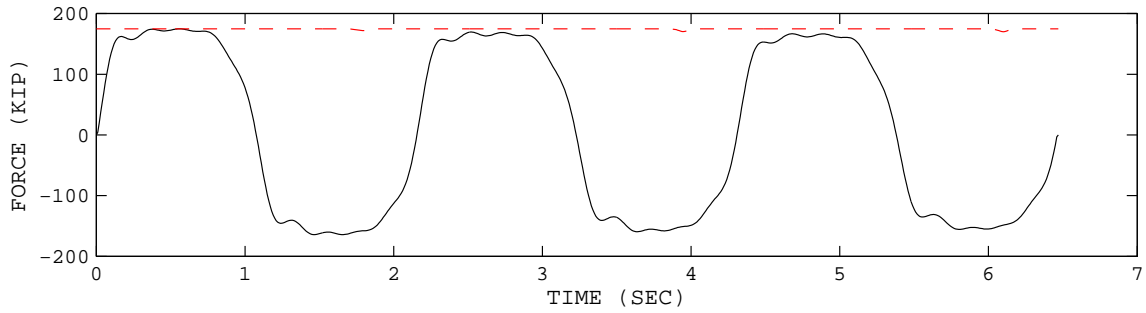


(a) Measured

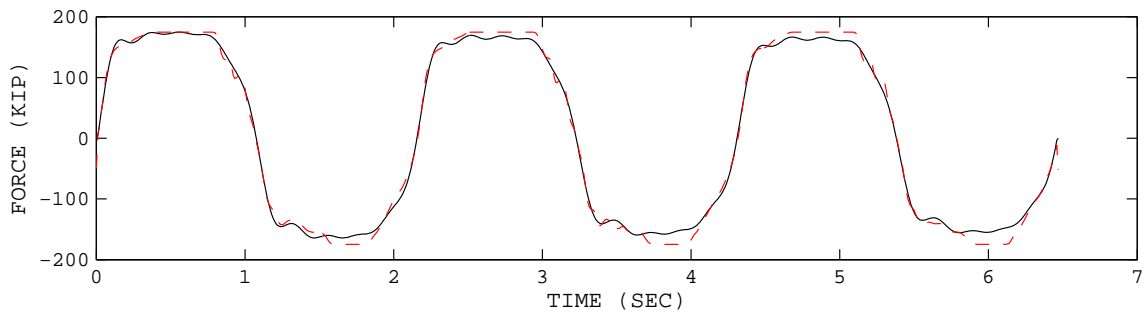


(b) Identified

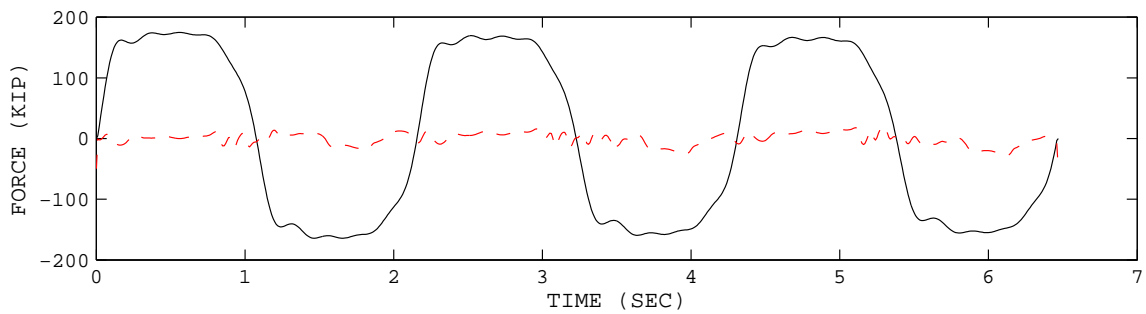
Figure C.41: Phase plots of measured and identified damper response using ANN in phase plot for the data set UCB1\_17\_5.



(a) Force before training

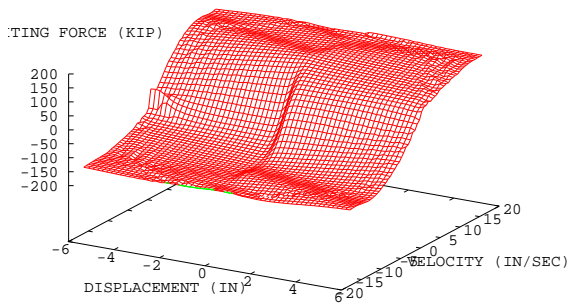


(b) Force after training

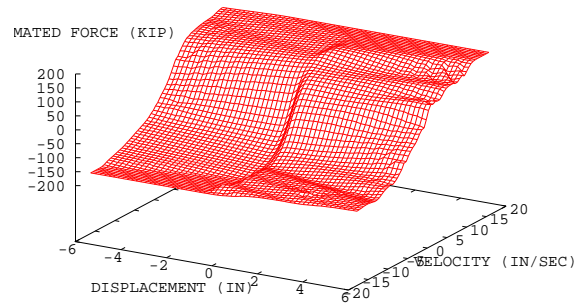


(c) Error after training

Figure C.42: Comparison of the measured and identified damper response using ANN in time history for the data set UCB1.17.6.

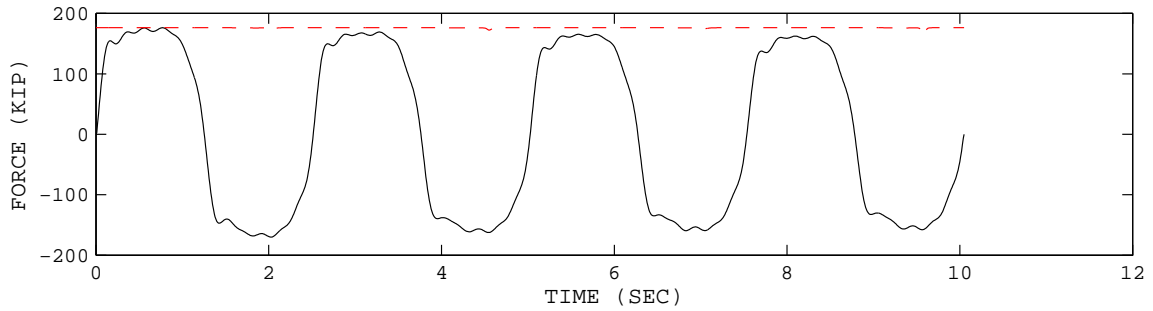


(a) Measured

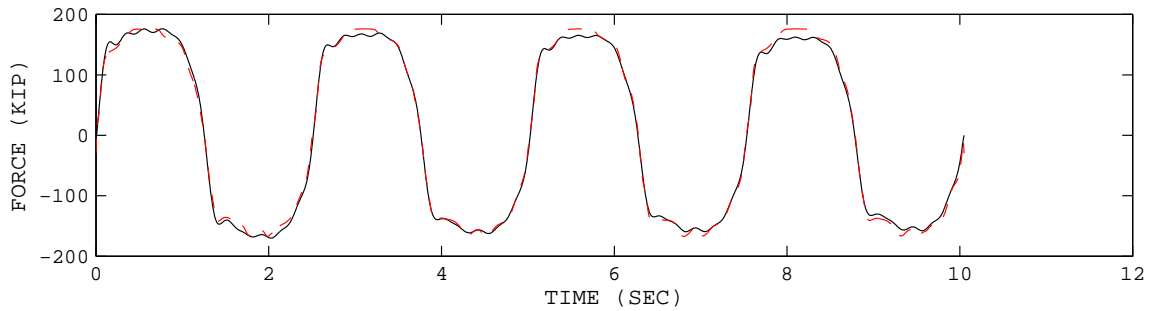


(b) Identified

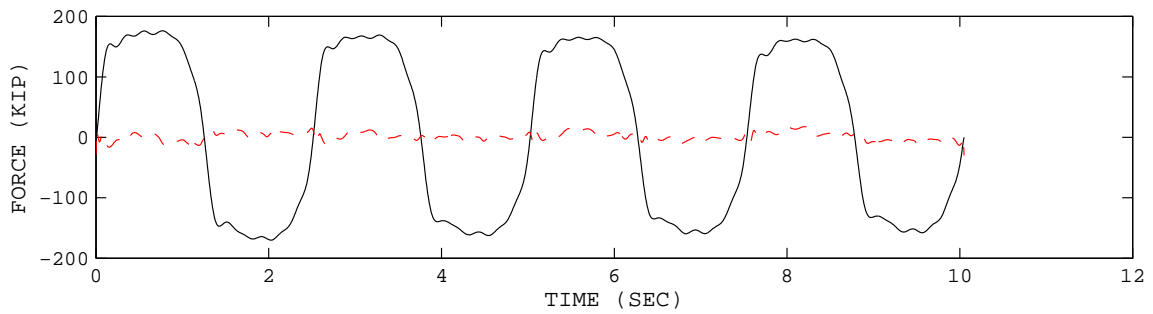
Figure C.43: Comparison of measured and identified damper response using ANN in phase plot for the data set UCB1\_17\_6.



(a) Force before training

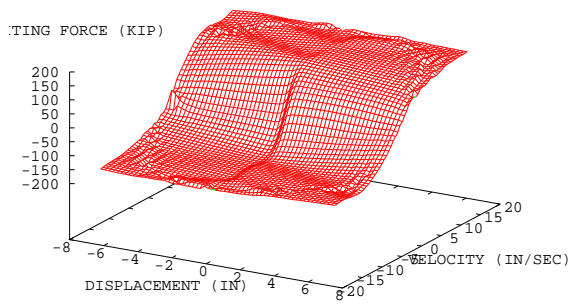


(b) Force after training

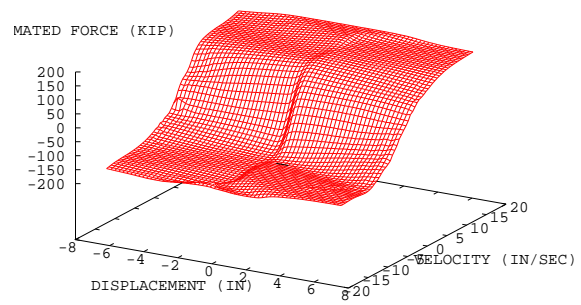


(c) Error after training

Figure C.44: Comparison of the measured and identified damper response using ANN in time history for the data set UCB1\_17\_7.



(a) Measured



(b) Identified

Figure C.45: Phase plots of measured and identified damper response using ANN in phase plot for the data set UCB1\_17\_7.



# Appendix D

## DATA ACQUISITION FOR THE 15 KIP VISCOUS DAMPER - FIRST ROUND

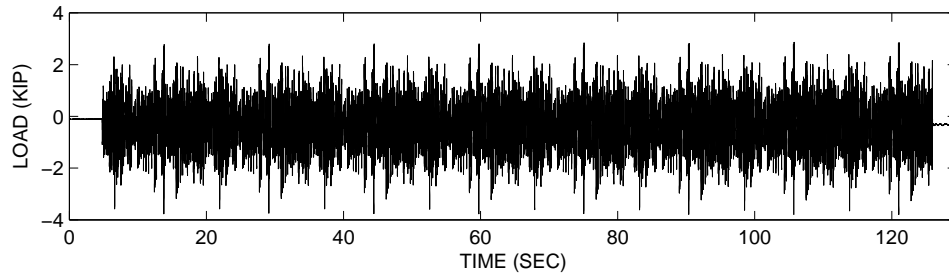
### D.1 Experimental Data (Raw) for the 15 Kip Viscoous Damper - First Round

The dynamic response of the 15 kip viscous damper in the first round experiments was obtained at the University of California, Berkeley by measuring the displacement and force. The first 20 rows of the obtained data (Qtr1\_01) is shown below. The entire data sets are provided in the accompanying CD in \data\UCB2\_1\raw\ folder. The measured data sets are illustrated in Figures D.1 to D.16.

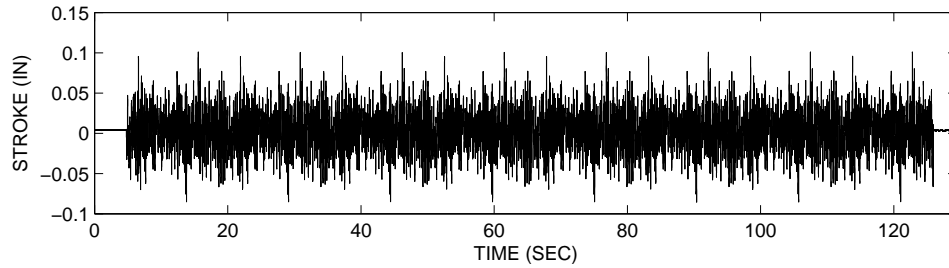
```
c:\damper2\ascii\ADAMP2A.001
06/05/10
09:36:41
12
999.928000
Time      Secs      Load      KIP      Stroke  IN      Oiltemp1 degF  Oiltemp2 degF  Tempex1 degF  Tempex2 degF  Tempex3 degF  Tempex4 degF
-1.0000720E-03  -1.0781250E-01  +4.3122703E-03  +6.5855652E+01  +6.8415062E+01  +6.6621284E+01  +6.8065056E+01  +6.6796288E+01  +6.8075996E+01
+0.0000000E+00  -1.0781250E-01  +3.9372901E-03  +6.5899399E+01  +6.8415062E+01  +6.6610352E+01  +6.8185371E+01  +6.6818169E+01  +6.8097870E+01
+1.0000720E-03  -1.0781250E-01  +3.9372901E-03  +6.5866585E+01  +6.8415062E+01  +6.6610352E+01  +6.8097870E+01  +6.6807228E+01  +6.8065056E+01
+2.0001440E-03  -1.0781250E-01  +4.3122703E-03  +6.5833778E+01  +6.8393188E+01  +6.6610352E+01  +6.7999435E+01  +6.6752541E+01  +6.8065056E+01
+3.0002160E-03  -1.0937500E-01  +4.4997600E-03  +6.5790024E+01  +6.8393188E+01  +6.6610352E+01  +6.7890053E+01  +6.6730667E+01  +6.8065056E+01
+4.0002880E-03  -1.0937500E-01  +4.3122703E-03  +6.5790024E+01  +6.8360374E+01  +6.6599411E+01  +6.7802551E+01  +6.6686913E+01  +6.8065056E+01
+5.0003600E-03  -1.0468750E-01  +4.3122703E-03  +6.5790024E+01  +6.8371315E+01  +6.6610352E+01  +6.7747864E+01  +6.6643166E+01  +6.8086937E+01
+6.0004320E-03  -1.0625000E-01  +4.3122703E-03  +6.5768150E+01  +6.8371315E+01  +6.6588470E+01  +6.7693176E+01  +6.6621284E+01  +6.8075996E+01
+7.0005040E-03  -1.0468750E-01  +4.3122703E-03  +6.5779091E+01  +6.8393188E+01  +6.6599411E+01  +6.7682243E+01  +6.6610352E+01  +6.8054123E+01
+8.0005760E-03  -1.0937500E-01  +4.1247802E-03  +6.5811897E+01  +6.8436935E+01  +6.6610352E+01  +6.7715050E+01  +6.6621284E+01  +6.8065056E+01
+9.0006480E-03  -1.0781250E-01  +4.1247802E-03  +6.5822838E+01  +6.8480690E+01  +6.6621284E+01  +6.7802551E+01  +6.6643166E+01  +6.8086937E+01
+1.0000720E-02  -1.0625000E-01  +4.1247802E-03  +6.5855652E+01  +6.8502563E+01  +6.6610352E+01  +6.7857246E+01  +6.6686913E+01  +6.8054123E+01
+1.1000792E-02  -1.1093750E-01  +3.7498001E-03  +6.5899399E+01  +6.8513504E+01  +6.6610352E+01  +6.7988495E+01  +6.6741600E+01  +6.8086937E+01
+1.2000864E-02  -1.1093750E-01  +3.9372901E-03  +6.5910339E+01  +6.8546318E+01  +6.6621284E+01  +6.8065056E+01  +6.6774414E+01  +6.8086937E+01
+1.3000936E-02  -1.1093750E-01  +3.9372901E-03  +6.5943153E+01  +6.8535378E+01  +6.6621284E+01  +6.8141624E+01  +6.6796288E+01  +6.8086937E+01
+1.4001008E-02  -1.0937500E-01  +4.1247802E-03  +6.5921280E+01  +6.8524437E+01  +6.6621284E+01  +6.8196312E+01  +6.6807228E+01  +6.8086937E+01
+1.5001080E-02  -1.0781250E-01  +4.1247802E-03  +6.5932213E+01  +6.8491631E+01  +6.6632225E+01  +6.8229126E+01  +6.6840042E+01  +6.8086937E+01
+1.6001152E-02  -1.0937500E-01  +4.1247802E-03  +6.5921280E+01  +6.8469749E+01  +6.6621284E+01  +6.8185371E+01  +6.6840042E+01  +6.8065056E+01
+1.7001224E-02  -1.0625000E-01  +3.9372901E-03  +6.5888466E+01  +6.8436935E+01  +6.6577538E+01  +6.8152557E+01  +6.6829102E+01  +6.8086937E+01
+1.8001296E-02  -1.0625000E-01  +4.1247802E-03  +6.5866585E+01  +6.8404129E+01  +6.6588470E+01  +6.8032242E+01  +6.6785355E+01  +6.8086937E+01

AccDamp  G      AccAct  G      Command  IN
+1.5624999E-03  -9.3749998E-04  +1.3124300E-03
+9.3749998E-04  -1.5624999E-03  +9.3745004E-04
+9.3749998E-04  -9.3749998E-04  +1.1249400E-03
+9.3749998E-04  -9.3749998E-04  +9.3745004E-04
-3.1249999E-04  -3.1249999E-04  +1.3124300E-03
-3.1249999E-04  -3.1249999E-04  +9.3745004E-04
```

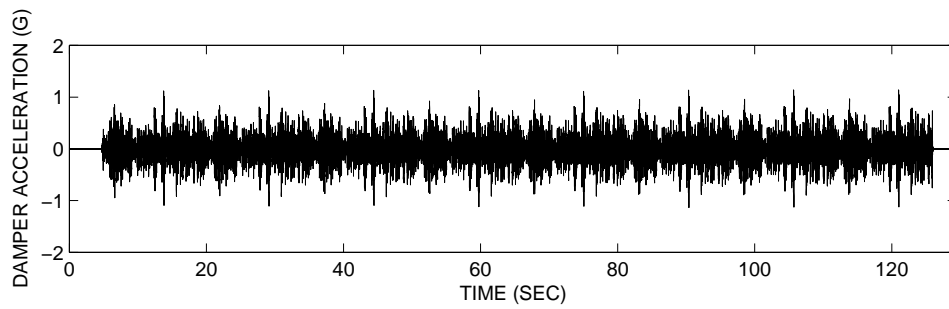
-3.1249999E-04	+1.5624999E-03	+1.1249400E-03
-9.3749998E-04	+1.5624999E-03	+1.1249400E-03
-1.5624999E-03	+2.1875000E-03	+1.1249400E-03
-1.8750000E-03	+2.4999999E-03	+1.3124300E-03
-2.1875000E-03	+1.8750000E-03	+1.1249400E-03
-1.5624999E-03	+1.5624999E-03	+9.3745004E-04
-1.8750000E-03	+9.3749998E-04	+1.1249400E-03
-9.3749998E-04	-3.1249999E-04	+1.1249400E-03
-9.3749998E-04	-3.1249999E-04	+1.3124300E-03
-3.1249999E-04	-6.2499999E-04	+9.3745004E-04
-3.1249999E-04	-9.3749998E-04	+1.3124300E-03
+9.3749998E-04	-1.5624999E-03	+1.1249400E-03
+9.3749998E-04	-1.5624999E-03	+9.3745004E-04
+1.2500000E-03	-6.2499999E-04	+1.1249400E-03



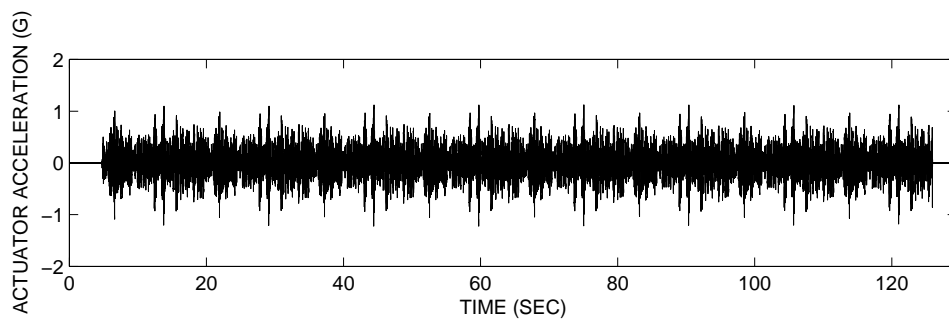
(a) Load (Force)



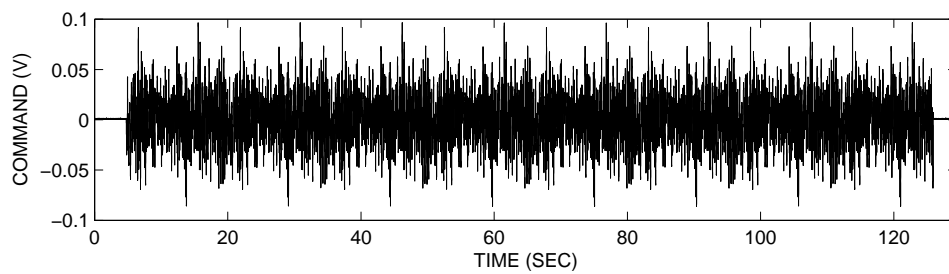
(b) Stroke (Displacement)



(c) Damper acceleration

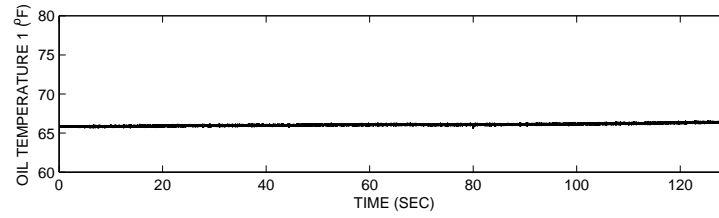


(d) Actuator acceleration

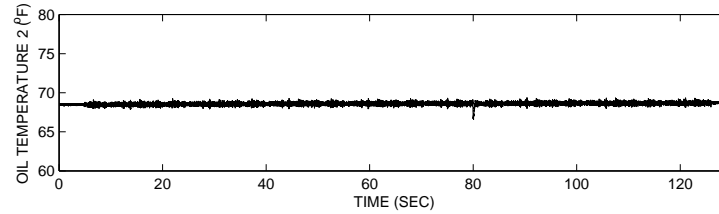


(e) Command Signal

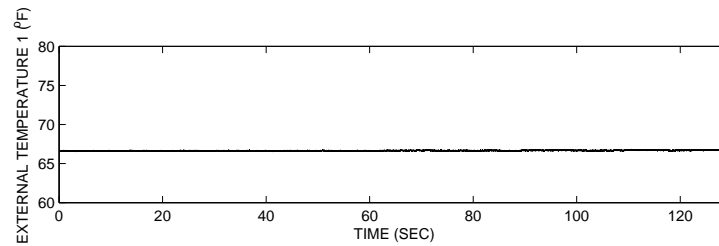
Figure D.1: Measured data of the 15 kip damper in the first round experiments for the data set Qrt1.01.



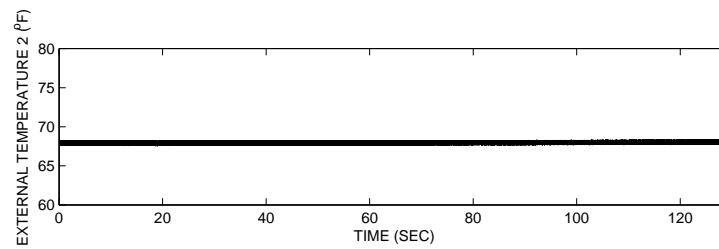
(a) Oil temperature 1



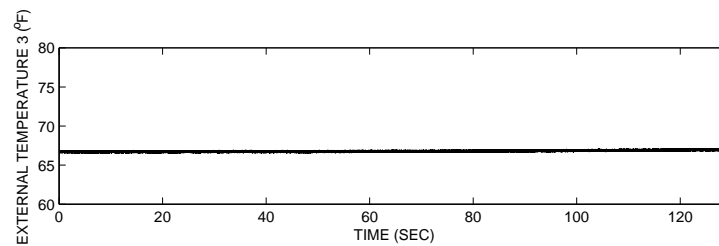
(b) Oil temperature 2



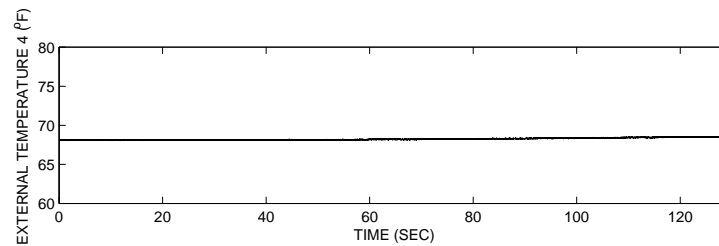
(c) Surface temperature 1



(d) Surface temperature 2

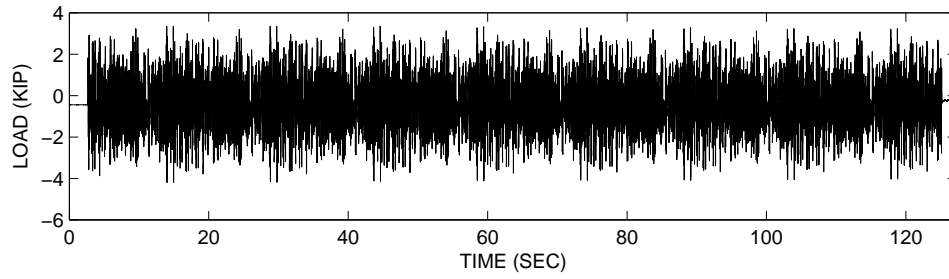


(e) Surface temperature 3

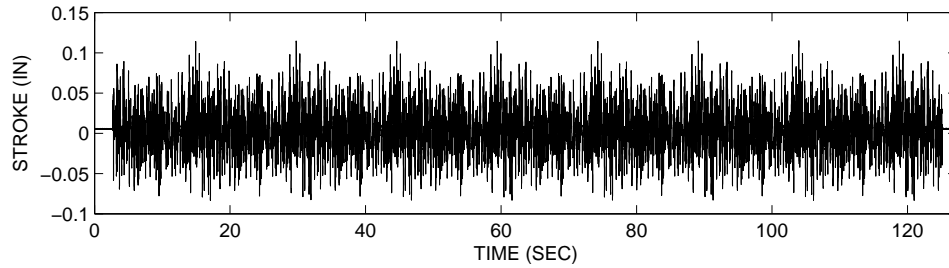


(f) Surface temperature 4

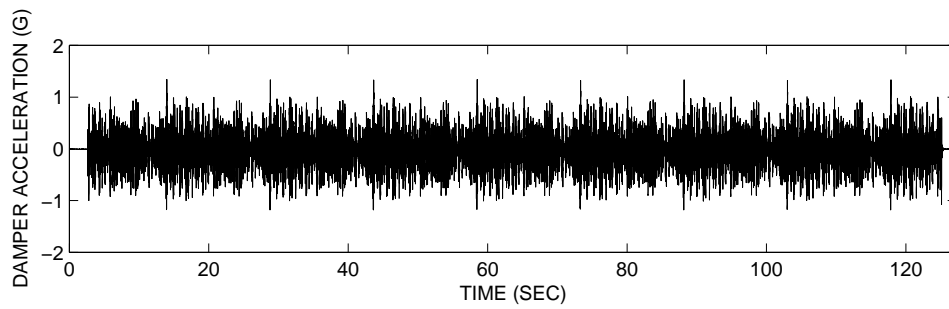
Figure D.2: Measured oil and surface temperatures of the 15 kip damper in the first round experiments for the data set Qrt1.01.



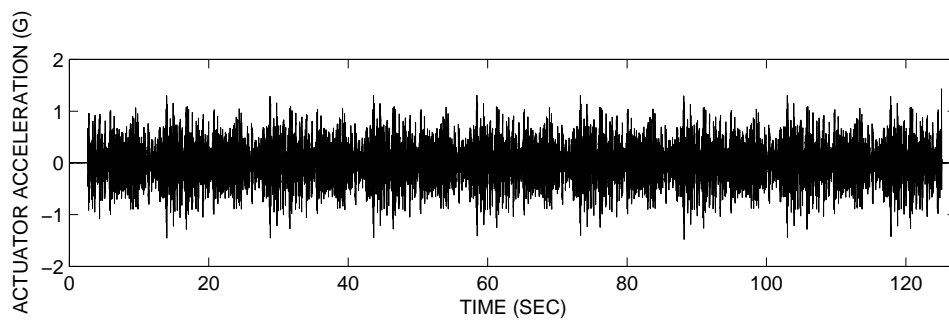
(a) Load (Force)



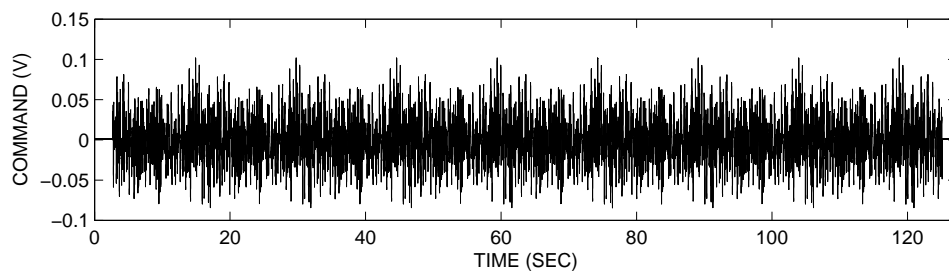
(b) Stroke (Displacement)



(c) Damper acceleration

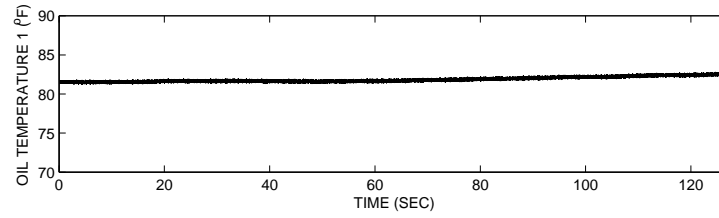


(d) Actuator acceleration

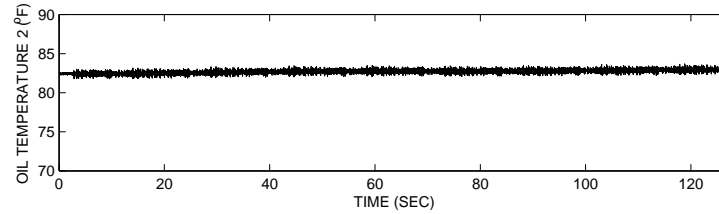


(e) Command Signal

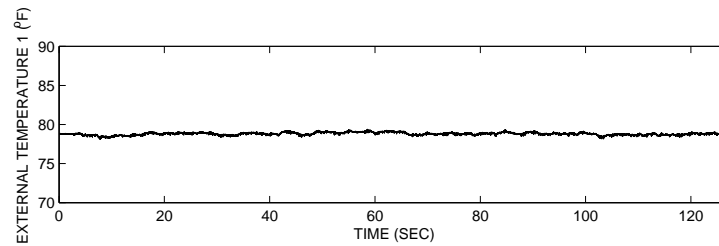
Figure D.3: Measured data of the 15 kip damper in the first round experiments for the data set Qrt2\_01.



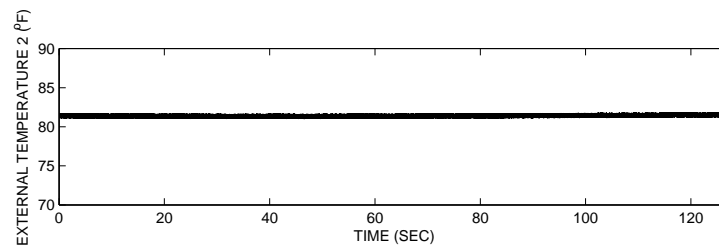
(a) Oil temperature 1



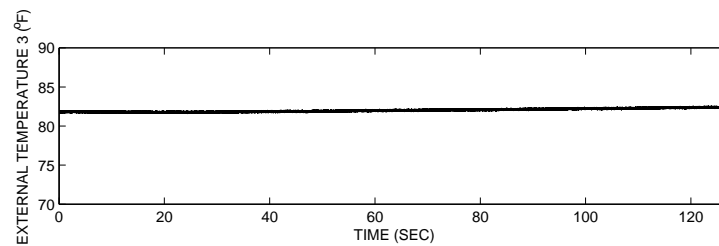
(b) Oil temperature 2



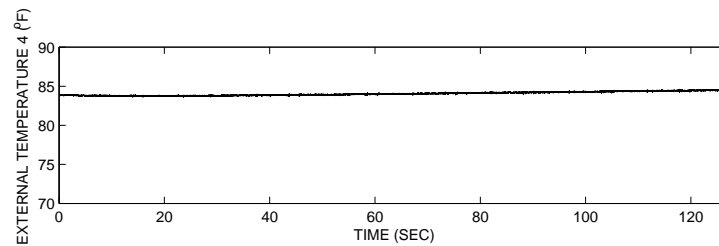
(c) Surface temperature 1



(d) Surface temperature 2

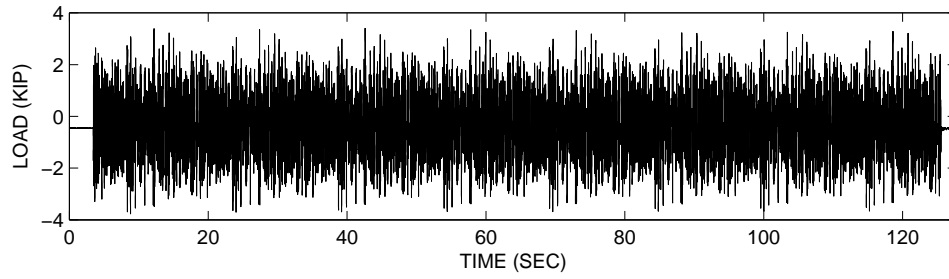


(e) Surface temperature 3

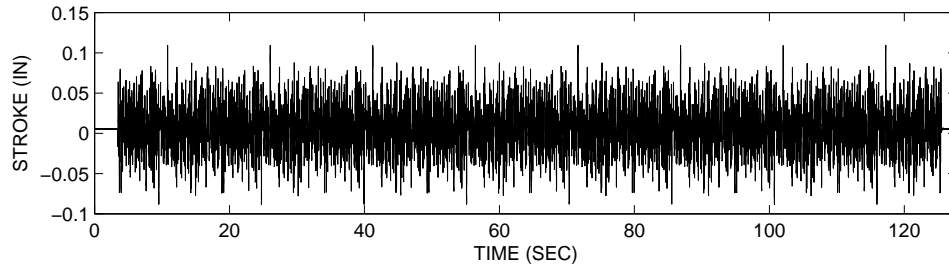


(f) Surface temperature 4

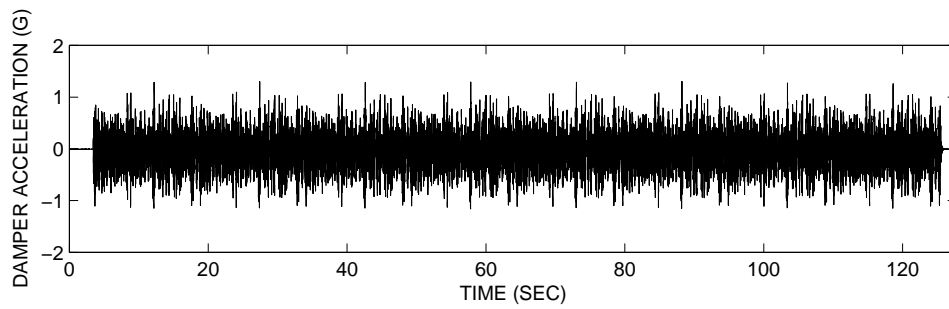
Figure D.4: Measured oil and surface temperatures of the 15 kip damper in the first round experiments for the data set Qrt2\_01.



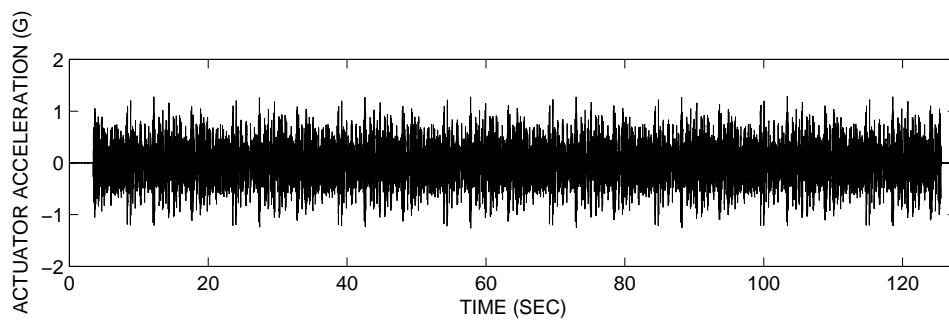
(a) Load (Force)



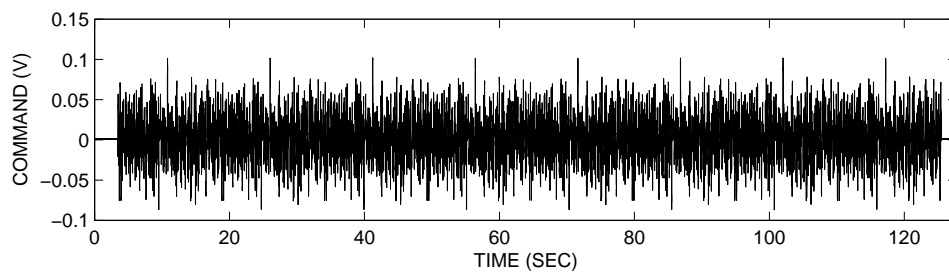
(b) Stroke (Displacement)



(c) Damper acceleration

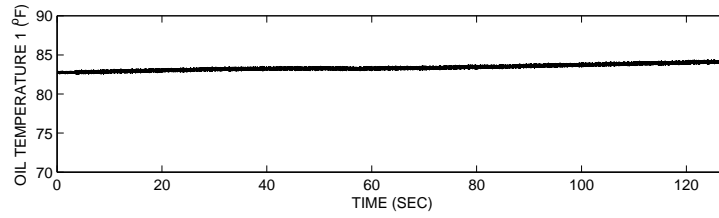


(d) Actuator acceleration

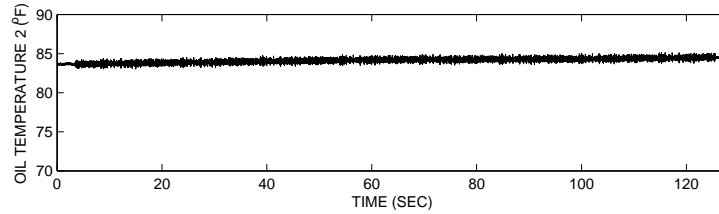


(e) Command Signal

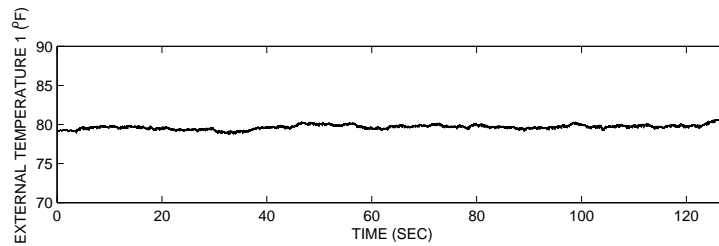
Figure D.5: Measured data of the 15 kip damper in the first round experiments for the data set Qrt3\_01.



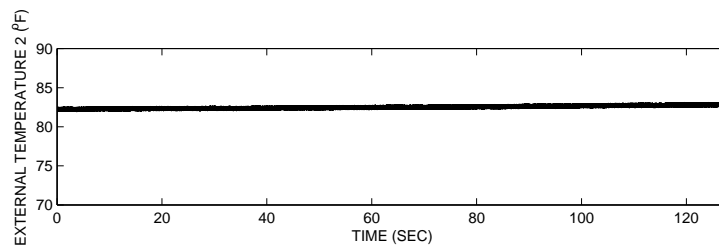
(a) Oil temperature 1



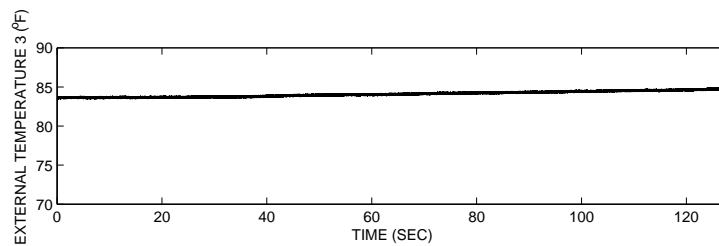
(b) Oil temperature 2



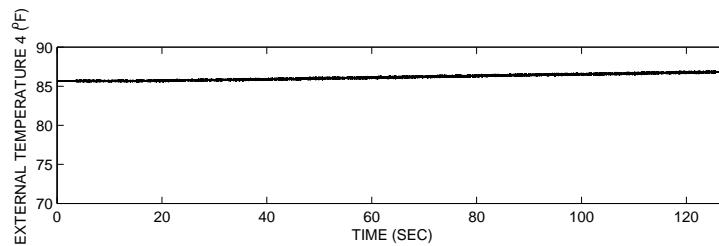
(c) Surface temperature 1



(d) Surface temperature 2

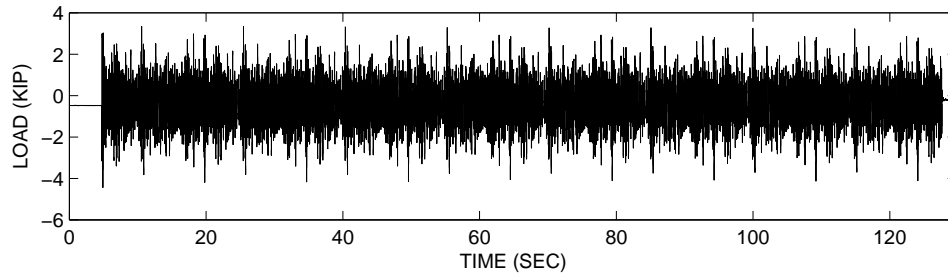


(e) Surface temperature 3

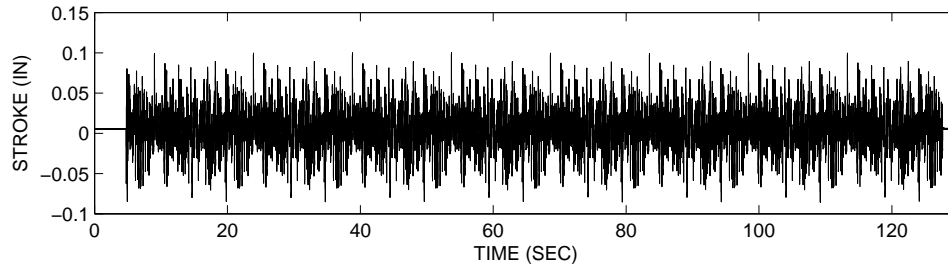


(f) Surface temperature 4

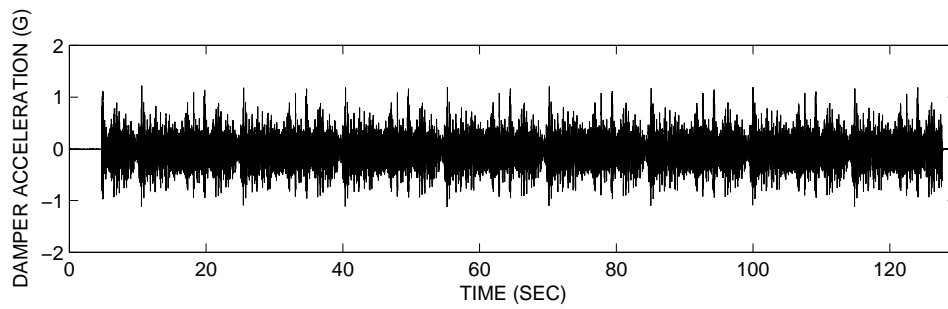
Figure D.6: Measured oil and surface temperatures of the 15 kip damper in the first round experiments for the data set Qrt3\_01.



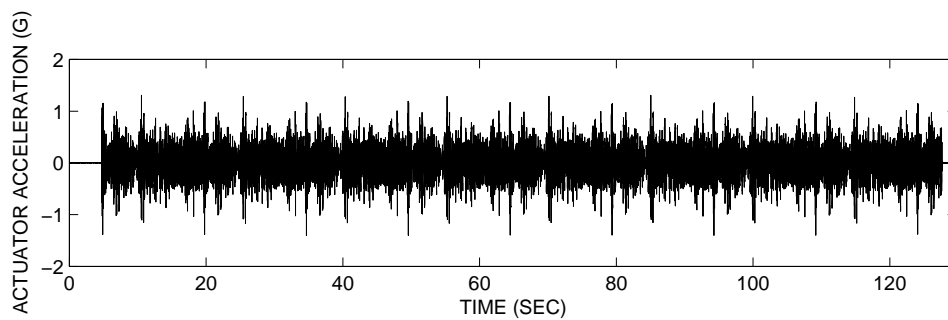
(a) Load (Force)



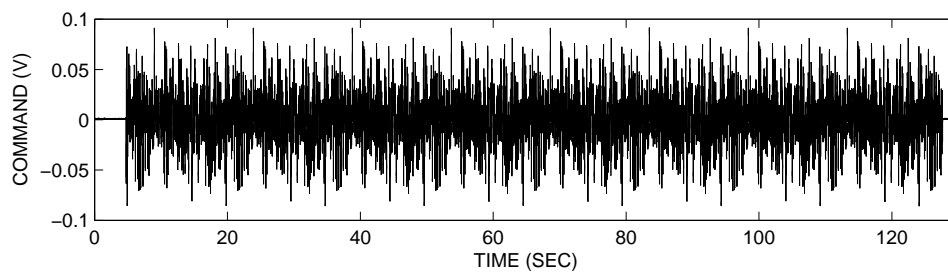
(b) Stroke (Displacement)



(c) Damper acceleration

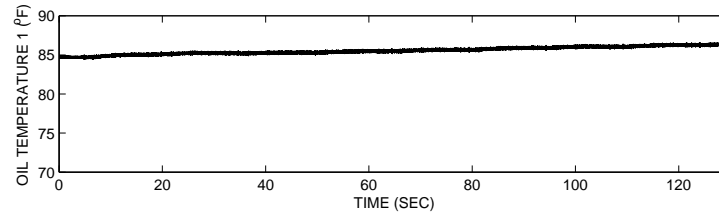


(d) Actuator acceleration

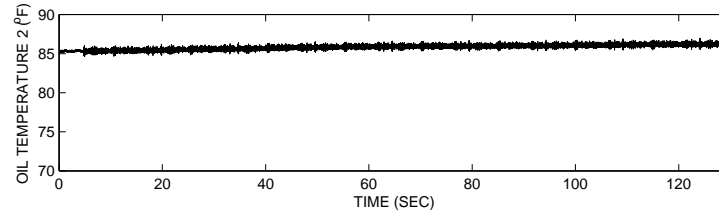


(e) Command Signal

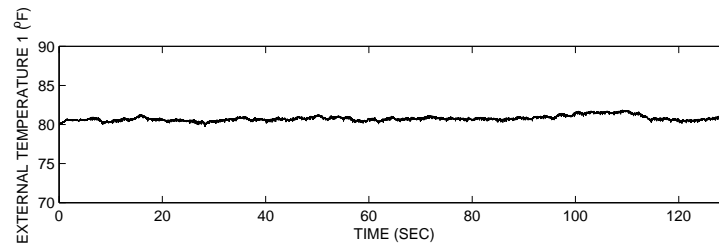
Figure D.7: Measured data of the 15 kip damper in the first round experiments for the data set Qrt4\_01.



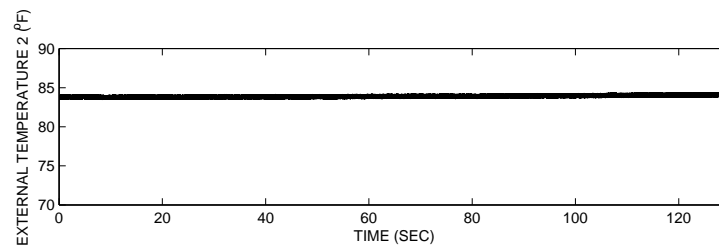
(a) Oil temperature 1



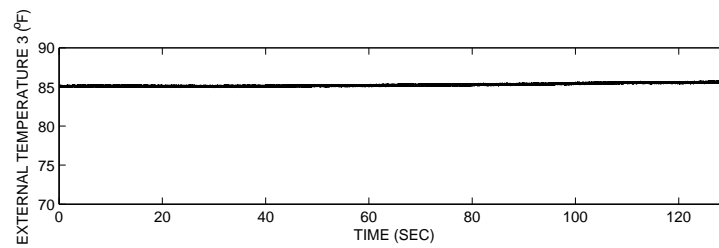
(b) Oil temperature 2



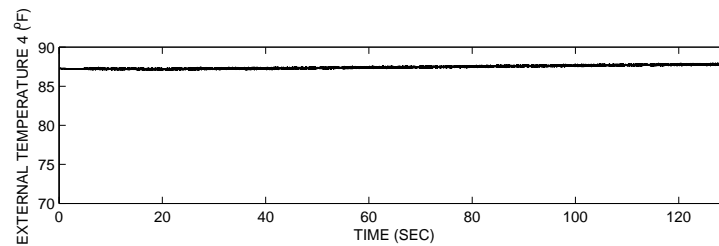
(c) Surface temperature 1



(d) Surface temperature 2

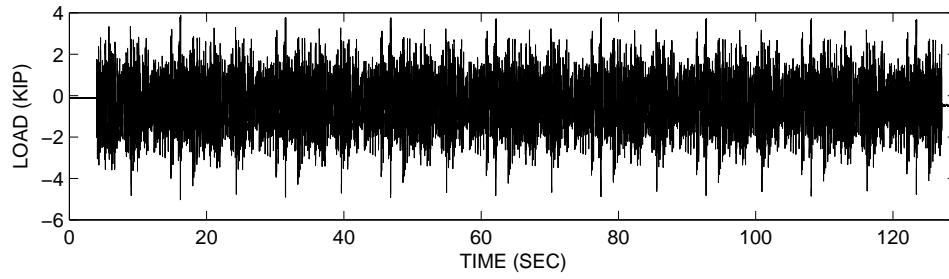


(e) Surface temperature 3

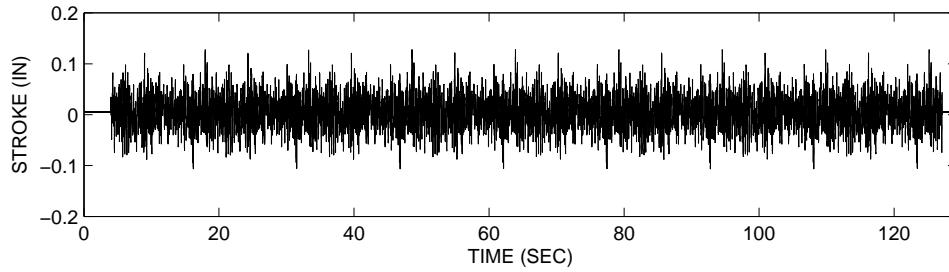


(f) Surface temperature 4

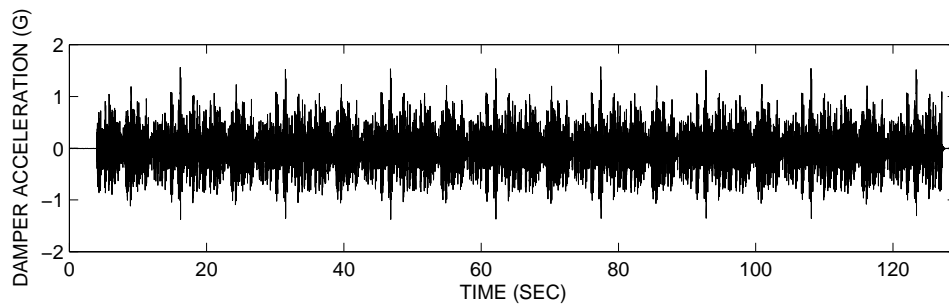
Figure D.8: Measured oil and surface temperatures of the 15 kip damper in the first round experiments for the data set Qrt4.01.



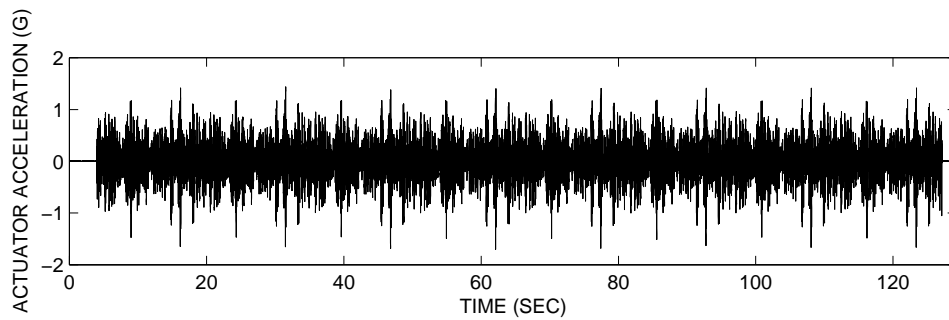
(a) Load (Force)



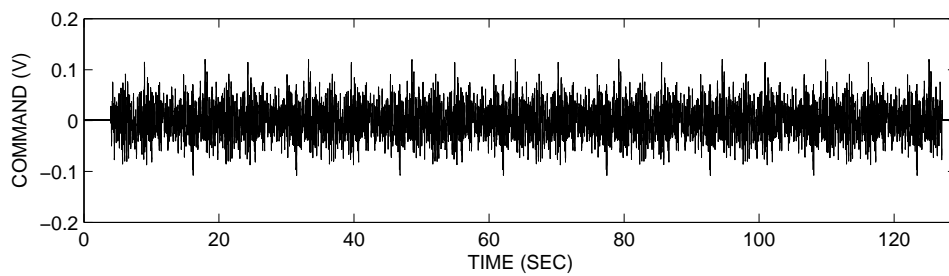
(b) Stroke (Displacement)



(c) Damper acceleration

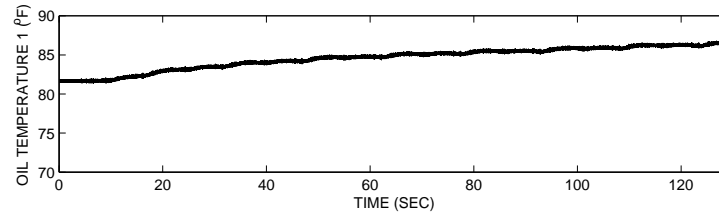


(d) Actuator acceleration

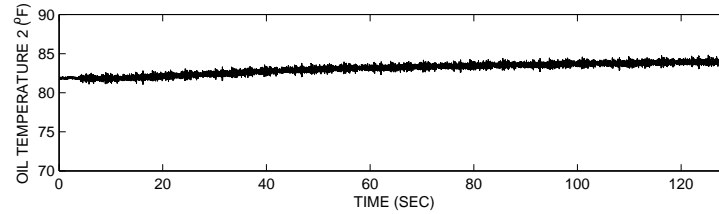


(e) Command Signal

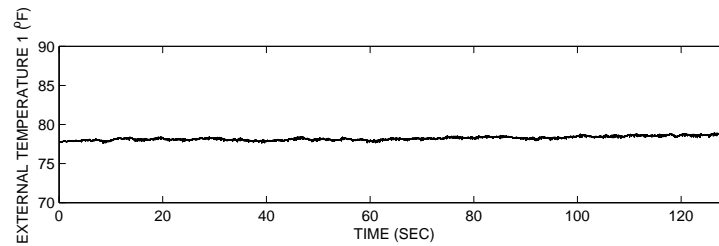
Figure D.9: Measured data of the 15 kip damper in the first round experiments for the data set Qrt1.0125.



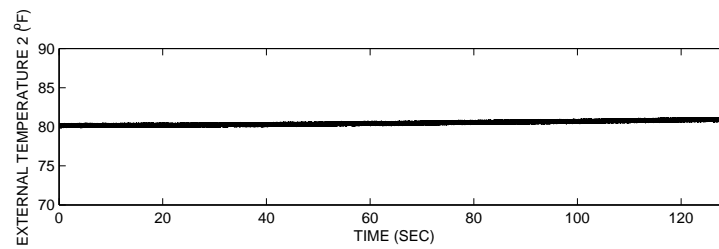
(a) Oil temperature 1



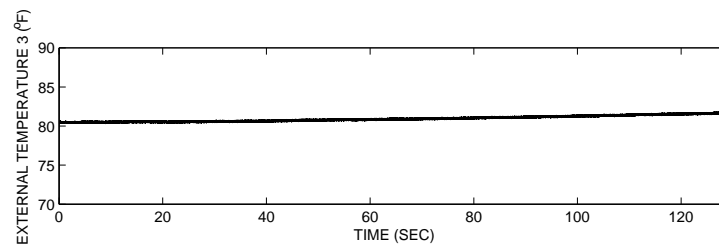
(b) Oil temperature 2



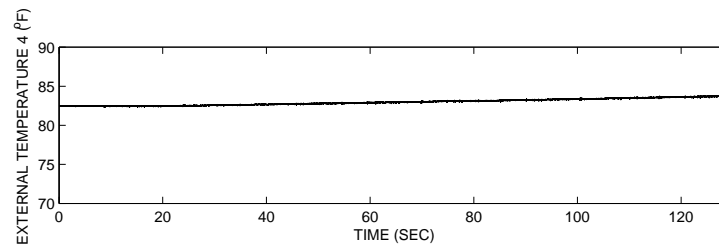
(c) Surface temperature 1



(d) Surface temperature 2

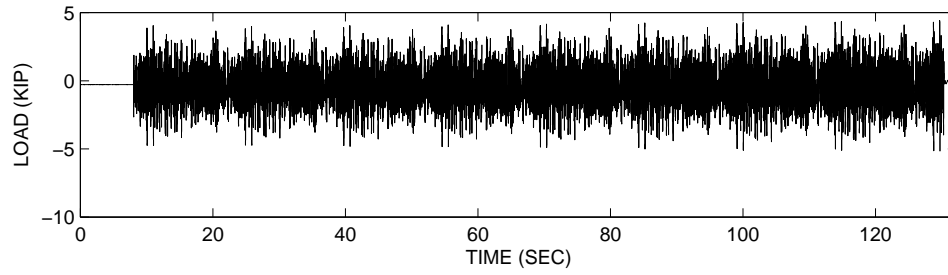


(e) Surface temperature 3

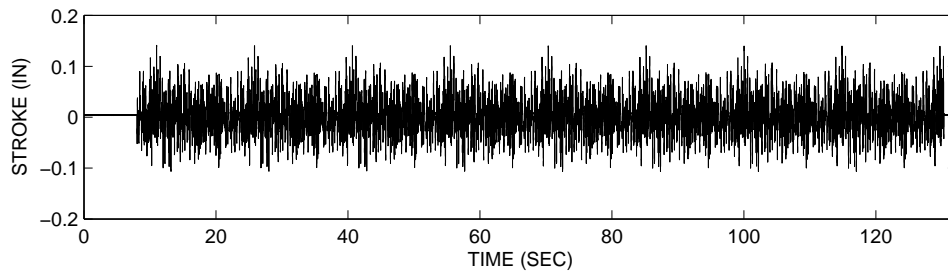


(f) Surface temperature 4

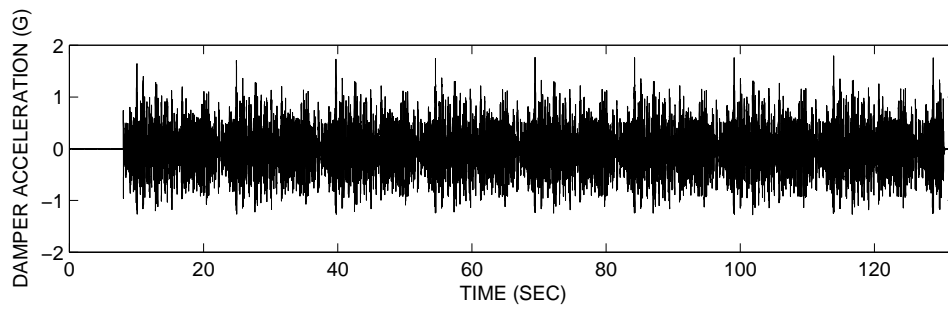
Figure D.10: Measured oil and surface temperatures of the 15 kip damper in the first round experiments for the data set Qrt1.0125.



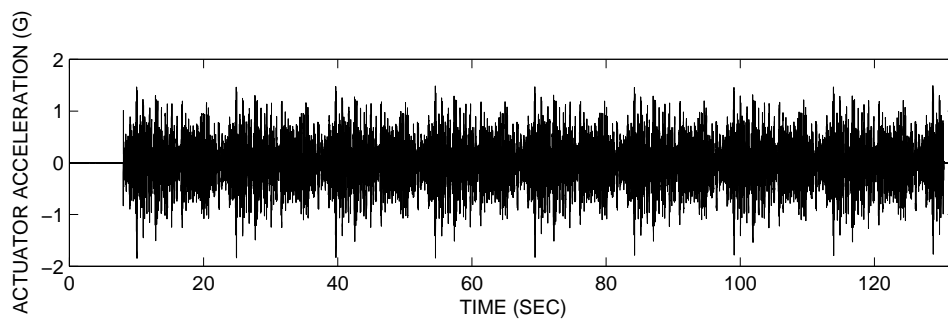
(a) Load (Force)



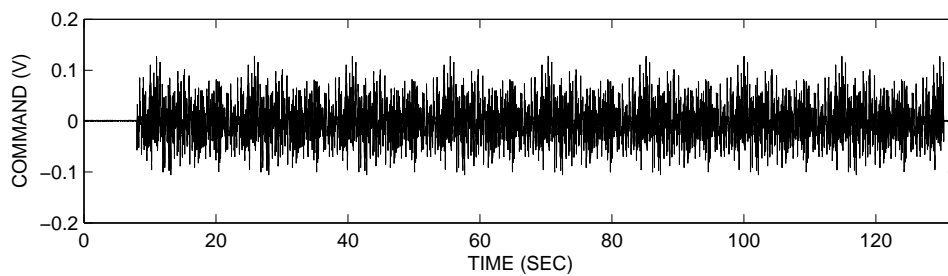
(b) Stroke (Displacement)



(c) Damper acceleration

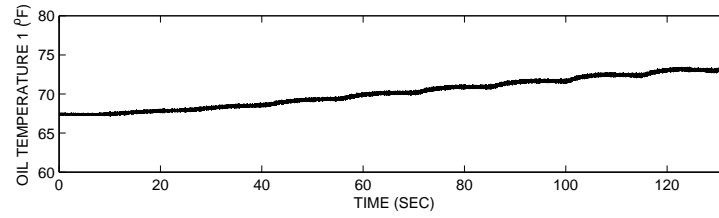


(d) Actuator acceleration

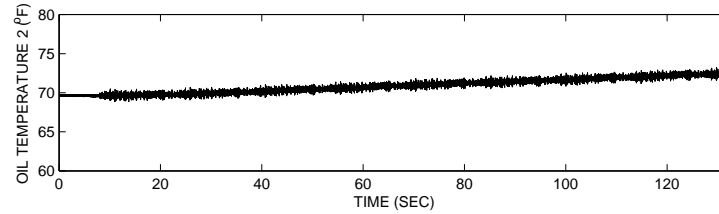


(e) Command Signal

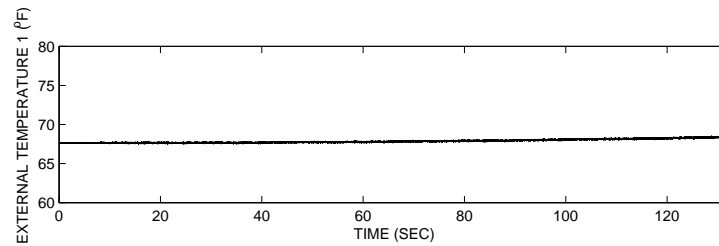
Figure D.11: Measured data of the 15 kip damper in the first round experiments for the data set Qrt2\_0125.



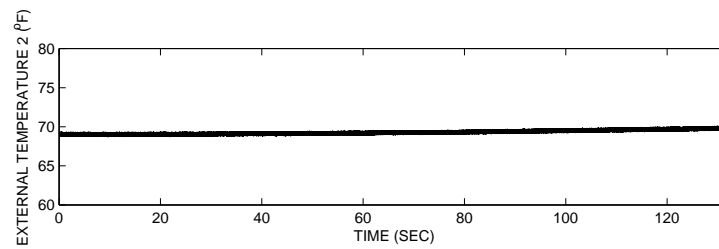
(a) Oil temperature 1



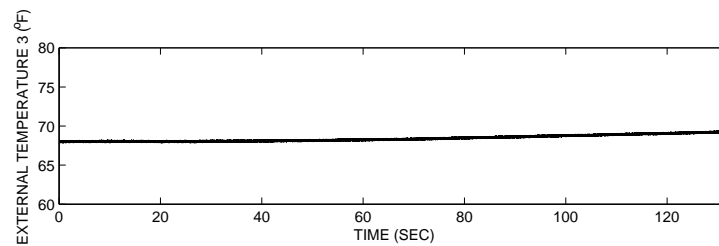
(b) Oil temperature 2



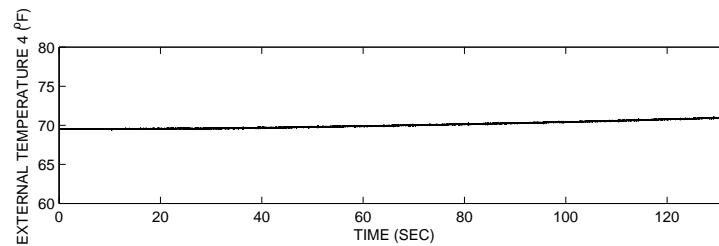
(c) Surface temperature 1



(d) Surface temperature 2

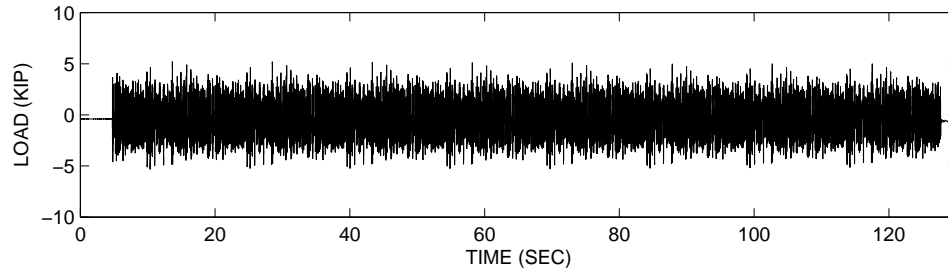


(e) Surface temperature 3

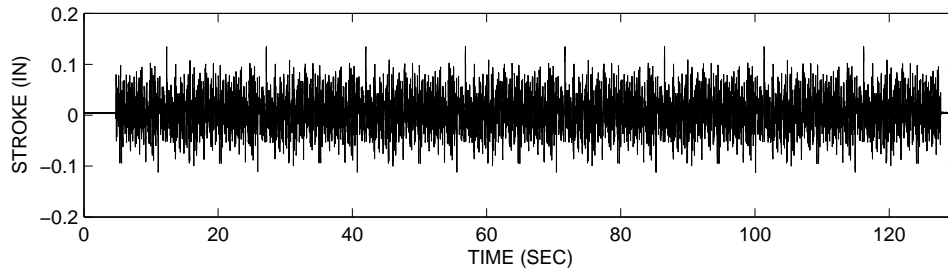


(f) Surface temperature 4

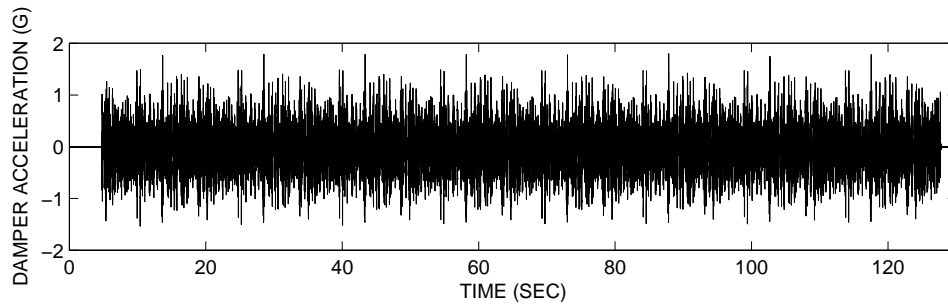
Figure D.12: Measured oil and surface temperatures of the 15 kip damper in the first round experiments for the data set Qrt2.0125.



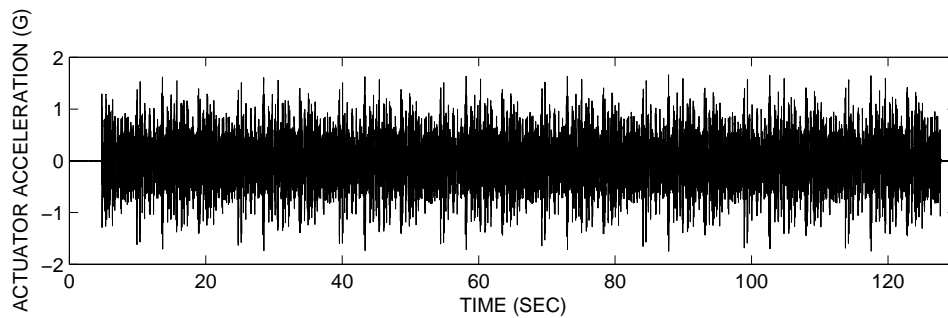
(a) Load (Force)



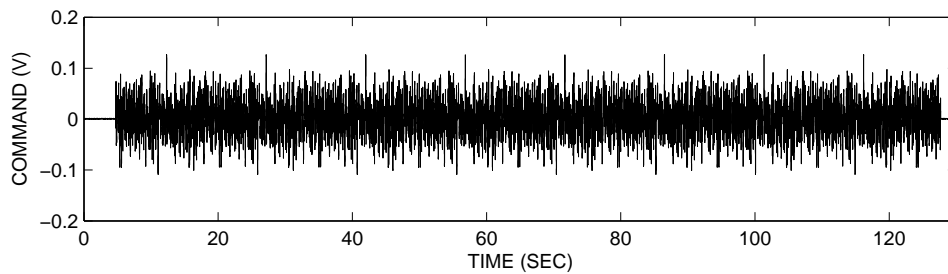
(b) Stroke (Displacement)



(c) Damper acceleration

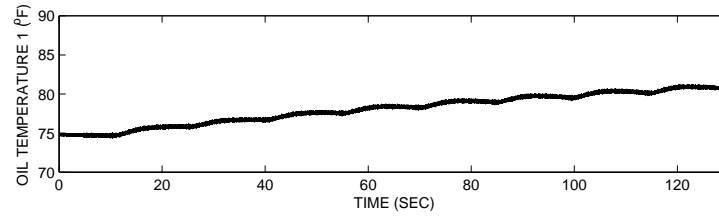


(d) Actuator acceleration

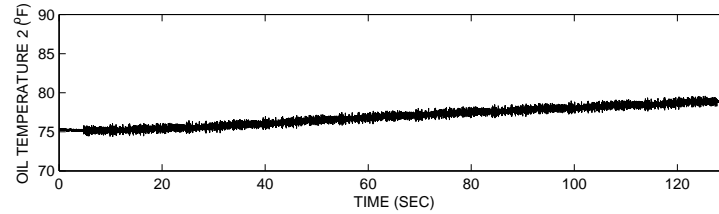


(e) Command Signal

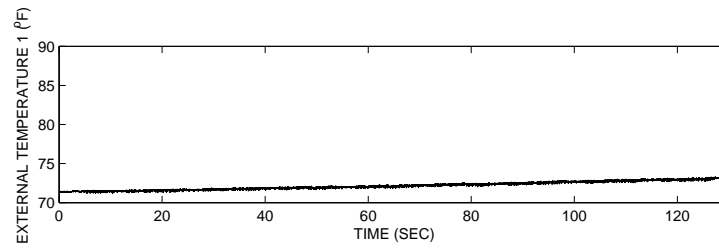
Figure D.13: Measured data of the 15 kip damper in the first round experiments for the data set Qrt3\_0125.



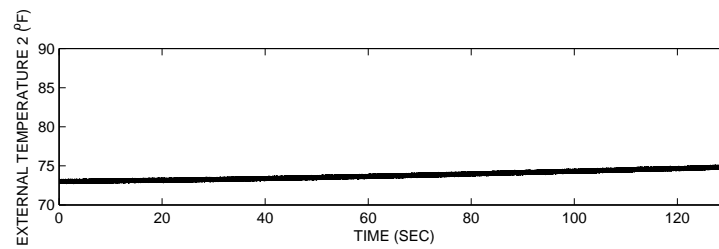
(a) Oil temperature 1



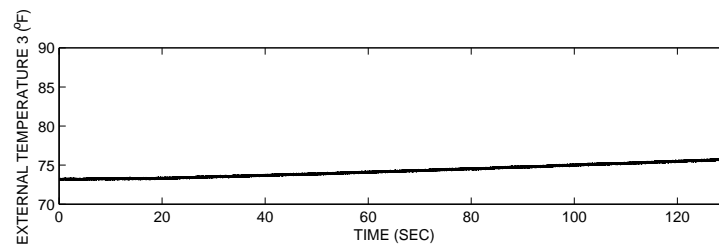
(b) Oil temperature 2



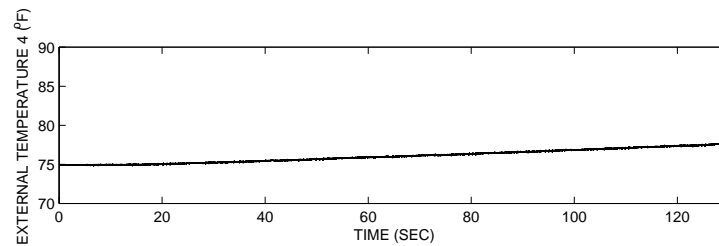
(c) Surface temperature 1



(d) Surface temperature 2

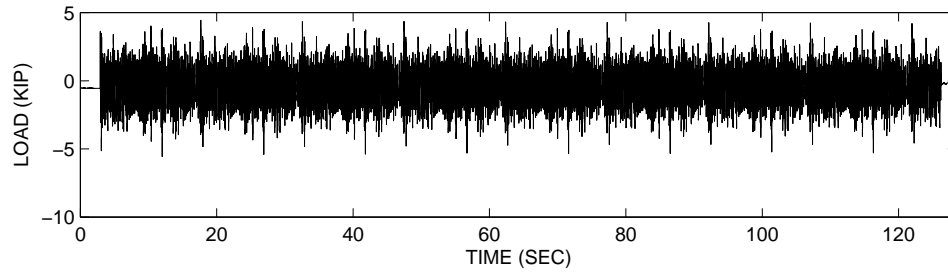


(e) Surface temperature 3

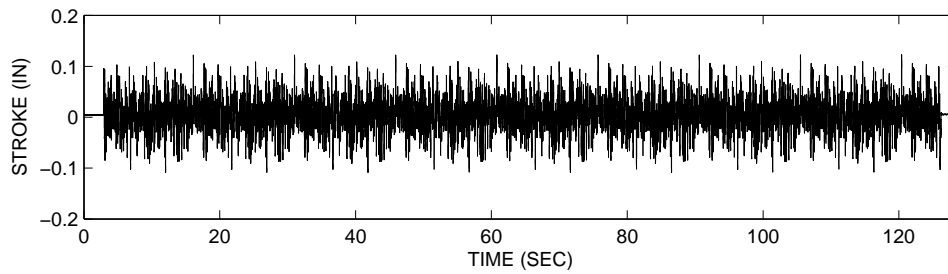


(f) Surface temperature 4

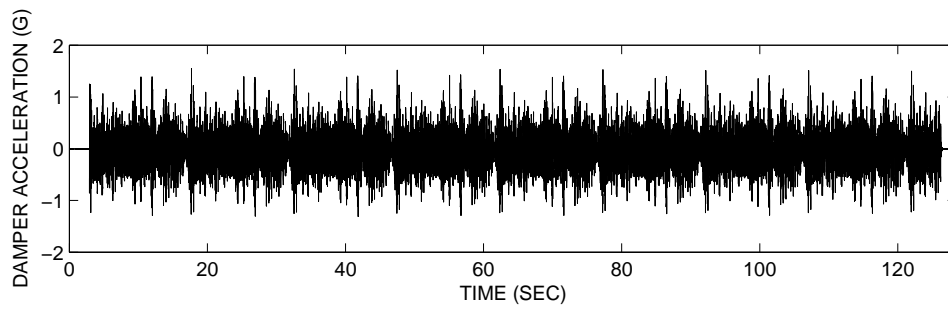
Figure D.14: Measured oil and surface temperatures of the 15 kip damper in the first round experiments for the data set Qrt3\_0125.



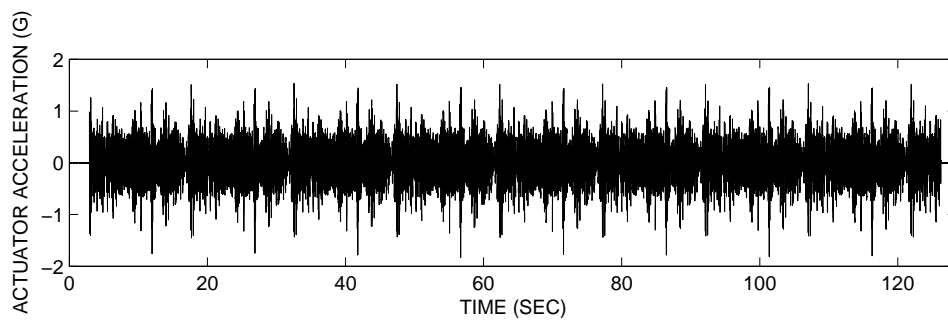
(a) Load (Force)



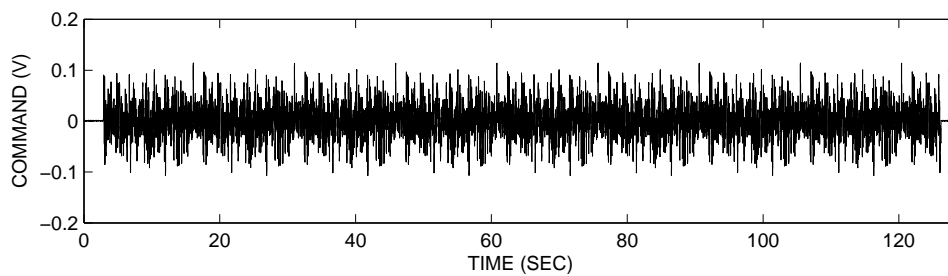
(b) Stroke (Displacement)



(c) Damper acceleration

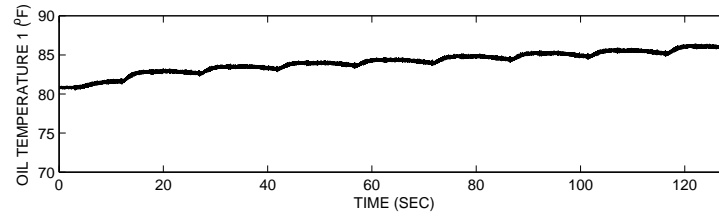


(d) Actuator acceleration

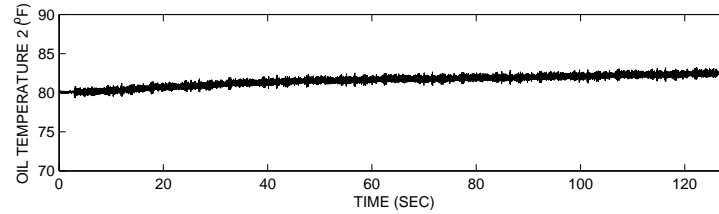


(e) Command Signal

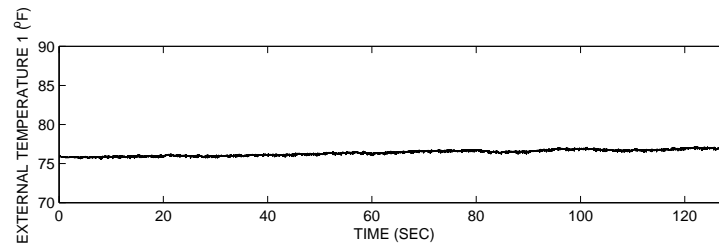
Figure D.15: Measured data of the 15 kip damper in the first round experiments for the data set Qrt4\_0125.



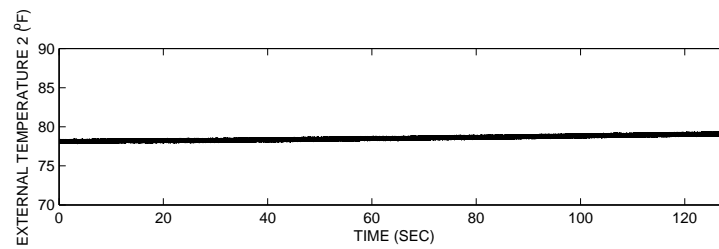
(a) Oil temperature 1



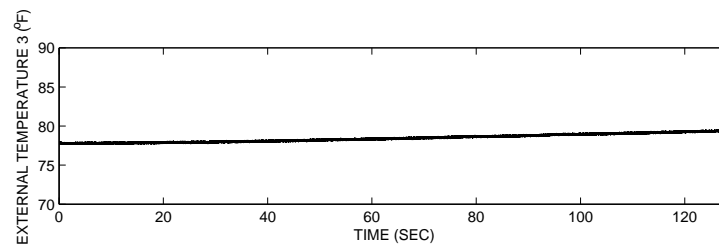
(b) Oil temperature 2



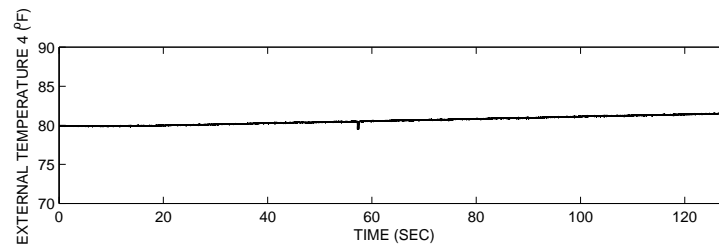
(c) Surface temperature 1



(d) Surface temperature 2



(e) Surface temperature 3



(f) Surface temperature 4

Figure D.16: Measured oil and surface temperatures of the 15 kip damper in the first round experiments for the data set Qrt4.0125.

# Appendix E

## DATA ACQUISITION FOR THE 15 KIP VISCOUS DAMPER - SECOND ROUND

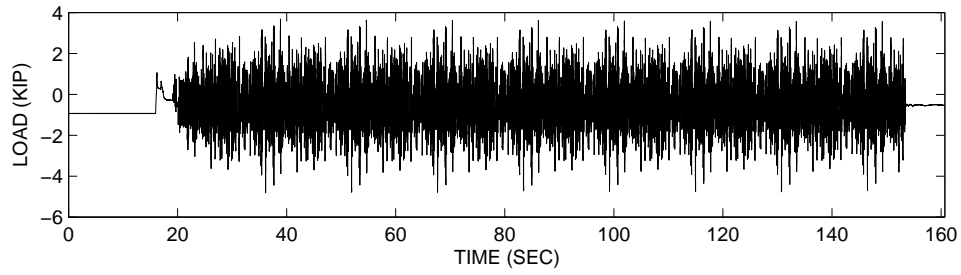
### E.1 Experimental Data (Raw) for the 15 Kip Viscous Damper - Second Round

The dynamic response of the 15 kip viscous damper in the second round experiments was obtained at the University of California, Berkeley by measuring the displacement and force. The first 20 rows of the obtained data (usc\_10175\_q1) is shown below. The entire data sets are provided in the accompanying CD in \data\UCB2\_2\raw\ folder. The measured data sets are illustrated in Figures E.1 to E.32.

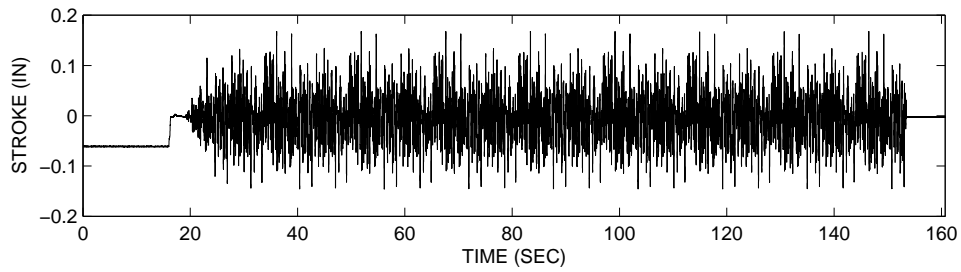
```
c:\damper2\ascii\ADAMP2A.001
11/26/10
13:00:37
12
999.928000
Time      Secs   Load    KIP   Stroke  IN      Oiltemp1 degF  Oiltemp2 degF  Tempex1 degF  Tempex2 degF  Tempex3 degF  Tempex4 degF
-1.0000720E-03  -1.6953125E+00  -1.2393089E-01  +8.2677773E+01  +8.4482483E+01  +8.5029366E+01  +8.5849693E+01  +3.5839432E+02  +3.5839432E+02
+0.0000000E+00  -1.6984376E+00  -1.2524332E-01  +8.2666832E+01  +8.4471550E+01  +8.5029366E+01  +8.5838753E+01  +3.5839432E+02  +3.5839432E+02
+1.0000720E-03  -1.7046875E+00  -1.2693073E-01  +8.2655899E+01  +8.4482483E+01  +8.5029366E+01  +8.5849693E+01  +3.5839432E+02  +3.5839432E+02
+2.0001440E-03  -1.7046875E+00  -1.2880564E-01  +8.2655899E+01  +8.4482483E+01  +8.5040306E+01  +8.5871567E+01  +3.5839432E+02  +3.5839432E+02
+3.0002160E-03  -1.7078125E+00  -1.3011806E-01  +8.2677773E+01  +8.4504364E+01  +8.5040306E+01  +8.5904381E+01  +3.5839432E+02  +3.5839432E+02
+4.0002880E-03  -1.7078125E+00  -1.3180548E-01  +8.2710587E+01  +8.4504364E+01  +8.5040306E+01  +8.5937195E+01  +3.5839432E+02  +3.5839432E+02
+5.0003600E-03  -1.7078125E+00  -1.3330540E-01  +8.2732460E+01  +8.4515297E+01  +8.5040306E+01  +8.6002823E+01  +3.5839432E+02  +3.5839432E+02
+6.0004320E-03  -1.7062501E+00  -1.3499281E-01  +8.2787148E+01  +8.4548111E+01  +8.5062180E+01  +8.6068443E+01  +3.5839432E+02  +3.5839432E+02
+7.0005040E-03  -1.7031250E+00  -1.3630523E-01  +8.2830902E+01  +8.4548111E+01  +8.5040306E+01  +8.6112198E+01  +3.5839432E+02  +3.5839432E+02
+8.0005760E-03  -1.7015625E+00  -1.3780515E-01  +8.2830902E+01  +8.4569984E+01  +8.5029366E+01  +8.6123138E+01  +3.5839432E+02  +3.5839432E+02
+9.0006480E-03  -1.6937500E+00  -1.3949256E-01  +8.2841835E+01  +8.4559052E+01  +8.5040306E+01  +8.6155945E+01  +3.5839432E+02  +3.5839432E+02
+1.0000720E-02  -1.6921875E+00  -1.4080499E-01  +8.2852776E+01  +8.4559052E+01  +8.5040306E+01  +8.6112198E+01  +3.5839432E+02  +3.5839432E+02
+1.1000792E-02  -1.6859375E+00  -1.4230491E-01  +8.2819962E+01  +8.4526237E+01  +8.5040306E+01  +8.6090324E+01  +3.5839432E+02  +3.5839432E+02
+1.2000864E-02  -1.6843750E+00  -1.4342986E-01  +8.2798088E+01  +8.4515297E+01  +8.5029366E+01  +8.6046570E+01  +3.5839432E+02  +3.5839432E+02
+1.3000936E-02  -1.6750001E+00  -1.4474228E-01  +8.2765274E+01  +8.4504364E+01  +8.5018433E+01  +8.5980942E+01  +3.5839432E+02  +3.5839432E+02
+1.4001008E-02  -1.6640625E+00  -1.4624220E-01  +8.2721519E+01  +8.4482483E+01  +8.4996559E+01  +8.5904381E+01  +3.5839432E+02  +3.5839432E+02
+1.5001080E-02  -1.6515626E+00  -1.4774212E-01  +8.2677773E+01  +8.4471550E+01  +8.5029366E+01  +8.5849693E+01  +3.5839432E+02  +3.5839432E+02
+1.6001152E-02  -1.6390625E+00  -1.4905456E-01  +8.2644958E+01  +8.4449677E+01  +8.5018433E+01  +8.5827820E+01  +3.5839432E+02  +3.5839432E+02
+1.7001224E-02  -1.6171875E+00  -1.5017949E-01  +8.2612144E+01  +8.4449677E+01  +8.5018433E+01  +8.5849693E+01  +3.5839432E+02  +3.5839432E+02
+1.8001296E-02  -1.6015625E+00  -1.5130444E-01  +8.2634018E+01  +8.4471550E+01  +8.5029366E+01  +8.5849693E+01  +3.5839432E+02  +3.5839432E+02

AccDamp  G      AccAct      G      Command  IN
-6.0312498E-02  +7.4999998E-03  -1.4286739E-01
-7.2187498E-02  +9.6875001E-03  -1.4436731E-01
-8.5000001E-02  +1.2187500E-02  -1.4549224E-01
-9.6562497E-02  +1.3437499E-02  -1.4680468E-01
```

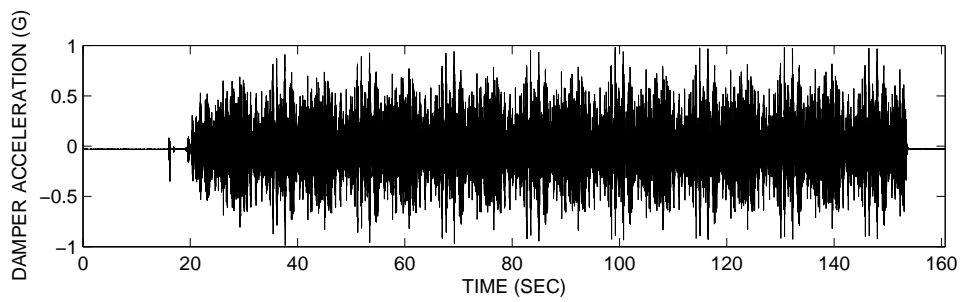
-1.0656250E-01	+1.4687500E-02	-1.4830460E-01
-1.1343750E-01	+1.5625000E-02	-1.4999200E-01
-1.1687500E-01	+1.7812500E-02	-1.5092945E-01
-1.1531249E-01	+2.1562500E-02	-1.5242937E-01
-1.0968750E-01	+2.3437500E-02	-1.5355432E-01
-9.8124996E-02	+2.5625000E-02	-1.5467925E-01
-8.3437495E-02	+2.9062500E-02	-1.5617917E-01
-6.7499995E-02	+3.2812499E-02	-1.5711662E-01
-5.2187499E-02	+3.8437501E-02	-1.5842906E-01
-4.0312499E-02	+4.4999998E-02	-1.5955399E-01
-3.1562500E-02	+4.9062498E-02	-1.6067894E-01
-2.6562499E-02	+5.0937500E-02	-1.6142890E-01
-2.5312500E-02	+5.3124998E-02	-1.6274132E-01
-2.7812500E-02	+5.6249999E-02	-1.6367878E-01
-3.1562500E-02	+6.0624998E-02	-1.6424124E-01
-3.7499998E-02	+6.3749999E-02	-1.6536619E-01



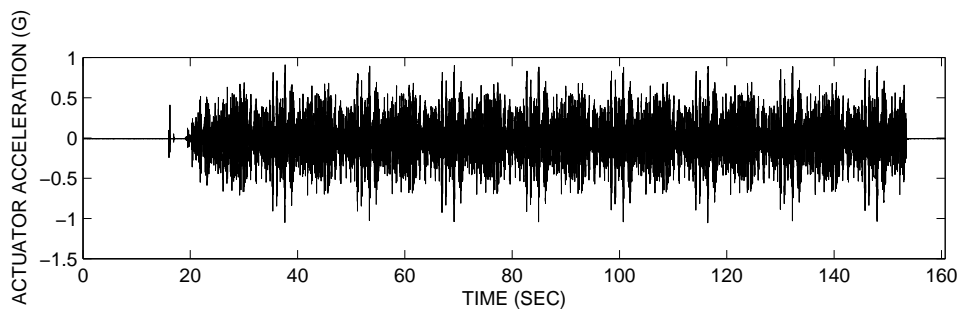
(a) Load (Force)



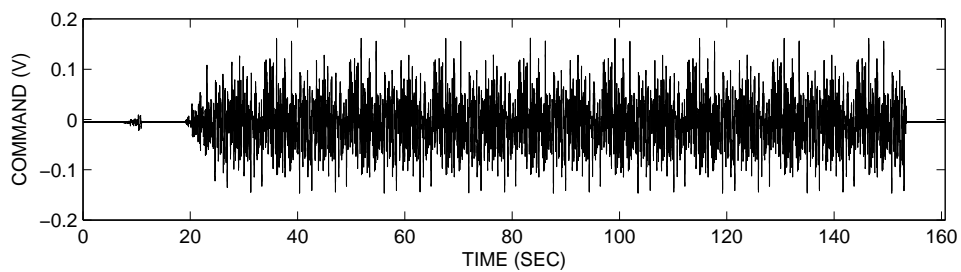
(b) Stroke (Displacement)



(c) Damper acceleration

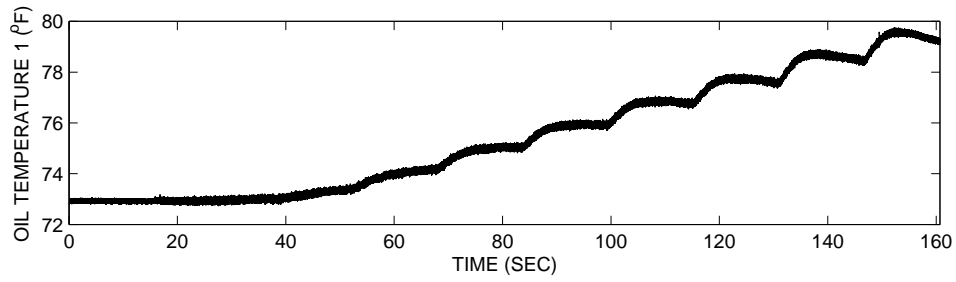


(d) Actuator acceleration

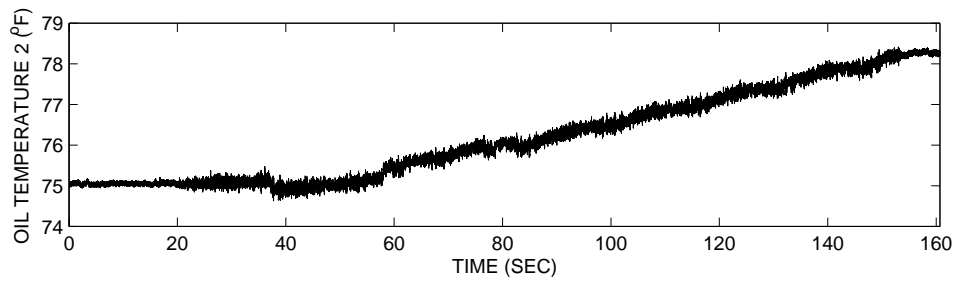


(e) Command Signal

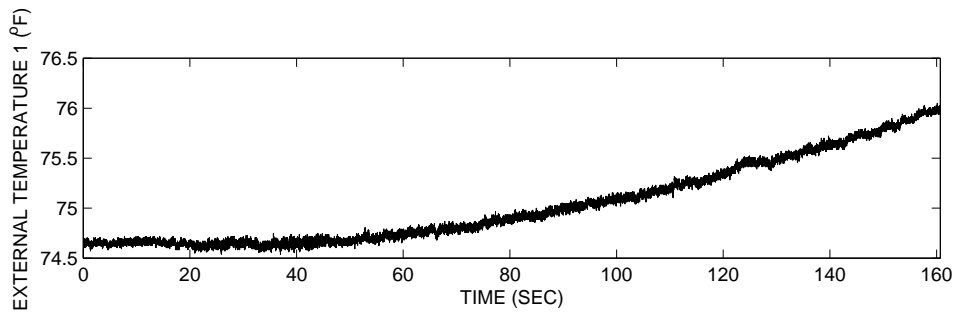
Figure E.1: Measured data of the 15 kip damper in the second round experiments for the data set usc\_10.175\_q1.



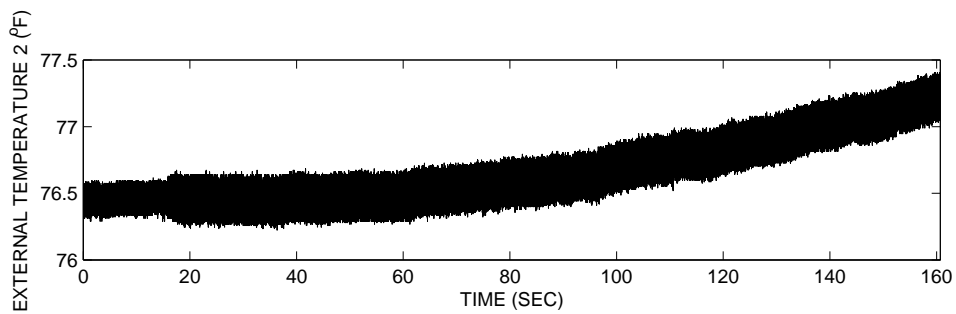
(a) Oil temperature 1



(b) Oil temperature 2

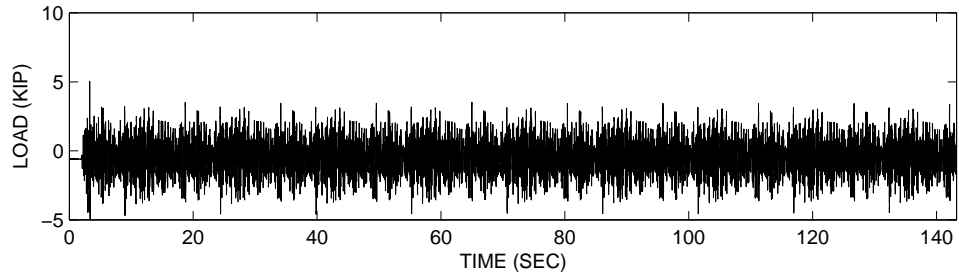


(c) Surface temperature 1

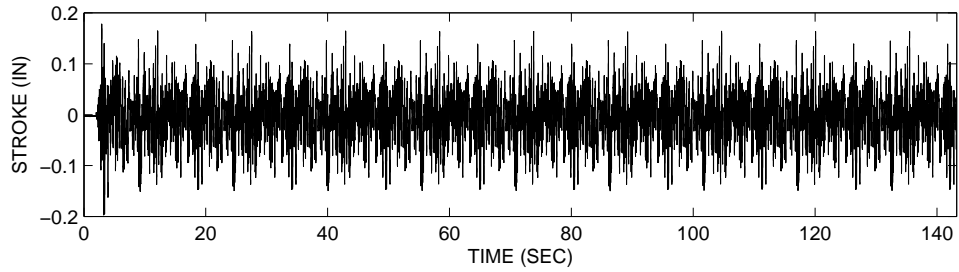


(d) Surface temperature 2

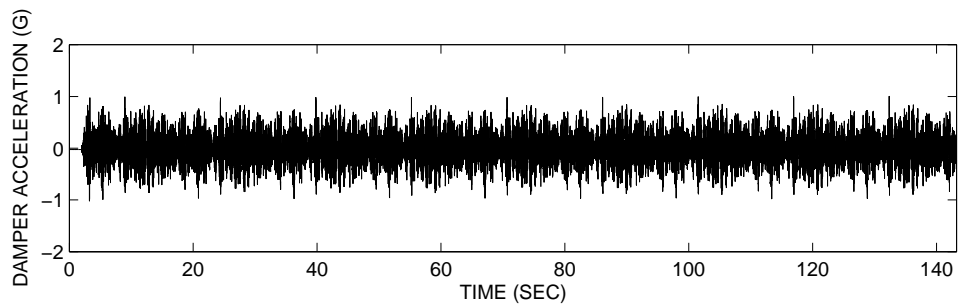
Figure E.2: Measured oil and surface temperatures of the 15 kip damper in the second round experiments for the data set usc\_10\_175\_q1.



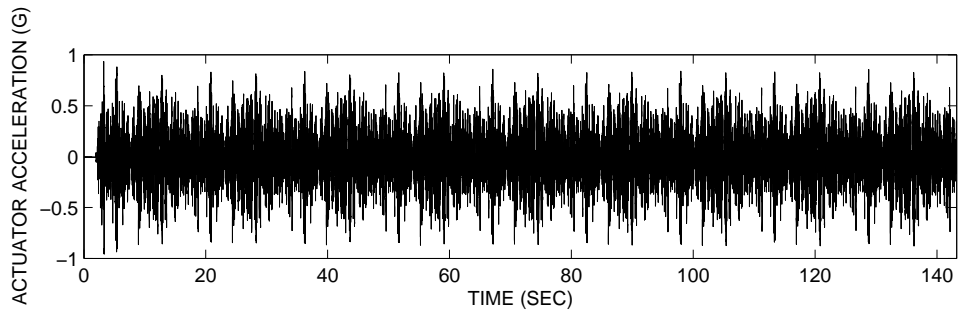
(a) Load (Force)



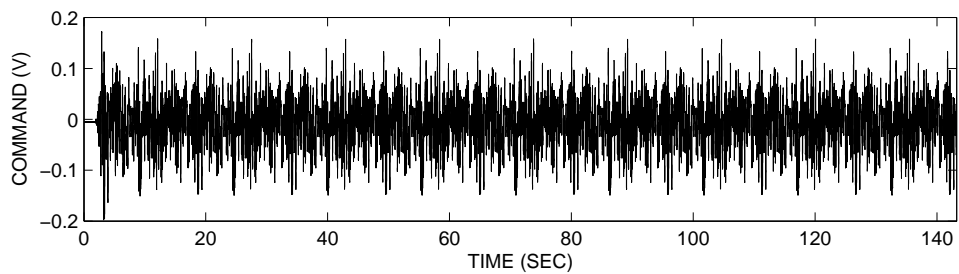
(b) Stroke (Displacement)



(c) Damper acceleration

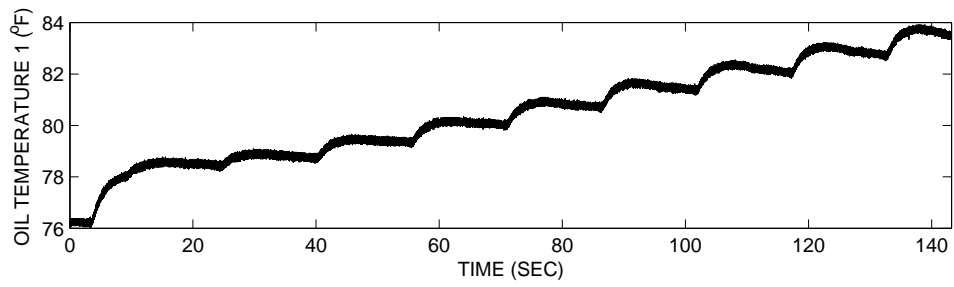


(d) Actuator acceleration

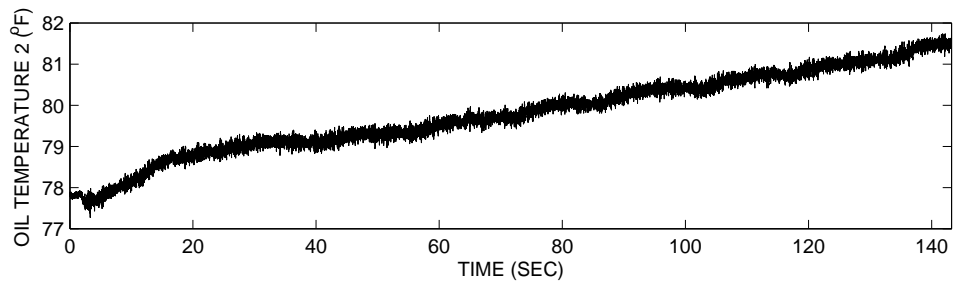


(e) Command Signal

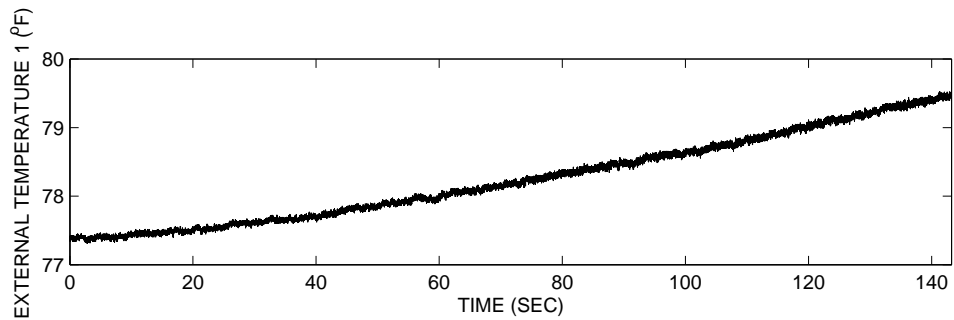
Figure E.3: Measured data of the 15 kip damper in the second round experiments for the data set usc\_10\_175\_q2.



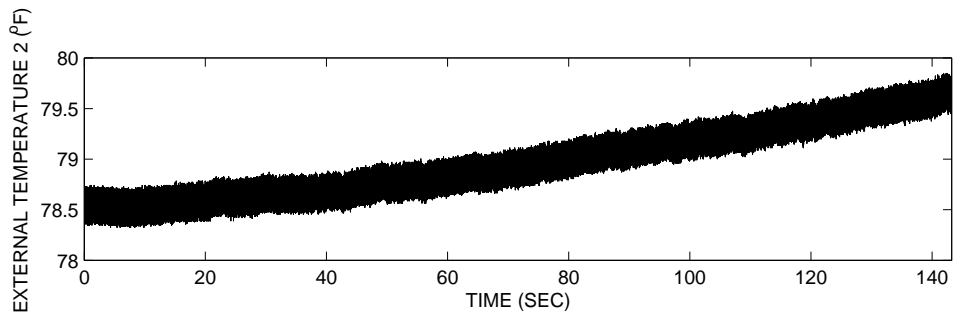
(a) Oil temperature 1



(b) Oil temperature 2

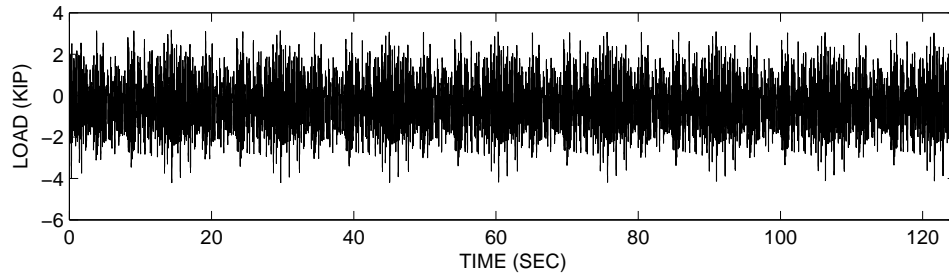


(c) Surface temperature 1

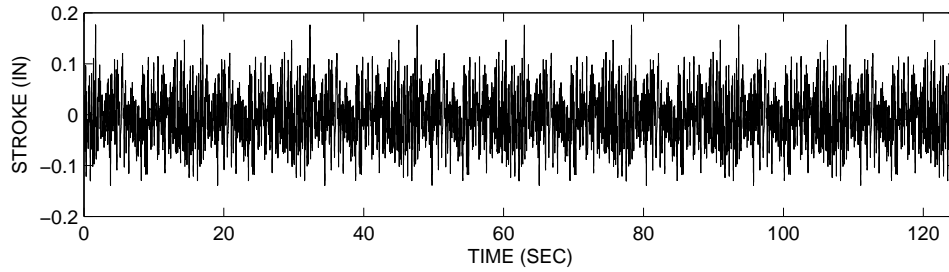


(d) Surface temperature 2

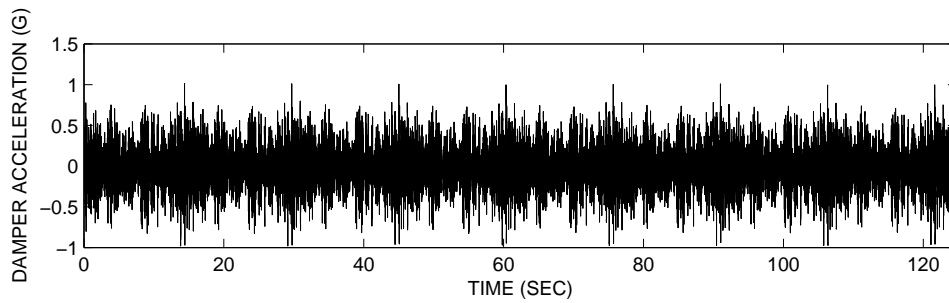
Figure E.4: Measured oil and surface temperatures of the 15 kip damper in the second round experiments for the data set usc\_10\_175-q2.



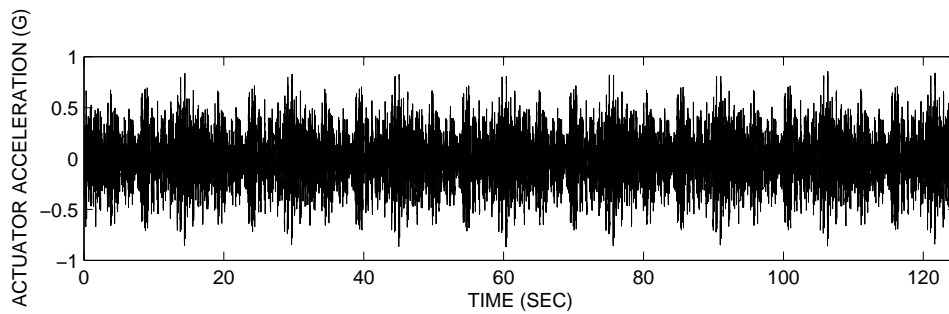
(a) Load (Force)



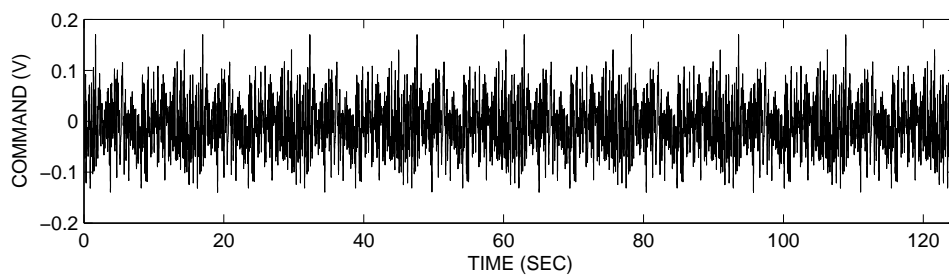
(b) Stroke (Displacement)



(c) Damper acceleration

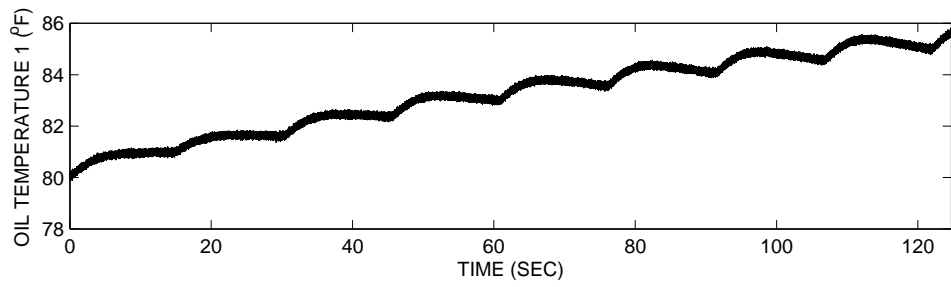


(d) Actuator acceleration

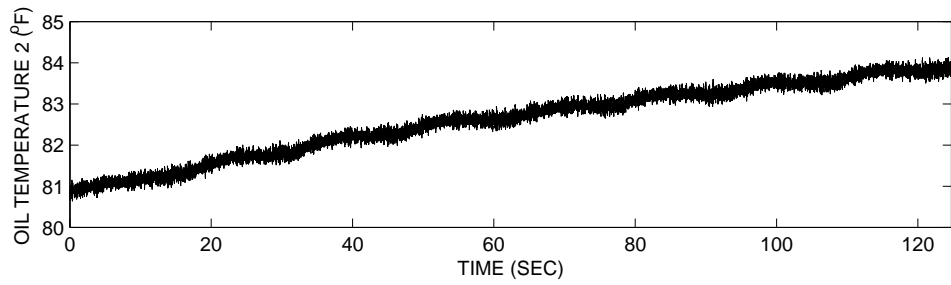


(e) Command Signal

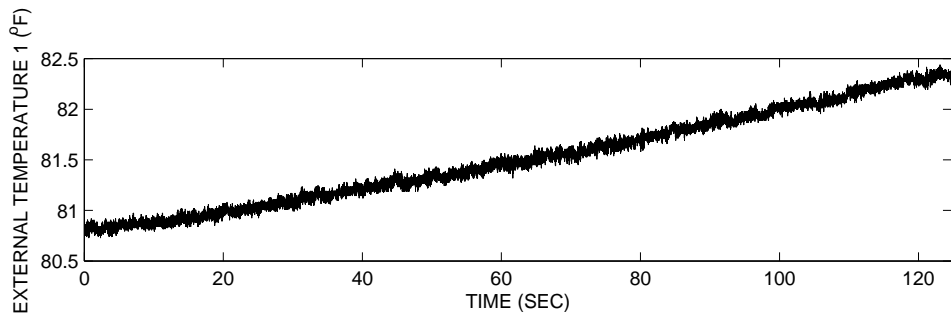
Figure E.5: Measured data of the 15 kip damper in the second round experiments for the data set usc\_10\_175\_q3.



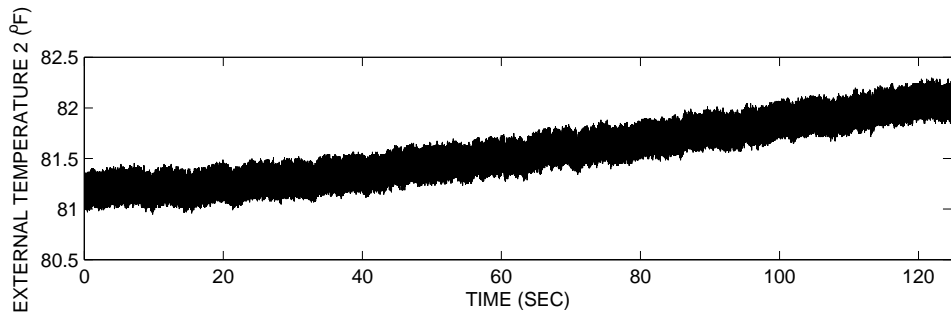
(a) Oil temperature 1



(b) Oil temperature 2

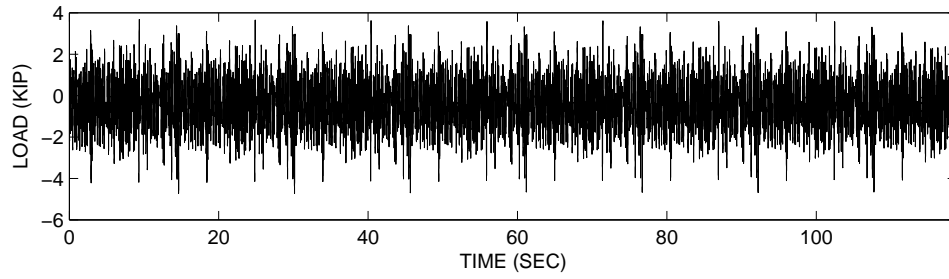


(c) Surface temperature 1

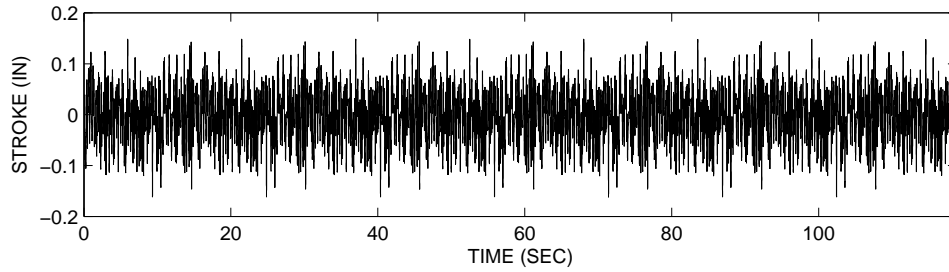


(d) Surface temperature 2

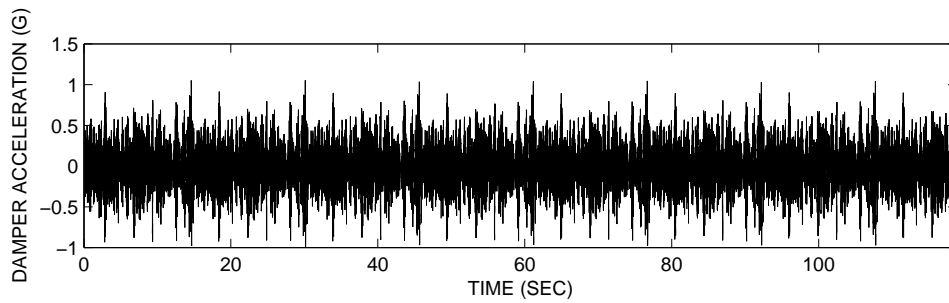
Figure E.6: Measured oil and surface temperatures of the 15 kip damper in the second round experiments for the data set usc\_10\_175\_q3.



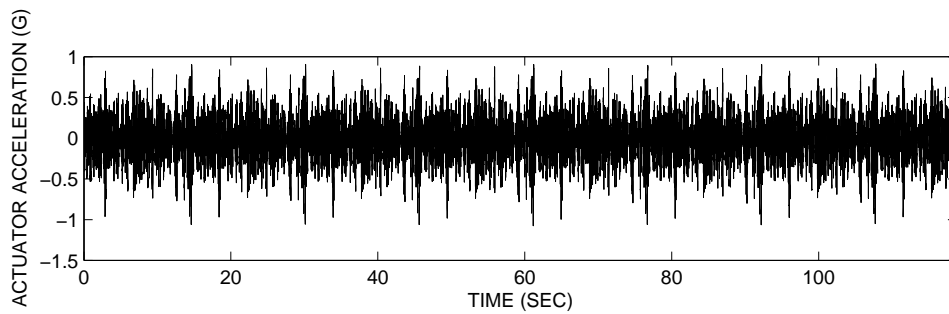
(a) Load (Force)



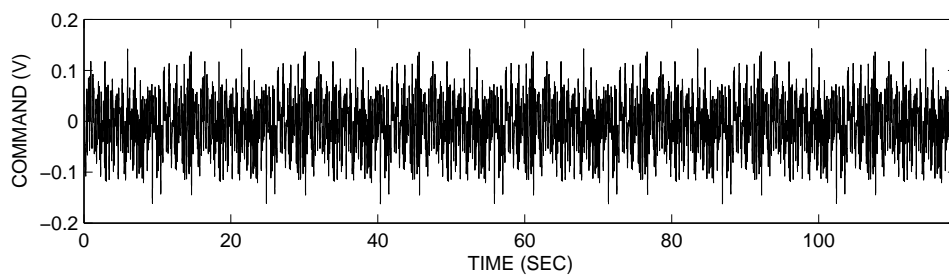
(b) Stroke (Displacement)



(c) Damper acceleration

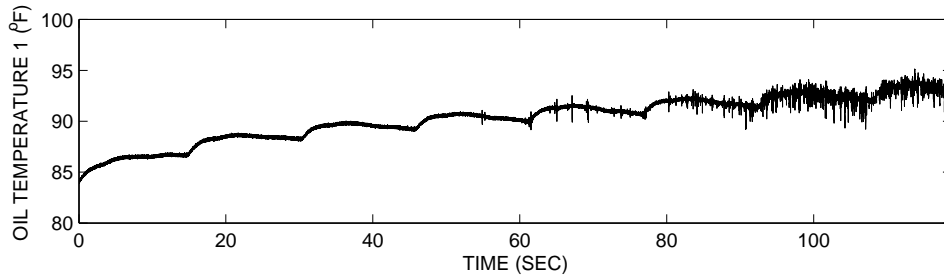


(d) Actuator acceleration

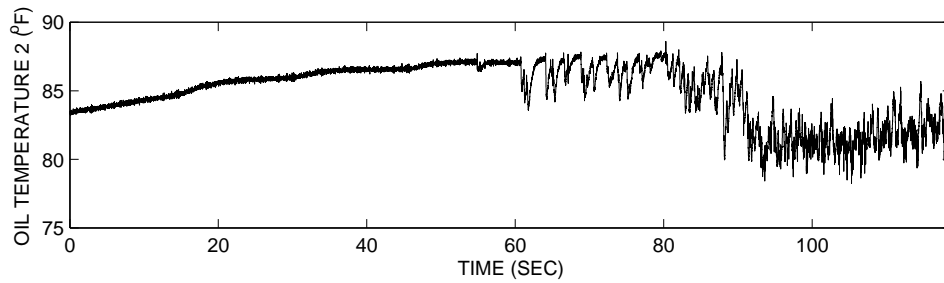


(e) Command Signal

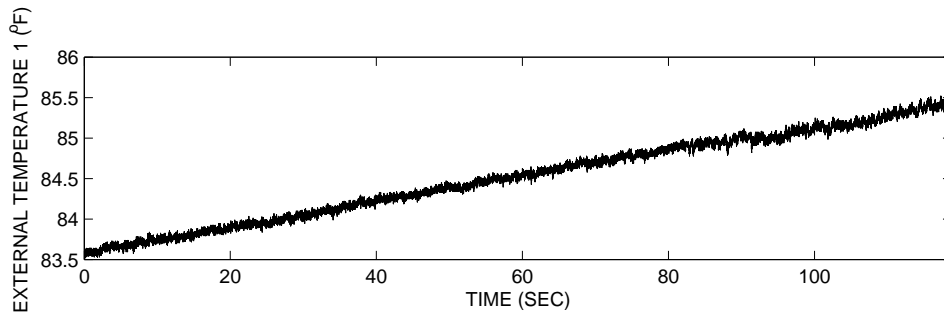
Figure E.7: Measured data of the 15 kip damper in the second round experiments for the data set usc\_10\_175\_q4.



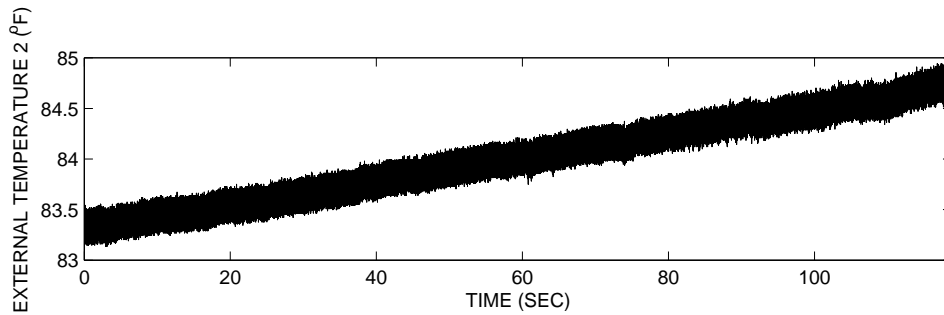
(a) Oil temperature 1



(b) Oil temperature 2

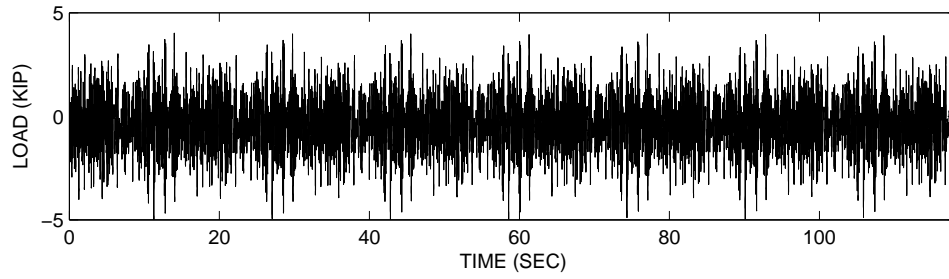


(c) Surface temperature 1

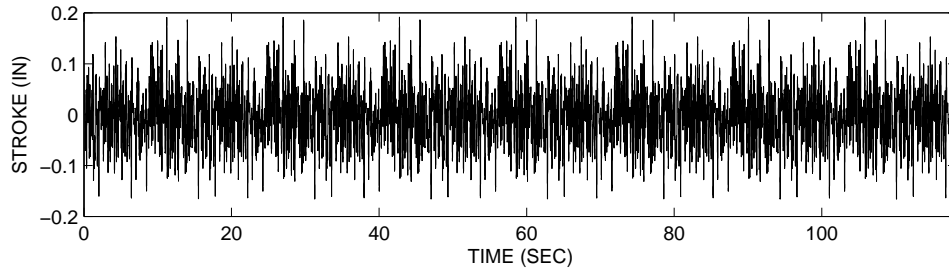


(d) Surface temperature 2

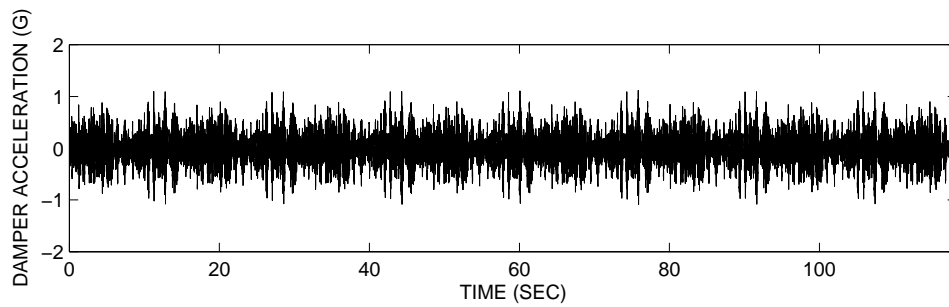
Figure E.8: Measured oil and surface temperatures of the 15 kip damper in the second round experiments for the data set usc\_10\_175\_q4.



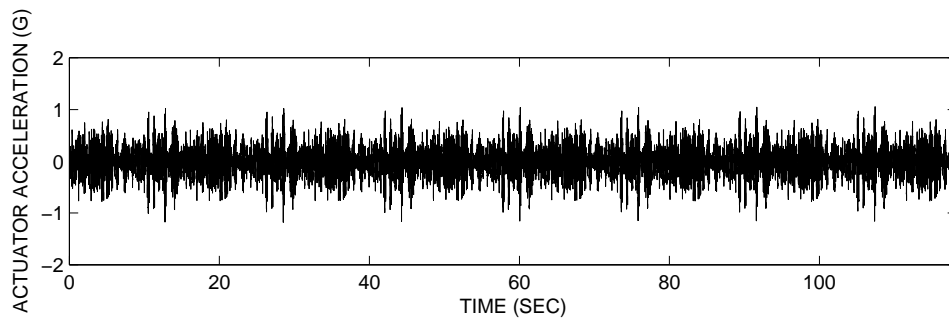
(a) Load (Force)



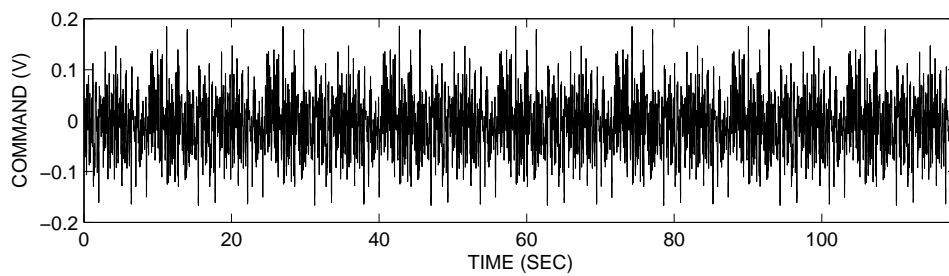
(b) Stroke (Displacement)



(c) Damper acceleration

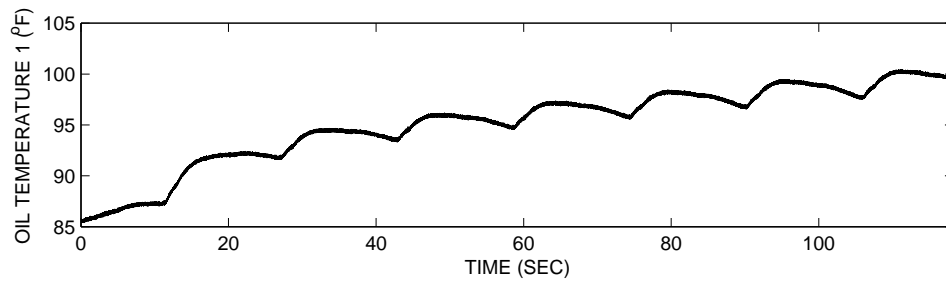


(d) Actuator acceleration

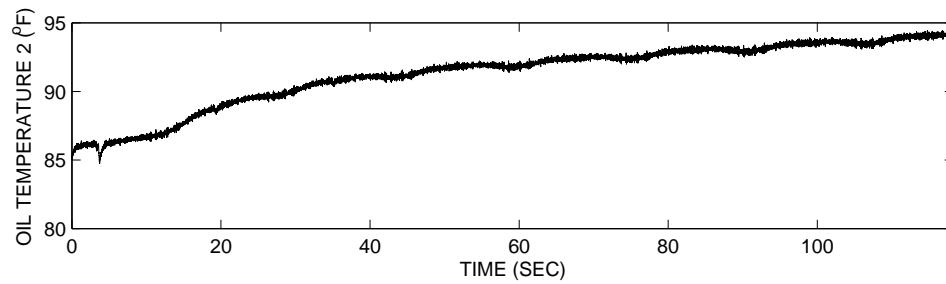


(e) Command Signal

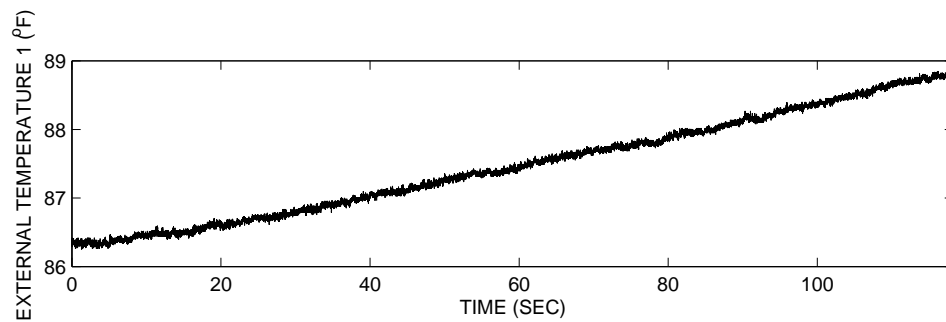
Figure E.9: Measured data of the 15 kip damper in the second round experiments for the data set usc\_10\_200\_q1.



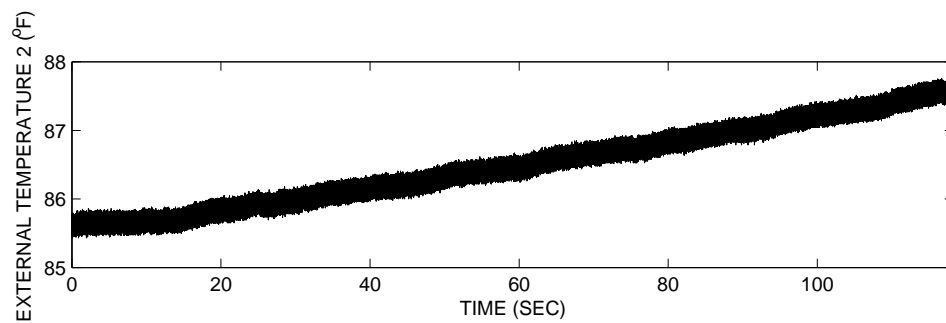
(a) Oil temperature 1



(b) Oil temperature 2

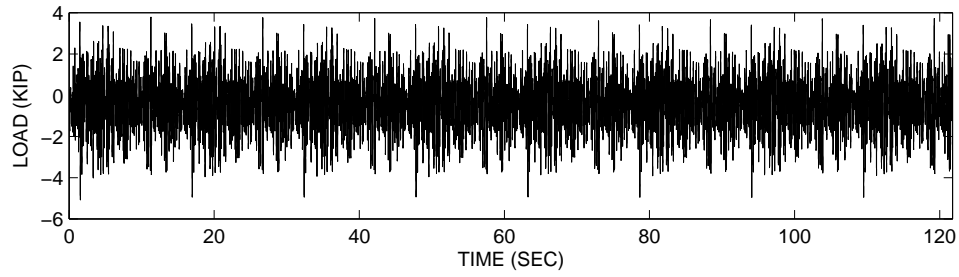


(c) Surface temperature 1

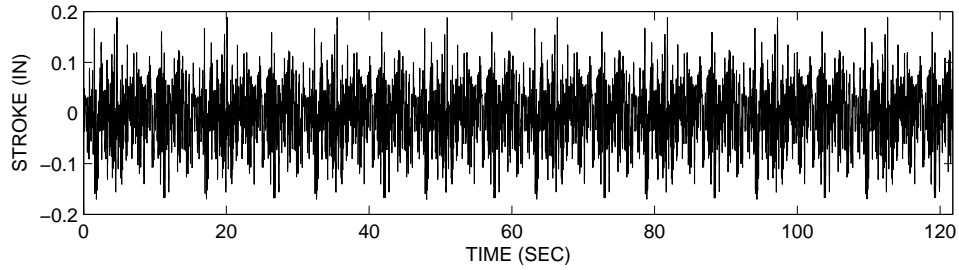


(d) Surface temperature 2

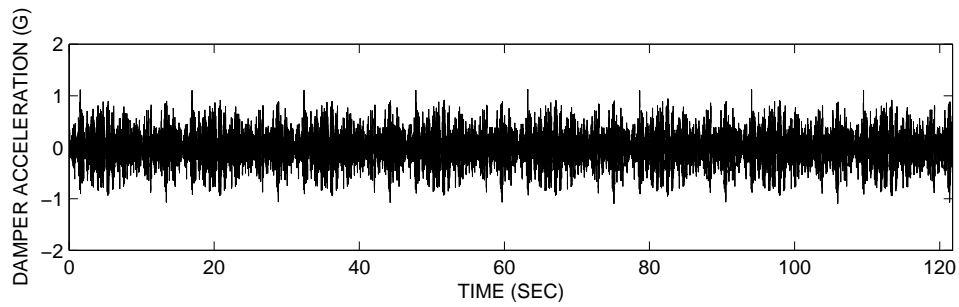
Figure E.10: Measured oil and surface temperatures of the 15 kip damper in the second round experiments for the data set usc\_10\_200\_q1.



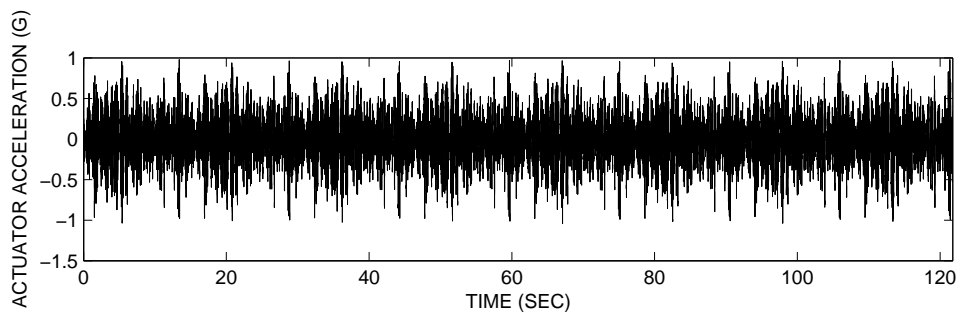
(a) Load (Force)



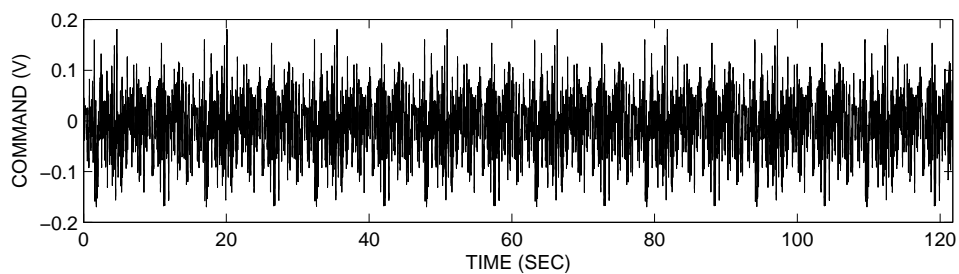
(b) Stroke (Displacement)



(c) Damper acceleration

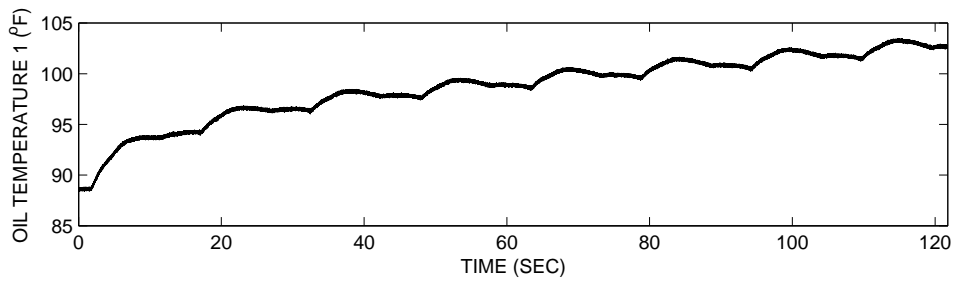


(d) Actuator acceleration

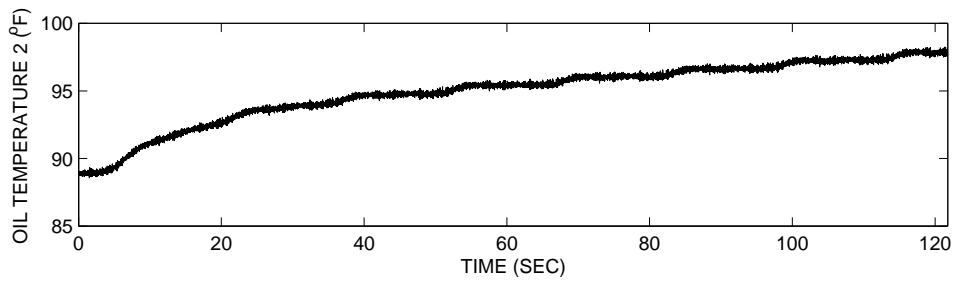


(e) Command Signal

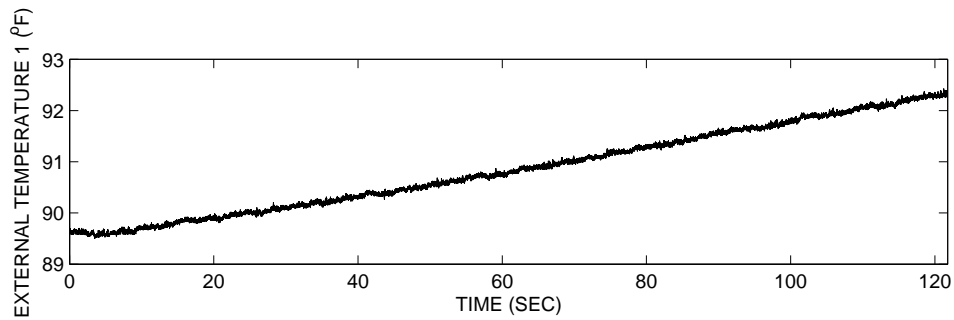
Figure E.11: Measured data of the 15 kip damper in the second round experiments for the data set usc\_10\_200\_q2.



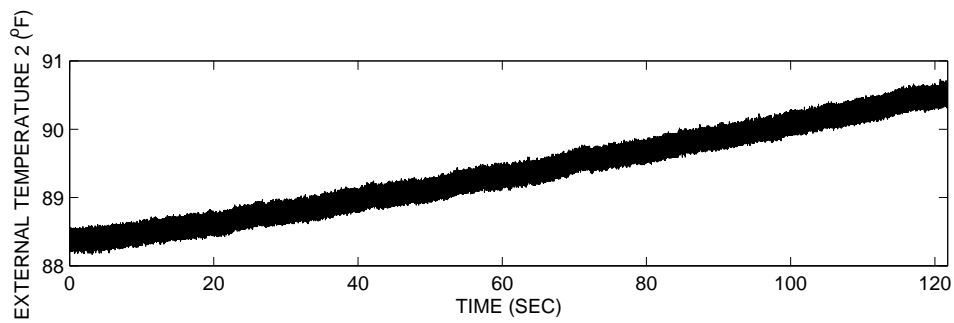
(a) Oil temperature 1



(b) Oil temperature 2

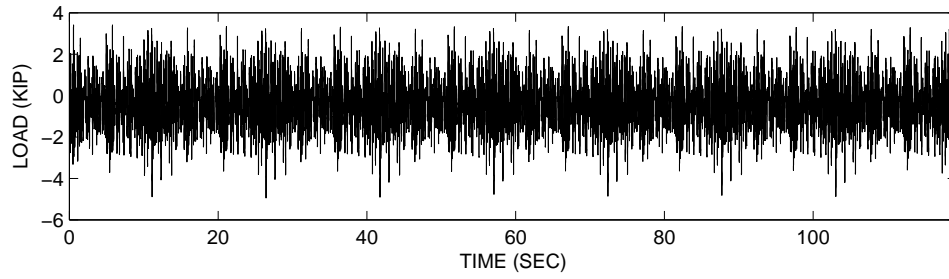


(c) Surface temperature 1

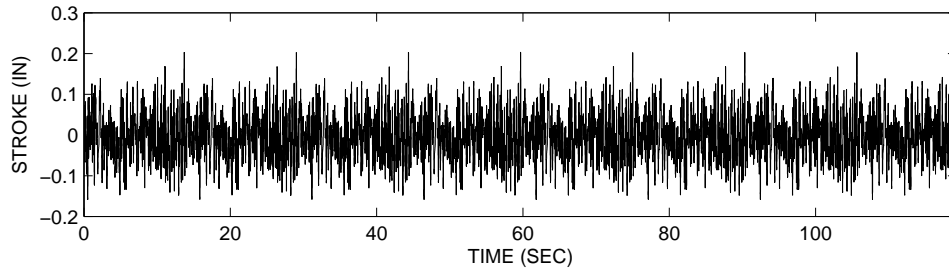


(d) Surface temperature 2

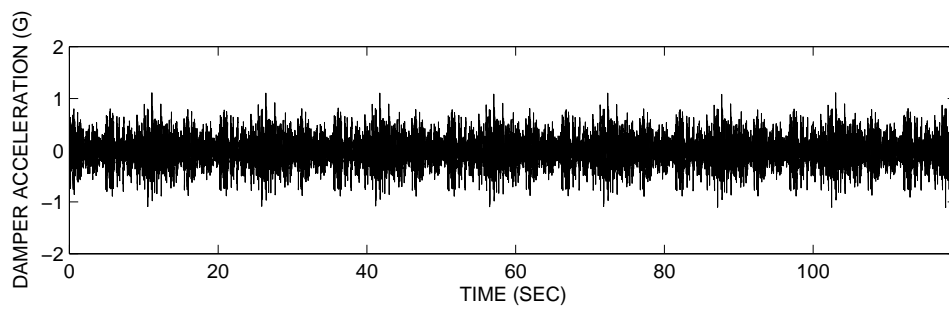
Figure E.12: Measured oil and surface temperatures of the 15 kip damper in the second round experiments for the data set usc\_10\_200\_q2.



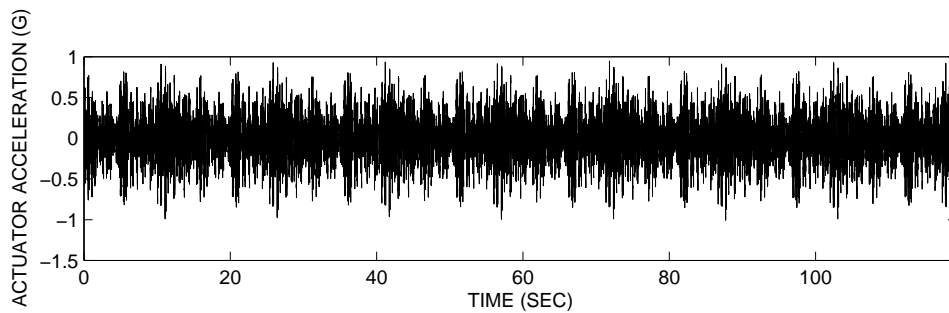
(a) Load (Force)



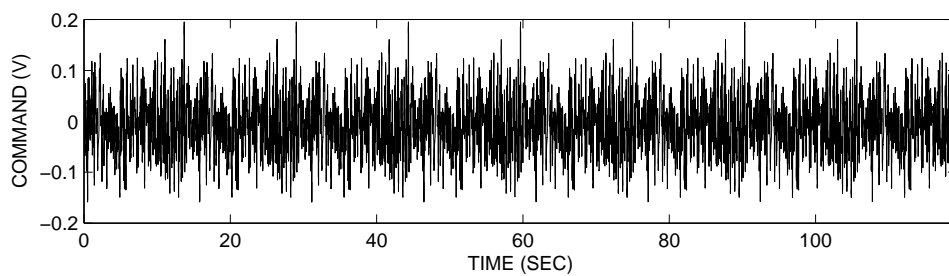
(b) Stroke (Displacement)



(c) Damper acceleration

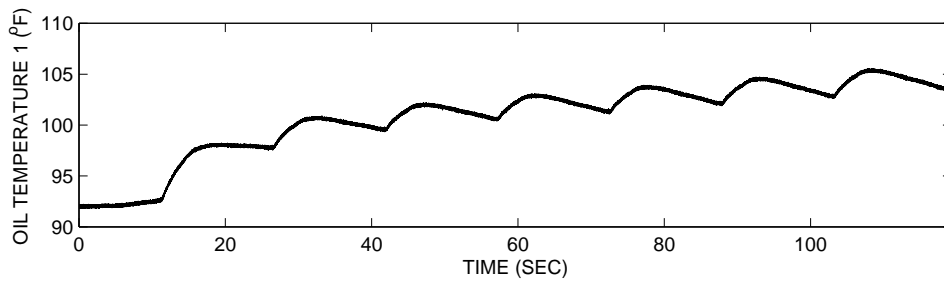


(d) Actuator acceleration

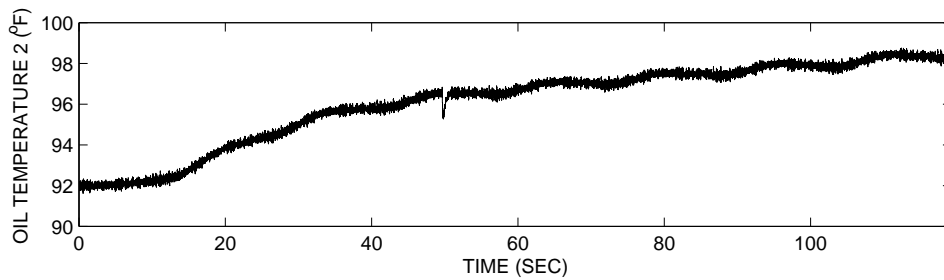


(e) Command Signal

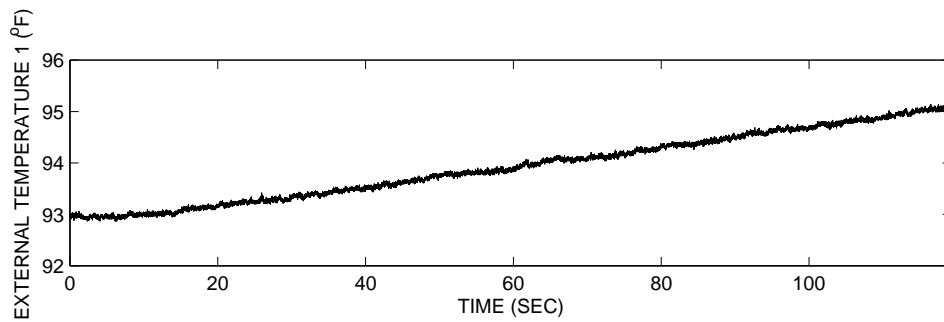
Figure E.13: Measured data of the 15 kip damper in the second round experiments for the data set usc\_10\_200\_q3.



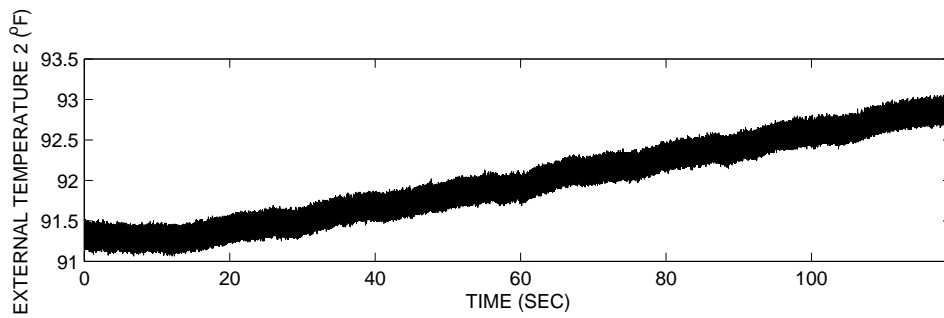
(a) Oil temperature 1



(b) Oil temperature 2

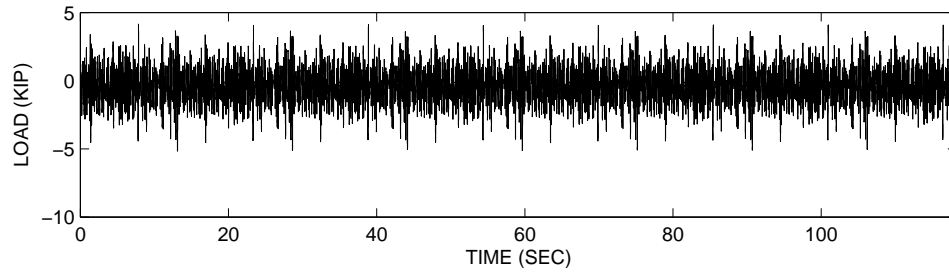


(c) Surface temperature 1

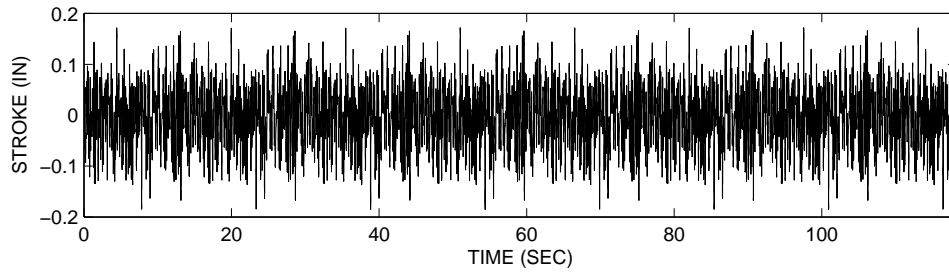


(d) Surface temperature 2

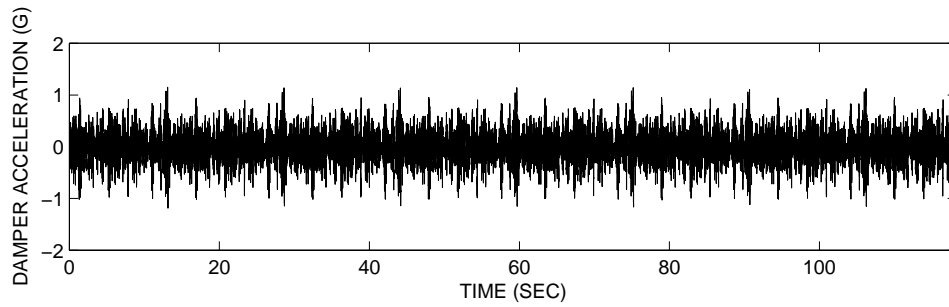
Figure E.14: Measured oil and surface temperatures of the 15 kip damper in the second round experiments for the data set usc\_10\_200\_q3.



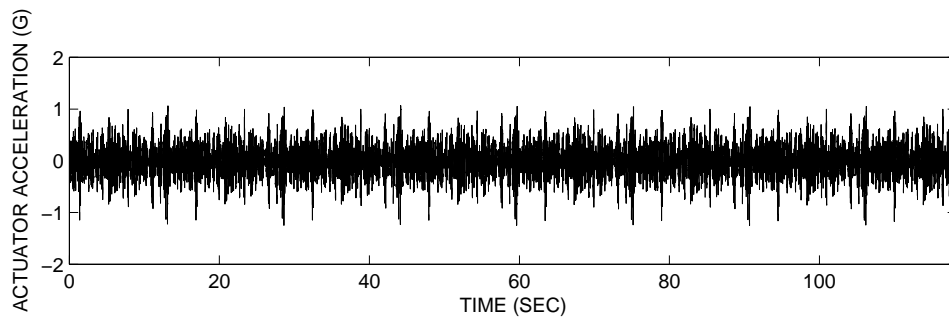
(a) Load (Force)



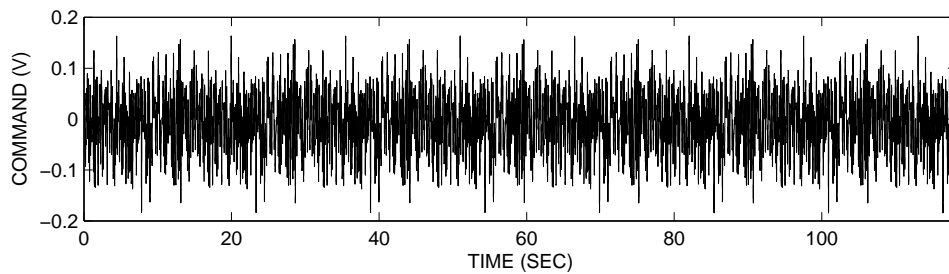
(b) Stroke (Displacement)



(c) Damper acceleration

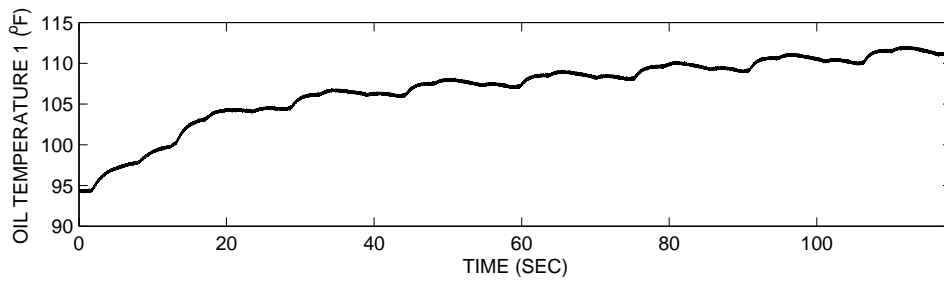


(d) Actuator acceleration

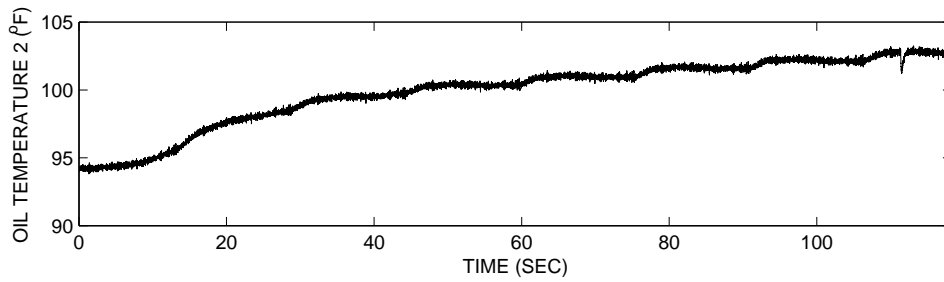


(e) Command Signal

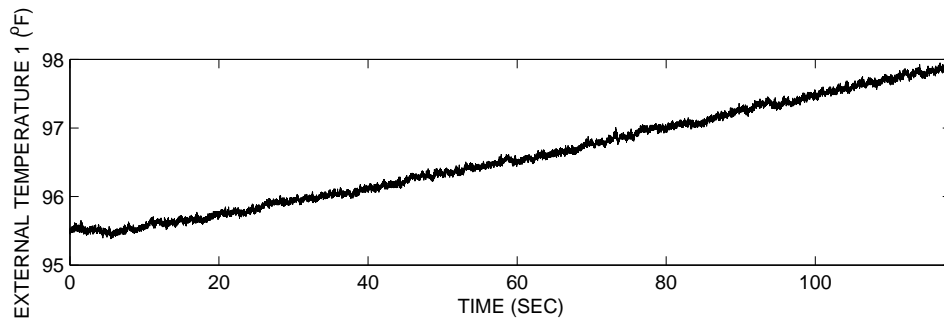
Figure E.15: Measured data of the 15 kip damper in the second round experiments for the data set usc\_10\_200\_q4.



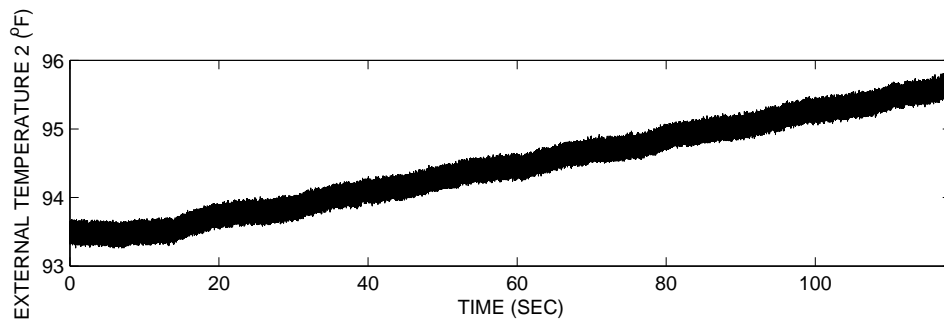
(a) Oil temperature 1



(b) Oil temperature 2

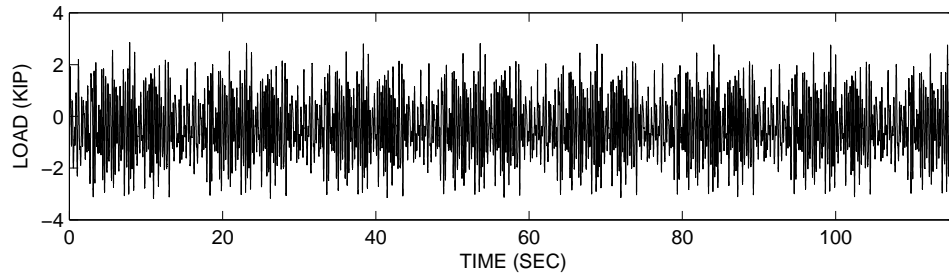


(c) Surface temperature 1

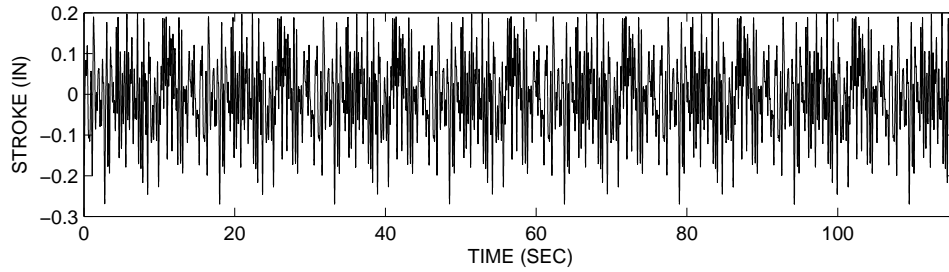


(d) Surface temperature 2

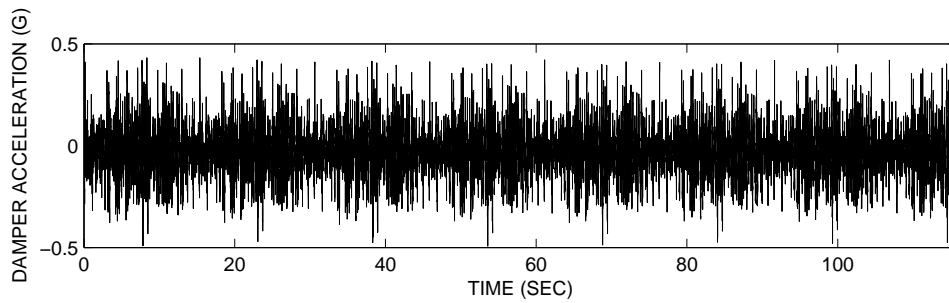
Figure E.16: Measured oil and surface temperatures of the 15 kip damper in the second round experiments for the data set usc\_10\_200\_q4.



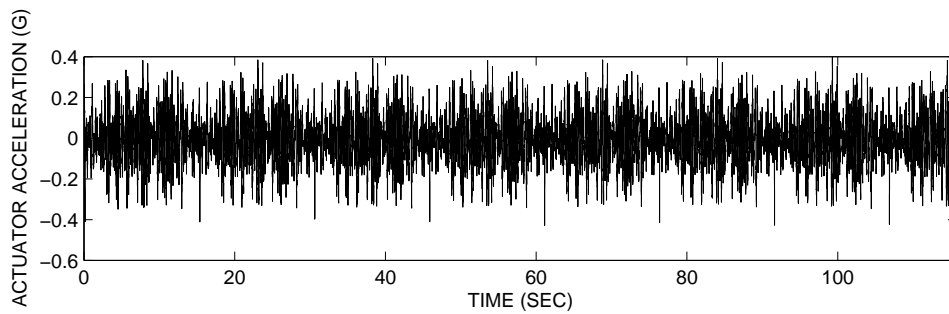
(a) Load (Force)



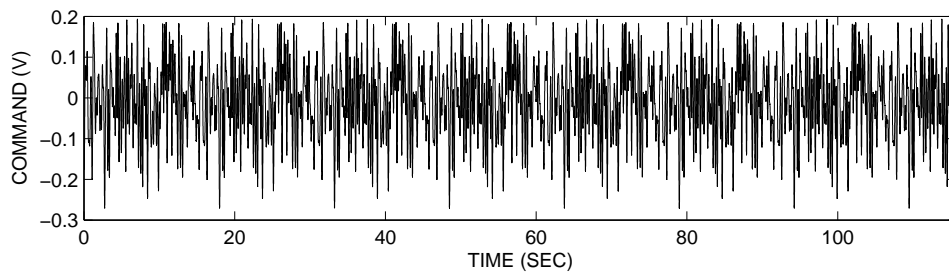
(b) Stroke (Displacement)



(c) Damper acceleration

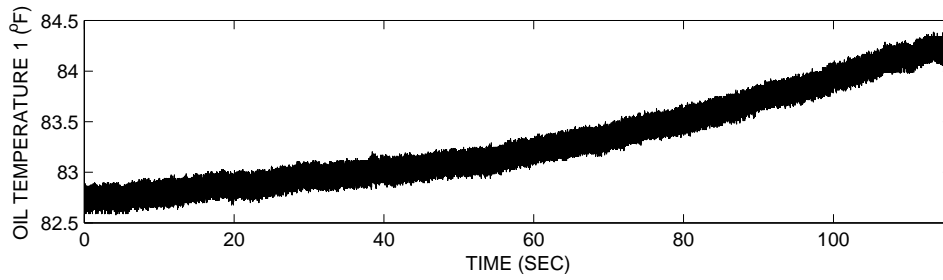


(d) Actuator acceleration

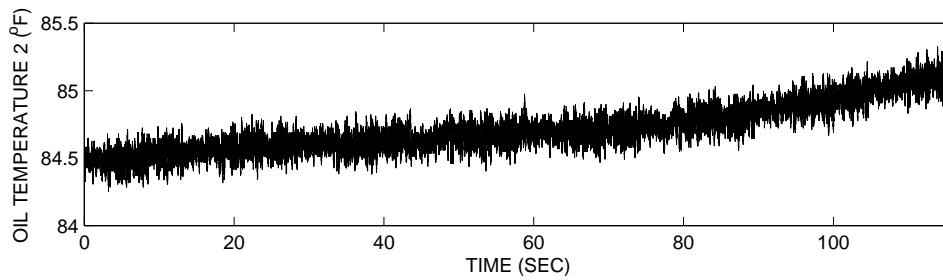


(e) Command Signal

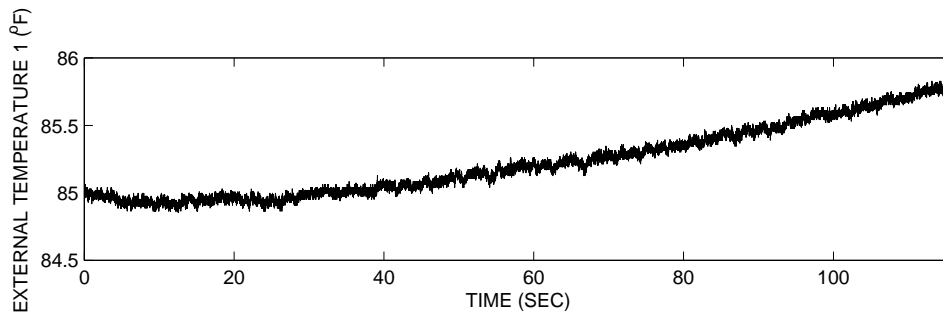
Figure E.17: Measured data of the 15 kip damper in the second round experiments for the data set usc\_5\_300\_q1.



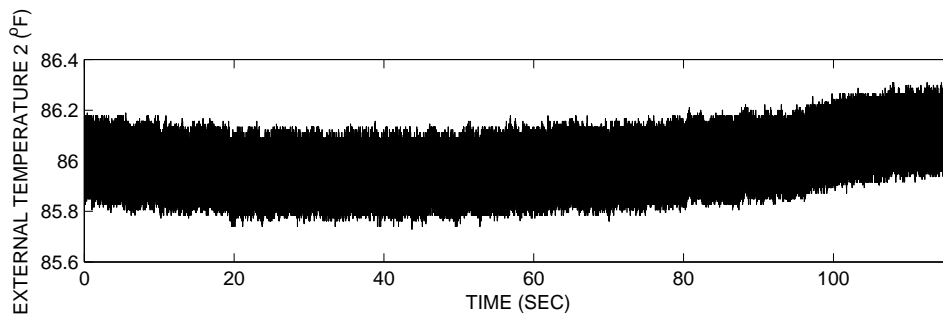
(a) Oil temperature 1



(b) Oil temperature 2

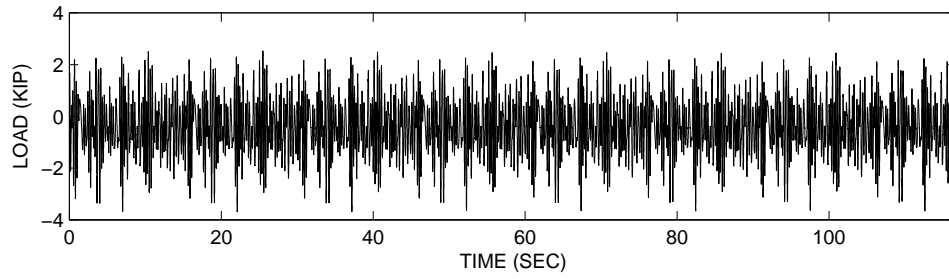


(c) Surface temperature 1

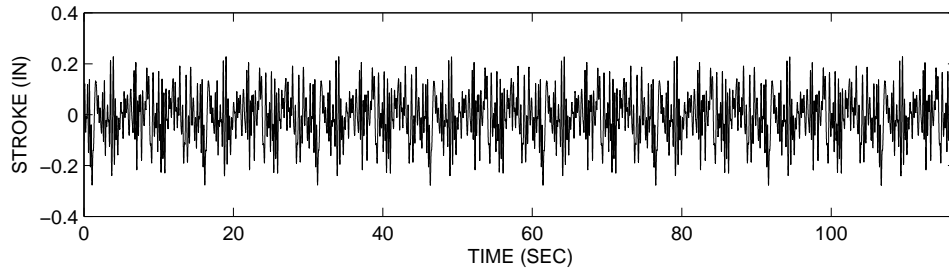


(d) Surface temperature 2

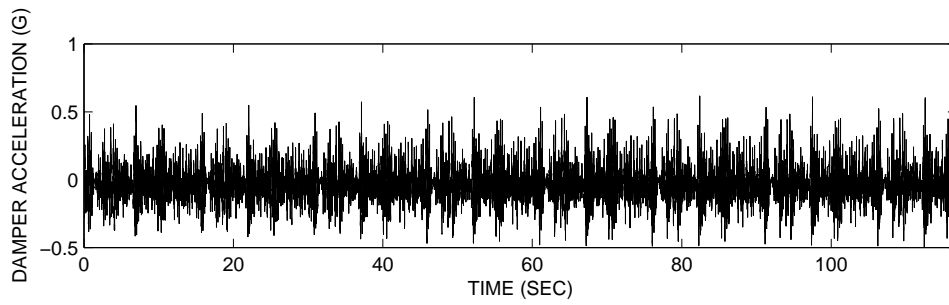
Figure E.18: Measured oil and surface temperatures of the 15 kip damper in the second round experiments for the data set usc\_5\_300\_q1.



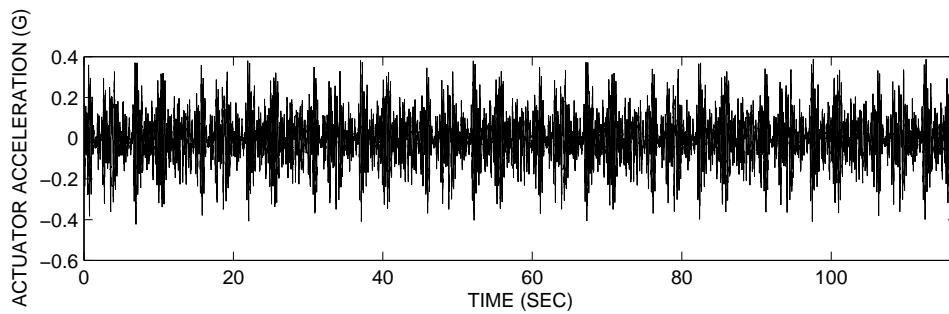
(a) Load (Force)



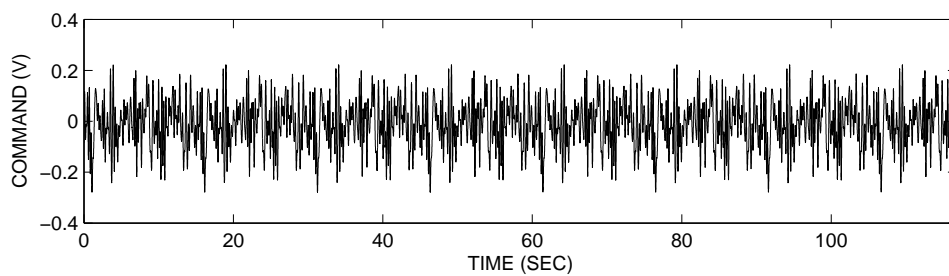
(b) Stroke (Displacement)



(c) Damper acceleration

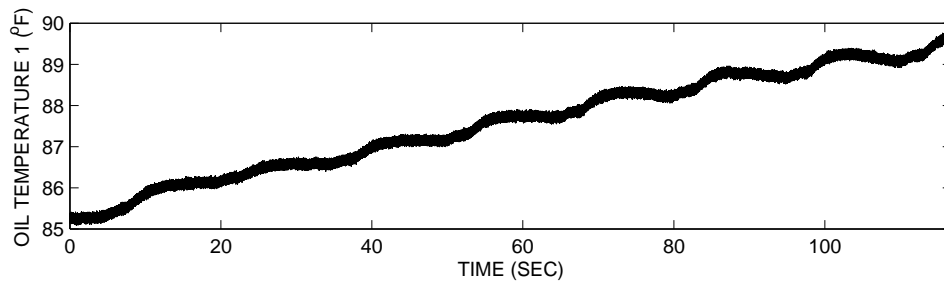


(d) Actuator acceleration

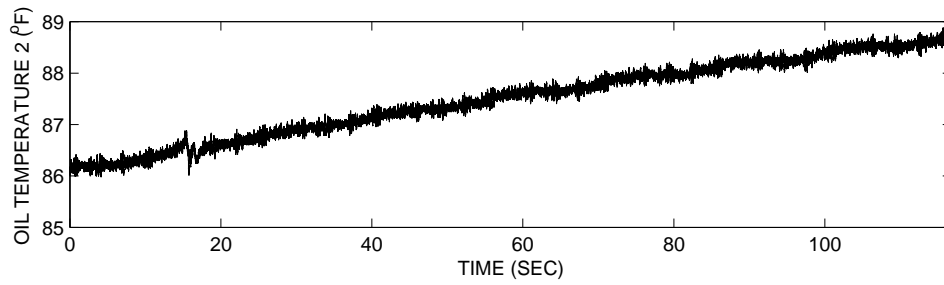


(e) Command Signal

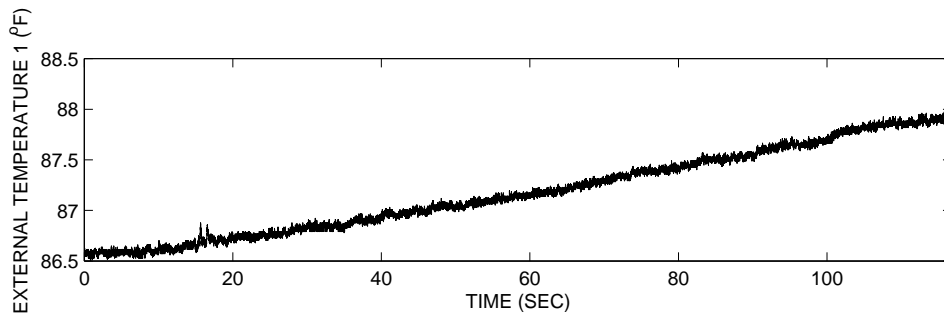
Figure E.19: Measured data of the 15 kip damper in the second round experiments for the data set usc\_5\_300\_q2.



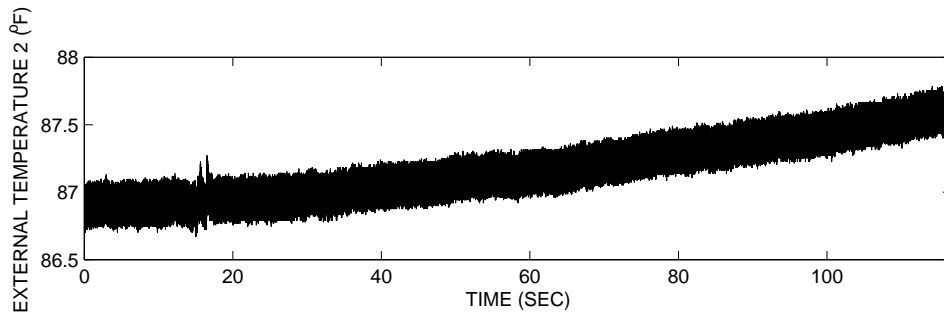
(a) Oil temperature 1



(b) Oil temperature 2

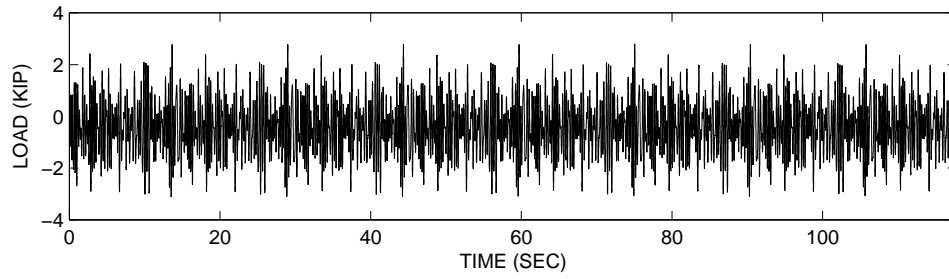


(c) Surface temperature 1

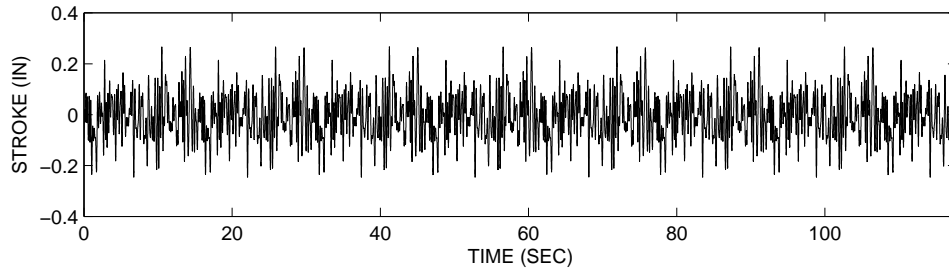


(d) Surface temperature 2

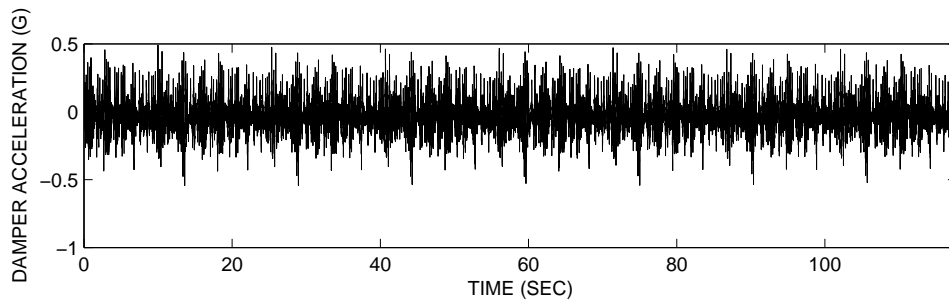
Figure E.20: Measured oil and surface temperatures of the 15 kip damper in the second round experiments for the data set usc\_5\_300\_q2.



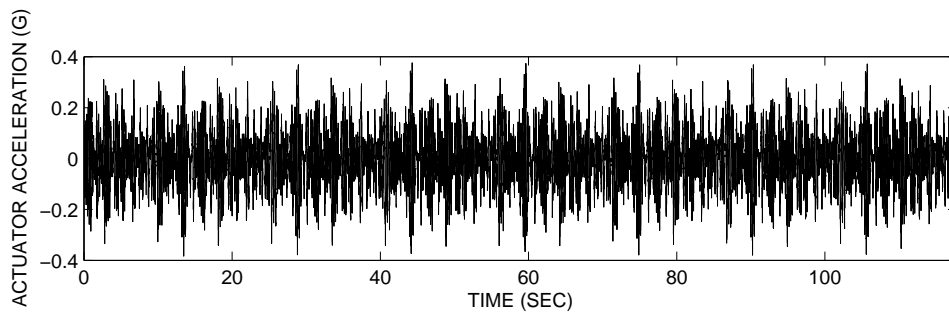
(a) Load (Force)



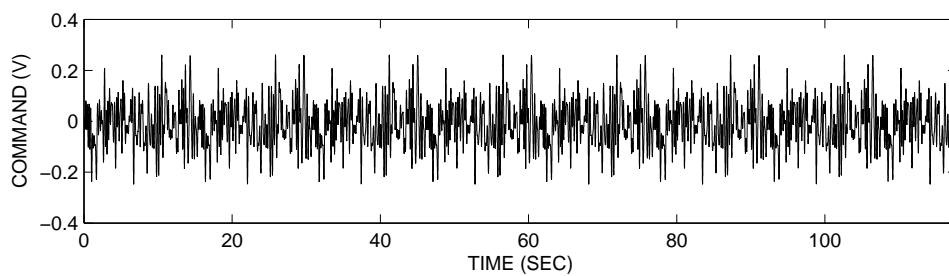
(b) Stroke (Displacement)



(c) Damper acceleration

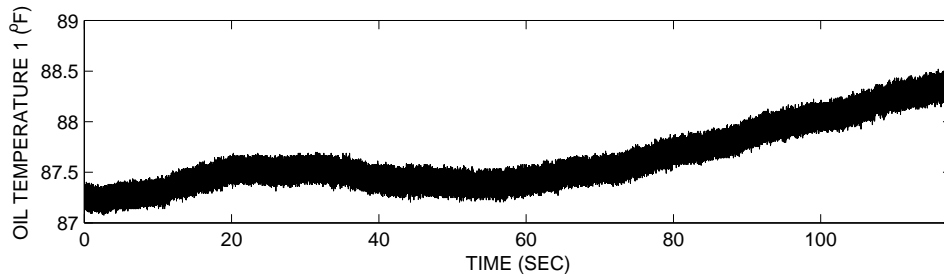


(d) Actuator acceleration

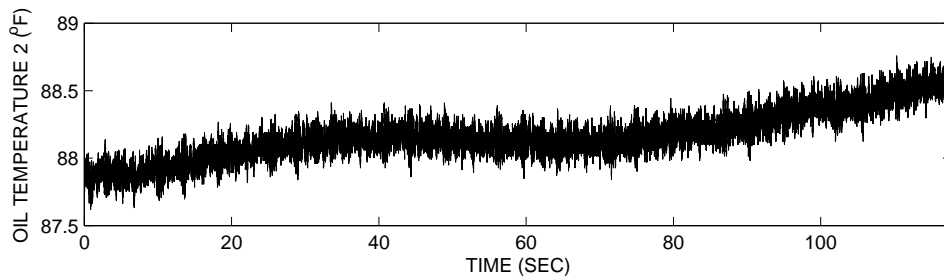


(e) Command Signal

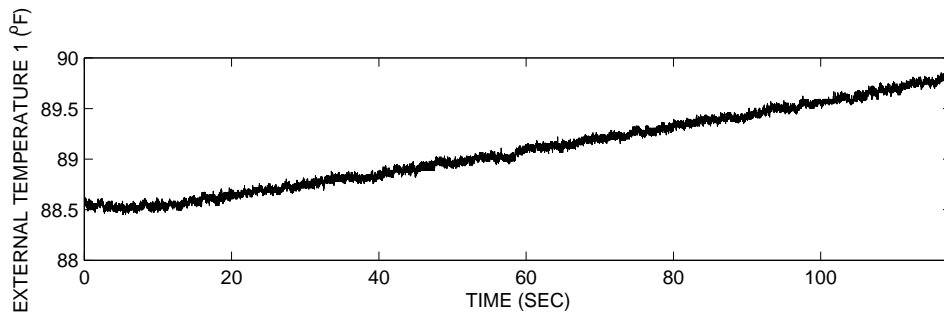
Figure E.21: Measured data of the 15 kip damper in the second round experiments for the data set usc\_5\_300\_q3.



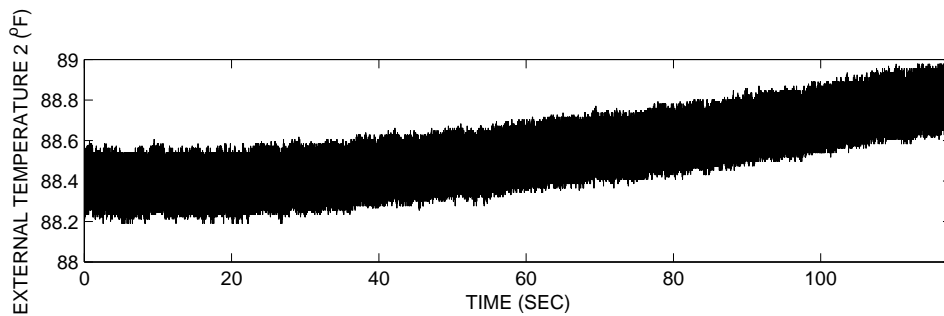
(a) Oil temperature 1



(b) Oil temperature 2

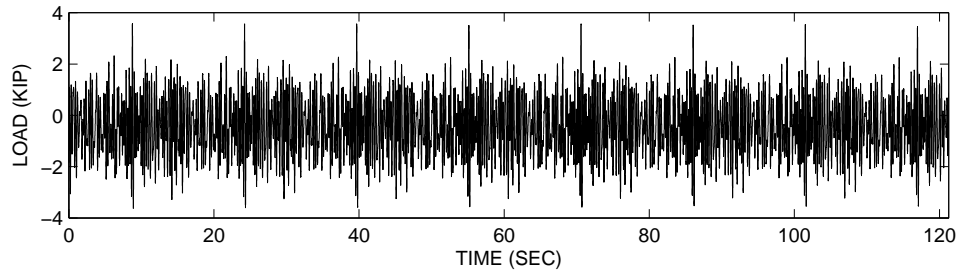


(c) Surface temperature 1

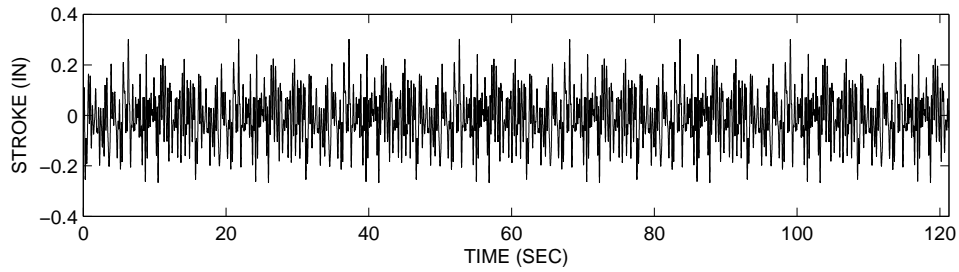


(d) Surface temperature 2

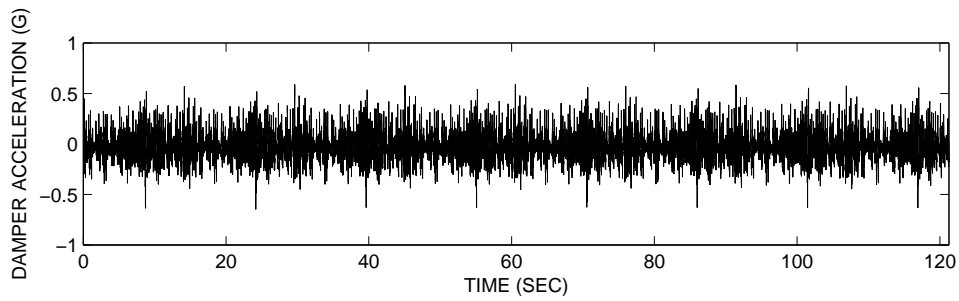
Figure E.22: Measured oil and surface temperatures of the 15 kip damper in the second round experiments for the data set usc\_5\_300\_q3.



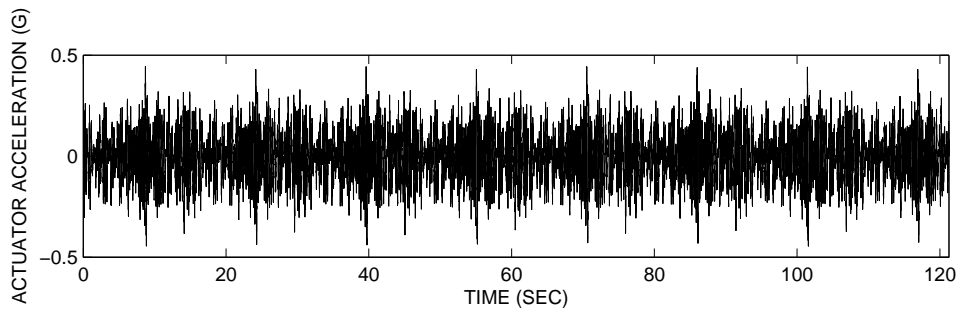
(a) Load (Force)



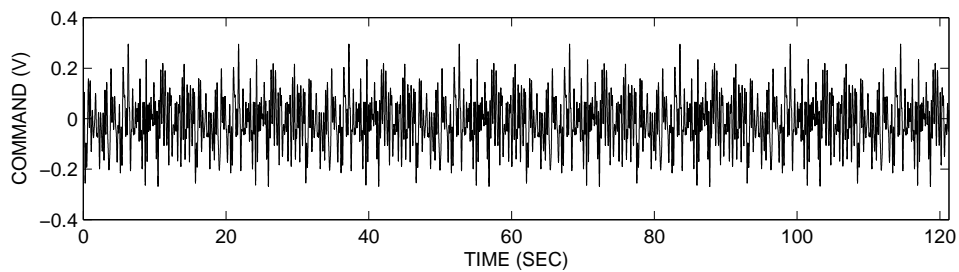
(b) Stroke (Displacement)



(c) Damper acceleration

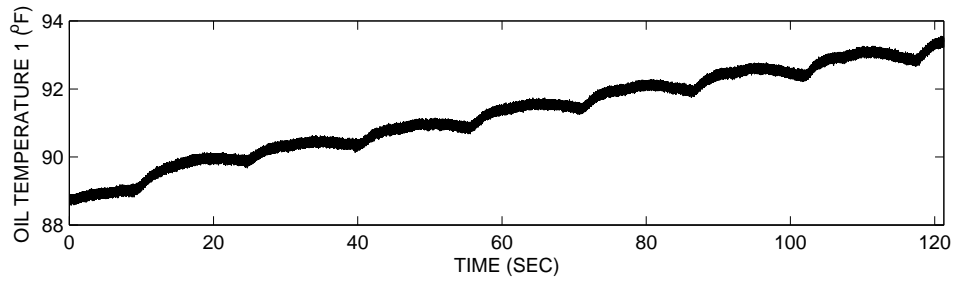


(d) Actuator acceleration

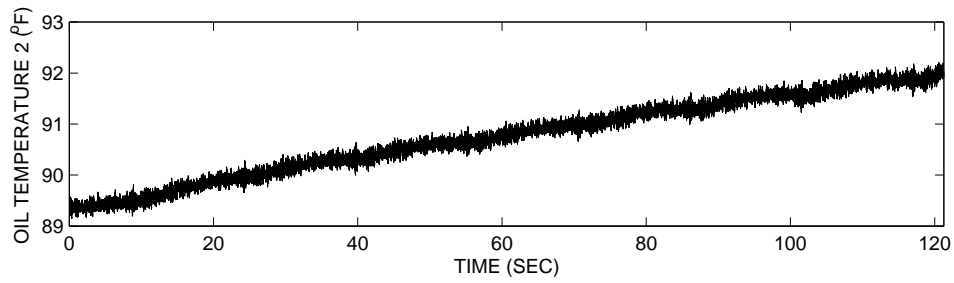


(e) Command Signal

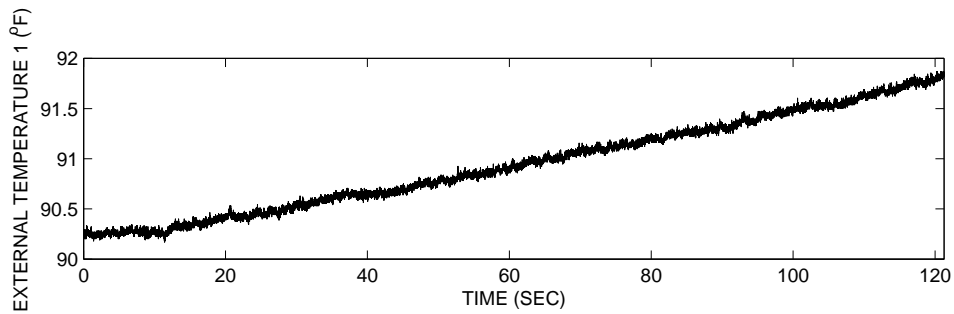
Figure E.23: Measured data of the 15 kip damper in the second round experiments for the data set usc\_5\_300\_q4.



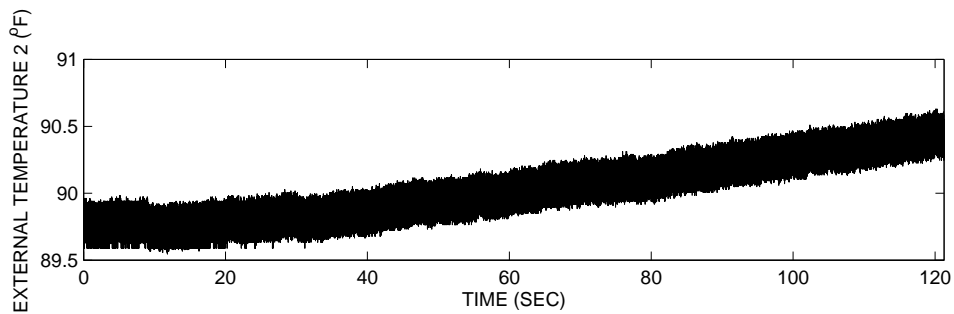
(a) Oil temperature 1



(b) Oil temperature 2

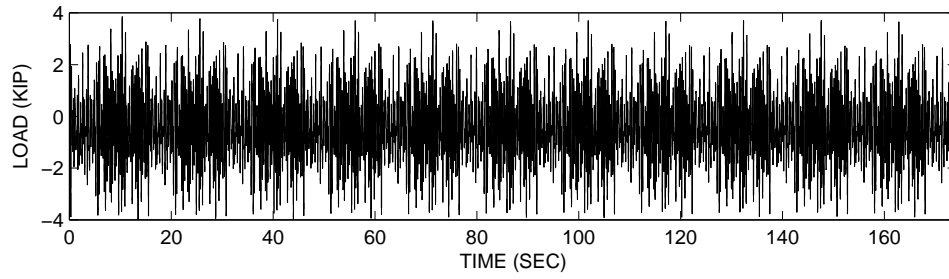


(c) Surface temperature 1

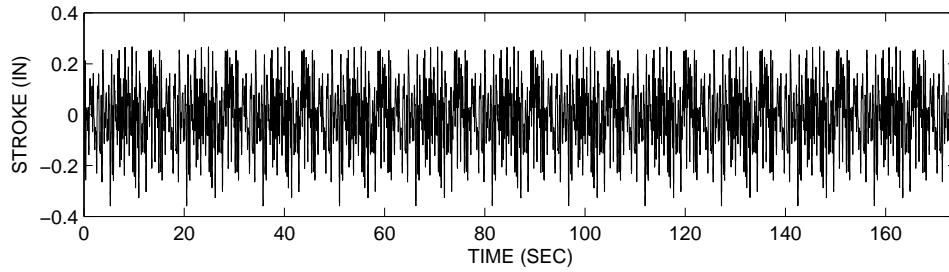


(d) Surface temperature 2

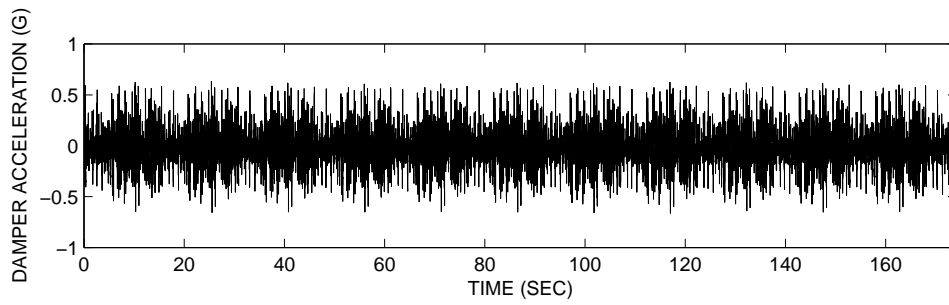
Figure E.24: Measured oil and surface temperatures of the 15 kip damper in the second round experiments for the data set usc\_5\_300\_q4.



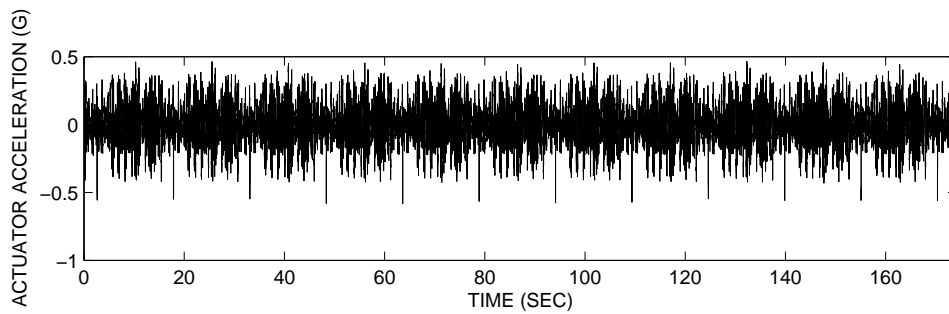
(a) Load (Force)



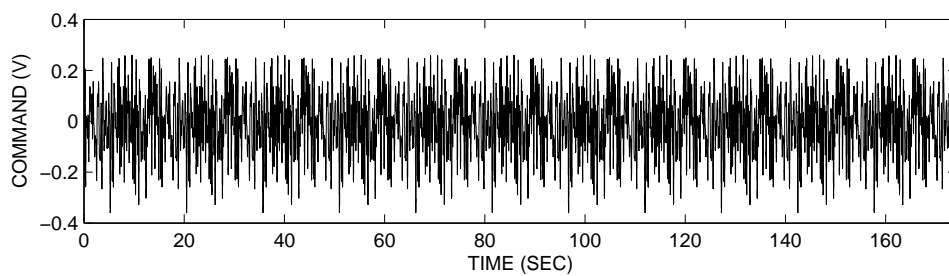
(b) Stroke (Displacement)



(c) Damper acceleration

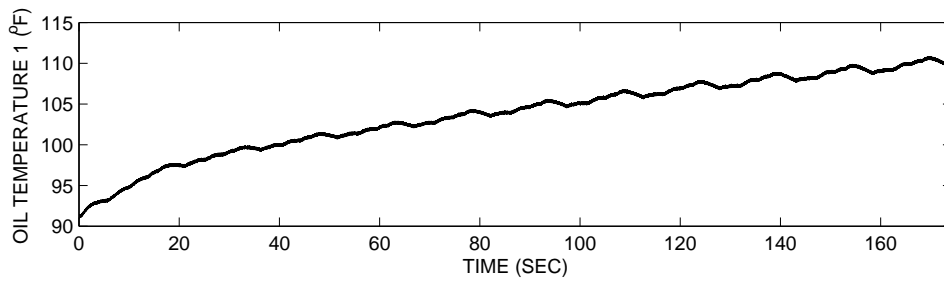


(d) Actuator acceleration

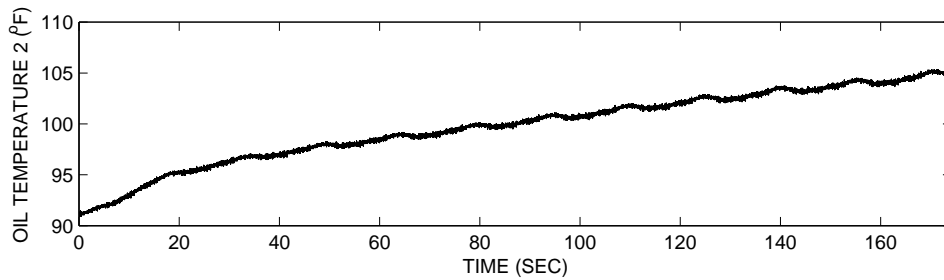


(e) Command Signal

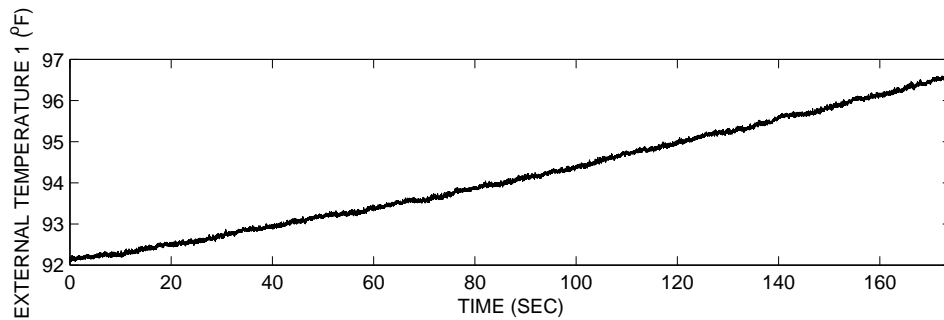
Figure E.25: Measured data of the 15 kip damper in the second round experiments for the data set usc\_5\_400\_q1.



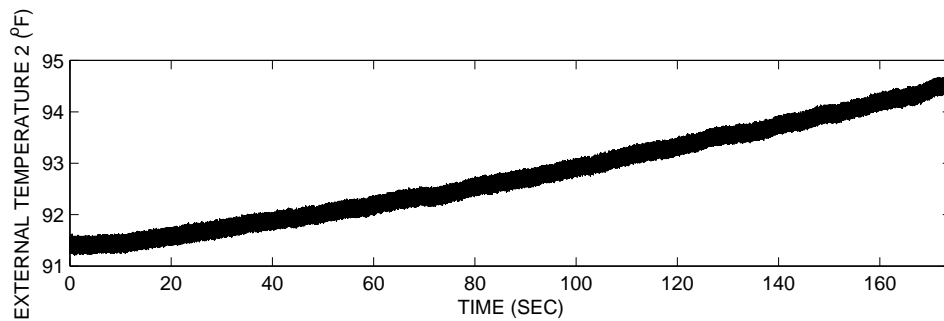
(a) Oil temperature 1



(b) Oil temperature 2

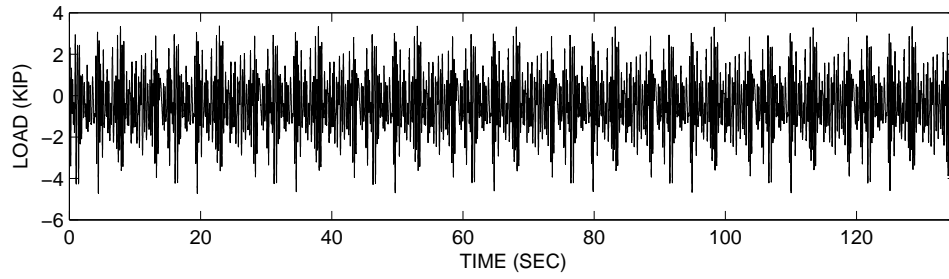


(c) Surface temperature 1

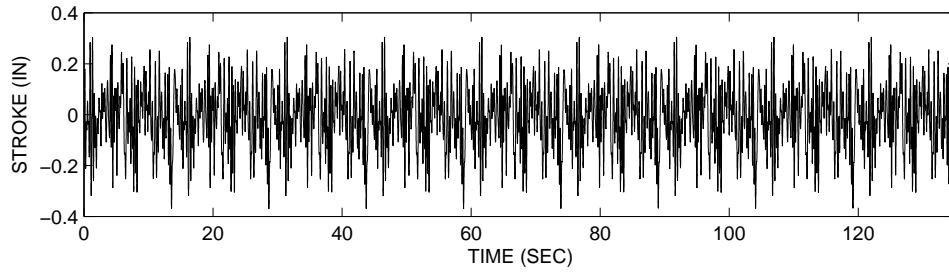


(d) Surface temperature 2

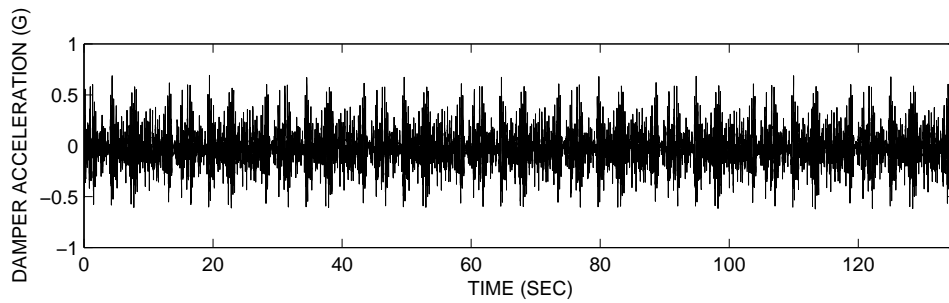
Figure E.26: Measured oil and surface temperatures of the 15 kip damper in the second round experiments for the data set usc\_5\_400\_q1.



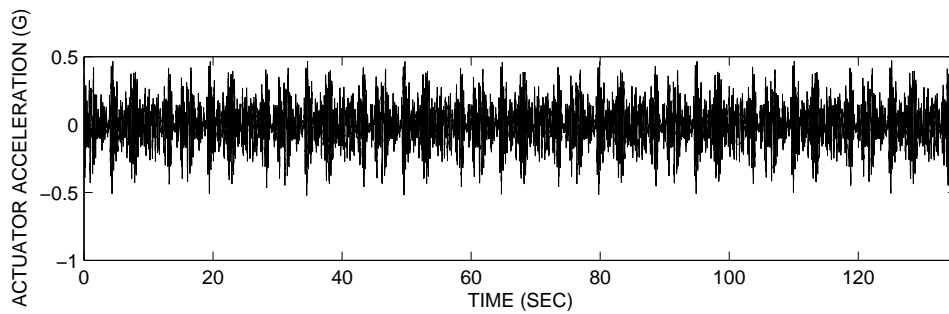
(a) Load (Force)



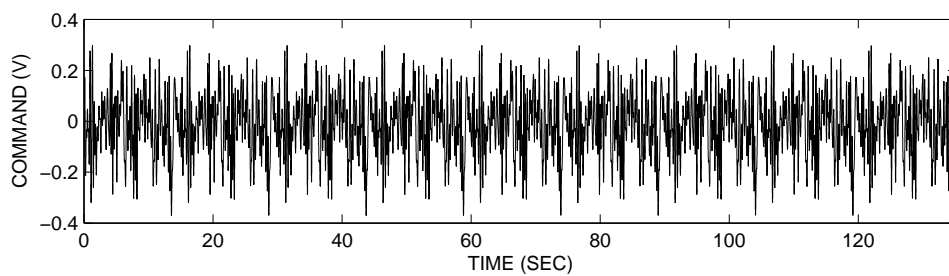
(b) Stroke (Displacement)



(c) Damper acceleration

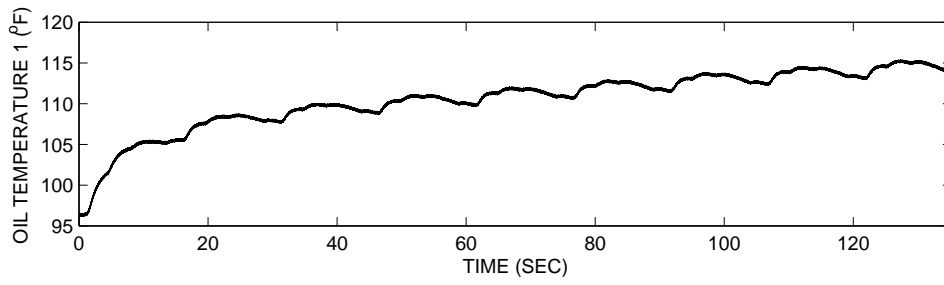


(d) Actuator acceleration

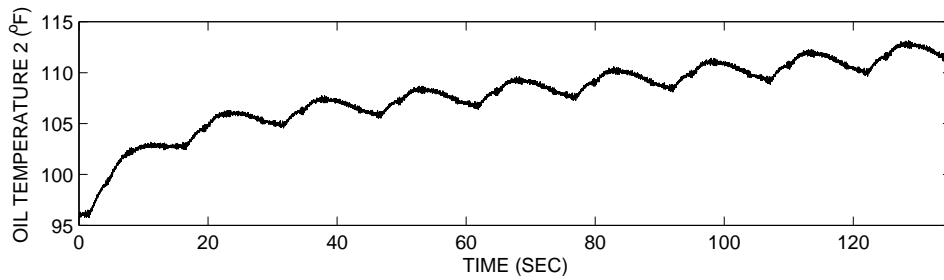


(e) Command Signal

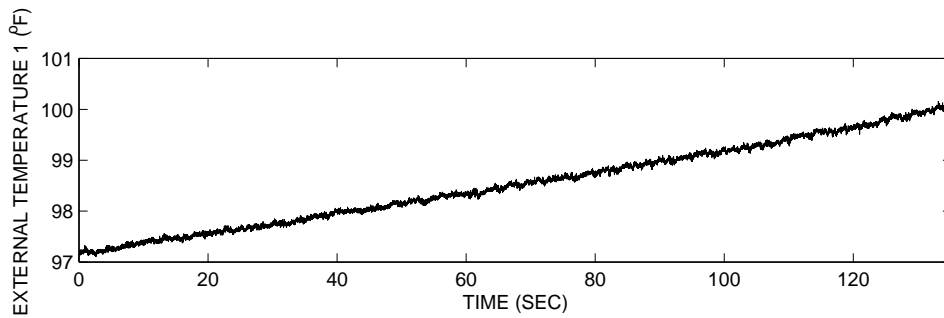
Figure E.27: Measured data of the 15 kip damper in the second round experiments for the data set usc\_5.400\_q2.



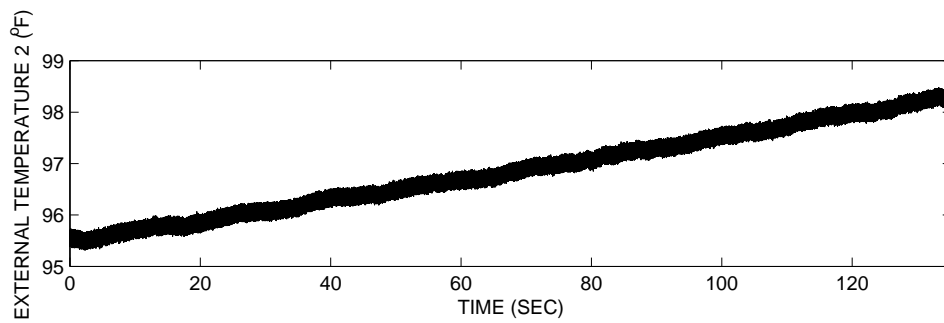
(a) Oil temperature 1



(b) Oil temperature 2

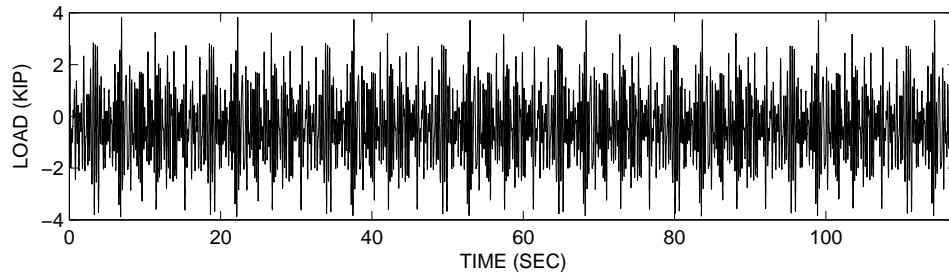


(c) Surface temperature 1

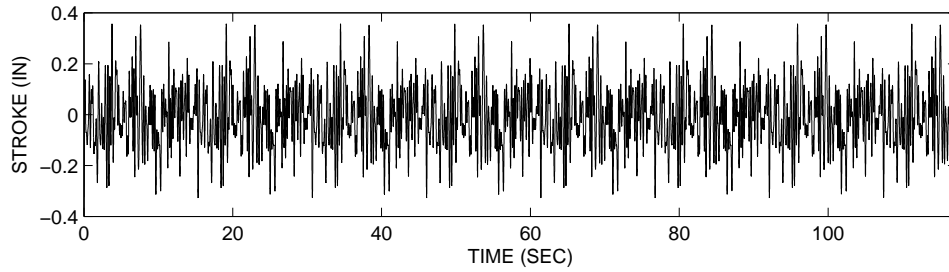


(d) Surface temperature 2

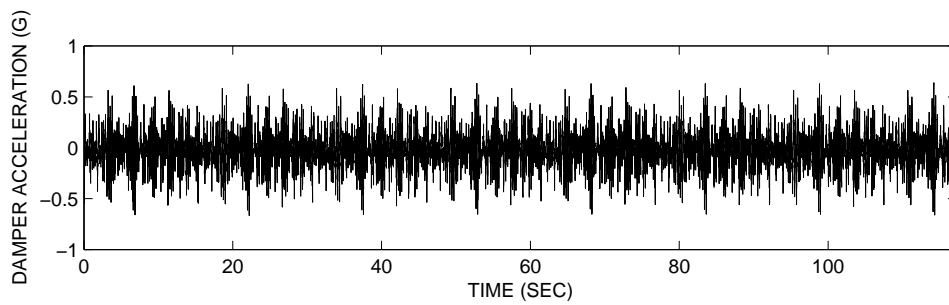
Figure E.28: Measured oil and surface temperatures of the 15 kip damper in the second round experiments for the data set usc\_5\_400\_q2.



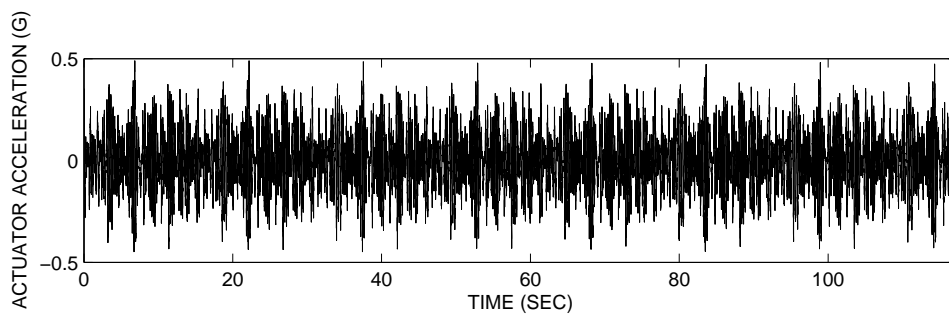
(a) Load (Force)



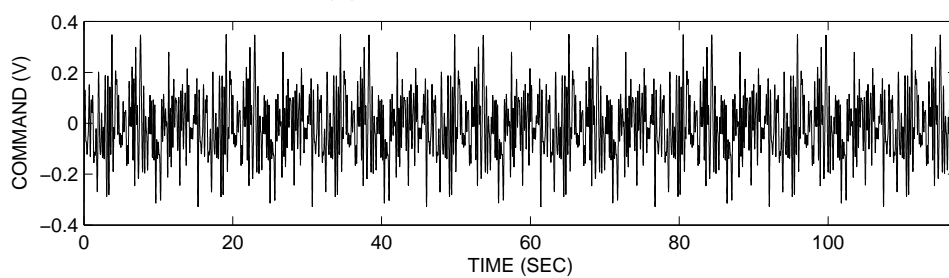
(b) Stroke (Displacement)



(c) Damper acceleration

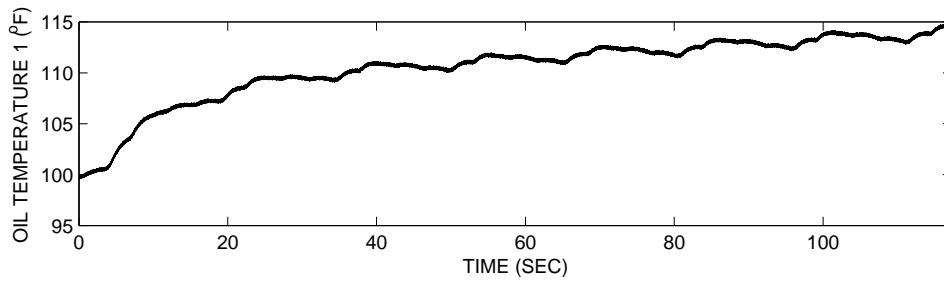


(d) Actuator acceleration

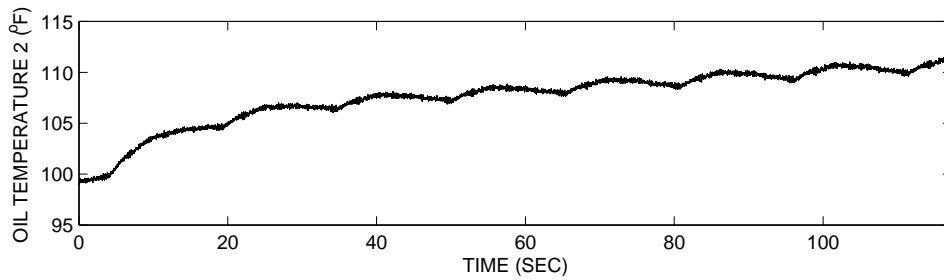


(e) Command Signal

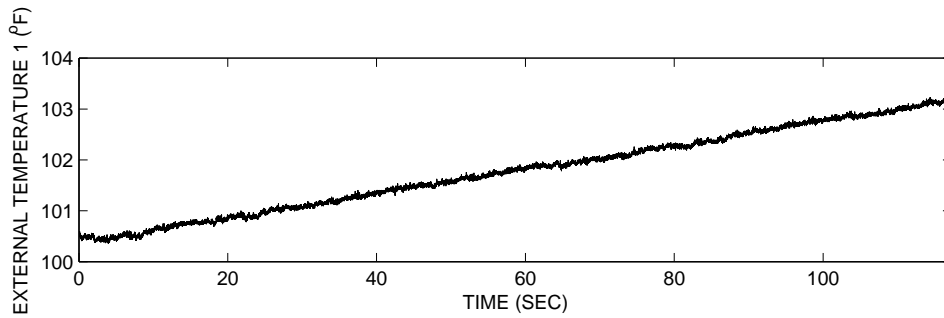
Figure E.29: Measured data of the 15 kip damper in the second round experiments for the data set usc\_5\_400\_q3.



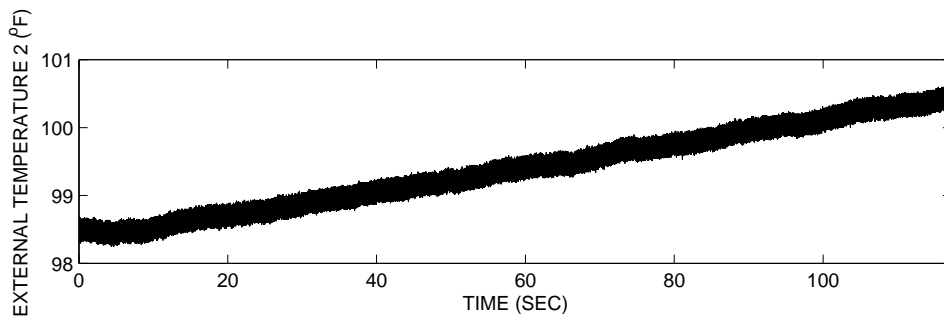
(a) Oil temperature 1



(b) Oil temperature 2

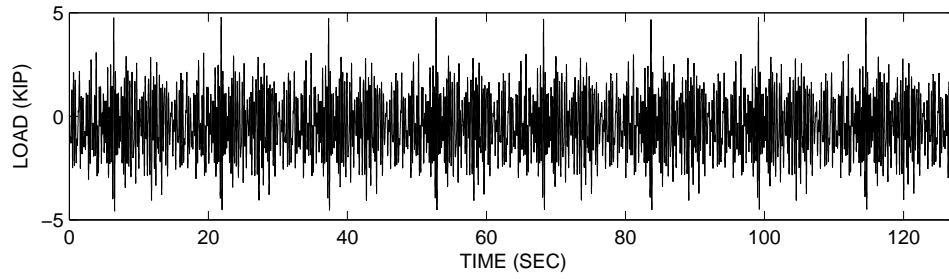


(c) Surface temperature 1

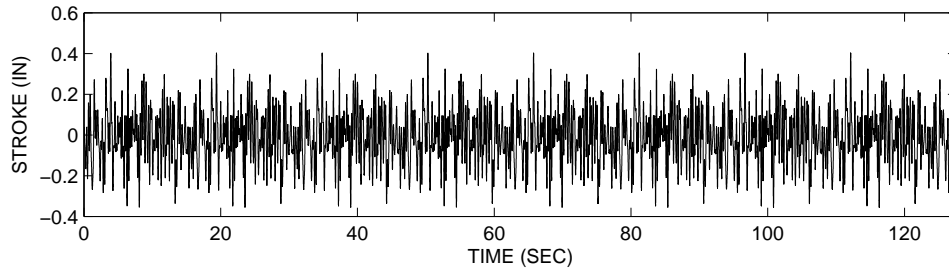


(d) Surface temperature 2

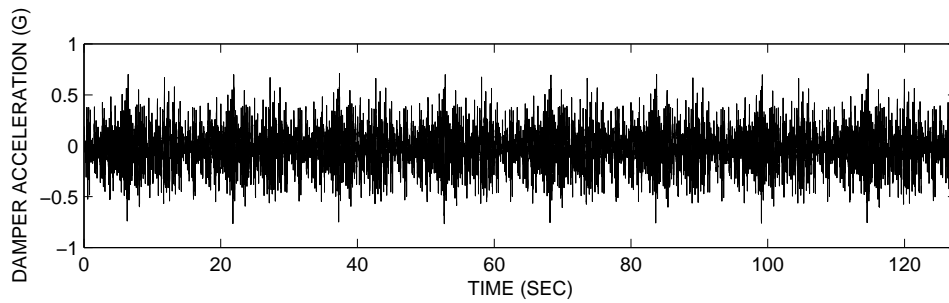
Figure E.30: Measured oil and surface temperatures of the 15 kip damper in the second round experiments for the data set usc\_5\_400\_q3.



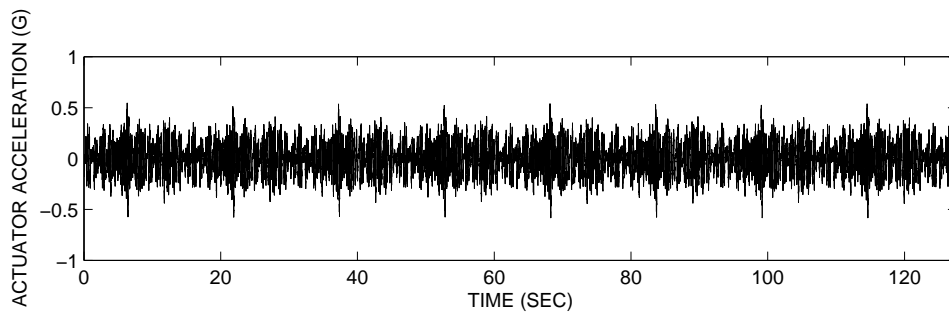
(a) Load (Force)



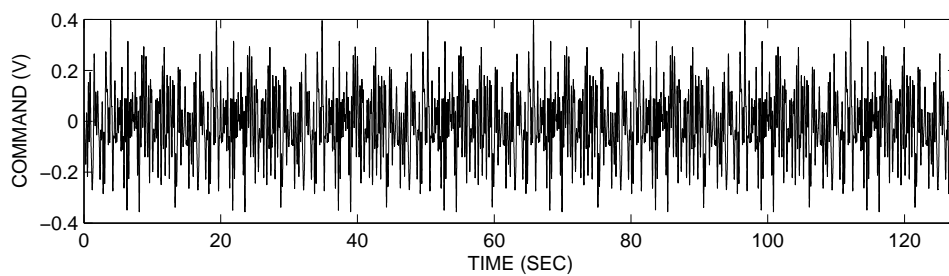
(b) Stroke (Displacement)



(c) Damper acceleration

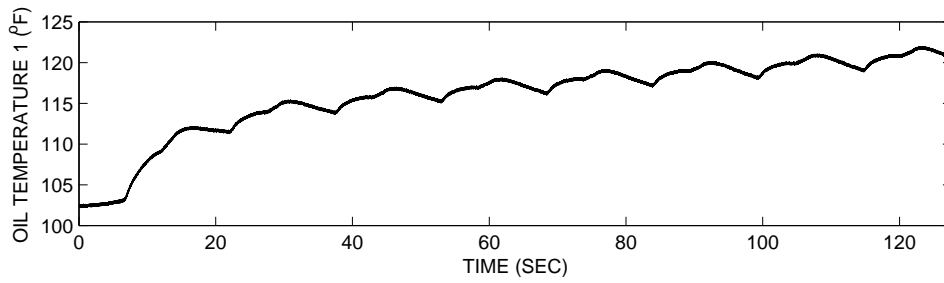


(d) Actuator acceleration

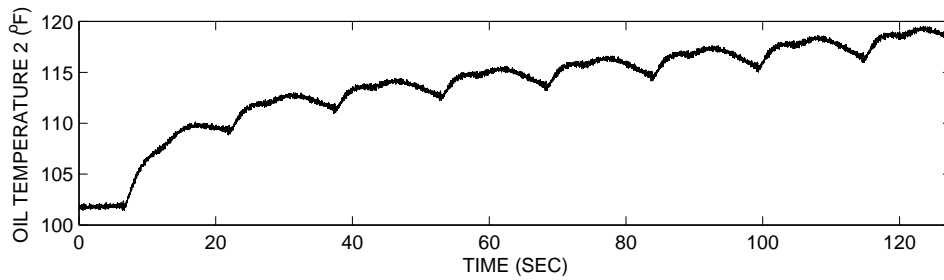


(e) Command Signal

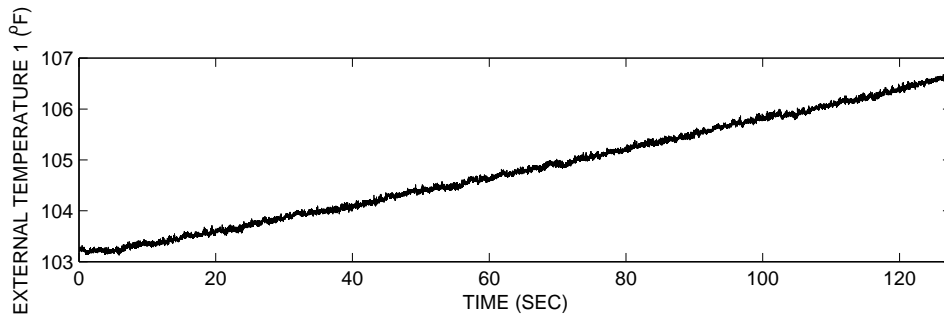
Figure E.31: Measured data of the 15 kip damper in the second round experiments for the data set usc\_5\_400\_q4.



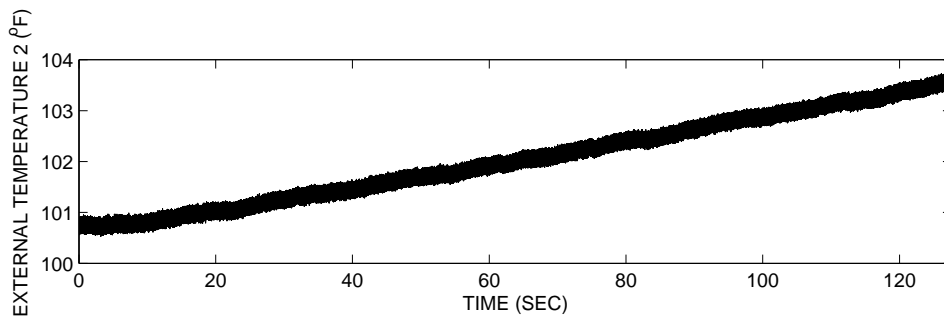
(a) Oil temperature 1



(b) Oil temperature 2



(c) Surface temperature 1



(d) Surface temperature 2

Figure E.32: Measured oil and surface temperatures of the 15 kip damper in the second round experiments for the data set usc\_5\_400\_q4.

## Appendix F

# PARAMETRIC IDENTIFICATION RESULTS OF THE 15 KIP VISCIOUS DAMPER

The results of the off-line and the on-line parametric identifications for the 15 kip viscous damper data sets are provided in this appendix. The test matrix of each data set is summarized in Tables F.1 and F.2.

Table F.1: The identification data sets of the 15 kip damper for the first round of testing.

Data set Name	Test Amplitude (in)	Cutoff Frequency (Hz)
Qtr4_01	0.1	15
Qtr4_0125	0.125	15

Table F.2: The identification data sets of the 15 kip damper for the second round of testing.

Data set Name	Test Amplitude (in)	Cutoff Frequency (Hz)
usc_10175_q4	0.175	10
usc_10200_q4	0.200	10
usc_5300_q4	0.300	5
usc_5400_q4	0.400	5

## F.1 Identification Results of 15 Kip Damper for the First Round of Testing

The plots of the on-line identification results are provided in section F.1.1, and the plots of the off-line identification results are provided in section F.1.2.

### F.1.1 On-Line Parametric Identification of the First Round of Testing

The on-line parametric identification results of the 15 kip damper for the first round of testing are summarized in Table F.3, where column 1 is the data set name, column 2 is the average value of the damping coefficient, column 3 is the average value of the exponent  $n$ , and column 4 is the normalized mean-square-error value of the difference between the predicted force and the measured force.

Table F.3: Summary of the on-line parametric identification results for the 15 kip damper of the data sets in the first round of testing. Column 1 is the data set name, column 2 is the manufacturer value for the damping coefficient  $C$ , column 3 is the average value of the identified damping coefficient  $\hat{C}$ , column 3 is the manufacturer specification value for the exponent  $n$ , column 4 is the average value of the identified exponent  $\hat{n}$  (Eqn. 2.6), column 5 is the selected value of the forgetting factor ( $\beta$ ) in the on-line identification algorithm (Eqn. 2.5), and column 6 is the normalized mean-square-error percentage of the difference between the predicted force and the measured force.

Data set Name	Damping Coeff. $C$ (kip sec/in)		Exponent $n$		$\beta$ forgetting factor	% MSE error
	Damper Spec.	Identified	Damper Spec.	Identified		
Qtr4.01	0.70	0.50	1.00	0.26	0.8	6.1
Qtr4.0125	0.70	0.59	1.00	0.34	0.8	6.4

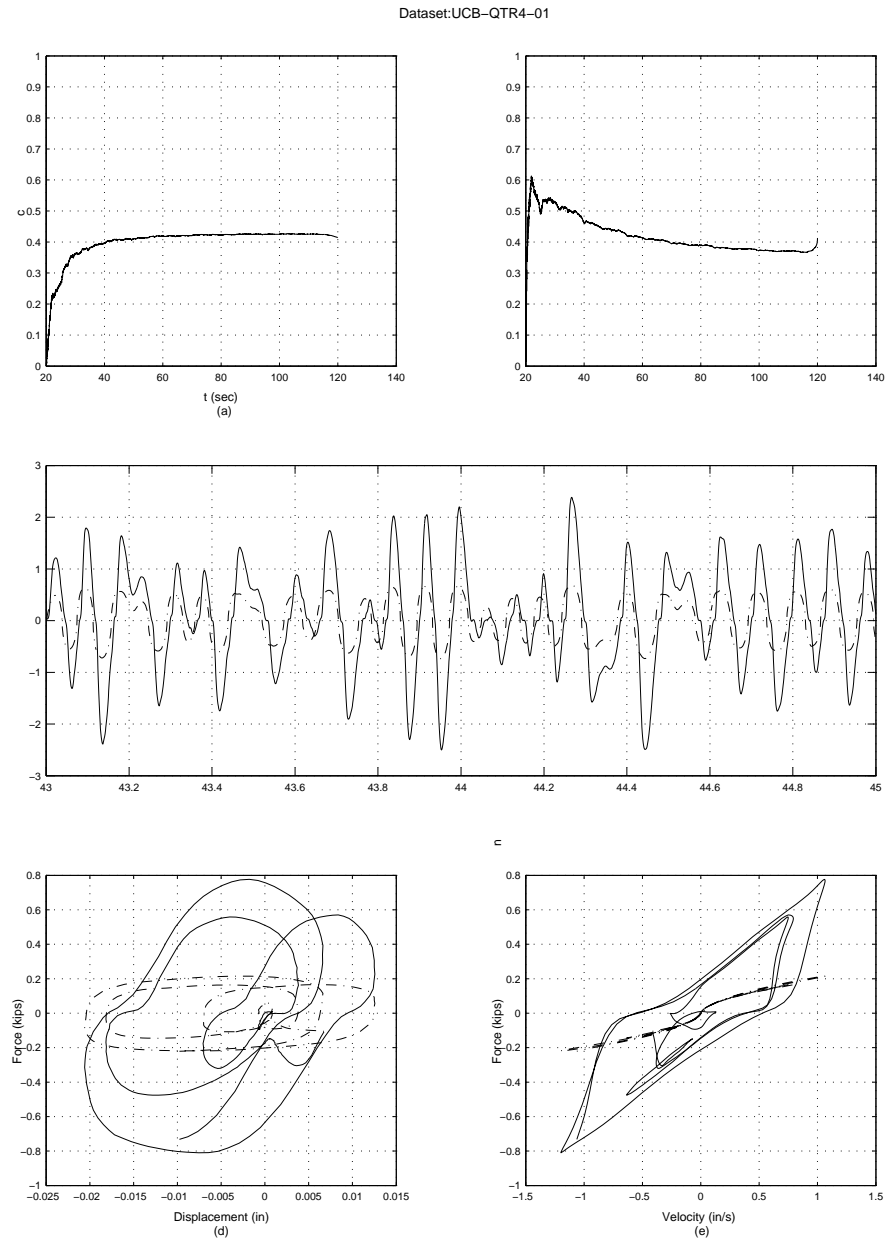


Figure F.1: On-line parametric identification results of the 15 kip damper for data set Qtr4.01. Part (a) and (b) show the filtered time-history of the unknown parameters, part (c) shows the time-history comparison of the measured force (solid line) and the predicted force (dash-dot line), part (d) is the displacement-force phase-plane comparison of the measured force (solid line) and the predicted force (dash-dot line), for one cycle, and part (e) is the velocity-force phase-plane comparison of the measured force (solid line) and the predicted force (dash-dot line), for one cycle.

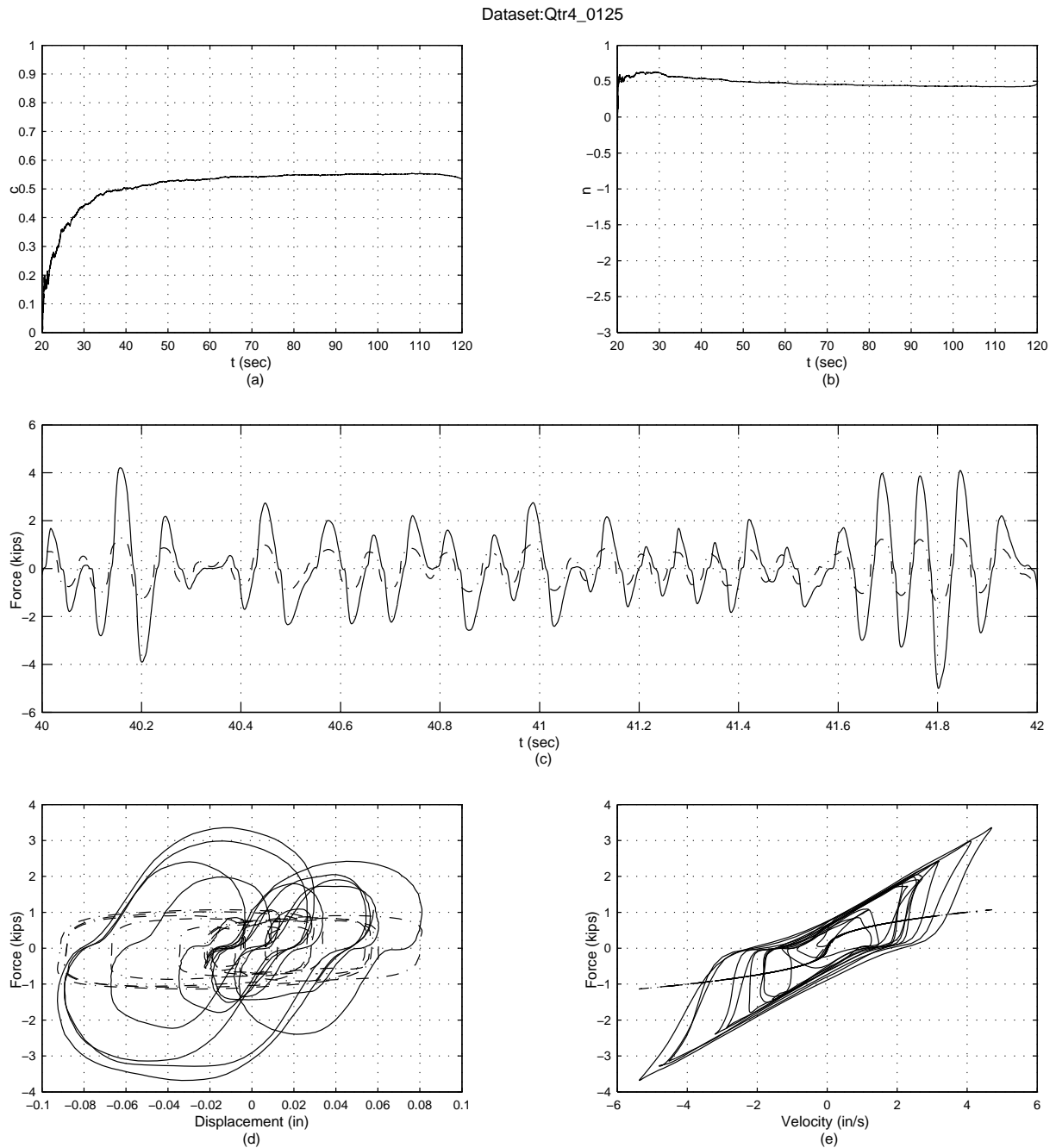


Figure F.2: On-line parametric identification results of the 15 kip damper for data set Qtr4\_0125. Part (a) and (b) show the filtered time-history of the unknown parameters, part (c) shows the time-history comparison of the measured force (solid line) and the predicted force (dash-dot line), part (d) is the displacement-force phase-plane comparison of the measured force (solid line) and the predicted force (dash-dot line), for one cycle, and part (e) is the velocity-force phase-plane comparison of the measured force (solid line) and the predicted force (dash-dot line), for one cycle.

### F.1.2 Off-Line Parametric Identification of the First Round of Testing

The off-line parametric identification results of the 15 kip damper for the first round of testing are summarized in Table F.4, where column 1 is the data set name, columns 2 to 6 give the optimum values of the initially unknown parameters for the optimization model (Eqn. 2.10), and the last column is the normalized mean-square-error value of the difference between the predicted force and the measured force.

Table F.4: Summary of the off-line parametric identification results for the 15 kip damper of the data sets in the first round of testing. Column 1 is the data set name, columns 2 to 7 give the optimum values of the initially unknown parameters (Eqn. 2.11), column 8 is the normalized mean-square-error (Eqn. 2.9).

Data set	$c$ (kip sec/in)	$k$ (kip/in)	$n$	$\theta_1$	$\theta_2$	$\theta_3$	% MSE
Qtr4_01	0.39	2.49	1.92	32.09	-216.10	162.00	4.72
Qtr4_0125	0.43	2.75	1.89	32.59	-197.10	160.00	4.62

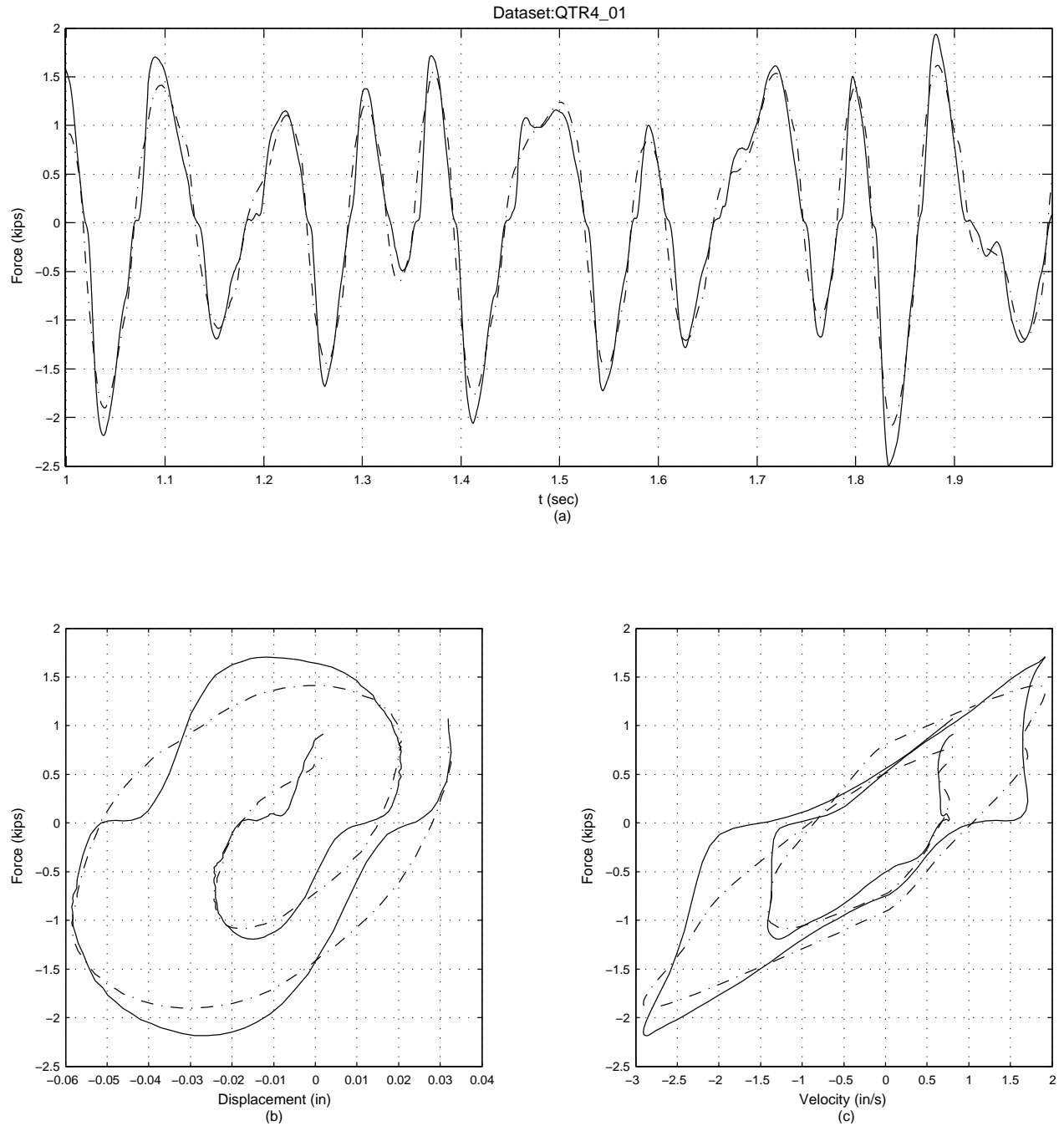


Figure F.3: Off-line parametric identification results of the 15 kip damper for data set Qtr4.01. Part (a) shows the time-history comparison of the measured force (solid line) and the predicted force (dash-dot line), part (b) shows the displacement-force phase-plane comparison of the measured force (solid line) and the predicted force (dash-dot line), for one cycle, and part (c) shows the velocity-force phase-plane comparison of the measured force (solid line) and the predicted force (dash-dot line), for one cycle.

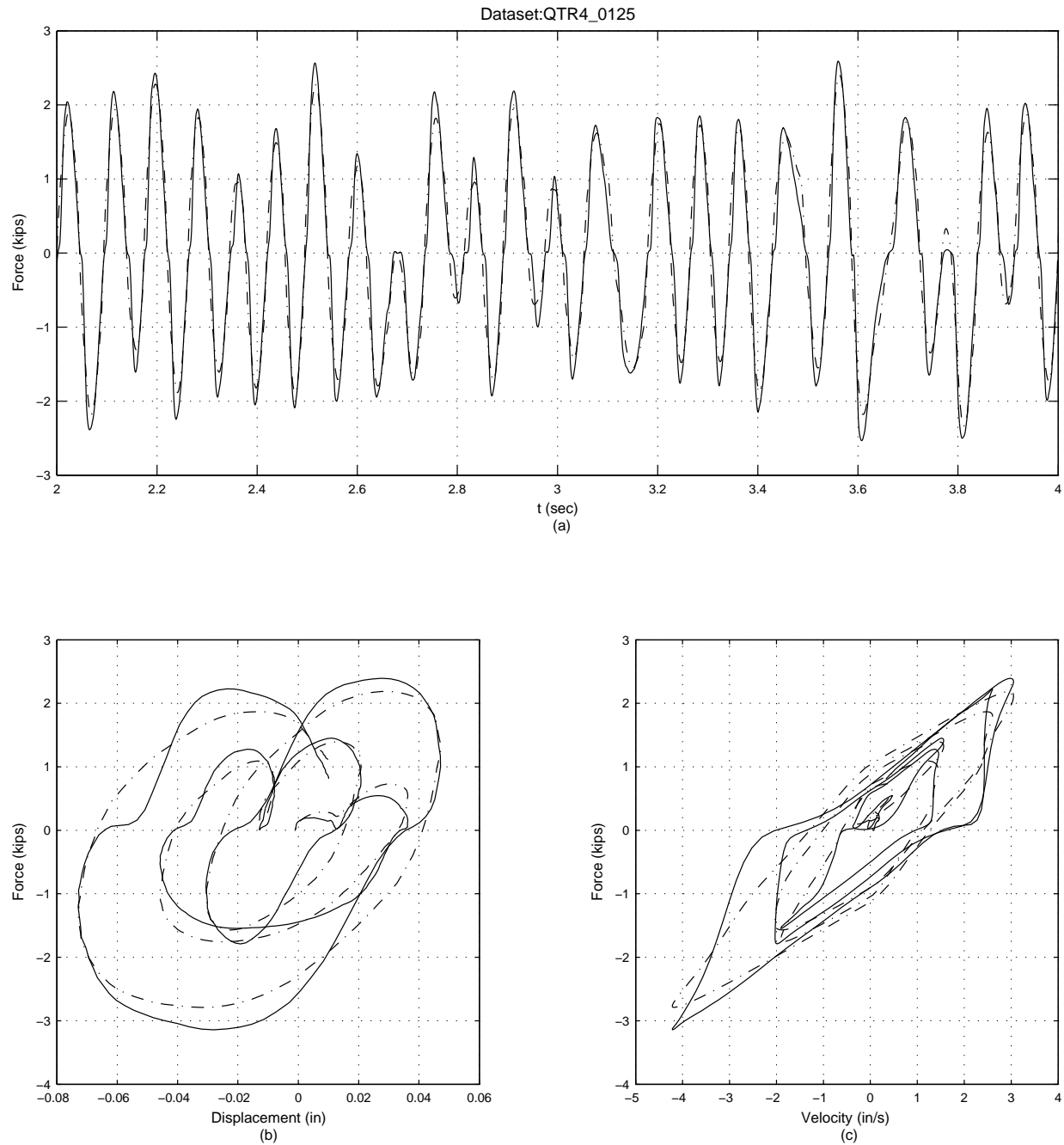


Figure F.4: Off-line parametric identification results of the 15 kip damper for data set Qtr4\_0125. Part (a) shows the time-history comparison of the measured force (solid line) and the predicted force (dash-dot line), part (b) shows the displacement-force phase-plane comparison of the measured force (solid line) and the predicted force (dash-dot line), for one cycle, and part (c) shows the velocity-force phase-plane comparison of the measured force (solid line) and the predicted force (dash-dot line), for one cycle.

## F.2 Identification Results of 15 kip Damper for the Second Round of Testing

The plots of the on-line identification results are provided in section F.2.1, and the plots of the off-line identification results are provided in section F.2.2.

### F.2.1 On-Line Parametric Identification Plots

The on-line parametric identification results of the 15 kip damper for the second round of testing are summarized in Table F.5, where column 1 is the data set name, column 2 is the average value of the damping coefficient, column 3 is the average value of the exponent  $n$ , column 4 is the value of the forgetting vector (Eqn. 2.5), and column 5 is the normalized mean-square-error value of the difference between the predicted force and the measured force.

Table F.5: Summary of the on-line parametric identification results for the 15 kip damper of the data sets in the first second of testing. Column 1 is the data set name, column 2 is the manufacturer value for the damping coefficient  $C$ , column 3 is the average value of the identified damping coefficient  $\hat{C}$ , column 3 is the manufacturer specification value for the exponent  $n$ , column 4 is the average value of the identified exponent  $\hat{n}$  (Eqn. 2.6), column 5 is the selected value of the forgetting factor ( $\beta$ ) in the on-line identification algorithm (Eqn. 2.5), and column 6 is the normalized mean-square-error percentage of the difference between the predicted force and the measured force.

Data set Name	Damping Coeff. $C$ (kip sec/in)		Exponent $n$		$\beta$ forgetting factor	% MSE error
	Damper Spec.	Identified	Damper Spec.	Identified		
usc_10175_q4	0.70	0.50	1.00	0.83	0.8	6.7
usc_10200_q4	0.70	0.80	1.00	0.69	0.8	6.4
usc_5300_q4	0.70	0.80	1.00	0.69	0.8	4.4
usc_5400_q4	0.70	0.50	1.00	0.89	0.8	6.0

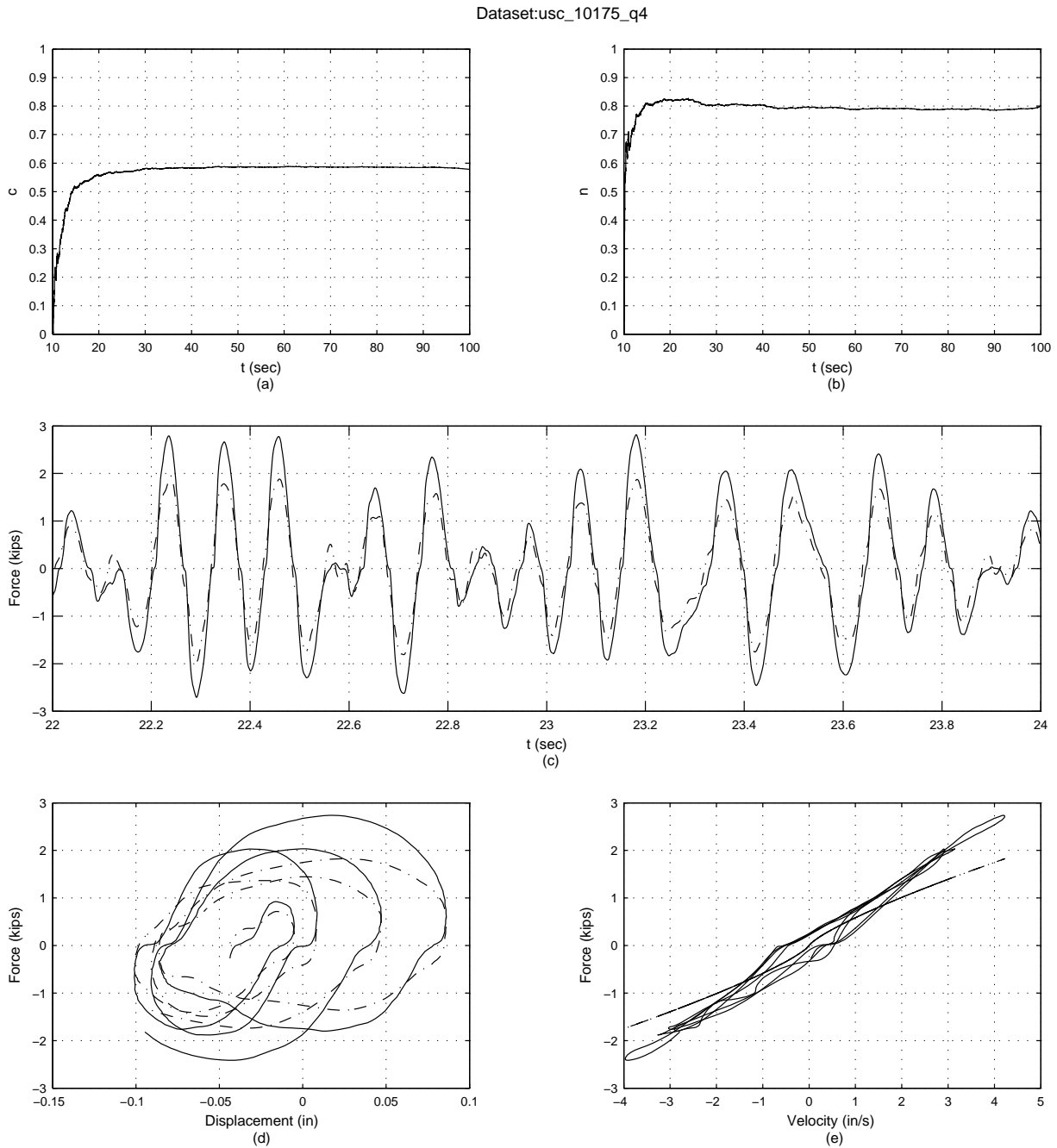


Figure F.5: On-line parametric identification results of the 15 kip damper for data set usc\_10175\_q4. Part (a) and (b) show the filtered time-history of the unknown parameters, part (c) shows the time-history comparison of the measured force (solid line) and the predicted force (dash-dot line), part (d) is the displacement-force phase-plane comparison of the measured force (solid line) and the predicted force (dash-dot line), for one cycle, and part (e) is the velocity-force phase-plane comparison of the measured force (solid line) and the predicted force (dash-dot line), for one cycle.

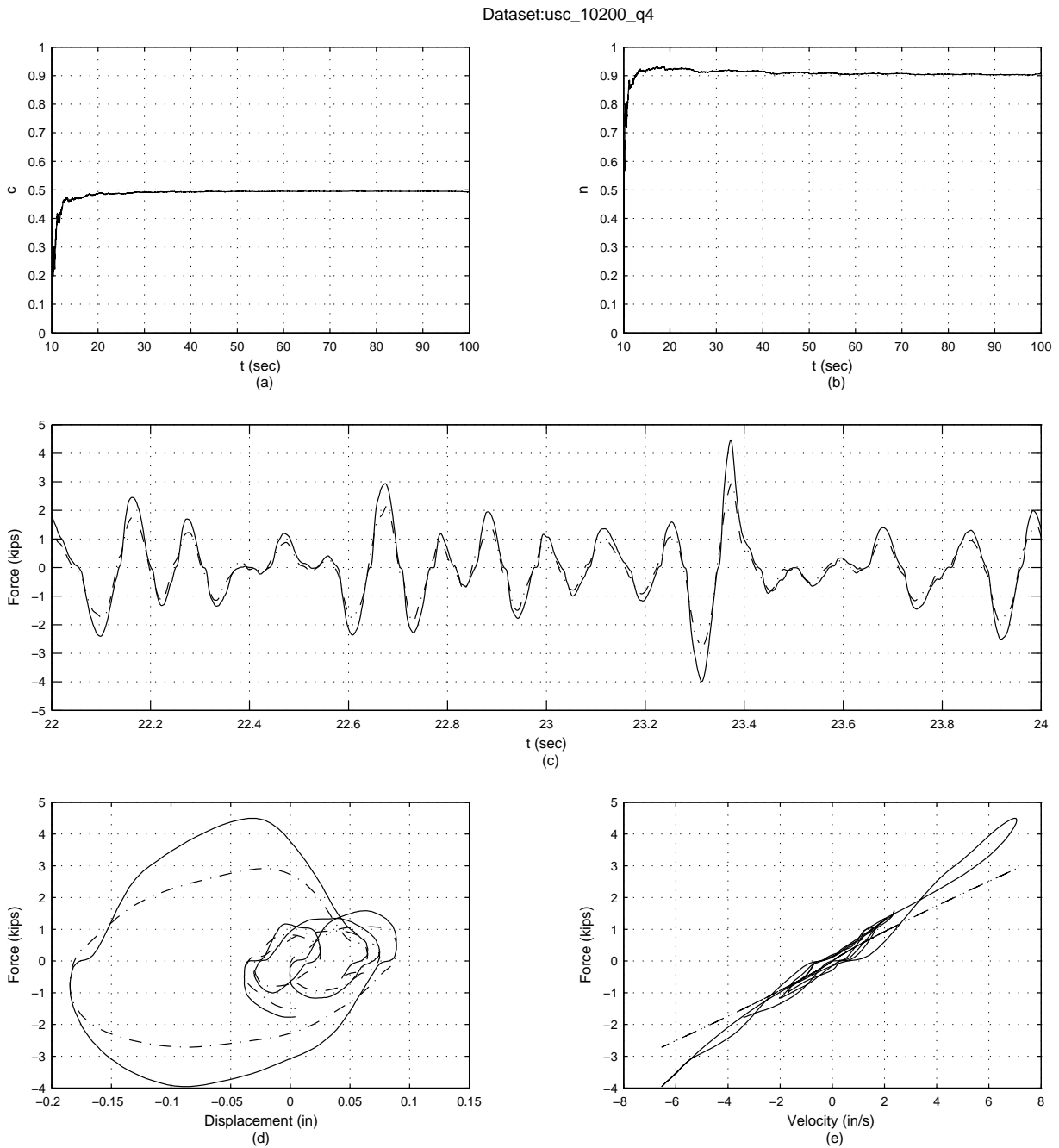


Figure F.6: On-line parametric identification results of the 15 kip damper for data set usc\_10200\_q4. Part (a) and (b) show the filtered time-history of the unknown parameters, part (c) shows the time-history comparison of the measured force (solid line) and the predicted force (dash-dot line), part (d) is the displacement-force phase-plane comparison of the measured force (solid line) and the predicted force (dash-dot line), for one cycle, and part (e) is the velocity-force phase-plane comparison of the measured force (solid line) and the predicted force (dash-dot line), for one cycle.

Dataset:usc\_5300\_q4

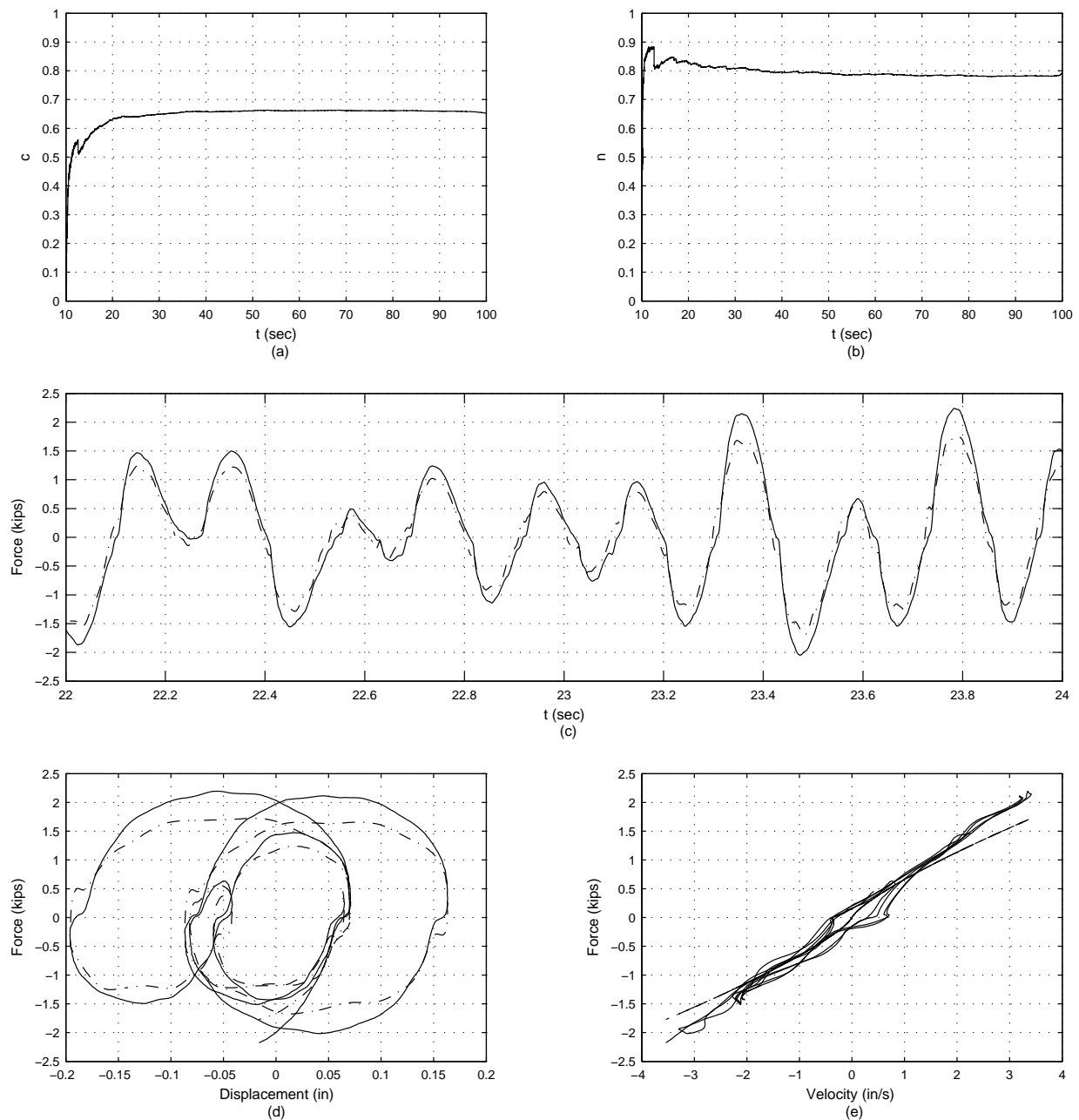


Figure F.7: On-line parametric identification results of the 15 kip damper for data set usc\_5300\_q4. Part (a) and (b) show the filtered time-history of the unknown parameters, part (c) shows the time-history comparison of the measured force (solid line) and the predicted force (dash-dot line), part (d) is the displacement-force phase-plane comparison of the measured force (solid line) and the predicted force (dash-dot line), for one cycle, and part (e) is the velocity-force phase-plane comparison of the measured force (solid line) and the predicted force (dash-dot line), for one cycle.

Dataset:usc\_5400\_q4

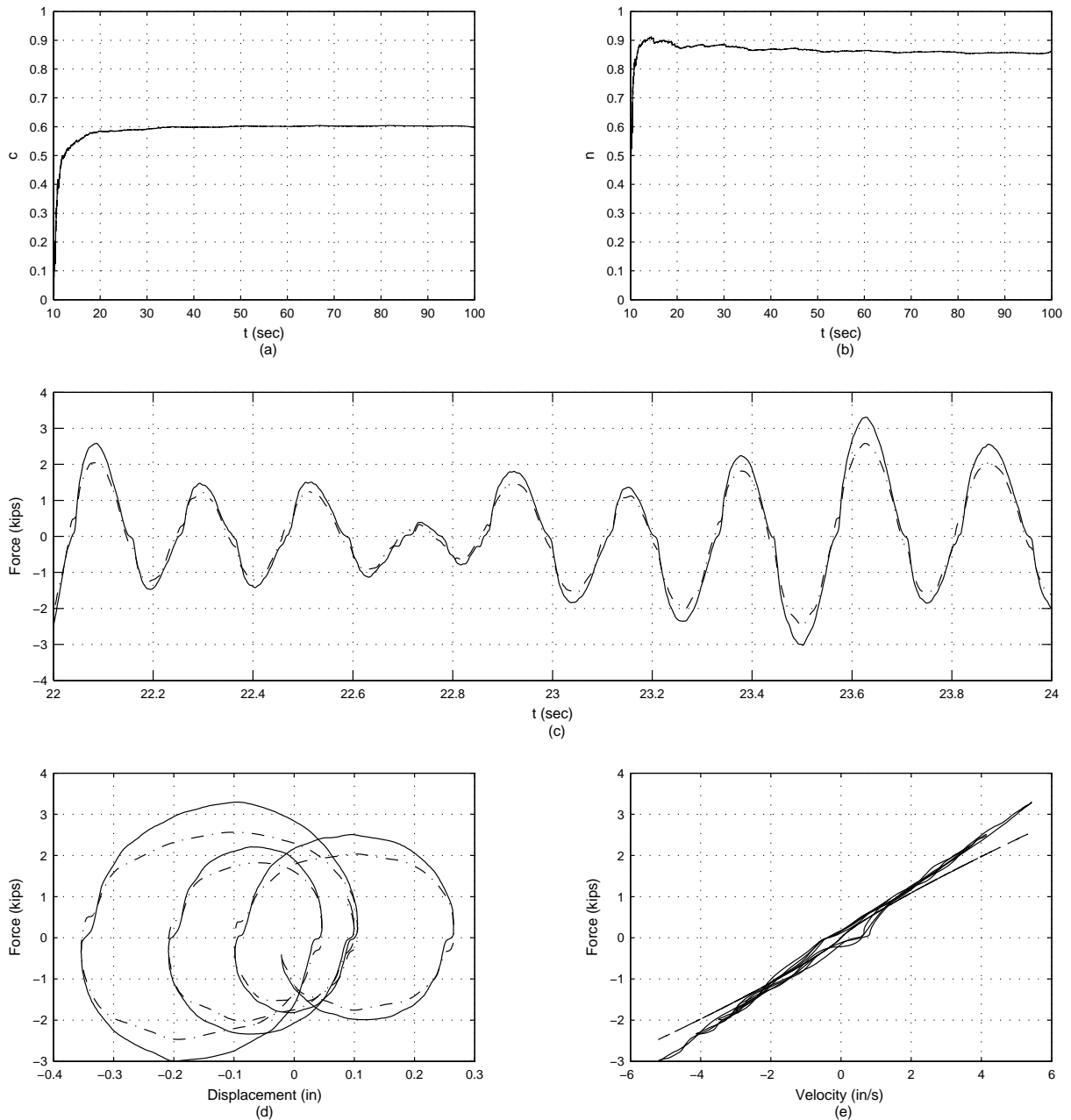


Figure F.8: On-line parametric identification results of the 15 kip damper for data set usc\_5400\_q4. Part (a) and (b) show the filtered time-history of the unknown parameters, part (c) shows the time-history comparison of the measured force (solid line) and the predicted force (dash-dot line), part (d) is the displacement-force phase-plane comparison of the measured force (solid line) and the predicted force (dash-dot line), for one cycle, and part (e) is the velocity-force phase-plane comparison of the measured force (solid line) and the predicted force (dash-dot line), for one cycle.

### F.2.2 Off-Line Parametric Identification Plots

The off-line parametric identification results of the 15 kip damper for the second round of testing are summarized in Table F.6, where column 1 is the data set name, columns 2 to 6 give the optimum values of the initially unknown parameters for the optimization model (Eqn. 2.10), and the last column is the normalized mean-square-error value of the difference between the predicted force and the measured force.

Table F.6: Summary of the off-line parametric identification results of the 15 kip damper for the data sets in the second round of testing. Column 1 is the data set name, columns 2 to 7 are the unknown parameters (Eqn. 2.11), column 8 is the normalized mean-square-error (Eqn. 2.9).

Data set	$c$ (kip sec/in)	$k$ (kip/in)	$n$	$\theta_1$	$\theta_2$	$\theta_3$	% MSE
usc_10175_q4	0.56	0.09	1.90	23.74	-411.40	153.80	3.26
usc_10200_q4	0.52	0.00	1.93	13.24	-362.80	162.00	3.28
usc_5300_q4	0.58	0.00	1.92	12.99	-402.80	164.10	2.47
usc_5400_q4	0.55	0.00	1.93	12.20	-384.60	163.10	2.38

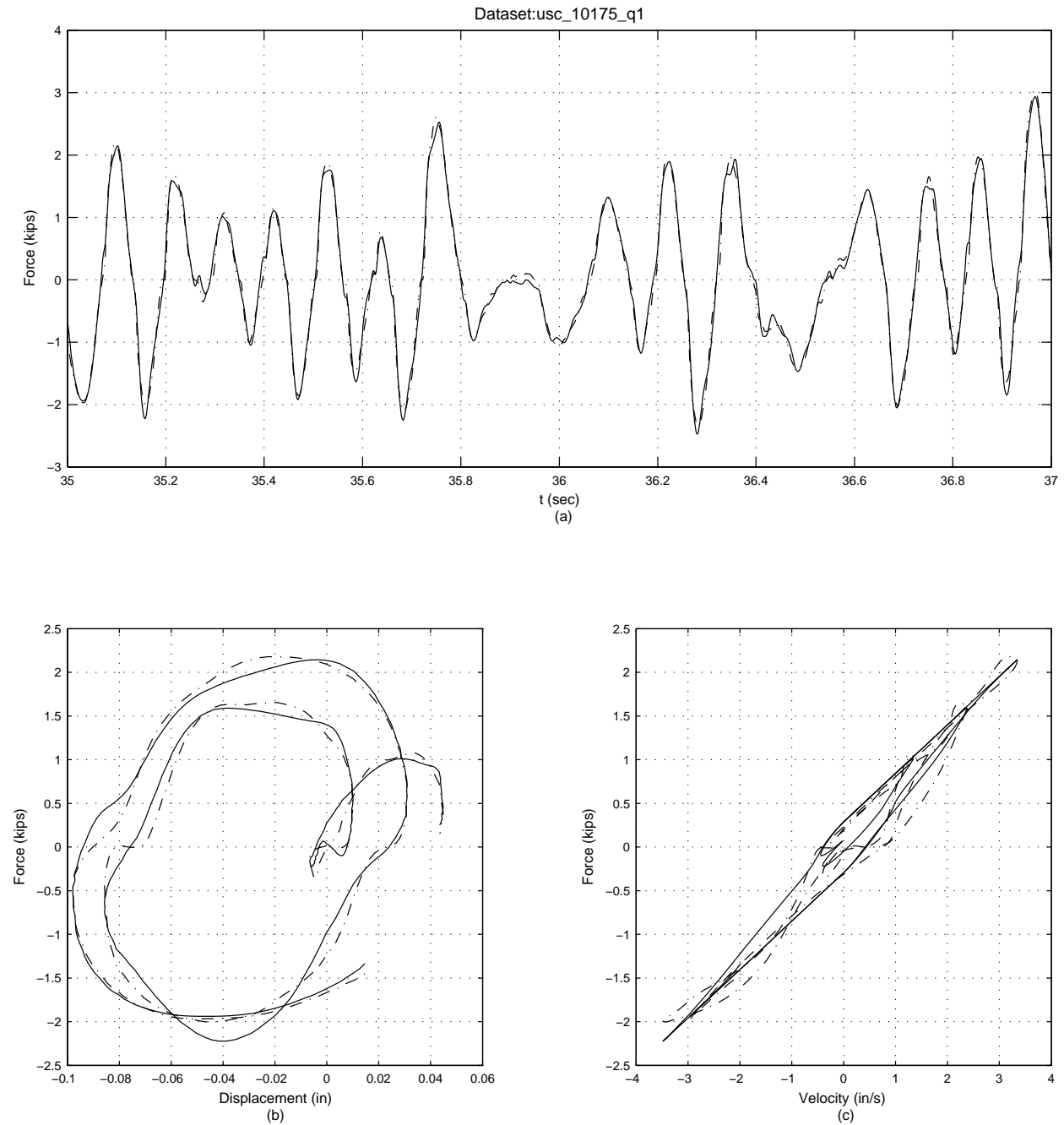


Figure F.9: Off-line parametric identification results of the 15 kip damper for data set usc\_10175\_q4. Part (a) shows the time-history comparison of the measured force (solid line) and the predicted force (dash-dot line), part (b) shows the displacement-force phase-plane comparison of the measured force (solid line) and the predicted force (dash-dot line), for one cycle, and part (c) shows the velocity-force phase-plane comparison of the measured force (solid line) and the predicted force (dash-dot line), for one cycle.

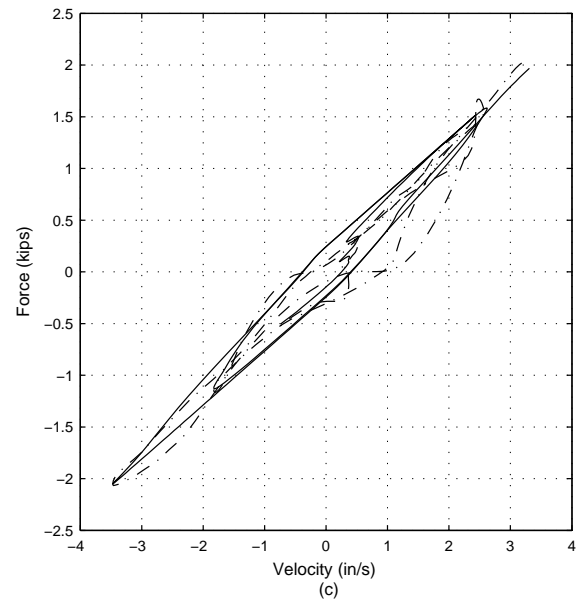
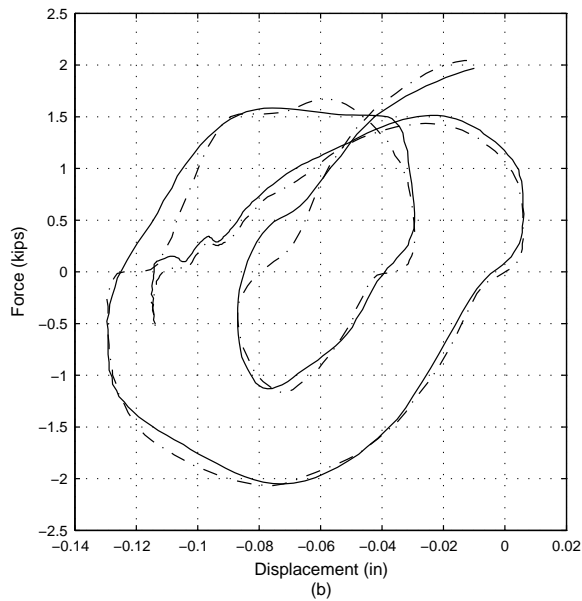
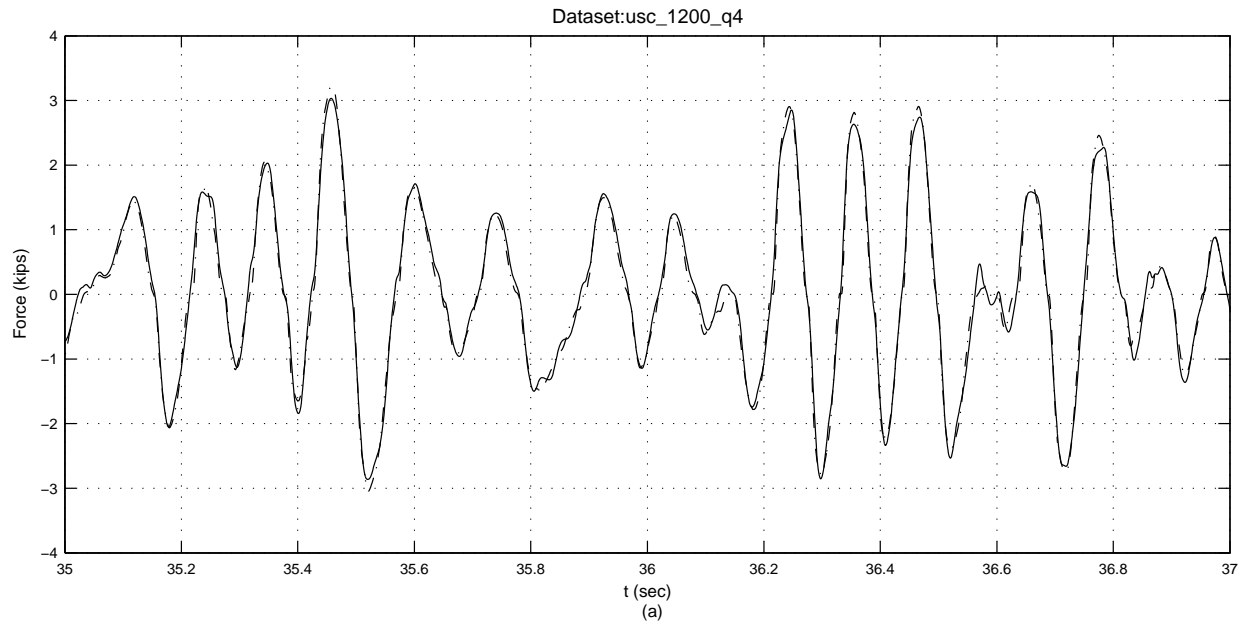


Figure F.10: Off-line parametric identification results of the 15 kip damper for data set usc\_10200\_q4. Part (a) shows the time-history comparison of the measured force (solid line) and the predicted force (dash-dot line), part (b) shows the displacement-force phase-plane comparison of the measured force (solid line) and the predicted force (dash-dot line), for one cycle, and part (c) shows the velocity-force phase-plane comparison of the measured force (solid line) and the predicted force (dash-dot line), for one cycle.

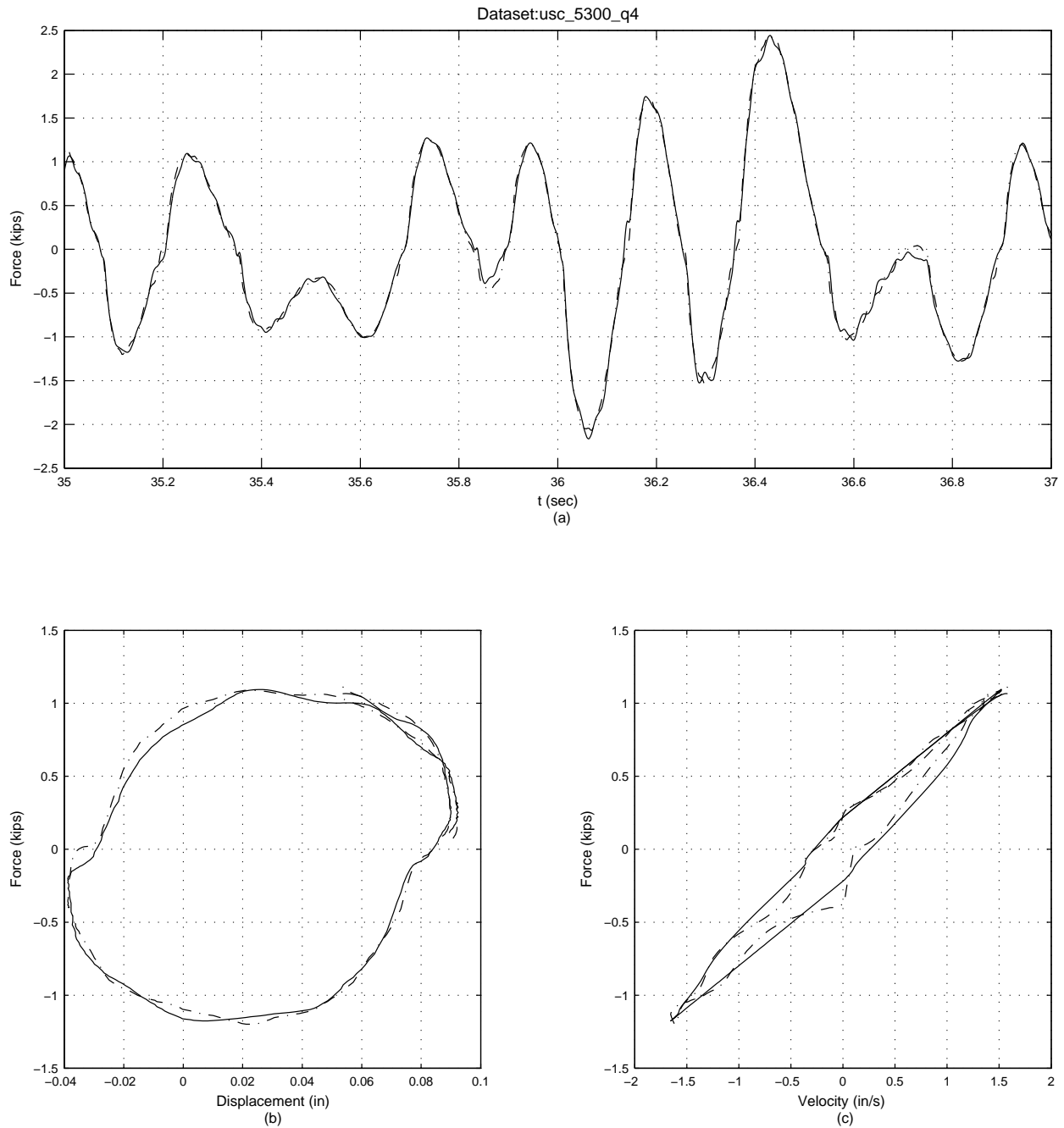


Figure F.11: Off-line parametric identification results of the 15 kip damper for data set usc\_5300\_q4. Part (a) shows the time-history comparison of the measured force (solid line) and the predicted force (dash-dot line), part (b) shows the displacement-force phase-plane comparison of the measured force (solid line) and the predicted force (dash-dot line), for one cycle, and part (c) shows the velocity-force phase-plane comparison of the measured force (solid line) and the predicted force (dash-dot line), for one cycle.

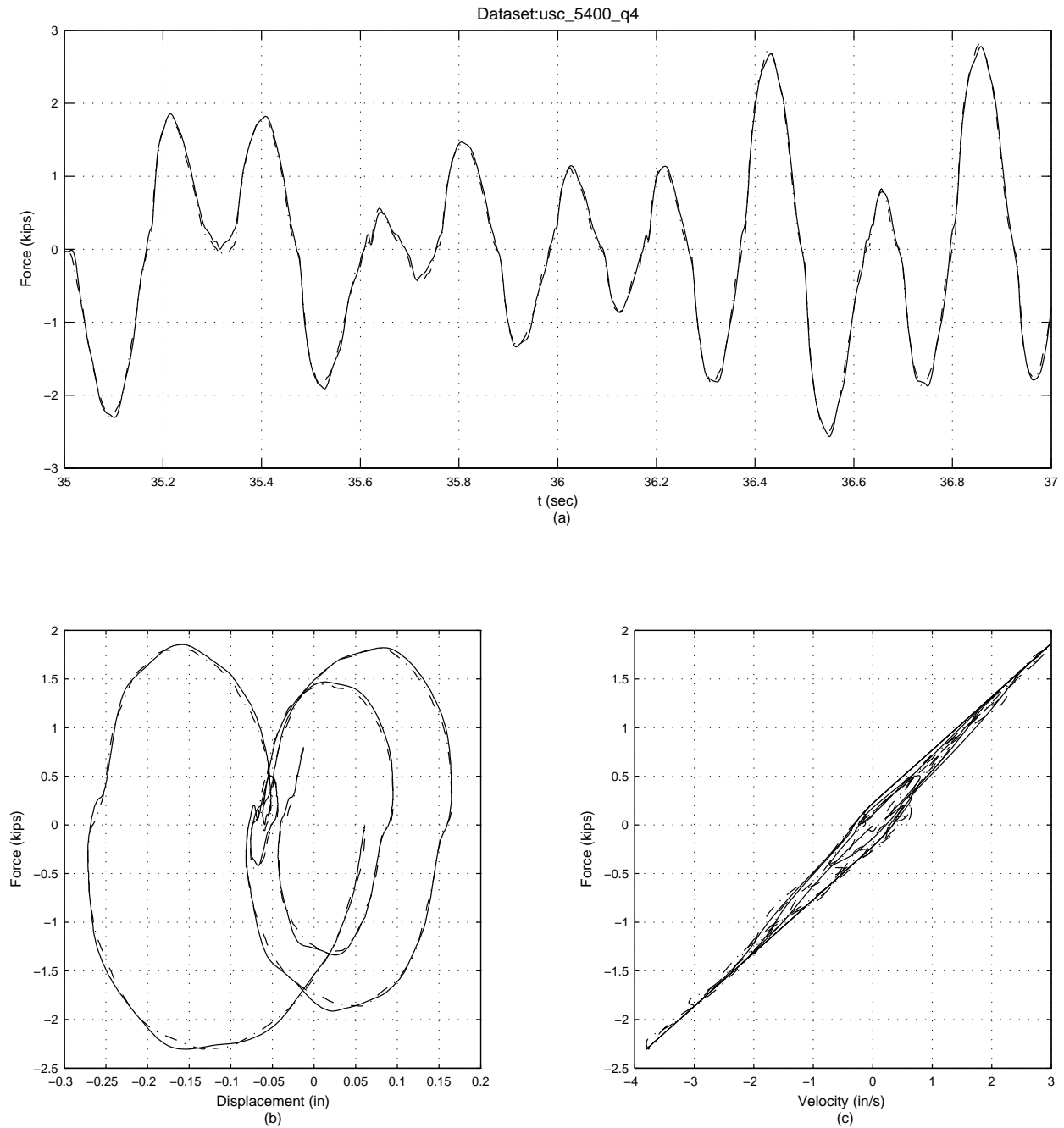


Figure F.12: Off-line parametric identification results of the 15 kip damper for data set usc\_5400\_q4. Part (a) shows the time-history comparison of the measured force (solid line) and the predicted force (dash-dot line), part (b) shows the displacement-force phase-plane comparison of the measured force (solid line) and the predicted force (dash-dot line), for one cycle, and part (c) shows the velocity-force phase-plane comparison of the measured force (solid line) and the predicted force (dash-dot line), for one cycle.



## Appendix G

# NONPARAMETRIC IDENTIFICATION RESULTS FOR THE 15 KIP VISCOUS DAMPER

### G.1 Restoring Force Method

#### G.1.1 Comparison of Measured and Identified Force for the 15 Kip Damper Using RFM

The plot comparisons of the measured and the identified force for a selected data set of the 15 kip viscous damper using the restoring force method are shown in this section (Figs. G.1 to G.10).

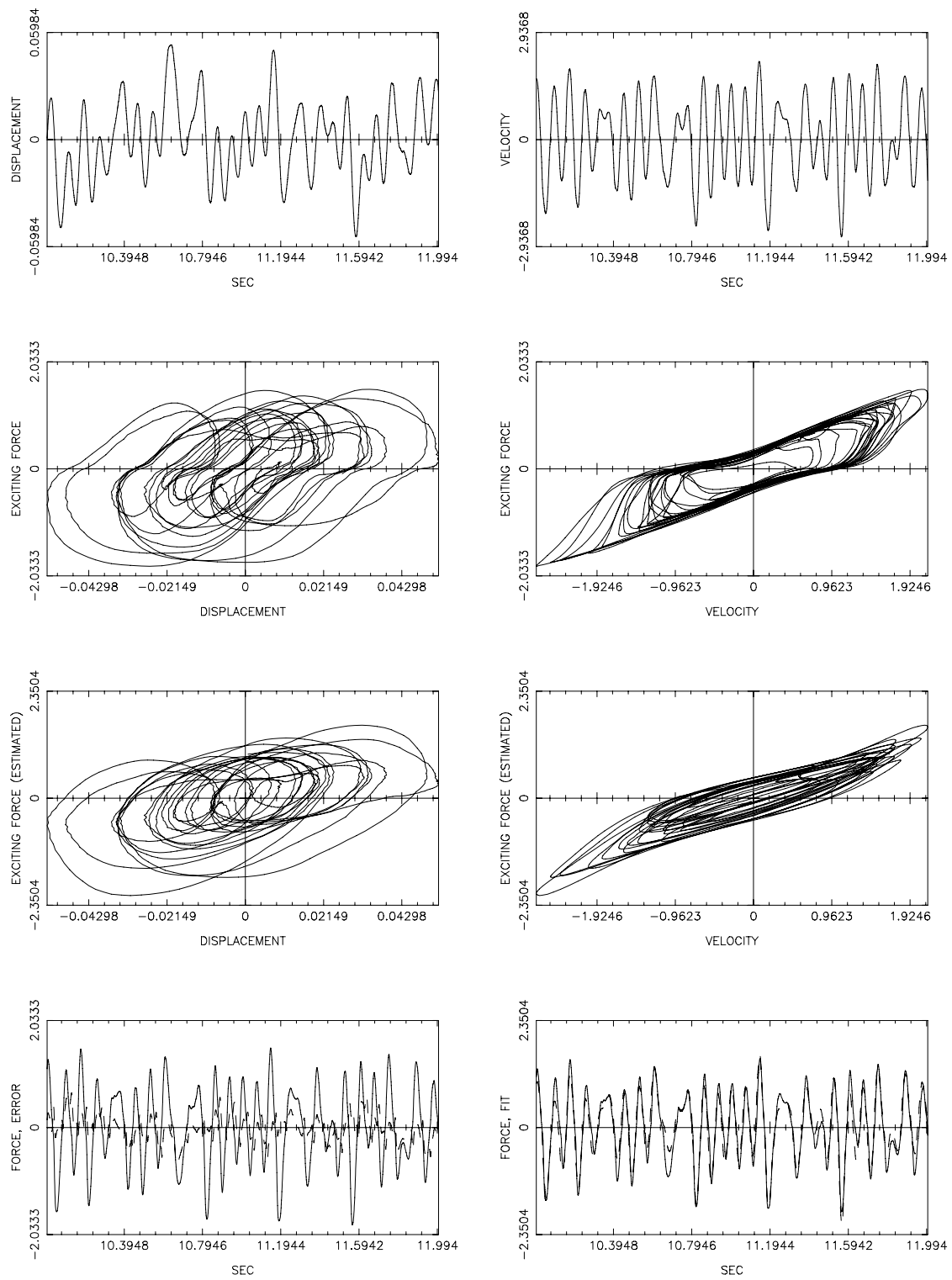


Figure G.1: Comparison of the measured and identified damper response using RFM for the data set Qtr1.01, segment No. 1.

## Restoring Force Method Analysis Results

---

Process Name	=	UCB-QTR1-01
Process Symbol	=	A00
Process Number	=	001
File Name	=	TBLA00001.ps
Process Date	=	Feb-02-2004 Mon
Process Time	=	03:32:11 PM

---

Starting data point	=	10001
Ending data point	=	12000
Data point increment	=	1
Min. displacement	=	-0.05
Max. displacement	=	0.05
Min. velocity	=	-2.67
Max. velocity	=	2.14
RMS level	=	0.73
Normalized RMS error	=	0.32

---

## Normalized Chebyshev Coefficients

I/J	0	1	2	3
0	-0.225	1.580	-0.097	0.167
1	0.464	0.000	-0.070	0.027
2	-0.023	0.061	0.013	0.067
3	-0.053	-0.008	0.087	-0.014

## Normalized Power Series Coefficients

I/J	0	1	2	3
0	-0.092	1.219	-0.220	0.399
1	0.957	-0.185	-0.664	0.280
2	-0.072	-0.277	0.051	0.533
3	-0.564	0.140	0.699	-0.231

## De-Normalized Power Series Coefficients

I/J	0	1	2	3
0	0.052	0.491	-0.017	0.029
1	17.250	-2.529	-1.821	0.393
2	-42.190	-33.940	14.990	13.050
3	-3486.000	764.500	695.100	-106.800

Figure G.2: Summary of the RFM identification of the 15 kip damper subjected to broadband excitation for the data set Qtr1\_01, segment No. 1.

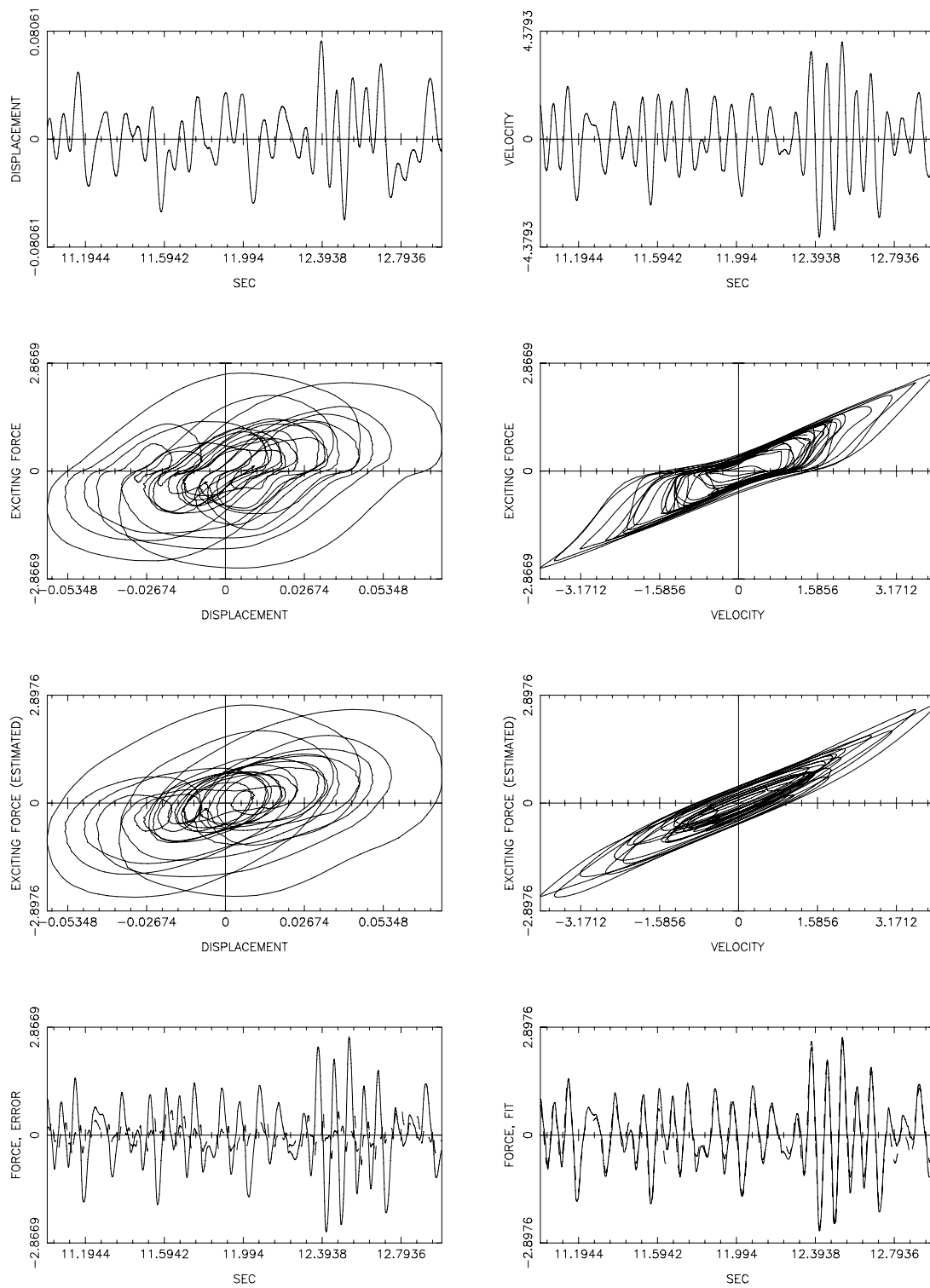


Figure G.3: Comparison of the measured and identified damper response using RFM for the data set Qtr1.01, segment No. 2.

## Restoring Force Method Analysis Results

---

Process Name	=	UCB-QTR1-01
Process Symbol	=	A00
Process Number	=	002
File Name	=	TBLA00002.ps
Process Date	=	Feb-02-2004 Mon
Process Time	=	03:33:28 PM

---

Starting data point	=	11001
Ending data point	=	13000
Data point increment	=	1

Min. displacement	=	-0.06
Max. displacement	=	0.07
Min. velocity	=	-3.98
Max. velocity	=	3.95
RMS level	=	0.88
Normalized RMS error	=	0.28

---

## Normalized Chebyshev Coefficients

I/J	0	1	2	3
0	-0.029	2.484	0.009	0.106
1	0.503	0.010	-0.061	-0.011
2	-0.086	0.047	-0.004	-0.028
3	-0.049	0.011	0.075	-0.039

## Normalized Power Series Coefficients

I/J	0	1	2	3
0	0.044	2.033	0.028	0.539
1	0.938	-0.342	-0.575	0.424
2	-0.164	0.264	-0.017	-0.227
3	-0.498	0.512	0.603	-0.622

## De-Normalized Power Series Coefficients

I/J	0	1	2	3
0	-0.038	0.522	0.006	0.008
1	14.270	-1.446	-0.522	0.108
2	-4.425	6.424	-2.739	-0.168
3	-1659.000	437.000	126.700	-33.460

Figure G.4: Summary of the RFM identification of the 15 kip damper subjected to broadband excitation for the data set Qtr1.01, segment No. 2.

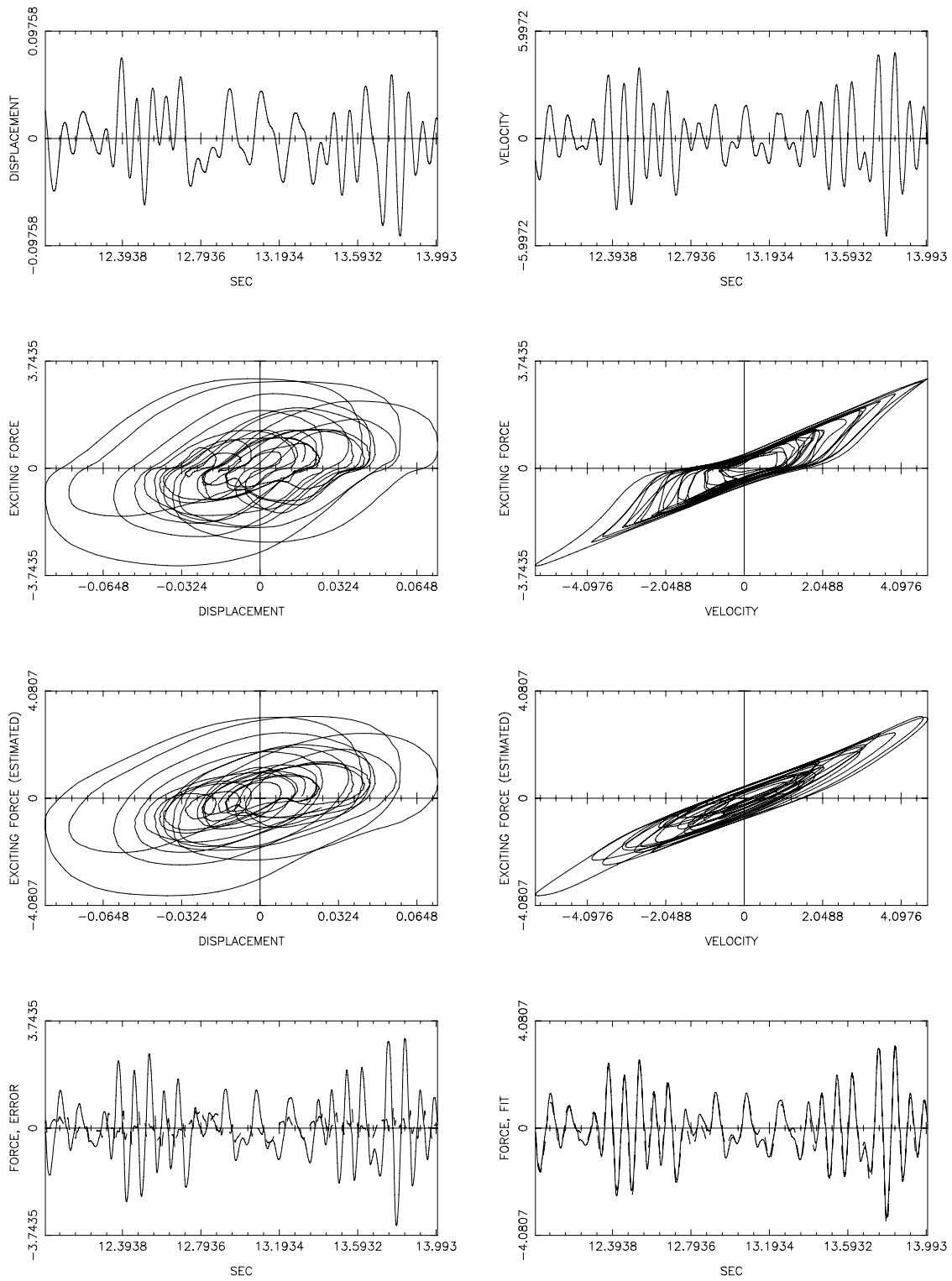


Figure G.5: Comparison of the measured and identified damper response using RFM for the data set Qtr1\_01, segment No. 3.

## Restoring Force Method Analysis Results

---

```

Process Name      =   UCB-QTR1-01
Process Symbol    =   A00
Process Number    =   003
File Name        =   TBLA00003.ps
Process Date     =   Feb-02-2004 Mon
Process Time     =   03:34:43 PM

```

---

```

Starting data point = 12001
Ending data point   = 14000
Data point increment = 1

Min. displacement   = -0.09
Max. displacement   = 0.07
Min. velocity       = -5.45
Max. velocity       = 4.79
RMS level           = 1.10
Normalized RMS error = 0.23

```

---

## Normalized Chebyshev Coefficients

I/J	0	1	2	3
0	-0.356	3.164	-0.003	0.144
1	0.607	0.046	-0.071	-0.043
2	-0.066	0.003	-0.022	0.036
3	-0.123	-0.007	0.082	-0.049

## Normalized Power Series Coefficients

I/J	0	1	2	3
0	-0.308	2.838	0.037	0.431
1	1.293	-0.246	-0.633	0.416
2	-0.089	-0.210	-0.087	0.289
3	-0.819	0.560	0.654	-0.783

## De-Normalized Power Series Coefficients

I/J	0	1	2	3
0	-0.006	0.550	0.003	0.004
1	15.230	-0.836	-0.256	0.041
2	-49.660	-1.066	0.655	0.074
3	-1469.000	233.300	36.090	-10.960

Figure G.6: Summary of the RFM identification of the 15 kip damper subjected to broadband excitation for the data set Qtr1\_01, segment No. 3.

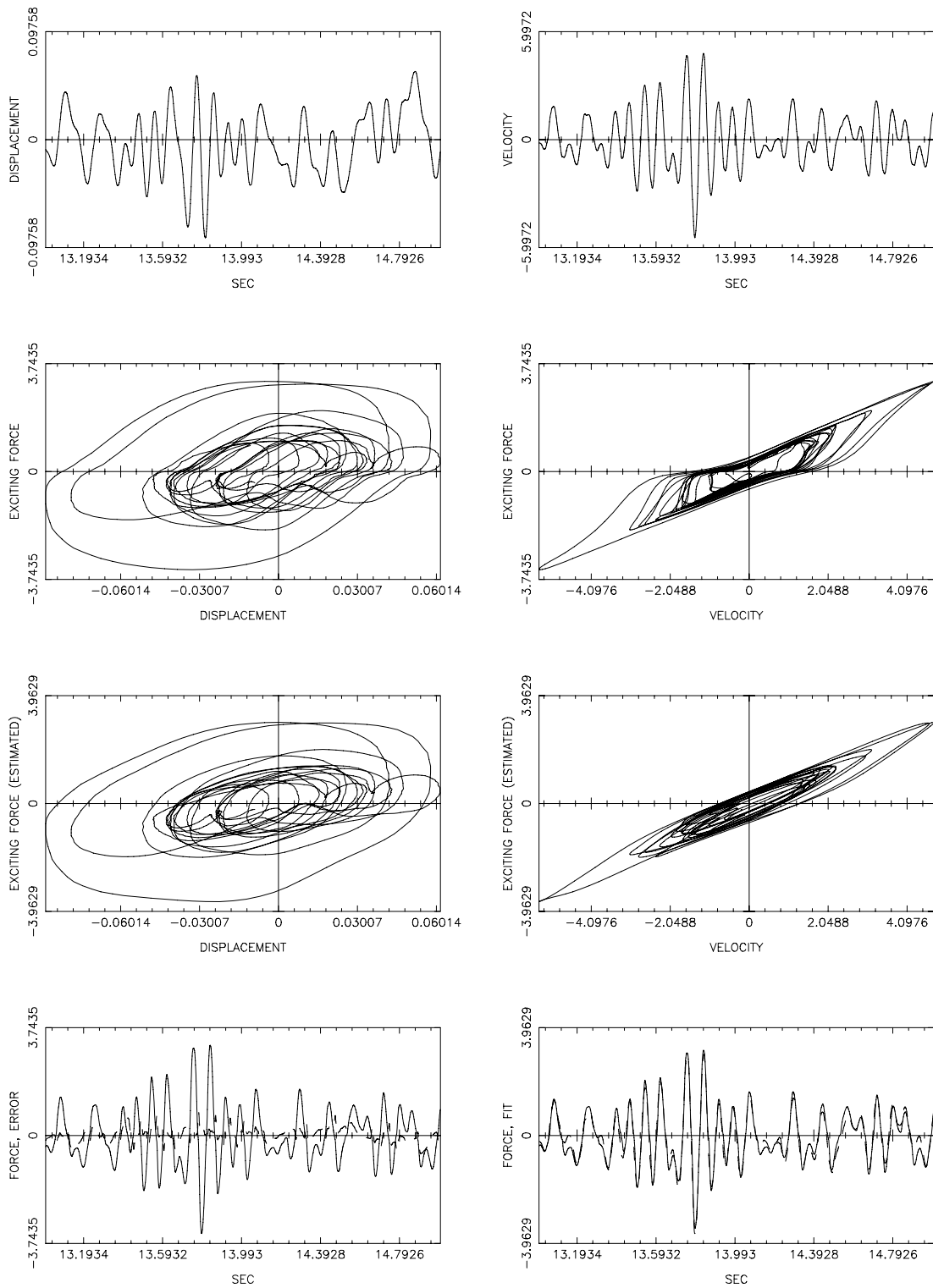


Figure G.7: Comparison of the measured and identified damper response using RFM for the data set Qtr1.01, segment No. 4.

## Restoring Force Method Analysis Results

---

Process Name	=	UCB-QTR1-01
Process Symbol	=	A00
Process Number	=	004
File Name	=	TBLA00004.ps
Process Date	=	Feb-02-2004 Mon
Process Time	=	03:36:04 PM

---

Starting data point	=	13001
Ending data point	=	15000
Data point increment	=	1

Min. displacement	=	-0.09
Max. displacement	=	0.06
Min. velocity	=	-5.45
Max. velocity	=	4.79
RMS level	=	0.99
Normalized RMS error	=	0.24

---

Normalized Chebyshev Coefficients				
I/J	0	1	2	3
0	-0.349	3.157	-0.025	0.119
1	0.560	0.055	-0.089	-0.039
2	0.003	-0.025	-0.031	0.016
3	0.000	-0.039	0.136	-0.038

Normalized Power Series Coefficients				
I/J	0	1	2	3
0	-0.357	2.874	0.012	0.410
1	1.058	-0.051	-0.996	0.295
2	0.067	-0.148	-0.123	0.131
3	-0.545	0.298	1.091	-0.603

De-Normalized Power Series Coefficients				
I/J	0	1	2	3
0	0.016	0.556	-0.003	0.003
1	13.570	-0.498	-0.446	0.028
2	-39.720	2.445	2.890	-0.257
3	-1227.000	198.000	87.420	-10.560

Figure G.8: Summary of the RFM identification of the 15 kip damper subjected to broadband excitation for the data set Qtr1\_01, segment No. 4.

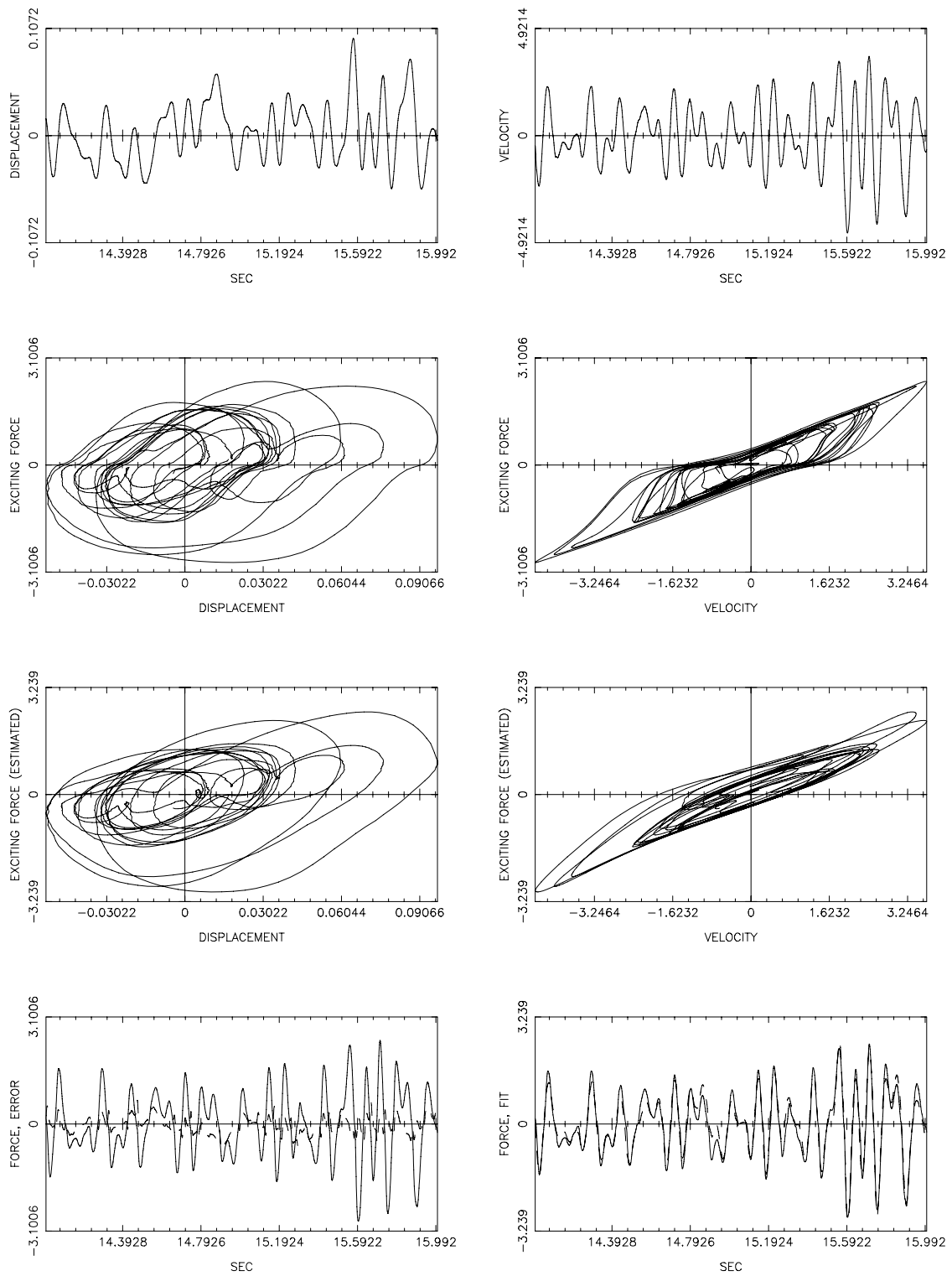


Figure G.9: Comparison of the measured and identified damper response using RFM for the data set Qtr1\_01, segment No. 5.

## Restoring Force Method Analysis Results

---

Process Name	=	UCB-QTR1-01
Process Symbol	=	A00
Process Number	=	005
File Name	=	TBLA00005.ps
Process Date	=	Feb-02-2004 Mon
Process Time	=	03:37:28 PM

---

Starting data point	=	14001
Ending data point	=	16000
Data point increment	=	1

Min. displacement	=	-0.05
Max. displacement	=	0.10
Min. velocity	=	-4.47
Max. velocity	=	3.64
RMS level	=	0.96
Normalized RMS error	=	0.26

---

## Normalized Chebyshev Coefficients

I/J	0	1	2	3
0	-0.088	2.424	-0.149	0.174
1	0.656	-0.058	-0.055	0.082
2	0.053	-0.018	0.079	0.083
3	-0.070	-0.003	0.062	0.018

## Normalized Power Series Coefficients

I/J	0	1	2	3
0	0.087	2.168	-0.456	0.366
1	1.106	-0.136	-0.481	0.115
2	-0.052	-0.535	0.318	0.664
3	-0.525	-0.223	0.493	0.283

## De-Normalized Power Series Coefficients

I/J	0	1	2	3
0	-0.006	0.522	-0.011	0.006
1	13.360	0.002	-0.483	-0.039
2	64.700	-15.130	0.183	1.097
3	-1258.000	-64.310	81.680	9.805

Figure G.10: Summary of the RFM identification of the 15 kip damper subjected to broadband excitation for the data set Qtr1.01, segment No. 5.

### **G.1.2 Histograms of Chebyshev and Power Series Coefficients for the 15 Kip Damper**

The histograms of the Chebyshev and power series coefficients of the 15 kip damper the second round of testing are shown in this section (Figs. G.11 to G.18).

PROCESS NAME : UCB-QTR1-01  
 PROCESS SYMBOL: A00  
 PROCESS DATE : FEB-03-2004 TUE  
 NO. PROCESSES : 108  
 START DATA PTS: 10,000  
 END DATA PTS : 119,000  
 DATA INCREMENT: 1  
 DATA OVERLAP : 50%

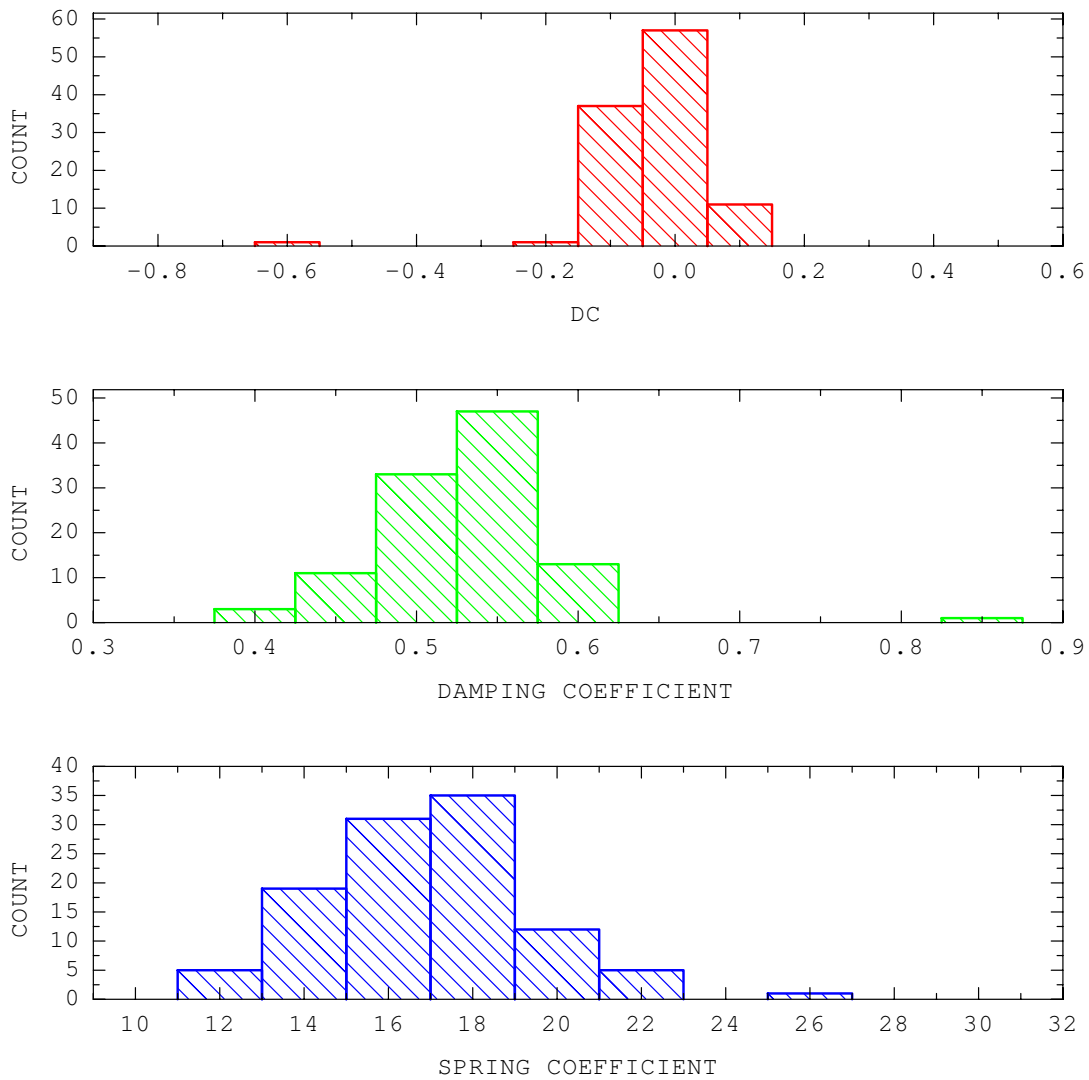


Figure G.11: Histogram of Chebyshev and power series coefficients for the data set Qtr1.01.

PROCESS NAME : UCB-QTR2-01  
 PROCESS SYMBOL: A04  
 PROCESS DATE : FEB-03-2004 TUE  
 NO. PROCESSES : 108  
 START DATA PTS: 10,000  
 END DATA PTS : 119,000  
 DATA INCREMENT: 1  
 DATA OVERLAP : 50%

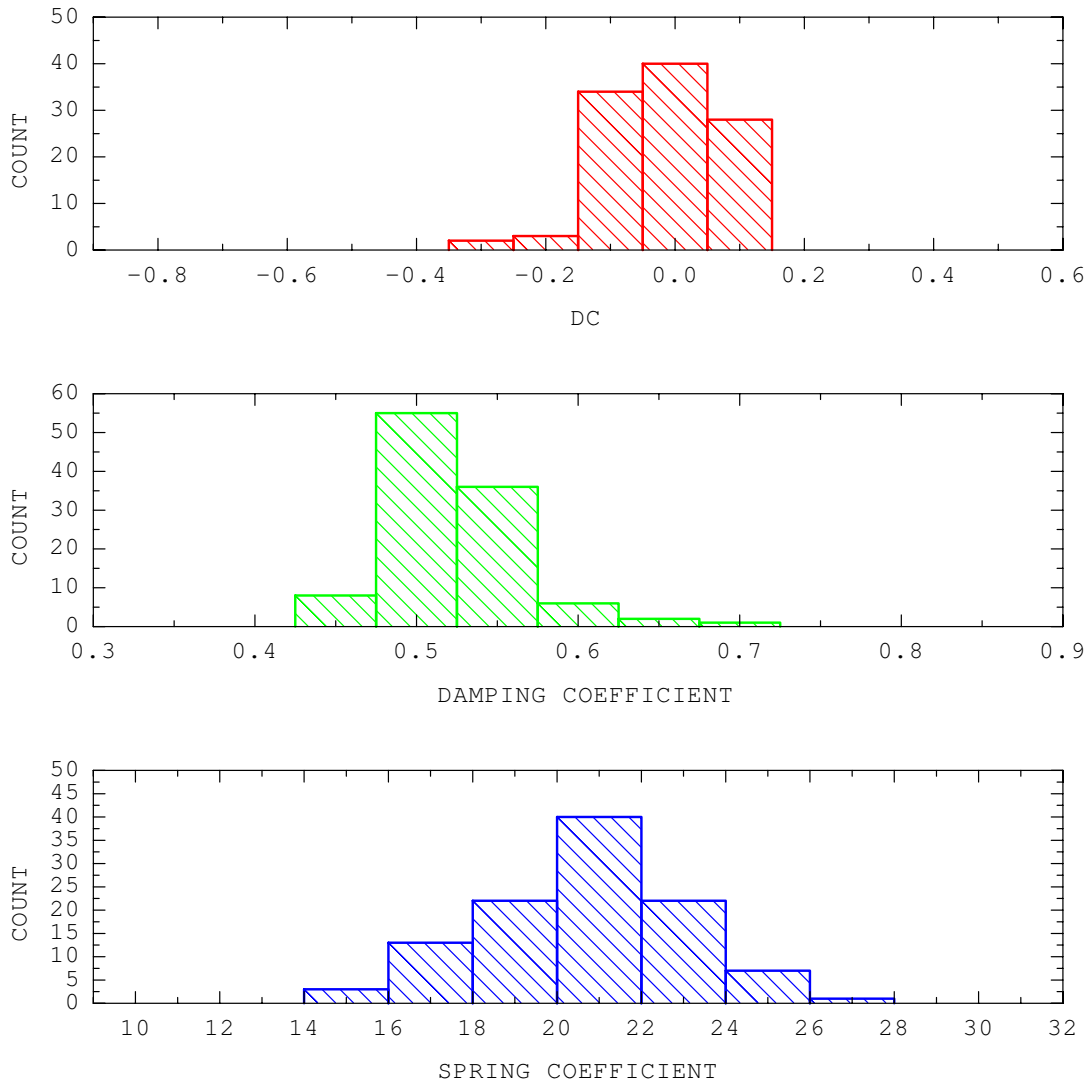


Figure G.12: Histogram of Chebyshev and power series coefficients for the data set Qtr2.01.

PROCESS NAME : UCB-QTR3-01  
 PROCESS SYMBOL: A06  
 PROCESS DATE : FEB-03-2004 TUE  
 NO. PROCESSES : 108  
 START DATA PTS: 10,000  
 END DATA PTS : 119,000  
 DATA INCREMENT: 1  
 DATA OVERLAP : 50%

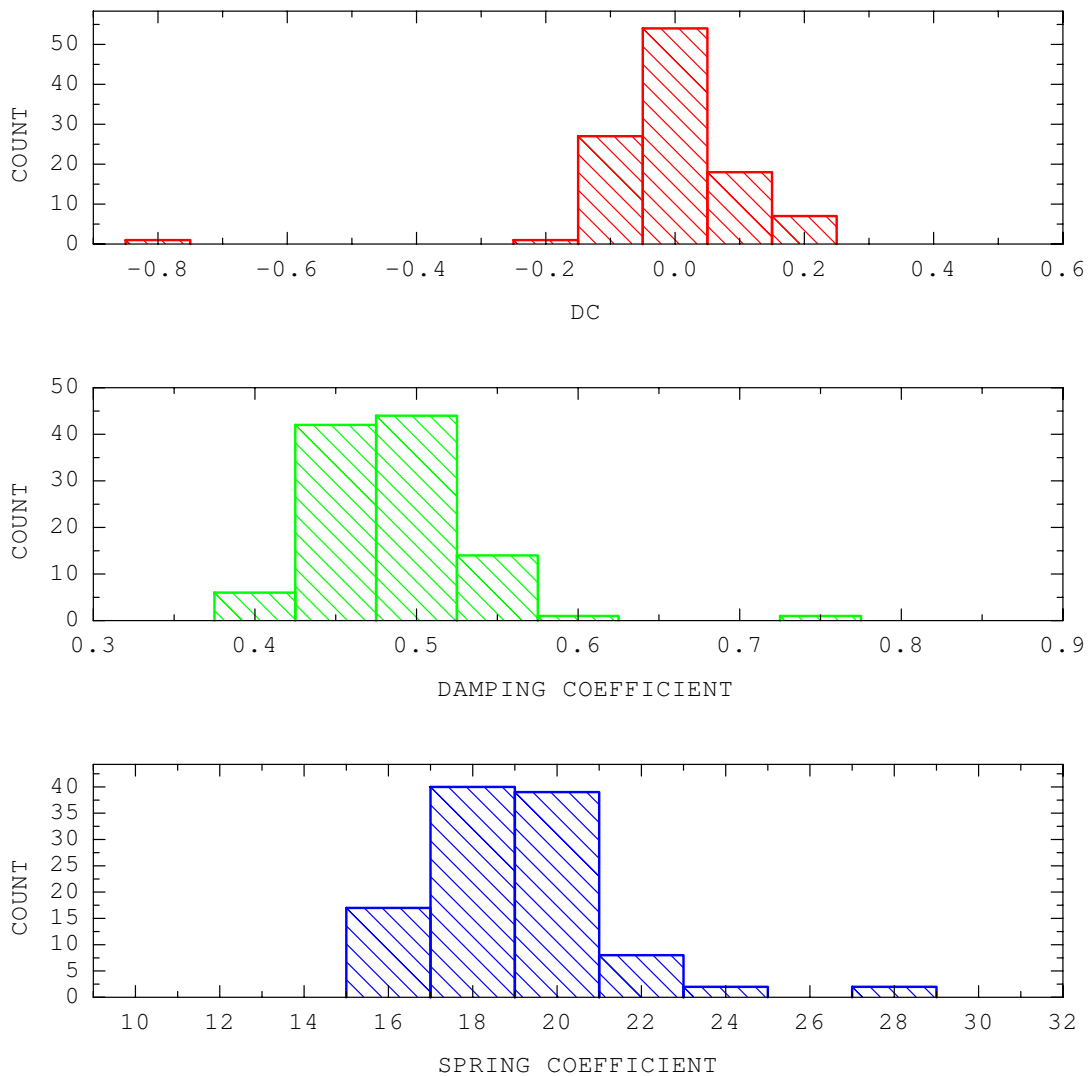


Figure G.13: Histogram of Chebyshev and power series coefficients for the data set Qtr3.01.

PROCESS NAME : UCB-QTR4-01  
 PROCESS SYMBOL: A08  
 PROCESS DATE : FEB-03-2004 TUE  
 NO. PROCESSES : 108  
 START DATA PTS: 10,000  
 END DATA PTS : 119,000  
 DATA INCREMENT: 1  
 DATA OVERLAP : 50%

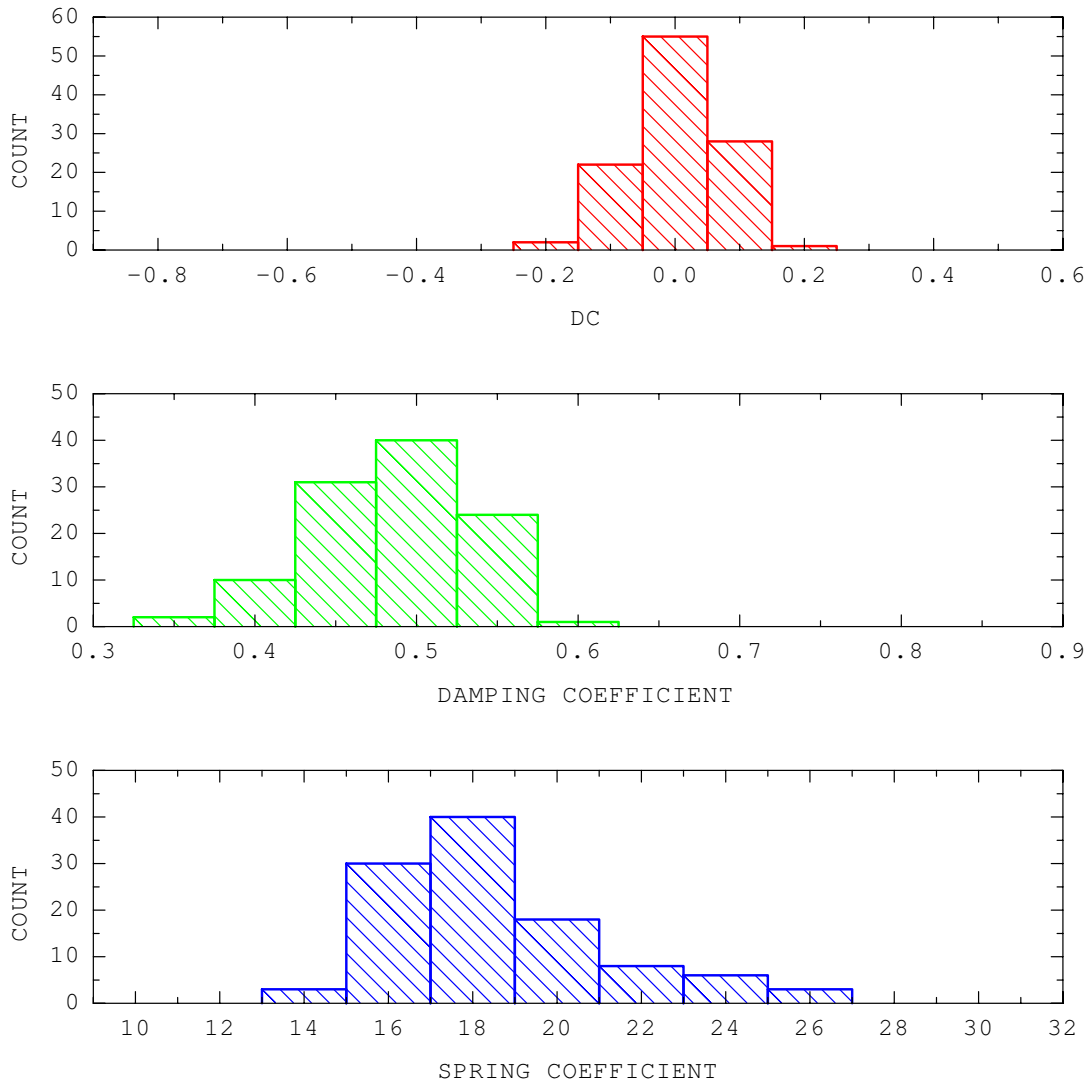


Figure G.14: Histogram of Chebyshev and power series coefficients for the data set Qtr4.01.

PROCESS NAME : UCB-QTR1-125  
 PROCESS SYMBOL: A03  
 PROCESS DATE : FEB-03-2004 TUE  
 NO. PROCESSES : 108  
 START DATA PTS: 10,000  
 END DATA PTS : 119,000  
 DATA INCREMENT: 1  
 DATA OVERLAP : 50%

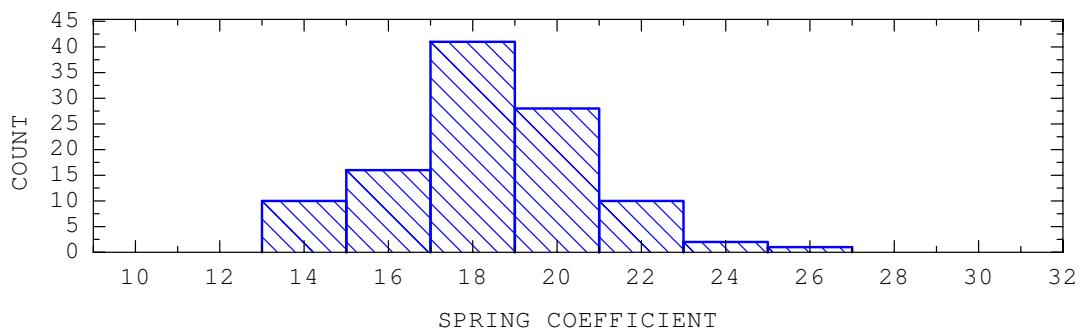
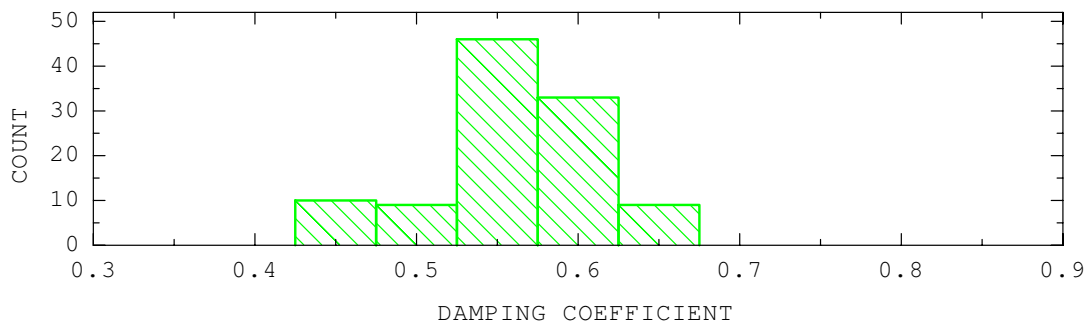
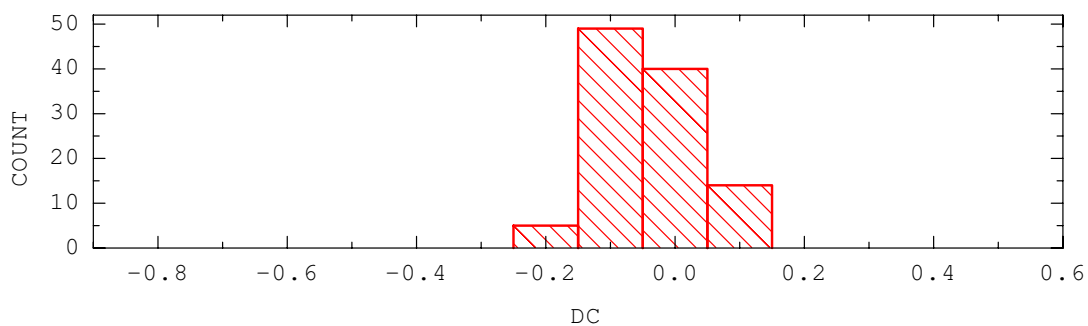


Figure G.15: Histogram of Chebyshev and power series coefficients for the data set Qtr1.0125.

PROCESS NAME : UCB-QTR2-125  
 PROCESS SYMBOL: A05  
 PROCESS DATE : FEB-03-2004 TUE  
 NO. PROCESSES : 107 (outlier #69 excluded)  
 START DATA PTS: 10,000  
 END DATA PTS : 119,000  
 DATA INCREMENT: 1  
 DATA OVERLAP : 50%

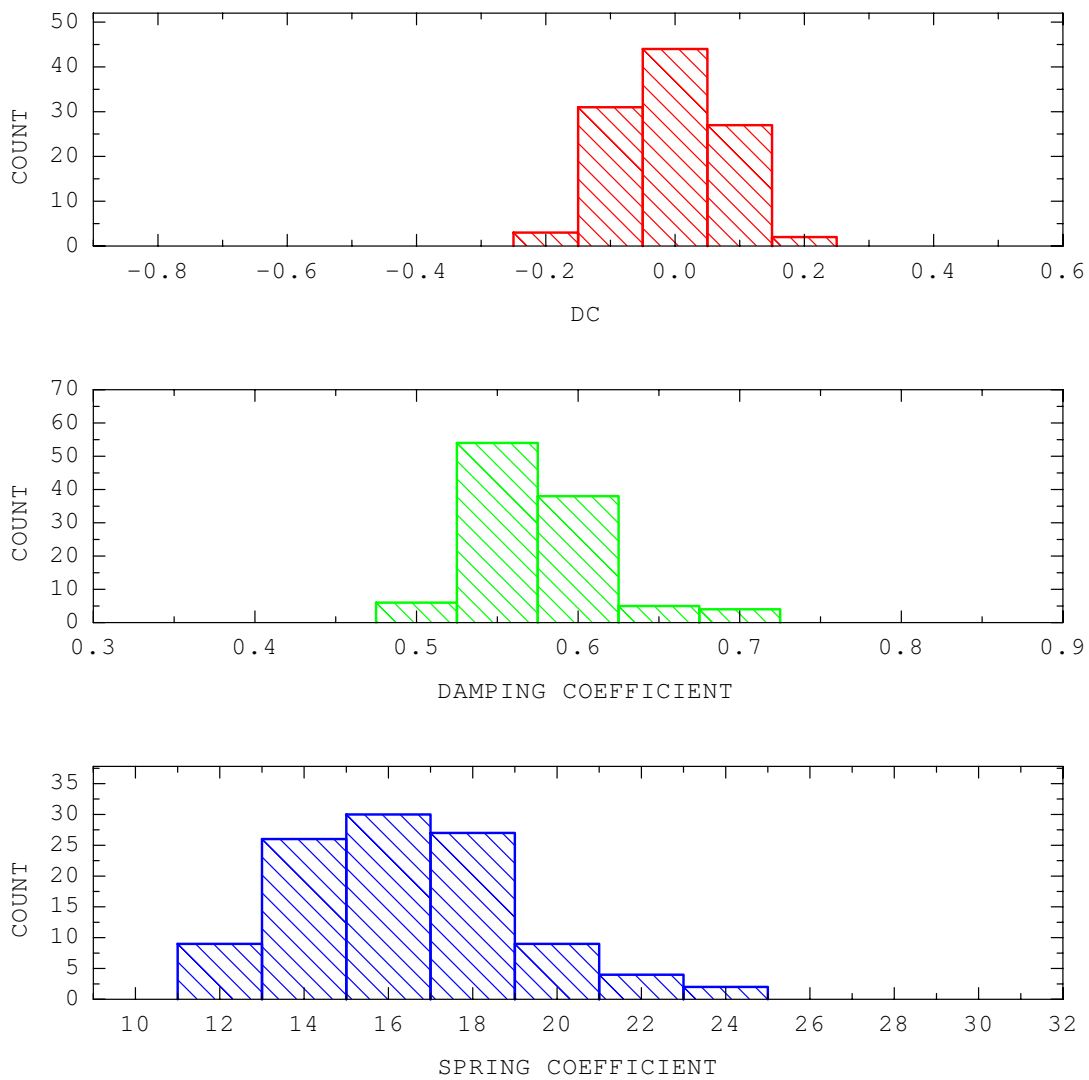


Figure G.16: Histogram of Chebyshev and power series coefficients for the data set Qtr2.0125.

PROCESS NAME : UCB-QTR3-125  
 PROCESS SYMBOL: A07  
 PROCESS DATE : FEB-03-2004 TUE  
 NO. PROCESSES : 105 (outliers #1, #90, #104 excluded)  
 START DATA PTS: 10,000  
 END DATA PTS : 119,000  
 DATA INCREMENT: 1  
 DATA OVERLAP : 50%

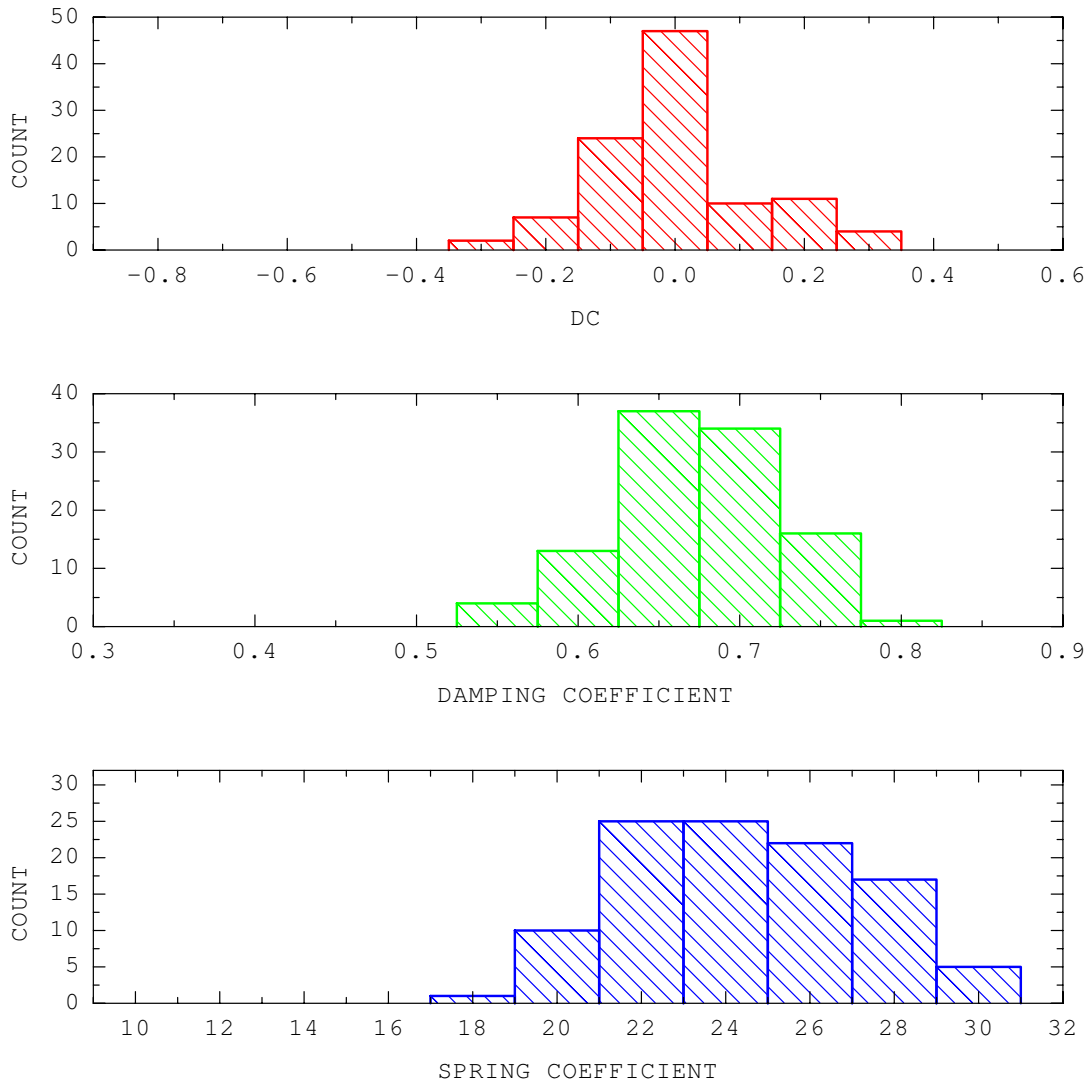


Figure G.17: Histogram of Chebyshev and power series coefficients for the data set Qtr3.0125.

PROCESS NAME : UCB-QTR4-125  
 PROCESS SYMBOL: A09  
 PROCESS DATE : FEB-03-2004 TUE  
 NO. PROCESSES : 108  
 START DATA PTS: 10,000  
 END DATA PTS : 119,000  
 DATA INCREMENT: 1  
 DATA OVERLAP : 50%

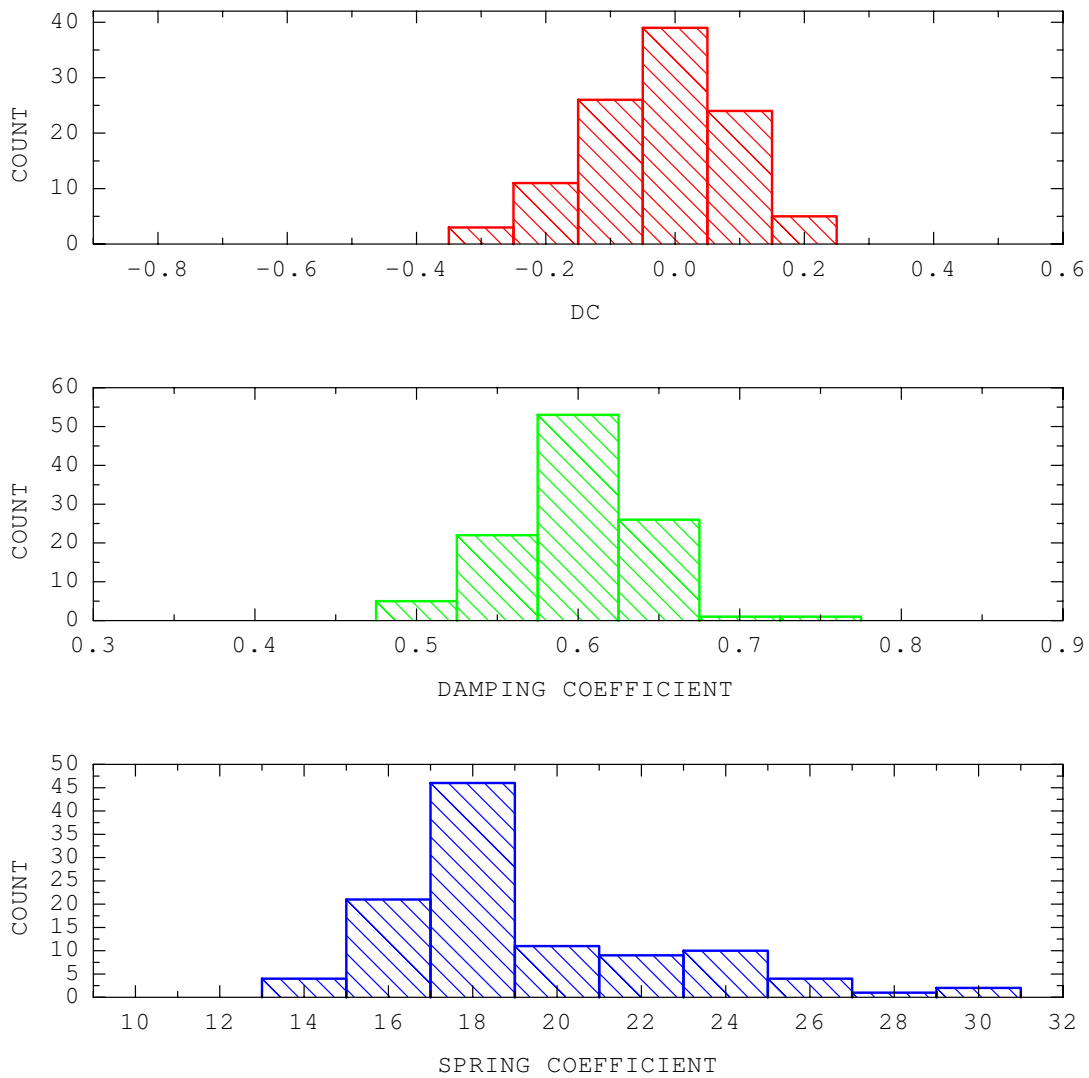


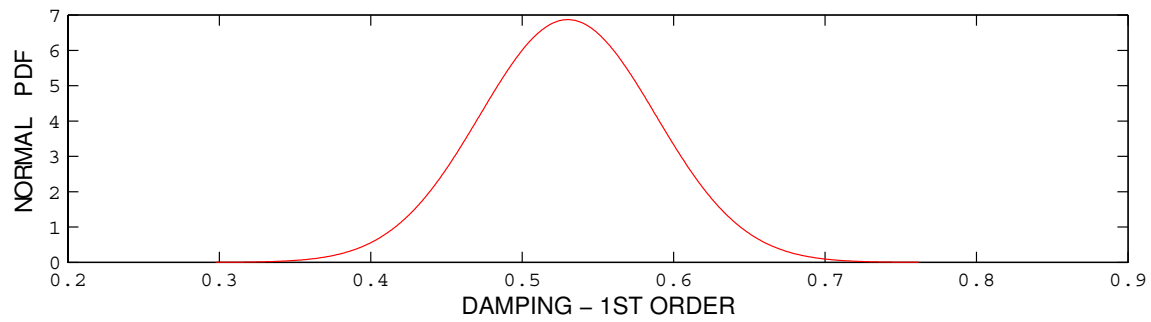
Figure G.18: Histogram of Chebyshev and power series coefficients for the data set Qtr4.0125.

Table G.1: The first and second order statistics of normalized Chebyshev coefficients of 15 kip viscous damper.

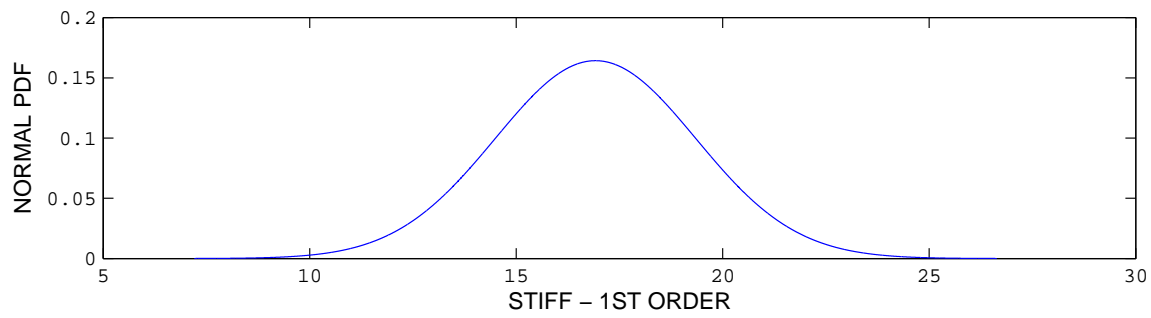
NO	Name	Coeff	Mean	STDV	Median	Max	Min
1	Qtr1_01	damp	0.5301	0.0581	0.5315	0.8620	0.3930
		stiff	16.9209	2.4287	16.9850	25.4500	11.9700
2	Qtr2_01	damp	0.5621	0.0494	0.5665	0.6750	0.4300
		stiff	18.3347	2.2832	18.5000	25.1900	13.4300
3	Qtr3_01	damp	0.5242	0.0419	0.5170	0.7000	0.4330
		stiff	20.6677	2.3276	21.0300	26.3600	14.9600
4	Qtr4_01	damp	0.5825	0.0805	0.5710	1.3020	0.4820
		stiff	15.7455	7.2014	16.3350	24.1800	-53.5800
5	Qtr1_0125	damp	0.4850	0.0455	0.4795	0.7450	0.3860
		stiff	19.0266	2.1301	18.8750	28.6600	15.1200
6	Qtr2_0125	damp	0.6865	0.1069	0.6735	1.3900	0.5380
		stiff	25.3739	6.3576	24.1900	72.2000	18.8900
7	Qtr3_0125	damp	0.4848	0.0460	0.4875	0.5810	0.3680
		stiff	18.5428	2.7797	17.8300	26.1000	13.2500
8	Qtr4_0125	damp	0.6008	0.0394	0.5985	0.7380	0.5150
		stiff	19.0851	3.2532	18.1450	30.2800	14.4000

### G.1.3 Probability Density Functions of Chebyshev Coefficients for the 15 Kip Damper

The probability density functions (pdf) determined from the histograms in Section G.1.2 are shown in this section (Figs G.19 to G.23). The first and second order statistics of the pdf's are summarized in Table G.1.

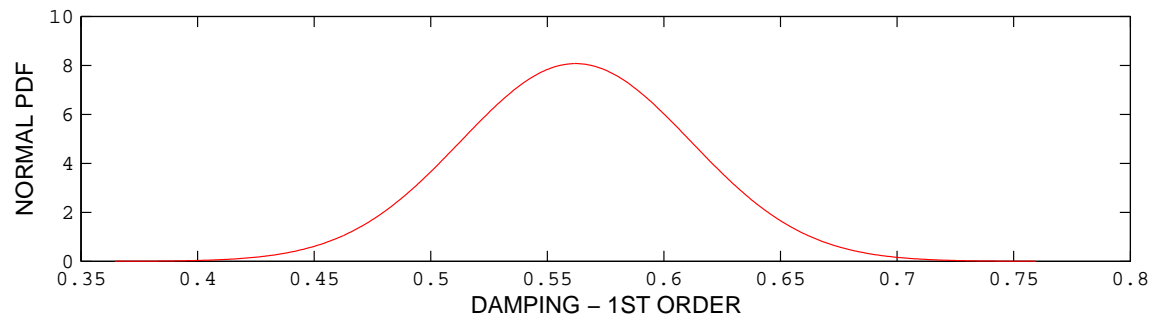


(a) First order damping coefficient

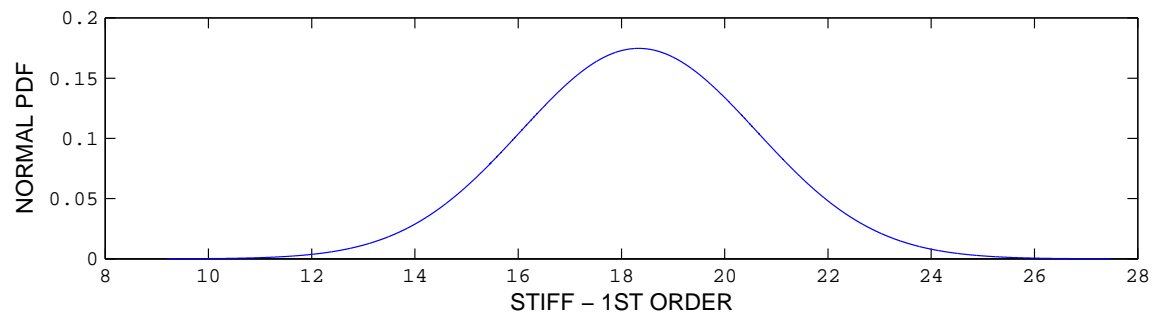


(b) First order stiffness coefficient

Figure G.19: Probability density function of the damping and stiffness Chebyshev coefficients for the data set Qtr1.01.

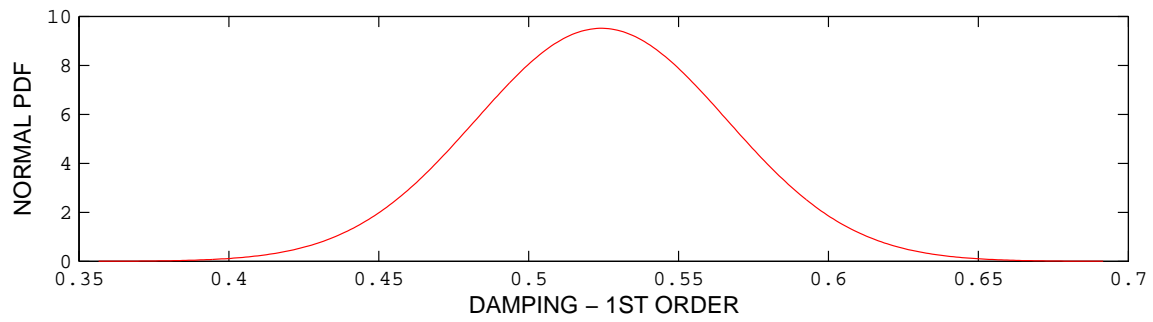


(a) First order damping coefficient

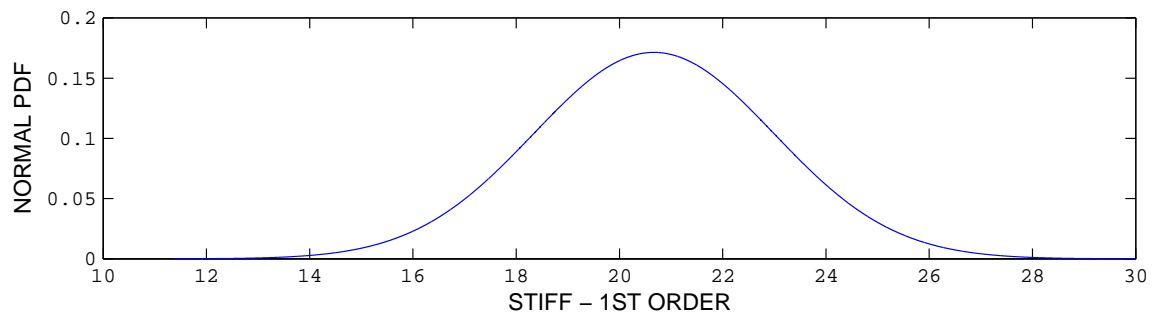


(b) First order stiffness coefficient

Figure G.20: Probability density function of the damping and stiffness Chebyshev coefficients for the data set Qtr2\_01.

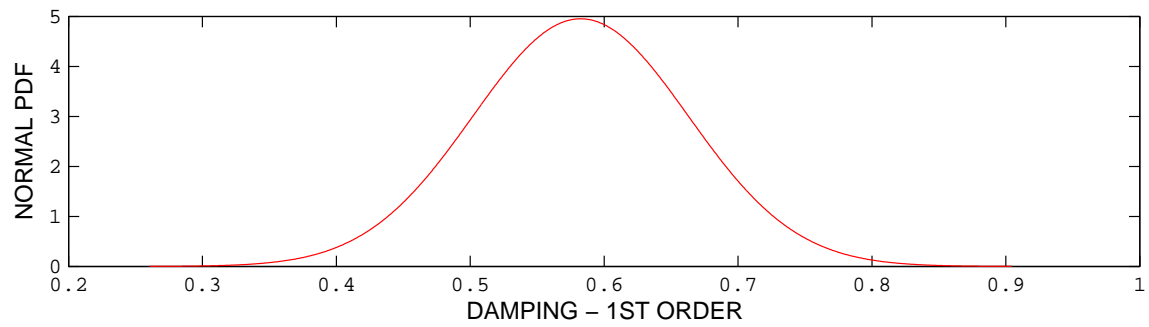


(a) First order damping coefficient

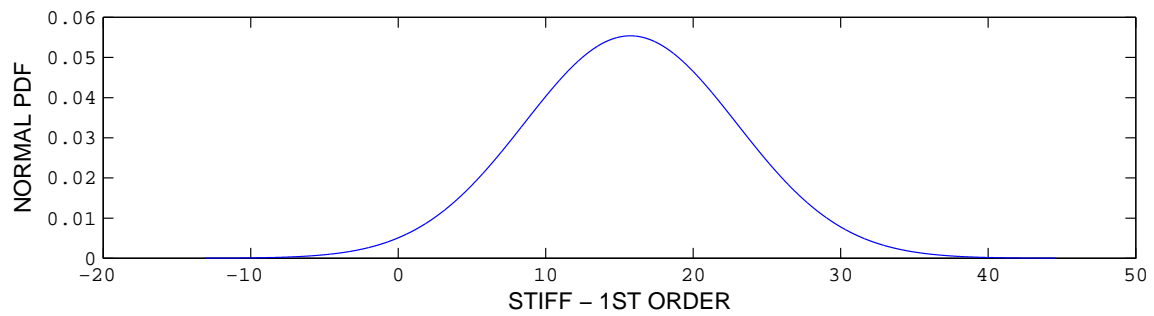


(b) First order stiffness coefficient

Figure G.21: Probability density function of the damping and stiffness Chebyshev coefficients for the data set Qtr3\_01.

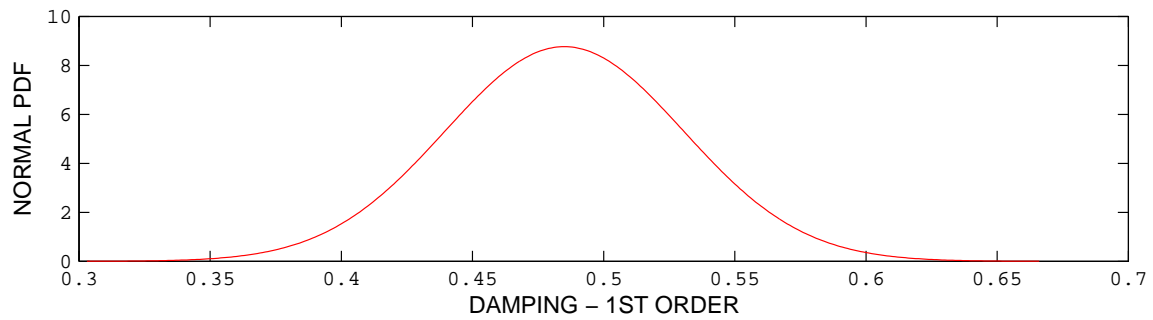


(a) First order damping coefficient

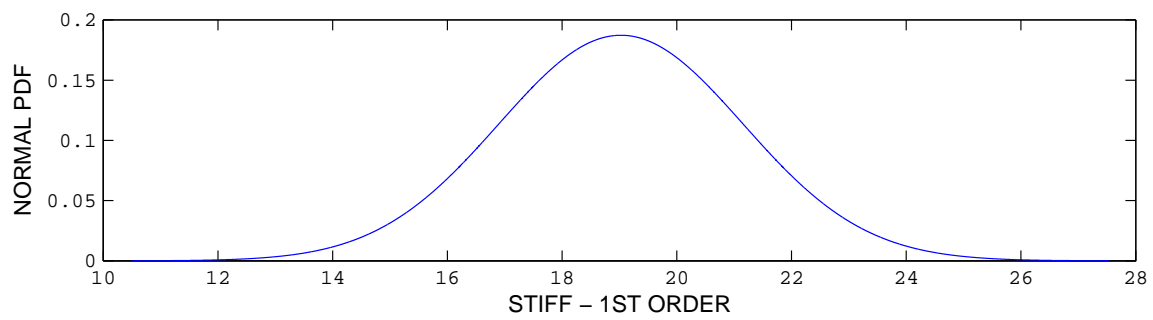


(b) First order stiffness coefficient

Figure G.22: Probability density function of the damping and stiffness Chebyshev coefficients for the data set Qtr1.01.

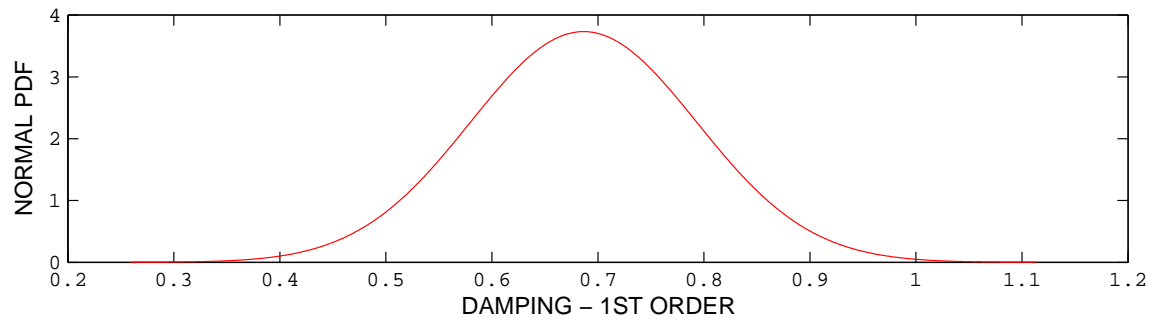


(a) First order damping coefficient

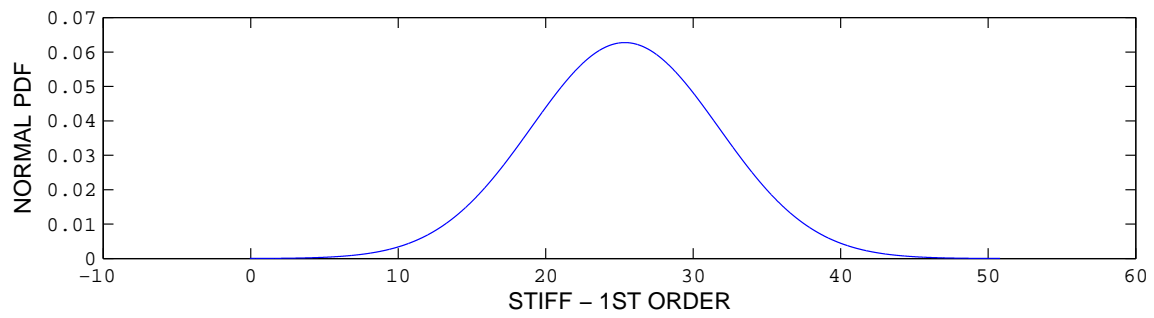


(b) First order stiffness coefficient

Figure G.23: Probability density function of the damping and stiffness Chebyshev coefficients for the data set Qtr1\_0125.

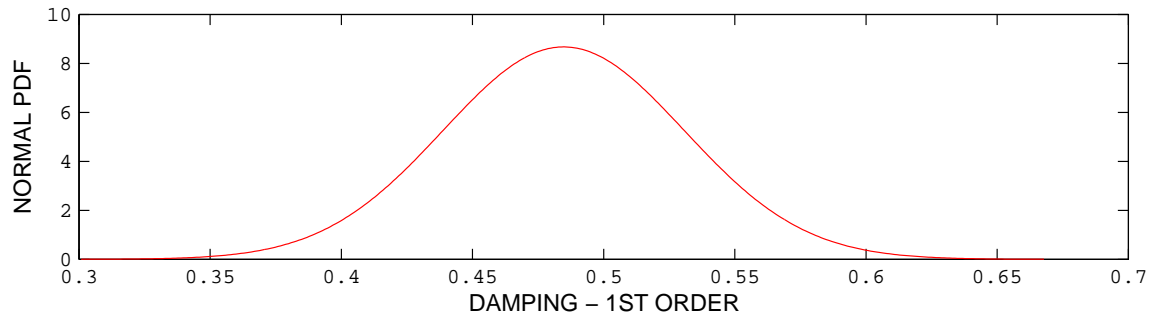


(a) First order damping coefficient

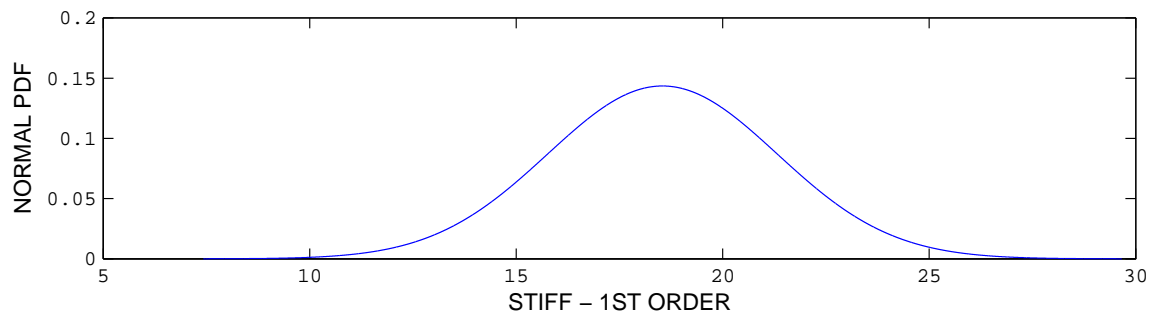


(b) First order stiffness coefficient

Figure G.24: Probability density function of the damping and stiffness Chebyshev coefficients for the data set Qtr2\_0125.

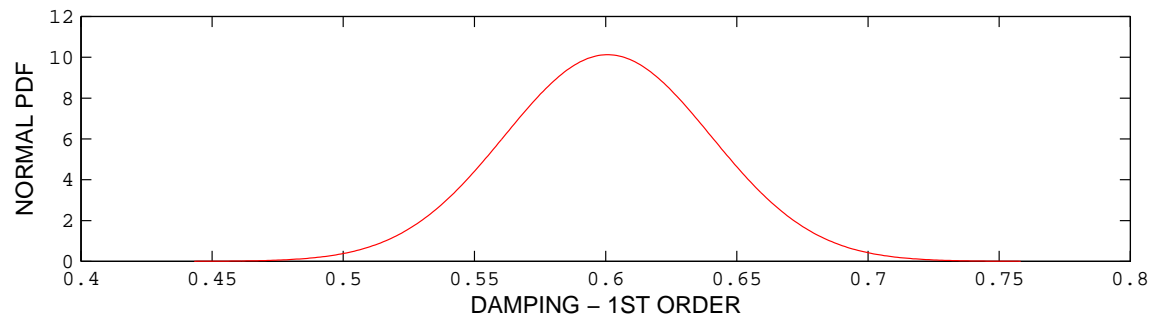


(a) First order damping coefficient

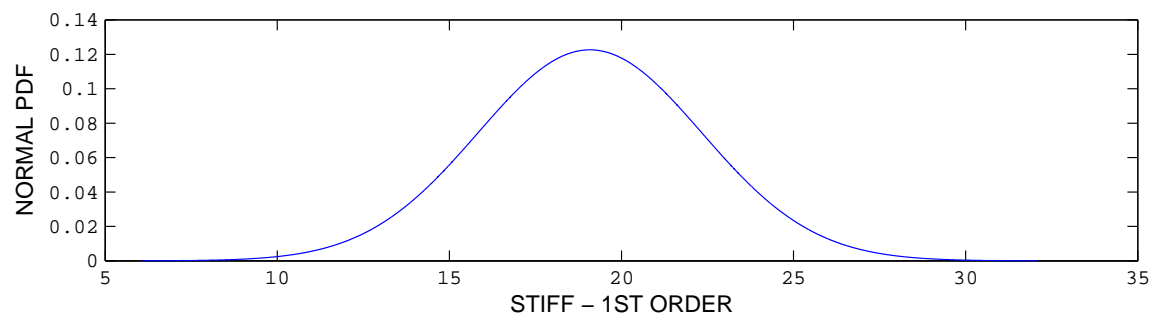


(b) First order stiffness coefficient

Figure G.25: Probability density function of the damping and stiffness Chebyshev coefficients for the data set Qtr3\_0125.



(a) First order damping coefficient



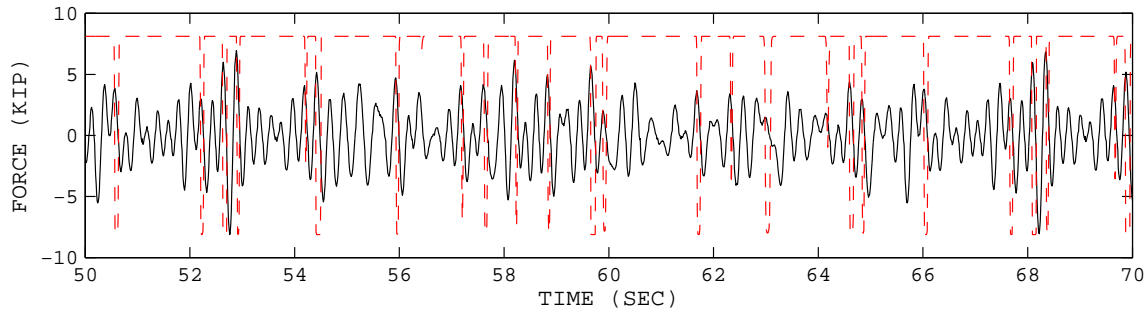
(b) First order stiffness coefficient

Figure G.26: Probability density function of the damping and stiffness Chebyshev coefficients for the data set Qtr4\_0125.

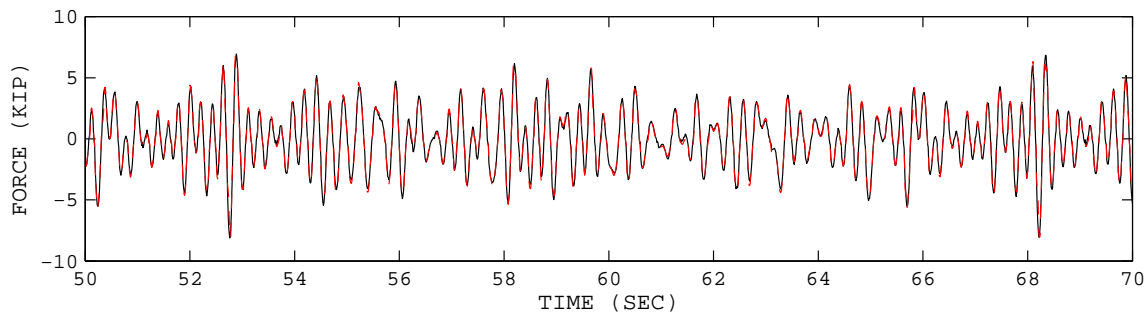
## **G.2 Restoring Force Method**

### **G.2.1 Comparison of Measured and Identified Force for the 15 Kip Damper Using ANN**

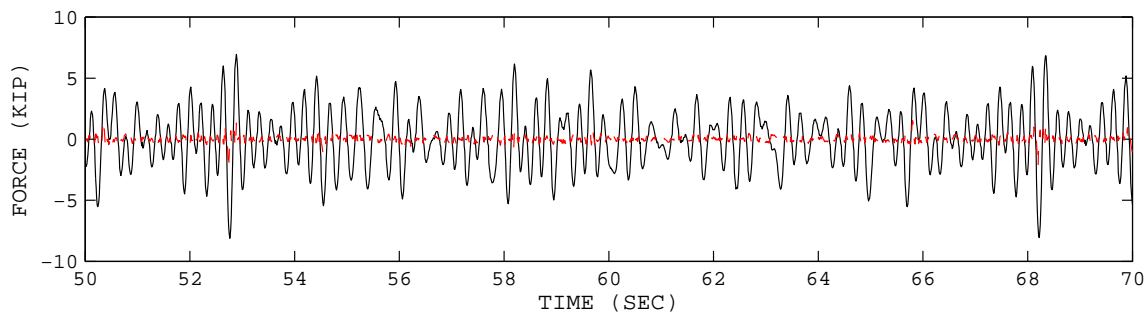
The plot comparisons of the measured and the identified force for selected data sets of the 15 kip viscous damper using the artificial neural networks are shown in this section (Figs G.27 to G.30).



(a) Force before training

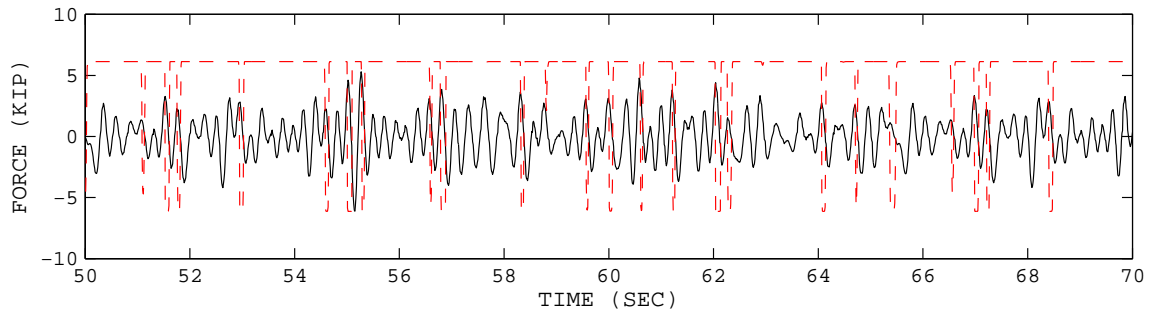


(b) Force after training

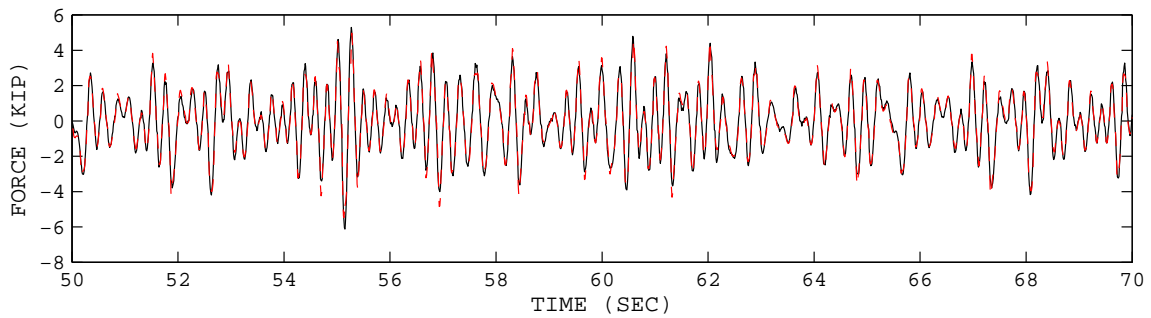


(c) Error after training

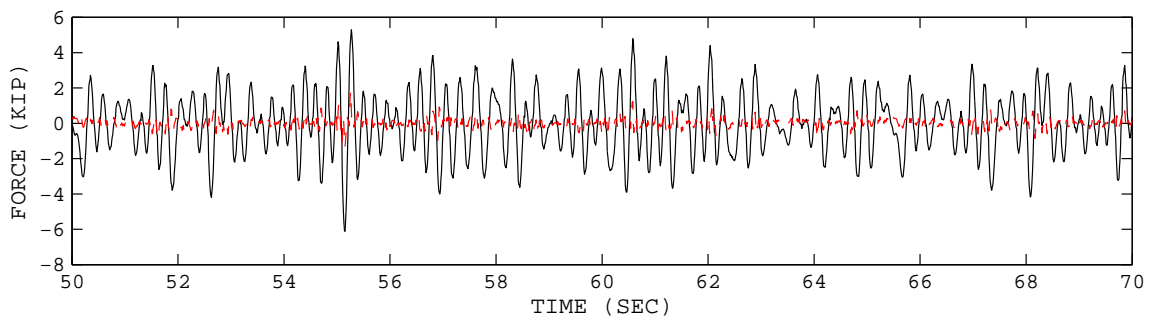
Figure G.27: Comparison of the measured and identified damper response using ANN in time history for the data set usc5400q4. The solid line is the measured force and the dot line is the identified force.



(a) Force before training

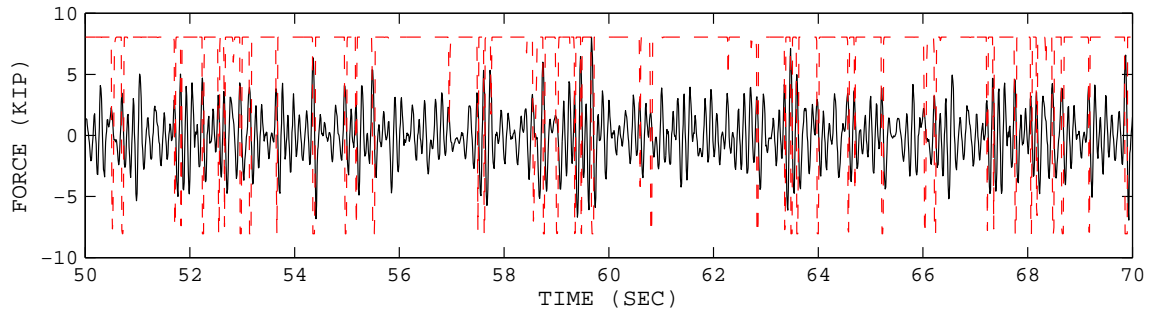


(b) Force after training

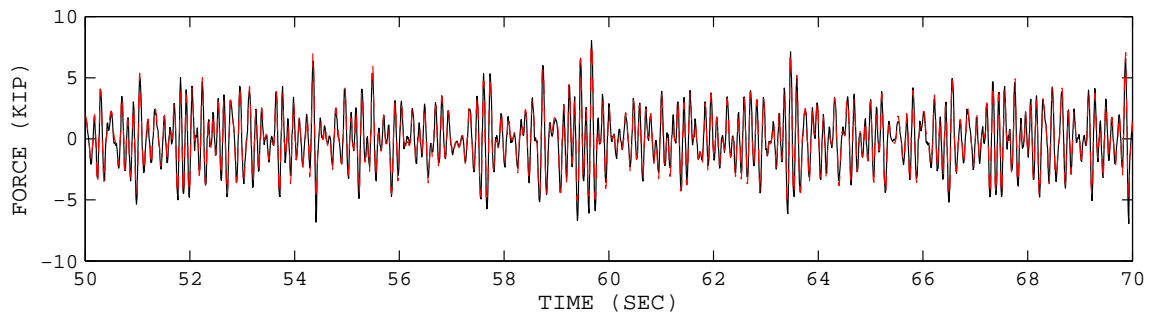


(c) Error after training

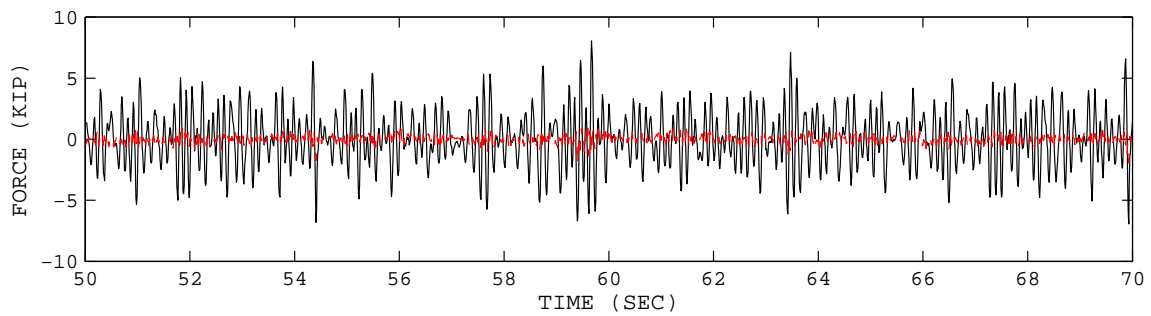
Figure G.28: Comparison of the measured and identified damper response using ANN in time history for the data set usc5300q4. The solid line is the measured force and the dot line is the identified force.



(a) Force before training

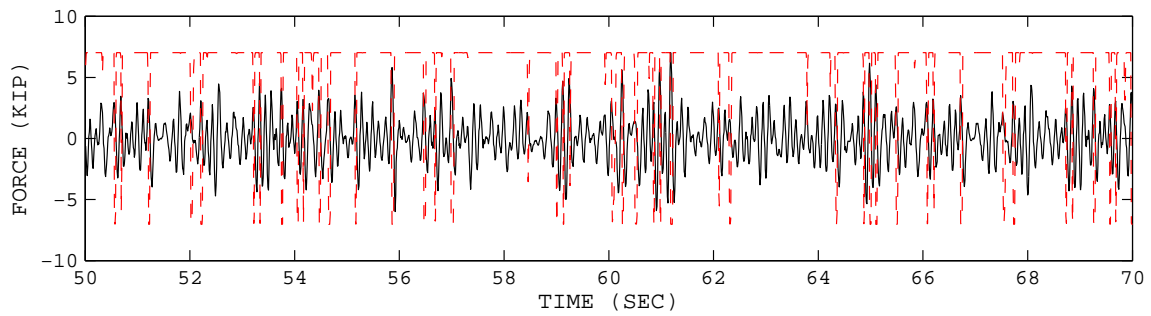


(b) Force after training

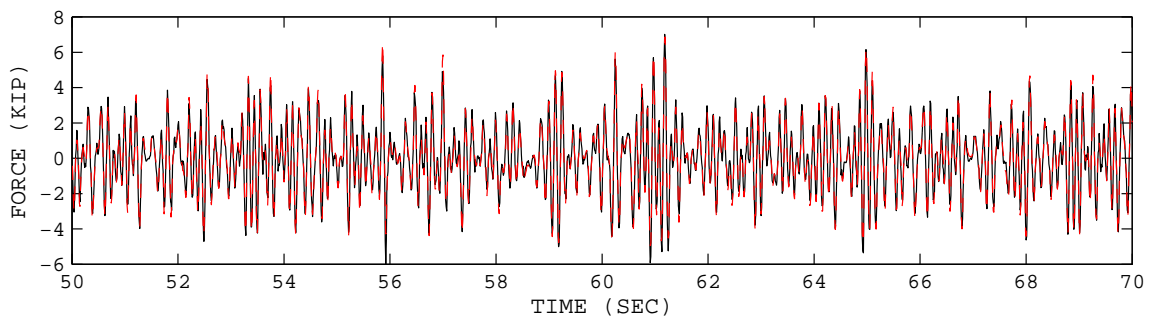


(c) Error after training

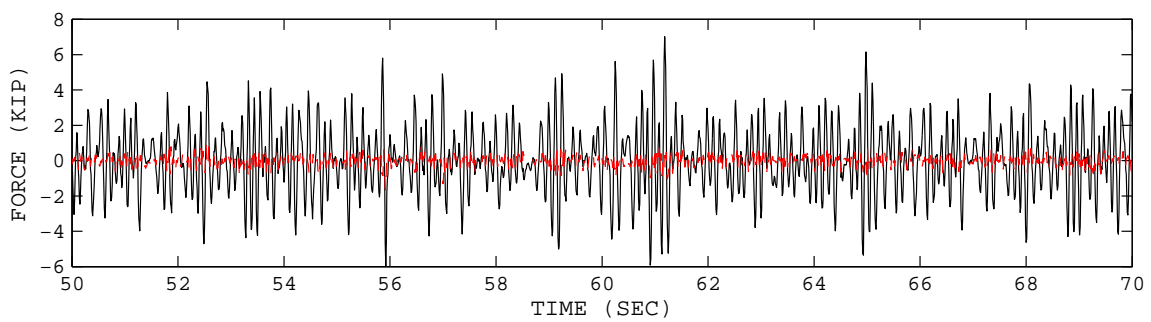
Figure G.29: Comparison of the measured and identified damper response using ANN in time history for the data set usc10200q4. The solid line is the measured force and the dot line is the identified force.



(a) Force before training



(b) Force after training



(c) Error after training

Figure G.30: Comparison of the measured and identified damper response using ANN in time history for the data set usc10175q4. The solid line is the measured force and the dot line is the identified force.

## Appendix H

# NONPARAMETRIC IDENTIFICATION RESULTS FOR THE MR DAMPER

### H.1 Data Acquisition and Preliminary Data Processing

#### H.1.1 Summary of Probability Density Functions for the MR Damper Excitation

The characteristics of the MR damper excitation signals are summarized in Table H.1.1.

Table H.1: Characteristics of the MR damper excitation.

No.	Name	Mean	STDV	Max	Min	Input Current
1	MRD1_X11V_M100_S00_00001	0.0005	0.0498	0.1739	-0.1893	1.0
2	MRD1_X11V_M100_S00_00002	0.0005	0.0473	0.1526	-0.1797	
3	MRD1_X11V_M100_S00_00003	0.0003	0.0459	0.1588	-0.1929	
4	MRD1_X11V_M100_S00_00004	0.0006	0.0478	0.1858	-0.1535	
5	MRD1_X11V_M100_S00_00005	0.0011	0.0453	0.1689	-0.1600	
6	MRD1_X11V_M100_S00_00006	0.0010	0.0473	0.1868	-0.1337	
7	MRD1_X11V_M100_S00_00007	0.0007	0.0495	0.1764	-0.1517	
8	MRD1_X11V_M100_S00_00008	0.0005	0.0470	0.1527	-0.1951	
9	MRD1_X11V_M100_S00_00009	0.0001	0.0453	0.1801	-0.1835	
10	MRD1_X11V_M100_S00_00010	0.0001	0.0481	0.1658	-0.1559	
11	MRD1_X11V_M095_S00_00001	0.0006	0.0498	0.1739	-0.1893	0.95
12	MRD1_X11V_M095_S00_00002	0.0006	0.0474	0.1525	-0.1798	
13	MRD1_X11V_M095_S00_00003	0.0004	0.0459	0.1590	-0.1928	
14	MRD1_X11V_M095_S00_00004	0.0007	0.0479	0.1858	-0.1534	
15	MRD1_X11V_M095_S00_00005	0.0010	0.0453	0.1687	-0.1601	
16	MRD1_X11V_M095_S00_00006	0.0006	0.0473	0.1863	-0.1341	
17	MRD1_X11V_M095_S00_00007	0.0002	0.0496	0.1760	-0.1520	
18	MRD1_X11V_M095_S00_00008	0.0002	0.0469	0.1523	-0.1953	
19	MRD1_X11V_M095_S00_00009	0.0001	0.0453	0.1800	-0.1833	
20	MRD1_X11V_M095_S00_00010	0.0001	0.0481	0.1658	-0.1558	
21	MRD1_X11V_M090_S00_00001	0.0007	0.0498	0.1740	-0.1892	0.90
22	MRD1_X11V_M090_S00_00002	0.0007	0.0474	0.1527	-0.1796	
23	MRD1_X11V_M090_S00_00003	0.0006	0.0460	0.1591	-0.1925	
24	MRD1_X11V_M090_S00_00004	0.0009	0.0478	0.1861	-0.1531	
25	MRD1_X11V_M090_S00_00005	0.0013	0.0453	0.1690	-0.1597	
26	MRD1_X11V_M090_S00_00006	0.0013	0.0474	0.1872	-0.1333	
27	MRD1_X11V_M090_S00_00007	0.0010	0.0496	0.1767	-0.1513	
28	MRD1_X11V_M090_S00_00008	0.0010	0.0470	0.1530	-0.1945	
29	MRD1_X11V_M090_S00_00009	0.0007	0.0453	0.1808	-0.1829	
30	MRD1_X11V_M090_S00_00010	0.0005	0.0481	0.1660	-0.1555	
31	MRD1_X11V_M075_S00_00001	0.0007	0.0499	0.1739	-0.1891	0.75
32	MRD1_X11V_M075_S00_00002	0.0007	0.0474	0.1527	-0.1795	
33	MRD1_X11V_M075_S00_00003	0.0005	0.0460	0.1591	-0.1924	
34	MRD1_X11V_M075_S00_00004	0.0009	0.0479	0.1860	-0.1532	
35	MRD1_X11V_M075_S00_00005	0.0012	0.0453	0.1690	-0.1598	
36	MRD1_X11V_M075_S00_00006	0.0012	0.0474	0.1870	-0.1334	
37	MRD1_X11V_M075_S00_00007	0.0010	0.0496	0.1767	-0.1515	
38	MRD1_X11V_M075_S00_00008	0.0010	0.0470	0.1530	-0.1946	
39	MRD1_X11V_M075_S00_00009	0.0009	0.0453	0.1808	-0.1826	
40	MRD1_X11V_M075_S00_00010	0.0009	0.0481	0.1665	-0.1550	

### H.1.2 MR Damper Response for 1.0 Ampere Input Current (Nominal Case, 100%)

Figures H.1 to H.3 show the MR damper response subjected to broadband excitation signals for 1.0 ampere input current.

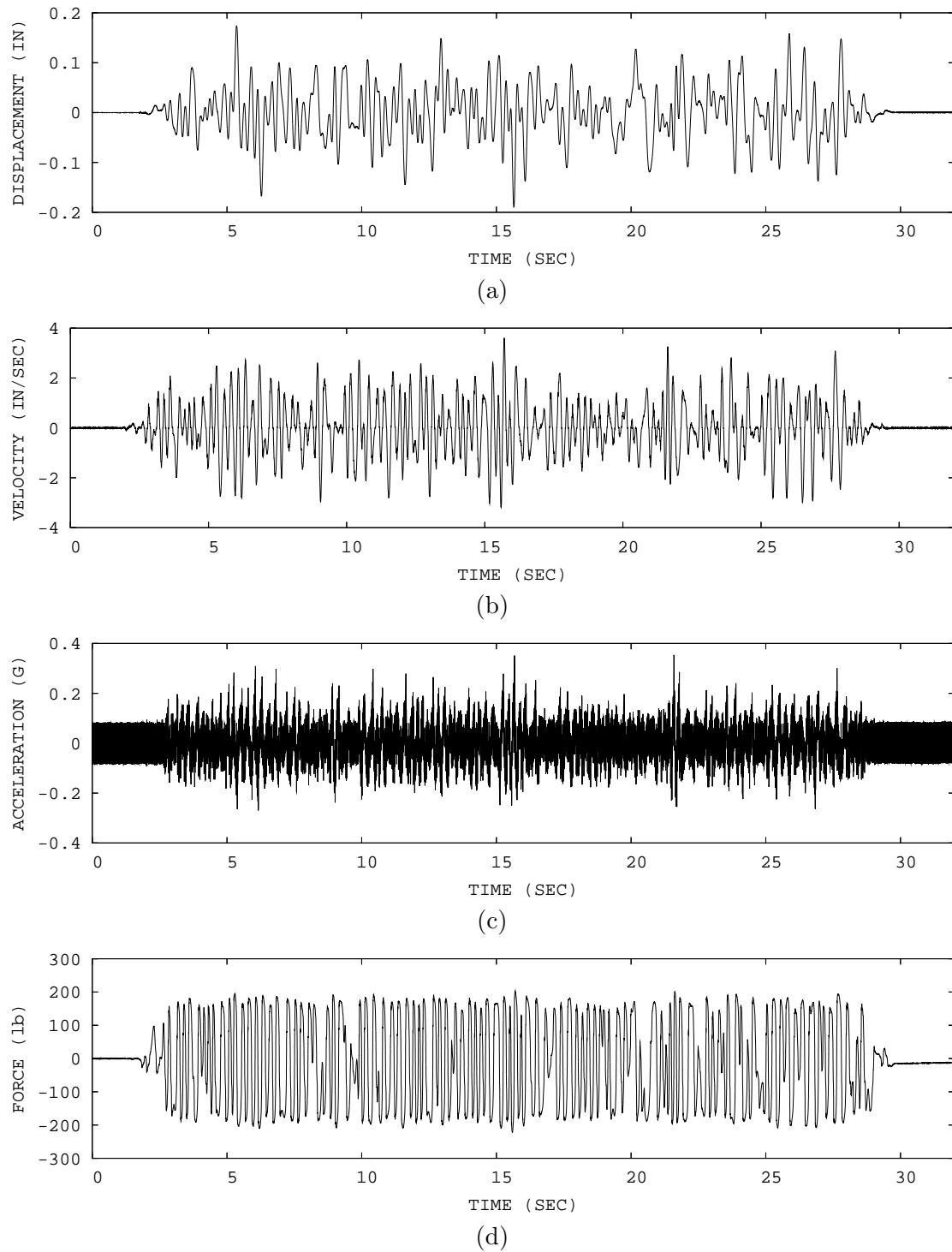
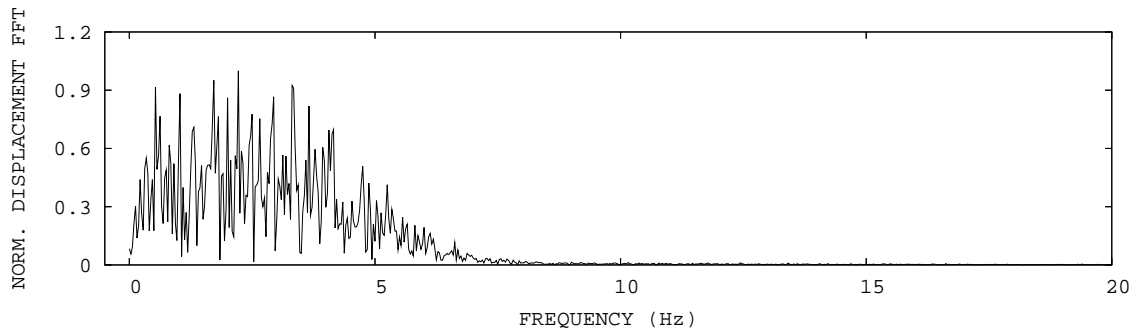
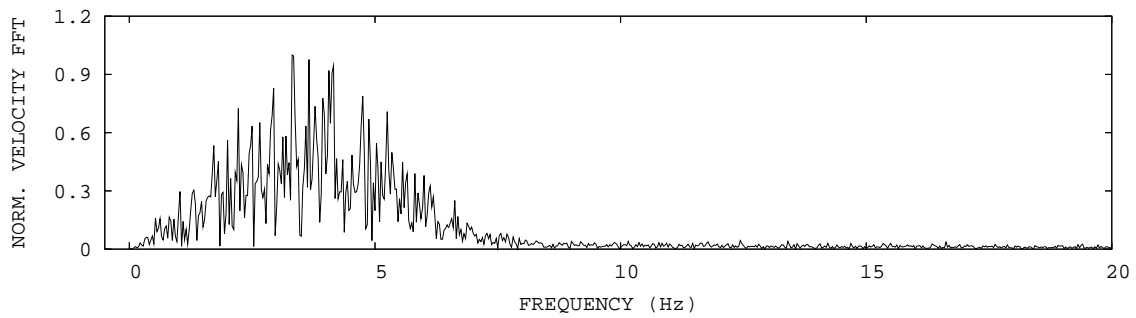


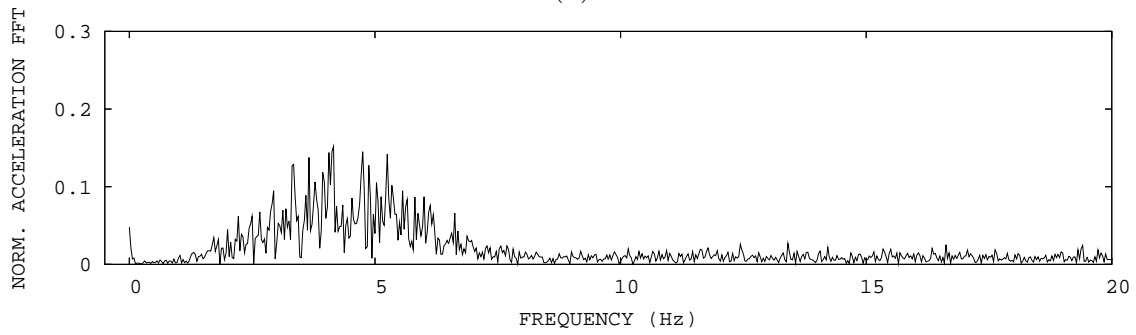
Figure H.1: Time history of the MR damper response subjected to broadband excitation for 1.0 ampere input current (MRD1\_X11V\_M100\_S00\_00001).



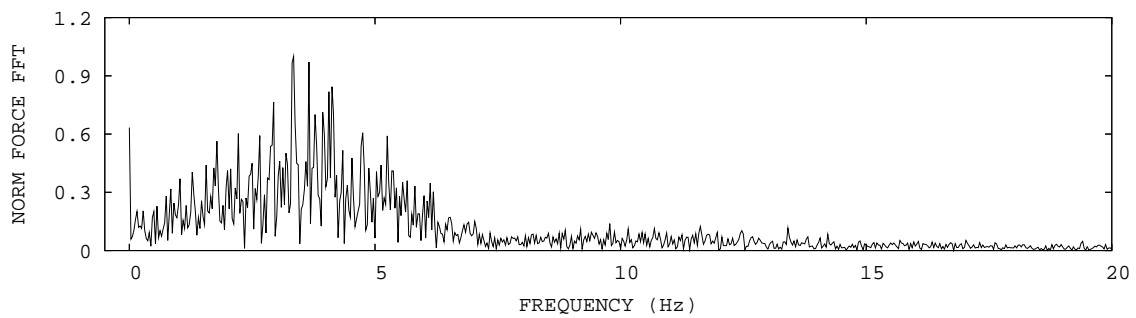
(a)



(b)



(c)



(d)

Figure H.2: FFT of the MR damper response subjected to broadband excitation for 1.0 ampere input current (MRD1\_X11V\_M100\_S00\_00001).

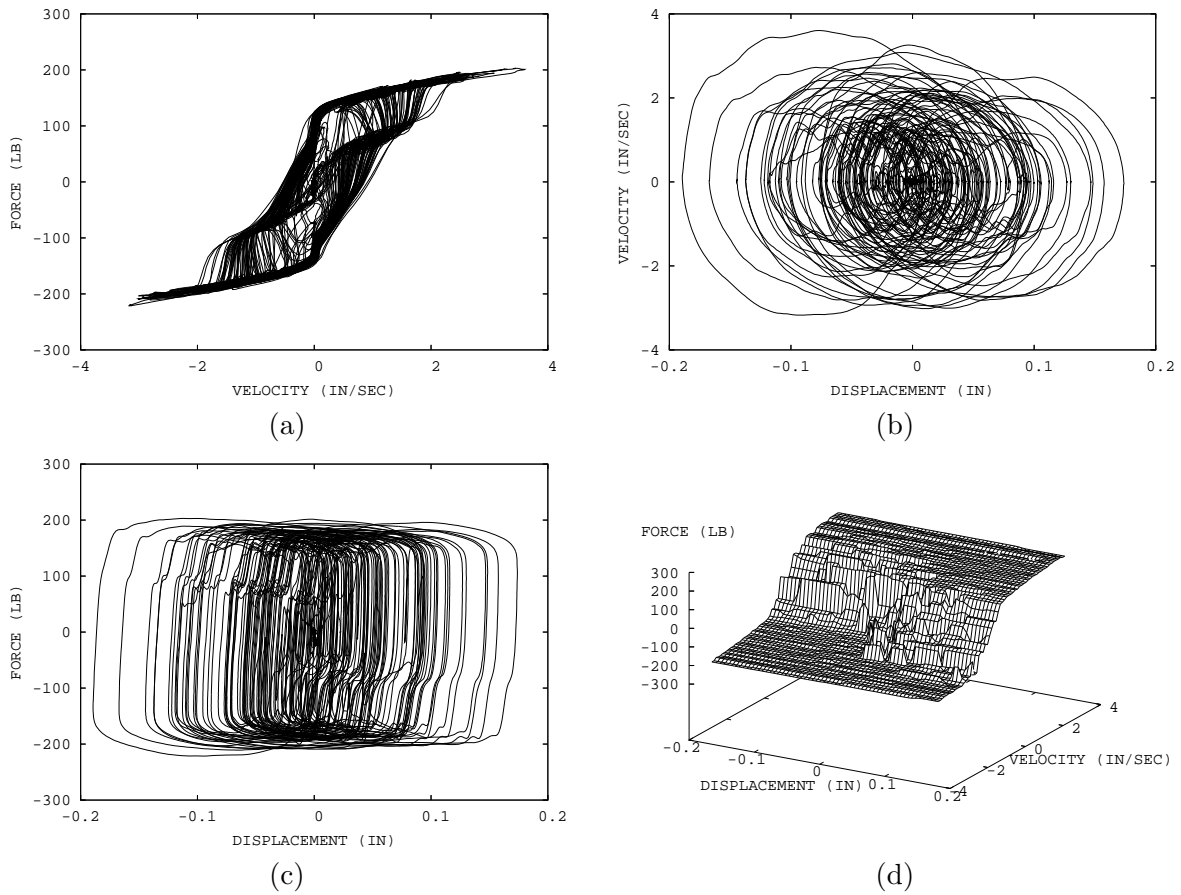


Figure H.3: Phase plot of the MR damper response subjected to broadband excitation for 1.0 ampere input current (MRD1\_X11V\_M100\_S00\_00001).

### H.1.3 MR Damper Response for 0.95 Ampere Input Current (95%)

Figures H.4 to H.6 show the MR damper response subjected to broadband excitation signals for 0.95 ampere input current.

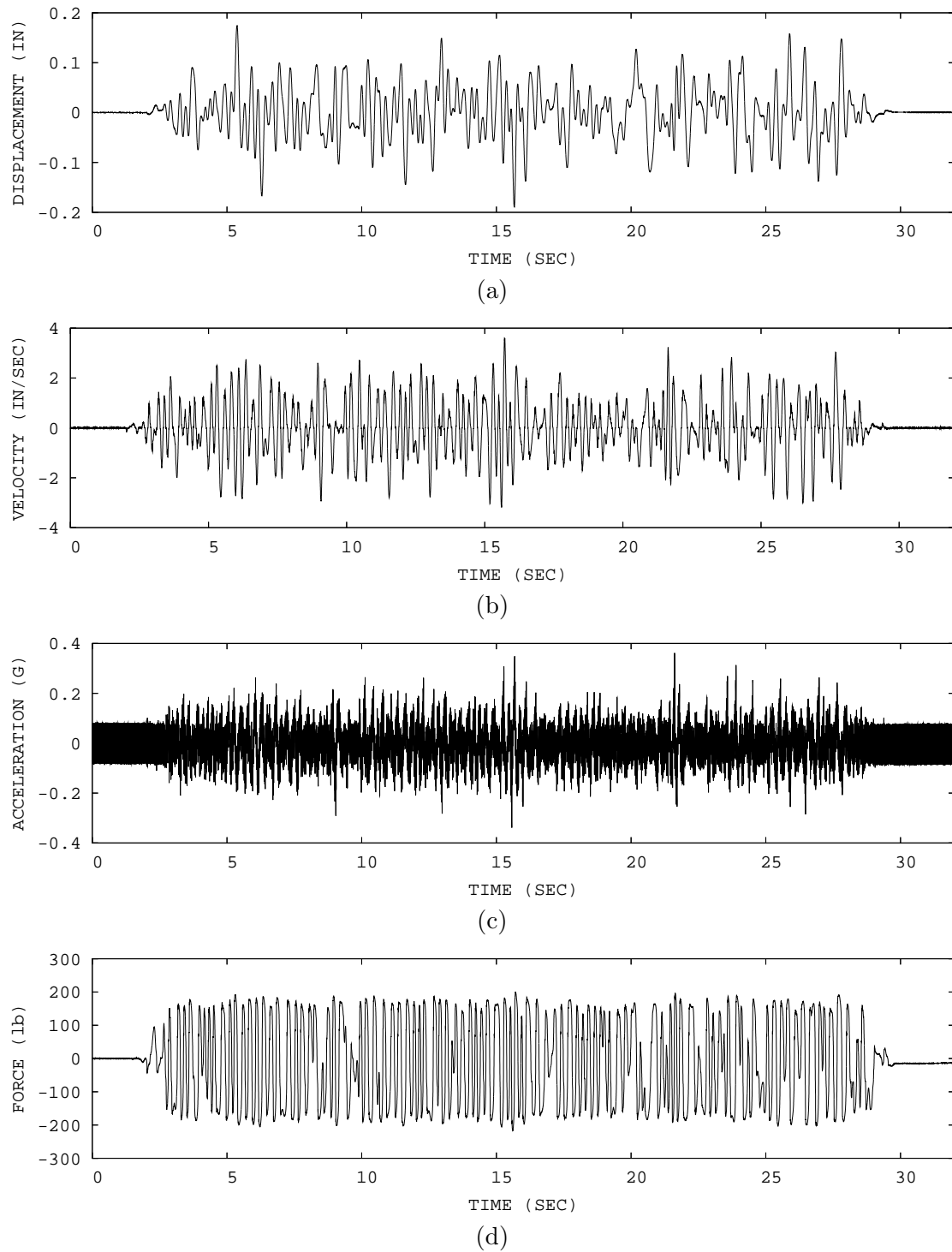
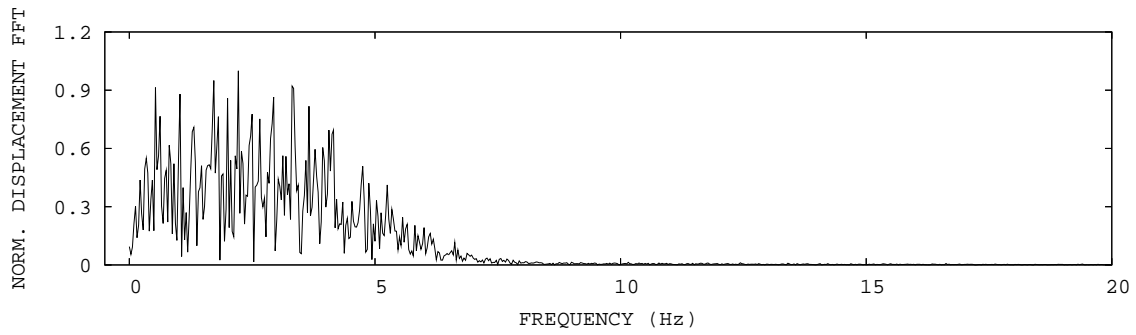
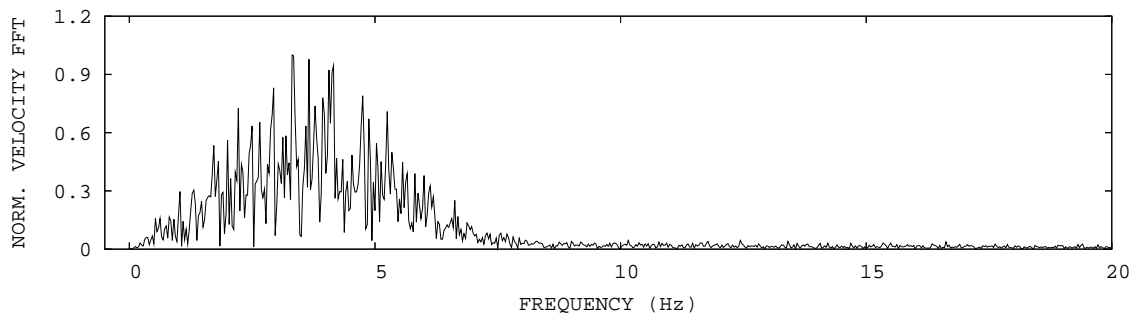


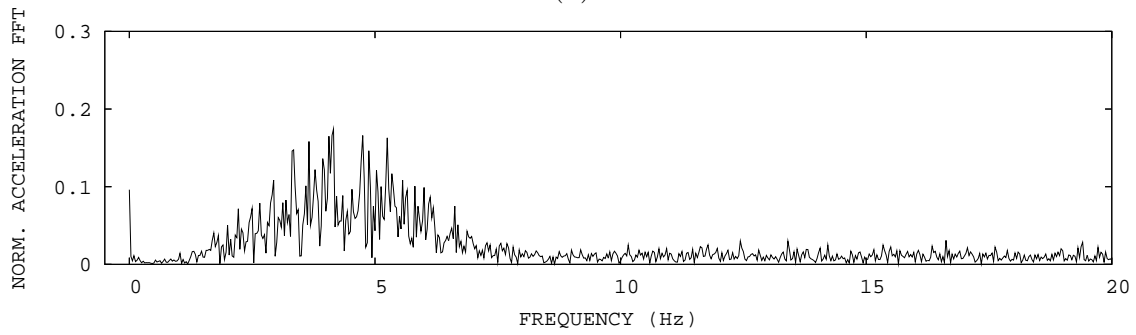
Figure H.4: Time history of the MR damper response subjected to broadband excitation for 0.95 ampere input current (MRD1\_X11V\_M095\_S00\_00001).



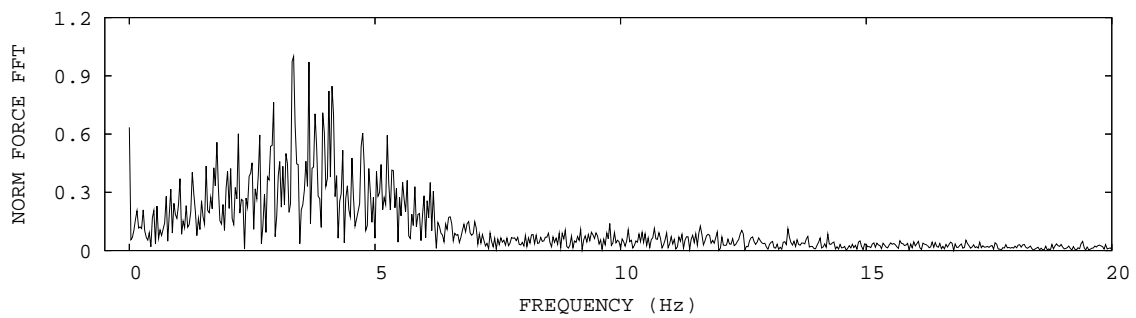
(a)



(b)



(c)



(d)

Figure H.5: FFT of the MR damper response subjected to broadband excitation for 0.95 ampere input current (MRD1\_X11V\_M095\_S00\_00001).

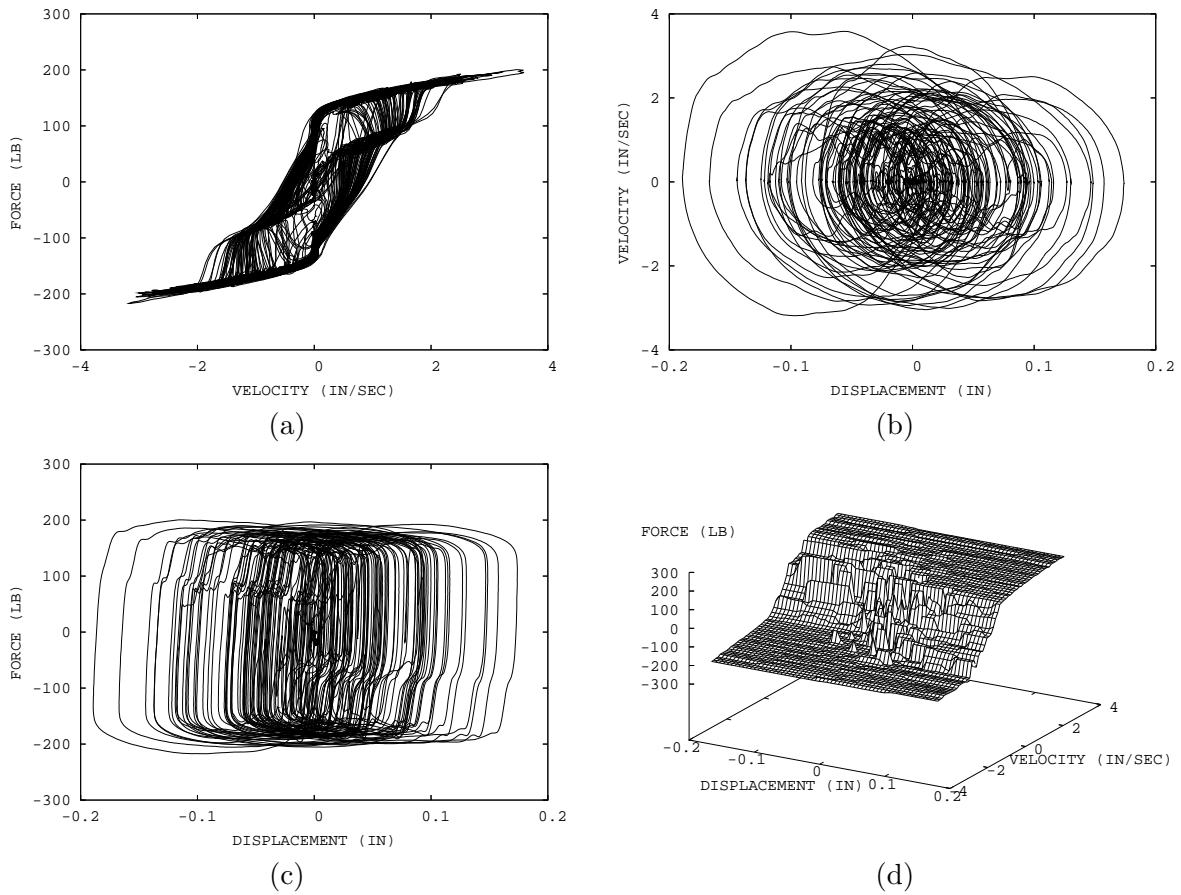


Figure H.6: Phase plot of the MR damper response subjected to broadband excitation for 0.95 ampere input current (MRD1\_X11V\_M095\_S00\_00001).

#### H.1.4 MR Damper Response for 0.90 Ampere Input Current (90%)

Figures H.7 to H.9 show the MR damper response subjected to broadband excitation signals for 0.90 ampere input current.

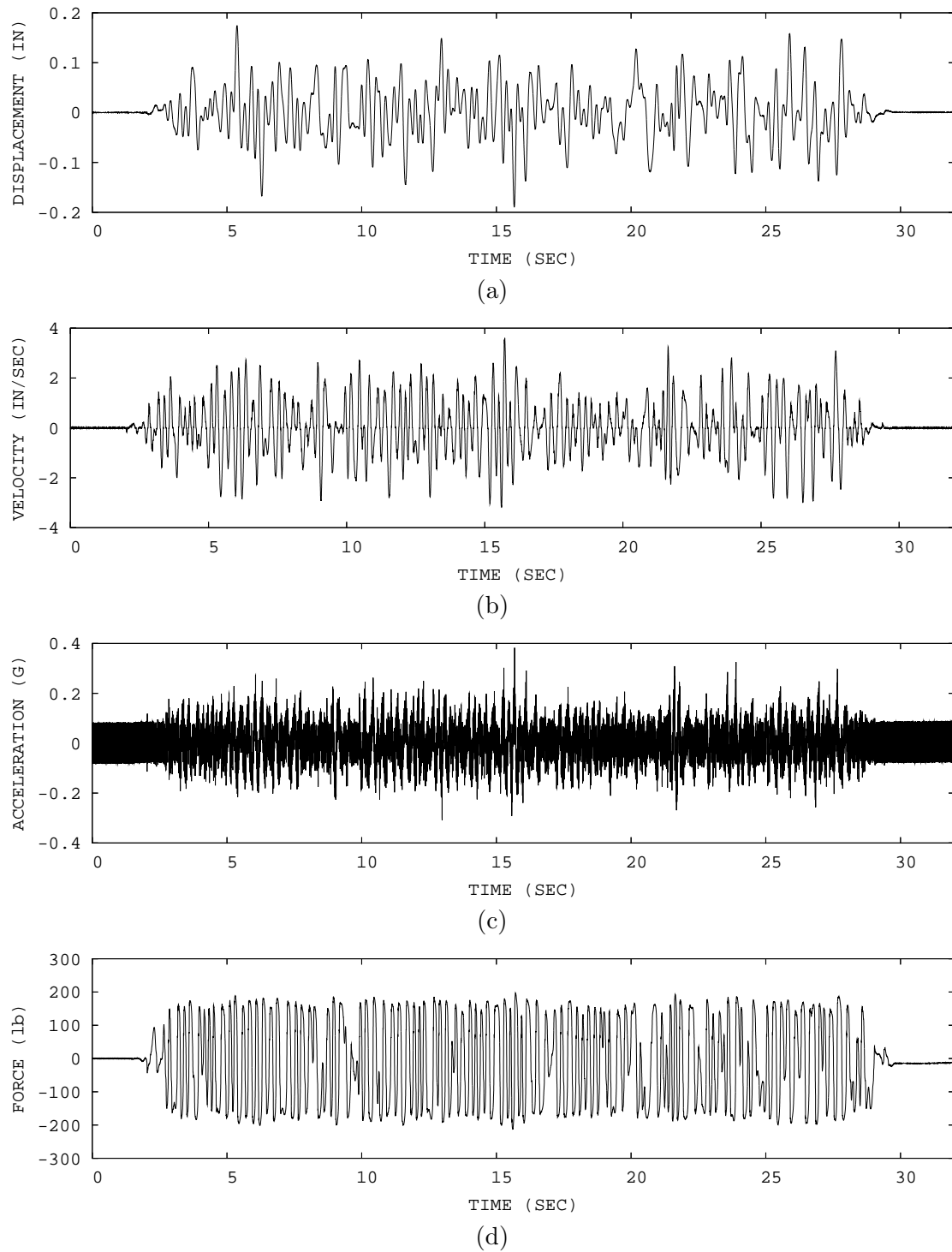
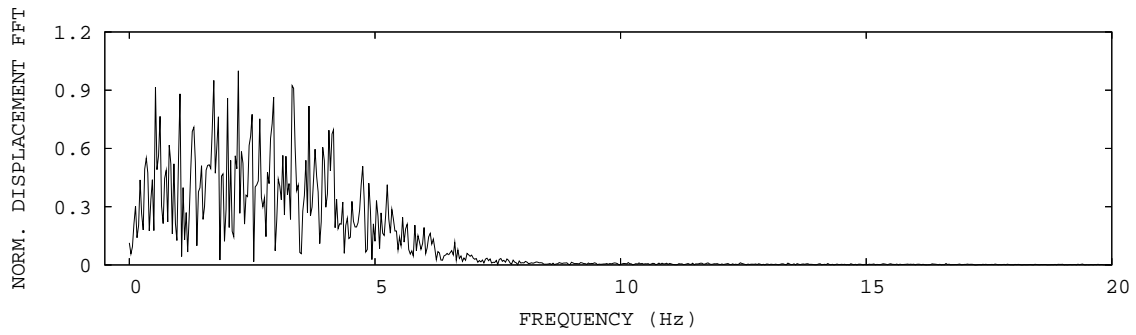
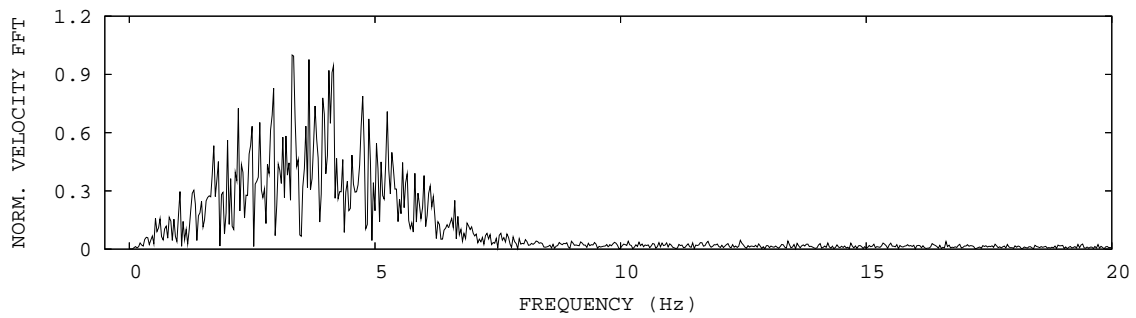


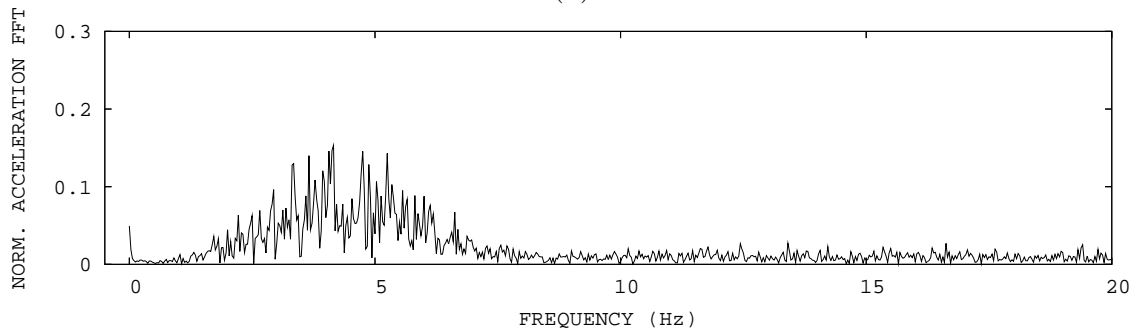
Figure H.7: Time history of the MR damper response subjected to broadband excitation for 0.90 ampere input current (MRD1\_X11V\_M090\_S00\_00001).



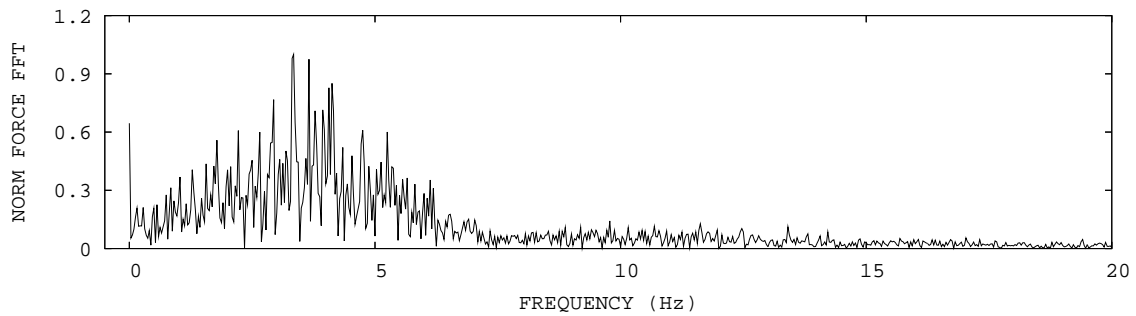
(a)



(b)



(c)



(d)

Figure H.8: FFT of the MR damper response subjected to broadband excitation for 0.90 ampere input current (MRD1\_X11V\_M090\_S00\_00001).

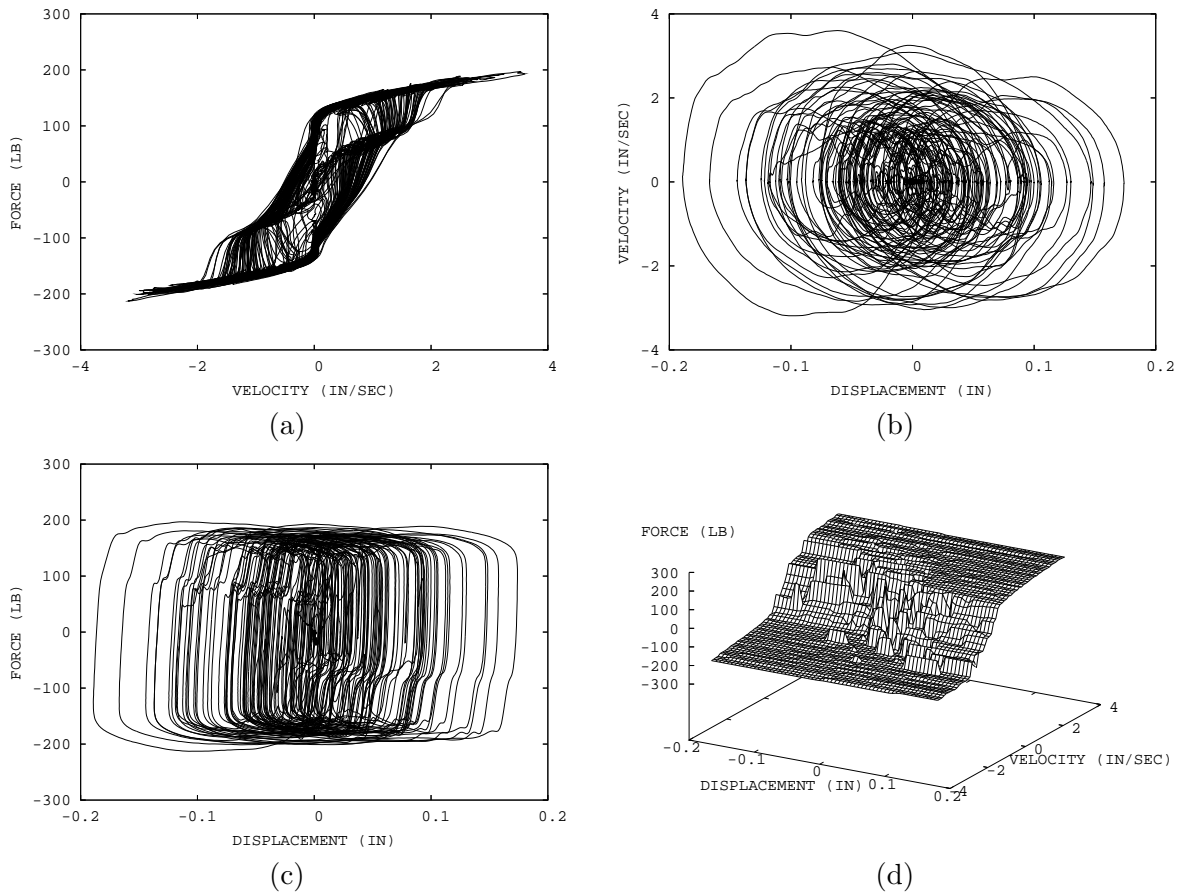


Figure H.9: Phase plot of the MR damper response subjected to broadband excitation for 0.90 ampere input current (MRD1\_X11V\_M090\_S00\_00001).

### H.1.5 MR Damper Response for 0.75 Ampere Input Current (75%)

Figures H.10 to H.12 show the MR damper response subjected to broadband excitation signals for 0.75 ampere input current.

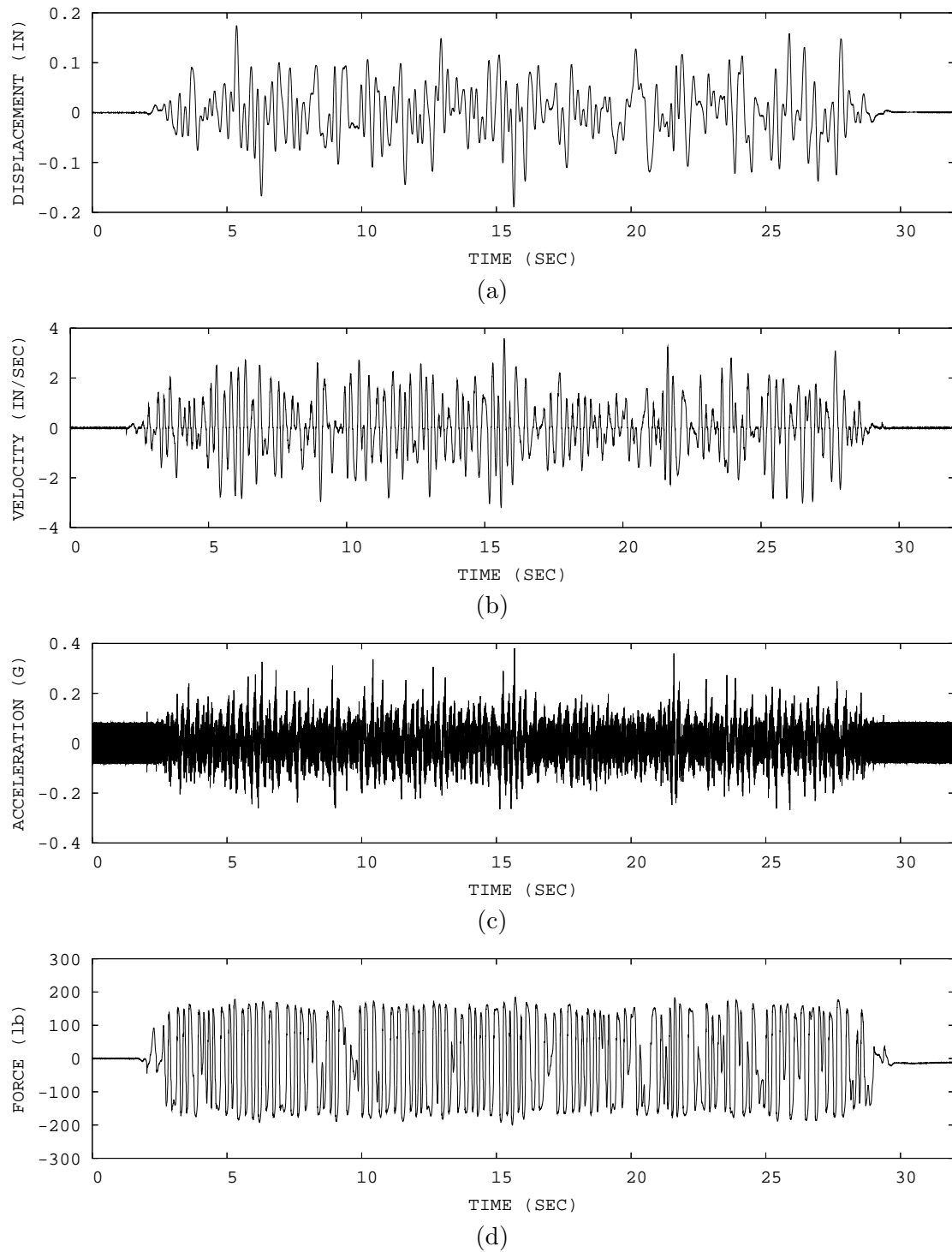


Figure H.10: Time history of the MR damper response subjected to broadband excitation for 0.75 ampere input current (MRD1\_X11V\_M075\_S00\_00001).

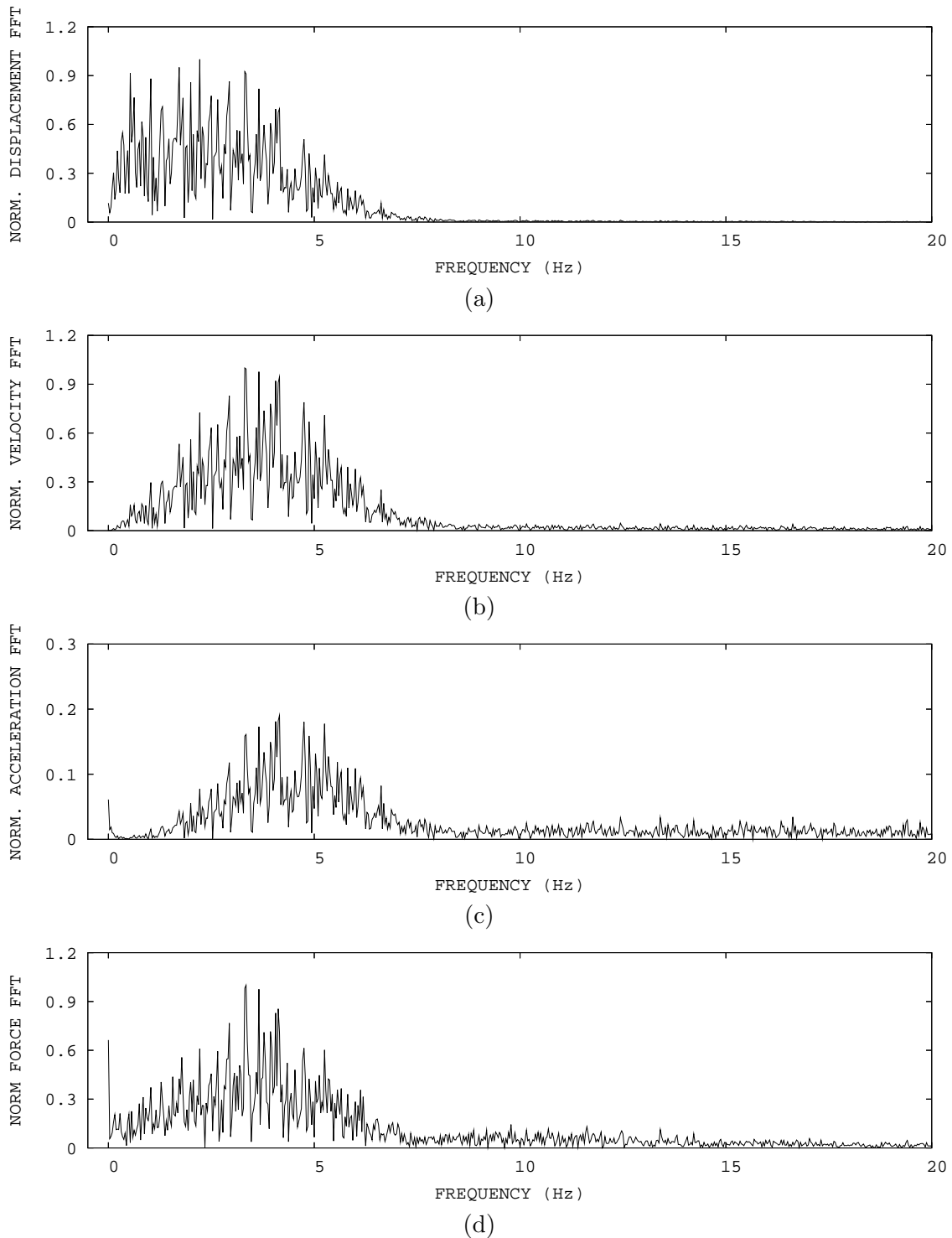


Figure H.11: FFT of the MR damper response subjected to broadband excitation for 0.75 ampere input current (MRD1\_X11V\_M075\_S00\_00001).

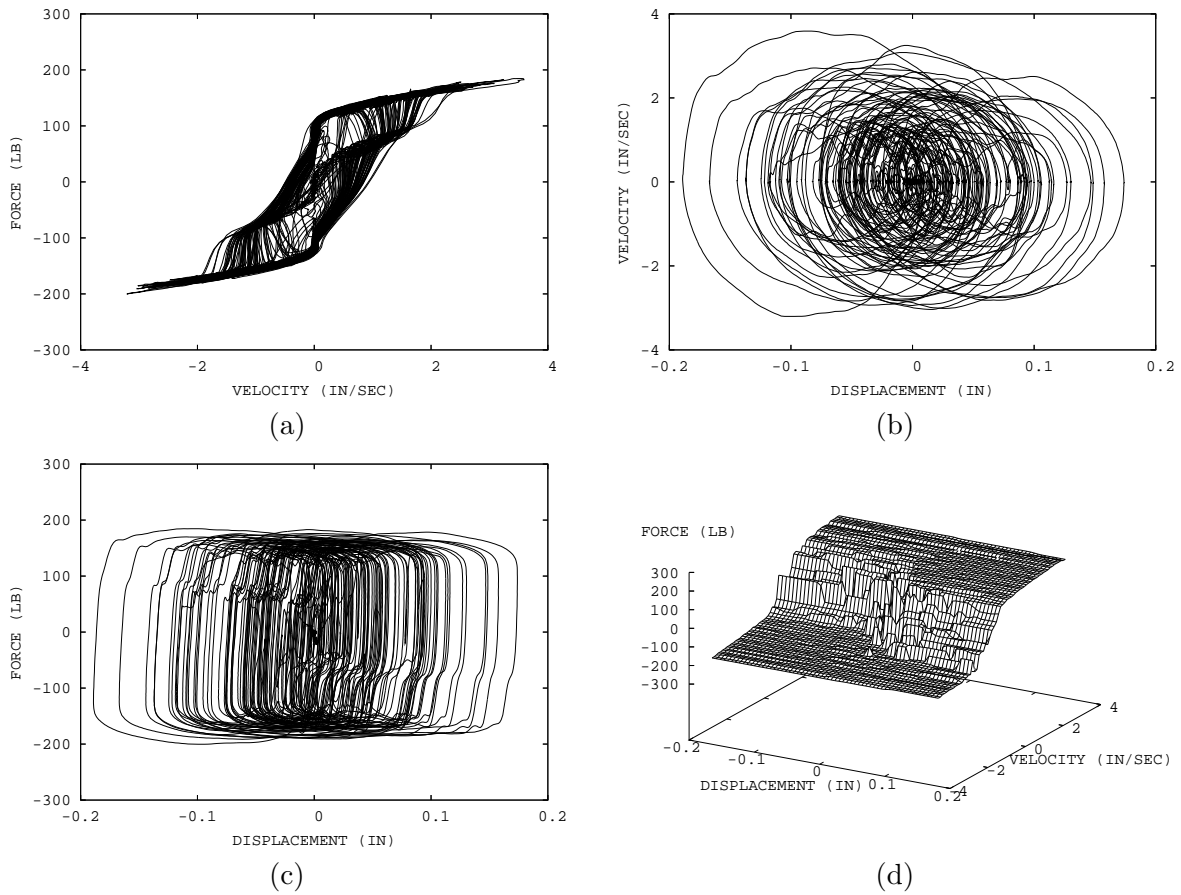


Figure H.12: Phase plot of the MR damper response subjected to broadband excitation for 0.75 ampere input current (MRD1\_X11V\_M075\_S00\_00001).

## H.2 Restoring Force Method

### H.2.1 Comparison of Measured and Identified MR Damper Force for 1.00 Ampere Input Current (100%)

Figures H.13 - H.22 show the comparison of the measured and identified damper response in time history using RFM for 1.0 ampere MR damper input current test No. 1 (MRD1\_X11V\_M100\_S00\_00001\_001) to test No. 10 (MRD1\_X11V\_M100\_S00\_00010\_001). The solid line is the measured force and the dashed line is the identified force.

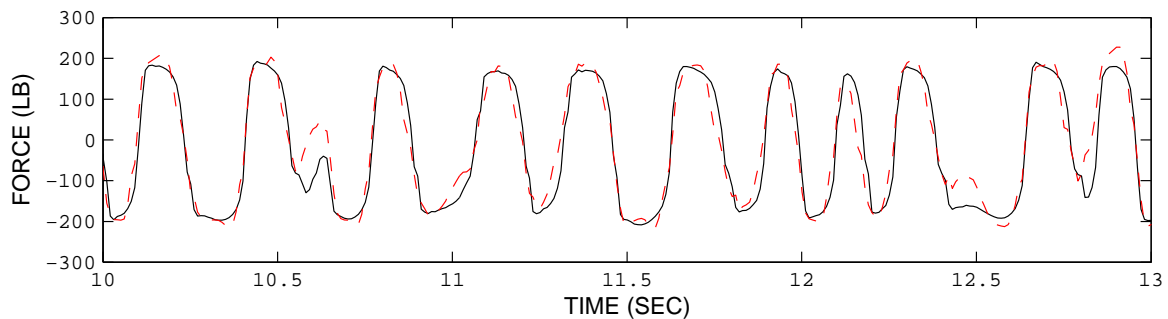


Figure H.13: Comparison of the measured and identified damper response in time history using RFM for 1.0 ampere MR damper input current test No. 1 (MRD1\_X11V\_M100\_S00\_00001\_001). The solid line is the measured force and the dashed line is the identified force.

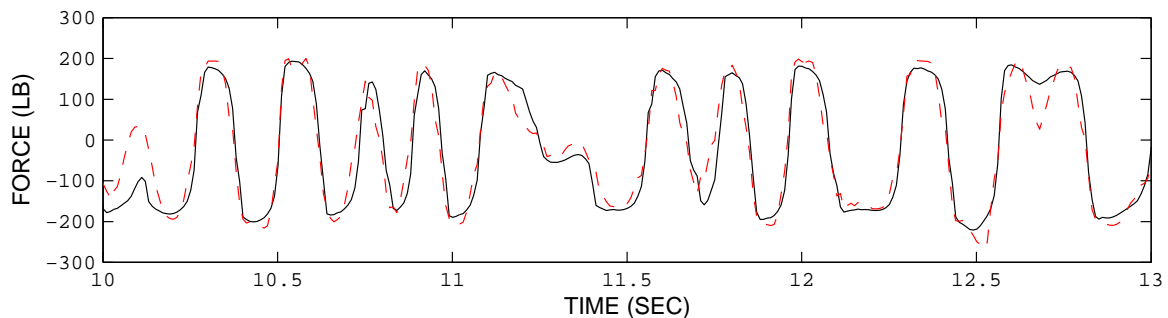


Figure H.14: Comparison of the measured and identified damper response in time history using RFM for 1.0 ampere MR damper input current test No. 2 (MRD1\_X11V\_M100\_S00\_00002\_001). The solid line is the measured force and the dashed line is the identified force.

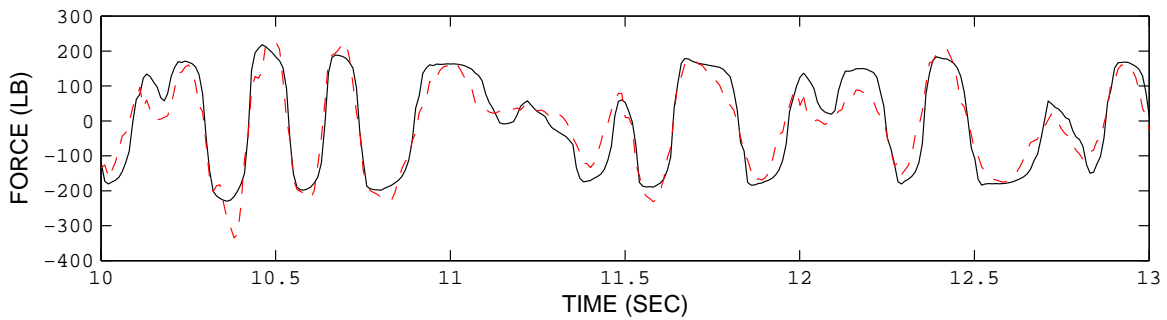


Figure H.15: Comparison of the measured and identified damper response in time history using RFM for 1.0 ampere MR damper input current test No. 3 (MRD1\_X11V\_M100\_S00\_00003\_001). The solid line is the measured force and the dashed line is the identified force.

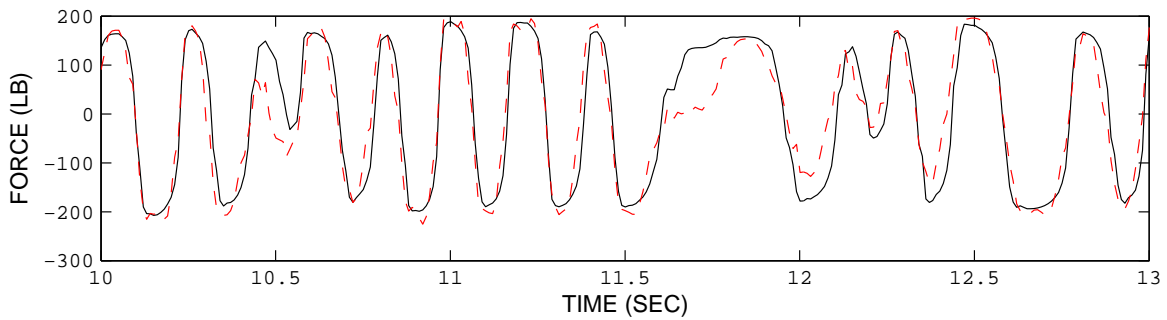


Figure H.16: Comparison of the measured and identified damper response in time history using RFM for 1.0 ampere MR damper input current test No. 4 (MRD1\_X11V\_M100\_S00\_00004\_001). The solid line is the measured force and the dashed line is the identified force.

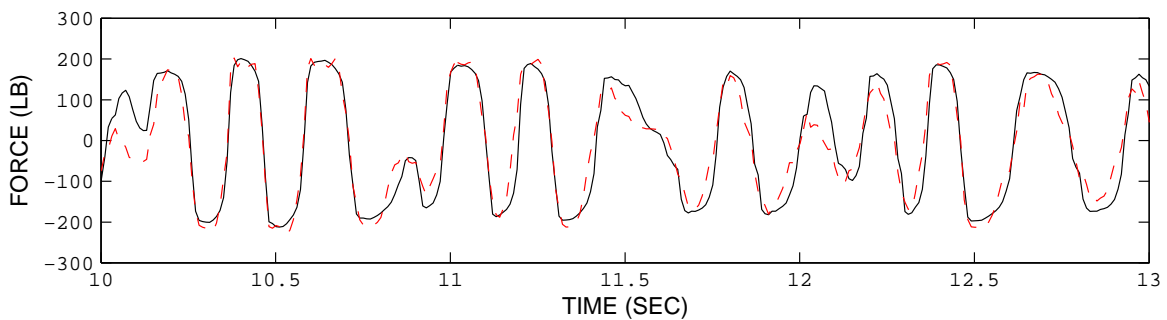


Figure H.17: Comparison of the measured and identified damper response in time history using RFM for 1.0 ampere MR damper input current test No. 5 (MRD1\_X11V\_M100\_S00\_00005\_001). The solid line is the measured force and the dashed line is the identified force.

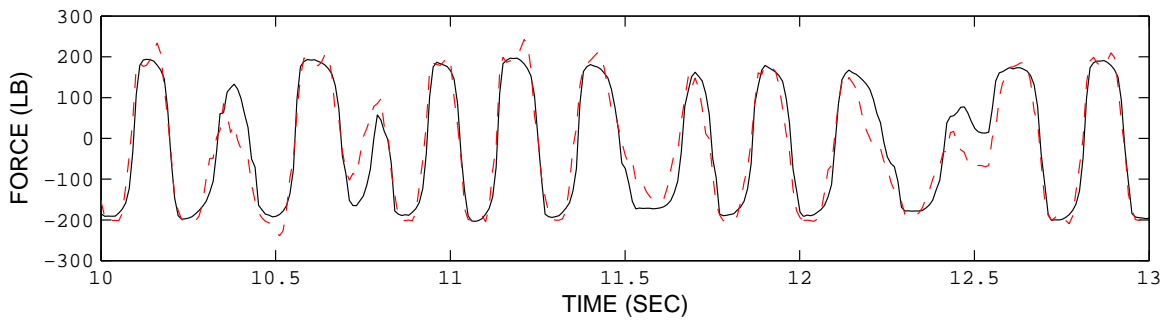


Figure H.18: Comparison of the measured and identified damper response in time history using RFM for 1.0 ampere MR damper input current test No. 6 (MRD1\_X11V\_M100\_S00\_00006\_001). The solid line is the measured force and the dashed line is the identified force.

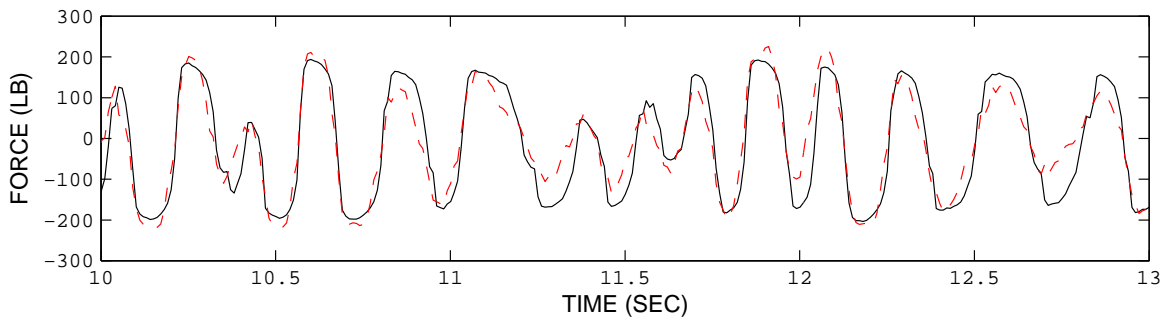


Figure H.19: Comparison of the measured and identified damper response in time history using RFM for 1.0 ampere MR damper input current test No. 7 (MRD1\_X11V\_M100\_S00\_00007\_001). The solid line is the measured force and the dashed line is the identified force.

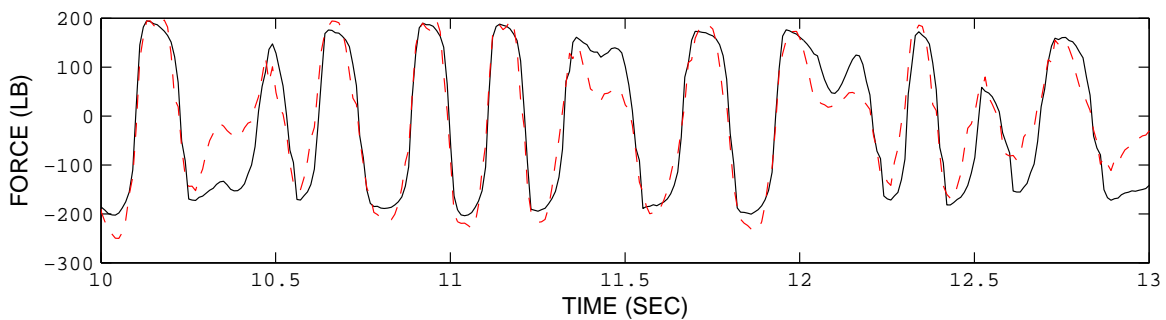


Figure H.20: Comparison of the measured and identified damper response in time history using RFM for 1.0 ampere MR damper input current test No. 8 (MRD1\_X11V\_M100\_S00\_00008\_001). The solid line is the measured force and the dashed line is the identified force.

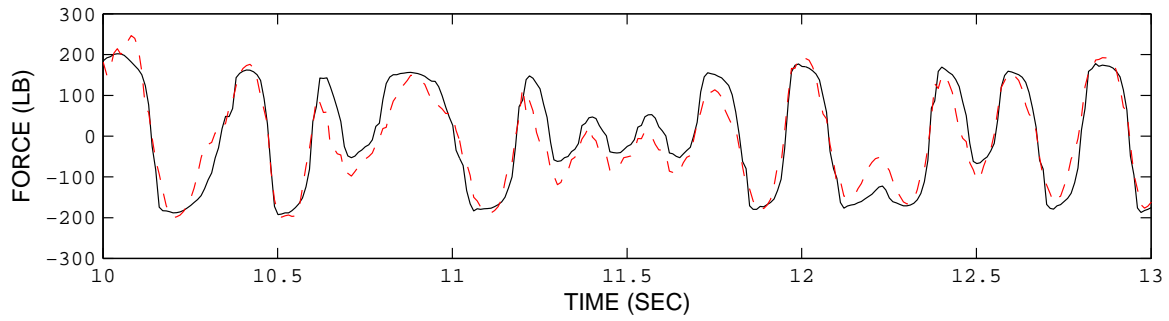


Figure H.21: Comparison of the measured and identified damper response in time history using RFM for 1.0 ampere MR damper input current test No. 9 (MRD1\_X11V\_M100\_S00\_00009\_001). The solid line is the measured force and the dashed line is the identified force.

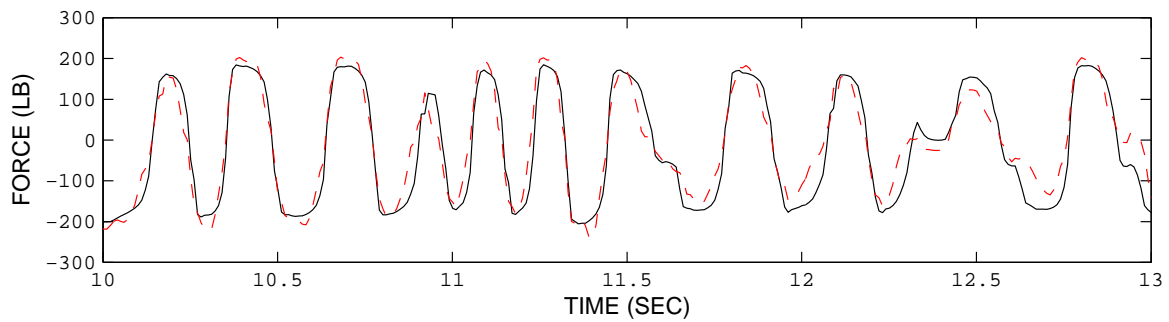


Figure H.22: Comparison of the measured and identified damper response in time history using RFM for 1.0 ampere MR damper input current test No. 10 (MRD1\_X11V\_M100\_S00\_00010\_001). The solid line is the measured force and the dashed line is the identified force.

## H.2.2 Comparison of Measured and Identified MR Damper Force for 0.95 Ampere Input Current (95%)

Figures H.23 - H.32 show the comparison of the measured and identified damper response in time history using RFM for 0.95 ampere MR damper input current test No. 1 (MRD1\_X11V\_M095\_S00\_00001\_001) to test No. 10 (MRD1\_X11V\_M095\_S00\_00010\_001). The solid line is the measured force and the dashed line is the identified force.

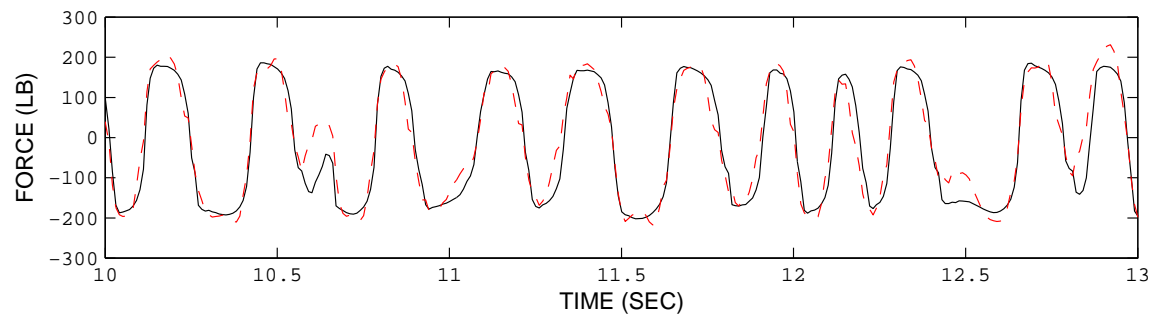


Figure H.23: Comparison of the measured and identified damper response in time history using RFM for 0.95 ampere MR damper input current test No. 1 (MRD1\_X11V\_M095\_S00\_00001\_001). The solid line is the measured force and the dashed line is the identified force.

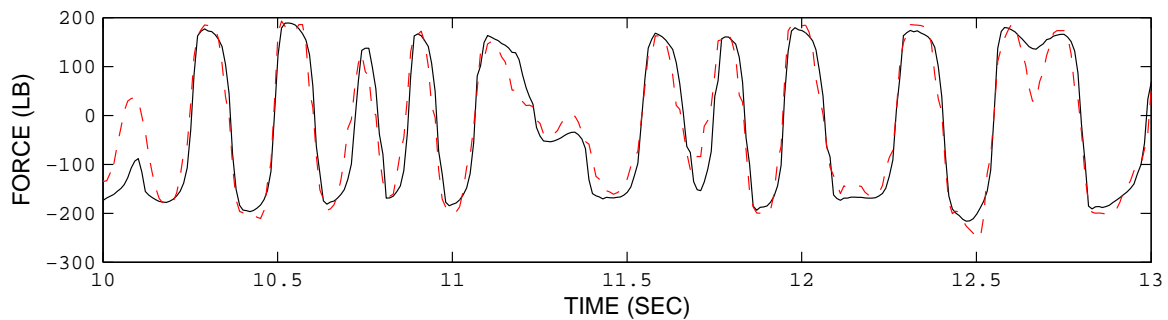


Figure H.24: Comparison of the measured and identified damper response in time history using RFM for 0.95 ampere MR damper input current test No. 2 (MRD1\_X11V\_M095\_S00\_00002\_001). The solid line is the measured force and the dashed line is the identified force.

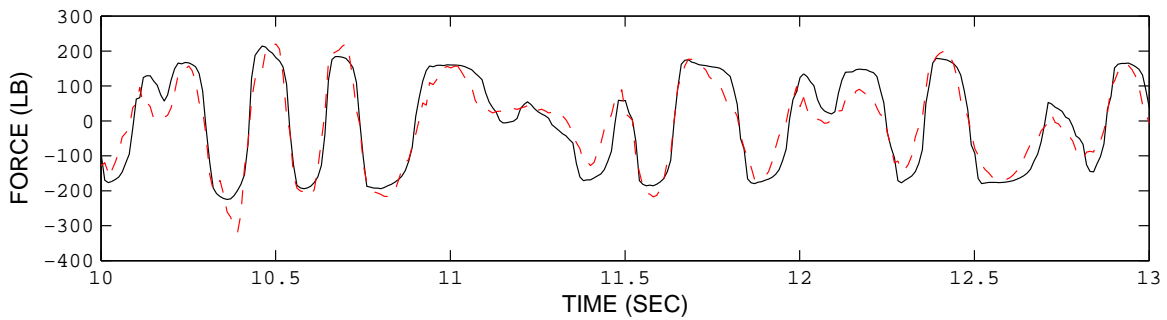


Figure H.25: Comparison of the measured and identified damper response in time history using RFM for 0.95 ampere MR damper input current test No. 3 (MRD1\_X11V\_M095\_S00\_00003\_001). The solid line is the measured force and the dashed line is the identified force.

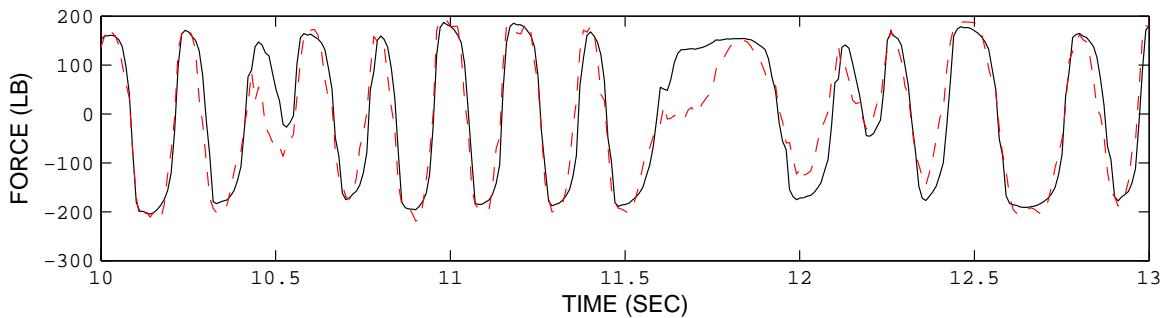


Figure H.26: Comparison of the measured and identified damper response in time history using RFM for 0.95 ampere MR damper input current test No. 4 (MRD1\_X11V\_M095\_S00\_00004\_001). The solid line is the measured force and the dashed line is the identified force.

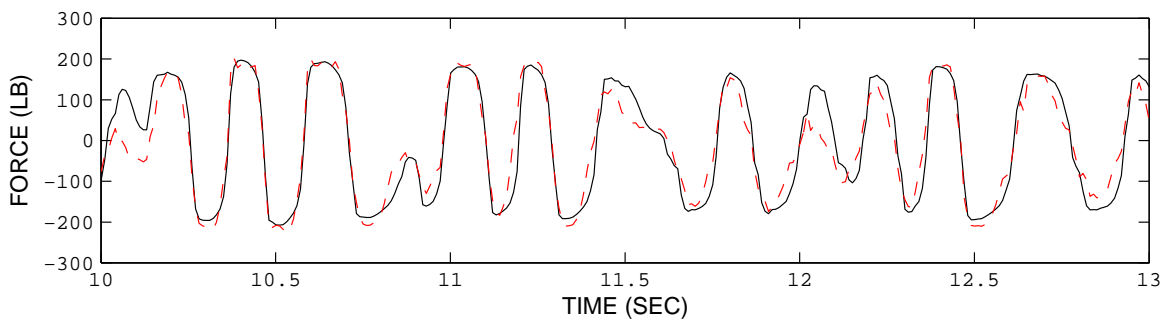


Figure H.27: Comparison of the measured and identified damper response in time history using RFM for 0.95 ampere MR damper input current test No. 5 (MRD1\_X11V\_M095\_S00\_00005\_001). The solid line is the measured force and the dashed line is the identified force.

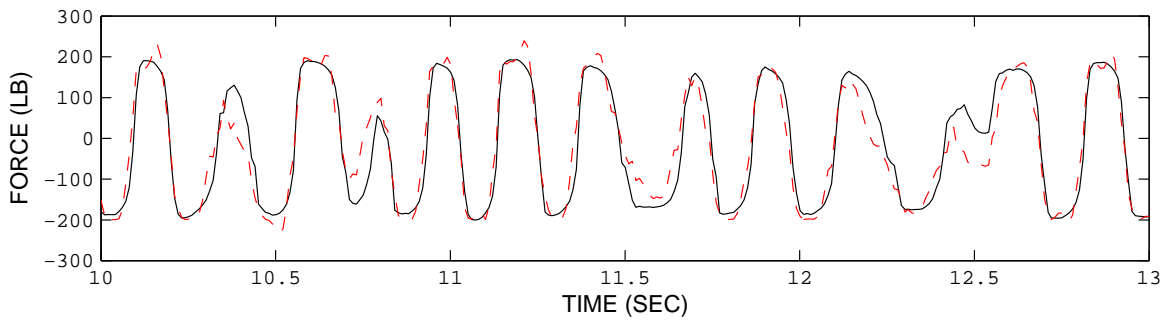


Figure H.28: Comparison of the measured and identified damper response in time history using RFM for 0.95 ampere MR damper input current test No. 6 (MRD1\_X11V\_M095\_S00\_00006\_001). The solid line is the measured force and the dashed line is the identified force.

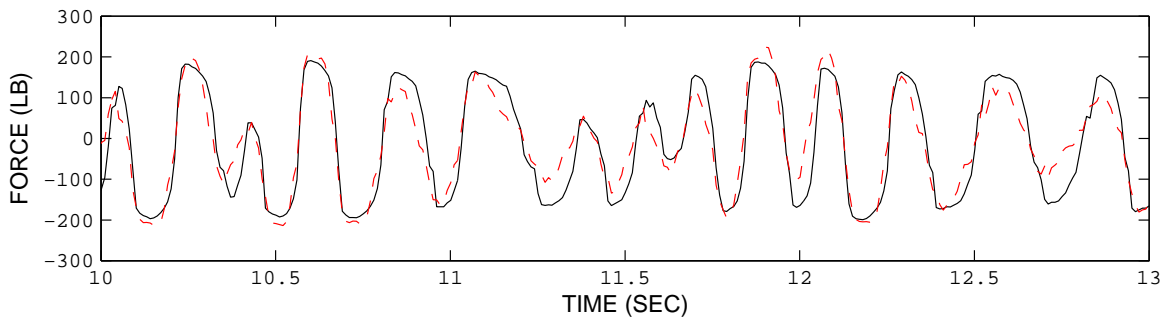


Figure H.29: Comparison of the measured and identified damper response in time history using RFM for 0.95 ampere MR damper input current test No. 7 (MRD1\_X11V\_M095\_S00\_00007\_001). The solid line is the measured force and the dashed line is the identified force.

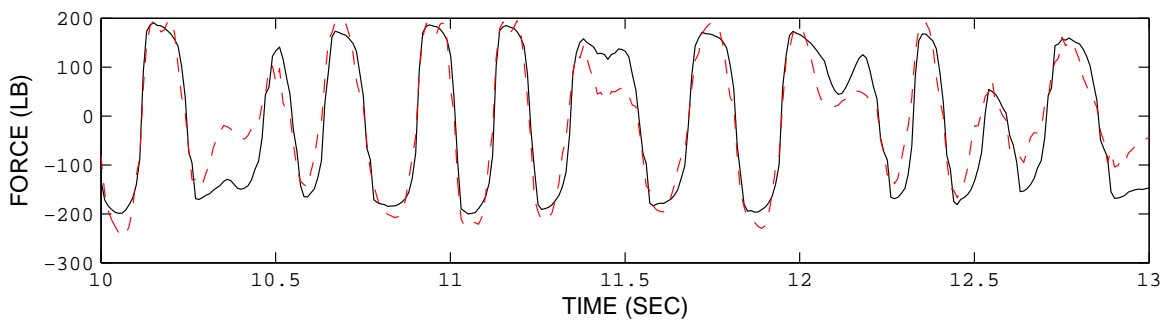


Figure H.30: Comparison of the measured and identified damper response in time history using RFM for 0.95 ampere MR damper input current test No. 8 (MRD1\_X11V\_M095\_S00\_00008\_001). The solid line is the measured force and the dashed line is the identified force.

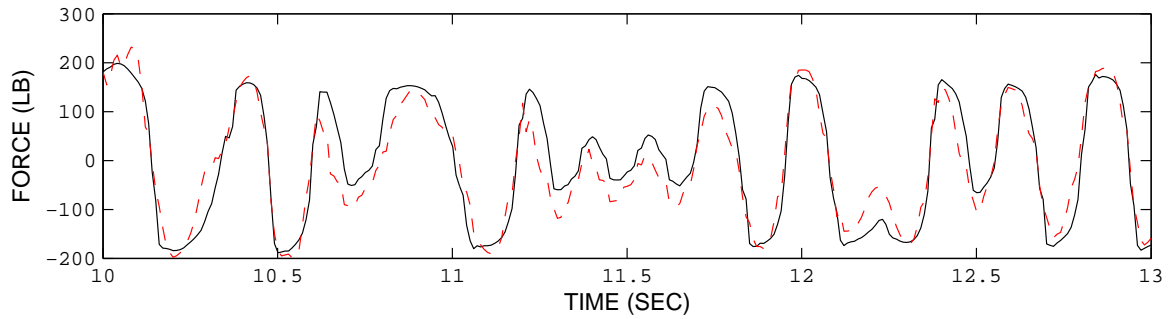


Figure H.31: Comparison of the measured and identified damper response in time history using RFM for 0.95 ampere MR damper input current test No. 9 (MRD1\_X11V\_M095\_S00\_00009\_001). The solid line is the measured force and the dashed line is the identified force.

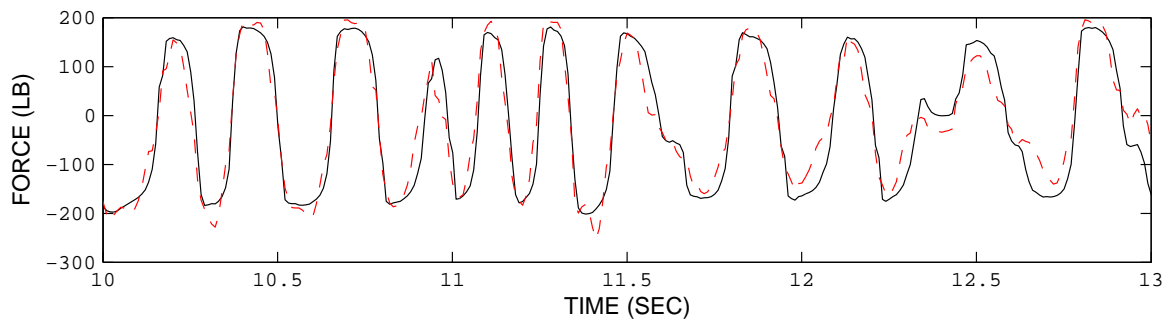


Figure H.32: Comparison of the measured and identified damper response in time history using RFM for 0.95 ampere MR damper input current test No. 10 (MRD1\_X11V\_M095\_S00\_00010\_001). The solid line is the measured force and the dashed line is the identified force.

### H.2.3 Comparison of Measured and Identified MR Damper Force for 0.90 Ampere Input Current (90%)

Figures H.33 - H.42 show the comparison of the measured and identified damper response in time history using RFM for 0.90 ampere MR damper input current test No. 1 (MRD1\_X11V\_M090\_S00\_00001\_001) to test No. 10 (MRD1\_X11V\_M090\_S00\_00010\_001). The solid line is the measured force and the dashed line is the identified force.

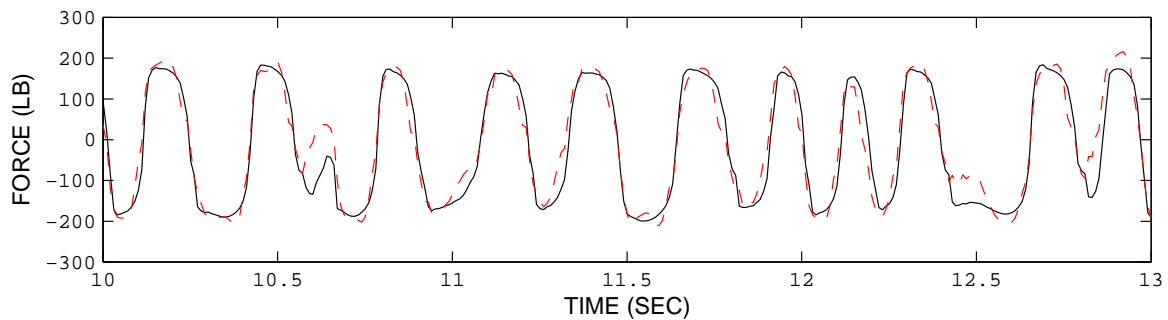


Figure H.33: Comparison of the measured and identified damper response in time history using RFM for 0.90 ampere MR damper input current test No. 1 (MRD1\_X11V\_M090\_S00\_00001\_001). The solid line is the measured force and the dashed line is the identified force.

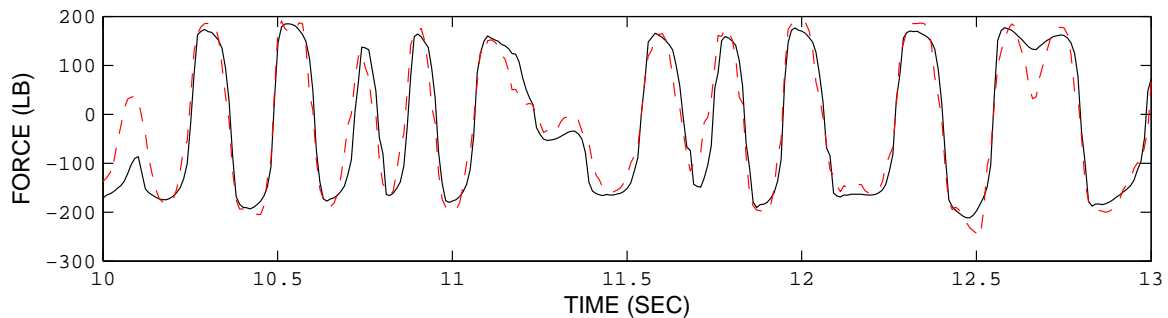


Figure H.34: Comparison of the measured and identified damper response in time history using RFM for 0.90 ampere MR damper input current test No. 2 (MRD1\_X11V\_M090\_S00\_00002\_001). The solid line is the measured force and the dashed line is the identified force.

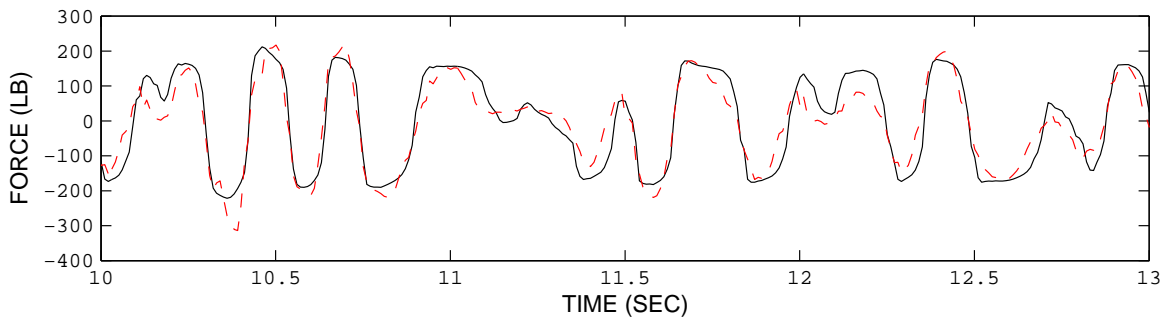


Figure H.35: Comparison of the measured and identified damper response in time history using RFM for 0.90 ampere MR damper input current test No. 3 (MRD1\_X11V\_M090\_S00\_00003\_001). The solid line is the measured force and the dashed line is the identified force.

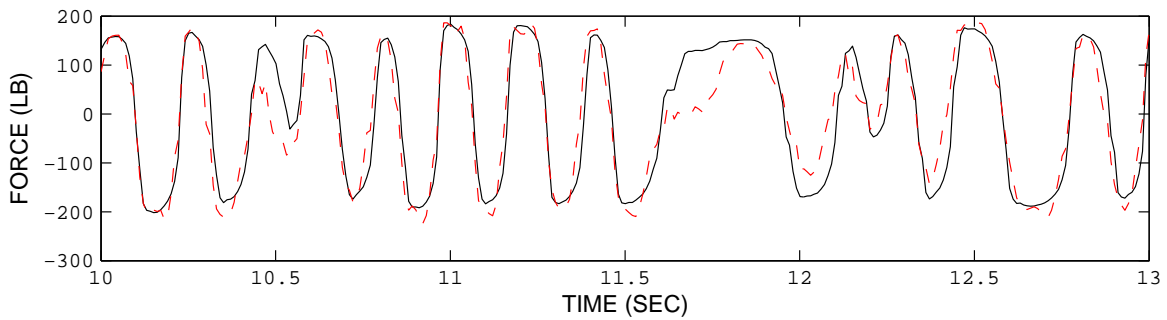


Figure H.36: Comparison of the measured and identified damper response in time history using RFM for 0.90 ampere MR damper input current test No. 4 (MRD1\_X11V\_M090\_S00\_00004\_001). The solid line is the measured force and the dashed line is the identified force.

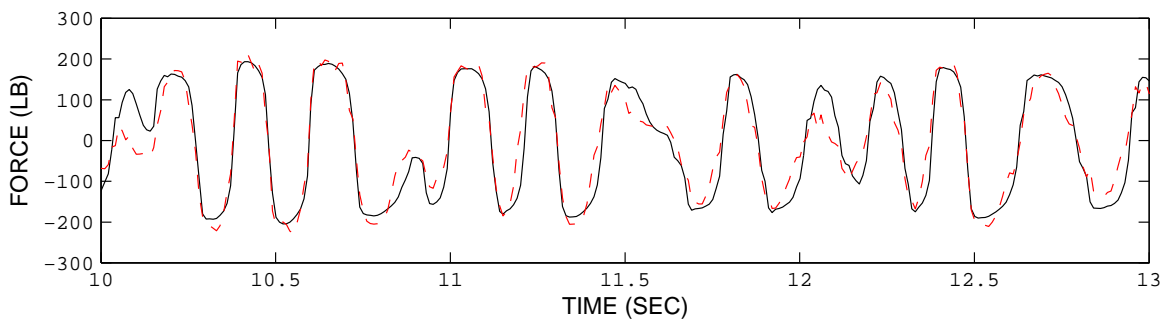


Figure H.37: Comparison of the measured and identified damper response in time history using RFM for 0.90 ampere MR damper input current test No. 5 (MRD1\_X11V\_M090\_S00\_00005\_001). The solid line is the measured force and the dashed line is the identified force.

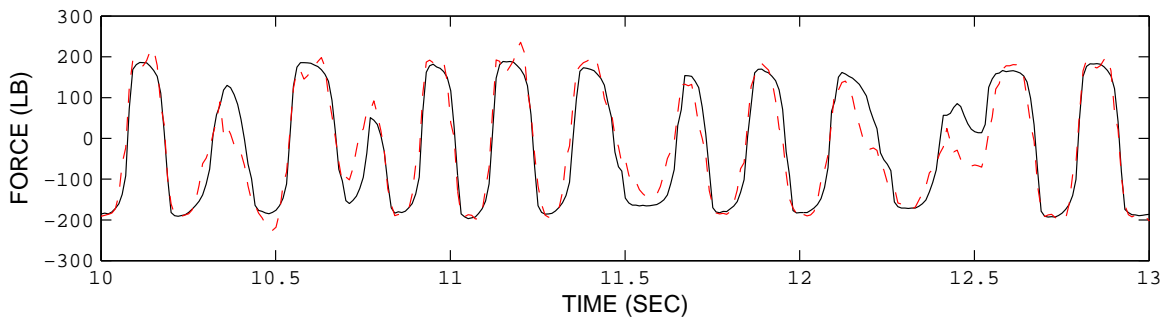


Figure H.38: Comparison of the measured and identified damper response in time history using RFM for 0.90 ampere MR damper input current test No. 6 (MRD1\_X11V\_M090\_S00\_00006\_001). The solid line is the measured force and the dashed line is the identified force.

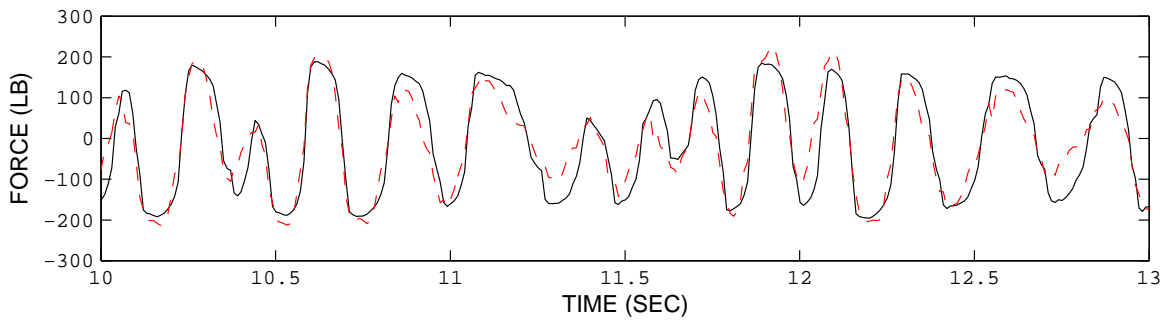


Figure H.39: Comparison of the measured and identified damper response in time history using RFM for 0.90 ampere MR damper input current test No. 7 (MRD1\_X11V\_M090\_S00\_00007\_001). The solid line is the measured force and the dashed line is the identified force.

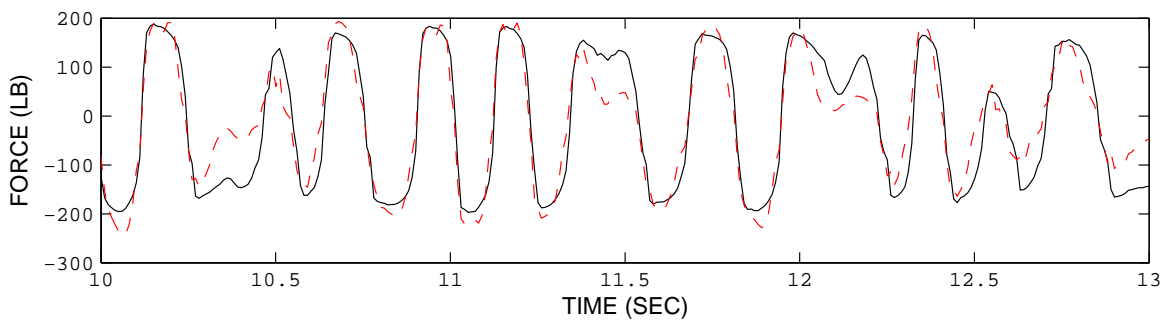


Figure H.40: Comparison of the measured and identified damper response in time history using RFM for 0.90 ampere MR damper input current test No. 8 (MRD1\_X11V\_M090\_S00\_00008\_001). The solid line is the measured force and the dashed line is the identified force.

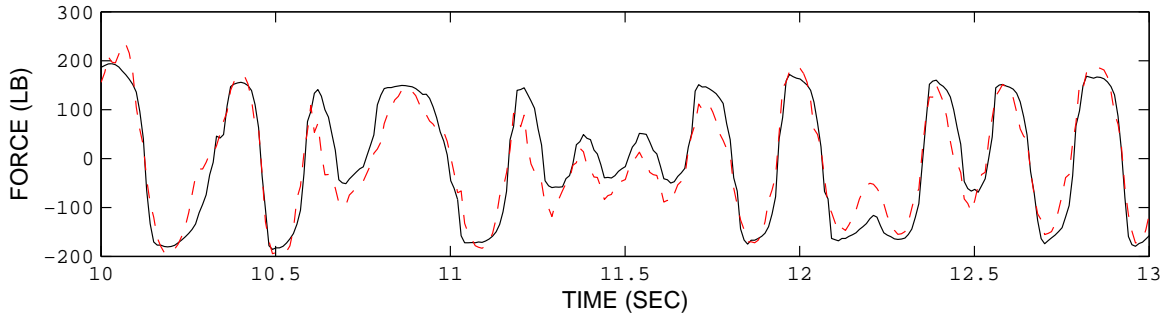


Figure H.41: Comparison of the measured and identified damper response in time history using RFM for 0.90 ampere MR damper input current test No. 9 (MRD1\_X11V\_M090\_S00\_00009\_001). The solid line is the measured force and the dashed line is the identified force.

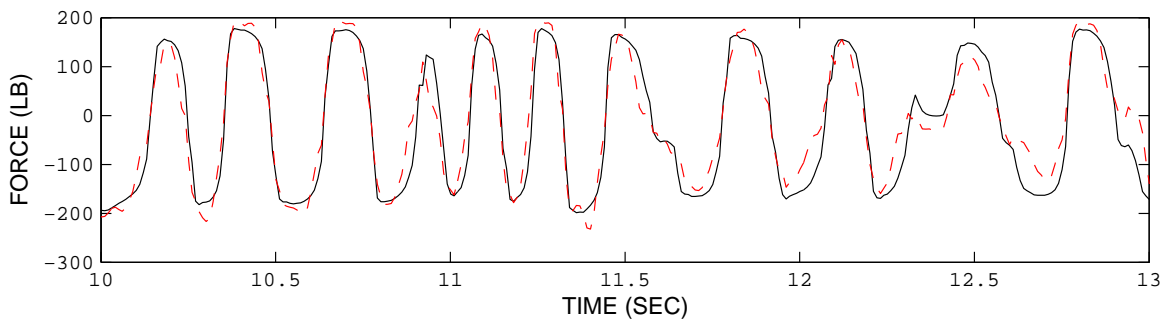


Figure H.42: Comparison of the measured and identified damper response in time history using RFM for 0.90 ampere MR damper input current test No. 10 (MRD1\_X11V\_M090\_S00\_00010\_001). The solid line is the measured force and the dashed line is the identified force.

## H.2.4 Comparison of Measured and Identified MR Damper Force for 0.75 Ampere Input Current (75%)

Figures H.43 - H.52 show the comparison of the measured and identified damper response in time history using RFM for 0.75 ampere MR damper input current test No. 1 (MRD1\_X11V\_M075\_S00\_00001\_001) to test No. 10 (MRD1\_X11V\_M075\_S00\_00010\_001). The solid line is the measured force and the dashed line is the identified force.

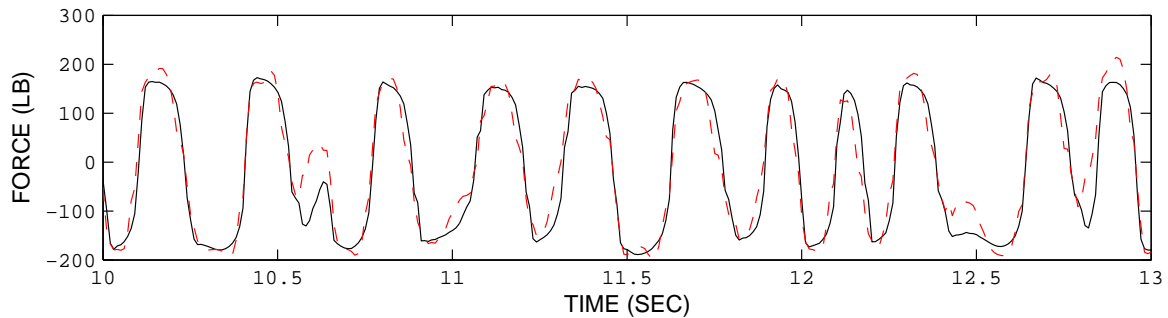


Figure H.43: Comparison of the measured and identified damper response in time history using RFM for 0.75 ampere MR damper input current test No. 1 (MRD1\_X11V\_M075\_S00\_00001\_001). The solid line is the measured force and the dashed line is the identified force.

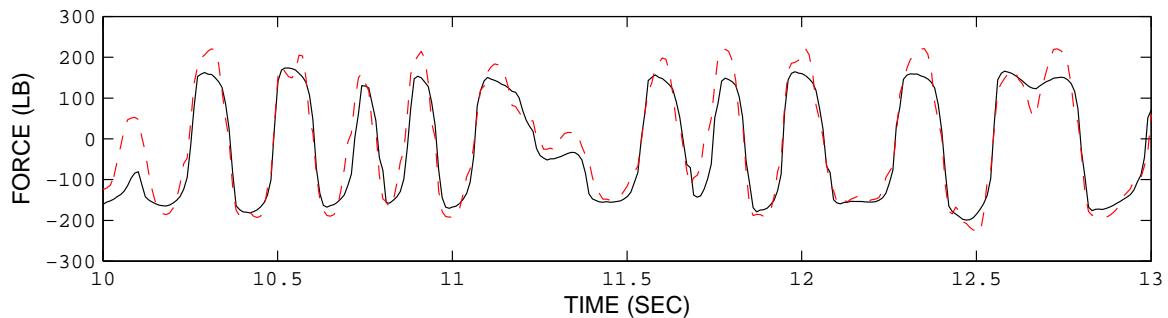


Figure H.44: Comparison of the measured and identified damper response in time history using RFM for 0.75 ampere MR damper input current test No. 2 (MRD1\_X11V\_M075\_S00\_00002\_001). The solid line is the measured force and the dashed line is the identified force.

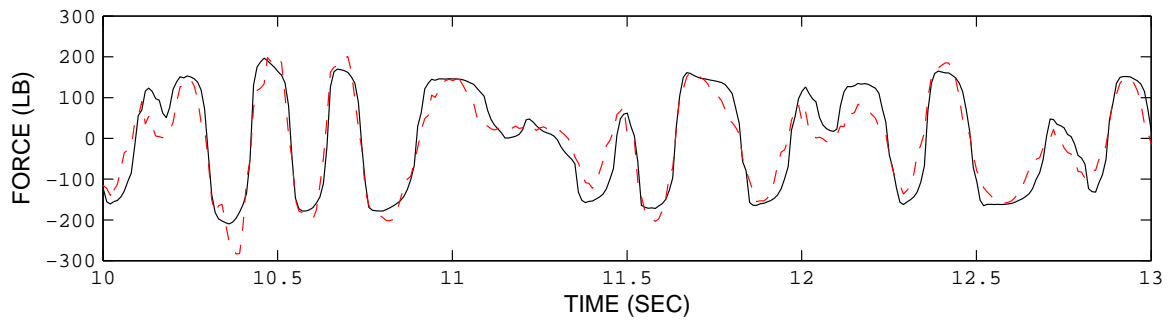


Figure H.45: Comparison of the measured and identified damper response in time history using RFM for 0.75 ampere MR damper input current test No. 3 (MRD1\_X11V\_M075\_S00\_00003\_001). The solid line is the measured force and the dashed line is the identified force.

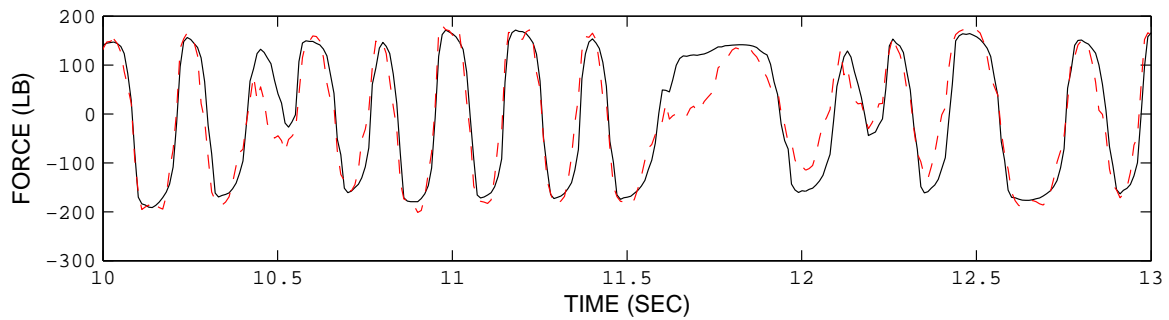


Figure H.46: Comparison of the measured and identified damper response in time history using RFM for 0.75 ampere MR damper input current test No. 4 (MRD1\_X11V\_M075\_S00\_00004\_001). The solid line is the measured force and the dashed line is the identified force.

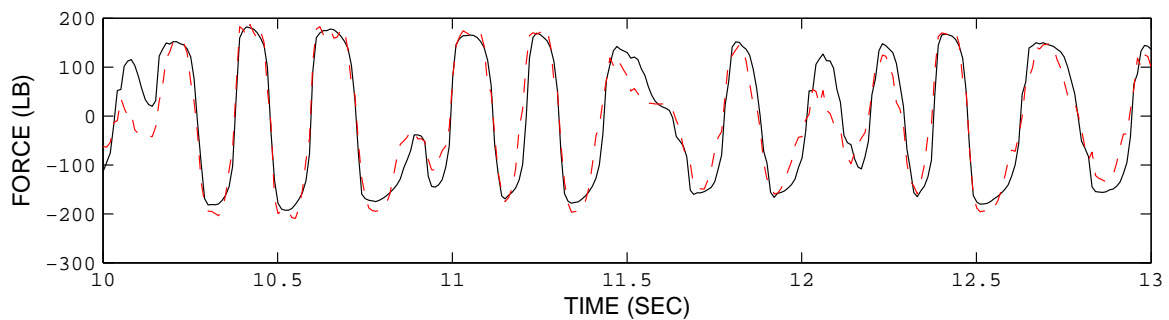


Figure H.47: Comparison of the measured and identified damper response in time history using RFM for 0.75 ampere MR damper input current test No. 5 (MRD1\_X11V\_M075\_S00\_00005\_001). The solid line is the measured force and the dashed line is the identified force.

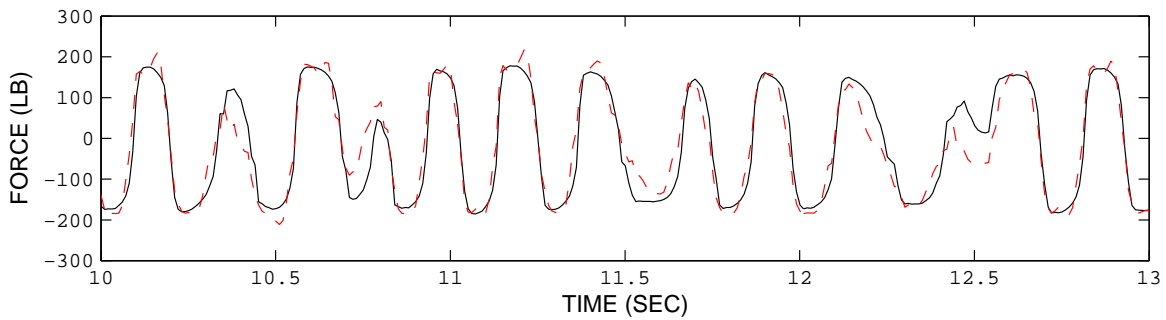


Figure H.48: Comparison of the measured and identified damper response in time history using RFM for 0.75 ampere MR damper input current test No. 6 (MRD1\_X11V\_M075\_S00\_00006\_001). The solid line is the measured force and the dashed line is the identified force.

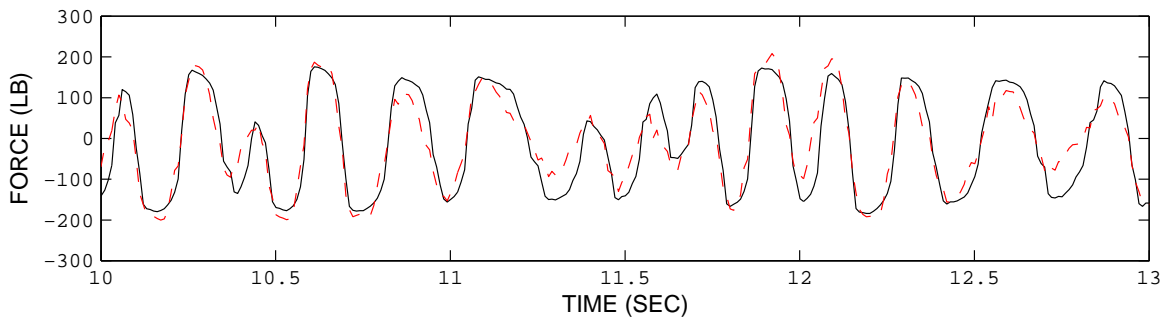


Figure H.49: Comparison of the measured and identified damper response in time history using RFM for 0.75 ampere MR damper input current test No. 7 (MRD1\_X11V\_M075\_S00\_00007\_001). The solid line is the measured force and the dashed line is the identified force.

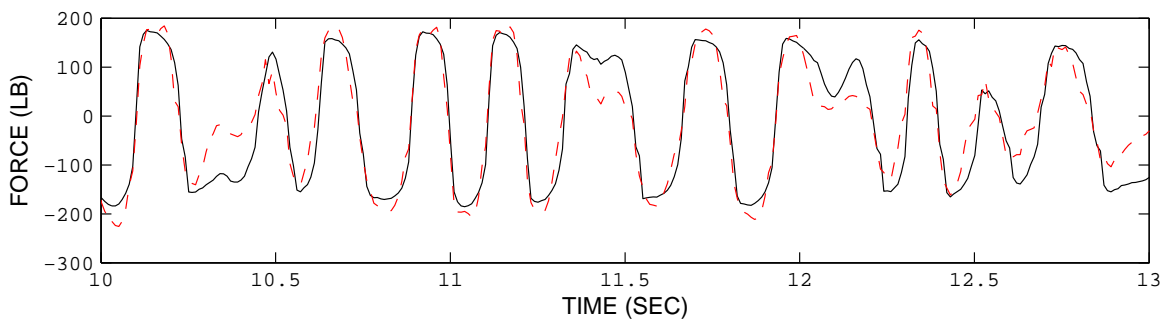


Figure H.50: Comparison of the measured and identified damper response in time history using RFM for 0.75 ampere MR damper input current test No. 8 (MRD1\_X11V\_M075\_S00\_00008\_001). The solid line is the measured force and the dashed line is the identified force.

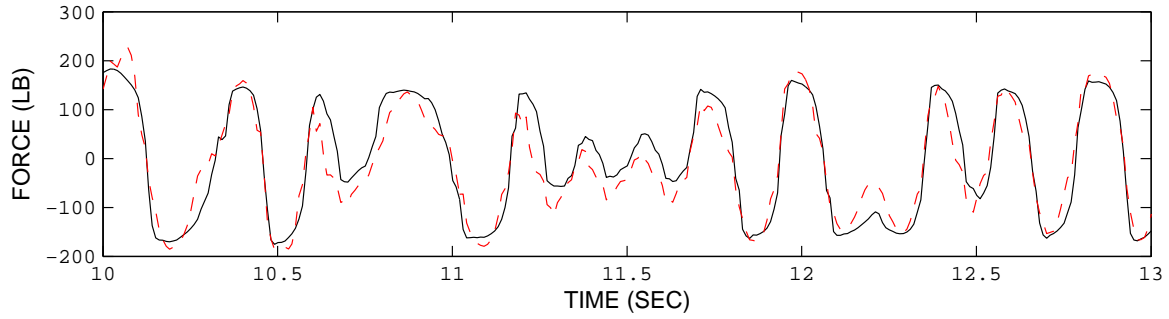


Figure H.51: Comparison of the measured and identified damper response in time history using RFM for 0.75 ampere MR damper input current test No. 9 (MRD1\_X11V\_M075\_S00\_00009\_001). The solid line is the measured force and the dashed line is the identified force.

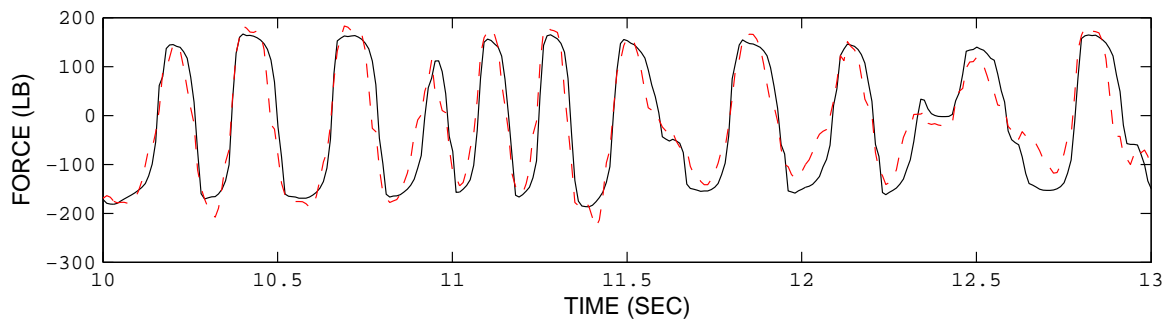
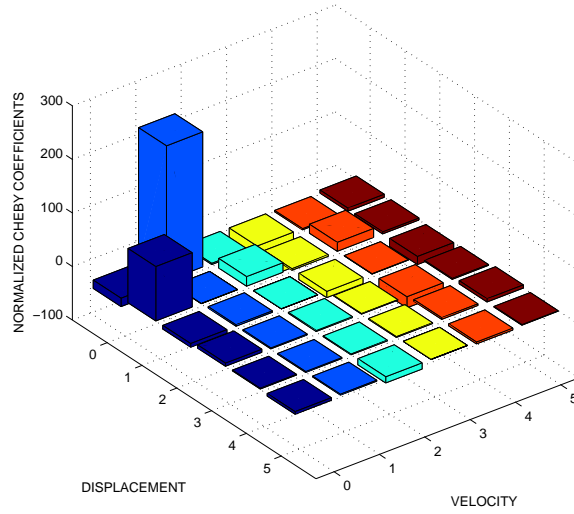
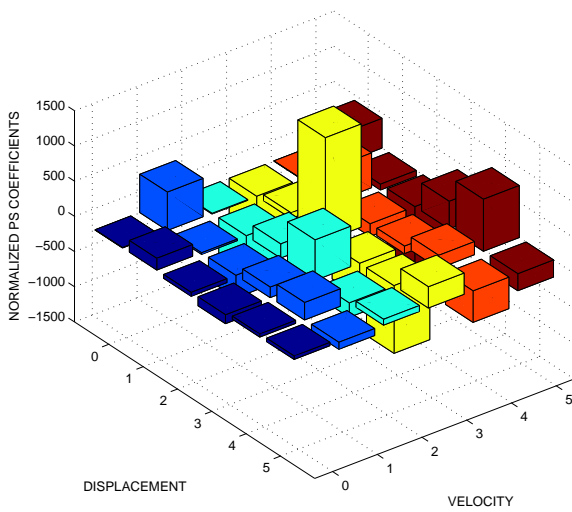


Figure H.52: Comparison of the measured and identified damper response in time history using RFM for 0.75 ampere MR damper input current test No. 10 (MRD1\_X11V\_M075\_S00\_00010\_001). The solid line is the measured force and the dashed line is the identified force.

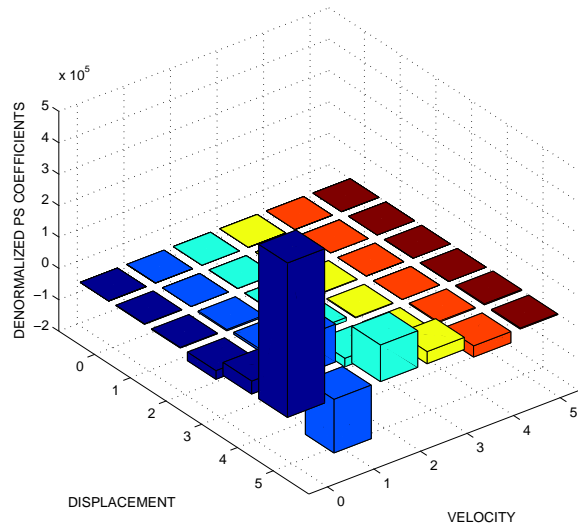
### H.2.5 Chebyshev Coefficients for the MR Damper



(a) Normalized Chebyshev coefficients

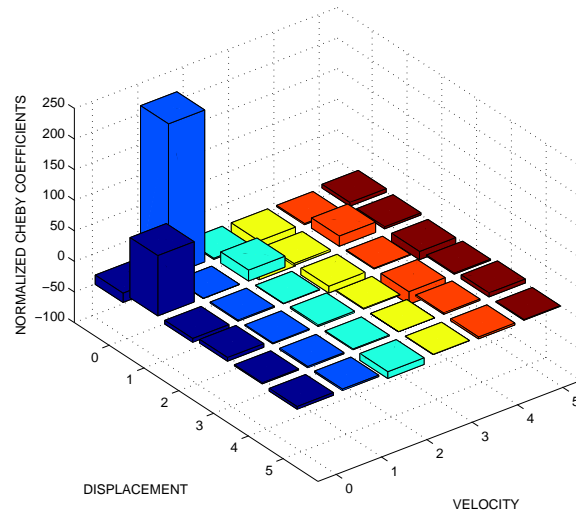


(b) Normalized power series coefficients

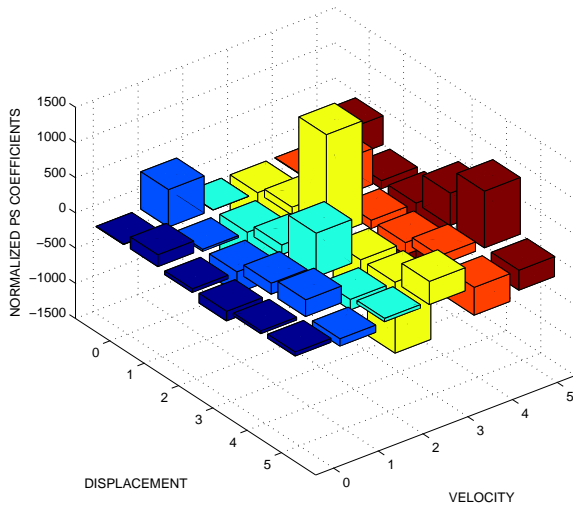


(c) Denormalized power series coefficients

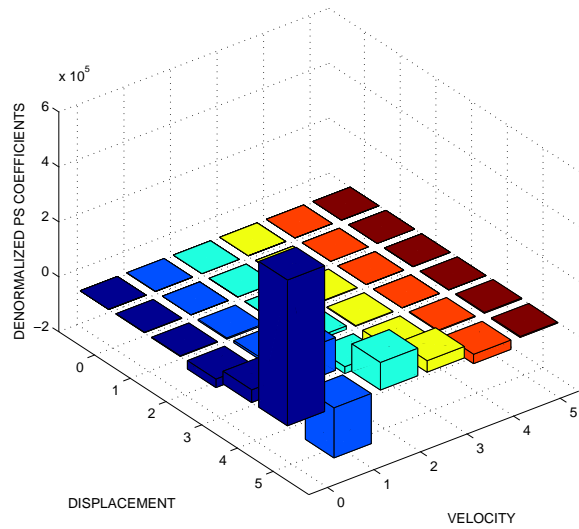
Figure H.53: The averaged restoring force coefficients for 1.0 ampere MR damper input current. The coefficients were averaged over MRD1\_X11V\_M100\_S00\_00001 to MRD1\_X11V\_M100\_S00\_00010.



(a) Normalized Chebyshev coefficients

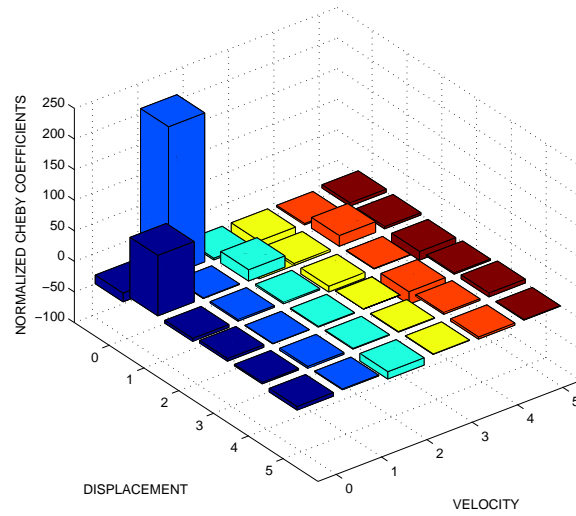


(b) Normalized power series coefficients

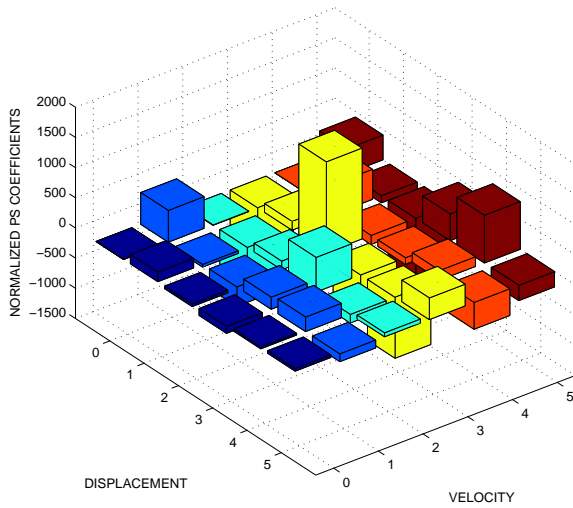


(c) Denormalized power series coefficients

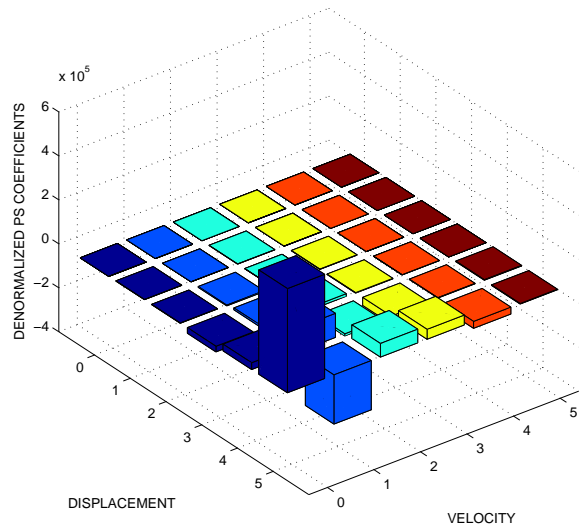
Figure H.54: The averaged restoring force coefficients for 0.95 ampere MR damper input current. The coefficients were averaged over MRD1\_X11V\_M095\_S00\_00001 to MRD1\_X11V\_M095\_S00\_00010.



(a) Normalized Chebyshev coefficients

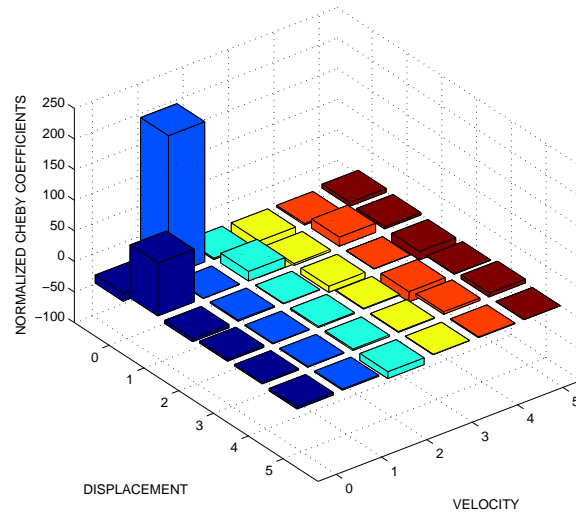


(b) Normalized power series coefficients

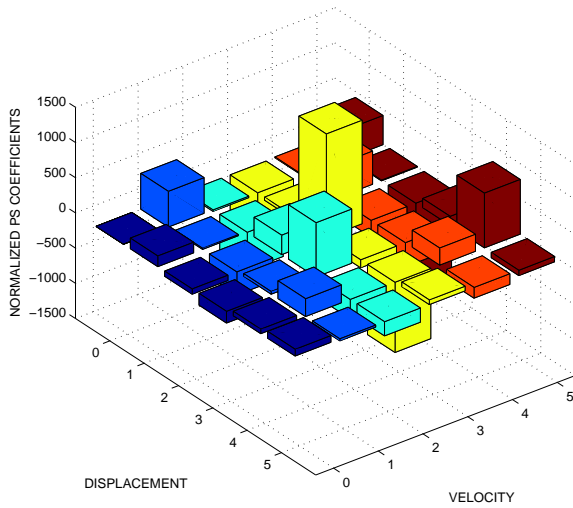


(c) Denormalized power series coefficients

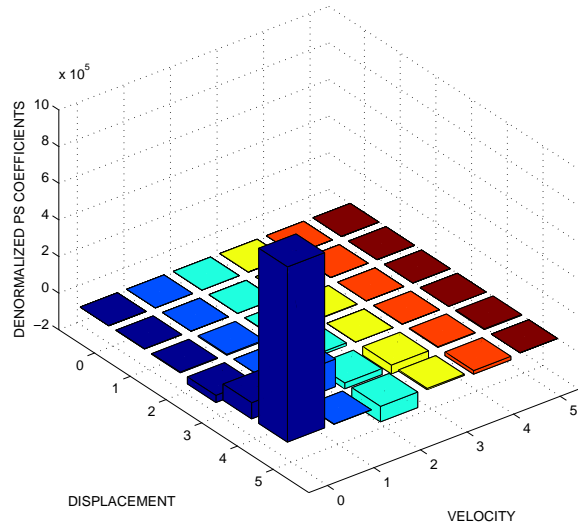
Figure H.55: The averaged restoring force coefficients for 0.90 ampere MR damper input current. The coefficients were averaged over MRD1\_X11V\_M090\_S00\_00001 to MRD1\_X11V\_M090\_S00\_00010.



(a) Normalized Chebyshev coefficients



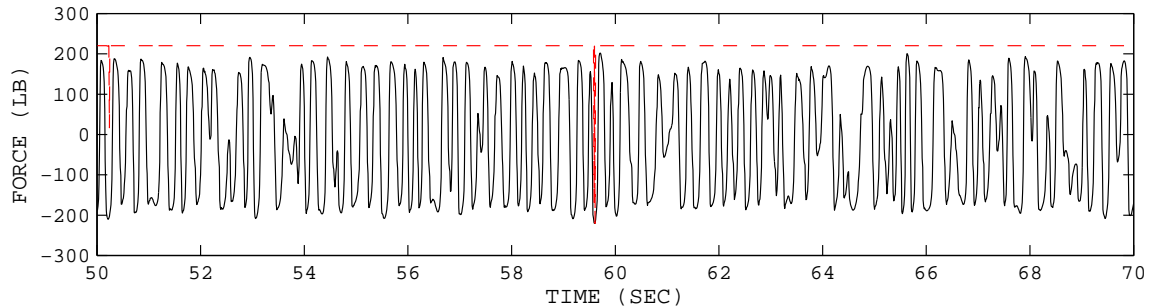
(b) Normalized power series coefficients



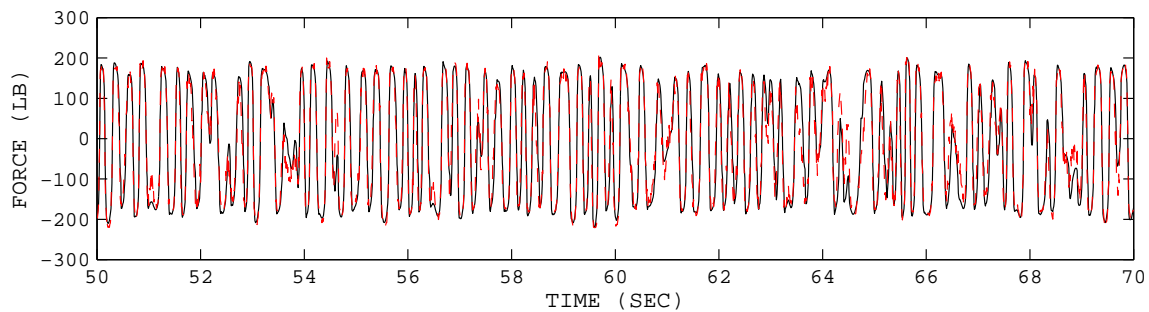
(c) Denormalized power series coefficients

Figure H.56: The averaged restoring force coefficients for 0.75 ampere MR damper input current. The coefficients were averaged over MRD1\_X11V\_M075\_S00\_00001 to MRD1\_X11V\_M075\_S00\_00010.

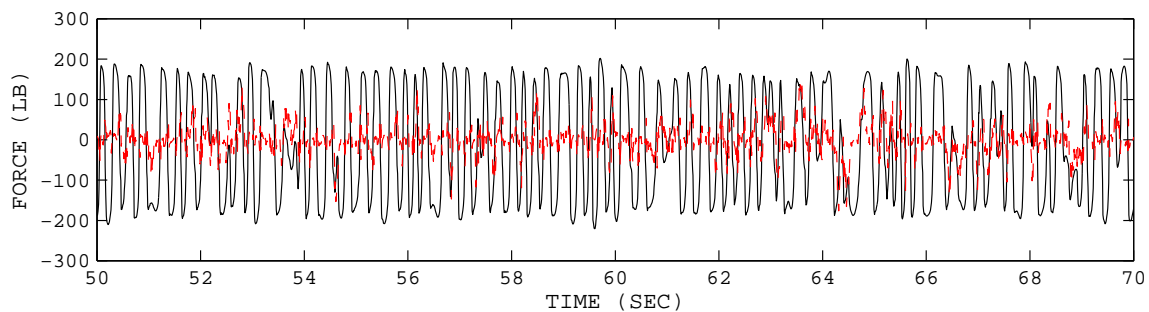
### H.3 Artificial Neural Networks



(a) Force before training

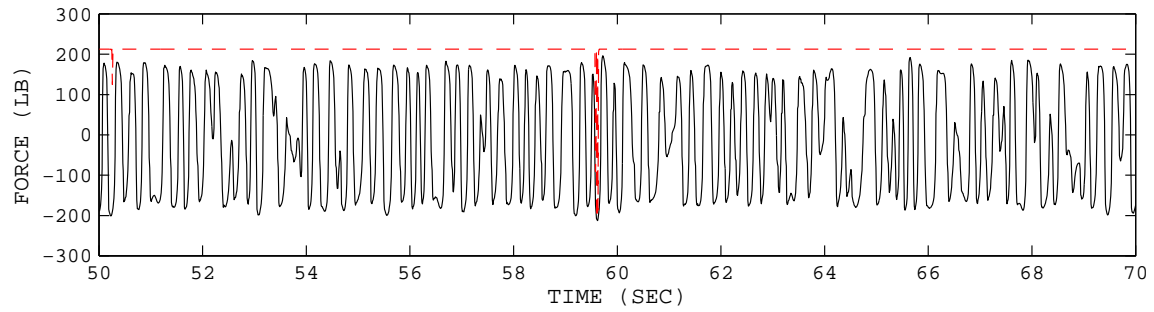


(b) Force after training

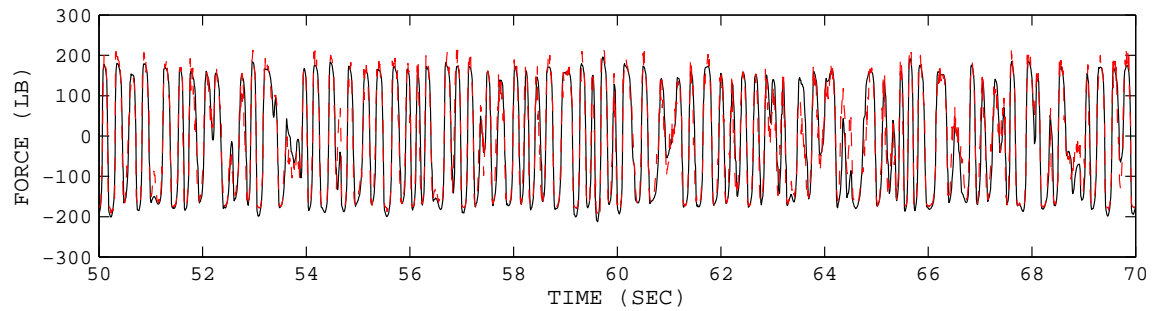


(c) Error after training

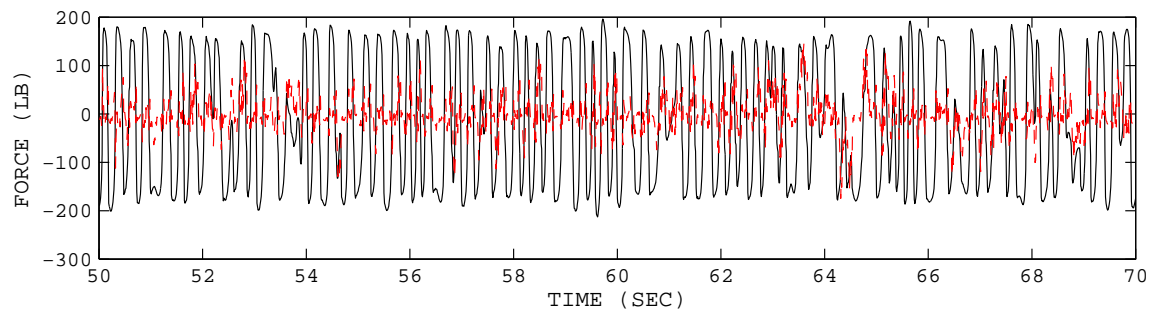
Figure H.57: Comparison of the measured and identified damper response in time history for 1.0 ampere MR damper input current (MRD1\_X11V\_M100\_S00-00001-001). The solid line is the measured force and the dashed line is the identified force.



(a) Force before training

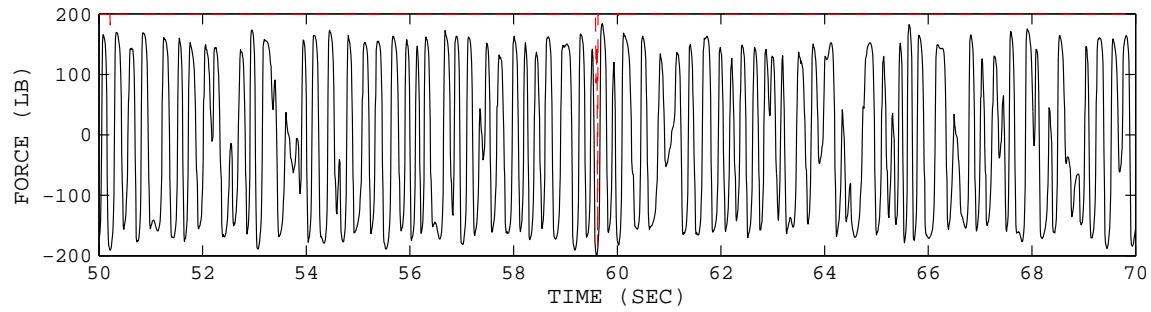


(b) Force after training

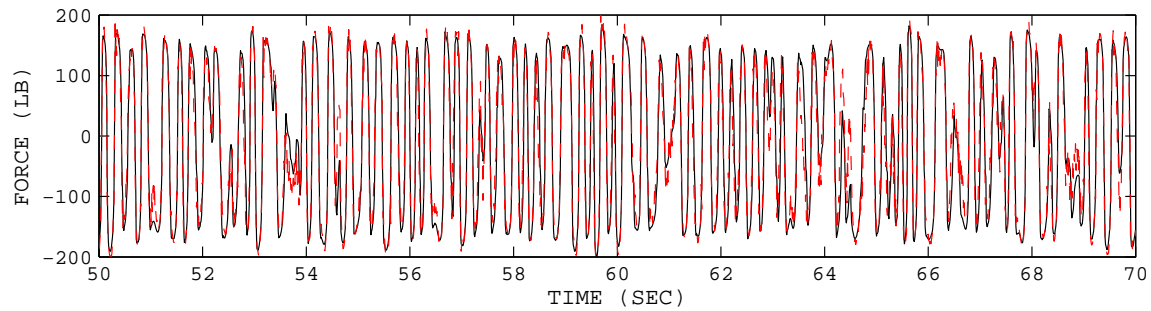


(c) Error after training

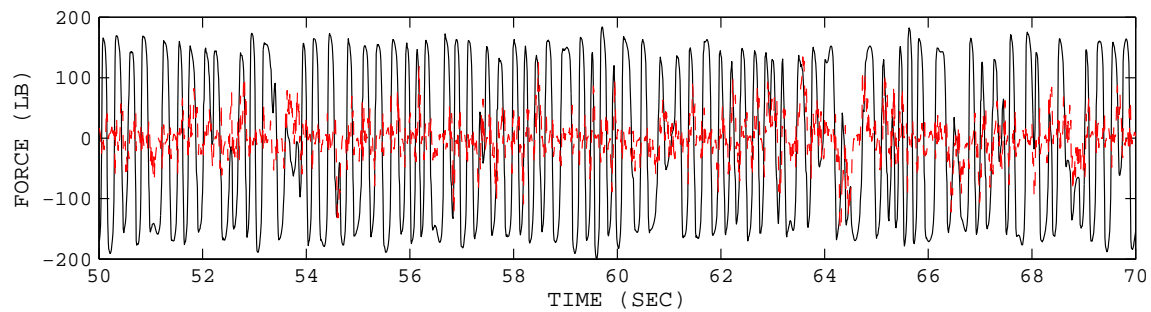
Figure H.58: Comparison of the measured and identified damper response in time history for 0.90 ampere MR damper input current (MRD1\_X11V\_M090\_S00\_00001.001). The solid line is the measured force and the dashed line is the identified force.



(a) Force before training



(b) Force after training



(c) Error after training

Figure H.59: Comparison of the measured and identified damper response in time history for 0.75 ampere MR damper input current (MRD1\_X11V\_M075\_S00\_00001\_001). The solid line is the measured force and the dashed line is the identified force.